

Universitat Jaume I
Department of Industrial Systems Engineering and Design



PREDICTION AND IMPROVEMENT OF
PART QUALITY IN MULTI-STATION
MACHINING SYSTEMS APPLYING THE
STREAM OF VARIATION MODEL

*A dissertation submitted in partial fulfillment of the requirements for the
degree of Doctor of Philosophy*

Author: José Vicente Abellán Nebot

Advisors: Dr. Fernando Romero Subirón
Dr. Roberto Sanchis Llopis

Castellón de la Plana, 2011

Universitat Jaume I
Departamento de Ingeniería de Sistemas Industriales y Diseño



PREDICCIÓN Y MEJORA DE LA CALIDAD
EN SISTEMAS DE MECANIZADO
MULTI-ESTACIÓN MEDIANTE EL MODELO
DE FLUJOS DE VARIACIÓN (STREAM OF
VARIATION)

*Documento remitido en cumplimiento parcial de los requisitos para la
obtención del grado de Doctor*

Autor: D. José Vicente Abellán Nebot

Directores: Dr. Fernando Romero Subirón
Dr. Roberto Sanchis Llopis

Castellón de la Plana, 2011

Resumen

En los últimos años, con objeto de integrar el conocimiento del proceso de fabricación en la etapa de desarrollo integrado de producto-proceso, se han realizado grandes esfuerzos hacia el desarrollo de modelos matemáticos que expliquen la relación entre las fuentes de variación en fabricación con las dispersiones producidas en la calidad dimensional y geométrica de las piezas fabricadas en sistemas de mecanizado multi-estación. Esta integración posibilita el desarrollo de un gran número de aplicaciones para la mejora del diseño del producto y del propio proceso de fabricación, como la detección de fuentes de variación críticas en el proceso, la selección de la estación donde realizar una inspección en proceso, la definición de planes de proceso robustos, el control activo de la variabilidad o el análisis/síntesis de tolerancias orientado al proceso. Sin embargo, en la actualidad existen todavía importantes limitaciones en el desarrollo de estos modelos e incluso algunas de sus aplicaciones potenciales no han sido, todavía, estudiadas y desarrolladas.

Con el propósito de mejorar estos modelos y su aplicabilidad, la investigación se ha dirigido hacia la definición de una metodología que incluya los errores de mecanizado a nivel uni-estación en modelos 3D de propagación de errores capaces de predecir con precisión la calidad de las piezas mecanizadas en sistemas multi-estación y hacia el desarrollo de nuevas estrategias para la mejora de la calidad.

Propósito que se concreta en los siguientes objetivos generales:

- Revisar las fuentes de error del mecanizado que más influyen en la calidad micro- y macro-geométrica de las piezas mecanizadas.
- Revisar los modelos analíticos que cuantifican el impacto de las principales fuentes de error sobre la calidad dimensional en procesos de mecanizado uni- y multi-estación.
- Extender los actuales modelos analíticos de predicción multi-estación, que sólo describen el impacto de algunos errores de mecanizado, incluyendo otras fuentes de error todavía no consideradas en este contexto. Para ello, los errores de mecanizado a nivel uni-estación se deberán formular de modo que sea factible su incorporación en los complejos modelos de propagación de errores a nivel multi-estación.
- Desarrollar nuevas aplicaciones para la mejora de la calidad en procesos de mecanizado multi-estación. En estas aplicaciones se propondrán procedimientos para el diseño robusto de sistemas de mecanizado multi-estación, la compensación de errores en estaciones aguas abajo de donde éstos aparecen, y la determinación de las tolerancias del proceso de fabricación que minimicen su coste.

Para conseguir estos objetivos, se ha seguido una metodología de investigación basada en los siguientes pasos: identificación y clarificación del problema; establecimiento de las hipótesis de trabajo; formulación matemática del problema; definición de la metodología a seguir para su resolución; validación del modelo matemático y de la metodología propuesta mediante la resolución numérica y/o experimental de un caso de estudio.

Las propuestas y resultados de la investigación, junto con los conceptos y antecedentes necesarios, se han plasmado en la presente memoria, organizada en tres partes. La primera parte presenta una revisión de la literatura donde se realiza un análisis detallado de las fuentes de error de mecanizado que producen errores micro- y macro-geométricos en las superficies mecanizadas a nivel de uni-estación. En ella, se presentan las principales fuentes de error así como los modelos físicos/analíticos empleados para la estimación de la calidad resultante tras el mecanizado. La formulación de los modelos estudiados ha sido adaptada con objeto de mantener la consistencia en la derivación de los modelos y facilitar así su comprensión y su posterior uso en la predicción de la calidad final a nivel multi-estación. Aunque la descripción se centra en los modelos analíticos, también se presentan brevemente otros modelos más complejos basados en datos experimentales y herramientas matemáticas como regresiones múltiples o técnicas de inteligencia artificial, mostrando así una visión general de la predicción de la calidad de la pieza en sistemas de mecanizado uni-estación. Al final de esta primera parte, se presenta una revisión de los dos modelos 3D de propagación de errores en sistemas de mecanizado multi-estación más populares: el modelo de flujos/cadenas de variación (Stream of Variation –SoV–) y el modelo de la pieza fabricada (Model of Manufactured Part –MoMP–). Con objeto de mostrar su aplicación práctica, ambos modelos se han aplicado a un sencillo caso de estudio 2D para la predicción de la calidad final de la pieza, analizándose las principales ventajas, inconvenientes y potenciales aplicaciones de cada uno de ellos.

En la segunda y tercera parte de la memoria se presentan las principales aportaciones: la extensión del actual modelo SoV y el desarrollo de nuevas metodologías, basadas en este mismo modelo, para la mejora de la calidad en procesos de mecanizado multi-estación. En la segunda parte se muestra, numérica y experimentalmente, la importancia que pueden tener los errores inducidos por el proceso de mecanizado en la calidad final, como es el caso de aquéllos inducidos por la expansión térmica de la máquina-herramienta, el desgaste de la herramienta de corte, etc., y la necesidad de incluir estos errores dentro del propio modelo SoV. La extensión del modelo SoV se formula en detalle al final de la segunda parte de la tesis, validándose experimentalmente con una mejora en la predicción del 67% para el caso de estudio analizado y abriéndose la puerta a un importante campo de aplicación para la predicción y mejora de la calidad en procesos de mecanizado multi-estación.

Por último, la tercera parte de la tesis presenta algunas de las potenciales aplicaciones del actual modelo SoV, y de su versión extendida, para la mejora de la calidad en sistemas multi-estación. La primera aplicación muestra el uso del modelo SoV en sistemas de mecanizado multi-estación con máquinas-herramientas basadas en CNC donde, estimando los errores generados en la pieza, es posible modificar las trayectorias de las herramientas de corte y compensar así, parcialmente, el error esperado en la pieza final. Para ello, se propone el uso de utillajes basados en sensores de precisión de forma que, optimizando la

distribución de los sensores en el utillaje, se maximice la información obtenida para poder así estimar los errores existentes en el proceso aguas arriba de la estación y compensar el efecto de estos errores mediante la modificación de la trayectoria de la herramienta de corte. La segunda aplicación se centra en la evaluación y mejora de los planes de proceso de fabricación mediante el uso del modelo SoV y datos de históricos de planta. La principal contribución de este trabajo es el uso de la información de los históricos de planta para la extracción de las capacidades de las máquinas-herramienta y el desarrollo de una metodología sistemática, basada en la evaluación de índices de sensibilidad, para la detección de componentes críticos del plan de procesos de fabricación (localizadores críticos en la localización de la pieza en máquina y máquinas-herramientas críticas por su limitada capacidad de fabricación). Finalmente, la tercera aplicación muestra el uso del modelo extendido SoV para la determinación de las tolerancias del proceso de fabricación en sistemas multi-estación. La síntesis de estas tolerancias, mediante el modelo SoV actual, únicamente determina la variabilidad admisible de los componentes del utillaje (por ejemplo, tolerancias admisible de los localizadores distribuidos según esquema 3-2-1) que aseguran una calidad geométrica de la pieza a un mínimo coste de fabricación. Al no considerarse otras fuentes de variabilidad en el proceso de fabricación, no es posible asegurar ni la consecución de una determinada calidad de la pieza final ni un coste de fabricación mínimo. La aplicación del modelo extendido SoV, al incluir nuevas variables de proceso como es el desgaste máximo admisible de la herramienta de corte o la máxima expansión térmica del husillo en las diferentes estaciones de mecanizado, permite una definición más general del problema de asignación de las tolerancias a las especificaciones del proceso de fabricación, estimando de forma más precisa el coste final.

Las aportaciones de esta tesis doctoral también abren la puerta a otras aplicaciones orientadas a la mejora de la calidad en procesos de mecanizado multi-estación. Entre estos trabajos futuros de investigación podemos citar los siguientes: diagnóstico de fallos en sistemas de fabricación multi-estación, contemplando las causas del propio proceso de mecanizado; identificación de las variables de proceso críticas que impiden obtener la calidad geométrica de la pieza durante la planificación de procesos; optimización global de los parámetros de corte, tales como profundidad de corte, velocidad de corte, avances, etc., con el objeto de minimizar el coste de fabricación y respetar unas determinadas especificaciones geométricas.

Adicionalmente, para salvar algunas de las hipótesis simplificadoras, se propone algunas líneas de trabajo futuro dirigidas a mejorar los modelos de propagación de errores multi-estación. Entre las propuestas de trabajo futuro, más detalladas en la memoria, destacamos las siguientes:

- Los modelos de propagación de la variación en procesos de mecanizado multi-estación (SoV y MoMP) han de ser expandidos con objeto de analizar la variación de la fabricación durante el mecanizado de piezas poco rígidas. Actualmente, estos modelos se restringen a piezas rígidas.
- De igual modo, estos modelos no tienen en cuenta los errores geométricos de forma de las piezas, lo que limita en parte su aplicación. Es por ello de interés el estudio

de la incorporación en estos modelos de los errores de forma, tanto de las superficies utilizadas durante la localización, como de las superficies resultantes del mecanizado.

- El modelo SoV está definido para utillajes basados en localizadores puntuales, de modo que resulta de interés analizar su expansión de forma que pueda incluirse en el modelo utillajes habituales a nivel industrial como mordazas, platos de garras, etc.
- El modelo SoV puede ser empleado en sistemas donde se emplea utillajes con localizadores puntuales basados en el principio de localización 3-2-1, aún presentando una disposición no ortogonal. Sin embargo, el posible uso de utillajes N-2-1 es un área inexplorada que debería ser objeto de estudio.

Estas futuras líneas de investigación ayudarán a la reducción total del tiempo de producción y a la mejora de la calidad en los sistemas de mecanizado multi-estación, permitiendo que el tránsito entre la idea, o el concepto, hasta el producto fabricado, se realice de la forma más eficaz y eficiente posible, haciendo posible la obtención de la primera pieza correcta a la primera.

Acknowledgments

I would like to express my sincere gratitude to my advisors, Professor Fernando Romero and Dr. Roberto Sanchis, for give me the opportunity to work on the multidisciplinary field of manufacturing and automation and guide, support and encourage me on my research along these hard years. I would also like to extent my sincere gratitude to my colleague Dr. Jian Liu, who has been a great mentor during my stage in U.S.A and from who I learnt invaluable knowledge and abilities. Without them, this dissertation would not have become possible.

I am grateful for the support of Universitat Jaume I to fellow researchers and its commitment to provide financial support for conducting research stages in top research centers. This support let me meet first level researches in my research stages at The University of Michigan, The University of Arizona, and Tecnológico de Monterrey. The invaluable experiences and friendships acquired during these stages benefit me so much in my own research and will benefit me in my future career development. My special gratitude goes to those people who hosted me in these research stages: my advisors Prof. Rubén Morales-Menéndez, Prof. Jianjun Shi and Prof. Elijah Kannatey-Asibu, and my lab-mates and colleagues Héctor Siller, Juil Yum, Mi Gan and Briggita Bodnar. All of them made me feel at home.

Furthermore, the work presented in this thesis has been made possible by countless colleagues, staff, and faculty members along my research period. Special mention goes to my colleagues Carlos Vila, Julio Serrano, Gracia Bruscas, Antonio Estruch and Miguel Ángel Aymerich.

Finally, my most profound gratitude goes to my great family, especially my parents, for always being there for me whenever needed, and to my lovely lady María del Lledó, for her patience and support along these hard years. This thesis is especially dedicated to them.

Abstract

Recent research efforts have been aimed toward deriving mathematical models to relate manufacturing sources of variation with part quality variations in multi-station machining systems in order to integrate design and manufacturing knowledge. Such integration would make it possible to create a large number of applications to improve product and process design and manufacturing in areas such as fault diagnosis, best placement of inspection stations, process planning, dimensional control and process-oriented tolerancing. However, nowadays there are still important limitations on the development of these models and even some of their potential applications have still not been studied in detail. The comprehensive research work described in this dissertation contributes to overcome some of the current limitations in this field.

The dissertation is divided into three parts. The first part presents a comprehensive literature review of machining sources of error that produce macro and/or micro-geometrical variations on machined surfaces, and the 3D manufacturing variation models (the Stream of Variation model – SoV – and the Model of the Manufactured Part – MoMP) applied in the literature to analyze the propagation of those variations in multi-station machining processes. The second part of the dissertation highlights the current limitation of the SoV model through an experimental study where fixture- and machining-induced variations are analyzed. To overcome this limitation, the extension of the SoV model is formulated by modeling and adding machining-induced variations. The third part of the dissertation presents some potential applications of the SoV model and its extended version for part quality improvement. The first application shows how to apply the SoV model together with sensor-based fixtures when there are CNC machine-tools in the multi-station machining system in order to modify the cutting-tool path and partially compensate the expected part quality error. The second developed application deals with the evaluation and improvement of manufacturing process plans by integrating the SoV model and historical shop-floor quality data. Finally, the third application shows the use of the extended SoV model for the improvement of process-oriented tolerancing in multi-station machining processes.

Contents

| | | |
|----------|---|-----------|
| 1 | Introduction | 1 |
| 1.1 | Motivation for the proposed research | 1 |
| 1.2 | Research objectives | 5 |
| 1.3 | Research methodology | 6 |
| 1.4 | Organization of the dissertation | 7 |
| | References | 8 |
| | | |
| I | Part Quality Prediction in Uni- and Multi-Station Machin- ing Systems | 11 |
| | | |
| 2 | Source of machining errors in machine-tools | 13 |
| 2.1 | Introduction | 13 |
| 2.2 | Sources of machining errors in macro-geometric part quality | 15 |
| 2.2.1 | Fixture-dependent errors or setup errors | 16 |
| 2.2.2 | Machine-tool errors: geometric and kinematic errors | 21 |
| 2.2.3 | Machine-tool errors: thermal-induced errors | 23 |
| 2.2.4 | Machine-tool errors: cutting force-induced errors | 24 |
| 2.2.5 | Machine-tool errors: cutting-tool wear-induced errors | 25 |
| 2.2.6 | Workpiece-dependent errors: cutting force-induced and thermal-induced errors | 26 |
| 2.3 | Sources of machining errors in micro-geometric part quality | 27 |
| 2.4 | Conclusions | 29 |
| | References | 29 |
| | | |
| 3 | Prediction of part quality in uni-station machining systems | 33 |
| 3.1 | Introduction | 33 |
| 3.2 | Physical models | 35 |
| 3.2.1 | Setup errors: fixture errors | 35 |
| 3.2.2 | Setup errors: datum feature errors | 45 |
| 3.2.3 | Setup errors: clamping errors | 51 |
| 3.2.4 | Machine-tool errors | 52 |
| 3.2.5 | Workpiece-dependent errors: cutting force-induced and thermal-induced errors | 59 |
| 3.2.6 | Surface roughness | 61 |
| 3.3 | Experimental models | 63 |

| | | |
|----------|---|-----------|
| 3.3.1 | Regression-based models | 63 |
| 3.3.2 | AI-based models | 65 |
| 3.4 | Conclusions | 67 |
| 3.5 | Appendix 3.1: Homogeneous Transformation Matrix | 67 |
| 3.6 | Appendix 3.2: Differential Transformation Matrix | 69 |
| 3.7 | Appendix 3.3: Corollaries | 71 |
| | References | 72 |
| 4 | Prediction of part quality in multi-station machining systems | 79 |
| 4.1 | Introduction | 79 |
| 4.2 | Variation modeling and propagation by the IO school: the Stream of Variation model | 81 |
| 4.2.1 | Fundamentals | 81 |
| 4.2.2 | Virtual part quality inspection and verification | 84 |
| 4.2.3 | Main applications | 87 |
| 4.3 | Variation modeling and propagation by the PD school: the Model of the Manufactured Part | 90 |
| 4.3.1 | Fundamentals | 90 |
| 4.3.2 | Virtual part quality measurement and verification | 94 |
| 4.3.3 | Main applications | 97 |
| 4.4 | Modeling examples | 98 |
| 4.4.1 | Modeling example: SoV model | 98 |
| 4.4.2 | Modeling example: MoMP model | 101 |
| 4.5 | Comparison and discussion | 106 |
| 4.6 | Conclusions | 109 |
| 4.7 | Appendix 4.1: Corollaries | 110 |
| 4.8 | Appendix 4.2: Comparison of SDTs with DMVs | 113 |
| 4.9 | Appendix 4.3: Derivation of SoV matrices | 115 |
| 4.10 | Appendix 4.4: SoV matrices for the case study | 118 |
| 4.11 | Appendix 4.5: SDTs for the case study | 120 |
| | References | 121 |

II Extension of the Stream of Variation model in multi-station machining processes **127**

| | | |
|----------|---|------------|
| 5 | Limitations of the current SoV model due to machining-induced variations | 129 |
| 5.1 | Introduction | 129 |
| 5.2 | Theoretical limitations of current SoV model | 130 |
| 5.3 | Experimental study | 131 |
| 5.4 | Discussion | 135 |
| 5.5 | Conclusions | 136 |
| | References | 137 |

| | | |
|----------|--|------------|
| 6 | Extension of the SoV model considering machining-induced variations | 139 |
| 6.1 | Introduction | 139 |
| 6.2 | Random Deviation Representation | 141 |
| 6.2.1 | Coordinate System Definition | 141 |
| 6.2.2 | Variation Representation | 142 |
| 6.3 | Extension of the State Space Model | 144 |
| 6.3.1 | Framework for Incorporating Machining-Induced Variations | 145 |
| 6.3.2 | Geometric, kinematic and thermal variations of machine-tool axes | 147 |
| 6.3.3 | Spindle thermal-induced variations | 150 |
| 6.3.4 | Cutting force-induced variations | 151 |
| 6.3.5 | Cutting-tool wear-induced variations | 152 |
| 6.4 | Case Study | 153 |
| 6.4.1 | Results and Discussion | 156 |
| 6.5 | Conclusions | 158 |
| 6.6 | Appendix 6.1: Proof of Lemma 1 | 159 |
| | References | 161 |

III Novel applications of the SoV model 163

| | | |
|----------|---|------------|
| 7 | Quality prediction and compensation in multi-station machining processes using sensor-based fixtures | 165 |
| 7.1 | Introduction | 165 |
| 7.2 | Active control for variation reduction | 168 |
| 7.2.1 | Step 1: identification of station-induced variations | 168 |
| 7.2.2 | Step 2: Sensor-based fixture design | 171 |
| 7.2.3 | Step 3: Compensability Analysis | 177 |
| 7.3 | Case Study | 180 |
| 7.3.1 | Identification of station-induced variations | 182 |
| 7.3.2 | Sensor-based fixture design and compensability analysis | 182 |
| 7.3.3 | Comparison of part quality variation according to sensor accuracy and sensor distribution | 183 |
| 7.4 | Conclusions | 185 |
| | References | 186 |
| 8 | Design of multi-station machining processes by integrating the SoV model and shop-floor data | 189 |
| 8.1 | Introduction | 189 |
| 8.2 | SoV model for process planning evaluation | 192 |
| 8.3 | Methodology | 195 |
| 8.3.1 | Extracting manufacturing capabilities from historical shop-floor quality data | 196 |
| 8.3.2 | Sensitivity analysis for adjusting process plan candidates | 197 |
| 8.3.3 | Process plan evaluation and selection | 202 |
| 8.4 | Case study | 203 |
| 8.4.1 | Problem description | 203 |
| 8.4.2 | Step 1: Estimation of manufacturing operation capabilities | 203 |

| | | |
|-----------|--|------------|
| 8.4.3 | Step 2: Sensitivity analysis | 206 |
| 8.4.4 | Step 3: Process plan evaluation and selection | 208 |
| 8.5 | Conclusions | 209 |
| | References | 209 |
| 9 | Process-oriented tolerancing using the extended Stream of Variation model | 213 |
| 9.1 | Introduction | 213 |
| 9.2 | Assumptions | 216 |
| 9.3 | Problem formulation | 216 |
| 9.4 | Definition of manufacturing cost functions | 218 |
| 9.4.1 | Fixture precision cost | 218 |
| 9.4.2 | Fixture maintenance cost | 218 |
| 9.4.3 | Cutting-tool replacement cost | 219 |
| 9.4.4 | Quality loss cost | 219 |
| 9.5 | Definition of constraints | 220 |
| 9.5.1 | Constraints of non-maintainable KCCs | 220 |
| 9.5.2 | Constraints of maintainable KCCs | 220 |
| 9.5.3 | Part quality constraints | 221 |
| 9.6 | Summary of the optimization problem | 223 |
| 9.7 | Case study | 223 |
| 9.7.1 | Problem description | 223 |
| 9.7.2 | Numerical analysis | 227 |
| 9.7.3 | Comparison with a traditional process - oriented tolerancing methodology | 227 |
| 9.8 | Conclusions | 231 |
| 9.9 | Appendix 9.1: Part quality constraints in direct measurements | 231 |
| 9.10 | Appendix 9.2: Part quality constraints in indirect measurements | 232 |
| 9.11 | Appendix 9.3: P.d.f. of tooling wear variables | 233 |
| | References | 234 |
| 10 | Conclusions and future work | 237 |
| 10.1 | Conclusions | 237 |
| 10.2 | Suggestions for future work | 240 |
| 11 | Appendix: Matlab code | 243 |
| 11.1 | SoV model and case study of Chapter 5 | 243 |
| 11.2 | Extended SoV model and case study of Chapter 6 | 267 |

List of Figures

| | | |
|------|--|----|
| 1.1 | Comparison of the traditional manufacturing paradigm and the new emerging time-based competition paradigm. | 2 |
| 1.2 | Rationale and goal of the thesis. | 5 |
| 1.3 | Organization of the dissertation and publications. | 8 |
| 2.1 | Form deviation, orientational deviation and locational deviation. | 14 |
| 2.2 | Part quality according to DIN 4760 Form Deviations, Concepts, Classification (1982). | 15 |
| 2.3 | Sources of errors affecting macro-geometric part quality. | 17 |
| 2.4 | Degrees of freedom of a workpiece in \mathcal{R}^3 space. | 18 |
| 2.5 | Examples of generic forms of location. a) plane location with fixture surfaces and locators; b) concentric location with concentric locators, V-blocks and 3-jaw chucks; c) radial location with concentric and radial locators. | 19 |
| 2.6 | Example of (a) locator/fixture errors, (b) locating datum errors and (c) clamping errors. | 21 |
| 2.7 | Six d.o.f. error motion of a machine-tool carriage system. | 22 |
| 2.8 | Example of a machine-tool structure deformed due to thermal effects. | 23 |
| 2.9 | Example of cutting force-induced error in a ball end milling operation. | 25 |
| 2.10 | Example of cutting-tool wear-induced error in machining. | 26 |
| 2.11 | Example of workpiece-dependent errors due to cutting forces. | 27 |
| 2.12 | Factors affecting generation of surface roughness -modified from Benardos and Vosniakos's (2003) research work-. | 28 |
| 3.1 | Typology of machining models according to van Luttervelt's (2001) research work. | 34 |
| 3.2 | Example of fixture errors: (a) nominal conditions, (b) conditions with fixture errors. | 36 |
| 3.3 | Fixture based on locators. Each i th locator is defined by its position r_i and the normal vector n_i of the locating surface where it contacts. | 38 |
| 3.4 | A generic fixture layout based on locators with a) a 3-2-1 locating scheme, and b) a plane-hole locating scheme. | 40 |
| 3.5 | A generic 3-2-1 locating scheme based on locating surfaces. CSs are centered at each face. | 41 |
| 3.6 | a) Nominal workpiece-fixture assembly. Sequence of small movements for locating the workpiece on the actual fixture over the: b) primary datum, c) secondary datum, and d) tertiary datum. | 42 |

| | | |
|------|--|-----|
| 3.7 | Relationships between CSs for the planar contact between locating surface and primary datum. | 43 |
| 3.8 | Example of datum feature errors: (a) nominal conditions, (b) conditions with datum errors. | 46 |
| 3.9 | Representation of the contact deformation of two elastic bodies with curved surfaces. | 51 |
| 3.10 | Deformation of a spherical locator due to clamping forces. | 52 |
| 3.11 | Ball-end mill and cantilever beam simplification. Adapted from Kim <i>et al.</i> 's (2003) research work. | 57 |
| 3.12 | Effect of cutting-tool flank wear on hole shrinkage in drilling composites. Extracted from Arul <i>et al.</i> 's (2007) research work. | 58 |
| 3.13 | Relationship between flank wear and machined surface deviation in: a) sharp, and b) rounded cutting inserts. | 59 |
| 3.14 | Turning deflection for a workpiece clamped in a chuck. | 60 |
| 3.15 | Surface roughness produced by a single-point cutting-tool geometry with a rounded corner. | 62 |
| 3.16 | Surface roughness produced by a single-point cutting-tool geometry with a sharp corner. | 62 |
| 3.17 | Illustration for determining the effective feed rate for traces parallel to the feed direction. | 63 |
| 3.18 | Frequency of usage of AI approaches in part quality prediction. References from ISI Web of Knowledge (2003-2008). | 65 |
| 3.19 | Basic guidelines for AI selection according to model requirements. | 67 |
| 3.20 | HTM from CS 2 to CS 1 if CS 2 is deviated from nominal values. | 70 |
| 3.21 | DTM from CS 2 to CS 1 if both CSs are deviated from nominal values. | 70 |
| 3.22 | HTM from CS 2 to CS 1 if CS 2 is deviated from nominal values due to a sequence of small deviations. | 72 |
| 4.1 | Dimensional deviation of a plane surface at station k using a DMV. | 82 |
| 4.2 | Propagation of manufacturing variation in an MMP. | 82 |
| 4.3 | Sources of variation and state space model formulation for station k | 83 |
| 4.4 | Gap distance of a boundary point on a deviated toleranced surface. | 86 |
| 4.5 | Diagram of the SoV model derivation and its applications. | 88 |
| 4.6 | Model of Manufactured Part throughout the MMP. | 94 |
| 4.7 | Virtual gauge and SDTs in virtual inspection. | 95 |
| 4.8 | 2D case study. Raw material and part design. Dimensions in mm | 99 |
| 4.9 | SoV example. Multi-station machining process used in the 2D case study. | 99 |
| 4.10 | MoMP example. Multi-station machining process to manufacture the 2D example. Dimensions in mm | 103 |
| 4.11 | DMVs among CSs if CS 1 and 2 are deviated from nominal values. | 110 |
| 4.12 | Surface S_i with a torsor deviation and frames D and F | 113 |
| 4.13 | Example for analyzing small displacements using SDTs and DMVs. | 113 |
| 4.14 | Torsors involved in the example for deriving $\mathbf{T}_{R,B}$ | 114 |
| 4.15 | DMVs involved in the example for deriving \mathbf{x}_B^R | 115 |
| 4.16 | Steps for deriving the SoV matrices \mathbf{A}_k and \mathbf{B}_k | 116 |
| 5.1 | Example of sources of variation in a MMP. | 131 |

| | | |
|------|--|-----|
| 5.2 | Case study. Coordinate systems of surfaces S_0 - S_8 | 132 |
| 5.3 | Case study. MMP adopted to manufacture the part. | 133 |
| 5.4 | CMM measurements and SoV model predictions after experimentation 1, 2 and 3 for each KPC. | 135 |
| 5.5 | Prediction errors of the SoV model after experimentation 1, 2 and 3 for each KPC. | 135 |
| 6.1 | Required modeling parameters for estimating machining-induced variations. | 140 |
| 6.2 | Example of the CSs involved in a 5-axis CNC machine-tool (type X-Y-Z-A-B). | 143 |
| 6.3 | Relationships between the different CSs in a n -axis machine-tool. | 145 |
| 6.4 | Summary of the procedure to derive the extended state space model. | 148 |
| 6.5 | Experimentation to model machining-induced variations due to a) spindle thermal effects, and b) cutting-tool wear. | 151 |
| 6.6 | Aluminum 6061 part investigated by the case study. Surface CSs from S_0 to S_8 | 153 |
| 6.7 | Case study. Part to be machined in a 3-station machining process. | 154 |
| 6.8 | Machined feature deviations measured experimentally along spindle thermal expansion. | 156 |
| 6.9 | Machined feature deviations measured when machining with: a) flank wear at the primary cutting-tool edge and b) flank wear at the secondary cutting-tool edge. | 157 |
| 6.10 | Average prediction error of the three KPCs for both conventional and extended SoV models in the five tested experimental conditions. | 158 |
| 7.1 | Active control for variation reduction: feed-back and feed-forward control strategies. | 166 |
| 7.2 | Diagram of the methodology conducted for quality prediction and compensation with sensor-based fixtures | 169 |
| 7.3 | Example of a sensor-based fixture with inductive precision sensors mounted on a 3-2-1 locating scheme. | 171 |
| 7.4 | Sensor-based fixture scheme. Position and normal vectors of locators and sensors. | 172 |
| 7.5 | Algorithm to place the optimal number of sensors in the sensor-based fixture. | 177 |
| 7.6 | Case study. Part to be machined in a 4-station machining process. | 180 |
| 7.7 | Case study. Surfaces S_0 to S_8 . Dimensions in mm | 181 |
| 7.8 | Identification of the impact of station-induced variations on the final part quality. | 183 |
| 7.9 | Variation of KPCs according to sensor-based fixture designs: (1) Non-sensor-based fixture; (2) sensor-based fixture with nine non-optimal sensors; (3) sensor-based fixture with nine optimal sensors; (4) sensor-based fixture with 14 optimal sensors. | 184 |
| 7.10 | Variation of a) KPC_1 and b) KPC_2 according to different sensor-based fixtures. | 185 |
| 7.11 | Compensability index according to sensor precision and the sensor-based fixture design. | 186 |

| | | |
|------|--|-----|
| 8.1 | Three-step methodology proposed for process plan evaluation, adjustment and selection. | 191 |
| 8.2 | Generic MMP with all potential datum schemes and machine-tools to be applied at each station. | 192 |
| 8.3 | Representation of the MMP according to the SoV nomenclature. | 194 |
| 8.4 | Flowchart for process plan adjustment through sensitivity analysis. | 198 |
| 8.5 | Case study. a) Proposed process plan number 1. b) Proposed process plan number 2. Process plan number 3 is the same than number 2 but machine-tool $M4$ is placed at the third station and machine-tool $M3$ at the fourth station. | 204 |
| 8.6 | Case study. Previous production line. | 206 |
| 8.7 | Comparison of actual and extracted values of the machining-induced variations at each manufacturing station. Figures a) and b) refer to linear and angular deviations respectively. | 207 |
| 8.8 | Sensitivity analysis results for process plans 1 and 2. | 208 |
| 8.9 | Graphical representation of the multivariate process capability indices of process plans 1, 2 and 3. | 209 |
| 9.1 | Example of the influence of machining-induced variations on the tolerance allocation problem. | 215 |
| 9.2 | Process-oriented tolerancing problem. | 224 |
| 9.3 | Final machined part for the case study (unit: mm). | 225 |
| 9.4 | Case study. Part to be machined in a 3-station machining process. | 225 |
| 9.5 | a) Design tolerances for fixture locators; b) Time between two consecutive fixture maintenance actions (in hours) at each machining station; c) Admissible cutting-tool wear at each cutting-tool edge before a cutting-tool replacement is conducted. | 229 |
| 9.6 | P.d.f of some of the KCCs for the case study and p.d.f of the resulting deviation of feature S_3 | 230 |
| 10.1 | Summary of thesis contributions, suggested future work and on-going research work. | 239 |

List of Tables

| | | |
|------|---|-----|
| 1.1 | Current state of art and future vision for product and process integration according to the IMTR Initiative. | 3 |
| 3.1 | Regression-based (SMR) and AI-based models applied to part quality prediction (surface roughness – Ra – and dimensional deviation – DD). | 64 |
| 4.1 | SDTs according to the type of surface and torsor constraints according to the type of tolerance. | 91 |
| 4.2 | SDTs (link torsors) according to the joint type of mating surfaces. | 93 |
| 4.3 | Nominal location and orientation of each local feature CS. | 100 |
| 4.4 | Nominal location and orientation of F_k at each station. Position of locators is also shown. | 100 |
| 4.5 | Ranges of locators and machining deviations for the SoV case study. Dimensional deviations in mm , angular deviations in rad | 102 |
| 4.6 | Numerical resolution according to the worst-case and the statistical analyses for the SoV case study. Dimensions in mm | 102 |
| 4.7 | Nominal location and orientation of F_k w.r.t. D , and nominal location and orientation of fixture surfaces w.r.t. F_k | 104 |
| 4.8 | Nominal location and orientation of G w.r.t. D , and nominal location and orientation of gauge surfaces w.r.t. G . Only primary datum surfaces are necessary for inspecting KPC_1 , KPC_2 and KPC_3 | 104 |
| 4.9 | Precision of part-holder surfaces (according to the planar tolerance size) and machined surfaces for the MoMP case study. Dimensional deviations in mm , angular deviations in rad | 107 |
| 4.10 | Numerical resolution according to the worst-case and the statistical analyses for the MoMP case study. Dimensions in mm | 107 |
| 4.11 | Generic comparison of the SoV and the MoMP models. | 109 |
| 4.12 | SDTs for station 1. | 120 |
| 4.14 | SDTs for inspection station. | 121 |
| 4.13 | SDTs for station 2. | 121 |
| 5.1 | Machined features and datum features according to the 3-2-1 locating scheme at each station. | 133 |
| 5.2 | Nominal location ($\mathbf{t}_{F_k}^{\circ D}$) and orientation ($\varphi_{F_k}^{\circ D}$) of fixture CS at each station and fixture layout. | 133 |
| 5.3 | Nominal location ($\mathbf{t}_{S_i}^{\circ D}$) and orientation ($\varphi_{S_i}^{\circ D}$) of each feature. | 134 |

| | | |
|-----|---|-----|
| 5.4 | Locators errors measured in machine-tool table before conducting experiment 1, 2 and 3. Note that locators errors apply to station 1, 2 and 3. . . . | 134 |
| 5.5 | CMM results after experimentation 1, 2 and 3. | 134 |
| 5.6 | SoV model prediction according to locator errors. | 134 |
| 5.7 | Model prediction error after experimentation 1, 2 and 3. | 134 |
| 6.1 | Machined features and datum features according to the 3-2-1 locating scheme at each station. | 154 |
| 6.2 | Nominal location ($\mathbf{t}_{F_k}^{\circ D}$) and orientation ($\varphi_{F_k}^{\circ D}$) of fixture CS at each station and fixture layout. | 154 |
| 6.3 | Nominal location ($\mathbf{t}_{S_i}^{\circ D}$) and orientation ($\varphi_{S_i}^{\circ D}$) of each feature. | 155 |
| 6.4 | Experimental conditions. Note that all deviations apply to stations 1, 2 and 3. | 156 |
| 7.1 | Machined features and datum features according to the 3-2-1 locating scheme at each station. | 181 |
| 7.2 | Nominal location ($\mathbf{t}_{F_k}^{\circ D}$) and orientation ($\varphi_{F_k}^{\circ D}$) of fixture CS at each station and fixture layout. | 182 |
| 7.3 | Nominal location ($\mathbf{t}_{S_i}^{\circ D}$) and orientation ($\varphi_{S_i}^{\circ D}$) of each feature. | 182 |
| 7.4 | Sensor distribution for the sensor-based fixture at station 4. | 183 |
| 7.5 | Results of the compensability analysis for the case study. | 184 |
| 8.1 | Summary of the sensitivity indices and physical meaning. | 202 |
| 8.2 | Nominal location ($\mathbf{t}_{S_i}^{\circ D}$) and orientation ($\varphi_{S_i}^{\circ D}$) of each feature. | 203 |
| 8.3 | Nominal location ($\mathbf{t}_{F_k}^{\circ D}$) and orientation ($\varphi_{F_k}^{\circ D}$) of fixture CS at each station and fixture layout. PP1: process plan 1; PP2,3: process plan 2 and 3. . . . | 204 |
| 8.4 | Nominal location ($\mathbf{t}_{S_i}^{\circ D}$) and orientation ($\varphi_{S_i}^{\circ D}$) of each feature for the previous part produced. | 205 |
| 8.5 | Nominal location ($\mathbf{t}_{F_k}^{\circ D}$) and orientation ($\varphi_{F_k}^{\circ D}$) of fixture CS at each station and fixture layout for the previous production line. | 205 |
| 9.1 | Machined features and datum features according to the 3-2-1 locating scheme at each station. | 225 |
| 9.2 | Nominal location ($\mathbf{t}_{F_k}^{\circ D}$) and orientation ($\varphi_{F_k}^{\circ D}$) of fixture CS at each station and fixture layout. | 226 |
| 9.3 | Nominal location ($\mathbf{t}_{S_i}^{\circ D}$) and orientation ($\varphi_{S_i}^{\circ D}$) of each feature. | 226 |
| 9.4 | Numerical values for manufacturing tolerance allocation in the case study. . . . | 227 |
| 9.5 | Parameters applied in the GA and the MADS algorithm. | 228 |

Introduction

1.1 Motivation for the proposed research

Manufacturers today face greater challenges than ever. Globalization has greatly expanded the availability of new markets, while simultaneously spurring intense competition in all sectors [1]. In this era, manufacturers have to deal with frequent and unpredictable market changes, shortened product cycles, and rapid-frequency introduction of new products [2]. As a result of this changing situation, manufacturing companies are moving to a new manufacturing paradigm characterized by the so-called time-based competition (TBC), where the time-to-market for a new product or the service responsiveness of a company has become the new cutting edge in global market competition [2, 3].

The essence of the TBC manufacturing paradigm involves recognition and careful management of time as a limited resource while continuously removing waste or non-value-added activities [3]. As shown in Figure 1.1, the TBC manufacturing paradigm involves compressing time in every phase of the product creation and delivery cycle generating a significant source of competitive advantage [4]. Therefore, concurrent engineering, lean and six sigma principles are applied in the TBC manufacturing paradigm. Manufacturing systems such as flexible and reconfigurable manufacturing systems (FMS and RMS) are also used together with tools like Taguchi methods and quality function deployment (QFD) in order to improve the efficiency of the production process by reducing lead time, lowering product cost, improving product quality, and enhancing product innovation.

A key issue to reduce the time required to introduce a product on the market (product development time, process development time, manufacturing lead time and ramp-up time) is the integration of product and process knowledge. This product-process integration allows engineers to: i) analyze, predict, and optimize the performance of manufacturing systems during the design phase; ii) eliminate or reduce product design changes after the design phase; and iii) rapidly identify and isolate root causes of all faults during ramp-up time. In fact the lack of comprehensive knowledge-based methods for product/process performance prediction and control is a major barrier hindering further progress in new product and process development and the main cause preventing manufacturers from achieving high rates of correct products the first time they are produced [2]. Despite the importance of product and process design integration, product design has traditionally been separated

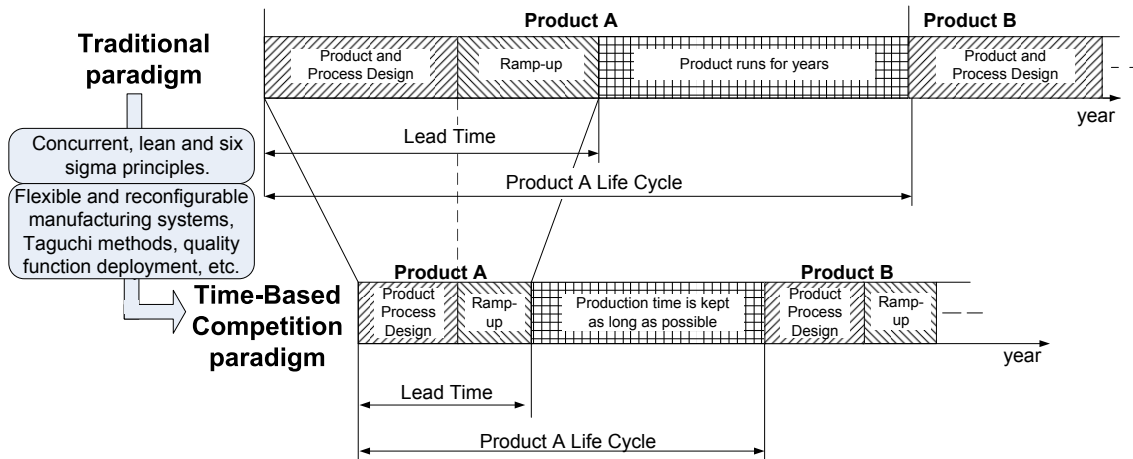


Figure 1.1: Comparison of the traditional manufacturing paradigm and the new emerging time-based competition paradigm.

from process design in many manufacturing companies. This product-oriented approach is referred to as over-the-wall design since there is no systematic integration of design and manufacturing. This outdated design philosophy is one of the reasons why companies still have lower first-time-right rates [2].

In order to overcome these limitations and concentrate research efforts, many public institutions around the world have created R&D roadmaps that define the path to the future for their industries, and identify technology advances that will help them reduce costs, increase profitability, improve quality, and shorten time-to-market [1]. In recent years, the Integrated Manufacturing Technology Roadmapping (IMTR) Initiative – launched in 1998 by U.S. institutions to develop a research and development agenda – defined the future requirements of the manufacturing technology for the period 2000-2015. In order to meet these requirements, the IMTR Initiative outlined reference paths through roadmaps in the following areas:

- Information systems for manufacturing enterprises.
- Modeling and simulation for manufacturing.
- Manufacturing processes and equipment.
- Technologies for enterprise integration.

The roadmaps developed in each area provide an assessment of the current state-of-art and state-of-practice in that technological field, a vision of the future state for 2015, and a series of goals, requirements, and tasks to achieve that vision. Many of the requirements of future manufacturing technology reported in these roadmaps are focused on the integration of product requirements, product design, and manufacturing process design. This integration is expected to be achieved by increasing the fundamental understanding of materials and processes and by improving the development of modeling and simulation

Table 1.1: Current state of art and future vision for product and process integration according to the IMTR Initiative.

| IMTR Area | Current State of Art | IMTR. Vision for 2015 |
|---------------------------------------|---|--|
| Manufacturing Processes and Equipment | -Few mathematical process models | -Knowledge-based advisory systems for processes and tools |
| | -Limited use of analytical models for process application | -Self-diagnosis/self-healing machine-tools |
| Manufacturing Processes and Equipment | -Limited intrusive, off-line and in-process inspection | -Integrated error compensation in machine-tools |
| | -Parametric acceptance as a basis for establishing quality | -All manufacturing operations contain in-process monitoring and inspection processes |
| | -Test and inspection based on empirical rather than analytical process models | -Many post-process inspection operations eliminated |
| | | -Elimination of rework |
| Modeling and simulating | -Poor understanding of underlying physics | -Multivariate performance analysis |
| | -Models from empirical data for statistical control | |

tools with which to capture and represent knowledge for confident manufacturing predictions. In this context, some of the most important current limitations of manufacturing enterprises refer to the area of manufacturing processes and equipment, as well as the area of modeling and simulating. In these areas there is a recognized lack of mathematical process models, a poor understanding of manufacturing processes, and a limited in-process versus post-process inspection, among other shortcomings. According to the IMTR vision for 2015, future manufacturing will overcome these limitations through knowledge-based advisory systems developed from the understanding of the processes, real-time error compensations, and in-process monitoring and inspection. A brief summary of some of these limitations and expected future capabilities, according to the IMTR vision, is shown in Table 1.1.

To achieve the IMTR vision, there are several major enablers that should be investigated in depth. Some of these enablers, also defined as critical capabilities for the manufacturers of the future, are listed in the IMTR roadmaps as follows [5–7]:

- Science-based manufacturing: in the future manufacturing will become more of a science and less of an art. Advances in the fundamental understanding of manufacturing will enable many future improvements in product and process design, modeling and simulation, and control of manufacturing processes. By improving the ability to construct valid analytical models of materials, processes and equipment based on scientific principles rather than observed behavior, new possibilities for optimizing manufacturing decisions will arise.
- Intelligent design and process advisors: building on advances in the scientific understanding of manufacturing and progress in simulation and modeling, information systems and knowledge-based technologies, the IMTR vision anticipates the proliferation of computer-based advisory systems to assist decision-makers in product and

process design, as well as tooling and equipment selection, production scheduling and control, material management, and other areas.

- First product correct: trial and error in product and process design is a very expensive and time-consuming fact of life in today's manufacturing enterprises. Manufacturers of the future will be able to generate the first product correctly, which means that companies will have the ability to make the transition from design concept to a finished product with absolute certainty of obtaining a correct result from the first unit onward [7].

Achieving these capabilities will have a major impact on manufacturing enterprises by enabling them to reduce the cost of developing and manufacturing products, enhance product quality and reliability, reduce the time required to move new products from concept to market, and improve responsiveness to changes in customer needs [5, 6].

From the IMTR Initiative roadmaps, one can conclude that there is a need to integrate product design and manufacturing processes through analytical models that describe the performance of manufacturing processes and their quality outcome based on scientific principles. This integration based on the understanding of manufacturing processes will increase the first-time-right rates moving toward the ideal goal of first product correct.

Besides the IMTR Initiative roadmaps, the current research literature confirms that, being focused on discrete multi-station manufacturing processes, a research gap exists in the development of analytical models that describe the manufacturing performance according to its sources of variation. In this field, variational models have been developed in the last decade to describe the performance of multi-station assembly processes analytically. These models have been used in a large number of applications such as fault diagnosis [8, 9], best placement of inspection stations [10, 11], process planning [12, 13] and dimensional control [14]. In multi-station machining systems, although less investigated, similar research works have been reported for fault diagnosis [15], machining process planning [16, 17] and process-oriented tolerancing [18, 19]. However, the 3D variational models reported in the literature describe the multi-station machining process by kinematic relationships according to previous workpiece datum errors and fixture errors, thus propagating the workpiece error station by station. With these models, operation-induced errors related to machining errors such as thermal errors, cutting force-induced errors, cutting-tool wear-induced errors, and so on, are completely overlooked, although these sources of variation are well-known in uni-station machining processes. Thus, there is a need to extend 3D variational models to include operation-induced deviations since nowadays there is no explicit integration of machining error models in the error propagation throughout multi-station machining processes. Hence, the sources of variation that modify the ideal machining conditions and generate macro- and micro-geometric part deviations should be explored in greater detail. Understanding the machining/machine-tool errors physically enables us to model the machining output in terms of macro- and micro-geometric part quality and, thus, allows us extend the 3D variational models to include machining errors.

In addition to the literature review, this research gap has been confirmed by important researchers in the field such as Professor Jianjun Shi from the University of Michigan and Dr. Jian Liu from the University of Arizona, who have collaborated in the research presented in this dissertation.

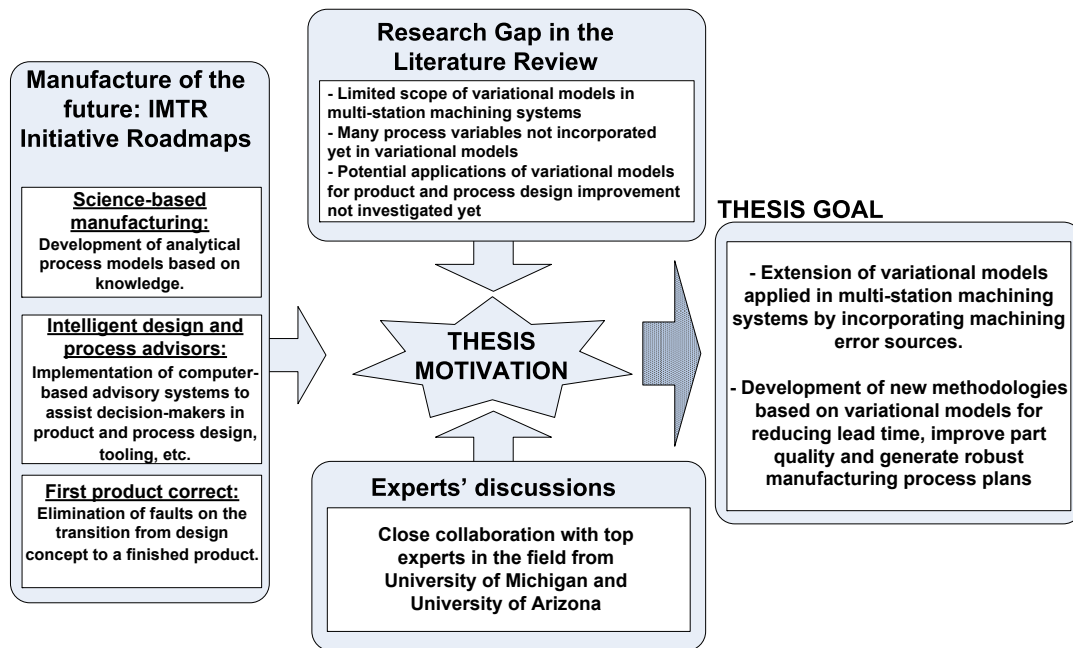


Figure 1.2: Rationale and goal of the thesis.

In conclusion, everything that has been outlined above, there is a clear motivation to investigate and partially fill this research gap and extend the 3D variational models applied in multi-station machining systems by incorporating machining error sources through scientific-based models (Figure 1.2 shows the idea underlying the rationale). Additionally, new potential applications for part quality improvement in multi-station machining processes can still be investigated and some of them are described in this thesis. With this research we expect to help improve part quality prediction and part quality itself through new strategies related to robust process planning design, prediction, and compensation of machining errors (e.g., cutting-tool path compensation at downstream stations) and process-oriented tolerancing.

1.2 Research objectives

The main purpose of the research presented in this dissertation is to derive a methodology for including machining errors in 3D variational models in order to accurately predict part quality in multi-station machining processes. This inclusion can also lead to the development of new strategies for part quality improvement, such as designing robust process planning, compensating errors at downstream stations, and allocating manufacturing tol-

erances for a minimum manufacturing cost. The main objectives of the dissertation can be listed as follows:

- Review the main sources of machining errors that influence the macro- and micro-geometric quality of machined parts.
- Review the analytical models that quantify the main sources of machining errors and evaluate their impact on machined part quality in both uni- and multi-station machining processes.
- Extend the current analytical models that describe the impact of some machining errors on part quality in multi-station machining systems in order to include additional machining errors that have not been considered yet in the context of multi-station. For this purpose, the challenge is to incorporate uni-station machining error models into the formulation of multi-station machining error models.
- Develop new methodologies for improving part quality in multi-station machining processes. The new methodologies will propose procedures to design robust multi-station machining systems that minimize part quality variability; methods for compensating fixture errors in multi-station systems at downstream stations; and cost-effective methods for allocating manufacturing tolerances.

1.3 Research methodology

The research methodology applied in this dissertation follows the methodology typically applied in scientific inquiries and is based on five main steps [20]:

- Identification of the problem. The problem may involve a question about something or a gap in knowledge.
- Statement of the problem. This step is the clarification of the problem, through a literature review.
- Definition of working hypotheses for solving the problem.
- Formulation of the mathematical model and the methodology for the possible solution to the problem.
- Prediction of consequences and testing the hypotheses. The researcher predicts the consequences of the hypotheses on applying them to a case study and gathers objective data to evaluate the adequacy of the hypotheses formulated.

In addition to these five steps, an initial step consisting in a literature review is mandatory in order to understand and contextualize the problem (or problems) to be dealt with.

This dissertation undertakes the experimental identification of the limitations of the Stream of Variation (SoV) model (a 3D manufacturing variation model) due to machining-induced variations. After the identification of the problem, the corresponding working hypotheses to overcome these limitations are formulated and tested, defining the extension

of the SoV model. Additionally, the dissertation analyzes three other problems related to part quality prediction and the improvement of multi-station machining processes. To deal with each problem, the previous five steps of the research methodology are followed. The proposed solution of each problem is formulated and validated through a case study using simulations.

It should be mentioned that part of the working hypotheses developed in this dissertation has been tested experimentally using a vertical milling center and a coordinate measuring machine (CMM). Other working hypotheses have been validated through simulations using Matlab and its global optimization toolbox, and ProEngineer.

1.4 Organization of the dissertation

This dissertation is divided into three parts. The first is an introductory part to give the reader a generic view of machining errors and macro- and micro-geometric part quality errors in machining processes. Within this part, Chapter 2 introduces the main sources of errors described in the literature, such as geometric and kinematic errors, fixture-induced errors, thermal errors, cutting force-induced errors, and cutting-tool wear-induced errors. Chapter 3 reviews the analytical models presented in the literature to evaluate these machining errors and estimate their impact on final part quality when machining operations are conducted in a single station with a single manufacturing setup. To describe the effect of some of these operation errors (mainly fixture-induced errors) in multi-station machining systems, Chapter 4 describes two analytical models used in the literature. The models reviewed are the Stream of Variation model (SoV) [21], developed at the University of Michigan for dealing with error propagation in the assembly process of automobiles, and the Model of the Manufactured Part (MoMP) [22], developed at different French universities for tolerance analysis/synthesis in product design. In that chapter, the comprehensive study of both models concludes with their most important advantages and drawbacks, and the potential research lines for their improvement.

The second part of the dissertation proposes the extension of the SoV model in order to estimate part quality in multi-station machining systems not only when fixture-induced errors occur but also when any other kind of machining errors occur. Within this part, Chapter 5 describes, experimentally, the limitations of the current SoV model in multi-station machining systems if machining-induced errors such as thermal errors or cutting-tool wear-induced errors are with the same order of magnitude as fixture-induced errors. To overcome these limitations, Chapter 6 presents the extension of the SoV model analytically in order to deal with other machining errors. This model extension could encourage research on overlooked problems in multi-station machining processes, such as machining error diagnosis, machining error compensation, complete manufacturing tolerance allocation, or new maintenance strategies, among others. A summarized version of the fundamentals of the SoV model and the addition of machining-induced variations can be found in the chapter book prepared by the author in Ref. [23].

The third part of the dissertation presents novel applications of the SoV model (extended and non-extended versions), overlooked in the past by other researchers. This

part comprises Chapters 7, 8 and 9 which are organized as individual research papers. Chapter 7 presents the potential application of the SoV model to improve part quality through cutting-tool path compensations in multi-station manufacturing processes by using sensor-based fixtures in critical machining stations. Chapter 8 presents the application of the SoV model for designing robust multi-station machining processes using historical shop-floor quality data about existing multi-station processes. As a final potential application, Chapter 9 presents the application of the extended SoV model developed in the dissertation for process-oriented tolerancing, where not only process variables such as fixture accuracy are allocated but also other process variables that still remain unconsidered in the process-oriented tolerance problem, such as the admissible cutting-tool wear. This process-oriented tolerancing approach also considers other non-allocable process variables such as the thermal expansion of the spindle and additional costs, such as those related to cutting-tool replacement.

Finally, Chapter 10 concludes the dissertation by summarizing its original contributions. Potential future research is also discussed. Figure 1.3 shows a graphic representation of the organization of the dissertation and the major publications.

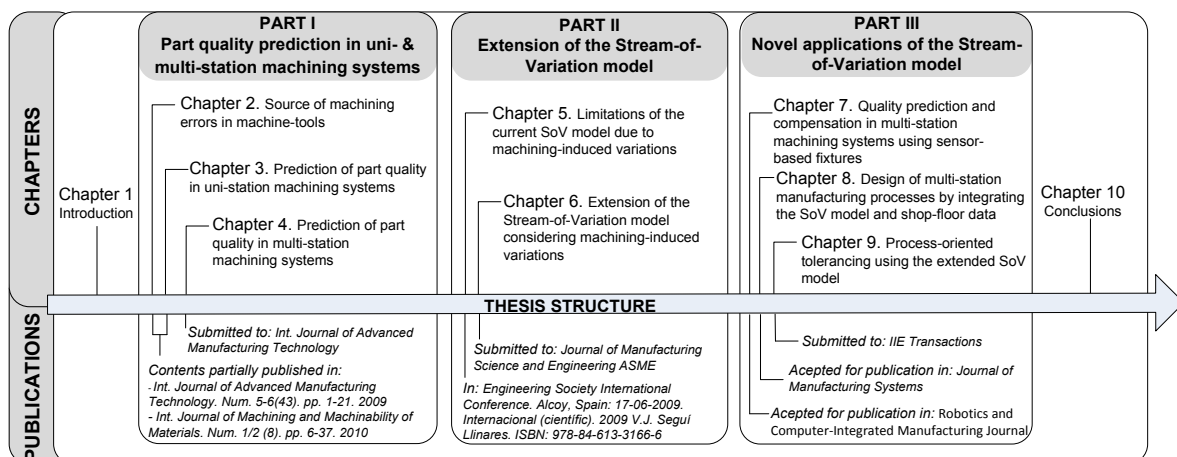


Figure 1.3: Organization of the dissertation and publications.

References

- [1] Integrated Manufacturing Technology Roadmapping Initiative, Integrated Manufacturing Technology Roadmapping Project: An Overview of the IMTR Roadmaps, 2000.
- [2] D. Ceglarek, W. Huang, S. Zhou, Y. Ding, R. Kumar, Y. Zhou, Time-based competition in multistage manufacturing: Stream-of-variation analysis (SOVA) methodology - review, *International Journal of Flexible Manufacturing Systems* 16 (1) (2004) 11–44.

-
- [3] K. L. Sim, A. P. Curatola, Time-based competition, *International Journal of Quality & Reliability Management* 16 (7) (1999) 659–674.
 - [4] S. H. Hum, H. H. Sim, Time-based competition: Literature review and implications for modelling, *International Journal of Operations and Production Management* 16 (1) (1996) 75–90.
 - [5] Integrated Manufacturing Technology Roadmapping Initiative, *Integrated Manufacturing Technology Roadmapping Project: Manufacturing Processes and Equipment*, Oak Ridge, TN, 2000.
 - [6] Integrated Manufacturing Technology Roadmapping Initiative, *Integrated Manufacturing Technology Roadmapping Project: Modeling and Simulation*, Oak Ridge, TN, 2000.
 - [7] Integrated Manufacturing Technology Roadmapping Initiative, *First Product Correct. Visions and Goals for the 21st Century Manufacturing Enterprise*, Oak Ridge, TN, 2000.
 - [8] Y. Ding, J. Shi, D. Ceglarek, Diagnosability analysis of multi-station manufacturing processes, *Journal of Dynamic Systems, Measurement, and Control* 124 (1) (2002) 1–13.
 - [9] S. Zhou, Y. Chen, Y. Ding, J. Shi, Diagnosability study of multistage manufacturing processes based on linear mixed-effects models, *Technometrics* 45 (4) (2003) 312–325.
 - [10] D. Djurdjanovic, J. Ni, Bayesian approach to measurement scheme analysis in multistation machining systems, *Proceedings of the Institution of Mechanical Engineers Part B-Journal of Engineering Manufacture* 217 (8) (2003) 1117–1130.
 - [11] D. Djurdjanovic, J. Ni, Stream-of-variation (SoV)-based measurement scheme analysis in multistation machining systems, *IEEE Transactions on Automation Science and Engineering* 3 (4) (2006) 407–422.
 - [12] Y. Ding, D. Ceglarek, J. J. Shi, Fault diagnosis of multistage manufacturing processes by using state space approach, *Journal of Manufacturing Science and Engineering-Transactions of the Asme* 124 (2) (2002) 313–322.
 - [13] H. Wang, D. Ceglarek, Quality-driven sequence planning and line configuration selection for compliant structure assemblies, *CIRP Annals - Manufacturing Technology* 54 (1) (2005) 31–35.
 - [14] L. Izquierdo, J. Shi, S. Hu, C. Wampler, Feedforward control of multistage assembly processes using programmable tooling, *NAMRI/SME Transactions* 35 (2007) 295–302.
 - [15] H. Wang, Q. Huang, R. Katz, Multi-operational machining processes modeling for sequential root cause identification and measurement reduction, *Journal of Manufacturing Science and Engineering* 127 (3) (2005) 512–521.

-
- [16] S. F. Zhang, Z. H. Sha, R. K. Kang, A physical machining accuracy predicting model in turning, *Key Engineering Materials* 329 (2007) 675–680.
 - [17] J. Liu, J. Shi, S. J. Hu, Quality-assured setup planning based on the stream-of-variation model for multi-stage machining processes, *IIE Transactions* 41 (2009) 323–334(12).
 - [18] Y. Ding, J. Jin, D. Ceglarek, J. Shi, Process-oriented tolerancing for multi-station assembly systems, *IIE Transactions* 37 (2005) 493–508.
 - [19] Y. Chen, Y. Ding, J. Jin, D. Ceglarek, Integration of process-oriented tolerancing and maintenance planning in design of multistation manufacturing processes, *IEEE Transactions on Automation Science and Engineering* 3 (4) (2006) 440–453.
 - [20] D. Ary, L. C. Jacobs, A. Razavieh, C. K. Sorensen, *Introduction to Research in Education*, 8th Edition, Wadsworth Publishing, 2009.
 - [21] J. Shi, *Stream of Variation Modeling and Analysis for Multistage*, CRC Press Taylor and Francis Group, 2007.
 - [22] F. Villeneuve, O. Legoff, Y. Landon, Tolerancing for manufacturing: a three-dimensional model, *International Journal of Production Research* 39 (8) (2001) 1625–1648.
 - [23] J. Abellan-Nebot, J. Liu, F. Romero, Stream-of-variation based quality assurance for multi-station machining processes - modeling and planning, in: *Statistical and computational techniques in manufacturing*, 2011 (In press), pp. –.

Part I

**Part Quality Prediction in Uni- and
Multi-Station Machining Systems**

Source of machining errors in machine-tools

The geometric quality of machined components is one of the most critical considerations for any manufacturer. Many key factors like cutting-tools and machining conditions, accuracy of machine-tools and fixture devices, etc., play an important role in whether it is accomplished or not. Machining errors are divided into quasi-static errors (geometric and kinematic errors; fixture-induced errors; thermal errors; cutting force-induced errors; cutting-tool wear-induced errors; etc.) and dynamic errors (spindle motion errors, vibrations, etc.). These machining errors produce errors on machined surfaces, which can be macro-geometric errors (dimension, form, and orientation errors) or micro-geometric errors (surface roughness or defects in material micro-structure). This chapter describes the principal sources of machining errors for each type of part quality error.

2.1 Introduction

In manufacturing, the condition of the surface of the part comprises the properties of that surface, which can be chemical, mechanical, and geometric properties [1]. The chemical and mechanical properties comprise chemical composition, grain, hardness, strength and inhomogeneities. Geometrical properties define the geometric part quality of manufacturing parts. These geometric properties are defined as deviations from ideal geometrical elements of the workpiece. Ideal geometrical elements have a geometric, unique and nominal form, such as planes, cylinders, spheres, cones, and tori. Geometric deviations can be macro-geometric deviations such as deviations in size, form, orientation, location, and deviations due to waviness, or micro-geometric deviations such as surface roughness and surface discontinuities [1].

On the one hand, macro-geometric deviations are those that can be assessed with usual measuring devices for the assessment of size, form, orientation, location, and waviness (e.g., dial indicator). As the main characteristics of these deviations, the following can be pointed out [1]:

- Size deviation is the difference between actual size and nominal size, and they are assessed over the entire geometric element. They are mainly originated by imprecise

adjustment of the machine-tool and by variations during the manufacturing process, e.g., due to tool wear, geometric inaccuracies of machine-tool axes, etc.

- Form deviation is the deviation of a feature (geometric element, surface or line) from its nominal form, as shown in Figure 2.1. Form deviations are originated, for example, by looseness or error in guidances and bearings of the machine-tool, deflections of the machine-tool or the workpiece, etc.
- Orientational deviation is the deviation of a feature from its nominal form and orientation with respect to (w.r.t.) a reference feature called a datum feature. Orientational deviation includes form deviation (Figure 2.1). Orientational deviations are originated by fixture errors and machining-errors such as geometric and kinematic machine-tool errors, cutting-tool deflections, etc.
- Locational deviation is the deviation of a feature from its nominal location. The location is related to one or more datum feature(s). Locational deviation also includes form deviation and orientational deviation (Figure 2.1). Locational deviations are originated in a similar way to size, form, and orientational deviations.
- Waviness is mostly more or less periodic irregularities of a workpiece surface with spacings greater than the spacings of its roughness [2]. Waviness is originated by form deviations of the cutter or by vibrations, and by eccentric fixture in turning processes [2].

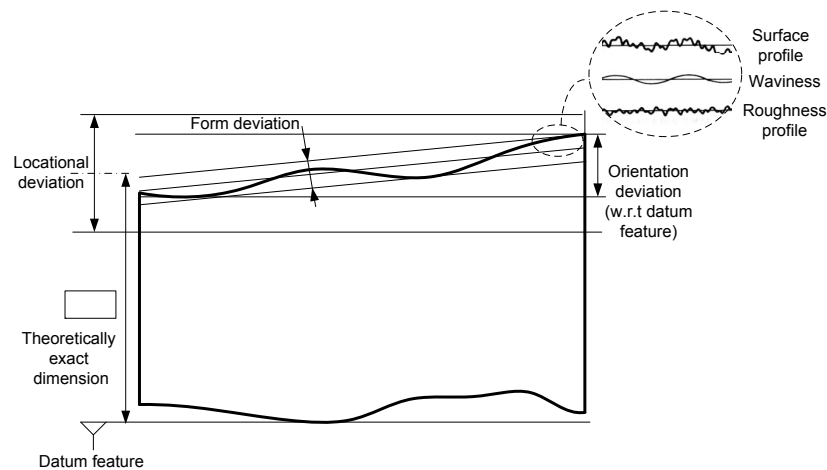


Figure 2.1: Form deviation, orientational deviation and locational deviation.

On the other hand, micro-geometric deviations are assessed from a representative part of the surface and they are defined by surface roughness and surface discontinuity. As the main characteristics of these deviations, the following can be highlighted [1]:

- Surface roughness is originated by the direct effect of the cutting edges, i.e., by imprinting the cutting edges on the surface. Other origins are related to vibrations,

variations in cutting conditions, defects in the structure of the workpiece material, and so forth.

- Surface discontinuity is an isolated imperfection in the surface like a crack, pore or lap. In general it is not taken into account when assessing deviations of size, form, orientation, location, waviness, and roughness.

According to DIN 4760 [2], macro-geometric part quality is defined as the first- and second-order deviations of the machined surface from nominal values. From third- to sixth-order deviations, the micro-geometric part quality is defined (see Figure 2.2). Within the micro-geometric part quality, surface roughness is defined by the third- to the fifth-order deviation. It is important to remark that there is no distinct borderline between macro- and micro-geometric deviations. Indeed, sometimes parts of the micro-deviations will contribute to the result of the measured macro-deviations and vice versa [1].






| Geometrical deviation and profile diagram | Description | Examples of source of error |
|--|--------------------|--|
| 1st order: Form  | Form deviation | Errors in guidance of machine-tool, deflections of machine-tool or workpiece, error in fixture of workpiece, wear. |
| 2nd order: Waviness  | Waviness | Eccentric fixture, form deviation of cutting-tool, vibrations. |
| 3rd order: Roughness  | Grooves | Form of tool cutting edge, cutting feed speed. |
| 4th order: Roughness  | Flakes | Cutting process (tear chip, shear chip), deformation from blasting, gemmation with galvanizing. |
| 5th order: Roughness Not presentable | Crystal structure | Crystallization process, corrosion, etc. |
| 6th order: Deviation of crystal structure Not presentable | Crystal structure | Crystal structure. Physical and chemical processes on crystal structure. |
|  Actual surface: Superposition of surface deviations | | |

Figure 2.2: Part quality according to DIN 4760 Form Deviations, Concepts, Classification (1982).

In the following subsections the main sources of machining errors that influence both macro- and micro-geometric part quality are described. The physical models used in the literature to estimate part quality according to the type of machining error will be described in Chapter 3.

2.2 Sources of machining errors in macro-geometric part quality

In the context of macro-geometric part quality, machining errors can be classified into two categories: quasi-static errors and dynamic errors [3]. Quasi-static errors are those that occur between the tool and the workpiece and slowly vary with time, such as geometric and kinematic errors, thermal errors, cutting force-induced errors, cutting-tool wear-induced errors, fixturing errors, etc. These errors account for about 70 percent of total machine-tool

inaccuracy [3, 4]. Dynamic errors, on the other hand, are fast-changing errors caused by sources such as spindle error motion, vibrations of the machine structure, controller errors, etc. These are more dependent on the particular operating conditions of the machine and they mainly generate form errors and surface roughness variations. A more general classification of machining errors used by different authors [3, 5, 6] divides the errors as (see Figure 2.3):

1. Quasi-static errors
 - (a) Fixture-dependent errors or setup errors
 - i. Fixture errors
 - ii. Locating datum errors
 - iii. Clamping errors
 - (b) Machine-tool errors
 - i. Geometric and kinematic errors
 - ii. Thermal errors
 - iii. Cutting force-induced errors
 - iv. Cutting-tool wear-induced errors
 - (c) Workpiece-dependent errors
 - i. Thermal errors
 - ii. Cutting force-induced errors
2. Dynamic errors
 - (a) Controller errors
 - (b) Spindle error motion
 - (c) Vibrations

The characteristics of these sources of error will be outlined in the subsections that follow.

2.2.1 Fixture-dependent errors or setup errors

As a solid body in \mathbb{R}^3 space, a workpiece has six degrees of freedom (d.o.f.), as shown in Figure 2.4. These six d.o.f. are composed of three axial d.o.f. that allow straight-line movement in both directions along the three principal axes (shown as X, Y, and Z), and three radial d.o.f. that allow rotational movement, in both clockwise and counterclockwise radial directions, around the same three axes. In order to locate a workpiece completely, the six d.o.f. must be constrained.

In a machining operation, fixture devices are applied to locate and hold the workpiece. Fixtures must correctly locate a workpiece in a given orientation with respect to a cutting-tool or measuring device. Such location must be invariant in the sense that the devices must clamp and secure the workpiece in that location for a particular processing

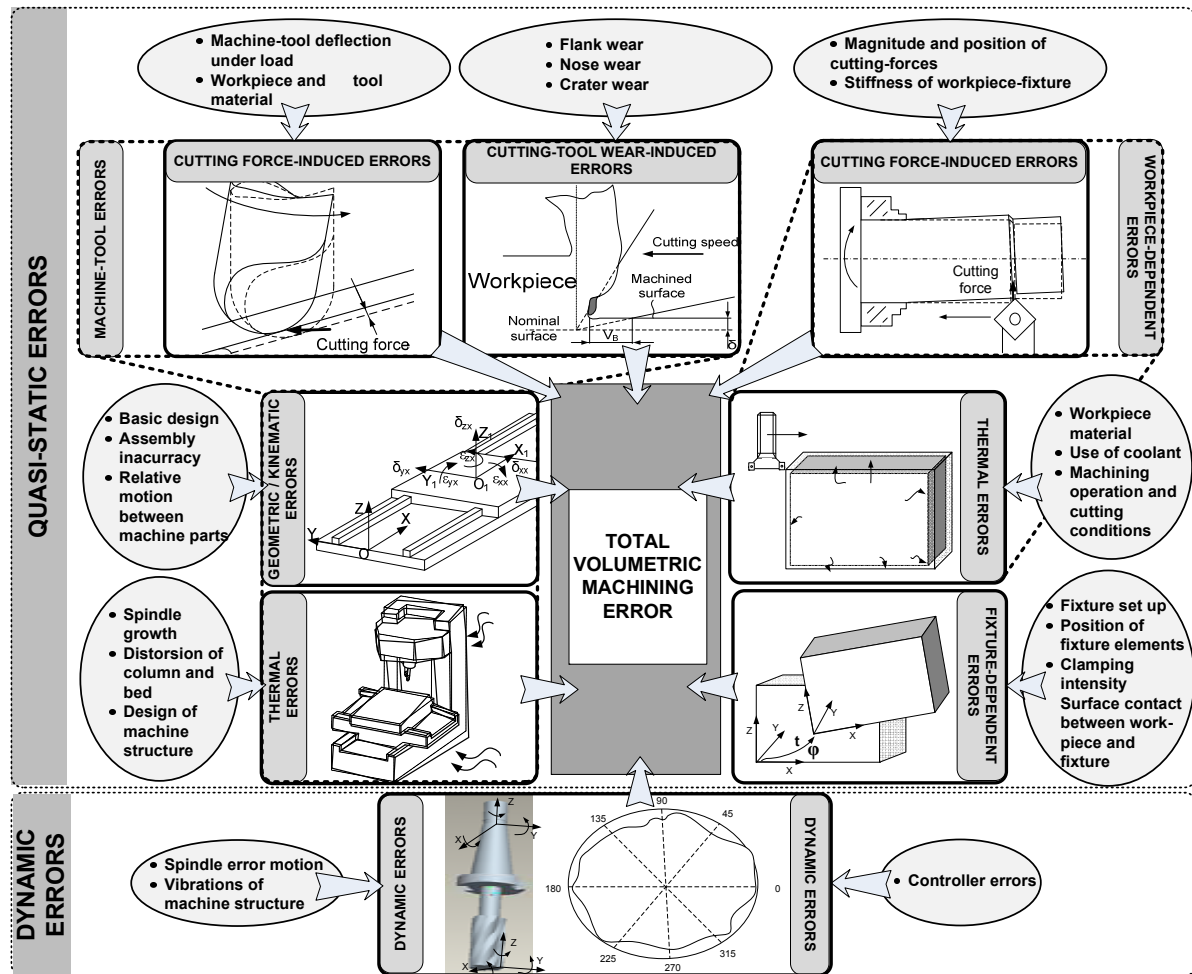


Figure 2.3: Sources of errors affecting macro-geometric part quality.

operation [7]. Fixtures are normally designed for a definite operation to process a specific workpiece and they are designed and manufactured individually. Jigs are similar to fixtures, but they not only locate and hold the part but also guide the cutting-tools in drilling and boring operations. Generally, all fixtures consist of the following elements: locators, clamps, supports, and fixture body [7]. A locator is usually a fixed component of a fixture. It is used to establish and maintain the position of a part in the fixture by constraining the movement of the part. A clamp is a force-actuating mechanism of a fixture. The forces exerted by the clamps hold a part securely in the fixture against all other external forces. A support is a fixed or adjustable element of a fixture. When severe part displacement/deflection is expected under the action of imposed clamping and processing forces, supports are added and placed below the workpiece so as to prevent or constrain deformation. The fixture body, or tool body, is the major structural element of a fixture. It maintains the spatial relationship between the fixturing elements mentioned above and the machine-tool on which the part will be processed.

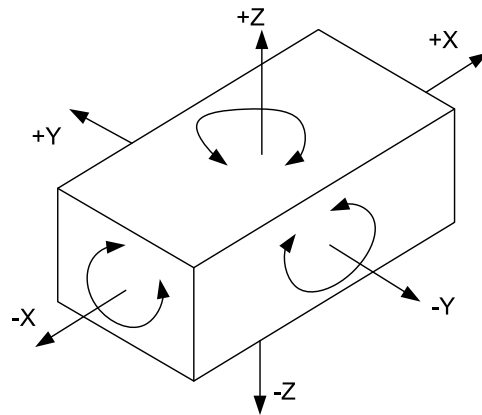


Figure 2.4: Degrees of freedom of a workpiece in \mathfrak{R}^3 space.

During fixturing, the workpiece surfaces are named according to their functionality as follows [7]:

- Active or machined surfaces: these are the surfaces to be machined.
- Locating datums: these are surfaces by means of which the workpiece is to be located.
- Clamping surfaces: these are surfaces subjected to the clamping forces.
- Measurement datums: these are reference surfaces where the dimensions are to be maintained and measured.
- Free surfaces: these surfaces are not involved in the setup for the particular machining operation.

In order to locate the part isostatically, three main generic forms of location can be distinguished: plane, concentric, and radial location [8].

In a plane location, the workpiece is located from any surface, which may be flat, curved, or have an irregular contour. Related to this form of location, a common fixture layout to locate prismatic objects is the 3-2-1 locating scheme. In this fixture layout, three locating surfaces are placed on fixture surfaces to constrain three d.o.f. on the first locating surface (primary locating datum), two d.o.f. on the second one (secondary locating datum) and one d.o.f. on the last locating surface (tertiary locating datum). To reduce the influence of geometric variations of locating surfaces on the locating accuracy, fixtures based on hemispherical point locators are commonly applied. To achieve the greatest stability, the first three points of location on the primary locating surface should be as far apart as possible, or the area enclosed by the three points as large as possible. For larger workpieces, the 4-2-1 locating principle is frequently used. Since this is an over-constrained fixture scheme, one of the locating points would act as a support [7]. Figure 2.5 (a) shows an example of plane location with fixture surfaces and locators in two dimensions.

In concentric location, the workpiece is located from a central axis which may or may not be in the center of the workpiece. Locating the workpiece from internal surfaces using a locating pin placed in a hole in the workpiece is the most common type of concentric location (Figure 2.5 (b)). An industrial fixture layout based on this location is the hole-plane locating scheme, which locates a workpiece from a central axis using a hole as a primary locating datum to constrain four d.o.f. and a plane to constrain one translational d.o.f. For cylindrical workpieces and external surface location, other fixture devices for concentric location, such as V-blocks or 3-jaw chucks, are applied [7].

In radial location, radial locators restrict the movement of a workpiece around a concentric locator (Fig 2.5 (c)). For this type of location, the common fixture layout is the plane-hole locating scheme, which locates the workpiece using a plane as a primary locating datum to constrain three d.o.f. (two rotational and one translational motion), a hole to constrain two d.o.f., and a slot to constrain the last d.o.f. Some of the fixture devices applied in radial location use two holes in the workpiece, one to locate the part with a concentric locator and the second to constrain the rotation of the part with a radial locator.

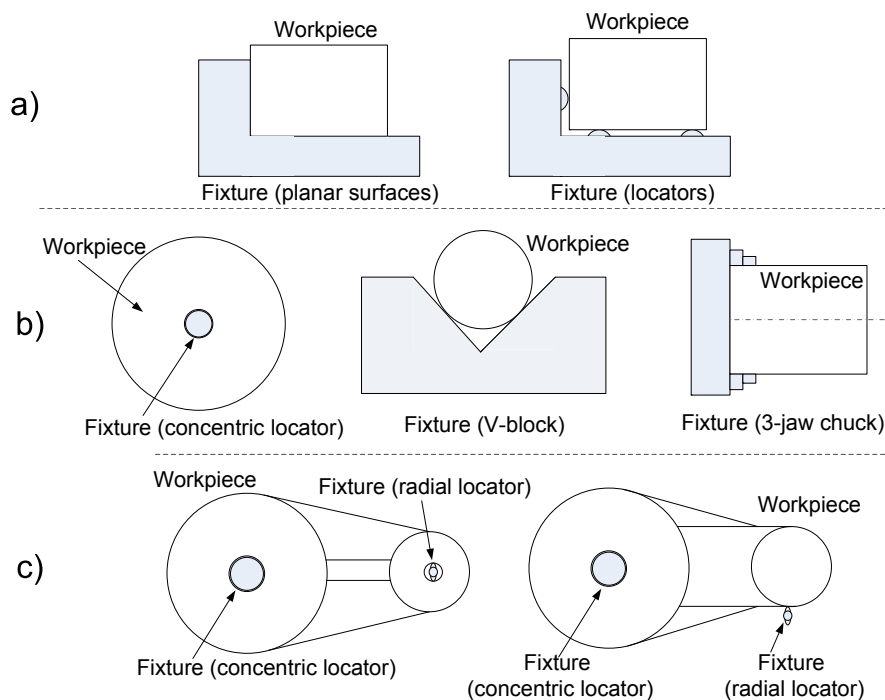


Figure 2.5: Examples of generic forms of location. a) plane location with fixture surfaces and locators; b) concentric location with concentric locators, V-blocks and 3-jaw chucks; c) radial location with concentric and radial locators.

In order to understand the importance of the fixture device and its setup on part quality, let us consider the normal preparation of a machining operation in a vertical machining center. First, a fixture device is placed on the machine-tool table, so the location coordinate system defined by the fixture layout, named FCS (fixture coordinate system),

is located w.r.t. the machine-tool coordinate system (MCS). Second, a workpiece is placed on the fixture device ensuring contact between the locating datums and the fixture locators or fixture surfaces. The features of the workpiece are defined w.r.t. the part reference coordinate system (RCS), and ideally this coordinate system coincides with the FCS and, thus, with the MCS [5]. Finally, the workpiece is clamped to ensure it is held firmly during machining.

Due to different setup errors, FCS and RCS may deviate from nominal values. In the literature, the effect of setup errors on workpiece location has been extensively investigated [5, 9–12]. According to these investigations, three main types of setup errors can be distinguished: locator/fixture errors, locating datum errors, and clamping errors. These types of setup errors are described as follows:

- Locator/fixture errors:

Locator/fixture errors refer to the deviation of locators or surfaces that make up the fixture away from their nominal positions. These deviations produce the deviation of the FCS from its nominal value, denoted as ${}^{\circ}\text{FCS}$. As cutting-tool movements in CNC programs are referenced to ${}^{\circ}\text{FCS}$ and not to FCS (when executing a CNC program, there is an internal off-setting of the MCS to realize the movements w.r.t. the ${}^{\circ}\text{FCS}$), a dimensional deviation of the machined part occurs. Figure 2.6 (a) shows how a dimensional deviation of a locator that makes up a fixture produces a position and orientation deviation of the FCS w.r.t. its nominal value, generating a dimensional deviation of the feature machined.

- Locating datum errors:

The locating surfaces of the workpiece may always present some degree of geometric imperfection (such as parallelism and perpendicularity errors, form errors, etc.) due to manufacturing variability in previous stations. Due to this imperfection, RCS will be deviated from its nominal value, denoted as ${}^{\circ}\text{RCS}$, and thus a dimensional deviation of the machined part will occur. Figure 2.6 (b) shows how a locating datum error can affect the final part location on the fixture, generating a dimensional deviation of the feature machined.

- Clamping errors:

Clamping errors refer to the deviation of workpiece location due to the clamping forces applied to hold the workpiece firmly in the fixture. These errors are generally explained by elastic/plastic deformations. Generally speaking, clamping deformations can be catalogued as two components: contacting deformation on the locators, and deflecting deformation on locating datums [5]. These two components will produce a deviation of FCS away from nominal values and a deviation of RCS away from nominal values, respectively. Figure 2.6 (c) shows how the force applied by a clamp deforms a locator, generating a dimensional deviation of the feature machined.

Additionally, the dimensions of part features are defined w.r.t. a design coordinate system (DCS). Under ideal conditions, the DCS and the FCS are coincident. However,

due to setup errors, FCS may be deviated away from nominal values. In the literature, the effect of setup errors on workpiece location has been extensively investigated [5, 9–12].

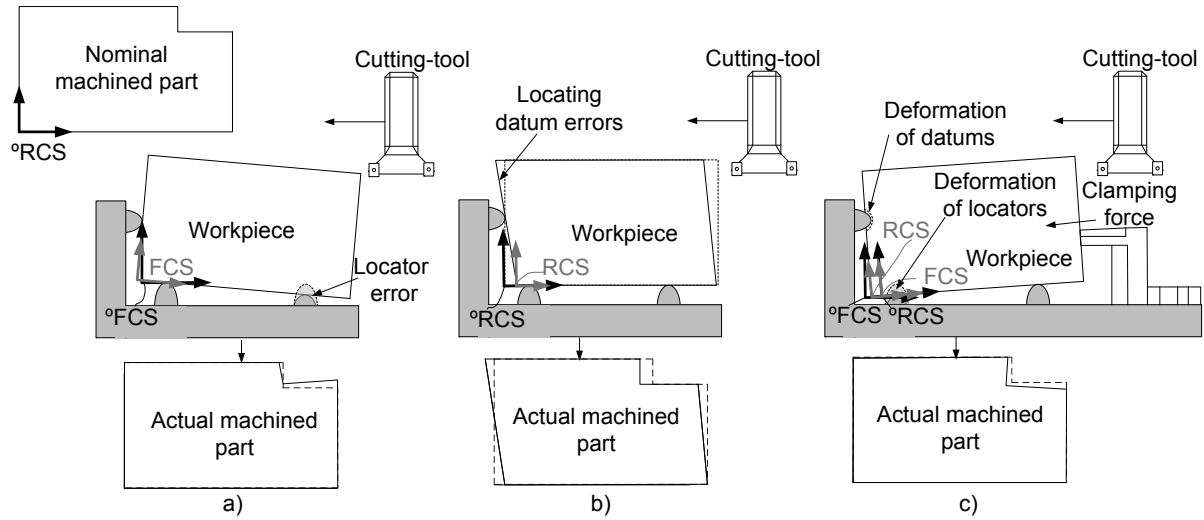


Figure 2.6: Example of (a) locator/fixture errors, (b) locating datum errors and (c) clamping errors.

2.2.2 Machine-tool errors: geometric and kinematic errors

Geometric errors are those errors that are extant in a machine-tool on account of its basic design, the inaccuracies built in during assembly, and as a result of the components used in the machine-tool [3]. Geometric errors are smooth and continuous, and they could exhibit hysteresis behavior. On the other hand, kinematic errors are concerned with the relative motion errors of several moving machine-tool components that need to move in accordance with precise functional requirements [3]. The geometric and kinematic errors identified in a machine-tool are defined as follows:

- Positioning error of each axis.
- Straightness of each axis in its perpendicular axes.
- Roll, yaw and pitch errors of each axis.
- Squareness error between axes.

In order to understand these errors, let us consider the X -axis carriage of a machine-tool, as shown in Figure 2.7. For this carriage system, movement is only allowed in the X direction. However, due to manufacturing and assembly imperfections, there are small displacements in the other five d.o.f. and so the coordinate system of the carriage system is deviated from its nominal value. These small deviations are: one positioning error along the X -axis, called $\delta_x(x)$; two straightness errors along the Y -axis and the Z -axis named

$\delta_y(x)$ and $\delta_z(x)$ respectively; and three angular errors defined as roll, yaw and pitch errors, which are rotational errors about the X -axis, Y -axis and Z -axis respectively, called $\varepsilon_x(x)$, $\varepsilon_y(x)$ and $\varepsilon_z(x)$ respectively. Note that ε represents angular error motions, δ represents the translational error motions, and for both errors the first subscripted letter represents the axis the motion rotates about and the second one represents the intended direction of motion. Now, let us consider a second carriage system, in this case in the Y -axis. Similar to the X -axis carriage system, translational and rotational errors arise, but now the translational error along the X -axis is also composed of an orthogonality (squareness) error, which is defined by the product $\varepsilon_z(y) \cdot y$, where y is the position of the carriage in the Y -axis.

If we consider an additional carriage system, for example a Z -axis carriage, again similar translational and rotational errors are defined but the translational error along the X - and Y -axes are also composed of orthogonality (squareness) errors ($\varepsilon_x(z) \cdot z$ and $\varepsilon_y(z) \cdot z$ respectively). Consequently, for a 3-axis machine-tool with three carriages in the X , Y and Z direction, 21 error components are generally identified [3, 13]. From these errors, there are three linear positioning errors (one for each carriage axis, called $\delta_i(j)$ when $i = j$), six straightness errors (two for each carriage axis, called $\delta_i(j)$ when $i \neq j$), nine angular errors (three for each carriage axis, called $\varepsilon_i(j)$), and three orthogonality (squareness) errors (called $\varepsilon_z(y) \cdot y$, $\varepsilon_x(z) \cdot z$ and $\varepsilon_y(z) \cdot z$).

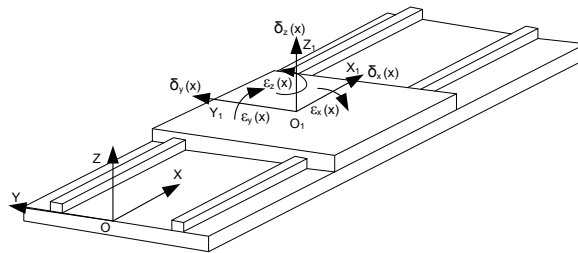


Figure 2.7: Six d.o.f. error motion of a machine-tool carriage system.

As can be noted, geometric and kinematic errors depend on the configuration of the machine-tool axes and the relative movement among them. For example, 5-axis machine-tools are composed of three translation axes (T) and two rotational axes (R). According to their configuration, 5-axis machine-tools can be configured as RRTTT, when the rotational axes are on the machine-tool table on a double turntable which rotates the workpiece, or as TTTRR when the machine-tool has two degrees of rotation freedom at the main spindle, and so on. Unlike the 3-axis machine-tool with three translational axes, in a 5-axis machine-tool there are two rotational axes. In a rotational axis there is a rotation about the i -th axis by the angle θ_i , but due to imperfections, angular and translational errors are also generated, which depend on the angle of rotation θ_i [14]. Following the same reasoning as shown above, different translational, angular and orthogonality errors can be defined.

Other geometric and kinematic sources of errors can be found in the literature, such as backlash errors and contouring errors of each axis. However, the study of these errors is beyond the scope of this work.

2.2.3 Machine-tool errors: thermal-induced errors

Thermal-induced errors are the main cause of inaccurate workpieces in precision engineering, where thermal factors account for 40-70% of the total dimensional and form errors [15]. Six heat sources that produce thermal-induced errors in the machine-tool are usually identified in the literature [16]: (i) heat from the cutting process; (ii) heat generated by the machine; (iii) the heating or cooling provided by the cooling systems; (iv) heating or cooling influence of the room; (v) the effect of people; and (vi) thermal memory from any previous situation. Critical among these sources is the heat generated at the moving elements by the continuous running of the machine-tool as a result of frictional resistance, in the motors, in pumps, etc. This heat causes relative expansion of the various elements of the machine-tool such as spindle, ballscrews and guideways, leading to inaccurate positioning of the cutting-tool tip which removes the workpiece material and gives the final dimension and geometry of the machined surface [17]. Figure 2.8 shows an example of how machine-tool structure is deformed due to thermal effects.

Thermal-induced errors are sensitive to varying spindle speeds and the temperature history (warm-up or cool-down cycles) owing to different thermal time constants of the various machine-tool components. For example, the thermal growth of a spindle is contributed not only by the thermal expansion of the spindle itself but also by the thermal bending of the machine column. The spindle heats up and cools down quickly but the column has a relatively sluggish response to generated heat [18].

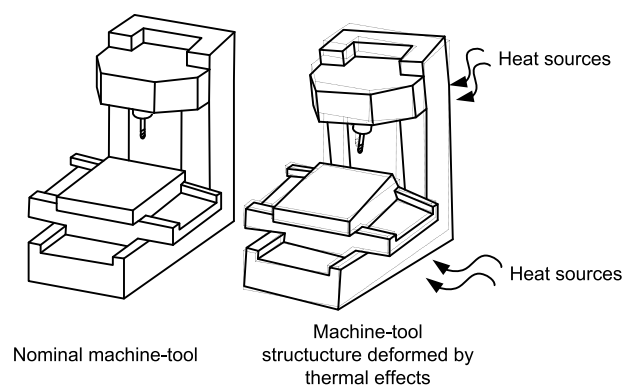


Figure 2.8: Example of a machine-tool structure deformed due to thermal effects.

In general, the thermal volumetric errors could be divided into two categories. In the first category are those errors that change depending on the temperature but not according to the axis position. These errors effectively change the machine offsets and are known as position independent thermal errors (PITE). The second category of errors deals with those that change according to axis position as well as temperature. They effectively alter

the linear positioning of the machine-tool and are known as position dependent thermal errors (PDTE) [17]. As presented in Chen *et al.* [18, 19], the total volumetric error in a 3-axis machine-tool can be broken down into 32 error components. In addition to the well-known 21 geometric and kinematic errors (excluding backlash and contouring errors), 11 additional thermal error components are identified. The first group of additional thermal errors accounts for thermal drifts at the tool-tip, which include three translational drifts and two inclinational drifts of the spindle axis. The second group of additional thermal errors is due to thermal shifts at the references of machine-tool axes, which include six translational errors if one axis is selected as the reference for the other two axes [18, 19].

2.2.4 Machine-tool errors: cutting force-induced errors

Traditionally, cutting force-induced errors have been neglected, since cutting forces are small during finish machining [15]. However, in recent years hard machining has been gaining increased popularity. In hard machining, hardened steel is cut directly to its final form and finish, thereby avoiding the customary grinding operations. In these operations, the cutting forces can be very high and the effect of cutting force-induced errors on macro-geometric part quality due to the deflection of machine-tool components cannot be neglected [20, 21]. In fact, in some applications cutting forces produce a significant deflection of the cutting-tool that deviates the cutting-tool tip away from nominal values, thus generating a deviation of the machined surfaces (Figure 2.9). These cutting force-induced errors depend on the stiffness of all the components of the machine-tool (such as the bed, column, cutting-tool, etc.) that are within the force-flux flow caused as a result of the cutting action. They also depend on the magnitude and direction of the cutting force. Thus, for a machine-tool with a given stiffness a heavy cut would generally produce more inaccurate components than a light cut, but applying cutting strategies that produce greater cutting forces may also give rise to smaller errors owing to the direction of the force w.r.t. the surface.

When considering cutting force-induced errors, one has to distinguish machining operations where there is a constant cutting force, such as turning operations, and those that involve variable cutting forces, such as milling operations. In the former, the error caused by deflection of the tool tip can be predicted relatively easily, using the equivalent stiffness value of the system. In the latter, a more complex derivation is required [22].

Special attention should be paid in drilling operations where cutting force-induced errors are an important factor related to form and positional/orientation errors. The cause is that, ideally, the cutting lips of standard drills (except for special asymmetric drills) ought to be identical to each other so that radial force components should cancel each other out and the drill should not observe any net radial force – only an axial force. However, in practice, due to inaccuracies in tool manufacturing, the drill lips are not identical and the resultant radial force produces cutting-tool deflections that generate non-perfect holes [23].

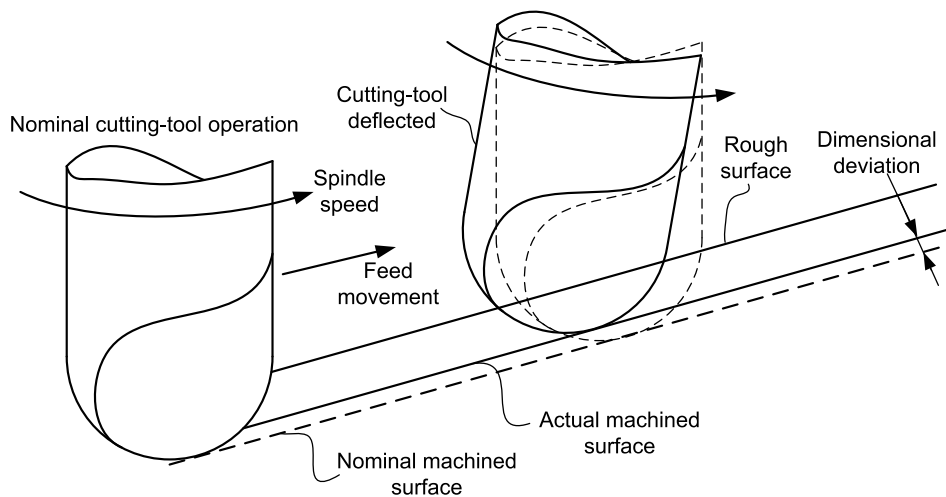


Figure 2.9: Example of cutting force-induced error in a ball end milling operation.

2.2.5 Machine-tool errors: cutting-tool wear-induced errors

Wear can be located on different zones of the cutting-tool edges. Edge wear and crater wear on the rake surface alter the state of stress and strain in the cutting region, thereby changing cutting forces and the mechanics associated with the chip-making process [24]. If cutting-tool wear is located on the tool rake face, cutting edge resistance is badly affected and the edge may break, but this type of wear does not have a direct consequence on the dimensions of the workpiece. On the other hand, if wear is located on the flank face, both the tool shape and dimension change, resulting in a loss of the effective depth of cut during machining (Figure 2.10). Both of these changes in the geometry of the cutting-tool could produce out-of-tolerance dimensions on machined parts [24].

Macro-geometric deviation of part dimensions due to flank wear depends mainly on the clearance angle of the cutting-tool as shown in Figure 2.10. In general, larger clearance angles produce a higher impact on part quality for a given flank wear value. However, for large clearance angles, the volume of wear to reach a particular width of flank wear is also increased and thus longer tool life values are obtained. On the other hand, large clearance angles produce weaker cutting edges and the more liable the tool is to chipping or fracture [25]. Experience has shown that with most work materials, clearance angles in the range of $5 - 8^\circ$ with high-speed steel (HSS) tools and $5 - 11^\circ$ with carbides give the best compromise between these conflicting requirements [26]. Furthermore, other factors that influence on the impact of flank wear on macro-geometric dimensions are the rake angle and, if rounded cutting inserts are applied, the nose radius of the cutting-tool [27].

Flank wear is measured by the V_B parameter. The cutting-tool tip deviation is proportional to the value of V_B and thus the higher the value of V_B is, the higher the inaccuracy of the machined part will be. However, depending on the machining operation and the geometry of the cutting-tool, the V_B has a greater or lesser impact on the quality dimension. Furthermore, flank wear is not always uniform along the primary and secondary

cutting edges, so the flank wear effect on part quality depends on which cutting edge is generating the final machined surface. For instance, in face milling, flank wear at the secondary edge is responsible for dimensional part quality [28], but in end milling operations the flank wear at the primary edge is the critical one in terms of dimensional part quality. For general applications, machining handbooks recommend cutting-tool replacement for specific maximum values of V_B . For example, in turning and face milling operations with carbide cutting-tools, it is recommended that V_B should be under 0.45 mm , whereas for end milling-slotting and end milling-peripheral operations V_B with carbide or HSS cutting-tools it should be under 0.3 mm [24].

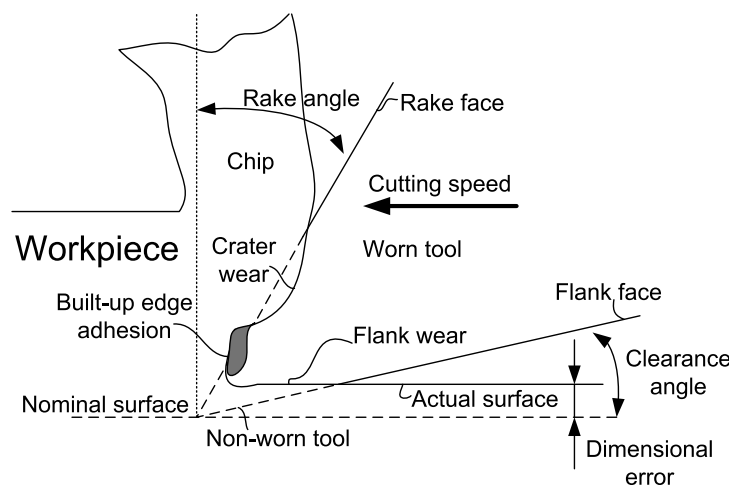


Figure 2.10: Example of cutting-tool wear-induced error in machining.

Apart from the direct impact of flank wear on dimensional part quality due to the loss of the effective depth of cut, cutting-tool wear also produces an increase in cutting forces due to the loss of a sharpened edge and increased rubbing. The increase in cutting forces (in some applications, such as hard machining, cutting forces can be increased by up to 200% [20]) may produce other macro-geometric errors due to deflections.

2.2.6 Workpiece-dependent errors: cutting force-induced and thermal-induced errors

Both cutting force-induced and thermal-induced errors are not only related to the machine-tool and can also have a significant effect on the workpiece. For instance, thermal effects may also be responsible for the expansion of the workpiece during the machining process. This expansion is usually important when cutting hardened steels without a coolant, although it may be considered negligible when coolant is applied [20]. In dry drilling operations, the thermal expansion of the workpiece should also be taken into account to obtain high quality holes [29].

Cutting force-induced errors can also produce workpiece deflections during machining. In turning operations, in the moment when the cutting-tool enters the workpiece (transi-

tion from air to material), the workpiece begins to deform elastically because of the force that the cutting-tool exerts on it [30] (see Figure 2.11). This elastic deformation results in the workpiece being pushed away from the cutting-tool, and thus the depth of cut is smaller than the desired one. The end result is that the produced part is over-dimensioned, which means that the part diameter is larger than that aimed for. Note that for some specific cutting-tool configurations and operations, the cutting-tool force component may be exerted towards the cutting-tool and thus the resulting part diameter may be smaller instead of larger.

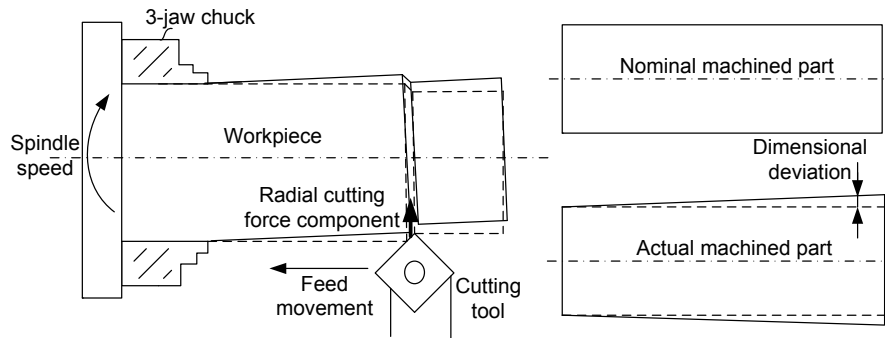


Figure 2.11: Example of workpiece-dependent errors due to cutting forces.

2.3 Sources of machining errors in micro-geometric part quality

As explained above, micro-geometric part quality refers to the deviation of the nominal surface from the third- up to the sixth-order deviation according to DIN4760 [2]. Surface roughness defines the micro-geometric part quality from the third- to the fifth-order deviation. Sixth-order deviation refers to workpiece material structure, which is connected to physical-chemical mechanisms acting on a grain and lattice scale (slip, diffusion, oxidation, residual stress, etc.). In this section we will focus on the source of machining errors related to surface roughness, without considering effects at the material structure level.

The importance of surface roughness in machining lies in the great influence it can have on the tribological properties, fatigue strength, corrosion resistance, and aesthetic appeal of the product [31]. Most of the factors that have a negative impact on surface roughness are well-known. According to the literature, the main factors that affect surface roughness are [32]:

- Nominal geometry of the cutting-tool. Surface roughness is mainly defined by the cutting-tool feed marks, which depends on the radius of the cutting-tool inserts and the feed rate of the cutting-tool.
- Mounting and manufacturing errors of cutting-tools. These errors are also called runout errors and they refer to the mounting errors of the cutter in its arbor, the

mounting errors of the cutter inserts in the cutter head, and manufacturing errors of the cutter inserts. Due to these mounting or manufacturing errors, multi-point cutting-tools, such as those used in milling operations, tend to generate higher surface roughness values than single-point cutting-tools, such as those used in turning operations.

- Errors in the cutting-tool edge geometry during cutting. Two main factors are distinguished: the cutting-tool flank wear and the built-up edge (BUE) formation. Flank wear modifies the shape of the cutting-tool edge due to micro-chipping, thus affecting the generation of surface roughness. Although in general flank wear produces an increase in surface roughness, in some specific applications low-middle values of flank wear may improve surface roughness due to rubbing effects [28]. The BUE formation during machining refers to the adhesion of material on the cutting-tool edge during machining, which modifies the cutting edge geometry and increases surface roughness.

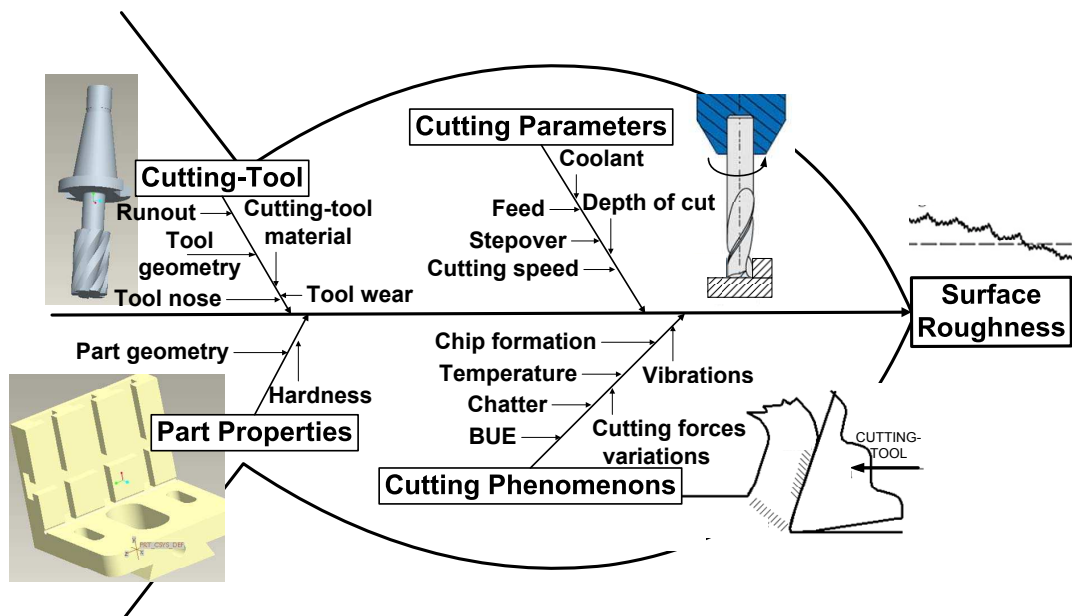


Figure 2.12: Factors affecting generation of surface roughness - modified from Benardos and Vosniakos's (2003) research work-.

Besides these factors, other important factors that influence surface roughness have been identified in the literature [26, 33]. Some of these factors are:

- The occurrence of chatter or vibrations during machining.
- Inaccuracies in machine-tool movements.
- Defects in the structure of the workpiece material.
- Hardness of workpiece material.

- Discontinuous chip formation when machining brittle materials.
- Tearing of the workpiece material when ductile metals are cut at low cutting speeds.
- Other cutting-tool geometry factors and variations in cutting conditions (cutting-tool rake angle, variations in depth of cut and cutting speed, etc.).

Figure 2.12 summarizes most of the factors described in the literature that affect surface roughness.

2.4 Conclusions

In this chapter we have briefly described the main sources of machining errors that have an impact on part quality at the macro-geometric and/or micro-geometric levels. The review is completed in Chapter 3, where some physical models defined in the literature to quantify the effect of these machining errors are described.

References

- [1] G. Henzold, *Geometrical Dimensioning and Tolerancing for Design, Manufacturing and Inspection*, Elsevier Ltd, 2006.
- [2] DIN4760, Form deviations; concepts; classification system, Deutsches Institut Fuer Normung.
- [3] R. Ramesh, M. A. Mannan, A. N. Poo, Error compensation in machine tools - a review part I: geometric, cutting-force induced and fixture-dependent errors, *International Journal of Machine Tools and Manufacture* 40 (9) (2000) 1235–1256.
- [4] J. Shi, *Stream of Variation Modeling and Analysis for Multistage*, CRC Press Taylor and Francis Group, 2007.
- [5] X. Huang, P. Gu, Tolerance analysis in setup and fixture planning for precision machining, in: *Proceedings of the Fourth International Conference on Computer Integrated Manufacturing and Automation Technology*, 1994, pp. 298–305.
- [6] Z. Q. Liu, Repetitive measurement and compensation to improve workpiece machining accuracy, *International Journal of Advanced Manufacturing Technology* 15 (2) (1999) 85–89.
- [7] A. Y. C. Nee, Z. J. Tao, A. S. Kumar, *An Advanced Treatise on Fixture Design and Planning*, World Scientific Publishing Co. Pte. Ltd, 2004.
- [8] CarrLane Manufacturing, *Jig and Fixture Handbook*, Carr Lane Mfg. Co. Available via <http://www.carrlane.com/>. Accessed 10 June 2010, 1992.
- [9] E. C. DeMeter, M. J. Hockenberger, The application of tool path compensation for the reduction of clamping-induced geometric errors, *International Journal of Production Research* 35 (12) (1997) 3415–3432.

-
- [10] M. Y. Wang, Characterizations of positioning accuracy of deterministic localization of fixtures, in: *Proceedings of the International Conference on Robotics and Automation*, Vol. 3, 2002, pp. 2894–2899.
- [11] M. Estrems, H. T. Sanchez, F. Faura, Influence of fixtures on dimensional accuracy in machining processes, *International Journal of Advanced Manufacturing Technology* 21 (5) (2003) 384–390.
- [12] A. Raghu, S. N. Melkote, Modeling of workpiece location error due to fixture geometric error and fixture-workpiece compliance, *Journal of Manufacturing Science and Engineering-Transactions of the ASME* 127 (1) (2005) 75–83.
- [13] A. C. Okafor, Y. M. Ertekin, Derivation of machine tool error models and error compensation procedure for three axes vertical machining center using rigid body kinematics, *International Journal of Machine Tools and Manufacture* 40 (8) (2000) 1199–1213.
- [14] A. K. Srivastava, S. C. Veldhuis, M. A. Elbestawit, Modelling geometric and thermal errors in a five-axis CNC machine tool, *International Journal of Machine Tools and Manufacture* 35 (9) (1995) 1321–1337.
- [15] J. C. Liang, H. F. Li, J. Ni, A comprehensive error compensation system for correcting geometric, thermal, and cutting force-induced errors, *International Journal of Advanced Manufacturing Technology* 13 (1997) 708–712.
- [16] J. Bryan, International status of thermal error research, *Annals of the CIRP* 39 (2) (1990) 645–656.
- [17] R. Ramesh, M. A. Mannan, A. N. Poo, Error compensation in machine tools - a review part II: thermal errors, *International Journal of Machine Tools and Manufacture* 40 (9) (2000) 1257–1284.
- [18] J. S. Chen, J. Yuan, J. Ni, Thermal error modelling for real-time error compensation, *International Journal of Advanced Manufacturing Technology* 12 (1996) 266–275.
- [19] J. S. Chen, J. Yuan, J. Ni, S. M. Wu, Real-time compensation of time-variant volumetric errors on a machining center, *Journal of Engineering for Industry* 115 (1993) 472–479.
- [20] H. K. Tonshoff, C. Arendt, R. Ben Amor, Cutting of hardened steel, *Annals of the Cirp* 49 (2000) 547–566.
- [21] L. N. López de Lacalle, A. Lamikiz, J. A. Sánchez, M. A. Salgado, Effects of tool deflection in the high-speed milling of inclined surfaces, *The International Journal of Advanced Manufacturing Technology* 24 (2004) 621–631.
- [22] L. N. López de Lacalle, A. Lamikiz, *Machine Tools for High Performance Machining*, Springer, 2009.
- [23] M. Pirtini, I. Lazoglu, Forces and hole quality in drilling, *International Journal of Machine Tools and Manufacture* 45 (2005) 1271–1281.

-
- [24] J. R. Davis, *Metals Handbook: Machining*, ASM International, 1989.
- [25] M. A. E. Baradie, The effect of varying the workpiece diameter on the cutting tool clearance angle in tool-life testing, *Wear* 195 (1-2) (1996) 201–205.
- [26] G. Boothroyd, *Fundamentals of Machining and Machine Tools*, Marcel Dekker, Inc., 1989.
- [27] X. Bi, Y. Liu, Y. Liu, Analysis and control of dimensional precision in turning process, in: *Control and Decision Conference*, 2009, pp. 3456–3459.
- [28] J. Gu, G. C. Barber, Q. Y. Jiang, S. Tung, Surface roughness model for worn inserts of face milling: Part I - factors that affect arithmetic surface roughness, *Tribology Transactions* 44 (1) (2001) 47–52.
- [29] M. Bono, J. Ni, The effects of thermal distortions on the diameter and cylindricity of dry drilled holes, *International Journal of Machine Tools and Manufacture* 41 (2001) 2261–2270.
- [30] P. G. Benardos, S. Mosialos, G. C. Vosniakos, Prediction of workpiece elastic deflections under cutting forces in turning, *Robotics and Computer-Integrated Manufacturing* 22 (2006) 505–514.
- [31] K. A. Risbood, U. S. Dixit, A. D. Sahasrabudhe, Prediction of surface roughness and dimensional deviation by measuring cutting forces and vibrations in turning process, *Journal of Materials Processing Technology* 132 (1-3) (2003) 203–214.
- [32] J. Kaczmarek, *Principles of machining by cutting, abrasion and erosion*, Peter Peregrinus, 1983.
- [33] P. G. Benardos, G. C. Vosniakos, Predicting surface roughness in machining: a review, *International Journal of Machine Tools and Manufacture* 43 (8) (2003) 833–844.

Prediction of part quality in uni-station machining systems

Improvement of machining accuracy requires an understanding of the sources of variation that modify the ideal machining conditions and generate macro- and micro-geometric part deviations. Understanding the machining/machine-tool errors physically allows us to model the machining output in terms of macro- and micro-geometric part quality, so that they can be predicted under specific conditions or making it possible to perform error compensation actions to improve part quality in uni-station machining systems. In this chapter, some physical models that relate the source of errors studied in Chapter 2 with part quality are reviewed. Additionally, a brief explanation of experimental models based on regressions and artificial intelligence techniques applied for the same purpose is also presented.

3.1 Introduction

In Chapter 2 the most important sources of machining errors that have a direct impact on macro- and micro-geometric part quality were described. In order to improve part quality, the effect of those sources of error should be limited by developing robust process plans, using robust machine-tools and proper cutting conditions, and so forth. In practice, there are many machining errors that it is not economically feasible to reduce (e.g., geometric and kinematic errors, thermal-induced errors, etc.), since this can mean an excessive cost during manufacturing and/or assembly of the machine-tool or during the machining operation itself [1]. For these cases, the prediction of part quality by specific models can be used to ensure whether part specifications can be met or to conduct cutting-tool path compensations in order to improve the expected part quality.

In the literature there are many different types of models for predicting the performance of machining operations [2]. Recently, a unified terminology for classifying machining models has been proposed by van Luttervelt [3]. His classification is based on five main properties: the type of operation (milling, turning, etc.); the predicted quantity (tool-wear, surface roughness, macro-geometric quality, etc.); the main purpose (predictive, descriptive, etc.); the time of application of the model (pre-process, in-process, etc.);

and the modeling approach applied (mechanistic, kinematic, numerical, regression-based, and artificial intelligence – AI-based – approaches). Figure 3.1 shows van Luttervelt’s classification of machining models according to these five properties.

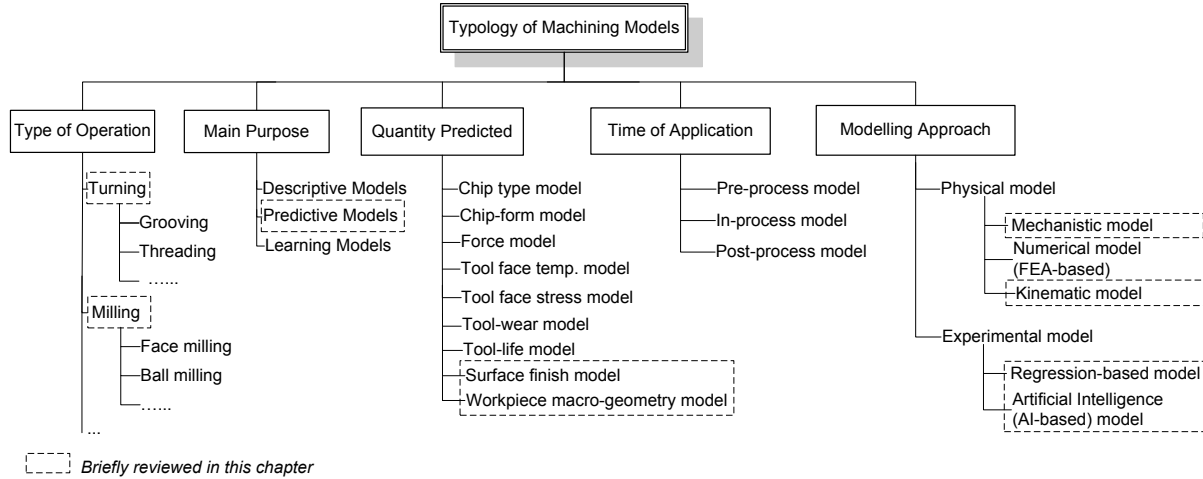


Figure 3.1: Typology of machining models according to van Luttervelt’s (2001) research work.

According to the modeling approach applied, machining models can be divided into two main groups: physical models and experimental models. Physical models are based on a thorough analysis of the basic physical principles [3]. A further subdivision of physical models is possible on the basis of the physical principle used. This subdivision is composed of [3]:

- **Mechanistic models:** the model takes into account only the mechanical aspects of an operation. For instance, only equilibrium of forces or only kinematics are considered. Mechanistic models are applied for modeling a large number of cutting aspects such as chip formation, cutting forces, chip-breaking, cutting-tool deflections, etc.
- **Numerical models:** the model analyzes the interaction between the tool and the workpiece taking into account dynamic effects, thermo-mechanical coupling, and friction [4]. These complex models are based on finite element analysis (FEA), and they are able to provide information about stresses and strain fields, shear zones, and temperature fields.
- **Kinematic models:** the model takes into account only the kinematic aspects of motions, and all elastic and plastic deformations related to workpieces, machine-tools and cutting-tools are neglected. Different kinematic models can be discerned on the basis of which motions and resulting geometry are modeled. For instance, different kinematic models can be derived for modeling fixture-induced errors, geometric and kinematic machine-tool errors, micro-geometric errors, etc.

In many practical situations, it can be difficult to obtain physical models or, if they can be obtained, the accuracy of the model may be low due to the influence of other

sources of errors that were previously assumed to be negligible. In those cases, models based on the experimental approach can be applied, where experimental data are used as the basis in formulating the models. Two main types of models can be distinguished based on experimental approaches: regression-based models, and AI-based models.

This chapter reviews some machining models used in the literature to describe the relationship between the sources of machining errors and the resulting part quality (surface roughness and macro-geometry) in uni-station machining systems. It should be remarked that, in this thesis, the term uni-station machining system refers to a machining station where one or more machining operations are conducted with the same fixture setup (same fixture device and locating datums). Without loss of generality, the review will focus on milling and to a lesser extent on turning, since similar models can be found for other applications such as drilling or grinding.

This chapter is organized as follows. Section 3.2 describes some physical models applied in the literature for macro- and micro-geometric part quality prediction. Some of these models, such as those for modeling fixture errors and geometric and kinematic machine-tool errors, are based on kinematic models, whereas those for modeling cutting force-induced errors and fixture clamping errors are based on mechanistic approaches. The models shown in this part will be used later on Chapter 6 to be included in 3D manufacturing variation models for quality prediction in multi-station machining systems. In Section 3.3, some experimental models applied in the literature for macro- and micro-geometric part quality prediction are briefly reviewed. These models, especially those based on AI, have gained in popularity in recent decades although many of the researchers in the mechanical field are skeptical of their use. However, it should be said that these models fill the gap left by physical models, since in some cases these models are too difficult or excessively expensive to be identified with enough accuracy. Finally, Section 3.4 concludes the chapter.

3.2 Physical models

In this section, some of the physical models that describe how the sources of machining errors analyzed in Chapter 2 influence micro- and macro-geometric part quality are described. Basically, the physical models reported in this section are based on kinematics and mechanistic approaches.

General assumptions: Datum surfaces and locating surfaces are assumed to be perfect in form (without form errors). Fixture locators are assumed to be punctual and when locating surfaces are applied, it is assumed that workpiece-fixture surfaces in contact are perfectly plane. Geometric errors are assumed to be small in comparison to nominal values and thus, the small-angle approximation can be applied.

3.2.1 Setup errors: fixture errors

Given a fixture, a workpiece should be localized with a unique position and orientation. The location (position and orientation) is considered to be deterministic if the workpiece

cannot make an infinitesimal motion while maintaining contact with all the locators / locating surfaces [5]. Due to manufacturing and assembly inaccuracies, tooling wear, etc., there is a deviation of the location of locators/locating surfaces. These inaccuracies produce a location deviation of the fixture coordinate system (FCS) with respect to (w.r.t.) its nominal value, denoted as ${}^{\circ}\text{FCS}$. Assuming small position and orientation errors, the FCS deviation is expressed by a differential motion vector (DMV), denoted as $\mathbf{x}_{FCS}^{\circ FCS}$ and abbreviated as $\mathbf{x}_F^{\circ F}$. This vector will be composed of a position deviation vector, defined by the vector $\mathbf{d}_F^{\circ F} = [d_{F_x}^{\circ F}, d_{F_y}^{\circ F}, d_{F_z}^{\circ F}]^T$, and an orientation deviation vector, defined by the vector $\boldsymbol{\theta}_F^{\circ F} = [\theta_{F_x}^{\circ F}, \theta_{F_y}^{\circ F}, \theta_{F_z}^{\circ F}]^T$. Thus, location deviation is defined as $\mathbf{x}_F^{\circ F} = [(\mathbf{d}_F^{\circ F})^T, (\boldsymbol{\theta}_F^{\circ F})^T]^T$. As was shown in Chapter 2, the cutting-tool trajectory is referenced from ${}^{\circ}\text{FCS}$. If FCS is deviated from its nominal value, the cutting-tool path will be deviated w.r.t. the location of the workpiece, and it will generate a deviation of machined surfaces w.r.t. their nominal values, as shown in Figure 3.2.

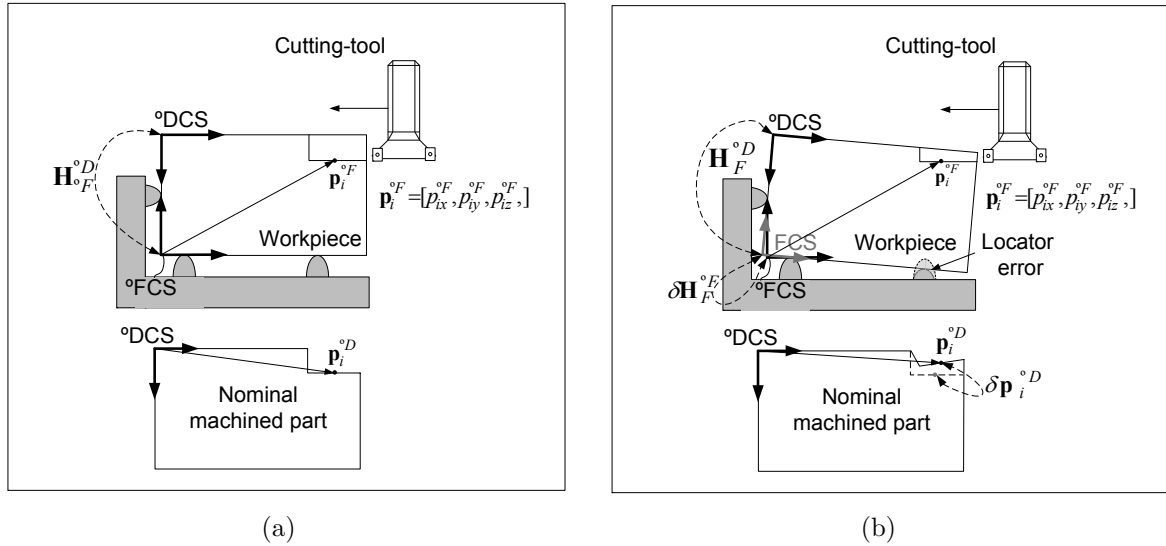


Figure 3.2: Example of fixture errors: (a) nominal conditions, (b) conditions with fixture errors.

In order to analyze how fixture errors influence this deviation and thus the macro-geometric part quality, let us consider an ideal machining operation and a point i on the feature generated by the cutting-tool, as shown in Figure 3.2 (a). As this point is generated by the cutting-tool, it is defined w.r.t. the ${}^{\circ}\text{FCS}$, and it is denoted as $\mathbf{p}_i^{\circ F} = [p_{ix}^{\circ F}, p_{iy}^{\circ F}, p_{iz}^{\circ F}]$. Let us define the vector $\tilde{\mathbf{p}}_i^{\circ F} = [\mathbf{p}_i^{\circ F}, 1]^T$. The point i w.r.t. the part design CS (a CS from which all workpiece features are referenced to), denoted as ${}^{\circ}\text{DCS}$, is defined as:

$$\tilde{\mathbf{p}}_i^{\circ D} = \mathbf{H}_{\circ F}^{\circ D} \cdot \tilde{\mathbf{p}}_i^{\circ F}, \quad (3.1)$$

where $\mathbf{H}_{\circ F}^{\circ D}$ is the homogeneous transformation matrix (HTM) of ${}^{\circ}\text{FCS}$ w.r.t. ${}^{\circ}\text{DCS}$ (see Appendix 3.1). However, due to fixture errors (neglecting any other errors) the actual FCS will be deviated and thus a point on the machined surface will be deviated w.r.t. the

°DCS, as shown in Figure 3.2 (b). Mathematically, the actual position of a point i w.r.t. the °DCS knowing the position of point i w.r.t. the °FCS is formulated as:

$$\tilde{\mathbf{p}}_i^{\circ D} = \mathbf{H}_F^{\circ D} \cdot \delta \mathbf{H}_{\circ F}^F \cdot \tilde{\mathbf{p}}_i^{\circ F}, \quad (3.2)$$

where $\delta \mathbf{H}_{\circ F}^F$ is the HTM for small position and orientation deviations of °FCS w.r.t. FCS. If there are no fixture errors, $\delta \mathbf{H}_{\circ F}^F$ is a 4×4 identity matrix. Thus, the deviation of the point i on the machined surface from nominal values due to fixture errors is obtained as:

$$\begin{aligned} \delta \tilde{\mathbf{p}}_i^{\circ D} &= \mathbf{H}_F^{\circ D} \cdot \delta \mathbf{H}_{\circ F}^F \cdot \tilde{\mathbf{p}}_i^{\circ F} - \mathbf{H}_F^{\circ D} \cdot \mathbf{I}_{4 \times 4} \cdot \tilde{\mathbf{p}}_i^{\circ F} \\ &= \mathbf{H}_F^{\circ D} \cdot (\delta \mathbf{H}_{\circ F}^F - \mathbf{I}_{4 \times 4}) \cdot \tilde{\mathbf{p}}_i^{\circ F}. \end{aligned} \quad (3.3)$$

Note that due to solid rigid movement, $\mathbf{H}_F^{\circ D}$ in Eq. (3.3) is equal to $\mathbf{H}_{\circ F}^{\circ D}$. Applying Eq. (3.3), the deviation of each point on the machined surface is formulated as a function of the deviation of the FCS from its nominal value expressed by the term $\delta \mathbf{H}_{\circ F}^F$. As shown in Appendix 3.2, matrix $\delta \mathbf{H}_{\circ F}^F$ is defined as:

$$\delta \mathbf{H}_{\circ F}^F = \mathbf{I}_{4 \times 4} + \Delta_F^F, \quad (3.4)$$

where $\Delta_F^F = -\Delta_F^{\circ F}$, and $\Delta_F^{\circ F}$ is the differential transformation matrix (DTM):

$$\Delta_F^{\circ F} = \begin{pmatrix} \hat{\boldsymbol{\theta}}_F^{\circ F} & \mathbf{d}_F^{\circ F} \\ \mathbf{0}_{1 \times 3} & 0 \end{pmatrix}, \quad (3.5)$$

and $\hat{\boldsymbol{\theta}}_F^{\circ F}$ is the skew matrix of vector $\boldsymbol{\theta}_F^{\circ F}$. Note that the DTM $\Delta_F^{\circ F}$ can be also expressed in vector form by a DMV as $\mathbf{x}_F^{\circ F} = [(\mathbf{d}_F^{\circ F})^T, (\boldsymbol{\theta}_F^{\circ F})^T]^T$.

In this section, we will show how to derive the deviation vector $\mathbf{x}_F^{\circ F}$ for fixtures based both on locators and on locating surfaces according to locator and surface deviations. For the first case, two fixture layouts will be analyzed: a 3-2-1 locating scheme and a plane-hole locating scheme. For the second case, only the 3-2-1 locating scheme will be studied.

Specific assumptions: Locators and locating surfaces are assumed to be rigid.

Fixtures based on locators

Suppose a fixture composed of j th locators, where \mathbf{r}_i defines the contact point between the i th locator and the workpiece, and \mathbf{n}_i defines the normal vector of the workpiece surface at the i th contact point, all expressed w.r.t. the nominal FCS (see Figure 3.3). Following the research work in [5], a small variation in a fixture locator in the direction of movement constraint, i.e., \mathbf{n}_i , denoted as Δl_i , will cause a small perturbation in the FCS, denoted as $\mathbf{x}_F^{\circ F}$. This small perturbation can be expressed mathematically as:

$$\Delta l_i = \mathbf{w}_i^T \cdot \mathbf{x}_F^{\circ F}, \quad (3.6)$$

where

$$\mathbf{w}_i^T = [\mathbf{n}_i^T, (\mathbf{r}_i \times \mathbf{n}_i)^T]. \quad (3.7)$$

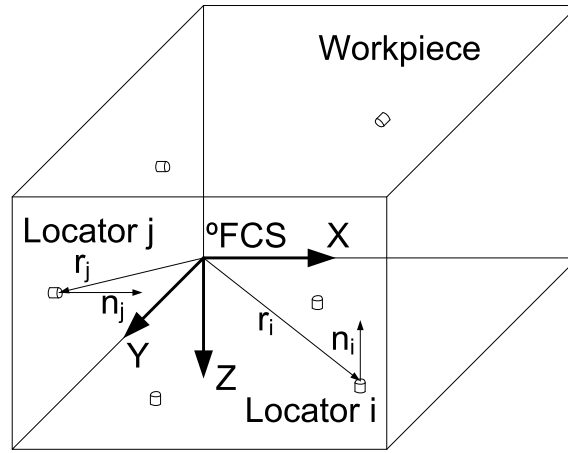


Figure 3.3: Fixture based on locators. Each i th locator is defined by its position r_i and the normal vector n_i of the locating surface where it contacts.

and \times is the cross product operator. Δl_i is defined by the equation:

$$\Delta l_i = \mathbf{n}_i^T \cdot \Delta \mathbf{r}_i, \quad (3.8)$$

where $\Delta \mathbf{r}_i$ is the position variation of locator i .

Considering the fixture to be made up of j locators, Eq. (7.15) becomes

$$\Delta \mathbf{l} = \mathbf{G}^T \cdot \mathbf{x}_F^{\circ F}, \quad (3.9)$$

where $\Delta \mathbf{l} = [\Delta l_1, \Delta l_2, \dots, \Delta l_j]^T$ and $\mathbf{G} = [\mathbf{w}_1, \mathbf{w}_2, \dots, \mathbf{w}_j]^T$, and j is the number of locators that compose the fixture. Matrix \mathbf{G} is called the *locator matrix* in [5].

On analyzing the locator matrix \mathbf{G} , one can discern three different possibilities during fixturing:

1. The row rank of \mathbf{G} is lower than six. For this case, not all the six degrees of freedom (d.o.f.) of the workpiece are constrained by fixture locators and thus $\mathbf{x}_F^{\circ F}$ is partially undetermined. In other words, the workpiece is not located deterministically.
2. The row rank of \mathbf{G} is equal to six and \mathbf{G} is a full rank matrix. For this case, the six d.o.f. of the workpiece are constrained by the six locators that compose the fixture and thus there is a unique solution to $\mathbf{x}_F^{\circ F}$. In other words, a deterministic localization of the workpiece is ensured.
3. The row rank of \mathbf{G} is greater than six. For this case, the six d.o.f. of the workpiece are constrained but how they are constrained depends on which locators are touching the workpiece. This case occurs when more than six locators composed the fixture and thus the solution to $\mathbf{x}_F^{\circ F}$ will depend on which combination of the six locators is actually touching the workpiece. In other words, the workpiece is over-constrained and the workpiece is not located deterministically.

Therefore, in order to ensure a deterministic localization, the fixture should be composed of six locators and $\{\mathbf{w}_1, \dots, \mathbf{w}_6\}$ should be linearly independent [5]. With this configuration, the locator matrix \mathbf{G} is full rank and invertible, and the deviation of FCS from nominal values due to the deviation of fixture locators can be expressed mathematically as:

$$\mathbf{x}_F^{\circ F} = (\mathbf{G}^T)^{-1} \cdot \Delta \mathbf{l}. \quad (3.10)$$

Eq. (3.10) can be rewritten in the form:

$$\mathbf{x}_F^{\circ F} = \mathbf{B}_{f_1} \cdot [\Delta l_1, \Delta l_2, \dots, \Delta l_6]^T, \quad (3.11)$$

where \mathbf{B}_{f_1} is defined as $(\mathbf{G}^T)^{-1}$ and its result depends on the layout of the fixture.

For a generic 3-2-1 locating scheme as shown in Figure 3.4 (a), matrix \mathbf{B}_{f_1} can be derived in a straight forward manner following the methodology explained above, resulting in the matrix:

$$\mathbf{B}_{f_1} = \begin{pmatrix} \frac{(l_{2y}-l_{3y}) \cdot l_{5z}}{C} & \frac{-(l_{1y}-l_{3y}) \cdot l_{5z}}{C} & \frac{(-l_{2y}+l_{1y}) \cdot l_{5z}}{C} & \frac{-l_{5y}}{(-l_{5y}+l_{4y})} & \frac{l_{4y}}{(-l_{5y}+l_{4y})} & 0 \\ \frac{-(l_{2x}-l_{3x}) \cdot l_{6z}}{C} & \frac{(l_{1x}-l_{3x}) \cdot l_{6z}}{C} & \frac{-(-l_{2x}+l_{1x}) \cdot l_{6z}}{C} & \frac{l_{6x}}{(-l_{5y}+l_{4y})} & \frac{-l_{6x}}{(-l_{5y}+l_{4y})} & 1 \\ \frac{(l_{3y}l_{2x}-l_{2y}l_{3x})}{C} & \frac{-(-l_{3x}l_{1y}+l_{3y}l_{1x})}{C} & \frac{(-l_{1y}l_{2x}+l_{2y}l_{1x})}{C} & 0 & 0 & 0 \\ \frac{-(l_{2x}-l_{3x})}{C} & \frac{(l_{1x}-l_{3x})}{C} & \frac{-(-l_{2x}+l_{1x})}{C} & 0 & 0 & 0 \\ \frac{-(l_{2y}-l_{3y})}{C} & \frac{(l_{1y}-l_{3y})}{C} & \frac{-(-l_{2y}+l_{1y})}{C} & 0 & 0 & 0 \\ 0 & 0 & 0 & \frac{-1}{(-l_{5y}+l_{4y})} & \frac{1}{(-l_{5y}+l_{4y})} & 0 \end{pmatrix}, \quad (3.12)$$

where $C = l_{3x}l_{1y} - l_{1y}l_{2x} + l_{3y}l_{2x} + l_{2y}l_{1x} - l_{2y}l_{3x} - l_{3y}l_{1x}$. Note that the position of the locator i th is described by the vector $\mathbf{r}_i = [l_{ix}, l_{iy}, l_{iz}]$ expressed in the ${}^{\circ}\text{FCS}$.

Similarly, for the generic plane-hole locating scheme based on locators shown in Figure 3.4 (b), the same methodology can be applied. For this case, the matrix \mathbf{B}_{f_1} is defined as:

$$\mathbf{B}_{f_1} = \begin{pmatrix} 0 & 0 & 0 & 1 & 0 & 0 \\ 0 & 0 & 0 & 0 & 1 & 0 \\ \frac{(l_{3y}l_{2x}-l_{2y}l_{3x})}{C} & \frac{-(-l_{3x}l_{1y}-l_{3y}l_{1x})}{C} & \frac{(-l_{1y}l_{2x}+l_{2y}l_{1x})}{C} & 0 & 0 & 0 \\ \frac{-(l_{2x}-l_{3x})}{C} & \frac{(l_{1x}-l_{3x})}{C} & \frac{-(-l_{2x}+l_{1x})}{C} & 0 & 0 & 0 \\ \frac{-(l_{2y}-l_{3y})}{C} & \frac{(l_{1y}-l_{3y})}{C} & \frac{-(-l_{1y}+l_{2y})}{C} & 0 & 0 & 0 \\ 0 & 0 & 0 & \frac{1}{l_{6y}} & 0 & \frac{-1}{l_{6y}} \end{pmatrix}. \quad (3.13)$$

Similar results can be found in [6], where these two types of fixtures are analyzed.

Fixtures based on locating surfaces

If the fixture device is based on locating surfaces instead of punctual locators, the deviation of the FCS from nominal values depends on the deviation of the locating surfaces according to the d.o.f. they constrain. Villeneuve and Vignat [7] proposed a generic procedure for evaluating the deviation of the workpiece location when it is placed in a fixture

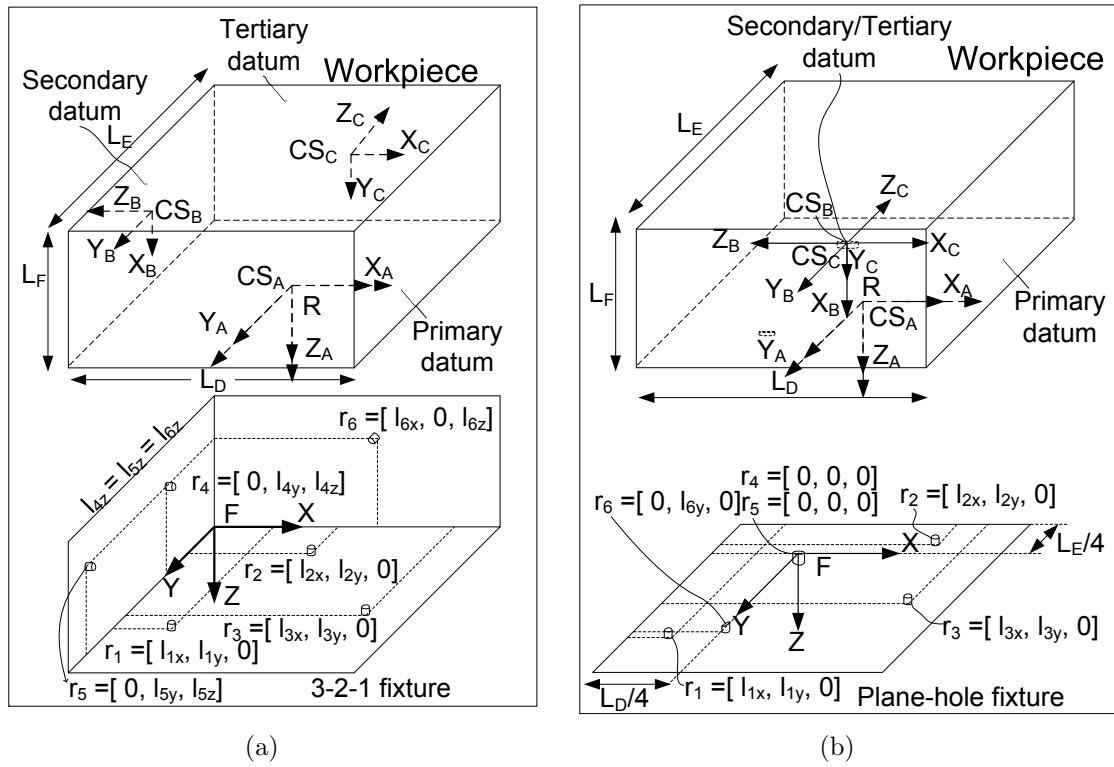


Figure 3.4: A generic fixture layout based on locators with a) a 3-2-1 locating scheme, and b) a plane-hole locating scheme.

based on locating surfaces. In this sub-section their work is adapted in order to make its formulation consistent with the rest of the models presented.

Let us consider the 3-2-1 locating scheme and the workpiece shown in Figure 3.5, where locating surfaces 1, 2 and 3 constrain three d.o.f., two d.o.f. and one d.o.f. respectively, being in contact with the workpiece datum *A* (primary datum), *B* (secondary datum) and *C* (tertiary datum) respectively. Under nominal conditions, CS 1, 2 and 3 coincide with CS *A*, *B* and *C*, respectively. Now consider the following sequence of workpiece placement: firstly, the *A* workpiece datum surface is placed on the fixture surface 1; secondly, the workpiece is moved over the primary datum until the workpiece is stopped by the contact between the *B* datum and the fixture surface 2; finally, the workpiece is moved over the primary datum while maintaining the contact between surfaces *B* and 2 until the workpiece is blocked due to the contact between the *C* datum and the fixture surface 3. Following this sequence and considering the previous general assumptions, the following restrictions always apply for 3-2-1 fixtures based on locating surfaces:

- In the primary datum, there is full contact between fixture surface 1 and datum surface *A*. The locating surface constrains three d.o.f. and thus position or orientation deviations of this fixture surface may deviate the final workpiece location. Assuming no form errors and a planar contact between fixture surface 1 and datum surface *A*, any point on datum surface *A*, denoted as A_k , will lie on fixture surface

1. Considering the CS of the surfaces with Z -axis pointing normal to the surface, the expression $[\tilde{\mathbf{p}}_{A_k}^1]_{(3)} = 0$ holds, where $[\cdot]_{(3)}$ refers to the third component of the vector. Note that $[\tilde{\mathbf{p}}_{A_k}^1]_{(3)} = 0$ means that the z coordinate of point A_k expressed in the CS of the fixture surface 1 is equal to 0, that is point A_k of the workpiece surface A is also on surface 1. Furthermore, as the primary datum is the first locating step, the position and orientation of the CS of fixture surface 1 and datum surface A will be coincident for the three constrained d.o.f.
- In the secondary datum, there are at least two contact points between fixture surface 2 and workpiece surface B . Thus, the constraints $[\tilde{\mathbf{p}}_{B_i}^2]_{(3)} = 0$ and $[\tilde{\mathbf{p}}_{B_j}^2]_{(3)} = 0$ can be defined, where B_i and B_j are two contact points that belong to the workpiece surface B . Furthermore, as it is assumed there is no penetration (i.e., no deformations) between surfaces, for any other points on surface B that are potential contact points, denoted as B_k for $k \neq i, j$, the expression $[\tilde{\mathbf{p}}_{B_k}^2]_{(3)} \leq 0$ holds.
 - In the tertiary datum, there is at least one contact point between fixture surface 3 and workpiece surface C . Similar to the above explanation, for this contact point defined as point C_l that belongs to the workpiece surface C , the expressions $[\tilde{\mathbf{p}}_{C_l}^3]_{(3)} = 0$ and $[\tilde{\mathbf{p}}_{C_k}^3]_{(3)} \leq 0$ hold, where C_k is any potential contact point between surface C and 3 except C_l .

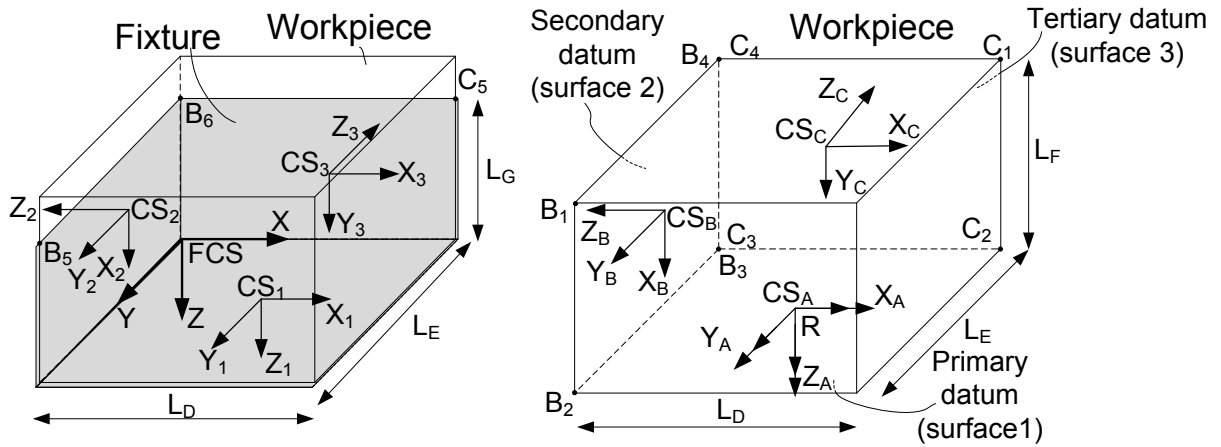


Figure 3.5: A generic 3-2-1 locating scheme based on locating surfaces. CSs are centered at each face.

These constraints make the location problem deterministic, so any deviation of locating surfaces will generate a deterministic deviation of the FCS. To evaluate the FCS deviation $\mathbf{x}_F^{\circ F}$ mathematically, the workpiece placement sequence explained above (shown in detail in Figure 3.6) should be analyzed step by step.

For the first step, the workpiece surface A is placed on the fixture surface 1. In this step, the deviation of the locating surface 1 along the three constrained d.o.f. will generate a deviation of the workpiece surface A in its three corresponding constrained d.o.f. As we

are considering small displacements, CS A is deviated in a similar way to the deviation of CS 1 and thus CS A is moved to A' . As shown in Figure 3.7, this small movement can be evaluated by the expression:

$$\delta \mathbf{H}_{A'}^{\circ A} = \mathbf{H}_{o_1}^{\circ A} \cdot \delta \mathbf{H}_1^{\circ 1} \cdot \mathbf{H}_{A'}^1. \quad (3.14)$$

Note that as there is a planar contact, $\mathbf{H}_{A'}^1 = \mathbf{H}_{o_A}^{\circ 1}$, and thus Eq. (3.14) becomes:

$$\delta \mathbf{H}_{A'}^{\circ A} = \mathbf{H}_{o_1}^{\circ A} \cdot \delta \mathbf{H}_1^{\circ 1} \cdot \mathbf{H}_{o_A}^{\circ 1}, \quad (3.15)$$

where $\mathbf{H}_{o_1}^{\circ A}$ and $\mathbf{H}_{o_A}^{\circ 1}$ are defined according to nominal part dimensions and nominal fixture layout. Note that this small movement is only carried out on the three constrained d.o.f. (for the example shown in Figure 3.5, the constrained d.o.f. are the position deviation in the Z -axis and the orientation deviation about the X - and Y -axis) and for the others there is a null movement.

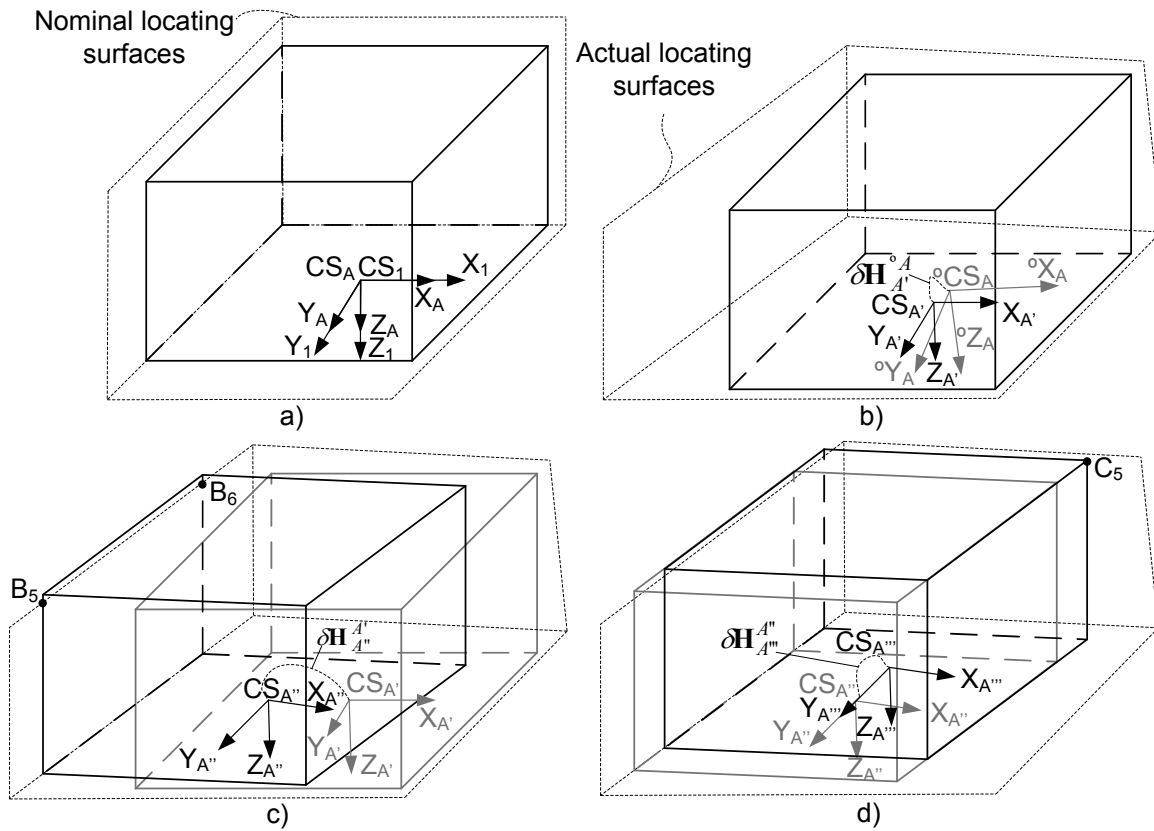


Figure 3.6: a) Nominal workpiece-fixture assembly. Sequence of small movements for locating the workpiece on the actual fixture over the: b) primary datum, c) secondary datum, and d) tertiary datum.

As the second step, the workpiece is moved to make contact between surface 2 and

surface B . In that moment, there are two contact points i and j that ensure:

$$[\tilde{\mathbf{p}}_{B_i}^2]_{(3)} = [\mathbf{H}_B^2 \cdot \tilde{\mathbf{p}}_{B_i}^B]_{(3)} = 0, \quad (3.16)$$

$$[\tilde{\mathbf{p}}_{B_j}^2]_{(3)} = [\mathbf{H}_B^2 \cdot \tilde{\mathbf{p}}_{B_j}^B]_{(3)} = 0, \quad (3.17)$$

$$[\tilde{\mathbf{p}}_{B_k}^2]_{(3)} = [\mathbf{H}_B^2 \cdot \tilde{\mathbf{p}}_{B_k}^B]_{(3)} \leq 0, \quad (3.18)$$

where B_i and B_j are points from surface B , and B_k is any other point on surface B that is not a contact point ($k \neq i, j$). As the workpiece is moved to make contact, the HTM \mathbf{H}_B^2 is defined as:

$$\begin{aligned} \mathbf{H}_B^2 &= \mathbf{H}_1^2 \cdot \mathbf{H}_A^1 \cdot \mathbf{H}_B^A \\ &= (\delta\mathbf{H}_{o_2}^2 \cdot \mathbf{H}_{o_1}^{o_2} \cdot \delta\mathbf{H}_1^{o_1}) \cdot \mathbf{H}_A^1 \cdot (\delta\mathbf{H}_{o_A}^A \cdot \mathbf{H}_{o_B}^{o_A} \cdot \delta\mathbf{H}_B^{o_B}). \end{aligned} \quad (3.19)$$

As we are only considering fixture errors (datum errors are neglected for this analysis), matrices $\delta\mathbf{H}_{o_A}^A$ and $\delta\mathbf{H}_B^{o_B}$ are considered to be 4×4 identity matrices. Furthermore, at the primary datum there is a planar contact between workpiece and fixture surfaces so $\mathbf{H}_A^1 = \mathbf{H}_{o_A}^{o_1}$ (see Figure 3.7). Considering that over the primary datum the workpiece is moved to make contact with the secondary datum (and thus there is an additional HTM $\delta\mathbf{H}_{A''}^{A'}$ that defines the small translational and rotational movement of the workpiece conducted over the primary datum to make the workpiece contact at points B_i and B_j), Eq. (3.19) can be rewritten as:

$$\mathbf{H}_B^2 = (\delta\mathbf{H}_{o_2}^2 \cdot \mathbf{H}_{o_1}^{o_2} \cdot \delta\mathbf{H}_1^{o_1}) \cdot (\mathbf{H}_{o_A}^{o_1} \cdot \delta\mathbf{H}_{A''}^{A'}) \cdot \mathbf{H}_{o_B}^{o_A}. \quad (3.20)$$

Note that for a common 3-2-1 fixture as shown in Figure 3.5, the HTM $\delta\mathbf{H}_{A''}^{A'}$ defines a small translation on the X -axis and a small rotation about the Z -axis according to CS A' (see Figure 3.6 (c)). Thus, matrix $\delta\mathbf{H}_{A''}^{A'}$ only presents the unknown parameters of the small translational deviation in the X direction and the small orientational deviation about the Z -axis; the other HTM parameters are zero. Solving Eqs. (3.16), (3.17) and (3.20) constrained by Eq. (3.18), matrix $\delta\mathbf{H}_{A''}^{A'}$ is evaluated.

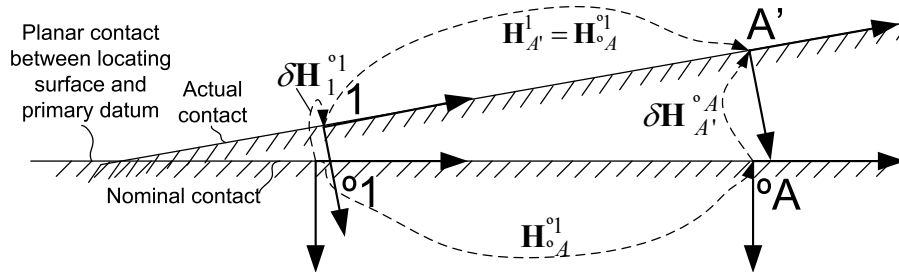


Figure 3.7: Relationships between CSs for the planar contact between locating surface and primary datum.

Similar procedure is conducted in the third step, when the workpiece is moved to make

contact between surfaces 3 and C . For this case, the contact point, denoted as C_l , ensures:

$$[\tilde{\mathbf{p}}_{C_l}^3]_{(3)} = [\mathbf{H}_C^3 \cdot \tilde{\mathbf{p}}_{C_l}^C]_{(3)} = 0, \quad (3.21)$$

$$[\tilde{\mathbf{p}}_{C_k}^3]_{(3)} = [\mathbf{H}_C^3 \cdot \tilde{\mathbf{p}}_{C_k}^C]_{(3)} \leq 0, \quad (3.22)$$

where C_k is any other point on surface C that is not a contact point ($k \neq l$). As the workpiece is moved over the primary and secondary datum to make contact, the HTM \mathbf{H}_C^3 is defined as:

$$\begin{aligned} \mathbf{H}_C^3 &= \mathbf{H}_1^3 \cdot \mathbf{H}_A^1 \cdot \mathbf{H}_C^A, \\ &= (\delta\mathbf{H}_{\circ 3}^3 \cdot \mathbf{H}_{\circ 1}^3 \cdot \delta\mathbf{H}_1^{\circ 1}) \cdot \mathbf{H}_A^1 \cdot (\delta\mathbf{H}_{\circ A}^A \cdot \mathbf{H}_{\circ C}^A \cdot \delta\mathbf{H}_C^{\circ C}). \end{aligned} \quad (3.23)$$

In this case, \mathbf{H}_A^1 is equal to $\mathbf{H}_{\circ A}^{\circ 1} \cdot \delta\mathbf{H}_{A''}^{A'} \cdot \delta\mathbf{H}_{A'''}^{A''}$, where $\delta\mathbf{H}_{A'''}^{A''}$ is the HTM that defines the small translational movement of the workpiece performed over the primary and secondary datum to make the workpiece contact at point C_l . For a common 3-2-1 fixture, like the one shown in Figure 3.5, this movement will be a small translation on the Y -axis according to CS A'' (see Figure 3.6 (d)) and thus $\delta\mathbf{H}_{A'''}^{A''}$ only presents one unknown parameter which is the small translation deviation in the Y direction; the other HTM parameters are zero. Considering only fixture errors, Eq. (3.23) can be rewritten as:

$$\mathbf{H}_C^3 = (\delta\mathbf{H}_{\circ 3}^3 \cdot \mathbf{H}_{\circ 1}^3 \cdot \delta\mathbf{H}_1^{\circ 1}) \cdot (\mathbf{H}_{\circ A}^{\circ 1} \cdot \delta\mathbf{H}_{A''}^{A'} \cdot \delta\mathbf{H}_{A'''}^{A''}) \cdot \mathbf{H}_{\circ C}^A. \quad (3.24)$$

Solving Eqs. (3.21) and (3.24) constrained by Eq. (3.22), matrix $\delta\mathbf{H}_{A'''}^{A''}$ is evaluated.

Finally, the deviation of the FCS w.r.t. nominal values can be obtained by knowing the position and orientation of CS A''' w.r.t. A by the following equation:

$$\delta\mathbf{H}_F^{\circ F} = \mathbf{H}_{\circ A}^{\circ F} \cdot \delta\mathbf{H}_{A'''}^{\circ A} \cdot \mathbf{H}_F^{A'''}, \quad (3.25)$$

which can also be expressed as:

$$\delta\mathbf{H}_F^{\circ F} = \mathbf{H}_{\circ A}^{\circ F} \cdot \delta\mathbf{H}_{A'}^{\circ A} \cdot \delta\mathbf{H}_{A''}^{\circ A'} \cdot \delta\mathbf{H}_{A'''}^{\circ A''} \cdot \mathbf{H}_F^{A'''}. \quad (3.26)$$

Applying Corollary 2 from Appendix 3.3 and considering that FCS is deviated in the same way as CS A and thus $\mathbf{H}_F^{A'''} = \mathbf{H}_{\circ F}^{\circ A}$, Eq. (3.26) becomes:

$$\delta\mathbf{H}_F^{\circ F} = \mathbf{H}_{\circ A}^{\circ F} \cdot \left(\mathbf{I}_{4 \times 4} + \Delta_{A'}^{\circ A} + \Delta_{A''}^{A'} + \Delta_{A'''}^{A''} \right) \cdot \mathbf{H}_{\circ F}^{\circ A}, \quad (3.27)$$

where $\Delta_{A'}^{\circ A} = \delta\mathbf{H}_{A'}^{\circ A} - \mathbf{I}_{4 \times 4}$, and $\Delta_{A''}^{A'}$ and $\Delta_{A'''}^{A''}$ can be defined similarly. The terms $\delta\mathbf{H}_{A'}^{\circ A}$, $\delta\mathbf{H}_{A''}^{\circ A'}$ and $\delta\mathbf{H}_{A'''}^{\circ A''}$ are obtained as explained above, and they depend on the locating surface errors $\delta\mathbf{H}_1^{\circ 1}$, $\delta\mathbf{H}_2^{\circ 2}$ and $\delta\mathbf{H}_3^{\circ 3}$. Considering Eqs. (3.4) and (3.5), from Eq. (3.27) the DMV $\mathbf{x}_F^{\circ F}$ can be extracted and expressed as follows:

$$\mathbf{x}_F^{\circ F} = \Upsilon_1 \cdot \mathbf{x}_1^{\circ 1} + \Upsilon_2 \cdot \mathbf{x}_2^{\circ 2} + \Upsilon_3 \cdot \mathbf{x}_3^{\circ 3}, \quad (3.28)$$

where $\mathbf{x}_1^{\circ 1}$, $\mathbf{x}_2^{\circ 2}$ and $\mathbf{x}_3^{\circ 3}$ represent the deviation of the CS of the locating surfaces 1, 2 and 3 respectively in a vector form, and Υ_1 , Υ_2 and Υ_3 are the resulting matrices after being

rewritten.

For illustrative purposes, the methodology shown above is applied to the example shown in Figure 3.5. Assuming that the locating surface errors produce a deterministic location problem where points B_5 , B_6 and C_5 are the contact points with the fixture surfaces, the FCS deviation is formulated by Eq. (3.28) with the following matrix coefficients:

$$\mathbf{\Upsilon}_1 = \begin{pmatrix} 0 & 0 & 0 & 0 & L_G & 0 \\ 0 & 0 & 0 & -L_G & 0 & 0 \\ 0 & 0 & 1 & -L_E/2 & L_D/2 & 0 \\ 0 & 0 & 0 & 1 & 0 & 0 \\ 0 & 0 & 0 & 0 & 1 & 0 \\ 0 & 0 & 0 & 0 & 0 & 0 \end{pmatrix}, \quad (3.29)$$

$$\mathbf{\Upsilon}_2 = \begin{pmatrix} 0 & 0 & -1 & L_E/2 & -L_G/2 & 0 \\ 0 & 0 & 0 & -L_D & 0 & 0 \\ 0 & 0 & 0 & 0 & 0 & 0 \\ 0 & 0 & 0 & 0 & 0 & 0 \\ 0 & 0 & 0 & 0 & 0 & 0 \\ 0 & 0 & 0 & 1 & 0 & 0 \end{pmatrix}, \quad (3.30)$$

$$\mathbf{\Upsilon}_3 = \begin{pmatrix} 0 & 0 & 0 & 0 & 0 & 0 \\ 0 & 0 & -1 & L_G/2 & L_D/2 & 0 \\ 0 & 0 & 0 & 0 & 0 & 0 \\ 0 & 0 & 0 & 0 & 0 & 0 \\ 0 & 0 & 0 & 0 & 0 & 0 \\ 0 & 0 & 0 & 0 & 0 & 0 \end{pmatrix}. \quad (3.31)$$

Note that if the locating surface deviations produce a workpiece location with contact points other than B_5 , B_6 and C_5 , matrices $\mathbf{\Upsilon}_1$, $\mathbf{\Upsilon}_2$ and $\mathbf{\Upsilon}_3$ should be re-evaluated.

3.2.2 Setup errors: datum feature errors

Datum features used for locating the workpiece may always present some degree of geometric imperfection (such as parallelism errors, perpendicularity errors, etc.) due to manufacturing variability in previous stations. Due to this imperfection, the part reference coordinate system (RCS) of the workpiece in the fixture setup will be deviated from its nominal value, denoted as ${}^\circ\text{RCS}$, and thus a dimensional deviation of the machined part will occur.

In order to analyze how datum feature errors influence this deviation and thus the macro-geometric part quality, let us consider an ideal machining operation and a point i on the feature generated by the cutting-tool, as shown in Figure 3.8 (a). Point i is referenced from the ${}^\circ\text{FCS}$. Thus, this point is denoted as $\mathbf{p}_i^{\circ F} = [p_{ix}^{\circ F}, p_{iy}^{\circ F}, p_{iz}^{\circ F}]$. In addition, let us define the vector $\tilde{\mathbf{p}}_i^{\circ F} = [\mathbf{p}_i^{\circ F}, 1]^T$. For simplicity, let us consider the primary datum

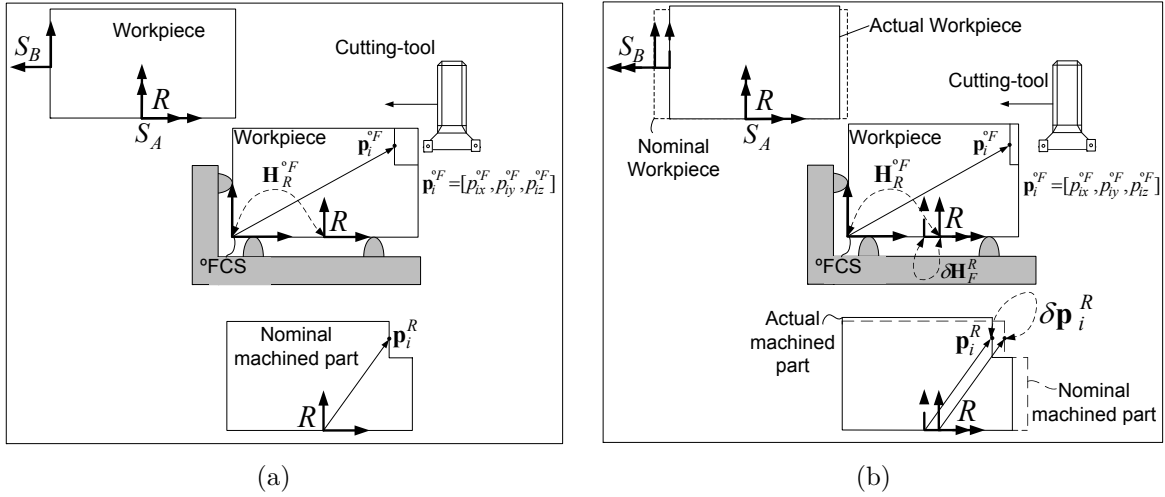


Figure 3.8: Example of datum feature errors: (a) nominal conditions, (b) conditions with datum errors.

(surface S_A) as the RCS from which the machined feature is defined. Then, the point i w.r.t. R is defined as:

$$\tilde{\mathbf{p}}_i^R = \mathbf{H}_{\circ F}^R \cdot \tilde{\mathbf{p}}_i^{\circ F}. \quad (3.32)$$

However, due to datum errors (neglecting any other errors) the position and orientation of S_A will be deviated w.r.t. $\circ\text{FCS}$ by the HTM $\delta\mathbf{H}_F^R$ and thus a point on the machined surface will be deviated, as shown in Figure 3.8 (b). Mathematically, the actual position of a point i w.r.t. R , knowing the position of point i w.r.t. the $\circ\text{FCS}$, is formulated as:

$$\tilde{\mathbf{p}}_i^R = \mathbf{H}_{\circ F}^R \cdot \delta\mathbf{H}_F^R \cdot \tilde{\mathbf{p}}_i^{\circ F}. \quad (3.33)$$

If there are no datum errors, $\delta\mathbf{H}_F^R$ is a 4×4 identity matrix. Thus, the deviation of the point i on the machined surface from nominal values due to datum errors is obtained as:

$$\delta\tilde{\mathbf{p}}_i^R = \mathbf{H}_{\circ F}^R \cdot \delta\mathbf{H}_F^R \cdot \tilde{\mathbf{p}}_i^{\circ F} - \mathbf{H}_{\circ F}^R \cdot \mathbf{I}_{4 \times 4} \cdot \tilde{\mathbf{p}}_i^{\circ F} \quad (3.34)$$

Applying Eq. (3.34), the deviation of each point of the machined surface is formulated as a function of the deviation of FCS w.r.t. the primary datum expressed by the term $\delta\mathbf{H}_F^R$. As shown in Appendix 3.2, matrix $\delta\mathbf{H}_F^R$ is defined as:

$$\delta\mathbf{H}_F^R = \mathbf{I}_{4 \times 4} + \Delta_F^R, \quad (3.35)$$

and the DTM Δ_F^R can also be expressed in vector form by a DMV as $\mathbf{x}_F^R = \left[(\mathbf{d}_F^R)^T, (\boldsymbol{\theta}_F^R)^T \right]^T$.

In this section, we will show how to derive the deviation vector \mathbf{x}_F^R for fixtures based on locators and based on locating surfaces according to their locator and surface deviations. For the first case, two fixture layouts will be analyzed: a 3-2-1 locating scheme and

a plane-hole locating scheme. For the second case, only the 3-2-1 locating scheme will be studied.

Specific assumptions: Locators and locating surfaces are assumed to be rigid. In order to facilitate the derivation of 3D manufacturing variation models in later chapters, the RCS will be defined as the primary datum CS, denoted as CS A . Thus, $\mathbf{x}_F^R \equiv \mathbf{x}_F^A$.

Fixtures based on locators

In a 3-2-1 locating scheme based on locators (see Figure 3.4 (a)), the deterministic location of the part is ensured when the workpiece touches the six locators. Considering only datum errors and assuming prismatic surfaces, the influence of the deviation of surfaces B and C on workpiece location can be obtained (note that the primary datum is placed touching three locators, and deviations of surfaces B and C are referred to as deviations from their respective nominal values w.r.t. the primary datum). At these surfaces, the following constraints apply:

- Locators 4 and 5 defined by vectors \mathbf{r}_4 and \mathbf{r}_5 touch workpiece surface B , and thus the third component of \mathbf{r}_4 and \mathbf{r}_5 w.r.t. CS B are zero. Mathematically, this is expressed as $\left[\tilde{\mathbf{p}}_{r_4}^B\right]_{(3)} = 0$ and $\left[\tilde{\mathbf{p}}_{r_5}^B\right]_{(3)} = 0$, where $\tilde{\mathbf{p}}_{r_i}^B = [l_{ix}^B, l_{iy}^B, l_{iz}^B, 1]^T$ and $[\cdot]_{(3)}$ denotes the third component of the vector.
- Similarly, locator \mathbf{r}_6 touches workpiece surface C , so $\left[\tilde{\mathbf{p}}_{r_6}^C\right]_{(3)} = 0$.

As described in [6], the influence of datum feature errors can be derived as follows. The contact points can be expressed mathematically as:

$$\tilde{\mathbf{p}}_{r_4}^B = \mathbf{H}_A^B \cdot \mathbf{H}_F^A \cdot \tilde{\mathbf{p}}_{r_4}^F, \quad (3.36)$$

$$\tilde{\mathbf{p}}_{r_5}^B = \mathbf{H}_A^B \cdot \mathbf{H}_F^A \cdot \tilde{\mathbf{p}}_{r_5}^F, \quad (3.37)$$

$$\tilde{\mathbf{p}}_{r_6}^C = \mathbf{H}_A^C \cdot \mathbf{H}_F^A \cdot \tilde{\mathbf{p}}_{r_6}^F. \quad (3.38)$$

The HTM \mathbf{H}_A^B is defined as:

$$\begin{aligned} \mathbf{H}_A^B &= (\mathbf{H}_{\circ B}^A \cdot \delta\mathbf{H}_B^A)^{-1} \\ &= (\delta\mathbf{H}_B^A)^{-1} \cdot (\mathbf{H}_{\circ A}^B), \end{aligned} \quad (3.39)$$

where $\delta\mathbf{H}_B^A$ is the HTM that defines the small translational and orientational deviations of CS B w.r.t. A due to the deviation from nominal values of B and A . From Corollary 1 in Appendix 3.3, as $(\delta\mathbf{H}_B^A)^{-1} = \mathbf{I}_{4 \times 4} - \Delta_B^A$, Eq. (3.39) becomes:

$$\mathbf{H}_A^B = (\mathbf{I}_{4 \times 4} - \Delta_B^A) \cdot (\mathbf{H}_{\circ A}^B), \quad (3.40)$$

On the other hand, the HTM \mathbf{H}_F^A is defined as:

$$\begin{aligned} \mathbf{H}_F^A &= \mathbf{H}_{\circ F}^A \cdot \delta\mathbf{H}_F^A, \\ &= \mathbf{H}_{\circ F}^A \cdot (\mathbf{I}_{4 \times 4} + \Delta_F^A) \end{aligned} \quad (3.41)$$

Substituting Eqs. (3.40) and (3.41) in Eq. (3.36):

$$\tilde{\mathbf{p}}_{r_4}^B = (\mathbf{I}_{4 \times 4} - \Delta_B^A) \cdot \mathbf{H}_{\circ A}^{\circ B} \cdot \mathbf{H}_{\circ F}^{\circ A} \cdot (\mathbf{I}_{4 \times 4} + \Delta_F^A) \cdot \tilde{\mathbf{p}}_{r_4}^F. \quad (3.42)$$

Neglecting the second-order small values and considering the contact between surfaces ($[\tilde{\mathbf{p}}_{r_4}^B]_{(3)} = 0$), the following equation applies:

$$[\tilde{\mathbf{p}}_{r_4}^B]_{(3)} = [(-\Delta_B^A \cdot \mathbf{H}_{\circ F}^{\circ B} + \mathbf{H}_{\circ F}^{\circ B} \cdot \Delta_F^A + \mathbf{H}_{\circ F}^{\circ B}) \cdot \tilde{\mathbf{p}}_{r_4}^F]_{(3)} = 0. \quad (3.43)$$

As the X coordinate of the location of locator 4 w.r.t. CS F is zero, through the HTM $\mathbf{H}_{\circ F}^{\circ B}$ the term $[\mathbf{H}_{\circ F}^{\circ B} \cdot \tilde{\mathbf{p}}_{r_4}^F]_{(3)}$ becomes zero, and thus Eq. (3.43) is rewritten as:

$$[-\Delta_B^A \cdot \mathbf{H}_{\circ F}^{\circ B} + \mathbf{H}_{\circ F}^{\circ B} \cdot \Delta_F^A] \cdot \tilde{\mathbf{p}}_{r_4}^F]_{(3)} = 0, \quad (3.44)$$

and thus:

$$[(\mathbf{H}_{\circ F}^{\circ B} \cdot \Delta_F^A) \cdot \tilde{\mathbf{p}}_{r_4}^F]_{(3)} = [\Delta_B^A \cdot \mathbf{H}_{\circ F}^{\circ B} \cdot \tilde{\mathbf{p}}_{r_4}^F]_{(3)}. \quad (3.45)$$

By following the same procedure, Eqs. (3.46) and (3.47) can be derived for locators 5 and 6, respectively.

$$[(\mathbf{H}_{\circ F}^{\circ B} \cdot \Delta_F^A) \cdot \tilde{\mathbf{p}}_{r_5}^F]_{(3)} = [\Delta_B^A \cdot \mathbf{H}_{\circ F}^{\circ B} \cdot \tilde{\mathbf{p}}_{r_5}^F]_{(3)}, \quad (3.46)$$

$$[(\mathbf{H}_{\circ F}^{\circ C} \cdot \Delta_F^A) \cdot \tilde{\mathbf{p}}_{r_6}^F]_{(3)} = [\Delta_C^A \cdot \mathbf{H}_{\circ F}^{\circ C} \cdot \tilde{\mathbf{p}}_{r_6}^F]_{(3)}. \quad (3.47)$$

Note that from Eqs. (3.45-3.47), we can evaluate the DTM Δ_F^A that shows the effect of datum fixture errors on workpiece location. Furthermore, note that from the six parameters of Δ_F^A (three translational and three orientation deviations), only three are unknown since datum deviations of surface B and C only influence the X and Y positioning of the workpiece and the rotation about the Z -axis, all expressed from CS A . Other parameters, such as rotation about the X - and Y -axis and positioning along Z -axis, are defined by the deviation of the CS A itself (primary datum). Thus, the three unknown parameters that depend on datum fixture errors of surfaces B and C can be obtained by solving Eqs. (3.45-3.47). After solving, the deviation of the FCS w.r.t. CS A can be rewritten considering the deviation of each datum feature in a vector form as:

$$\mathbf{x}_F^A = \Phi_1 \cdot \mathbf{x}_B^A + \Phi_2 \cdot \mathbf{x}_C^A. \quad (3.48)$$

For the 3-2-1 locating scheme based on the locators shown in Figure 3.4 (a), Eqs. (3.45-3.47) were solved and the following matrices Φ_1 and Φ_2 were obtained:

$$\Phi_1 = \begin{pmatrix} 0 & 0 & -1 & L_E/2 & l_{5z} + L_F/2 + \frac{l_{5y} \cdot (l_{5z} - l_{4z})}{(l_{4y} - l_{5y})} & 0 \\ 0 & 0 & 0 & -l_{6x} & \frac{l_{6x} \cdot (l_{4z} - l_{5z})}{l_{4y} - l_{5y}} & 0 \\ 0 & 0 & 0 & 0 & 0 & 0 \\ 0 & 0 & 0 & 0 & 0 & 0 \\ 0 & 0 & 0 & 0 & 0 & 0 \\ 0 & 0 & 0 & 1 & \frac{-(l_{4z} - l_{5z})}{l_{4y} - l_{5y}} & 0 \end{pmatrix}, \quad (3.49)$$

$$\Phi_2 = \begin{pmatrix} 0 & 0 & 0 & 0 & 0 & 0 \\ 0 & 0 & -1 & -l_{6z} - L_F/2 & l_{6x} - L_D/2 & 0 \\ 0 & 0 & 0 & 0 & 0 & 0 \\ 0 & 0 & 0 & 0 & 0 & 0 \\ 0 & 0 & 0 & 0 & 0 & 0 \\ 0 & 0 & 0 & 0 & 0 & 0 \end{pmatrix}. \quad (3.50)$$

Similarly, for the plane-hole locating scheme based on locators shown in Figure 3.4 (b), the resulting matrices Φ_1 and Φ_2 are:

$$\Phi_1 = \begin{pmatrix} 0 & 0 & -1 & 0 & 0 & 0 \\ 0 & 0 & 0 & 0 & 0 & 0 \\ 0 & 0 & 0 & 0 & 0 & 0 \\ 0 & 0 & 0 & 0 & 0 & 0 \\ 0 & 0 & 0 & 0 & 0 & 0 \\ 0 & 0 & 0 & 1 & 0 & 0 \end{pmatrix}, \quad (3.51)$$

$$\Phi_2 = \begin{pmatrix} 0 & 0 & 0 & 0 & 0 & 0 \\ 0 & 0 & -1 & 0 & 0 & 0 \\ 0 & 0 & 0 & 0 & 0 & 0 \\ 0 & 0 & 0 & 0 & 0 & 0 \\ 0 & 0 & 0 & 0 & 0 & 0 \\ 0 & 0 & 0 & 0 & 0 & 0 \end{pmatrix}. \quad (3.52)$$

Similar results for both 3-2-1 fixture layouts can be found in [6].

Fixtures based on locating surfaces

Datum feature errors in fixtures based on locating surfaces can be obtained by following the same procedure as shown when fixture errors occur in locating surfaces (subsection 3.2.1), but now datum feature errors are significant whereas fixture errors are negligible. For this case, we are interested in obtaining the deviation of FCS w.r.t. RCS as a function of the small position and orientation deviations of secondary and tertiary datum surfaces.

Without loss of generality, let us consider the fixture layout based on locating surfaces shown in Figure 3.5, where primary, secondary and tertiary datums are A , B , and C , respectively. According to the workpiece placement sequence explained above, the first step refers to the placement of datum A over 1. As only datum errors are assumed, and the contact between surfaces is assumed perfectly plane, $\mathbf{H}_1^A = \mathbf{H}_{o_1}^{\circ A}$, and $\delta\mathbf{H}_{A'}^A$ is $\mathbf{I}_{4 \times 4}$. For the second step, the workpiece is moved to make contact between surface 2 and surface B . This small translational and rotational movement of the workpiece is defined by the HTM $\delta\mathbf{H}_{A''}^A$. In that moment, there are two contact points i and j that ensure Eqs. (3.16-3.18). Thus, the HTM \mathbf{H}_B^2 can be defined as:

$$\begin{aligned} \mathbf{H}_B^2 &= \mathbf{H}_1^2 \cdot \mathbf{H}_A^1 \cdot \mathbf{H}_B^A \\ \mathbf{H}_B^2 &= \mathbf{H}_{o_1}^{\circ 2} \cdot (\mathbf{H}_{o_A}^{\circ 1} \cdot \delta\mathbf{H}_{A''}^A) \cdot (\mathbf{H}_{o_B}^{\circ A} \cdot \delta\mathbf{H}_B^A), \end{aligned} \quad (3.53)$$

since no fixture errors are present. Following the same procedure as that shown in sub-section 3.2.1, matrix $\delta\mathbf{H}_{A''}^{A'}$ can be evaluated.

Similarly, for the third step the workpiece is moved to make contact between surfaces 3 and C , and then, Eqs. (3.21) and (3.22) hold. As the workpiece is moved over the primary and secondary datum to make contact, the HTM \mathbf{H}_C^3 is defined as:

$$\begin{aligned}\mathbf{H}_C^3 &= \mathbf{H}_1^3 \cdot \mathbf{H}_A^1 \cdot \mathbf{H}_C^A \\ \mathbf{H}_C^3 &= \mathbf{H}_{\circ 1}^{\circ 3} \cdot (\mathbf{H}_{\circ A}^{\circ 1} \cdot \delta\mathbf{H}_{A''}^{A'} \cdot \delta\mathbf{H}_{A''}^{A''}) \cdot (\mathbf{H}_{\circ C}^{\circ A} \cdot \delta\mathbf{H}_C^A),\end{aligned}\quad (3.54)$$

where $\delta\mathbf{H}_{A''}^{A''}$ is the HTM that defines the small translational movement of the workpiece performed over the primary and secondary datum to make the workpiece contact at point C_l . Following the same procedure as that shown in sub-section 3.2.1, matrix $\delta\mathbf{H}_{A''}^{A''}$ can be evaluated.

After the three steps, and applying Corollary 2 from Appendix 3.3, the deviation of A w.r.t. 1 is defined as:

$$\mathbf{H}_A^1 = \mathbf{H}_{\circ A}^{\circ 1} \cdot \left(\mathbf{I}_{4 \times 4} + \Delta_{A''}^{A'} + \Delta_{A''}^{A''} \right), \quad (3.55)$$

and thus, $\delta\mathbf{H}_A^1 = \mathbf{I}_{4 \times 4} + \Delta_{A''}^{A'} + \Delta_{A''}^{A''}$. As we are interested in the deviation of F w.r.t. A and since $\delta\mathbf{H}_1^F = \mathbf{I}_{4 \times 4}$ (no fixture errors), according to Eq. (3.56), one can observed that $\delta\mathbf{H}_A^F = \delta\mathbf{H}_A^1$.

$$\begin{aligned}\mathbf{H}_A^F &= \mathbf{H}_1^F \cdot \mathbf{H}_A^1 \\ \mathbf{H}_A^F \cdot \delta\mathbf{H}_A^F &= \mathbf{H}_{\circ 1}^{\circ F} \cdot \mathbf{H}_{\circ A}^{\circ 1} \cdot \delta\mathbf{H}_A^1.\end{aligned}\quad (3.56)$$

Finally, evaluating $\Delta_{A''}^{A'}$ and $\Delta_{A''}^{A''}$, the expression $\delta\mathbf{H}_A^F = \delta\mathbf{H}_A^1$ can be rewritten considering the datum errors in a vector form as:

$$\mathbf{x}_F^A = \Psi_1 \cdot \mathbf{x}_B^A + \Psi_2 \cdot \mathbf{x}_C^A, \quad (3.57)$$

where \mathbf{x}_B^A and \mathbf{x}_C^A represent the deviation of the CS of the locating datum surfaces B and C respectively in vector form, and Ψ_1 and Ψ_2 are the resulting matrices after solving.

By applying this methodology in the example illustrated in Figure 3.5 and assuming that the locating surface errors produce a deterministic location problem where points B_5 , B_6 and C_5 are the contact points with the fixture surfaces, the following matrix coefficients for Eq. (3.57) are obtained:

$$\Psi_1 = \begin{pmatrix} 0 & 0 & 1 & 0 & L_G - L_F/2 & 0 \\ 0 & 0 & 0 & L_D/2 & 0 & 0 \\ 0 & 0 & 0 & 0 & 0 & 0 \\ 0 & 0 & 0 & 0 & 0 & 0 \\ 0 & 0 & 0 & 0 & 0 & 0 \\ 0 & 0 & 0 & -1 & 0 & 0 \end{pmatrix}, \quad (3.58)$$

$$\Psi_2 = \begin{pmatrix} 0 & 0 & 0 & 0 & 0 & 0 \\ 0 & 0 & 1 & L_F/2 - L_G & -L_D/2 & 0 \\ 0 & 0 & 0 & 0 & 0 & 0 \\ 0 & 0 & 0 & 0 & 0 & 0 \\ 0 & 0 & 0 & 0 & 0 & 0 \\ 0 & 0 & 0 & 0 & 0 & 0 \end{pmatrix}. \quad (3.59)$$

3.2.3 Setup errors: clamping errors

Under clamping forces, both workpiece and fixture may deform, especially when fixtures based on spherical locators are applied. This deformation causes a deviation of the workpiece location from nominal values and thus a dimensional and geometric error will be generated after machining.

Specific assumptions: Without loss of generality, it is assumed that fixtures are based on spherical locators and datum surfaces are plane surfaces.

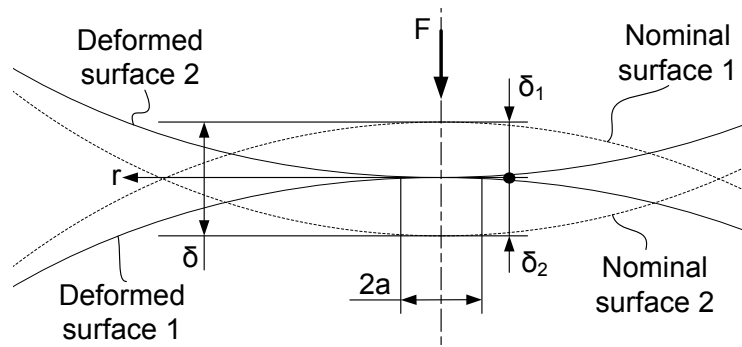


Figure 3.9: Representation of the contact deformation of two elastic bodies with curved surfaces.

According to Hertz's contact theory [8], the displacement of the points on the surface in a contact between two elastic bodies with curved surfaces (see Figure 3.9) is equal to:

$$\delta = \left(\frac{9}{16 \cdot R_* \cdot E_*^2} \right)^{1/3} \cdot F^{2/3}, \quad (3.60)$$

where δ is the contact deformation; F is the total compression load; R_* is the equivalent radius of the two contact bodies; and E_* is the equivalent Young's modulus of the two contact bodies. These parameters are defined by the expressions [8]:

$$\frac{1}{R_*} = \frac{1}{R_1} + \frac{1}{R_2}, \quad (3.61)$$

$$\frac{1}{E_*} = \frac{1 - \nu_1^2}{E_1} + \frac{1 - \nu_2^2}{E_2}, \quad (3.62)$$

$$a^2 = R_* \cdot \delta, \quad (3.63)$$

where a is the radius of the contact circle; R_1 and R_2 are the radii of the two contact bodies; E_1 and E_2 are the Young's modulus of the two contact bodies; and ν_1 and ν_2 are the Poisson's ratios of the two contact bodies. Note that the pressure is assumed to be exerted on a circle-shaped area with radius a and the pressure distribution is defined as:

$$p(r) = p_0 \cdot \left(1 - \frac{r^2}{a^2}\right)^{1/2}, \quad (3.64)$$

where p_0 is the maximum pressure that acts at the center and it is defined as $p_0 = 3 \cdot F / 2 \cdot \pi \cdot a^2$, and r is the distance from the center of the contact circle where the pressure is evaluated.

Applying Hertz's theory for a fixture based on spherical locators and assuming that workpieces are composed of planar surfaces, as shown in Figure 3.10, Eq. (3.60) applies, and R_* is equal to the radius of the spherical locator R_1 . Note that for any other type of contact between fixture locators (or locating surfaces) and workpiece surfaces, Eq. (3.60) can be modified accordingly. For example, the analysis of contact surfaces between two cylinders, between a block and a cylinder, or between an elastic planar surface and a rigid cone-shape surface can be conducted considering the modifications shown in [8, 9].

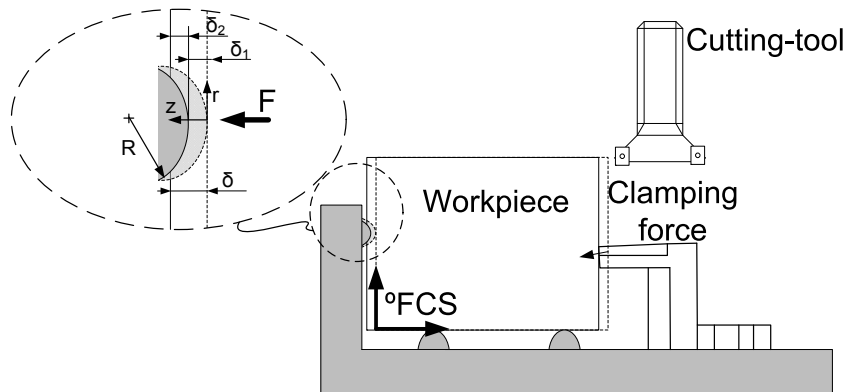


Figure 3.10: Deformation of a spherical locator due to clamping forces.

It is important to remark that Eq. (3.60) gives the total deformation of the two bodies, which is the sum of the deformation of both bodies. Due to these deformations, the FCS will be deviated from its nominal value. In order to analyze the effect of clamping errors on the final part quality, the total contact deformation can be considered as an additional fixture error, and the final part deviation can be evaluated as described in sub-section 3.2.1.

3.2.4 Machine-tool errors

The final deviation of a machined surface due to machine-tool errors depends on a large number of errors that can be identified along the chain of elements that guide and transmit the translational and rotational movement from the axis carriages to the cutting-tool edge, which is in charge of the removal of material. In this chain of elements, the following errors can be identified:

- Geometric and kinematic errors that define the translational and orientation deviation of the machine-tool spindle w.r.t. the machine-tool CS (reference CS) due to geometric inaccuracies and misalignments.
- Thermal errors that define the translational and orientation deviation of the machine-tool spindle w.r.t. the machine-tool CS due to the thermal state of the machine-tool structure.
- Cutting force-induced errors that define the deviation of the cutting-tool tip w.r.t. the machine-tool spindle due to deflections.
- Cutting-tool wear-induced errors that define the deviation of the cutting-tool edge w.r.t. the cutting-tool tip due to the wear of the cutting-tool edge.

The common physical models used in vertical machining centers (similar models can be derived for other types of machine-tools) to estimate these errors are outlined in the following sub-sections.

Specific assumptions: The geometric, kinematic and thermal-induced errors of the axis carriages of the machine-tool are assumed to be small in comparison to nominal values, and thus the small-angle approximation can be applied. The geometric and kinematic errors of the axis carriages due to cutting force-induced deformations are assumed to be negligible. Cutting-tool flank wear is assumed to be homogeneous and there is no generation of a built-up edge.

Geometric and kinematic errors

Machine-tools are typically composed of multiple linear or rotational moving elements that are designed to have only one d.o.f. in the moving or rotating direction. However, due to geometric inaccuracy and misalignment, all rigid bodies present deviations along six d.o.f. (three translational errors and three rotational errors). Using rigid body kinematics, the location of each axis of a machine-tool relative to each other or to the reference frame can be modeled using HTMs.

As a machine-tool is composed of multiple axes, the final deviation of the last axis can be derived by formulating the HTM of each axis w.r.t. the previous one. Thus, the resulting HTM that defines the position of the cutting-tool with respect to the reference CS can be obtained by successively multiplying the HTMs of neighboring links in the kinematic chain from the reference CS to the last axis CS. For example, let us consider a 3-axis vertical machine-tool where the CS of the axes are oriented identically according to the common convention of machine-tools (X-Y-Z direction according to the machine-tool table dimensions of length-width-height and Z points upwards, X points rightwards w.r.t. the front operation view of the machine-tool, and Y points according to the right-hand rule). Consider that the axis movements are conducted in the X, Y and Z order. Ideally,

the pure translation of the X -axis carriage can be formulated by the HTM:

$$\mathbf{H}_{\circ X}^{\circ M} = \begin{pmatrix} 1 & 0 & 0 & x \\ 0 & 1 & 0 & 0 \\ 0 & 0 & 1 & 0 \\ 0 & 0 & 0 & 1 \end{pmatrix}, \quad (3.65)$$

where x denotes the position of the X -axis carriage CS w.r.t. the machine-tool reference CS, denoted as $\circ M$. However, due to geometric and kinematic errors, the carriage has errors in its six d.o.f. With the assumption of rigid body kinematics and small-angle approximation, the small position and orientation errors of the carriage can be defined by the HTM [10–12]:

$$\delta \mathbf{H}_X^{\circ X} = \begin{pmatrix} 1 & -\varepsilon_{zx} & \varepsilon_{yx} & \delta_{xx} \\ \varepsilon_{zx} & 1 & -\varepsilon_{xx} & \delta_{yx} \\ -\varepsilon_{yx} & \varepsilon_{xx} & 1 & \delta_{zx} \\ 0 & 0 & 0 & 1 \end{pmatrix} \cdot \begin{pmatrix} 1 & -\varepsilon_z(x) & \varepsilon_y(x) & \delta_x(x) \\ \varepsilon_z(x) & 1 & -\varepsilon_x(x) & \delta_y(x) \\ -\varepsilon_y(x) & \varepsilon_x(x) & 1 & \delta_z(x) \\ 0 & 0 & 0 & 1 \end{pmatrix}. \quad (3.66)$$

The first HTM on the right hand side of Eq. (3.66) describes the mounting errors of the X -axis. The mounting errors are positioning and orientational errors due to assembly errors, and they are not dependent on the carriage position. For a prismatic joint, these errors can be represented by three possible angular deviations ε_{xx} (rotation around the X -axis), ε_{yx} (rotation around the Y -axis) and ε_{zx} (rotation around the Z -axis), and three offsets (δ_{xx} , δ_{yx} , δ_{zx}). The second HTM on the right hand side of Eq. (3.66) represents the motional deviations, which include the terms $\delta_p(q)$ and $\varepsilon_p(q)$. $\delta_p(q)$ refers to the positional deviation in the P -axis direction when the prismatic joint moves along the Q -axis and is a function of the position of the Q -axis, denoted as q . $\varepsilon_p(q)$ refers to the angular deviation around the P -axis when the Q -axis moves and it is also a function of the position of the Q -axis. Thus, the actual HTM for an X -axis linear motion carriage can be formulated as $\mathbf{H}_X^{\circ M} = \mathbf{H}_{\circ X}^{\circ M} \cdot \delta \mathbf{H}_X^{\circ X}$. Similarly, the following nominal and error HTM are defined for the Y -axis and Z -axis [10, 11]:

$$\mathbf{H}_{\circ Y}^X = \begin{pmatrix} 1 & 0 & 0 & 0 \\ 0 & 1 & 0 & y \\ 0 & 0 & 1 & 0 \\ 0 & 0 & 0 & 1 \end{pmatrix}, \quad \mathbf{H}_{\circ Z}^Y = \begin{pmatrix} 1 & 0 & 0 & 0 \\ 0 & 1 & 0 & 0 \\ 0 & 0 & 1 & z \\ 0 & 0 & 0 & 1 \end{pmatrix}, \quad (3.67)$$

$$\delta \mathbf{H}_Y^{\circ Y} = \begin{pmatrix} 1 & -\varepsilon_{zy} & \varepsilon_{yy} & \delta_{xy} \\ \varepsilon_{zy} & 1 & -\varepsilon_{xy} & \delta_{yy} \\ -\varepsilon_{yy} & \varepsilon_{xy} & 1 & \delta_{zy} \\ 0 & 0 & 0 & 1 \end{pmatrix} \cdot \begin{pmatrix} 1 & -\varepsilon_z(y) & \varepsilon_y(y) & \delta_x(y) \\ \varepsilon_z(y) & 1 & -\varepsilon_x(y) & \delta_y(y) \\ -\varepsilon_y(y) & \varepsilon_x(y) & 1 & \delta_z(y) \\ 0 & 0 & 0 & 1 \end{pmatrix}. \quad (3.68)$$

$$\delta \mathbf{H}_Z^{\circ Z} = \begin{pmatrix} 1 & -\varepsilon_{zz} & \varepsilon_{yz} & \delta_{xz} \\ \varepsilon_{zz} & 1 & -\varepsilon_{xz} & \delta_{yz} \\ -\varepsilon_{yz} & \varepsilon_{xz} & 1 & \delta_{zz} \\ 0 & 0 & 0 & 1 \end{pmatrix} \cdot \begin{pmatrix} 1 & -\varepsilon_z(z) & \varepsilon_y(z) & \delta_x(z) \\ \varepsilon_z(z) & 1 & -\varepsilon_x(z) & \delta_y(z) \\ -\varepsilon_y(z) & \varepsilon_x(z) & 1 & \delta_z(z) \\ 0 & 0 & 0 & 1 \end{pmatrix}. \quad (3.69)$$

The resulting deviation of the last axis (or the machine-tool spindle) w.r.t. the reference CS can be represented by the following matrix multiplication:

$$\mathbf{H}_Z^{\circ M} = \mathbf{H}_{\circ X}^{\circ M} \cdot \delta \mathbf{H}_X^{\circ X} \cdot \mathbf{H}_{\circ Y}^X \cdot \delta \mathbf{H}_Y^{\circ Y} \cdot \mathbf{H}_{\circ Z}^Y \cdot \delta \mathbf{H}_Z^{\circ Z}. \quad (3.70)$$

The actual position of the last axis can be obtained by extracting the translational vector $[d_{Z_x}^{\circ M}, d_{Z_y}^{\circ M}, d_{Z_z}^{\circ M}]^T$ from the resulting $\mathbf{H}_Z^{\circ M}$.

Similar geometric-kinematic models for part quality prediction can be derived for other machine-tools with a different number of axes and different configurations [13–15].

Thermal-induced errors

The effect of thermal variations on the machining accuracy may be determined by analyzing the geometric and kinematic errors of the machine-tool (as explained in the previous section), but also considering the current temperature distribution over the whole machine-tool [16]. As was shown in Chapter 2, two types of thermal errors are distinguished: the position independent thermal errors (PITE) and the position dependent thermal errors (PDTE). Therefore, in addition to geometric and kinematic errors, each axis is deviated from nominal values due to thermal effects.

With the assumption of rigid body kinematics and small-angle approximation, the small position and orientation error of the Q -axis carriage due to thermal components can be defined by the following HTM [17]:

$$\delta \mathbf{H}_Q^{\circ Q} = \begin{pmatrix} 1 & -\varepsilon_z^t(t, T_1, \dots, T_m, q) & \varepsilon_y^t(t, T_1, \dots, T_m, q) & \delta_x^t(t, T_1, \dots, T_m, q) \\ \varepsilon_z^t(t, T_1, \dots, T_m, q) & 1 & -\varepsilon_x^t(t, T_1, \dots, T_m, q) & \delta_y^t(t, T_1, \dots, T_m, q) \\ -\varepsilon_y^t(t, T_1, \dots, T_m, q) & \varepsilon_x^t(t, T_1, \dots, T_m, q) & 1 & \delta_z^t(t, T_1, \dots, T_m, q) \\ 0 & 0 & 0 & 1 \end{pmatrix}. \quad (3.71)$$

This HTM describes the geometric deviations due to thermal effects, whose components are defined as $\delta_p^t(t, T_1, \dots, T_m, q)$ and $\varepsilon_p^t(t, T_1, \dots, T_m, q)$ for position and angular deviations, respectively. Mathematically, these terms can be defined in a general way by the expressions [17, 18]:

$$\delta_p^t(t, T_1, \dots, T_m, q) = f_0^{pq}(T_1, \dots, T_m, t) + f_1^{pq}(T_1, \dots, T_m, t) \cdot q + f_2^{pq}(T_1, \dots, T_m, t) \cdot q^2 + \dots \quad (3.72)$$

$$\varepsilon_p^t(t, T_1, \dots, T_m, q) = g_0^{pq}(T_1, \dots, T_m, t) + g_1^{pq}(T_1, \dots, T_m, t) \cdot q + g_2^{pq}(T_1, \dots, T_m, t) \cdot q^2 + \dots \quad (3.73)$$

The terms $f_0^{pq}(T_1, \dots, T_m, t)$ and $g_0^{pq}(T_1, \dots, T_m, t)$ are the PITE components that model the position deviation on the P -axis when the Q -axis moves and it is a function of the operation time from the machine-tool startup, denoted as t , and the temperatures at different locations on the machine-tool structure, denoted as T_1, \dots, T_m . The terms $f_1^{pq}(T_1, \dots, T_m, t) \cdot q + f_2^{pq}(T_1, \dots, T_m, t) \cdot q^2 + \dots$ and $g_1^{pq}(T_1, \dots, T_m, t) \cdot q + g_2^{pq}(T_1, \dots, T_m, t) \cdot q^2 + \dots$ are the PDTE components that model the position and angular deviation on the P -axis when the Q -axis moves and it is a function of operation time, machine-tool temperatures and position at the Q -axis, denoted as q .

Cutting force-induced errors

During machining, cutting forces produce the deflection of the cutting-tool thereby generating geometric errors on the machined workpiece surfaces. In the literature, the simplest model for describing cutting-tool deflection is based on a unique cantilever beam where the cutting force is applied at the end of the beam (the depth of cut is assumed to be insignificant in comparison to the length of the overhang). López de Lacalle *et al.* [19] applied this model to estimate macro-geometric errors in high-speed milling finishing of moulds by ball-end mills. They defined the beam diameter by an equivalent tool diameter, since the helicoidal shape of the two edges reduces the resistant section. By these assumptions, the final tool deflection in radial direction, denoted as δ_r , and the rotation of the tool tip along the axis θ perpendicular to the cutting-tool axis, denoted as δ_θ , can be evaluated, respectively, as [20, Chapter 7]:

$$\delta_r = \frac{F \cdot L^3}{3 \cdot E \cdot I} = \frac{64 \cdot F \cdot L^3}{3 \cdot \pi \cdot E \cdot D^4}, \quad (3.74)$$

$$\delta_\theta = \frac{F \cdot L^2}{2 \cdot E \cdot I} = \frac{64 \cdot F \cdot L^2}{2 \cdot \pi \cdot E \cdot D^4}, \quad (3.75)$$

where E is the Young's modulus for the material tool; L^3/D^4 is the tool slenderness parameter; D is the equivalent tool diameter; L is the overhang length; and F is the cutting force perpendicular to the plane defined by the axis θ and the cutting-tool axis.

Similarly, cutting-tool deflections in the axial direction can also be estimated by the same cantilever beam but considering the force in the axial direction. For this case, the axial deflection is formulated as [21]:

$$\delta_a = \frac{F \cdot L}{E \cdot A}, \quad (3.76)$$

where A is the cross-sectional area of the tool.

A more general model for ball-end milling operations was proposed by Kim *et al.* [22]. For these types of machining operations, the cutting force component perpendicular to the cutting-tool axis is known as the major reason of the cutting-tool deflection. Although axial force is also acting on the cutter, the axial deflection of the tooling system can be ignored because the stiffness in the axial direction is relatively high. Kim *et al.* modeled the cutting-tool deflection in the radial direction as:

$$\delta_r = \delta_t + \delta_c, \quad (3.77)$$

where δ_t is the cutter bending deflection; and δ_c is the deflection of the cutting-tool clamping system. Assuming the cutter to be a cantilever with an overhang length L and considering that the cutting force acts at a distance z_f from the cutting-tool tip, the cutter bending deflection can be derived as [22]:

$$\delta_t(z) = \frac{F}{6 \cdot E \cdot I} \cdot \left[(z_f - z)^3 - (L - z)^3 + 3 \cdot (L - z)^2 \cdot (L - z_f) \right], \quad (3.78)$$

where z is the position w.r.t. the cutting-tool tip where the deflection is evaluated. The clamping deflection δ_c is modeled directly as F/K_c , where K_c is the cutter clamping

stiffness, which can be obtained experimentally. Eq. (3.78) can be modified considering that the end-ball cutting-tool is better represented by a two step cylindrical cantilever beam since a ball-end mill consists of two parts, the flute and the shank (see Figure 3.11). For this case, the resulting cutter bending deflection is reformulated as [22]:

$$\begin{aligned}
 \delta_t(z) &= \delta_s + \delta_f + \theta_s \cdot (L_f - z) \\
 &= \frac{F}{6 \cdot E \cdot I} \cdot \left[-(L - L_f)^3 + 3 \cdot (L - L_f)^2 \cdot (L - z_f) \right] + \frac{F}{6 \cdot E \cdot I_f} \cdot \left[(z_f - z)^3 \right. \\
 &\quad \left. -(L_f - z)^3 + 3 \cdot (L_f - z)^2 \cdot (L_f - z_f) \right] + \frac{F}{2 \cdot E \cdot I} \cdot \left[-(L - L_f)^2 \right. \\
 &\quad \left. + 2 \cdot (L - L_f) \cdot (L - z_f) \right] \cdot (L_f - z),
 \end{aligned} \tag{3.79}$$

where δ_s is the deflection of the shank; δ_f is the deflection of the flute; θ_s is the deflection angle of the shank; L_f is the length of the flute; and I_f is the moment of inertia of the flute.

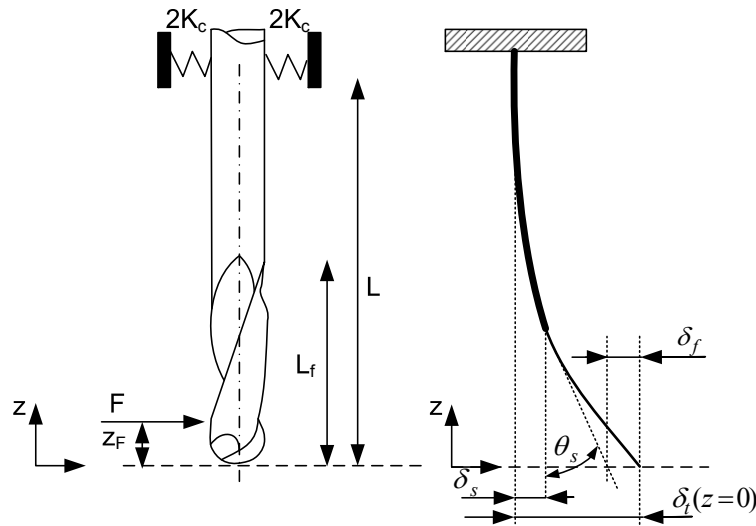


Figure 3.11: Ball-end mill and cantilever beam simplification.
Adapted from Kim *et al.*'s (2003) research work.

Cutting-tool wear-induced errors

The relationship of flank wear and dimensional deviation of machined parts depends on the machining operation and the geometry of the cutting-tool, as has been shown in Chapter 2. For example, the experimental work conducted by Zhou *et al.* [23] to identify the cutting errors in hard turning processes showed how the progressive tool wear on the cutting-tool increased the loss of the effective depth of cut up to $40 \mu m$, the relationship between flank wear and dimensional deviation being almost linear. Similarly, in drilling operations, the negative impact of the drill wear on the hole dimensions was observed in different research works [24, 25]. In Arul *et al.*'s research work [24], the flank wear due to abrasion during drilling decreased the effective cutting diameter, which produced a shrinkage of the drilled hole (see Figure 3.12). In Nourai *et al.*'s research work [25], drilling was

performed without coolant and due to adhesion and diffusion wear mechanisms, the holes drilled tended to increase considerably (up to an increase of $70 \mu m$ in diameter) instead of decreasing. In milling operations, the effect of flank wear from primary and secondary cutting edges depends on the type of milling operation. In face milling operations, flank wear at the primary cutting edge does not influence, since the face-milled surface is generated by the secondary cutting edge. However, in slotting or end milling operations the primary cutting edge has a direct impact on machined surface dimension since end-milled or slotted surfaces are generated by the cutting action of the primary cutting edge.

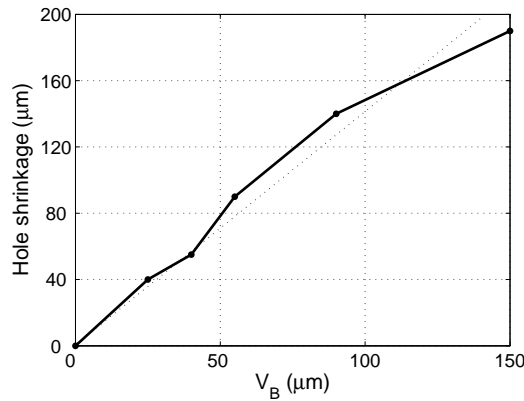


Figure 3.12: Effect of cutting-tool flank wear on hole shrinkage in drilling composites. Extracted from Arul *et al.*'s (2007) research work.

Analytically, two models are used to identify the relationship between flank wear and dimensional errors, assuming that there is homogeneous flank wear and no other factors such as the generation of a built-up edge are present. For sharp cutting inserts, the deviation of the machined surface in its normal direction from its nominal value is formulated as follows (see Figure 3.13 (a)):

$$\delta = \frac{\tan(\alpha)}{(1 - \tan(\gamma) \cdot \tan(\alpha))} \cdot V_B, \quad (3.80)$$

where α is the clearance angle; γ is the rake angle, and V_B is the flank wear value. Similarly, according to [26], for rounded cutting inserts the deviation of the machined surface is formulated as follows (see Figure 3.13 (b)):

$$\delta = \frac{r_e + V_B \cdot \cot(\alpha) - \sqrt{(r_e + V_B \cdot \cot(\alpha))^2 - V_B^2 \cdot (1 + \cot^2(\alpha))}}{1 + \cot^2(\alpha)}, \quad (3.81)$$

where r_e is the nose radius of the cutting insert. Note that Eqs. (3.80) and (3.81) can be applied for both primary and secondary cutting edges considering their respective values of α , γ and V_B . It should also be noted that, if the mechanism of tool wear presents adhesion (built-up edge or other similar effects), the resulting machined surface deviation may be different from that resulting from Eqs. (3.80) and (3.81).

expressed by $\delta_x(z)$ and $\delta_\theta(z)$, where $\delta_x(z)$ is the tool deflection in the radial direction, and $\delta_\theta(z)$ is the rotation of the workpiece along the θ -axis, which is perpendicular to the workpiece axis and to the cutting-force F_i .

A more complete model can be proposed by considering the workpiece deflection due to the shear stress and the deflection of the spindle. For this case, the overall workpiece deflection can be calculated as [29]:

$$\delta_x(z) = \frac{F_i \cdot z^2}{6 \cdot E \cdot I} \cdot (3a - z) + \chi \cdot \frac{F_i}{G \cdot A} \cdot z + c_s \cdot F_i, \quad \text{for } z \in [0, a] \quad (3.86)$$

$$\delta_x(z) = \frac{F_i \cdot a^2}{6 \cdot E \cdot I} \cdot (3z - a) + \chi \cdot \frac{F_i}{G \cdot A} \cdot z + c_s \cdot F_i, \quad \text{for } z \in [a, L] \quad (3.87)$$

where χ is the shear factor, G is the shear modulus, A is the total tool-workpiece interference area of cut, and c_s is the inverse function of the stiffness of the chuck. In Eqs. (3.86) and (3.87), the bending, shearing and spindle shift contributions are the first, second and third terms of each equation, respectively. Other models for different types of fixtures in turning, such as chuck-center or between centers, are described in [29].

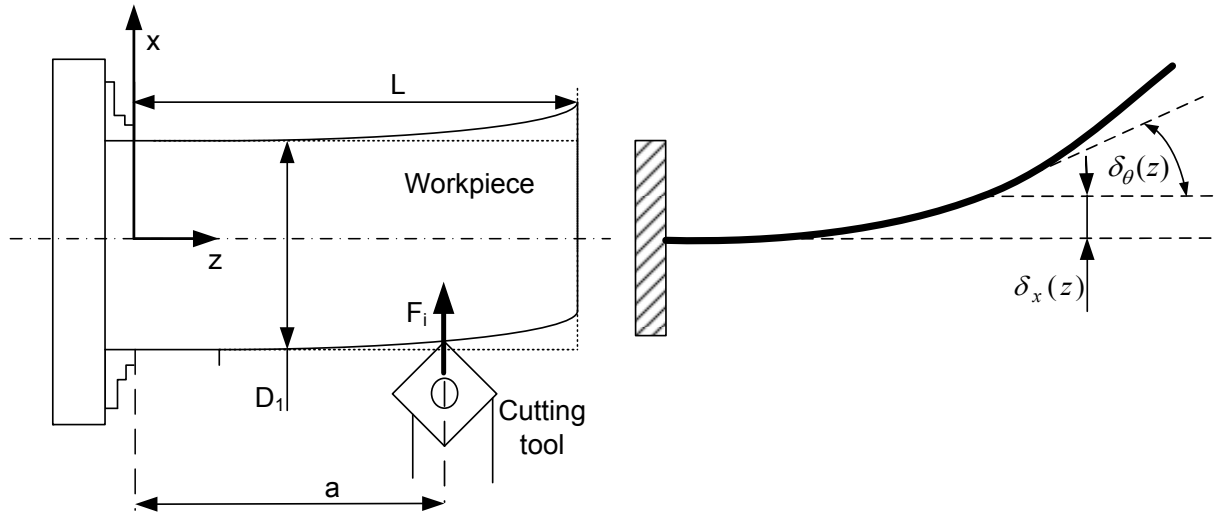


Figure 3.14: Turning deflection for a workpiece clamped in a chuck.

On the other hand, workpiece thermal-induced errors can be important when machining materials with high thermal expansion capabilities and no coolant is applied (dry conditions) [30]. Although this topic is a less explored field, the modeling approaches for predicting the dimensional and geometric errors of machined surfaces are also based on FEA models. Readers interested in this FEA model application can refer to [31].

3.2.6 Surface roughness

In machining, surface roughness may be considered as the sum of two independent effects [32, Chapter 5]:

- the “ideal” surface roughness, which is the result of the geometry of the cutting-tool and the feed speed,
- and the “natural” surface roughness, which is the result of the irregularities in the cutting operation.

The ideal surface roughness represents the best possible finish that may be obtained for a given tool shape and feed, and it can be approached only if built-up edge, chatter, inaccuracies in machine-tool movements, and so on, are not present.

For single-point cutting-tools such as those used in turning operations, the ideal surface roughness can be analytically obtained knowing the cutting-tool geometry and the feed rate. As reported in [32, Chapter 5], for cutting-tools with a rounded corner, the theoretical equation that gives the geometric peak-to-valley roughness (R_{zt}) is given by:

$$R_{zt} = \frac{f^2}{8 \cdot r_e}, \quad (3.88)$$

where f is the feed rate and r_e is the corner radius of the cutting-tool (Figure 3.15). For this cutting-tool geometry, the average surface roughness parameter R_a is usually determined from the expression [32, Chapter 5]:

$$R_a = \frac{0.0321 \cdot f^2}{r_e}. \quad (3.89)$$

For single-point cutting-tools but with a sharp corner (no rounded radius), the ideal surface roughness parameter R_{zt} is defined as [32, Chapter 5]:

$$R_{zt} = \frac{f}{\cot(\kappa_{r_e}) + \cot(\kappa'_{r_e})}, \quad (3.90)$$

where κ_{r_e} and κ'_{r_e} are the working major and minor cutting-edges angles, respectively (Figure 3.16). For this case, since the contact region between the tool and part is triangular, the average geometric roughness R_a is equal to $R_{zt}/4$.

For multi-point cutting-tools such as those applied in milling operations, the surface roughness is also affected by setup errors, since the cutting edges all cut at slightly different feed rates and depths of cut, especially with indexable cutters [33, Chapter 10]. Vibration due to the interrupted nature of the process and changes in cutter position caused by spindle and/or cutter runout and stability of part and fixture produce further variations in the effective feed rate and depth of cut of each cutting edge. As a result of all these effects, the surface finish in milling is less uniform than that in turning and boring.

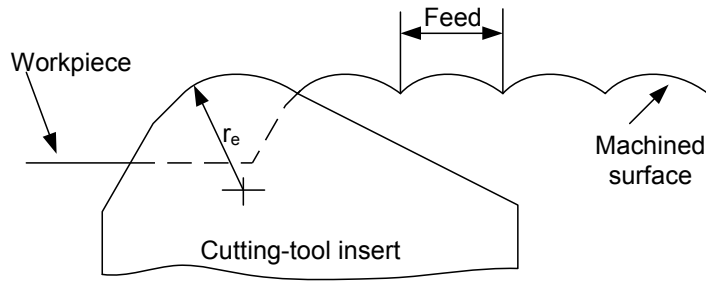


Figure 3.15: Surface roughness produced by a single-point cutting-tool geometry with a rounded corner.

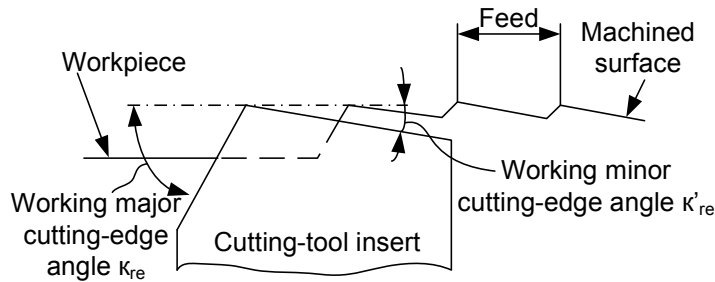


Figure 3.16: Surface roughness produced by a single-point cutting-tool geometry with a sharp corner.

For up and down peripheral milling operations, the peak-to-valley roughness can be obtained by the expression [34, Chapter 5]:

$$R_{zt} = \frac{f_z^2}{8 \cdot \left(\frac{d_t}{2} \pm \frac{f_z \cdot n_t}{\pi} \right)}, \quad (3.91)$$

where f_z is the feed rate per tooth; d_t is the diameter of the cutter; and n_t is the rotational frequency of the cutter. The sign (+) is valid for up milling and (−) for down milling. For face milling operations with rounded inserts, the surface roughness depends on the insert radius and on the effective feed rate. The geometric peak-to-valley roughness and the average surface roughness can be obtained from Eqs. (3.88) and (3.89), but substituting the feed rate f by the effective feed rate f_{eff} defined as [33, Chapter 10]:

$$f_{eff} = f \cdot \cos \left(\frac{r}{d_t} \right), \quad (3.92)$$

where r is the distance between the measurement trace and the centerline of the cutter (Figure 3.17). If the face milling operation is conducted using corner chamfer inserts, the estimated peak-to-valley roughness height is defined as:

$$R_{zt} = \frac{f_z}{\tan(l_a) + \cot(c_a)}, \quad (3.93)$$

where l_a and c_a are the lead angle and the face clearance angle of the tool, respectively. This expression is explained similarly as Eq. (3.90).

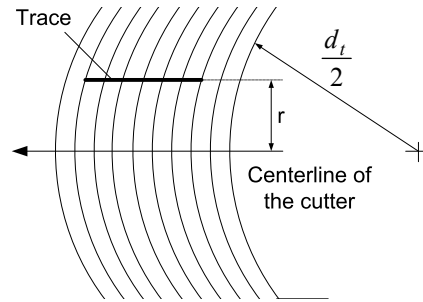


Figure 3.17: Illustration for determining the effective feed rate for traces parallel to the feed direction.

Other researchers have studied surface roughness generation when machining at low feed rates (feed rates lower than 0.1 mm per tooth). Under these conditions, the actual surface roughness moves away from the ideal roughness due to the limit of material plastic deformation [35]. At these feed rates, some authors have proposed alternative physical models to estimate the actual surface roughness by adding a purely geometric term to the ideal surface roughness. This additional term was first proposed by Brammertz [36], who defined the surface roughness parameter R_{zt} as:

$$R_{zt} = \frac{f^2}{8 \cdot r_e} + \frac{h_{min}}{2} \cdot \left(1 + \frac{r_e \cdot h_{min}}{f^2} \right), \quad (3.94)$$

where h_{min} is the minimum undeformed chip thickness. Interesting research studies have been published on this topic, in which the effect of material plastic flow has been analyzed [35, 37].

3.3 Experimental models

In many practical situations, it can be difficult to obtain physical models or, if they can be obtained, the accuracy of the model may be low due to the influence of other sources of errors that were previously assumed to be negligible. In those cases, more complex models based on experimental data such as those based on statistical regression techniques or AI techniques can be developed. In this section, some regression-based models and AI-based models applied in part quality prediction are outlined. Some important research works in the field are also reported.

3.3.1 Regression-based models

After conducting a sequence of experiments according to a previous design of experiments, experimental data can be fitted to estimate the relationship between the source of error analyzed and the machining performance in terms of part quality. For instance, Lee and Yang [38] proposed a thermal error modeling of CNC machine-tools based on a successive linear regression analysis. To model cutting-tool force-induced errors, Fuh and Chang [39]

Table 3.1: Regression-based (SMR) and AI-based models applied to part quality prediction (surface roughness – Ra – and dimensional deviation – DD).

| <i>Reference</i> | <i>Process</i> | <i>Modeling technique</i> | <i>Ra</i> | <i>DD</i> |
|------------------|----------------|---------------------------|-----------|-----------|
| [38] | M | SMR | - | ✓ |
| [39] | M | SMR | - | ✓ |
| [43] | M | SMR | ✓ | - |
| [44] | M | SMR, ANN | ✓ | - |
| [46] | M | SMR, ANN | ✓ | - |
| [47] | T | ANN | ✓ | ✓ |
| [48] | T | ANN | - | ✓ |
| [49] | T | ANN | ✓ | ✓ |
| [50] | T | ANN | - | ✓ |
| [51] | M | ANN | ✓ | - |
| [52] | M | ANN | ✓ | - |
| [53] | T | Fuzzy | ✓ | - |
| [54] | T | Fuzzy | ✓ | - |
| [55] | T | ANFIS | - | ✓ |
| [56] | M | ANFIS | ✓ | - |
| [57] | M | ANFIS | ✓ | - |
| [58] | M | BN | ✓ | - |

T: Turning; **M:** Milling.

proposed an experimental model based on a quadratic regression to estimate the machined surface deviation by considering the Brinell hardness of the workpiece, the cutting speed, the feed, and the radial and axial depth of cut. Dimensional errors induced by cutting-tool wear were also analyzed by experimental models in [26], which also took into account the deflection of the workpiece during turning. In [40], a compensation formulation for geometric and cutting force-induced errors was developed based on polynomial regressions.

For the prediction of micro-geometric part quality some experimental models have been applied in the literature instead of physical models. Their use is justified because, in reality, surface roughness generation is influenced by additional mechanisms such as vibrations, engagement of the cutting-tool, built-up edge, tool wear, etc., especially in high quality machining operations [41], so physical models may be inaccurate. For these cases, in the literature there are several surface roughness experimental models obtained from experimental procedures that are based on regressions. A common regression-based model applied in the literature for surface roughness prediction is reported in [42], and it is defined as:

$$Ra = k \cdot V_c^{x_1} \cdot f^{x_2} \cdot a_p^{x_3}, \quad (3.95)$$

where V_c , f and a_p denote the cutting speed, the feed rate and the depth of cut, respectively, and k , x_1 , x_2 and x_3 are empirical coefficients that can be obtained after fitting experimental data. Other experimental models based on quadratic functions [43] or surface response models [44, 45] can be found in the literature.

Table 3.1 summarizes some experimental research works conducted in the literature for modeling macro- and micro-geometric part quality based on regressions.

3.3.2 AI-based models

AI techniques can be used to learn complex non-linear relationships among process variables and machining performance variables from experimental data, providing models with high accuracy prediction. AI models are usually applied with sensor systems in order to extract information about the machining process from the sensors so that it can be used to help predict machining performance variables, such as surface roughness or dimensional part quality. The most common sensors applied for part quality prediction are dynamometers, accelerometers, acoustic emission sensors and current/power sensors, although the most significant for predicting dimensional part quality and surface roughness are dynamometers and accelerometers, respectively [59]. For modeling both micro- and macro-geometric part quality, four main AI approaches have been applied, representing more than the 90% of the research works reported in the literature (see Figure 3.18 and Abellan-Nebot's research work in [60]). These approaches are Artificial Neural Networks, Fuzzy Logic, Neuro-Fuzzy systems, and Bayesian Networks. As can be noted, researchers have paid special interest to Artificial Neural Networks, which has been applied in more than half of the references related to part quality prediction.

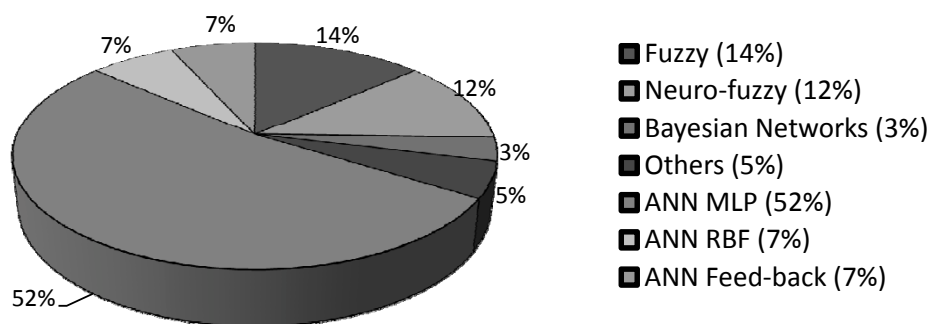


Figure 3.18: Frequency of usage of AI approaches in part quality prediction. References from ISI Web of Knowledge (2003-2008).

The literature review distinguishes the AI application according to micro- and macro-geometric predictions. Micro-geometric estimation should deal with an important stochastic behavior and non-linear relationships between many different cutting parameters and process variables, especially in milling operations, which means that many different AI techniques could be applied properly. However, macro-geometric estimations tend to be more heuristic and they are mostly restricted to the application of ANN approaches, where the main goal is to adjust non-linear functions according to clearly defined variables such as temperatures (thermal expansions) or forces (deflections), among others. According to the literature review, the recommended applications for each AI technique are defined as follows [60]:

- Artificial Neural Networks (ANNs) are recommended in applications where:
 - There is no purpose of knowledge extraction, and there is no previous knowledge of the process (or if there is previous knowledge, this knowledge is not intended to be added to the model).

- High accuracy prediction is required.
- There is no extrapolation and a good generalization is required.
- The experimental data set is composed of a medium-sized number of samples.
- Only the prediction is required and the inverse problem, such as cutting parameters evaluation to ensure a specific output value, is not considered.

In general, ANNs are the main tool for both surface roughness and dimensional deviation prediction.

- Fuzzy inference systems are recommended in applications where:
 - There is enough knowledge from the process and this knowledge is intended to be added to the model.
 - The understanding of the process prevails over the model accuracy.
 - Extrapolation can occur and the general process behavior is expected to be smooth.
 - The experimental data set is composed of a low/medium-sized number of samples, since part of the model is developed using previous knowledge.
 - Apart from specific variable prediction, the inverse problem also has to be solved.

In general, fuzzy inference systems are used for surface roughness prediction and cutting parameter selection given a surface roughness specification.

- Adaptive Neuro-fuzzy Inference Systems (ANFIS) are recommended in applications where:
 - There is a desire to add previous knowledge and/or to extract hidden knowledge from experimental data in a rule-form.
 - Ability for extrapolation and generalization are demanded.
 - A moderate rate of accuracy is required.
 - The experimental data set is composed of a medium-sized number of samples.
 - Apart from a specific variable prediction, the inverse problem has to be solved.

Since ANFIS are a hybridization of ANNs and fuzzy systems, the recommended applications are similar to both ANNs and fuzzy applications.

- Bayesian Networks (BNs) are recommended in applications where:
 - There is a desire to add previous knowledge and/or to extract hidden knowledge in the form of causal relationships and probabilities.
 - Low accuracy prediction is required but with a high degree of reliability.
 - An important stochastic component of the process is presented.
 - The experimental data set is composed of a large/very large number of samples.

- Partial observations are required, i.e., not all the variables in the model are available to estimate the output variable.

BNs are recommended for the prediction of surface roughness ranges in order to evaluate the probability of parts' being within or outside specifications. BNs are also recommended for cutting parameter selection to meet part specifications.

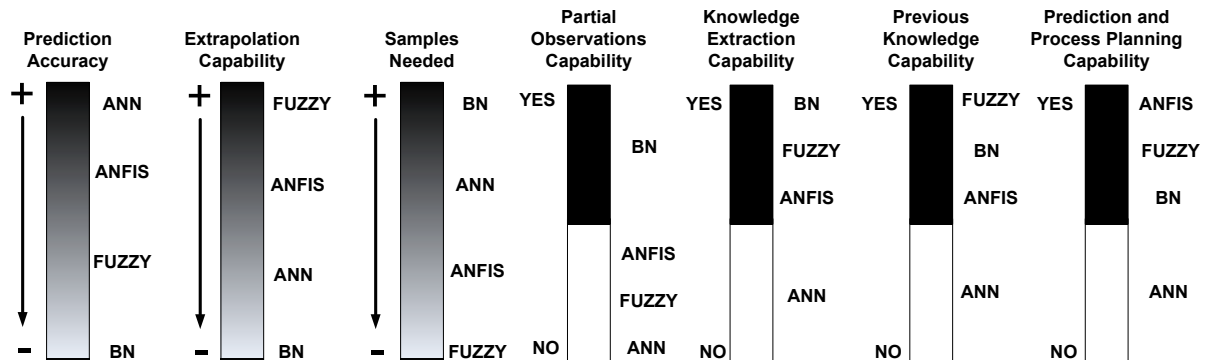


Figure 3.19: Basic guidelines for AI selection according to model requirements.

Figure 3.19 summarizes some of the main characteristics of the AI techniques applied in part quality prediction in machining systems. Furthermore, the most relevant research works conducted on part quality prediction in uni-station machining systems by using the above AI techniques are summarized in Table 3.1.

3.4 Conclusions

This chapter has briefly presented some of the physical models used in the literature to describe macro- and micro-geometric part quality errors due to machining errors such as those related to geometric and kinematic errors, fixture-induced errors, thermal-induced errors, cutting force-induced errors or cutting-tool wear-induced errors. Although there are other research works presented in the literature to deal with some of these machining errors, the ones shown in this chapter are the most representative. In addition, experimental models based on regressions and AI techniques have been briefly described since, on some occasions, these advanced models based on experimental data and process information from sensors are an interesting alternative method for modeling machining errors.

The models reported in this chapter will be later used in Chapter 6 for expanding 3D variation propagation models in multi-station machining processes.

3.5 Appendix 3.1: Homogeneous Transformation Matrix

A Homogeneous Transformation Matrix (HTM) in the 3D space is a 4×4 matrix that is used to represent one CS w.r.t. another CS. For illustrative purposes, let us consider two

CS, 1 and 2. Given the position and orientation vector of CS 1 w.r.t. CS 2, CS 1 can be expressed in 2 by a nominal HTM as [10]:

$$\mathbf{H}_1^2 = \bar{\mathbf{T}}_1^2 \cdot \bar{\mathbf{R}}_1^2, \quad (3.96)$$

where $\bar{\mathbf{T}}_1^2$ and $\bar{\mathbf{R}}_1^2$ are the translational and rotational matrix respectively. For a HTM, the superscript represents the CS we want the results to be represented in, and the subscript represents the CS we are transferring from. In Eq. (3.96) the translational matrix is defined as:

$$\bar{\mathbf{T}}_1^2 = \begin{pmatrix} 1 & 0 & 0 & t_{1x}^2 \\ 0 & 1 & 0 & t_{1y}^2 \\ 0 & 0 & 1 & t_{1z}^2 \\ 0 & 0 & 0 & 1 \end{pmatrix} = \begin{pmatrix} \mathbf{I}_{3 \times 3} & \mathbf{t}_1^2 \\ \mathbf{0}_{1 \times 3} & 1 \end{pmatrix}, \quad (3.97)$$

where \mathbf{t}_1^2 is the position vector of the origin of CS 1 expressed in 2 defined as $\mathbf{t}_1^2 = [t_{1x}^2, t_{1y}^2, t_{1z}^2]^T$. The rotational matrix is defined according to the rotation representation used. According to the Euler angles conversion, three Euler angles ($\bar{\varphi}$, $\bar{\theta}$, and $\bar{\psi}$) are used to define the rotational matrix. The orientation of CS 1 w.r.t. CS 2 can be obtained by three successive rotations as follows. First, CS 2 is rotated about the Z -axis by the angle $\bar{\varphi}$. Then, the resulting CS is rotated around the new Y -axis by angle $\bar{\theta}$, and finally the resulting CS is rotated around the new Z -axis by $\bar{\psi}$. According to this representation, the rotational matrix is formulated as [61, Chapter 2]:

$$\bar{\mathbf{R}}_1^2 = \begin{pmatrix} \mathbf{R}_1^2 & \mathbf{0}_{3 \times 1} \\ \mathbf{0}_{1 \times 3} & 1 \end{pmatrix}, \quad (3.98)$$

where

$$\mathbf{R}_1^2 = \mathbf{R}_{z, \bar{\varphi}} \cdot \mathbf{R}_{y, \bar{\theta}} \cdot \mathbf{R}_{z, \bar{\psi}}, \quad (3.99)$$

and

$$\mathbf{R}_{z, \bar{\varphi}} = \begin{pmatrix} \cos \bar{\varphi} & -\sin \bar{\varphi} & 0 \\ \sin \bar{\varphi} & \cos \bar{\varphi} & 0 \\ 0 & 0 & 1 \end{pmatrix}, \quad (3.100)$$

$$\mathbf{R}_{y, \bar{\theta}} = \begin{pmatrix} \cos \bar{\theta} & 0 & \sin \bar{\theta} \\ 0 & 1 & 0 \\ -\sin \bar{\theta} & 0 & \cos \bar{\theta} \end{pmatrix}, \quad (3.101)$$

$$\mathbf{R}_{z, \bar{\psi}} = \begin{pmatrix} \cos \bar{\psi} & -\sin \bar{\psi} & 0 \\ \sin \bar{\psi} & \cos \bar{\psi} & 0 \\ 0 & 0 & 1 \end{pmatrix}. \quad (3.102)$$

For this case, the rotational matrix is defined as:

$$\mathbf{R}_1^2 = \begin{pmatrix} c\bar{\varphi} \cdot c\bar{\theta} \cdot c\bar{\psi} - s\bar{\varphi} \cdot s\bar{\psi} & -c\bar{\varphi} \cdot c\bar{\theta} \cdot s\bar{\psi} - s\bar{\varphi} \cdot c\bar{\psi} & c\bar{\varphi} \cdot s\bar{\theta} \\ s\bar{\varphi} \cdot c\bar{\theta} \cdot c\bar{\psi} + c\bar{\varphi} \cdot s\bar{\psi} & -s\bar{\varphi} \cdot c\bar{\theta} \cdot s\bar{\psi} + c\bar{\varphi} \cdot c\bar{\psi} & s\bar{\varphi} \cdot s\bar{\theta} \\ -s\bar{\theta} \cdot c\bar{\psi} & s\bar{\theta} \cdot s\bar{\psi} & c\bar{\theta} \end{pmatrix}, \quad (3.103)$$

where c and s refer to \cos and \sin respectively. As a result, Eq. (3.96) can be rewritten as

$$\mathbf{H}_1^2 = \begin{pmatrix} \mathbf{R}_1^2 & \mathbf{t}_1^2 \\ \mathbf{0}_{1 \times 3} & 1 \end{pmatrix}. \quad (3.104)$$

Using the HTM, an i th point in CS 1, defined as $\mathbf{p}_i^1 = [p_{ix}^1, p_{iy}^1, p_{iz}^1]$, is related to the same point expressed in CS 2, defined as \mathbf{p}_i^2 , by the following equation:

$$\tilde{\mathbf{p}}_i^2 = \mathbf{H}_1^2 \cdot \tilde{\mathbf{p}}_i^1, \quad (3.105)$$

where $\tilde{\mathbf{p}}$ is equal to $[\mathbf{p}, 1]^T$.

Some useful properties of HTMs are listed as follows [62, Chapter 2]:

- Rotational matrices are orthogonal, and thus $(\mathbf{R}_2^1)^{-1} = (\mathbf{R}_2^1)^T$.
- From basic matrix properties, $(\mathbf{H}_2^1 \cdot \mathbf{H}_3^2)^{-1} = (\mathbf{H}_3^2)^{-1} \cdot (\mathbf{H}_2^1)^{-1}$, and $(\mathbf{H}_2^1 \cdot \mathbf{H}_3^2)^T = (\mathbf{H}_3^2)^T \cdot (\mathbf{H}_2^1)^T$.

3.6 Appendix 3.2: Differential Transformation Matrix

A Differential Transformation Matrix (DTM) in the 3D space is a 4×4 matrix that is used to represent the small position and orientation deviation of one CS w.r.t. another CS. For illustrative purposes, let us consider two CSs, 1 and 2, as shown in Figure 3.20. If CS 2 is deviated from nominal values by a small position and orientation deviation defined as $\mathbf{d}_2^{\circ 2} = [d_{2x}^{\circ 2}, d_{2y}^{\circ 2}, d_{2z}^{\circ 2}]^T$ and $\boldsymbol{\theta}_2^{\circ 2} = [\theta_{2x}^{\circ 2}, \theta_{2y}^{\circ 2}, \theta_{2z}^{\circ 2}]^T$ respectively, the HTM between the nominal CS $^{\circ 1}$ and the actual CS 2, called $\mathbf{H}_2^{\circ 1}$, is defined as:

$$\mathbf{H}_2^{\circ 1} = \mathbf{H}_{\circ 2}^{\circ 1} \cdot \delta \mathbf{H}_2^{\circ 2}, \quad (3.106)$$

where $\mathbf{H}_{\circ 2}^{\circ 1}$ is the HTM between the nominal CSs $^{\circ 1}$ and $^{\circ 2}$, and $\delta \mathbf{H}_2^{\circ 2}$ is a small deviation of the CS 2 from nominal values, and is defined as:

$$\delta \mathbf{H}_2^{\circ 2} = \begin{pmatrix} 1 & -\theta_{2z}^{\circ 2} & \theta_{2y}^{\circ 2} & d_{2x}^{\circ 2} \\ \theta_{2z}^{\circ 2} & 1 & -\theta_{2x}^{\circ 2} & d_{2y}^{\circ 2} \\ -\theta_{2y}^{\circ 2} & \theta_{2x}^{\circ 2} & 1 & d_{2z}^{\circ 2} \\ 0 & 0 & 0 & 1 \end{pmatrix}. \quad (3.107)$$

Note that the rotational matrix in $\delta \mathbf{H}_2^{\circ 2}$ is defined as Eq. (3.103) using the approximation of $\cos(\theta) \approx 1$ and $\sin(\theta) \approx \theta$ and neglecting second-order small values, since only small rotational deviations are considered. Eq. (3.107) can be rewritten as:

$$\delta \mathbf{H}_2^{\circ 2} = \mathbf{I}_{4 \times 4} + \boldsymbol{\Delta}_2^{\circ 2}, \quad (3.108)$$

where $\boldsymbol{\Delta}_2^{\circ 2}$ is called the DTM. The DTM is defined as:

$$\boldsymbol{\Delta}_2^{\circ 2} = \begin{pmatrix} \hat{\boldsymbol{\theta}}_2^{\circ 2} & \mathbf{d}_2^{\circ 2} \\ \mathbf{0}_{1 \times 3} & 0 \end{pmatrix}, \quad (3.109)$$

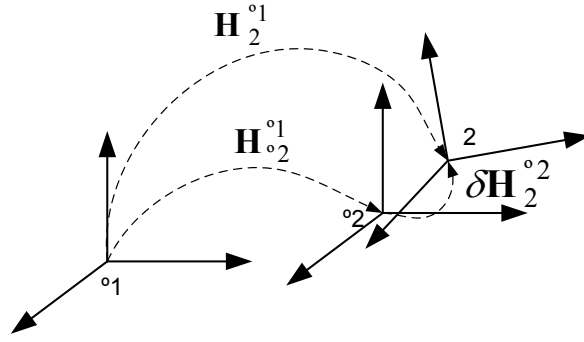


Figure 3.20: HTM from CS 2 to CS 1 if CS 2 is deviated from nominal values.

where $\hat{\theta}_2^{\circ 2}$ is the skew matrix of $\theta_2^{\circ 2}$ and is defined as:

$$\hat{\theta}_2^{\circ 2} = \begin{pmatrix} 0 & -\theta_{2z}^{\circ 2} & \theta_{2y}^{\circ 2} \\ \theta_{2z}^{\circ 2} & 0 & -\theta_{2x}^{\circ 2} \\ -\theta_{2y}^{\circ 2} & \theta_{2x}^{\circ 2} & 0 \end{pmatrix}. \quad (3.110)$$

For a more generic case, let us consider two CSs, 1 and 2, as shown in Figure 3.21. If both CSs are deviated from nominal values, the HTM between the actual CS 1 and CS 2 can be defined as:

$$\mathbf{H}_2^1 = \mathbf{H}_{o_2}^{o_1} \cdot \delta \mathbf{H}_2^1, \quad (3.111)$$

where $\delta \mathbf{H}_2^1$ is the HTM that defines the small position and orientation deviations of CS 2 w.r.t. 1 due to the deviation from their nominal values, and its DTM is defined as:

$$\Delta_2^1 = \begin{pmatrix} \hat{\theta}_2^{o_1} & \mathbf{d}_2^1 \\ \mathbf{0}_{1 \times 3} & 0 \end{pmatrix}, \quad (3.112)$$

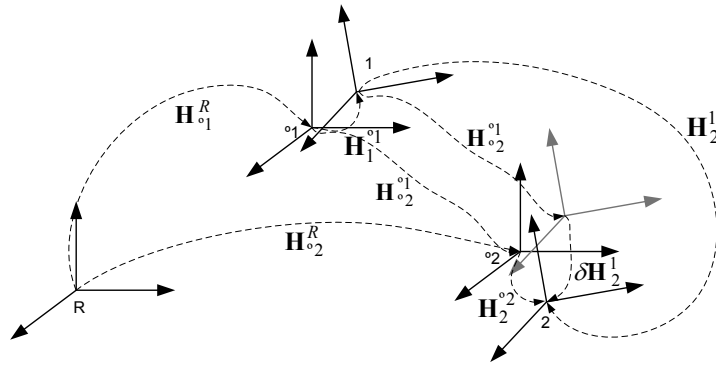


Figure 3.21: DTM from CS 2 to CS 1 if both CSs are deviated from nominal values.

It is important to remark that any DTM defines the small position and orientation deviation of one CS w.r.t. another CS, and these deviations can also be expressed as a

differential motion vector (DMV) in vector form. Indeed, given the DTM of CS 2 w.r.t. 1, denoted as Δ_2^1 , a DMV is straightforwardly defined as:

$$\mathbf{x}_2^1 = \begin{pmatrix} \mathbf{d}_2^1 \\ \boldsymbol{\theta}_2^1 \end{pmatrix}. \quad (3.113)$$

3.7 Appendix 3.3: Corollaries

Corollary 1: Consider a CS 1 and 2. Given a small deviation of CSs 1 and 2 from nominal values, and given the DTM of CS 2 w.r.t. 1 as Δ_2^1 , then the inverse of the HTM that defines the small position and orientation deviation of CS 2 w.r.t. 1 is defined as:

$$(\delta\mathbf{H}_2^1)^{-1} = \mathbf{I}_{4 \times 4} - \Delta_2^1. \quad (3.114)$$

Proof of Corollary 1: Assuming small deviations, the CS 2 is deviated w.r.t. 1 from nominal values by a small translational vector of $\mathbf{d}_2^1 = [d_{2x}^1, d_{2y}^1, d_{2z}^1]^T$ and a small rotational vector of $\boldsymbol{\theta}_2^1 = [\theta_{2x}^1, \theta_{2y}^1, \theta_{2z}^1]^T$ following the Euler angles conversion. Thus,

$$\begin{aligned} \delta\mathbf{H}_2^1 &= \bar{\mathbf{T}}_2^1 \cdot \mathbf{R}_{z, \bar{\varphi}} \cdot \mathbf{R}_{y, \bar{\theta}} \cdot \mathbf{R}_{z, \bar{\psi}}, \\ &= \begin{pmatrix} 1 & -\theta_{2z}^1 & \theta_{2y}^1 & d_{2x}^1 \\ \theta_{2z}^1 & 1 & -\theta_{2x}^1 & d_{2y}^1 \\ -\theta_{2y}^1 & \theta_{2x}^1 & 1 & d_{2z}^1 \\ 0 & 0 & 0 & 1 \end{pmatrix} = \mathbf{I}_{4 \times 4} + \Delta_2^1. \end{aligned} \quad (3.115)$$

If we evaluate the inverse of these small movements, the deviation of the nominal CS 1 w.r.t. the actual CS 2 can be approximated as the same previous values but negative, thus $\mathbf{d}_1^2 = [-d_{2x}^1, -d_{2y}^1, -d_{2z}^1]^T$. Similarly, the rotational deviations w.r.t. the actual CS 1 can be approximated as $\boldsymbol{\theta}_1^2 = [-\theta_{2x}^1, -\theta_{2y}^1, -\theta_{2z}^1]^T$. Therefore, $(\delta\mathbf{H}_{\circ 2}^1)^{-1}$ is formulated as:

$$\begin{aligned} (\delta\mathbf{H}_{\circ 2}^1)^{-1} &= \bar{\mathbf{T}}_1^2 \cdot \mathbf{R}_{z, \bar{\varphi}} \cdot \mathbf{R}_{y, \bar{\theta}} \cdot \mathbf{R}_{z, \bar{\psi}}, \\ &= \begin{pmatrix} 1 & \theta_{2z}^1 & -\theta_{2y}^1 & -d_{2x}^1 \\ -\theta_{2z}^1 & 1 & \theta_{2x}^1 & -d_{2y}^1 \\ \theta_{2y}^1 & -\theta_{2x}^1 & 1 & -d_{2z}^1 \\ 0 & 0 & 0 & 1 \end{pmatrix}, \end{aligned} \quad (3.116)$$

and from Eq. (3.116) it is obtained that $(\delta\mathbf{H}_2^1)^{-1} = \mathbf{I}_{4 \times 4} - \Delta_2^1$.

Corollary 2: Consider CS 1 and 2 shown in Figure 3.22. Consider now that CS 2 is deviated from nominal values by a sequence of n small translation and orientation deviations, resulting after each deviation in the CS $2'$, $2''$, \dots , $2^{n'}$. Noting Δ_i as the DTM of the i th small translation and orientation deviation, the HTM $\mathbf{H}_2^{\circ 1}$ can be formulated as:

$$\mathbf{H}_2^{\circ 1} = \mathbf{H}_{\circ 2}^{\circ 1} \cdot \left(\mathbf{I}_{4 \times 4} + \sum_{i=1}^n \Delta_i \right). \quad (3.117)$$

Proof of Corollary 2: As shown in Figure 3.22, the HTM $\mathbf{H}_2^{\circ 1}$ is defined as:

$$\mathbf{H}_2^{\circ 1} = \mathbf{H}_{2^{n'}}^{\circ 1} = \mathbf{H}_{\circ 2}^{\circ 1} \cdot \delta\mathbf{H}_{2'}^{\circ 2} \cdot \delta\mathbf{H}_{2''}^{\circ 2'} \cdot \dots \cdot \delta\mathbf{H}_{2^{n'}}^{\circ 2^{(n-1)'}}. \quad (3.118)$$

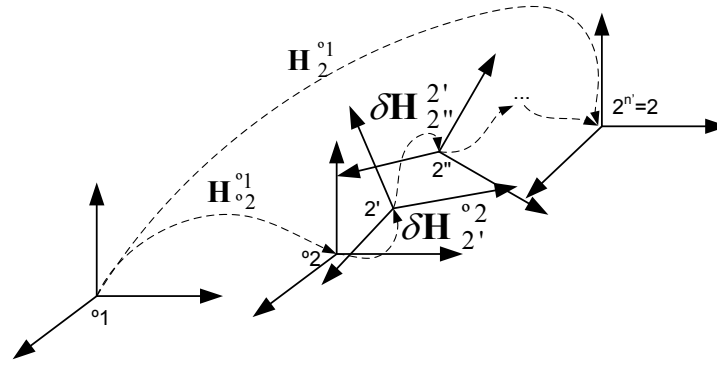


Figure 3.22: HTM from CS 2 to CS 1 if CS 2 is deviated from nominal values due to a sequence of small deviations.

As small translation and orientation deviations are assumed, Eq. (3.118) can be rewritten as:

$$\mathbf{H}_2^{\circ 1} = \mathbf{H}_{\circ 2}^{\circ 1} \cdot (\mathbf{I}_{4 \times 4} + \Delta_{2'}^{\circ 2}) \cdot (\mathbf{I}_{4 \times 4} + \Delta_{2''}^{2'}) \cdot \dots \cdot (\mathbf{I}_{4 \times 4} + \Delta_{2^{(n-1)'}}^{2^{(n-1)'}}), \quad (3.119)$$

and thus:

$$\mathbf{H}_2^{\circ 1} = \mathbf{H}_{\circ 2}^{\circ 1} \cdot (\mathbf{I}_{4 \times 4} + \Delta_{2'}^{\circ 2} + \Delta_{2''}^{2'} + \dots + \Delta_{2^{(n-1)'}}^{2^{(n-1)'}} + \Delta_{2'}^{\circ 2} \cdot \Delta_{2''}^{2'} + \Delta_{2''}^{2'} \cdot \Delta_{2'''}^{2''} + \dots). \quad (3.120)$$

If we assume the second-order (and higher) small values to be negligible, Eq. (3.120) can be approximated to Eq. (3.117).

References

- [1] R. Ramesh, M. A. Mannan, A. N. Poo, Error compensation in machine tools - a review part I: geometric, cutting-force induced and fixture-dependent errors, *International Journal of Machine Tools and Manufacture* 40 (9) (2000) 1235–1256.
- [2] C. A. van Luttervelt, T. Childs, I. Jawahir, F. Klocke, P. Venuvinod, Y. Altintas, E. Armarego, D. Dornfeld, I. Grabec, J. Leopold, B. Lindstrom, D. Lucca, T. Obikawa, Shirakashi, H. Sato, Present situation and future trends in modelling of machining operations progress report of the cirp working group modelling of machining operations, *CIRP Annals - Manufacturing Technology* 47 (2) (1998) 587–626.
- [3] C. A. van Luttervelt, Typology of models and simulation methods for machining operations, *Machining Science and Technology* 5 (3) (2001) 415–428.
- [4] O. Pantale, J. L. Bacaria, O. Dalverny, R. Rakotomalala, S. Caperaa, 2D and 3D numerical models of metal cutting with damage effects, *Computer Methods in Applied Mechanics and Engineering* 193 (39-41) (2004) 4383–4399.

-
- [5] M. Y. Wang, Characterizations of positioning accuracy of deterministic localization of fixtures, in: *Proceedings of the International Conference on Robotics and Automation*, Vol. 3, 2002, pp. 2894–2899.
- [6] S. Zhou, Q. Huang, J. Shi, State space modeling of dimensional variation propagation in multistage machining process using differential motion vectors, *IEEE Transactions on Robotics and Automation* 19 (2) (2003) 296–309.
- [7] F. Villeneuve, F. Vignat, Simulation of the manufacturing process in a tolerancing point of view: Generic resolution of the positioning problem, in: *Models for Computer Aided Tolerancing in Design and Manufacturing*, 2007, pp. 179–189.
- [8] V. L. Popov, *Contact Mechanics and Friction*, Springer, 2010.
- [9] J. H. Yeh, F. W. Liou, Contact condition modelling for machining fixture setup processes, *International Journal of Machine Tools and Manufacture* 39 (5) (1999) 787–803.
- [10] A. C. Okafor, Y. M. Ertekin, Derivation of machine tool error models and error compensation procedure for three axes vertical machining center using rigid body kinematics, *International Journal of Machine Tools and Manufacture* 40 (8) (2000) 1199–1213.
- [11] J. P. Choi, S. J. Lee, H. D. Kwon, Roundness error prediction with a volumetric error model including spindle error motions of a machine tool, *International Journal of Advanced Manufacturing Technology* 21 (2003) 923–928.
- [12] W. T. Lei, Y. Y. Hsu, Accuracy test of five-axis CNC machine tool with 3D probe-ball. Part I: design and modeling, *International Journal of Machine Tools and Manufacture* 42 (10) (2002) 1153–1162.
- [13] G. Chen, Rapid volumetric error mapping and compensation for a three-axis machining center, Thesis/dissertation (2000).
- [14] S. H. Yang, K. H. Kim, Y. K. Park, S. G. Lee, Error analysis and compensation for the volumetric errors of a vertical machining centre using a hemispherical helix ball bar test, *International Journal of Advanced Manufacturing Technology* 23 (2004) 495–500.
- [15] C. Raksiri, M. Parnichkun, Kinematic and geometric error verification and compensation of a three axes vertical machining center, in: *IEEE International Conference on Industrial Technology*, Vol. 2, 2002, pp. 1008–1012.
- [16] R. Ramesh, M. A. Mannan, A. N. Poo, Error compensation in machine tools - a review part II: thermal errors, *International Journal of Machine Tools and Manufacture* 40 (9) (2000) 1257–1284.
- [17] J. S. Chen, J. Yuan, J. Ni, Thermal error modelling for real-time error compensation, *International Journal of Advanced Manufacturing Technology* 12 (1996) 266–275.

-
- [18] J. C. Liang, H. F. Li, J. Ni, A comprehensive error compensation system for correcting geometric, thermal, and cutting force-induced errors, *International Journal of Advanced Manufacturing Technology* 13 (1997) 708–712.
- [19] L. N. López de Lacalle, A. Lamikiz, J. A. Sánchez, M. A. Salgado, Effects of tool deflection in the high-speed milling of inclined surfaces, *The International Journal of Advanced Manufacturing Technology* 24 (2004) 621–631.
- [20] J. M. Gere, S. P. Timoshenko, *Mecanics of Materials*, PWS Publishers; Second Edition, 1984.
- [21] T. A. Dow, E. L. Miller, K. Garrard, Tool force and deflection compensation for small milling tools, *Precision Engineering* 28 (2004) 31–45.
- [22] G. M. Kim, B. H. Kim, C. N. Chu, Estimation of cutter deflection and form error in ball-end milling processes, *International Journal of Machine Tools and Manufacture* 43 (2003) 917–924.
- [23] J. Zhou, M. Andersson, J. E. Stahl, Identification of cutting errors in precision hard turning process, *Journal of Materials Processing Technology* 153-154 (2004) 746–750.
- [24] S. Arul, L. Vijayaraghavan, S. K. Malhotra, Online monitoring of acoustic emission for quality control in drilling of polymeric composites, *Journal of Materials Processing Technology* 185 (2007) 184–190.
- [25] M. Nouari, G. List, F. Girot, D. Gehin, Effect of machining parameters and coating on wear mechanisms in dry drilling of aluminium alloys, *International Journal of Machine Tools and Manufacture* 45 (2005) 1436–1442.
- [26] X. Bi, Y. Liu, Y. Liu, Analysis and control of dimensional precision in turning process, in: *Control and Decision Conference*, 2009, pp. 3456–3459.
- [27] S. Ratchev, E. Govender, S. Nikov, K. Phuah, G. Tsiklos, Force and deflection modelling in milling of low-rigidity complex parts, *Journal of Materials Processing Technology* 143-144 (2003) 796–801.
- [28] M. Wan, W. Zhang, G. Qin, Z. Wang, Strategies for error prediction and error control in peripheral milling of thin-walled workpiece, *International Journal of Machine Tools and Manufacture* 48 (12-13) (2008) 1366–1374.
- [29] L. Carrino, G. Giorleo, W. Polini, U. Prisco, Dimensional errors in longitudinal turning based on the unified generalized mechanics of cutting approach. Part II: Machining process analysis and dimensional error estimate, *International Journal of Machine Tools and Manufacture* 42 (14) (2002) 1517–1525.
- [30] P. S. Sreejith, B. K. A. Ngoi, Dry machining: Machining of the future, *Journal of Materials Processing Technology* 101 (1-3) (2000) 287–291.
- [31] J. Rai, P. Xirouchakis, FEM-based prediction of workpiece transient temperature distribution and deformations during milling, *The International Journal of Advanced Manufacturing Technology* 42 (2009) 429–449.

-
- [32] G. Boothroyd, *Fundamentals of Machining and Machine Tools*, Marcel Dekker, Inc., 1989.
- [33] D. A. Stephenson, J. S. Agapiou, *Metal cutting theory and practice*, Marcel Dekker, Inc., 1997.
- [34] J. P. Davim, *Surface integrity in machining*, 1st Edition, Springer, 2010.
- [35] W. Grzesik, A revised model for predicting surface roughness in turning, *Wear* 194 (1-2) (1996) 143–148.
- [36] P. H. Brammerz, Die entstehung der oberflächenrauheit beim feindrehen, *Industrieanzeiger* (1961) 25–32.
- [37] K. Liu, S. N. Melkote, Effect of plastic side flow on surface roughness in micro-turning process, *International Journal of Machine Tools and Manufacture* 46 (14) (2006) 1778–1785.
- [38] J.-H. Lee, S.-H. Yang, Statistical optimization and assessment of a thermal error model for CNC machine tools, *International Journal of Machine Tools and Manufacture* 42 (1) (2002) 147–155.
- [39] K.-H. Fuh, H.-Y. Chang, An accuracy model for the peripheral milling of aluminum alloys using response surface design, *Journal of Materials Processing Technology* 72 (1) (1997) 42–47.
- [40] Z. Lechniak, A. Werner, K. Skalski, K. Kedzior, Methodology of off-line software compensation for errors in the machining process on the CNC machine tool, *Journal of Materials Processing Technology* 76 (1998) 42–48.
- [41] H. Siller, C. Vila, C. Rodríguez, J. Abellán, Study of face milling of hardened AISI D3 steel with a special design of carbide tools, *The International Journal of Advanced Manufacturing Technology* 40 (2009) 12–25.
- [42] F. Cus, J. Balic, Optimization of cutting process by GA approach, *Robotics and Computer-Integrated Manufacturing* 19 (1-2) (2003) 113–121.
- [43] G. C. Barber, R. Gu, Q. Jiang, J. Gu, S. Tung, Surface roughness model for worn inserts of face milling: Part II - an empirical model, *Tribology Transactions* 44 (1) (2001) 142–146.
- [44] T. Erzurumlu, H. Oktem, Comparison of response surface model with neural network in determining the surface quality of moulded parts, *Materials and Design* 28 (2) (2007) 459–465.
- [45] J. Vivancos, C. J. Luis, L. Costa, J. A. Ortíz, Optimal machining parameters selection in high speed milling of hardened steels for injection moulds, *Journal of Materials Processing Technology* 155-156 (2004) 1505–1512.
- [46] Y. H. Tsai, J. C. Chen, S. J. Lou, An in-process surface recognition system based on neural networks in end milling cutting operations, *International Journal of Machine Tools and Manufacture* 39 (4) (1999) 583–605.

- [47] R. Azouzi, M. Guillot, On-line prediction of surface finish and dimensional deviation in turning using neural network based sensor fusion, *International Journal of Machine Tools and Manufacture* 37 (9) (1997) 1201–1217.
- [48] A. E. Ouafi, M. Guillot, A. Bedrouni, Accuracy enhancement of multi-axis CNC machines through on-line neurocompensation, *Journal of Intelligent Manufacturing* 11 (2000) 535–545.
- [49] K. A. Risbood, U. S. Dixit, A. D. Sahasrabudhe, Prediction of surface roughness and dimensional deviation by measuring cutting forces and vibrations in turning process, *Journal of Materials Processing Technology* 132 (1-3) (2003) 203–214.
- [50] G. Warnecke, R. Kluge, Control of tolerances in turning by predictive control with neural networks, *Journal of Intelligent Manufacturing* 9 (4) (1998) 281–287.
- [51] H. Oktem, T. Erzurumlu, F. Erzincanli, Prediction of minimum surface roughness in end milling mold parts using neural network and genetic algorithm, *Materials and Design* 27 (9) (2006) 735–744.
- [52] Q. Huang, J. Shi, Simultaneous tolerance synthesis through variation propagation modeling of multistage manufacturing processes, *NAMRI/SME Transactions*, 31 (2003) 515–522.
- [53] N. R. Abburi, U. S. Dixit, A knowledge-based system for the prediction of surface roughness in turning process, *Robotics and Computer-Integrated Manufacturing* 22 (4) (2006) 363–372.
- [54] E. D. Kirby, J. C. Chen, Development of a fuzzy-nets-based surface roughness prediction system in turning operations, *Computers and Industrial Engineering* 53 (1) (2007) 30–42.
- [55] Y. Jiao, Z. J. Pei, S. Lei, E. S. Lee, G. R. Fisher, Fuzzy adaptive networks in machining process modelling: dimensional error prediction for turning operations, *International Journal of Production Research* 43 (14) (2005) 2931–2948.
- [56] F. Dweiri, M. Al-Jarrah, H. Al-Wedyan, Fuzzy surface roughness modeling of CNC down milling of alumic-79, *Journal of Materials Processing Technology* 133 (3) (2003) 266–275.
- [57] W. Ho, J. Tsai, B. Lin, J. Chou, Adaptive network-based fuzzy inference system for prediction of surface roughness in end milling process using hybrid Taguchi-genetic learning algorithm, *Expert Systems with Applications* 36 (2, Part 2) (2009) 3216–3222.
- [58] M. Correa, C. Bielza, M. de Ramirez, J. Alique, A Bayesian network model for surface roughness prediction in the machining process, *International Journal of Systems Science* 39 (12) (2008) 1181–1192.
- [59] J. V. Abellan-Nebot, F. Romero Subirón, A review of machining monitoring systems based on artificial intelligence process models, *The International Journal of Advanced Manufacturing Technology* 47 (2010) 237–257.

-
- [60] J. V. Abellan-Nebot, A review of artificial intelligent approaches applied to part quality prediction, *International Journal of Machining and Machinability of Materials* 8 (2010) 6–37(32).
 - [61] M. W. Spong, S. Hutchinson, M. Vidyasagar, *Robot modeling and control*, Hoboken, NJ: John Wiley and Sons, 2006.
 - [62] J. Shi, *Stream of Variation Modeling and Analysis for Multistage*, CRC Press Taylor and Francis Group, 2007.

Prediction of part quality in multi-station machining systems

In the fields of product design and quality improvement, the development of reliable 3D machining variation models for multi-station machining processes is a key issue to be able to estimate the resulting geometrical and dimensional quality of manufactured parts, generate robust process plans, eliminate downstream manufacturing problems, and reduce ramp-up times. In the literature, two main 3D machining variation models have been studied: the Stream of Variation model, oriented toward product quality improvement (fault diagnosis, process planning evaluation and selection, etc.), and the Model of the Manufactured Part, which is oriented toward product and manufacturing design activities (manufacturing and product tolerance allocation, geometric product validation, etc.). This chapter reviews the fundamentals of each model and describes, step-by-step, how to derive them using a simple case study. The chapter analyzes both models and compares their main characteristics and applications. A discussion about the drawbacks and limitations of each model and some potential research lines in this field are also presented.

4.1 Introduction

Traditionally, product design has been separated from manufacturing process design throughout the product development cycle increasing ramp-up times, product change costs, and variability of product quality. This product-oriented approach, called *over-the-wall design* due to the sequential nature of the design activities, prevents the integration of design and manufacturing activities to improve product development. In order to overcome this limitation, manufacturers have begun to investigate ways to evaluate product designs and manufacturing processes simultaneously, in an attempt to eliminate downstream manufacturing problems and reduce ramp-up times. For this purpose, product design requires the application of process-oriented approaches through 3D manufacturing variation models in order to integrate product and manufacturing process information. However, the application of 3D manufacturing variation models is currently limited, especially in multi-station machining processes (MMPs), where a large number of machining operations are conducted in different stations with different fixture devices. Due to this limitation on design and manufacturing integration, lengthy and costly trial and error approaches are usually

applied to decrease product quality variability [1]. In fact, in the fields of product design and quality improvement, the development of reliable 3D variation models of MMPs is a key issue to estimate the resulting geometrical and dimensional quality of manufactured parts.

In the literature, two important groups of researchers dealing with the development of 3D variation models for MMPs can be distinguished: i) one group of researchers who focus more on the quality improvement field (mostly universities from the USA), and ii) a second group of researchers focused on product design, mostly from universities in France and Canada. The research conducted by the first group, which we call the “IO school” (Industrial Operations school) hereinafter, is focused on modeling the dimensional and geometrical variation of manufactured parts by the state space model, which is commonly applied in control theory [2]. Through this model, the geometrical and dimensional deviation of machined surfaces at each station is related to its main sources of variation and the deviation from previous stations is considered by propagating them through the locating datums. Modeling explicitly the relationship between the sources of variation at each station and part quality, a large number of quality improvement activities can be conducted such as part active control for variation reduction, optimal placement of inspection stations, robust process planning, process-oriented tolerancing, and so forth. The research conducted by the second group, which we call the “PD school” (Product Design school) hereinafter, is focused on modeling variations in dimensional and geometrical part quality by considering the workpiece/fixture/machine-tool system as a mechanical assembly. Thus, well-known approaches for the analysis of mechanical assemblies can be applied. Specifically, the PD school applies the concept of small displacement torsors (SDTs) to describe and propagate surface deviations throughout different machining stations. The applications of the research conducted by the PD school are mainly focused on part quality prediction and manufacturing, and product tolerance allocation.

The purpose of this chapter is to review the 3D manufacturing variation models proposed by the IO and the PD school for MMPs, and to analyze their main drawbacks and advantages together with their future lines of research. The chapter is organized as follows. Section 4.2 describes the fundamentals of the 3D manufacturing variation model applied by the IO school and its main applications. Similarly, Section 4.3 describes the 3D manufacturing variation model applied by the PD school, together with its main applications. Section 4.4 presents two examples of 2D modeling (extendable to any 3D case study) to show, step-by-step, the implementation of both models, while analyzing them symbolically and numerically. Section 4.5 discusses both 3D variation models, and compares their main drawbacks and advantages. Finally, Section 4.6 concludes the chapter and outlines some potential lines of research in the field.

Note to readers: In this chapter, the nomenclature used in the 3D manufacturing variation models is the same as that used in the literature. Although the models analyzed are quite similar, the nomenclature has not been unified in order to facilitate the readers the understanding and the application of each model independently.

General assumptions: The 3D manufacturing variation models described in this

chapter are based on the following assumptions: i) datum surfaces and locating surfaces are assumed to be perfect in form (without form errors); ii) fixture locators are assumed to be punctual; iii) errors in fixtures and cutting-tool movements are assumed to be small in comparison to nominal values and thus, the small-angle approximation can be applied; and iv) workpieces and fixtures components are considered rigid.

4.2 Variation modeling and propagation by the IO school: the Stream of Variation model

4.2.1 Fundamentals

Manufacturing variability in MMPs and its impacts on part quality can be modeled by capturing the mathematical relationships between the sources of variation of manufacturing process variables that are critical to part quality (called key control characteristics -KCCs- of the process) and the deviations of the functional features of the product (called key product characteristics -KPCs-). These relationships can be modeled with a non-linear function $y_1 = f_1(\mathbf{u})$, where y_1 is the value of a KPC and $\mathbf{u} = [u_1, u_2, \dots, u_n]^T$ are the KCCs in the MMP. By assuming small variations, the non-linear model can be linearized through a Taylor series expansion, and the value of a KPC can be defined as

$$y_1 = f_1(\bar{\mathbf{u}}) + \left. \frac{\delta f_1(\mathbf{u})}{\delta u_1} \right|_{\mathbf{u}=\bar{\mathbf{u}}} \cdot (u_1 - \bar{u}_1) + \dots + \left. \frac{\delta f_1(\mathbf{u})}{\delta u_n} \right|_{\mathbf{u}=\bar{\mathbf{u}}} \cdot (u_n - \bar{u}_n) + \varepsilon_1, \quad (4.1)$$

where ε_1 contains the high-order non-linear residuals of the linearization, and the linearization point is defined by $\bar{\mathbf{u}} = [\bar{u}_1, \bar{u}_2, \dots, \bar{u}_n]^T$. This linear approximation can be considered good enough for many MMPs [3]. From Eq. (4.1), the dimensional variation of a KPC from its nominal value is defined as

$$\Delta y_1 = \left. \frac{\delta f_1(\mathbf{u})}{\delta u_1} \right|_{\mathbf{u}=\bar{\mathbf{u}}} \cdot \Delta u_1 + \dots + \left. \frac{\delta f_1(\mathbf{u})}{\delta u_n} \right|_{\mathbf{u}=\bar{\mathbf{u}}} \cdot \Delta u_n + \varepsilon_1, \quad (4.2)$$

where $\Delta y_1 = y_1 - f_1(\bar{\mathbf{u}})$, defines the variations of the KPC, and $\Delta u_j = u_j - \bar{u}_j$, for $j = 1, \dots, n$, defines the small variations of the KCCs in a MMP. Considering that there are M KPCs in the part which is stacked in the vector $\mathbf{Y} = [\Delta y_1, \dots, \Delta y_M]^T$, Eq. (4.2) can be re-written in matrix form as

$$\mathbf{Y} = \mathbf{\Gamma} \cdot \mathbf{U} + \boldsymbol{\varepsilon}, \quad (4.3)$$

where $\mathbf{U} = [\Delta u_1, \dots, \Delta u_n]^T$; $\boldsymbol{\varepsilon}$ is the stacked vector of the high-order non-linear residuals; and $\mathbf{\Gamma}$ is the matrix $\left[\left[\left. \frac{\delta f_1(\mathbf{u})}{\delta u_1} \right|_{\mathbf{u}=\bar{\mathbf{u}}}, \dots, \left. \frac{\delta f_1(\mathbf{u})}{\delta u_n} \right|_{\mathbf{u}=\bar{\mathbf{u}}} \right]; \dots; \left[\left. \frac{\delta f_M(\mathbf{u})}{\delta u_1} \right|_{\mathbf{u}=\bar{\mathbf{u}}}, \dots, \left. \frac{\delta f_M(\mathbf{u})}{\delta u_n} \right|_{\mathbf{u}=\bar{\mathbf{u}}} \right] \right]$.

For MMPs, obtaining Eq. (4.3) is a challenging task. Researchers from US universities have proposed the adoption of the well-known state space model from control theory [2, Chapter 11] to create a mathematical representation of the relationship between the sources of variation of an MMP and the deviation of the machined surfaces at each station. This also includes how the deviation of previously machined surfaces influences the current station when these surfaces are used as locating datums. In this representation,

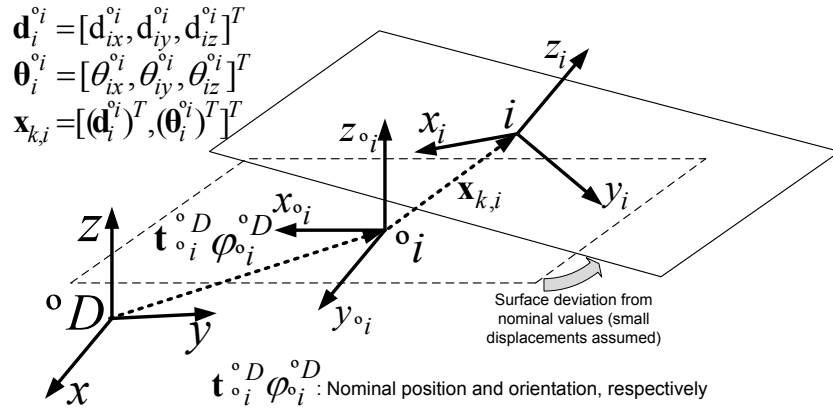


Figure 4.1: Dimensional deviation of a plane surface at station k using a DMV.

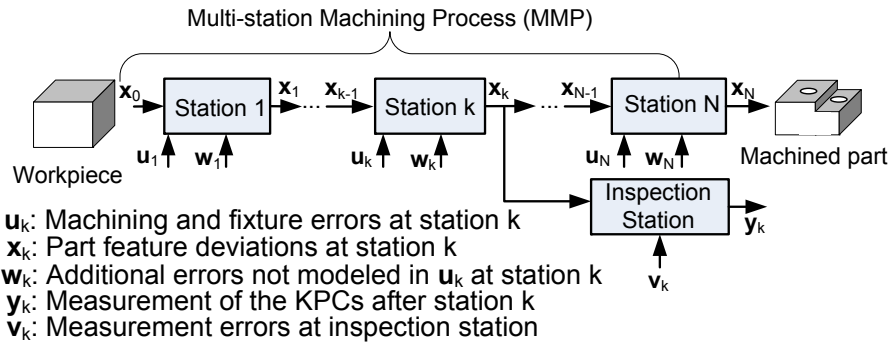


Figure 4.2: Propagation of manufacturing variation in an MMP.

dimensional deviations of part surfaces from nominal values are defined by 6×1 vectors called differential motion vectors (DMVs), which have the form of $\mathbf{x}_{k,i} = [(\mathbf{d}_i^{o_i})^T, (\boldsymbol{\theta}_i^{o_i})^T]^T$, where $\mathbf{d}_i^{o_i} = [d_{ix}^{o_i}, d_{iy}^{o_i}, d_{iz}^{o_i}]^T$ is the small translational deviation and $\boldsymbol{\theta}_i^{o_i} = [\theta_{ix}^{o_i}, \theta_{iy}^{o_i}, \theta_{iz}^{o_i}]^T$ is the small orientation deviation of the local CS of the i th part surface, as it is shown in Figure 4.1. For this example, ${}^o i$ refers to the nominal CS and i to the actual CS. The deviation of all part surfaces at station k are stacked in the vector $\mathbf{x}_k = [\mathbf{x}_{k,1}^T, \dots, \mathbf{x}_{k,i}^T, \dots]^T$. Note that each feature deviation, $\mathbf{x}_{k,i}$, is expressed in its own CS.

In a machining station, three main sources of variation can be distinguished: datum-induced deviations, fixture-induced deviations and machining-induced deviations. The state space model defines analytically how these three main sources of error influence on the final part quality deviation. To illustrate how these three main sources of variation influence on part quality, we consider an N -station machining process shown in Figure 4.2 and the k th machining station with the workpiece and the fixture device shown in Figure 4.3. At this k th station, the following sources of variation exist.

First, the deviations of the datum surfaces used for locating the workpiece deviate the workpiece location from its nominal value. This term can be estimated as $\mathbf{x}_k^d = \mathbf{A}_k \cdot \mathbf{x}_{k-1}$,

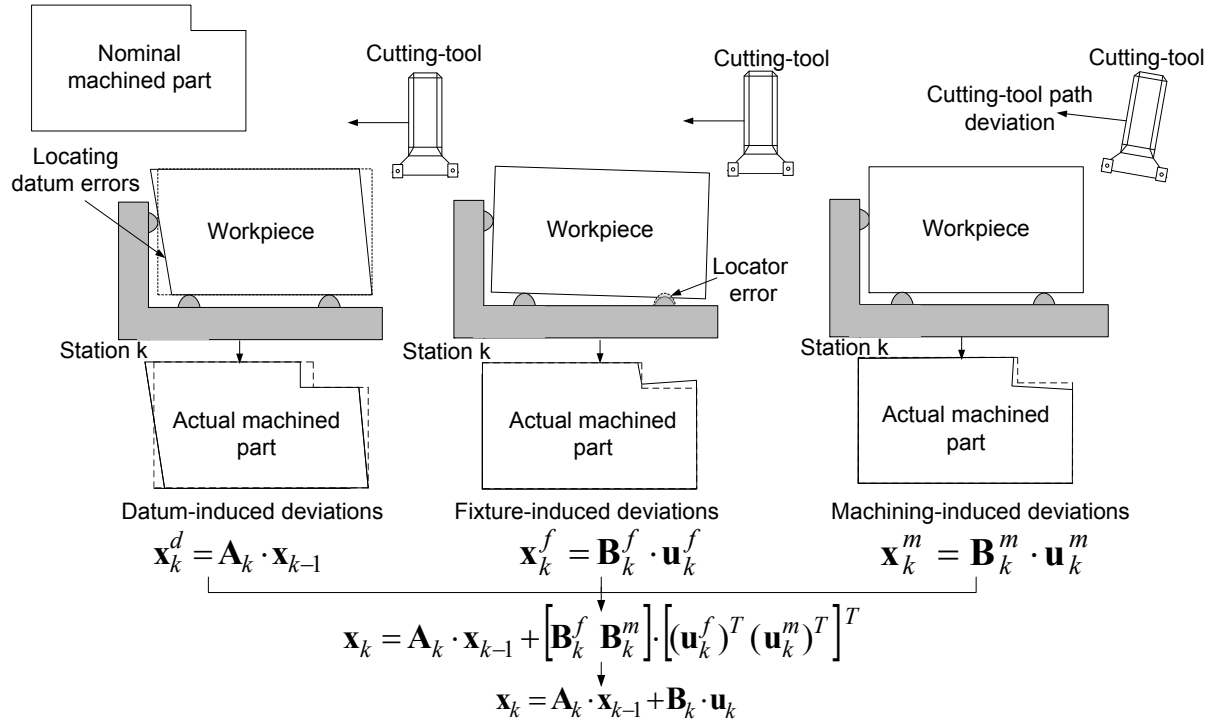


Figure 4.3: Sources of variation and state space model formulation for station k .

where \mathbf{x}_{k-1} is the vector of part surface deviations from upstream machining stations and \mathbf{A}_k linearly relates the datum deviations with the machined surface deviation due to the locating deviation of the workpiece.

Secondly, the fixture-induced deviations deviate the workpiece location on the machine-tool table and produce a machined surface deviation. This term can be estimated as $\mathbf{x}_k^f = \mathbf{B}_k^f \cdot \mathbf{u}_k^f$, where \mathbf{u}_k^f is the vector of locator deviations and \mathbf{B}_k^f is a matrix that linearly relates locator deviations with the machined surface deviation.

Thirdly, the operation or machining deviations such as those due to geometrical and kinematic errors, tool-wear errors, etc., deviate the cutting-tool tip during machining and thus, the machined surface is deviated from its nominal value. This term is modeled as $\mathbf{x}_k^m = \mathbf{B}_k^m \cdot \mathbf{u}_k^m$, where \mathbf{u}_k^m is the vector that defines the KCCs related to operation or machining deviations and \mathbf{B}_k^m is a matrix that linearly relates these KCCs with the machined surface deviations.

Therefore, for an N -station machining process the derivation of the state space model can be defined in a generic form as

$$\mathbf{x}_k = \mathbf{A}_k \cdot \mathbf{x}_{k-1} + \mathbf{B}_k \cdot \mathbf{u}_k + \mathbf{w}_k, \quad k = 1, \dots, N, \quad (4.4)$$

where $\mathbf{B}_k \cdot \mathbf{u}_k$ represents the deviations introduced within station k due to the KCCs (related to fixturing and machining) and it is defined as $[\mathbf{B}_k^f \quad \mathbf{B}_k^m] \cdot [(\mathbf{u}_k^f)^T, (\mathbf{u}_k^m)^T]^T$;

and \mathbf{w}_k is the unmodeled system noise and linearization errors.

The derivation of the state space model in MMPs, called the stream of variation (SoV) model, was firstly presented by Huang *et al.* [4]. Djurjanovic *et al.* [5] expanded on Huang's work in order to derive, in an explicit manner, the linear equations that model the relationships between fixtures, locating datum, and measurement datum features. In their research work, a complex mathematical derivation was required and the application of the proposed methodology was not straight forward. The SoV model derivation was improved by [3], who applied the DMV concept from robotics to represent the geometric deviation of each machined feature. In their work, a step by step methodology was proposed in order to derive the matrices \mathbf{A}_k and \mathbf{B}_k at each station using product and process information (i.e., part geometry and fixture layouts). However, the model was limited to 3-2-1 orthogonal fixture layouts based on locators and generic cutting-tool path deviations without explicitly including machining-induced errors. In a recent work, Loose *et al.* [6] extended the state space model formulation by including general non-orthogonal fixture layouts based on locators.

4.2.2 Virtual part quality inspection and verification

Somewhere along the MMP, an inspection station can be placed in order to inspect the KPCs and verify whether the workpiece/part is within specifications. Following the state space model formulation from control theory [2], a virtual inspection after the k th machining station can be conducted using the expression:

$$\mathbf{y}_k = \mathbf{C}_k \cdot \mathbf{x}_k + \mathbf{v}_k, \quad (4.5)$$

where \mathbf{y}_k represents the deviations of the inspected KPCs; $\mathbf{C}_k \cdot \mathbf{x}_k$ are the deviations of the KPCs that are defined as a linear combination of the deviations of workpiece features at the k th station; and \mathbf{v}_k is the measurement noise of the inspection process. In a similar way to \mathbf{x}_k , vector \mathbf{y}_k is defined as $[\mathbf{y}_{k,1}^T, \dots, \mathbf{y}_{k,q}^T, \dots, \mathbf{y}_{k,M}^T]^T$, where $\mathbf{y}_{k,q}$ is the inspected deviation of the q th KPC (denoted as S_q) defined by the vector $\mathbf{y}_{k,q} = [(\mathbf{d}_{S_q}^{S_m})^T, (\boldsymbol{\theta}_{S_q}^{S_m})^T]^T$, where S_m is the measurement datum surface and M is the number of KPCs inspected. In Eq. (4.5), matrix \mathbf{C}_k depends on what KPCs they are and which measurement datums are used to locate the part in the inspection station. How to derive matrix \mathbf{C}_k is explained in detail in [3].

In order to express part quality measurements by means of an explicit linear function of the KCCs presented throughout the MMP and considering that the inspection station is placed at the end of the MMP (after machining station N), Eqs. (4.4) and (4.5) can be combined and rewritten in the input–output form as:

$$\mathbf{Y} = \mathbf{\Gamma} \cdot \mathbf{U} + \boldsymbol{\varepsilon}, \quad (4.6)$$

where vectors \mathbf{Y} and \mathbf{U} are the stacking quality vectors after inspection and the vectors of sources of error respectively from stations $k = 1, 2, \dots, N$. In Eq. (4.6), vector \mathbf{Y} is defined as $\mathbf{Y} = [\mathbf{y}_{N,1}^T, \mathbf{y}_{N,2}^T, \dots, \mathbf{y}_{N,M}^T]^T$, vector \mathbf{U} is defined as $\mathbf{U} = [\mathbf{u}_1^T, \mathbf{u}_2^T, \dots, \mathbf{u}_N^T]^T$, and

matrices $\mathbf{\Gamma}$ and $\boldsymbol{\varepsilon}$ are defined as:

$$\mathbf{\Gamma} = [\mathbf{M}_{N,1}, \mathbf{M}_{N,2}, \dots, \mathbf{M}_{N,N}], \quad \boldsymbol{\varepsilon} = [\bar{\mathbf{M}}_{N,1}, \bar{\mathbf{M}}_{N,2}, \dots, \bar{\mathbf{M}}_{N,N}] \cdot [\mathbf{w}_1, \mathbf{w}_2, \dots, \mathbf{w}_N]^T + \mathbf{v}_N, \quad (4.7)$$

where

$$\begin{aligned} \bar{\mathbf{M}}_{N,j} &= \mathbf{C}_N \cdot \boldsymbol{\Phi}_{N,j} \cdot \mathbf{B}_j, & j \leq N, \\ \bar{\mathbf{M}}_{N,j} &= \mathbf{C}_N \cdot \boldsymbol{\Phi}_{N,j}, & j = N, \end{aligned} \quad (4.8)$$

$$\boldsymbol{\Phi}_{N,j} = \begin{cases} \mathbf{A}_{N-1} \cdot \mathbf{A}_{N-2} \cdots \mathbf{A}_j, & \text{if } j < N \\ \mathbf{I}, & \text{if } j = N \end{cases} \quad (4.9)$$

Using Eq. (4.6), the deviation of the local CS of an inspected KPC S_q w.r.t. the measurement datum S_m can be estimated. However, if one wants to verify whether an inspected KPC is within its tolerance zone according to geometric dimensioning and tolerancing (GD&T) practices, the deviation of the boundary points of the inspected KPC w.r.t. the measurement datum should be evaluated. For this purpose, the deviation of the r th boundary point P_r of the inspected q th KPC w.r.t. S_m can be evaluated according to the Corollary 3 (Appendix 4.1):

$$\mathbf{y}_{N,P_r} = \begin{pmatrix} \mathbf{I}_{3 \times 3} & -(\hat{\mathbf{t}}_{P_r}^{S_q}) \\ \mathbf{0}_{3 \times 3} & \mathbf{I}_{3 \times 3} \end{pmatrix} \cdot \mathbf{y}_{N,S_q}, \quad (4.10)$$

where \mathbf{y}_{N,S_q} is the deviation of the q th KPC obtained from Eq. (4.6); $\mathbf{I}_{3 \times 3}$ is the 3×3 identity matrix; $\mathbf{0}_{3 \times 3}$ is the 3×3 zero matrix; and $\hat{\mathbf{t}}_{P_r}^{S_q}$ is the skew matrix of the nominal position vector $\mathbf{t}_{P_r}^{S_q}$ which describes the position of the point P_r w.r.t. S_q . The resulting deviation of point P_r w.r.t. S_m is then defined by a 6×1 deviation vector in the form of $\mathbf{y}_{N,P_r} = [(\mathbf{d}_{P_r}^{S_m})^T, (\boldsymbol{\theta}_{P_r}^{S_m})^T]^T$. The deviation of the r th point on the toleranced surface following the direction of part verification, defined by the unit vector $\mathbf{n} = [n_x, n_y, n_z]^T$, is evaluated by the expression:

$$\left[\mathbf{y}_{N,P_r} \right]_{\mathbf{n}} = \mathbf{n}^T \cdot \mathbf{d}_{P_r}^{S_m}. \quad (4.11)$$

The tolerance zone where the variability of the manufactured feature will lie can be obtained by analyzing the deviation from nominal values of all boundary points of the KPC. If the tolerance of a KPC is defined from design specifications, then one can be interested in verifying the part virtually for a given MMP. For this purpose, the distance between each deviated boundary point and the specified tolerance zone from the design should be evaluated. For the point P_r , this distance is defined as the gap distance Gap_r and it is formulated as:

$$Gap_r = \min \left(\tau + \left[\mathbf{y}_{N,P_r} \right]_{\mathbf{n}}, \tau - \left[\mathbf{y}_{N,P_r} \right]_{\mathbf{n}} \right), \quad (4.12)$$

where τ is the maximum deviation of the r th point according to the tolerance value (e.g., for a dimensional tolerance of size for a plane, τ is $t/2$, where t is the dimensional tolerance value defined by the distance between two parallel planes). The r th point of the inspected

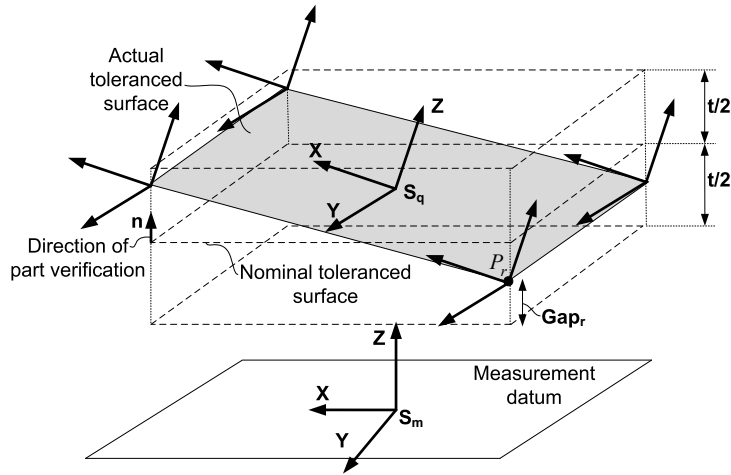


Figure 4.4: Gap distance of a boundary point on a deviated tolerated surface.

surface will be within the tolerance zone if Gap_r remains positive or null (see Figure 4.4). The verification of the GD&T tolerances applied to the KPC can be conducted by analyzing the deviation of all boundary points of the KPC. In the literature, the integration of positional, orientation and form tolerances into the SoV model has been conducted by Loose *et al.* [7], although other GD&T characteristics such as the profile of a surface and the inclusion of material condition modifiers are still unaddressed.

It should be remarked that the virtual measurement and verification can be conducted following two main approaches: the worst-case approach, and the statistical approach. Depending on which type of approach is applied, the estimation of the KPC deviation, and thus the estimation of the deviation of its boundary points in order to analyze a functional specification, will be more or less conservative. For each approach, the resulting estimation is derived as follows:

- Worst-case approach: the estimated deviation of the q th KPC will be the maximum according to the expected sources of variation. In accordance with Eq. (4.6), the worst-case analysis can be conducted assuming that all coefficients from matrix $\mathbf{\Gamma}$ and vector \mathbf{U} are positive and that the measurement error also increases the expected deviation. In other words, that all sources of errors act in the same direction, so the expected part quality will be the worst possible. The worst-case deviation of the S_q CS is:

$$\mathbf{y}_{N,S_q-wc} = \pm (|\mathbf{\Gamma}| \cdot |\mathbf{U}| + |\boldsymbol{\varepsilon}|), \quad (4.13)$$

and the worst possible part quality considering the point boundary deviation is defined as:

$$Gap_{wc} = \min(Gap_{r_{wc}}) \quad \forall r \in \text{boundary points}, \quad (4.14)$$

where $Gap_{r_{wc}}$ is evaluated by Eqs. (4.10) and (4.12) considering \mathbf{y}_{N,S_q-wc} instead of \mathbf{y}_{N,S_q} .

- Statistical approach: the worst-case analysis produces an estimation that is highly improbable, especially for a large number of sources of variation, due to the randomness of the sources of variation in MMPs. To estimate a more probable scenario, statistical analysis is commonly applied. In this analysis, the sources of variation are assumed to be independent from each other and distributed normally. Under these assumptions, the covariance of the S_q CS can be estimated as:

$$\Sigma_{\mathbf{y}_{N,S_q}} = \Gamma \cdot \Sigma_{\mathbf{U}} \cdot \Gamma^T + \Sigma_{\boldsymbol{\varepsilon}}, \quad (4.15)$$

where Σ_{\bullet} is the covariance matrix of \bullet . Therefore, the deviation of the KPC is estimated, according to 6σ , as:

$$\mathbf{y}_{N,S_{q-st}} = \pm 3 \sqrt{\text{diag}(\Sigma_{\mathbf{y}_{N,S_q}})}. \quad (4.16)$$

The part quality considering the point boundary deviations is defined as:

$$\text{Gap}_{st} = \min(\text{Gap}_{r_{st}}) \quad \forall r \in \text{boundary points}, \quad (4.17)$$

where $\text{Gap}_{r_{st}}$ is evaluated by Eqs. (4.10) and (4.12), considering $\mathbf{y}_{N,S_{q-st}}$ instead of \mathbf{y}_{N,S_q} .

4.2.3 Main applications

The SoV model, defined by Eqs. (4.4) and (4.5), let the integration of KPCs and KCCs through product and process information such as fixture layout, part geometry, sequence of machining and inspection operations, etc. Based on this model, the use of advanced control theory, multivariate statistics and Monte Carlo simulations enables a large number of applications along product-life cycle (Figure 4.5). In the literature, interesting research works can be found about part quality estimation and process planning [3, 5, 8, 9], manufacturing fault identification [10–18], active control for variation reduction [19–21] and process-oriented tolerancing [22, 23]. In the next subsections, we will briefly describe some of these applications and the main research works on the field.

Part quality estimation and process planning

The straight forward application of the SoV model is for part quality estimation (i.e., tolerance analysis), which allows the designer to estimate whether the MMP is able to manufacture parts within specifications. By this analysis, the process planner can search for the MMP that is most robust to manufacturing disturbances from a group of candidates, and conduct specific modifications to improve the manufacturing process. Zhang *et al.* [8] presented a sensitivity analysis based on the SoV model to assess how sensitive the KPCs are to certain fixture-induced variations in an MMP. Through the sensitivity indices, the robustness of each process plan candidate can be evaluated, and the critical stations and fixture components of each MMP can be detected and modified. Liu *et al.* [9] proposed a quality-assured setup planning to select the optimal process plan from a group of process plan candidates with different fixture layouts. The optimal process plan was referred to as the process plan candidate that minimizes the cost related to process precision and satisfies the quality specifications.

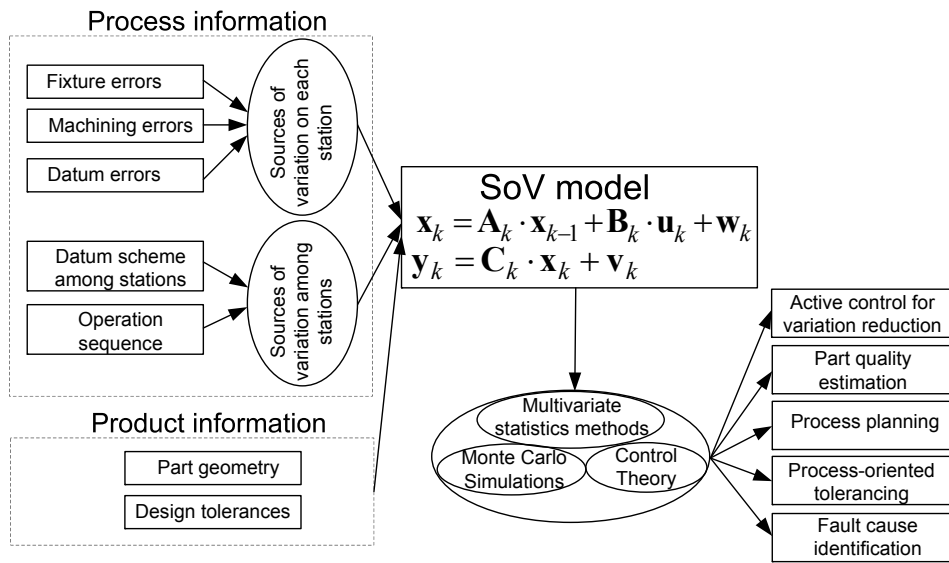


Figure 4.5: Diagram of the SoV model derivation and its applications.

Fault cause identification

The issue of diagnosability refers to the problem of whether the measurements of the KPCs contain enough information for the diagnosis of critical process faults [12]. For instance, by knowing the SoV model defined by Eq. (4.6) and measuring different KPCs (vector \mathbf{Y}), it may be possible to infer the sources of variation (vector \mathbf{U}). However, the MMPs are not usually diagnosable due to the inherent dimensional coupling between cutting-tool deviations and fixture deviations in each machining station. That is, fixture-induced deviations and machining-induced deviations may produce the same pattern deviation on KPCs. Consequently, it is difficult to distinguish between error sources in MMPs. To overcome this limitation, Wang *et al.* [10] applied the SoV model and proposed the concept of equivalent fixture error. With this concept, datum-induced and machining-induced errors are transformed into equivalent fixture-induced errors at each station. Using this approach, a sequential root cause identification can be conducted minimizing the number of measurements required, isolating firstly the faulty station. A similar approach was conducted by Zhang *et al.* [8] applying the station-level error decomposition method. Assuming measurement and un-modeled noises to be negligible, Ding *et al.* [11] studied the diagnosability of an MMP through the definition of a diagnosability matrix. According to this matrix, three different types of diagnosability were defined: i) diagnosability within MMP, ii) diagnosability within station, and iii) diagnosability between stations. Zhou *et al.* [12] extended the diagnosability analysis of MMPs when measurement and un-modeled noises are not negligible. Besides analyzing the diagnosis capability of the MMP, other research works have also studied how to identify a specific root fault cause when it is diagnosable. For this purpose, pattern recognition techniques [14] and direct estimation methods [13] have been tested.

The definition of at which station an inspection of part/workpiece quality should be conducted and which features should be inspected is crucial for a successful identification

of the root fault causes and process improvement. Djurdjanovic and Ni [17] proposed a Bayesian-based method to analyze the measurement schemes (i.e. placement of the inspection station and features to be inspected) in a MMP. Later, the same authors presented in [18] other non-Bayesian methods for analyzing different measurement schemes when only statistical characteristics of the sensor noise term ε are known. Other research works such as [15, 16] tackle the synthesis problem to define which is the optimal placement of the inspection stations for a given MMP.

Active control for variation reduction

As an extension of diagnosis methodologies, some researchers have developed an in-line process adjustment technique to reduce variability in MMPs. The basic idea is to control the product quality through in-line adjustments of certain process parameters such as the fixture locations or the cutting-tool path itself. The SoV model is applied to estimate the impact that those potential control actions will have on the quality of the final product. Active control for variation reduction requires two enablers [19]: in-line dimensional measurement sensors to measure actual part deviation, and real-time actuators such as CNC machining stations or flexible tooling [24] to act on the manufacturing process. Furthermore, dimensional quality control can be based on feed-back control or feed-forward control. Feed-back control implies that the control actions (corrections) are determined using downstream measurements obtained at the end of the process or at certain intermediate stations. This dimensional quality control can only be used to compensate mean shifts, but not to reduce variability. On the other hand, feed-forward control uses in-line measurements to determine the current deviation of the workpiece in order to subsequently apply control actions so as to minimize the effect of this deviation on the quality of the final part. In this way, feed-forward control compensates current deviations instead of reacting to past deviations as feed-back control does [19].

Izquierdo *et al.* [19] designed a feed-forward dimensional control based on programmable tooling and in-line measurements, although its application was focused on multi-station assembly processes. In MMPs, Djurdjanovic and Ni [21] developed a feed-forward control scheme based on flexible tooling adjustments and in-process product measurements. The control law is devised so that the dimensional product quality at the end of the line is as close to the nominal as possible in the least squares sense, taking into account the measurement and process noise, as well as the accuracy of actuation of flexible tooling elements.

Process-oriented tolerancing

Process-oriented tolerancing is a new approach that attempts to overcome the traditional limitations of the product-oriented tolerancing approach. Unlike product-oriented tolerancing, where part tolerances are optimally allocated considering only an associated manufacturing cost from very generic process planning guide-lines, process-oriented tolerancing optimally allocates tolerances of manufacturing process variables bearing in mind their associated manufacturing costs and their relationship with product quality. Process-oriented tolerancing is essentially a tolerance synthesis problem where the quality specification of the final product is ensured by allocating tolerances of manufacturing process variables for

a minimum cost. The framework of process-oriented tolerance synthesis was first proposed by Ding *et al.* in different research works [23, 25]. In these works, the tolerances of process variables in an MMP are allocated optimally by solving a non-linear constrained optimization problem defined by: cost functions, the SoV model, a process degradation model of fixture components, a tolerance accumulation model, and several constraints related to part specifications (tolerances). Chen *et al.* [22] expanded the work in [23] to integrate process-oriented tolerancing with maintenance planning in multi-station assembly processes. They incorporated tool fabrication cost, fixture maintenance cost, and quality loss functions to optimize the tolerance allocation of manufacturing process variables and the frequency of fixture maintenance operations. Compared to other process-oriented tolerance approaches, the integration of maintenance policies showed a more desirable system performance with a significant reduction in production cost.

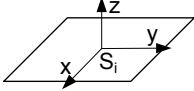
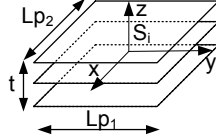
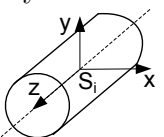
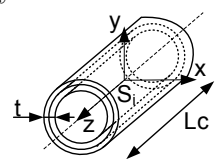

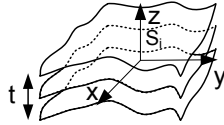
4.3 Variation modeling and propagation by the PD school: the Model of the Manufactured Part

4.3.1 Fundamentals

The PD school deals with the manufacturing variation analysis in MMPs by applying some of the concepts used in analyzing the geometrical variations of mechanical assemblies due to the imperfections of their components. The main idea of the PD school is to consider the manufacturing setup in a machining station as a mechanism, so that the knowledge related to dimensional and geometrical variation analysis in mechanisms can be applied. In the literature, the study of the propagation of variation in mechanisms can be conducted through different modeling approaches, depending on the nature of the model. The most commonly applied approaches are: i) kinematic models, such as models based on small displacement torsors (SDTs) [26] or vector-loop based models [27, 28], and ii) degree of freedom models, such as the tolerance maps models (T-Maps) [29]. The PD school has mainly applied the SDT approach to model and propagate the surface variations from parts, fixtures and cutting-tools, deriving the so-called Model of the Manufactured Part (MoMP) [30].

The aim of the MoMP is to simulate the deviations generated in the manufacturing process considering two independent phenomena: positioning deviations and machining deviations. These deviations are accumulated over successive setups and, as a result, propagate the manufacturing variability. Positioning deviations are caused by fixture surface deviations and locating datum surface deviations that have been generated in previous setups. Machining deviations are caused by multiple sources of error such as geometric and kinematic errors, thermal errors, cutting force-induced errors, cutting-tool wear-induced errors, and so forth. The positioning and machining deviations of part surfaces are modeled by the SDT approach assuming that the expected manufacturing variations are small and parts behave as a rigid solid. In this approach, dimensional and geometrical variations of manufactured parts are obtained by propagating the deviations of the elements that take part in the manufacturing process, modeled as a chain of SDTs.

Table 4.1: SDTs according to the type of surface and torsor constraints according to the type of tolerance.

| Surface | Surface torsor | Tolerance zone | Torsor constraints |
|--|---|---|---|
| Plane  | $\mathbf{T}_{S_i, N_i} = \begin{Bmatrix} \alpha & U \\ \beta & U \\ U & w \end{Bmatrix}$ | Planar size tolerance  | $\begin{aligned} -\frac{t}{2} &\leq w \leq \frac{t}{2}, \\ \frac{-t}{Lp_1} &\leq \alpha \leq \frac{t}{Lp_1}, \\ \frac{-t}{Lp_2} &\leq \beta \leq \frac{t}{Lp_2} \end{aligned}$ |
| Cylinder  | $\mathbf{T}_{S_i, N_i} = \begin{Bmatrix} \alpha & u \\ \beta & v \\ U & U \end{Bmatrix}$ | Cylindrical annulus  | $\begin{aligned} u^2 + v^2 &\leq \left(\frac{t}{2}\right)^2, \\ -\frac{t}{L_c} &\leq \alpha \leq \frac{t}{L_c}, \\ -\frac{t}{L_c} &\leq \beta \leq \frac{t}{L_c} \end{aligned}$ |
| Generic surface  | $\mathbf{T}_{S_i, N_i} = \begin{Bmatrix} \alpha & u \\ \beta & v \\ \gamma & w \end{Bmatrix}$ | Offsetting of a surface  | Undefined |

The dimensional and geometrical deviation of each element, described by an SDT, depends on the types of surfaces and tolerances involved. An SDT of a surface is composed of the small translation and orientation deviations that define the deviation between the nominal surface and the substitute surface, which is an ideal representation of the real one. For instance, a surface with a planar geometry can only present translation variations on the Z -axis, and orientation variations around the X - and Y -axes, considering the normal vector of the planar surface in Z direction of its local CS. Other variations (translation in X - and Y -axes and rotations around the Z -axis) keep the surface invariant and thus, these deviations are considered to be undetermined. The SDT that describes the deviation between the substitute plane S_i and the nominal plane N_i , denoted as \mathbf{T}_{S_i, N_i} , is thus defined as a translation deviation vector $\mathbf{D} = U \cdot x + U \cdot y + w \cdot z$ and an orientation deviation vector $\mathbf{\Omega} = \alpha \cdot x + \beta \cdot y + U \cdot z$. This SDT is defined as:

$$\mathbf{T}_{S_i, N_i} = \begin{Bmatrix} \mathbf{\Omega} \\ \mathbf{D} \end{Bmatrix} = \begin{Bmatrix} \alpha \cdot x + \beta \cdot y + U \cdot z \\ U \cdot x + U \cdot y + w \cdot z \end{Bmatrix} = \begin{Bmatrix} \alpha & U \\ \beta & U \\ U & w \end{Bmatrix}, \quad (4.18)$$

where U is an undetermined component, w is the translation deviation around the Z -axis, and α and β are the orientation deviations around the X - and Y -axes, respectively. Similar SDTs have been defined in the literature [30–32] for other types of surfaces, and some of them are shown in Table 4.1. Note that the torsor components are constrained to keep the surface within the tolerance range.

In addition to the surface torsors, it is also defined the link torsor and the part torsor. The link torsor represents the link between two substitute surfaces from different parts and shows the degrees of freedom constrained by the link (joint). The part torsor represents the part's displacement within the assembly in relation with geometric errors, joints

and its the nominal position of the part. For each part, a part torsor is defined and for each contact between parts, a link torsor is defined.

In assemblies, the resulting deviation of a part of an assembly can be directly computed from the summation of torsors of the assembled parts that define the position of the part analyzed. For instance, consider an assembly of two parts, A and B . The computation of the part torsor $\mathbf{T}_{R,B}$ (SDT of part B w.r.t. frame R) is evaluated for any set of joints between parts A and B (i.e., for any set of two interacting surfaces A_i, B_j) as follows [30]:

$$\begin{aligned}\mathbf{T}_{R,B} &= \mathbf{T}_{R,A} + \mathbf{T}_{A,A_i} + \mathbf{T}_{A_i,B_j} + \mathbf{T}_{B_j,B} \\ &= \mathbf{T}_{R,A} + \mathbf{T}_{A,A_i} + \mathbf{T}_{A_i,B_j} - \mathbf{T}_{B,B_j}.\end{aligned}\quad (4.19)$$

where \mathbf{T}_{A,A_i} and \mathbf{T}_{B,B_j} are the surface torsors that represent the deviation of surface A_i and B_j of part A and B respectively in the reference frame R ; \mathbf{T}_{A_i,B_j} is the link torsor that represents the deviation of the link between surface A_i and surface B_j in the reference frame R ; and $\mathbf{T}_{R,A}$ is the SDT of part A w.r.t. frame R . Note that $\mathbf{T}_{R,B}$ is identical whatever the contact surface is considered, i.e., if there are n interacting surfaces A_i-B_j that compose the joints in the assembly of parts A and B , thus there are n equations defined as Eq. (4.19) that result in the same value of $\mathbf{T}_{R,B}$. In the system of n linear equations, the unknown parameters are the link torsors. Obviously, different joints suppress different degrees of mobility, so for isostatic assemblies the resulting system of linear equations can be solved. Appendix 4.2 shows in detail the use of SDTs and their difference in comparison with DMVs.

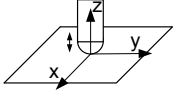
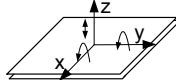
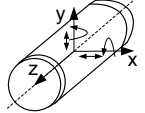
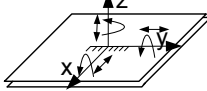
In the MoMP, the resulting variation in part quality at the end of the MMP is obtained by evaluating the chain of torsors that influence the manufacturing performance at each station, expressed all torsors in the same CS. Corollary 4 in Appendix 4.1 show the basics of the evaluation of surface torsors at different points in the surface and referenced in different frames. This chain of torsors considers both the positioning and the machining deviation at each station. Following the research work in [30], the positioning and machining deviation can be evaluated as follows:

- Positioning deviation: the positioning deviation, expressed as the torsor $\mathbf{T}_{F_k,D}$, is the deviation of the workpiece (the design reference $-D-$) w.r.t. the fixture setup (F_k) and it is formulated as:

$$\mathbf{T}_{F_k,D} = -\mathbf{T}_{D,S_l} + \mathbf{T}_{F_k,H_{k,j}} + \mathbf{T}_{H_{k,j},S_l}.\quad (4.20)$$

In this expression, \mathbf{T}_{D,S_l} is the SDT of locating datum surfaces (S_l) at D and it is obtained from previous stations. For the first station, \mathbf{T}_{D,S_l} represents the deviations of the raw surfaces S_l that are used as locating datums in this station. Torsor $\mathbf{T}_{F_k,H_{k,j}}$ indicates the j th part-holder surface deviation at the k station and the maximum values of the parameters of this torsor represent the part-holder precision (maximum deviations expected from part-holder surfaces). The link torsor $\mathbf{T}_{H_{k,j},S_l}$ represents the relative position between the locating datum surface S_l and the j th part-holder surface which depends on how both surfaces contact (joint type). Depending on the joint type of each pair of mating surfaces in the workpiece/part-holder assembly, different parameters of the link torsors are defined [32]. Some of these torsors

Table 4.2: SDTs (link torsors) according to the joint type of mating surfaces.

| Joint type | Link torsor | Joint type | Link torsor |
|---|---|--|--|
|  Punctual | $\mathbf{T}_{H_{k,j},S_l} = \begin{Bmatrix} U & U \\ U & U \\ U & w \end{Bmatrix}$ |  Plane-Plane | $\mathbf{T}_{H_{k,j},S_l} = \begin{Bmatrix} \alpha & U \\ \beta & U \\ U & w \end{Bmatrix}$ |
|  Cyl-Cyl | $\mathbf{T}_{H_{k,j},S_l} = \begin{Bmatrix} \alpha & u \\ \beta & v \\ U & U \end{Bmatrix}$ |  Rigid pair | $\mathbf{T}_{H_{k,j},S_l} = \begin{Bmatrix} \alpha & u \\ \beta & v \\ \gamma & w \end{Bmatrix}$ |

are shown in Table 4.2. The methodology used to obtain the values of the link parameters for a generic workpiece/part-holder assembly (over-constrained or isostatic assembly) is shown in detail in [33]. Note that Eq. (4.20) should be accomplished for any pair of locating datum and part-holder surfaces S_l and $H_{k,j}$ that define the workpiece/part-holder assembly. In case that the positioning is over-constrained, the hierarchy of the connection links (i.e. the order of placement between part and fixture and the degrees of freedom constrained by each link -primary, secondary and tertiary datums-) is considered to obtain the so-called compatibility equations for Eq. (4.20), so a unique positioning deviation of the workpiece $\mathbf{T}_{F_k,D}$ is evaluated.

- Machining deviation: machining deviation, expressed as the SDT \mathbf{T}_{F_k,S_i} for machining station k , is the deviation of the machining operation (M_{k,o_i} that generates surface S_i) w.r.t. the machine-tool setup (i.e., F_k) and it is formulated as:

$$\mathbf{T}_{F_k,S_i} = \mathbf{T}_{F_k,M_{k,o_i}} = \mathbf{T}_{F_k,M_{k,o}} + \mathbf{T}_{M_{k,o},M_{k,o_i}}, \quad (4.21)$$

where $\mathbf{T}_{F_k,M_{k,o}}$ is the SDT of the o th machining operation due to geometrical-kinematic variations and thermal distortions of the machine-tool; $\mathbf{T}_{M_{k,o},M_{k,o_i}}$ is the SDT of the machining operation due to cutting-tool wear or cutting force-induced deviations when machining the surface S_i . It is considered that \mathbf{T}_{F_k,S_i} is equal to $\mathbf{T}_{F_k,M_{k,o_i}}$, that is to say, that there is an identity between the surface generated by the machining operation and the surface machined on the part. Note that the parameters of the torsors $\mathbf{T}_{F_k,M_{k,o}}$ and $\mathbf{T}_{M_{k,o},M_{k,o_i}}$ and their constraints (maximum values) represent the machine-tools and tooling capabilities (i.e., maximum expected deviations of the cutting-tool path due to machining inaccuracies). The torsor $\mathbf{T}_{F_k,M_{k,o_i}}$ will be defined according to the type of surface geometry generated and the capability of the manufacturing process. For instance, for a face milling operation that generates a planar surface parallel to the machine-tool table, the following torsor

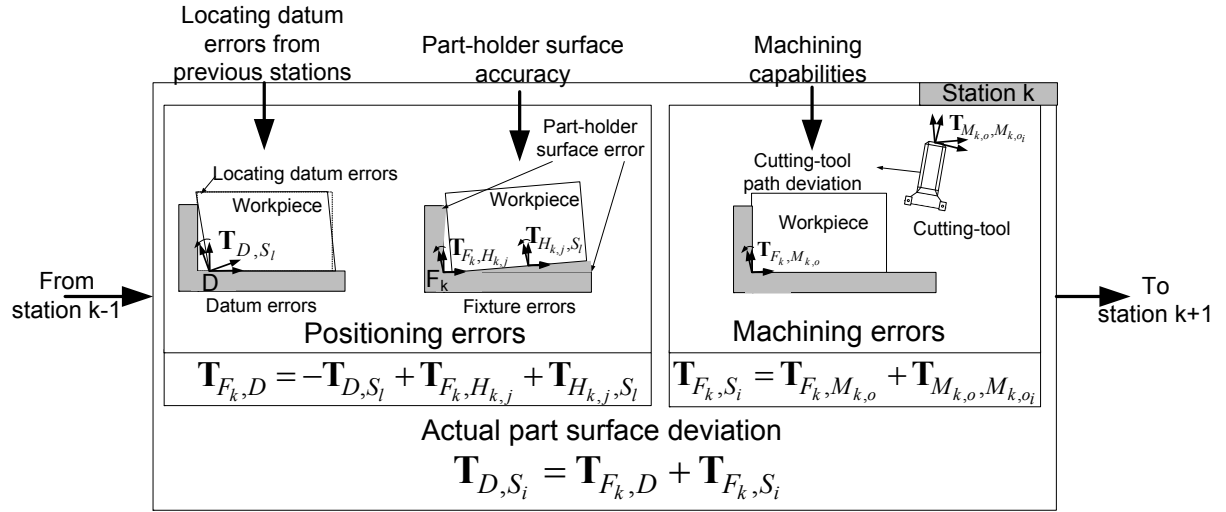


Figure 4.6: Model of Manufactured Part throughout the MMP.

will be defined:

$$\mathbf{T}_{F_k, M_{k,o_i}} = \begin{Bmatrix} \alpha_{M_i}^k & U \\ \beta_{M_i}^k & U \\ U & w_{M_i}^k \end{Bmatrix}, \quad (4.22)$$

where $w_{M_i}^k$, $\alpha_{M_i}^k$ and $\beta_{M_i}^k$ are machining deviations (translation and orientation deviations).

According to the positioning deviation and the machining deviation, the deviation of the part surface in a single setup is defined by the SDT \mathbf{T}_{D, S_i} , and it can be evaluated as follows:

$$\mathbf{T}_{D, S_i} = -\mathbf{T}_{F_k, D} + \mathbf{T}_{F_k, S_i}. \quad (4.23)$$

Note that the resulting torsors \mathbf{T}_{D, S_i} , $\mathbf{T}_{D, S_{i+1}}$, ... related to the i th, $(i+1)$ th, ... machining features at one station may be used as inputs in subsequent stations if these features are used as locating datums. Thus, the deviations of machined surfaces are propagated in the subsequent stations through the SDT $\mathbf{T}_{F_k, D}$. As shown in Figure 4.6, the station-by-station evaluation of all torsors defines the MoMP.

4.3.2 Virtual part quality measurement and verification

The formulation of the MoMP ends with the inclusion of the virtual inspection of the part using a virtual gauge. The virtual gauge is a perfect gauge made up of positioning surfaces and tolerance zone surfaces. The gauge and the resulting part from the MoMP are assembled and, similar to the assembly process of the workpiece/part-holder in the machining setup, a positioning deviation can be defined when the virtual inspection is conducted (see Figure 4.7). For the virtual gauge, the gauge CS G and gauge surfaces

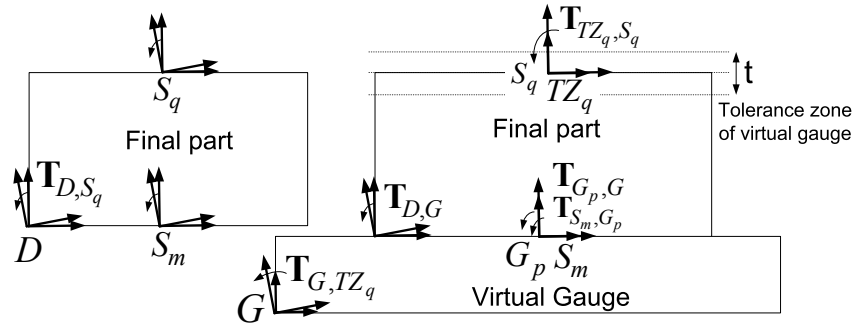


Figure 4.7: Virtual gauge and SDTs in virtual inspection.

are defined, the p th gauge surface being defined as G_p . The gauge positioning deviation is defined as:

$$\mathbf{T}_{D,G} = -\mathbf{T}_{G,G_p} + \mathbf{T}_{D,S_m} + \mathbf{T}_{S_m,G_p}, \quad (4.24)$$

where torsor \mathbf{T}_{G,G_p} indicates the deviation of the positioning surface p of the gauge and the maximum values of the parameters of this torsor represent the gauge precision (if we assume the inaccuracy of the gauge to be negligible, $\mathbf{T}_{G,G_p} = \{\mathbf{0}_{3 \times 1} \quad \mathbf{0}_{3 \times 1}\}$); torsor \mathbf{T}_{D,S_m} represents the deviation of the measurement datum surface S_m ; and the link torsor \mathbf{T}_{S_m,G_p} represents the relative position between S_m and the positioning gauge surface G_p , which depends on the part/gauge assembly condition (joint type).

After assembling the gauge and the final part, the functional tolerance compliance is verified by measuring the signed distance between the virtual gauge and the inspected surface S_q . This distance is evaluated at the boundary points of the tolerated surface projected along the inspection direction, obtaining the distance Gap_r for each r th boundary point. To calculate the Gap_r distance, first, the deviation between the inspected surface and its tolerance zone (defined as TZ_q) should be calculated. This deviation is expressed with the SDT \mathbf{T}_{TZ_q,S_q} , and it is evaluated following the Eq. (4.25) (see Ref. [34]):

$$\mathbf{T}_{TZ_q,S_q} = -\mathbf{T}_{D,G} + \mathbf{T}_{D,S_q} - \mathbf{T}_{G,TZ_q}, \quad (4.25)$$

where \mathbf{T}_{D,S_q} represents the deviation of the surface to be inspected S_q and \mathbf{T}_{G,TZ_q} is the deviation of the tolerance zone of the inspected surface w.r.t. the gauge CS, which is assumed to be $\{\mathbf{0}_{3 \times 1} \quad \mathbf{0}_{3 \times 1}\}$ if gauge errors are negligible. Considering the SDT \mathbf{T}_{TZ_q,S_q} as follows:

$$\mathbf{T}_{TZ_q,S_q} = \left\{ \begin{array}{c} \Omega_{TZ_q,S_q} \\ \mathbf{D}_{TZ_q,S_q} \end{array} \right\}, \quad (4.26)$$

the SDT that defines the deviation of the r th boundary point of the tolerated surface S_q is expressed as:

$$\mathbf{T}_{TZ_q,P_r} = \left\{ \begin{array}{c} \Omega_{TZ_q,P_r} \\ \mathbf{D}_{TZ_q,P_r} \end{array} \right\} = \left\{ \begin{array}{c} \Omega_{TZ_q,S_q} \\ \mathbf{D}_{TZ_q,S_q} + \Omega_{TZ_q,S_q} \times \mathbf{t}_{P_r}^{S_q} \end{array} \right\}, \quad (4.27)$$

where $\mathbf{t}_{P_r}^{S_q}$ is the translation vector from S_q to P_r , and \times is the cross product operator. By knowing the SDT \mathbf{T}_{TZ_q, P_r} , the deviation of the r th point of the toleranced surface along the direction of part verification, defined by the vector $\mathbf{n} = [n_x, n_y, n_z]^T$, is evaluated by the expression:

$$\left[\mathbf{T}_{TZ_q, P_r} \right]_{\mathbf{n}} = \mathbf{n} \cdot \mathbf{D}_{TZ_q, P_r}. \quad (4.28)$$

Analyzing the distance between the point deviation and the tolerance zone, the gap distance defined as Gap_r is formulated as:

$$Gap_r = \min \left(\tau + \left[\mathbf{T}_{TZ_q, P_r} \right]_{\mathbf{n}}, \tau - \left[\mathbf{T}_{TZ_q, P_r} \right]_{\mathbf{n}} \right) \quad (4.29)$$

where τ is the maximum deviation of the r th boundary point according to the tolerance value. The r th boundary point of the inspected surface will be within the tolerance zone if Gap_r remains positive or null.

In a similar way to the virtual verification by the SoV model, the virtual measurement and verification by the MoMP can be conducted following two main approaches: the worst-case approach and the statistical approach. For each approach, the resulting estimation is derived as follows:

- Worst-case approach:

Villeneuve and Vignat [35] reported that for a worst-case analysis, the tolerance compliance is conducted by solving an optimization problem in which the minimum gap distance from Eq. (4.29) at all boundary points of the toleranced surface is evaluated. This optimization problem is defined as:

$$Gap_{wc} = \min_{DM, DH, LHP}^{CM, CH, CGP} \left(\max_{LGP}^{CGP} (Gap_{min}) \right), \quad (4.30)$$

where

$$Gap_{min} = \min (Gap_r), \quad \forall r \in \text{boundary points}. \quad (4.31)$$

In Eq. (4.30), the term Gap_{min} is the minimum distance between the virtual gauge and the toleranced surface inspected after measuring the distance at all boundary points. The expression $\max_{LGP}^{CGP} (Gap_{min})$ defines the inspection process, where the gauge is assembled with the part according to the standard ISO or ASME tolerance specifications shown in the design drawings. The resulting assembly depends on how the part is inspected (defined by the link parameters denoted as LGP, which are the parameters of the torsi \mathbf{T}_{S_m, G_p}) and the positioning limits defined by the constraints of the positioning algorithm (denoted as CGP), as explained in [33]. Within the limits of these displacements, the most favorable position for the virtual gauge relative to the part can be found by maximizing the Gap_{min} value. In Eq. (4.30), material condition modifiers or incomplete datum frames can be considered in the tolerance verification, since they are related to the link parameters LGP of the gauge/part assembly and the positioning constraints CGP. The term $\min_{DM, DH, LHP}^{CM, CH, CGP} (\cdot)$ is the search expression of the worst-case combination of the manufacturing defects DM,

DH, LHP (machining, part-holder, and workpiece-fixtured assembly deviations, respectively) within the estimated range of variations expressed by the constraints CM, CH, CHP (machining, part-holder, and workpiece-fixtured assembly constraints, respectively, which are related to machine-tool and fixture capabilities and workpiece-fixtured configurations). According to this worst-case analysis, a process plan will be considered able to satisfy the functional tolerance if Gap_{wc} remains positive or null, which means that the deviation of the inspected surface is within the tolerance zone defined in the part drawing.

- Statistical approach: As reported above, the worst-case search is defined in Eq. (4.30) by the term $\min_{DM, DH, LHP}^{CM, CH, CHP}(\cdot)$. For a statistical analysis, instead of conducting a search for the worst-case combination, a large number of simulations are conducted in which the sources of variation DM, DH, LHP (machining, part-holder, and workpiece-fixtured assembly deviations, respectively) are simulated following a specific probability distribution function. For each simulation, the Gap_{min} is evaluated. After running thousands of simulations, the resulting probability distribution of the variable Gap_{min} defines whether, statistically, the parts comply with the functional tolerances [36].

4.3.3 Main applications

Basically, four main applications of the MoMP can be distinguished: part quality estimation, process planning, tolerance transfer and manufacturing tolerance synthesis.

Part quality estimation and process planning

In part quality estimation, the effect of individual variations along the manufacturing process (e.g., part-holder surface deviations and machining deviations) on functional part features is studied in order to check if parts are within specifications, ensuring product functionality. In general, the purpose of part quality estimation is the geometric product validation when designing MMPs. Villeneuve *et al.* [30] presented the MoMP and derived the equations to be applied for part quality estimation considering manufacturing process variations. The mathematical derivation was defined for milling operations, taking into account both isostatic and hyperstatic fixtures, the latter with a specific hierarchy of positioning surfaces (primary, secondary and tertiary positioning surfaces). Similar research but applied to turning processes was conducted by Vignat *et al.* [37], where they adapted the MoMP to turning processes considering the vibration effects and the rotation defect of the lathe to be negligible.

The estimation of part quality according to a specific MMP configuration helps the designer to select the most appropriate process plan (machining processes and production equipment) that ensures part specifications subjected to various criteria such as cost, time, and quality [38]. In this field, Nejad *et al.* [34] proposed the use of the MoMP for a rapid and accurate evaluation of alternative candidate process plans. Similar work was carried out by Louati *et al.* [39], who applied the MoMP to conduct a sensitivity analysis and

select, from a group of fixture candidates based on 3-2-1 fixture schemes, the one with the highest robustness to manufacturing disturbances.

Tolerance transfer and manufacturing tolerance synthesis

Tolerance transfer is intended to determine the intermediate geometrical and dimensional states of the part during its manufacturing process [40]. The manufacturing dimensions serve to satisfy not only the functional requirements given in the definition drawing, but also the manufacturing constraints (e.g., limitations of fixture and machine-tool accuracy). The basic idea of tolerance transfer is to convert functional (or design) tolerances into manufacturing tolerances, i.e., the tolerances of intermediate working dimensions throughout the MMP, including the identification of the defect parameters to be limited for each manufacturing setup and their corresponding ISO tolerances. The derived tolerances should guarantee the functional tolerances of the part and minimize the cost of the manufacturing process. In this field, Vignat and Villeneuve [41] studied the influence of each manufacturing defect on the final part quality in a turning process and, depending on the set of defects analyzed, they proposed a set of ISO tolerances for the workpieces at each station throughout the MMP that ensure part specifications.

On the other hand, manufacturing tolerance synthesis seeks to define the admissible variability of the manufacturing tools that are used in the manufacturing process such as machine-tools, cutting-tools, fixtures, etc., in order to ensure that the final part quality will be within specifications. In the literature there is no research work directly dealing with this topic applying the MoMP. However, its resolution is similar to the tolerance transfer problem, but being focused on manufacturing tools instead of intermediate workpiece states.

4.4 Modeling examples

4.4.1 Modeling example: SoV model

For illustrative purposes of the SoV model derivation, consider the part design and its associated raw material shown in Figure 4.8, and the 2-station machining process used in the manufacturing process shown in Figure 4.9. In order to evaluate the final part variability due to both fixture- and machining-induced deviations, the SoV methodology was applied. The methodology used to derive the SoV model can be summarized in the following steps:

- Step 1: Define the CSs of fixtures and part surfaces. The CS of reference from design is defined as the Design CS, denoted as D , the local CSs of part surfaces are defined as $\{S_1, \dots, S_7\}$, and the fixture CS is defined as F_k , where k is the machining station. Part surface CSs and fixture CSs are defined w.r.t. D CS. For the case study, Tables 4.3 and 4.4 are defined.
- Step 2: Define the coordinates of fixture locators w.r.t. F_k , as it is also shown in Table 4.4.

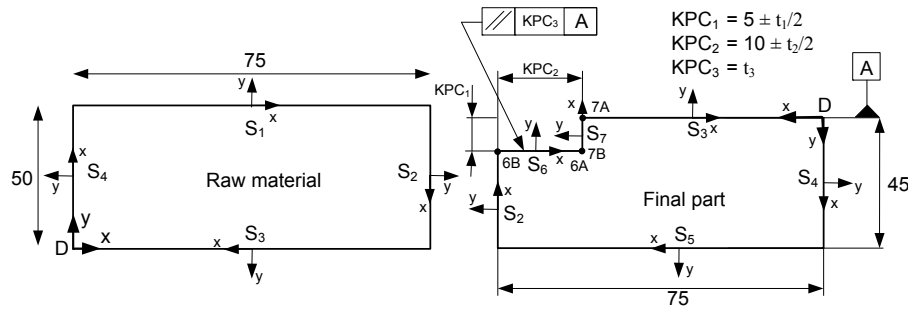


Figure 4.8: 2D case study. Raw material and part design. Dimensions in mm.

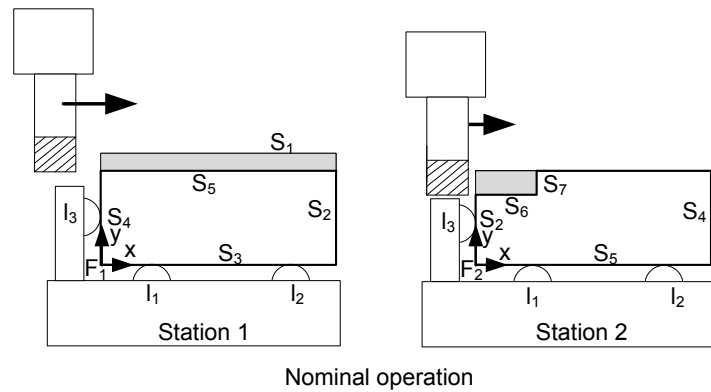


Figure 4.9: SoV example. Multi-station machining process used in the 2D case study.

- Step 3: For the first station, define the deviation of the raw part surfaces from nominal values. This means to derive the vector \mathbf{x}_0 , which is composed of the DMVs of all part features in their raw state. For the case study, $\mathbf{x}_0 = [\mathbf{x}_{0,1}^T, \mathbf{x}_{0,2}^T, \dots, \mathbf{x}_{0,7}^T]^T$. At the first station, only the raw surfaces can present an initial surface deviation, so only the DMVs $\{\mathbf{x}_{0,1}^T, \mathbf{x}_{0,2}^T, \mathbf{x}_{0,3}^T, \mathbf{x}_{0,4}^T\}$ should be defined, leaving the rest as $\mathbf{0}_{6 \times 1}$ vectors. Without loss of generality, we assume nominal values of raw material surfaces (initial surface deviations are negligible), so $\mathbf{x}_0 = \mathbf{0}_{42 \times 1}$.
- Step 4: For the k th station, derive the vector \mathbf{u}_k which defines the sources of errors due to fixture or machining deviations at the station k . For the case study, the vector \mathbf{u}_k is defined as $[(\mathbf{u}_k^f)^T, (\mathbf{u}_k^m)^T]^T$, where \mathbf{u}_k^f are the locator deviations at station k defined by $[\Delta l_{1y}^k, \Delta l_{2y}^k, \Delta l_{3x}^k]^T$, and Δl_{j*}^k refers to the deviation of the j th locator in the $*$ direction. \mathbf{u}_k^m are the machining deviations when machining surface i , defined by $[u_{M_i}^k, v_{M_i}^k, 0, 0, 0, \gamma_{M_i}^k]^T$, where $u_{M_i}^k$, $v_{M_i}^k$ and $\gamma_{M_i}^k$ refer to the translation deviation of the cutting-tool path along the X - and Y -axes, and orientation deviations around the Z -axis, respectively. Note that as we are assuming small deviations, it is only considered the locator deviation along the direction where the workpiece location is constrained (the influence of other small locator deviations on part quality is negligible). Appendix 4.4 shows the resulting matrices for the 2D case study.

Table 4.3: Nominal location and orientation of each local feature CS.

| Feature | $\varphi_{S_i}^{\circ D}$ (rad) | $\mathbf{t}_{S_i}^{\circ D}$ (mm) | Feature | $\varphi_{S_i}^{\circ D}$ (rad) | $\mathbf{t}_{S_i}^{\circ D}$ (mm) |
|---------|---------------------------------|-----------------------------------|---------|---------------------------------|-----------------------------------|
| S_1 | [0, 0, 0] | [37.5, 50, 0] | S_5 | [0, 0, 0] | [37.5, 45, 0] |
| S_2 | [0, 0, $\pi/2$] | [75, 25, 0] | S_6 | [0, 0, π] | [70, 5, 0] |
| S_3 | [0, 0, π] | [37.5, 0, 0] | S_7 | [0, 0, $\pi/2$] | [65, 2.5, 0] |
| S_4 | [0, 0, $-\pi/2$] | [0, 25, 0] | | | |

Table 4.4: Nominal location and orientation of F_k at each station. Position of locators is also shown.

| Fixture | $\varphi_{F_k}^{\circ D}$ (rad) | $\mathbf{t}_{F_k}^{\circ D}$ (mm) | Locators w.r.t. F_k (mm) |
|---------|---------------------------------|-----------------------------------|---|
| F_1 | [0, 0, 0] | [0, 0, 0] | $l_{1x} = 25, l_{1y} = 0, l_{2x} = 50, l_{2y} = 0, l_{3x} = 0, l_{3y} = 22.5$ |
| F_2 | [0, 0, π] | [75, 45, 0] | $l_{1x} = 25, l_{1y} = 0, l_{2x} = 50, l_{2y} = 0, l_{3x} = 0, l_{3y} = 22.5$ |

- Step 5: For each k station, derive the matrices $\mathbf{A}_k, \mathbf{B}_k$. Please, refer to Appendix 4.3 for deriving the SoV matrices. Appendix 4.4 shows the resulting matrices for the case study.
- Step 6: Derive the matrix \mathbf{C}_K , where K is the inspection station. Please, refer to Appendix 4.3 for deriving the SoV matrices. Appendix 4.4 shows the resulting matrices for measuring KPC_1 - KPC_3 and KPC_2 in the case study.
- Step 7: For each KPC, evaluate the deviation of the boundary points of each tolerated surface w.r.t. the measurement datum by Eqs. (4.10) and (4.11).

Symbolic resolution

By applying the SoV model in the 2D case study, the resulting deviation of each KPC due to fixture- and machining-induced deviations is defined as follows:

- KPC_1 : the deviation of the KPC_1 is defined as

$$KPC_1 = \max \left(\left| \left[\mathbf{y}_{3,P_{6A}} \right]_{\mathbf{y}} \right|, \left| \left[\mathbf{y}_{3,P_{6B}} \right]_{\mathbf{y}} \right| \right), \quad (4.32)$$

where these deviations are related to fixture and machining deviations as:

$$\begin{aligned} \left[\mathbf{y}_{3,P_{6A}} \right]_{\mathbf{y}} &= -27.5\gamma_{M_5}^1 + 5\gamma_{M_6}^2 - 1.6\Delta l_{1y}^2 + 0.6\Delta l_{2y}^2 - 0.6\Delta l_{1y}^1 + 1.6\Delta l_{2y}^1 \\ &\quad - v_{M_5}^1 + v_{M_6}^2, \end{aligned} \quad (4.33)$$

$$\left[\mathbf{y}_{3,P_{6B}} \right]_{\mathbf{y}} = -37.5\gamma_{M_5}^1 - 5\gamma_{M_6}^2 - 2\Delta l_{1y}^2 + 2\Delta l_{2y}^1 + \Delta l_{2y}^2 - \Delta l_{1y}^1 - v_{M_5}^1 + v_{M_6}^2. \quad (4.34)$$

Note that most of the deviations at the first station are propagated downstream, thus affecting the KPC_1 . However, note also that locator deviations Δl_{3x}^1 and Δl_{3x}^2

and machining deviations along the X direction ($u_{M_5}^1$ and $u_{M_6}^2$) do not influence KPC_1 .

- KPC_2 : the deviation of the KPC_2 is defined as

$$KPC_2 = \max \left(\left| \left[\mathbf{y}_{4,P_{7A}} \right]_{\mathbf{y}} \right|, \left| \left[\mathbf{y}_{4,P_{7B}} \right]_{\mathbf{y}} \right| \right), \quad (4.35)$$

where

$$\begin{aligned} \left[\mathbf{y}_{4,P_{7A}} \right]_{\mathbf{y}} &= +22.5\gamma_{M_5}^1 + 2.5\gamma_{M_7}^2 + 0.9\Delta l_{1y}^1 - 0.9\Delta l_{2y}^1 - 0.9\Delta l_{2y}^2 + 0.9\Delta l_{1y}^2 \\ &\quad + \Delta l_{3x}^2 - u_{M_7}^2, \end{aligned} \quad (4.36)$$

$$\begin{aligned} \left[\mathbf{y}_{4,P_{7B}} \right]_{\mathbf{y}} &= +17.5\gamma_{M_5}^1 - 2.5\gamma_{M_7}^2 + 0.7\Delta l_{1y}^1 - 0.7\Delta l_{2y}^1 - 0.7\Delta l_{2y}^2 + 0.7\Delta l_{1y}^2 \\ &\quad + \Delta l_{3x}^2 - u_{M_7}^2. \end{aligned} \quad (4.37)$$

In this case, note that the locator deviations Δl_{3x}^1 do not influence this KPC, although the same locator deviation at station 2 (Δl_{3x}^2) does exert an influence. Furthermore, only machining deviations when milling surface S_7 have an influence on the KPC (except deviation $v_{M_7}^2$), and the machining deviations when milling surfaces S_6 and S_5 have no influence at all.

- KPC_3 : the deviation of KPC_3 is defined as

$$KPC_3 = \left| \left[\mathbf{y}_{3,P_{6A}} \right]_{\mathbf{y}} - \left[\mathbf{y}_{3,P_{6B}} \right]_{\mathbf{y}} \right|, \quad (4.38)$$

where $\left[\mathbf{y}_{3,P_{6A}} \right]_{\mathbf{y}}$ and $\left[\mathbf{y}_{3,P_{6B}} \right]_{\mathbf{y}}$ are defined by Eqs. (4.33) and (4.34) respectively. By substitution, the deviation of KPC_3 is defined as $|10\gamma_{M_5}^1 + 10\gamma_{M_6}^2 + 0.4\Delta l_{1y}^1 - 0.4\Delta l_{2y}^1 - 0.4\Delta l_{2y}^2 + 0.4\Delta l_{1y}^2|$. Note that, since this KPC is a relationship of parallelism, locator deviations Δl_{3x}^1 and Δl_{3x}^2 , and translational machining deviations at any station do not exert an influence.

Numerical resolution

The case study is numerically solved by analyzing both the worst-case and the statistical approaches. The expected variability range for each manufacturing process variable is shown in Table 4.5 and all manufacturing process variables are assumed to be independent from each other. For the statistical analysis, the manufacturing process variables are assumed to be distributed normally and the ranges shown in Table 4.5 cover the 6σ interval. Furthermore, the worst-case is also resolved using a CAD software application. The prediction of the deviation of each KPC is shown in Table 4.6 depending on the type of analysis conducted.

4.4.2 Modeling example: MoMP model

For illustrative purposes, the same 2D case study shown in Figure 4.8 is used to describe the use of the MoMP. Unlike the previous example, the current 2-station manufacturing process applies fixture surfaces instead of fixture locators, as shown in Figure 4.10,

Table 4.5: Ranges of locators and machining deviations for the SoV case study. Dimensional deviations in *mm*, angular deviations in *rad*.

| Station 1 | | | | | | | | | | | |
|-------------------|------------|-------------------|------------|-------------------|-------------|-------------|------------|-------------|------------|------------------|-------------|
| Δl_{1y}^1 | ± 0.02 | Δl_{2y}^1 | ± 0.02 | Δl_{3x}^1 | ± 0.02 | $u_{M_5}^1$ | ± 0.01 | $v_{M_5}^1$ | ± 0.01 | $\gamma_{M_5}^1$ | ± 0.001 |
| Station 2 | | | | | | | | | | | |
| Δl_{1y}^2 | ± 0.02 | Δl_{2y}^2 | ± 0.02 | Δl_{3x}^2 | ± 0.02 | $u_{M_6}^2$ | ± 0.01 | $v_{M_6}^2$ | ± 0.01 | $\gamma_{M_6}^2$ | ± 0.001 |
| $u_{M_7}^2$ | ± 0.01 | $v_{M_7}^2$ | ± 0.01 | $\gamma_{M_7}^2$ | ± 0.001 | | | | | | |

Table 4.6: Numerical resolution according to the worst-case and the statistical analyses for the SoV case study. Dimensions in *mm*.

| | KPC_1 | KPC_2 | KPC_3 |
|-----------------------------------|-------------|-------------|-------------|
| Worst-case (CAD) | ± 0.183 | ± 0.127 | ± 0.051 |
| Worst-case | ± 0.182 | ± 0.127 | ± 0.052 |
| Statistical (6σ interval) | ± 0.075 | ± 0.048 | ± 0.021 |

since this modeling approach allows surface-based fixtures to be modeled. The MoMP is built by applying a methodology composed of the following steps (the resulting SDTs are summarized in Appendix 4.5):

- Step 1: Define the CSs for parts, fixtures, gauge, part surfaces, fixture surfaces and gauge surfaces. Design CS is defined as D ; local CSs of part surfaces are defined as $\{S_1, \dots, S_7\}$; fixture CS is defined as F_k ; local CSs of the j th fixture or part-holder surface is defined as $H_{k,j}$; gauge CS is defined as G ; and local CS of the p th gauge surface is defined as G_p . Part surface CSs and fixture and gauge CSs are defined w.r.t. the D CS. For this example, Tables 4.3 (the same as in the SoV example), 4.7 and 4.8 apply.
- Step 2: Define the coordinates of fixture surfaces w.r.t. the fixture CS and the coordinates of gauge surfaces w.r.t. the G CS. For the case study, Tables 4.7 and 4.8 also show this information.
- Step 3: For the first station, define the SDTs of the raw surfaces expressed in the CS D . This means to derive the SDTs $\{\mathbf{T}_{D,S_l}\}_D$. Without loss of generality, we assume nominal values of raw material surfaces, so $\{\mathbf{T}_{D,S_l}\}_D = \{\mathbf{0}_{3 \times 1} \quad \mathbf{0}_{3 \times 1}\}$ for $l = 1, 2, 3$ and 4.
- Step 4: For the next k th machining station (starting from station 1), derive the following torsors:
 - SDT associated to part-holder deviation according to fixture accuracy, expressed in the D CS ($\{\mathbf{T}_{F_k, H_{k,j}}\}_D$).
 - SDT associated to each joint workpiece/part-holder according to how the part is located and fixed in the fixture setup, expressed in the D CS ($\{\mathbf{T}_{H_{k,j}, S_l}\}_D$).

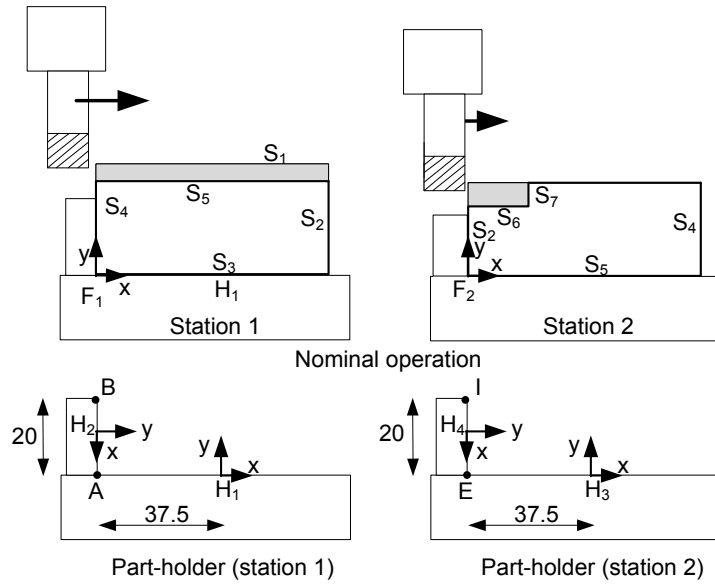


Figure 4.10: MoMP example. Multi-station machining process to manufacture the 2D example. Dimensions in *mm*.

- SDT associated to surface deviations acting as locating datums, which are obtained from surface deviations in previous stations, expressed in the D CS ($\{\mathbf{T}_{D,S_i}\}_D$).
- Step 5: Derive the positioning deviation torsor $\{\mathbf{T}_{F_k,D}\}_D$ by Eq. (4.20) following the methodology shown in [33], taking into account the datum hierarchy (primary and secondary datums).
- Step 6: Derive the machining deviation torsor $\{\mathbf{T}_{F_k,M_k,o_i}\}_{F_k}$ by Eq. (4.21) according to the machine-tool precision.
- Step 7: Derive the torsor $\{\mathbf{T}_{D,S_i}\}_D$ by Eq. (4.23).
- Step 8: Repeat steps 4-7 for all machining stations. Note that some SDTs in one station depend on other SDTs from previous stations, so the resolution of the problem should be station-by-station, starting from upstream stations and propagating the results to downstream stations.
- Step 9: To measure the deviation of the KPCs by a virtual gauge, derive the following torsors:
 - SDT associated to gauge surface deviation according to gauge accuracy, expressed in the D CS ($\{\mathbf{T}_{G,G_p}\}_D$). Without loss of generality, we can assume this deviation to be negligible, so $\{\mathbf{T}_{G,G_p}\}_D = \{\mathbf{0}_{3 \times 1} \quad \mathbf{0}_{3 \times 1}\}$.
 - SDT associated to each joint part/gauge-surface according to how the part is located and fixed in the inspection station, expressed in the D CS ($\{\mathbf{T}_{S_m,G_p}\}_D$).

Table 4.7: Nominal location and orientation of F_k w.r.t. D , and nominal location and orientation of fixture surfaces w.r.t. F_k .

| Fixture | $\varphi_{F_k}^{\circ D}$ (rad) | $\mathbf{t}_{F_k}^{\circ D}$ (mm) | Fixture Surface | $\varphi_{H_j}^{F_k}$ (rad) | $\mathbf{t}_{H_j}^{F_k}$ (mm) |
|---------|---------------------------------|-----------------------------------|-------------------|-----------------------------|-------------------------------|
| F_1 | [0, 0, 0] | [0, 0, 0] | H_1 (primary) | [0,0,0] | [37.5,0,0] |
| | | | H_2 (secondary) | [0,0, $\pi/2$] | [0,10,0] |
| F_2 | [0, 0, π] | [75, 45, 0] | H_3 (primary) | [0,0,0] | [37.5,0,0] |
| | | | H_4 (secondary) | [0,0, $\pi/2$] | [0,10,0] |

Table 4.8: Nominal location and orientation of G w.r.t. D , and nominal location and orientation of gauge surfaces w.r.t. G . Only primary datum surfaces are necessary for inspecting KPC_1 , KPC_2 and KPC_3 .

| KPC inspected | $\varphi_G^{\circ D}$ (rad) | $\mathbf{t}_G^{\circ D}$ (mm) | Gauge Surface | $\varphi_{G_p}^G$ (rad) | $\mathbf{t}_{G_p}^G$ (mm) |
|---------------------|-----------------------------|-------------------------------|---------------|-------------------------|---------------------------|
| KPC_1 and KPC_3 | [0, 0, 0] | [0, 0, 0] | G_1 | [0,0,0] | [37.5,0,0] |
| KPC_2 | [0, 0, $\pi/2$] | [75, 45, 0] | G_2 | [0,0,0] | [-25,0,0] |

- SDT associated to surface deviations that act as measurement datums, which are obtained from surface deviations in previous stations, expressed in the D CS ($\{\mathbf{T}_{D,S_m}\}_D$).

By these SDTs and applying Eq. (4.24), the positioning deviation torsor for the gauge/part assembly ($\{\mathbf{T}_{D,G}\}_D$) can be evaluated. Then, the deviation torsor between the actual toleranced surface and its tolerance zone is evaluated by Eq. (4.25). Finally, the deviation of each r th boundary point of the toleranced surface from its nominal value is evaluated by Eq. (4.29).

Symbolic resolution

Following this methodology, the final part variability of each KPC due to fixture- and machining-induced deviations can be obtained. For the 2D case study shown in Figure 4.10, the resulting torsor of positioning deviation at each station depends on the contact between the part and the secondary part-holder surface. In fact, there are different possible workpiece/fixture configurations, since the workpiece can be located in the X direction by making contact at point B or A at station 1, and point I or E at station 2, assuming no form error exists. The point at which the workpiece contacts the secondary part-holder surface depends on the deviations of the part-holder and workpiece surfaces. For the 2D case study, contact at point B at the first station and at point I at the second station occurs if, applying the resolution of the generic positioning problem shown in [33], Eqs. (4.39) and (4.40) apply for station 1 and 2 respectively.

$$\gamma_{H_2,S_4}^1 = (\gamma_{H_1}^1 - \gamma_{H_2}^1) > 0, \quad (4.39)$$

$$\gamma_{H_4,S_2}^2 = (\gamma_{H_3}^2 - \gamma_{M_5}^1 + \gamma_{H_1}^1 - \gamma_{H_4}^2) > 0. \quad (4.40)$$

If Eqs. (4.39) and (4.40) hold, the deviation of the joint workpiece/fixture at the secondary locating datum in the X direction (expressed in the fixture CS) at each station

is defined as:

$$v_{H_2, S_4}^1 = -p_B^{F_1} \cdot (\gamma_{H_1}^1 - \gamma_{H_2}^1), \quad (4.41)$$

$$v_{H_4, S_2}^2 = -p_I^{F_2} \cdot (\gamma_{H_3}^2 - \gamma_{M_5}^1 + \gamma_{H_1}^1 - \gamma_{H_4}^2). \quad (4.42)$$

For these workpiece/fixture configurations at station 1 and 2, the resulting final part variability is defined as follows:

- KPC_1 : the deviation of KPC_1 is defined as

$$KPC_1 = \max \left(\left| \left[\mathbf{T}_{TZ_1, P_{6A}} \right]_{\mathbf{y}} \right|, \left| \left[\mathbf{T}_{TZ_1, P_{6B}} \right]_{\mathbf{y}} \right| \right), \quad (4.43)$$

where

$$\left[\mathbf{T}_{TZ_1, P_{6A}} \right]_{\mathbf{y}} = -v_{H_1}^1 + v_{M_5}^1 + v_{H_3}^2 - v_{M_6}^2 - 5\gamma_{M_6}^2 + 27.5 \cdot (\gamma_{M_5}^1 - \gamma_{H_3}^2 - \gamma_{H_1}^1), \quad (4.44)$$

$$\left[\mathbf{T}_{TZ_1, P_{6B}} \right]_{\mathbf{y}} = -v_{H_1}^1 + v_{M_5}^1 + v_{H_3}^2 - v_{M_6}^2 + 5\gamma_{M_6}^2 + 37.5 \cdot (\gamma_{M_5}^1 - \gamma_{H_3}^2 - \gamma_{H_1}^1), \quad (4.45)$$

Note that deviations of part-holder surfaces H_2 and H_4 do not influence this KPC.

- KPC_2 : the deviation of KPC_2 is defined as

$$KPC_2 = \max \left(\left| \left[\mathbf{T}_{TZ_2, P_{7A}} \right]_{\mathbf{y}} \right|, \left| \left[\mathbf{T}_{TZ_2, P_{7B}} \right]_{\mathbf{y}} \right| \right), \quad (4.46)$$

where

$$\left[\mathbf{T}_{TZ_2, P_{7A}} \right]_{\mathbf{y}} = -v_{H_4}^2 - v_{M_7}^2 - 10\gamma_{H_4}^2 - 2.5\gamma_{M_7}^2 - 25 \cdot (\gamma_{M_5}^1 - \gamma_{H_3}^2 - \gamma_{H_1}^1), \quad (4.47)$$

$$\left[\mathbf{T}_{TZ_2, P_{7B}} \right]_{\mathbf{y}} = -v_{H_4}^2 - v_{M_7}^2 - 10\gamma_{H_4}^2 + 2.5\gamma_{M_7}^2 - 20 \cdot (\gamma_{M_5}^1 - \gamma_{H_3}^2 - \gamma_{H_1}^1) \quad (4.48)$$

In this case, note that deviations of the part-holder surface H_2 do not influence this KPC. Furthermore, the machining deviations of surface S_6 have no influence either.

- KPC_3 : the deviation of KPC_3 is defined as

$$KPC_3 = \left| \left[\mathbf{T}_{TZ_1, P_{6A}} \right]_{\mathbf{y}} - \left[\mathbf{T}_{TZ_1, P_{6B}} \right]_{\mathbf{y}} \right|, \quad (4.49)$$

where $\left[\mathbf{T}_{TZ_1, P_{6A}} \right]_{\mathbf{y}}$ and $\left[\mathbf{T}_{TZ_1, P_{6B}} \right]_{\mathbf{y}}$ are defined by Eq. (4.44) and (4.45) respectively.

By substitution, the deviation is defined as $|10\gamma_{M_5}^1 + 10\gamma_{M_6}^2 - 10\gamma_{H_3}^2 - 10\gamma_{H_1}^1|$. In a similar manner to the example shown previously, as this KPC is a relationship of parallelism, translational machining deviations at any station have no influence. Furthermore, deviations of part-holder surfaces H_1 and H_3 in the X or Y direction do not exert an influence, and only their orientation deviation has an influence on the relationship of parallelism.

Note that if Eqs. (4.39) and (4.40) do not apply, it means that the workpiece-fixture assembly is different from the configurations analyzed, and the resulting positioning deviation torsor varies. To analyze those cases, the same methodology shown above can be followed but the deviation of the joint workpiece/fixture at the secondary locating datum in X direction defined by Eqs. (4.41) and (4.42) should be re-evaluated considering points A and E as contact points between workpiece and part-holder at stations 1 and 2 respectively.

Numerical resolution

In a similar way to the SoV case study, the case study of the MoMP is solved numerically by analyzing the worst-case and the statistical approaches. The variability range for each manufacturing process variable is shown in Table 4.9. Unlike the SoV case study, where the variabilities of locators are independent from each other, in the MoMP the variability of a surface depends on different torsor parameters and those parameters are not independent from each other, since they are subjected to the geometrical/dimensional tolerance of the surface. For this case study, part-holder surfaces are planar and a planar size tolerance applies for each one.

The numerical resolution for the worst-case analysis requires a search algorithm. In this case study two algorithms are applied sequentially. Firstly, a genetic algorithm (GA) is used to find a region close to the optimal solution. Secondly, the solution provided by the GA is used as the starting point in a mesh adaptive direct search (MADS) algorithm for tuning the optimal solution. The resolution was repeated 10 times to ensure optimization convergence, so the global minimum reached provides the worst-case solution. The numerical resolution for the statistical analysis requires the evaluation of thousands of samples through Monte Carlo simulations. For this case study, 5,000 Monte Carlo simulations were run assuming that all torsor parameters are distributed normally with the 6σ ranges shown in Table 4.9 subjected to their tolerance constraints. Furthermore, the worst-case analysis was also solved using a CAD software. The prediction of each KPC is shown in Table 4.10 depending on the type of analysis conducted.

4.5 Comparison and discussion

Both SoV and MoMP models are based on engineering-driven approaches since they are built by using accurate process and product knowledge. Indeed, these models require comprehensive information about the product and the manufacturing process, such as the geometry of nominal part surfaces, manufacturing and fixture capabilities, geometric information about fixture configurations, placement of the inspection stations, capability of the inspection systems, and so forth. The large amount of a priori engineering knowledge required and its level of accuracy have an important impact on the robustness and reliability of the models, which might prevent their application in industry [42]. In fact, for a large-scale system it would be very difficult to build up a comprehensive physical model following the SoV or the MoMP derivation, and even if it was possible, the effect of small modeling errors and their propagation along a large number of stations can be an important source of inaccuracy that may lead to unreliable or misleading estimation

Table 4.9: Precision of part-holder surfaces (according to the planar tolerance size) and machined surfaces for the MoMP case study. Dimensional deviations in *mm*, angular deviations in *rad*.

| Station 1 | | | |
|--|---|----------------------------------|---|
| Precision of part-holder surface 1: $t = 0.1$ mm; torsor constraints: | $-\frac{0.1}{2} \leq v_{H_1}^1 + 37.5 \cdot \gamma_{H_1}^1 \leq +\frac{0.1}{2}$ | | |
| Precision of part-holder surface 2: $t = 0.02$ mm; torsor constraints: | $-\frac{0.02}{2} \leq v_{H_2}^1 + 10 \cdot \gamma_{H_2}^1 \leq \frac{0.02}{2}$ | | |
| Machining precision: | $-0.01 \leq u_{M_5}^1 \leq 0.01$ | $-0.01 \leq v_{M_5}^1 \leq 0.01$ | $-0.001 \leq \gamma_{M_5}^1 \leq 0.001$ |
| Station 2 | | | |
| Precision of part-holder surface 3: $t = 0.1$ mm; torsor constraints: | $-\frac{0.1}{2} \leq v_{H_3}^2 + 37.5 \cdot \gamma_{H_3}^2 \leq \frac{0.1}{2}$ | | |
| Precision of part-holder surface 4: $t = 0.02$ mm; torsor constraints: | $-\frac{0.02}{2} \leq v_{H_4}^2 + 10 \cdot \gamma_{H_4}^2 \leq \frac{0.02}{2}$ | | |
| Machining precision: | $-0.01 \leq u_{M_6}^2 \leq 0.01$ | $-0.01 \leq v_{M_6}^2 \leq 0.01$ | $-0.001 \leq \gamma_{M_6}^2 \leq 0.001$ |
| Machining precision: | $-0.01 \leq u_{M_7}^2 \leq 0.01$ | $-0.01 \leq v_{M_7}^2 \leq 0.01$ | $-0.001 \leq \gamma_{M_7}^2 \leq 0.001$ |

Table 4.10: Numerical resolution according to the worst-case and the statistical analyses for the MoMP case study. Dimensions in *mm*.

| | KPC_1 | KPC_2 | KPC_3 |
|-----------------------------------|-------------|-------------|-------------|
| Worst-case (CAD) | ± 0.163 | ± 0.114 | ± 0.047 |
| Worst-case | ± 0.162 | ± 0.114 | ± 0.047 |
| Statistical (6σ interval) | ± 0.091 | ± 0.037 | ± 0.018 |

results. However, for low- and medium-scale systems the application of SoV and MoMP models is highly recommended to eliminate downstream manufacturing problems and reduce ramp-up times.

Considering the modeling mechanism, both the SoV and MoMP models are based on kinematic chains and homogeneous transformation matrices. Both assume solid rigid parts and they cannot deal with form errors (intrinsic part tolerances), so they are focused on position and orientation errors (extrinsic part tolerances). However, some interesting differences can be found between both models that should be remarked on in order to select the most appropriate for each particular application.

The SoV model is preferred to the MoMP model when the applicability of the model is focused mainly on part quality improvement activities such as fault diagnosis, process diagnosability analysis, active control for variation reduction in flexible multi-station machining systems, and fixture maintenance planning. The derivation of the SoV model is, in the authors' opinion, more oriented toward multi-station systems due to the adoption of the state space model of control theory, and it is more easily automated due to its matrix formulation. Furthermore, the multi-station representation by the SoV model is clearer than that from the MoMP, and the inclusion of the inspection stations is also straight forward. The research work presented in [3], greatly facilitates the derivation of

the SoV model by the definition, step by step, of the matrices components. However, the application of the SoV model is still limited to MMPs with specific characteristics. Indeed, its application have been mainly conducted in milling operations with isostatic fixtures composed of six locators based on orthogonal 3-2-1 layouts. Although other configurations have been studied in [6], only fixtures based on locators (point-based fixtures) have been analyzed, thus leaving general fixture devices such as vises or 4-jaw chucks unaddressed [34].

The variation modeling tool used in the SoV model is the DMV, and it is used to model the three position and three orientation deviations of the local CS that is attached to any part surface. With this tool, the SoV model is oriented toward vectorial dimensioning and tolerancing (VD&T) specifications, and common product design specifications based on GD&T should be translated in order to be applied correctly, as shown in [7]. For virtual measurement and verification, the SoV model analyzes the deviation of the CS of the inspected surfaces, so their inspection is a point-based process similar to that conducted by a coordinate measuring machine. Virtual measurement and verification can be conducted for a worst-case or statistical analysis, but material conditioners for virtual verification are not considered. Both analyses are conducted in a straight forward manner by evaluating one single expression (without conducting a large number of simulations or using an optimization algorithm).

Unlike the SoV model, the MoMP is oriented toward product design activities. One of the main benefits of the MoMP is that the derivation of the manufacturing variations due to fixture devices is more generic and it can lead to the modeling of complex fixture devices such as vises or chucks. However, the methodology used to obtain the model is less straight forward than the SoV methodology, and it can be harder to apply if a large-medium number of stations is present. The variation modeling tool used in the MoMP is the SDT. The SDT models the deviation of the surface CS in a global frame constraining the deviations according to the tolerance specified in the surface. Therefore, tolerance zones can be modeled by an associated SDT as it is shown in [31]. This characteristic makes the MoMP friendlier for dealing with GD&T specifications than SoV models, although both models are in conformance with VD&T specifications due to their vectorial nature.

For virtual measurement and verification, the MoMP analyzes the deviation of the inspected surfaces through a virtual gauge. The inspection is therefore a surface-based process where the precision of the gauge system can be considered together with material conditioners or incomplete datum frames [37]. According to the accumulation of tolerance, the MoMP can conduct both worst-case and statistical analyses [37]. However, the worst-case analysis requires the resolution of a complex optimization problem where the overall minimum solution (and thus, the real worst-case solution) may not be reached. On the other hand, the statistical analysis requires time-consuming Monte Carlo simulations to infer the statistical results of the virtual inspection from thousands of simulated samples. Thus, the resolution of both worst-case and statistical analyses is quite complex in comparison with the same analysis conducted under the SoV model. This is because the SoV model includes the individual source of errors in the manufacturing process (e.g., in-

Table 4.11: Generic comparison of the SoV and the MoMP models.

| | SoV model | MoMP model |
|--------------------------------|---|--|
| Point of view | Process improvement | Product and manufacturing design |
| Standard conformance | VD&T and less friendly with GD&T | VD&T and more friendly with GD&T |
| Variation modeling tool | Differential motion vectors (DMV) applied to CS deviations expressed in local CSs | Small displacement torsors (SDT) applied to surface deviations expressed in global CSs |
| Worst-case analysis | ✓ | ✓ |
| Statistical analysis | ✓ | ✓* |
| Virtual inspection | Point-based as in coordinate measuring machine practices | Surface-based as in gauges practices |
| Material conditioners | X | ✓ |
| Form error modeling | X | X |
| Fixture devices | Isostatic fixtures based on locators. (Point-based fixtures) | Any type of fixture. (Surface-based fixtures) |

*: Through Monte Carlo simulations

dividual locator errors in isostatic fixture devices) which are independent from each other, whereas the MoMP models the deviations of surfaces by the SDT, whose parameters are not independent. In other words, the SoV model is applied only in simple isostatic fixture configurations based on locators, which greatly facilitates both worst-case and statistical analyses. For more complex fixtures, the SoV cannot be applied and the resolution should be conducted applying the MoMP. In fact, one important drawback of the MoMP is the complex resolution of the optimization problem shown in Eq. (4.30) for virtual measurement and verification.

4.6 Conclusions

The development of 3D manufacturing variation models for integrating product and manufacturing process design is essential to improve product development, eliminate downstream manufacturing problems, and reduce ramp-up times. In the literature, two main 3D manufacturing variation models in MMPs have been studied according to the nature of the problem to be analyzed: the Stream of Variation (SoV) model, and the Model of the Manufactured Part (MoMP). The SoV model has been developed to deal with product quality improvement whereas the MoMP has been developed to deal with product design activities. This chapter has presented both SoV and MoMP models, and their main characteristics and applications have been analyzed and compared. Furthermore, the methodology to derive both models has been described step-by-step by a simple 2D case study (applicable to any 3D part).

The SoV model will be extended in Chapter 6 incorporating specific machining-induced variations such as those due to geometric-kinematic variations, thermal distortions, cutting-tool deflexions, cutting-tool wear, etc. Furthermore, novel applications of the SoV model for quality improvement will be presented in detail in Chapters 7-9.

4.7 Appendix 4.1: Corollaries

Corollary 1: Consider the CS R , 1 and 2 as shown in Figure 4.11. Consider now that the CS 1 and 2 are deviated from nominal values. Noting the deviation of CS 1 w.r.t. R , expressed in vector form, as \mathbf{x}_1^R , and the deviation of CS 2 w.r.t. CS 1 as \mathbf{x}_2^1 , then the deviation of CS 2 w.r.t. R can be formulated in vector form as:

$$\mathbf{x}_2^R = \begin{pmatrix} (\mathbf{R}_{\circ 2}^{\circ 1})^T & -(\mathbf{R}_{\circ 2}^{\circ 1})^T \cdot (\hat{\mathbf{t}}_{\circ 2}^{\circ 1}) & \mathbf{I}_{3 \times 3} & \mathbf{0}_{3 \times 3} \\ \mathbf{0}_{3 \times 3} & (\mathbf{R}_{\circ 2}^{\circ 1})^T & \mathbf{0}_{3 \times 3} & \mathbf{I}_{3 \times 3} \end{pmatrix} \cdot \begin{pmatrix} \mathbf{x}_1^R \\ \mathbf{x}_2^1 \end{pmatrix} \quad (4.50)$$

This Corollary and its proof are also given in [3].

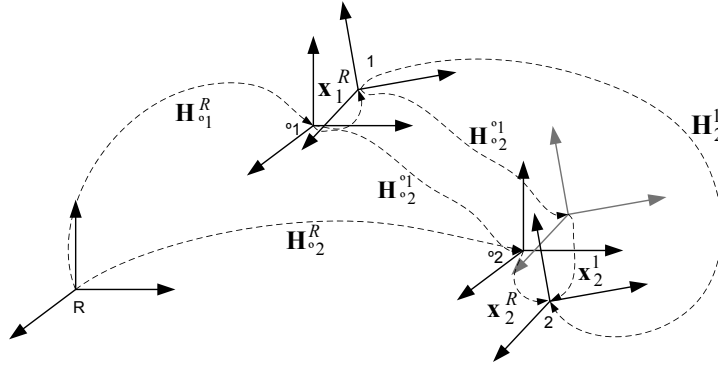


Figure 4.11: DMVs among CSs if CS 1 and 2 are deviated from nominal values.

Proof of Corollary 1: Noting $\mathbf{H}_1^R = \mathbf{H}_{\circ 1}^R \cdot \delta \mathbf{H}_1^R$, we have $\mathbf{H}_R^1 = (\mathbf{H}_1^R)^{-1} = (\delta \mathbf{H}_1^R)^{-1} \cdot \mathbf{H}_R^{\circ 1}$. Then, considering $\mathbf{H}_2^1 = \mathbf{H}_R^1 \cdot \mathbf{H}_2^R$, we have:

$$\mathbf{H}_2^1 = (\delta \mathbf{H}_1^R)^{-1} \cdot \mathbf{H}_R^{\circ 1} \cdot \mathbf{H}_2^R. \quad (4.51)$$

As $\mathbf{H}_2^R = \mathbf{H}_{\circ 2}^R \cdot \delta \mathbf{H}_2^R$, Eq. (4.51) is rewritten as:

$$\mathbf{H}_2^1 = (\delta \mathbf{H}_1^R)^{-1} \cdot \mathbf{H}_R^{\circ 1} \cdot \mathbf{H}_{\circ 2}^R \cdot \delta \mathbf{H}_2^R, \quad (4.52)$$

and thus by Corollary 1 from Appendix 3.3:

$$\mathbf{H}_2^1 = (\mathbf{I}_{4 \times 4} - \Delta_1^R) \cdot \mathbf{H}_{\circ 2}^{\circ 1} \cdot (\mathbf{I}_{4 \times 4} + \Delta_2^R). \quad (4.53)$$

As $\mathbf{H}_2^1 = \mathbf{H}_{\circ 2}^{\circ 1} \cdot \delta \mathbf{H}_2^1$, from Eq. (4.53) we can derive $\delta \mathbf{H}_2^1$ as:

$$\delta \mathbf{H}_2^1 = (\mathbf{H}_{\circ 2}^{\circ 1})^{-1} \cdot (\mathbf{H}_{\circ 2}^{\circ 1} - \Delta_1^R \cdot \mathbf{H}_{\circ 2}^{\circ 1} + \mathbf{H}_{\circ 2}^{\circ 1} \cdot \Delta_2^R - \Delta_1^R \cdot \mathbf{H}_{\circ 2}^{\circ 1} \cdot \Delta_2^R). \quad (4.54)$$

Neglecting the second-order small values:

$$\delta \mathbf{H}_2^1 = \mathbf{I}_{4 \times 4} - (\mathbf{H}_{\circ 2}^{\circ 1})^{-1} \cdot \Delta_1^R \cdot \mathbf{H}_{\circ 2}^{\circ 1} + \Delta_2^R. \quad (4.55)$$

As $\Delta_2^1 = \delta \mathbf{H}_2^1 - \mathbf{I}_{4 \times 4}$, Eq. (4.55) is rewritten as:

$$\Delta_2^R = (\mathbf{H}_{o_2}^{\circ 1})^{-1} \cdot \Delta_1^R \cdot \mathbf{H}_{o_2}^{\circ 1} + \Delta_2^1. \quad (4.56)$$

Considering the components of the matrices, Eq. (4.56) becomes:

$$\begin{aligned} \begin{pmatrix} \hat{\boldsymbol{\theta}}_2^R & \mathbf{d}_2^R \\ \mathbf{0}_{1 \times 3} & 0 \end{pmatrix} &= \begin{pmatrix} (\mathbf{R}_{o_2}^{\circ 1})^T & -(\mathbf{R}_{o_2}^{\circ 1})^T \cdot \mathbf{t}_{o_2}^{\circ 1} \\ \mathbf{0}_{1 \times 3} & 1 \end{pmatrix} \cdot \begin{pmatrix} \hat{\boldsymbol{\theta}}_1^R & \mathbf{d}_1^R \\ \mathbf{0}_{1 \times 3} & 0 \end{pmatrix} \cdot \begin{pmatrix} \mathbf{R}_{o_2}^{\circ 1} & \mathbf{t}_{o_2}^{\circ 1} \\ \mathbf{0}_{1 \times 3} & 1 \end{pmatrix} + \begin{pmatrix} \hat{\boldsymbol{\theta}}_2^1 & \mathbf{d}_2^1 \\ \mathbf{0}_{1 \times 3} & 0 \end{pmatrix}, \\ &= \begin{pmatrix} (\mathbf{R}_{o_2}^{\circ 1})^T \cdot \hat{\boldsymbol{\theta}}_1^R \cdot \mathbf{R}_{o_2}^{\circ 1} + \hat{\boldsymbol{\theta}}_2^R & (\mathbf{R}_{o_2}^{\circ 1})^T \cdot \hat{\boldsymbol{\theta}}_1^R \cdot \mathbf{t}_{o_2}^{\circ 1} + (\mathbf{R}_{o_2}^{\circ 1})^T \cdot \mathbf{d}_1^R + \mathbf{d}_2^R \\ \mathbf{0}_{1 \times 3} & 0 \end{pmatrix}. \end{aligned} \quad (4.57)$$

Therefore,

$$\hat{\boldsymbol{\theta}}_2^R = (\mathbf{R}_{o_2}^{\circ 1})^T \cdot \hat{\boldsymbol{\theta}}_1^R \cdot \mathbf{R}_{o_2}^{\circ 1} + \hat{\boldsymbol{\theta}}_2^1 \quad (4.58)$$

$$\mathbf{d}_2^R = (\mathbf{R}_{o_2}^{\circ 1})^T \cdot \hat{\boldsymbol{\theta}}_1^R \cdot \mathbf{t}_{o_2}^{\circ 1} + (\mathbf{R}_{o_2}^{\circ 1})^T \cdot \mathbf{d}_1^R + \mathbf{d}_2^1. \quad (4.59)$$

Considering that $\hat{\mathbf{a}} \cdot \mathbf{b} = -\hat{\mathbf{b}} \cdot \mathbf{a}$, and that if $\mathbf{c} = \mathbf{B} \cdot \mathbf{a}$, the skew matrix of \mathbf{c} is $\hat{\mathbf{c}} = |\mathbf{B}| \cdot (\mathbf{B}^T)^{-1} \cdot \hat{\mathbf{a}} \cdot (\mathbf{B})^{-1}$, then Eqs. (4.58) and (4.59) can be rewritten in vector form, resulting in Eq. (4.50).

Corollary 2: Consider the CS R , 1 and 2 as shown in Figure 4.11. Consider now that the CS 1 and 2 are deviated from nominal values. Noting the deviation of the CS 1 and 2 w.r.t. R , expressed in vector form, as \mathbf{x}_1^R and \mathbf{x}_2^R , then the deviation of CS 2 w.r.t. 1 in vector form can be formulated as:

$$\mathbf{x}_2^1 = \begin{pmatrix} -(\mathbf{R}_{o_2}^{\circ 1})^T & (\mathbf{R}_{o_2}^{\circ 1})^T \cdot (\hat{\mathbf{t}}_{o_2}^{\circ 1}) & \mathbf{I}_{3 \times 3} & \mathbf{0}_{3 \times 3} \\ \mathbf{0}_{3 \times 3} & -(\mathbf{R}_{o_2}^{\circ 1})^T & \mathbf{0}_{3 \times 3} & \mathbf{I}_{3 \times 3} \end{pmatrix} \cdot \begin{pmatrix} \mathbf{x}_1^R \\ \mathbf{x}_2^R \end{pmatrix}. \quad (4.60)$$

This Corollary and its proof are also given in [3].

Proof of Corollary 2: As shown in Eq. (4.55), the deviation of CS 2 from nominal values can be defined by the expression:

$$\Delta_2^R = (\mathbf{H}_{o_2}^{\circ 1})^{-1} \cdot \Delta_1^R \cdot \mathbf{H}_{o_2}^{\circ 1} + \delta \mathbf{H}_2^1 - \mathbf{I}_{4 \times 4}. \quad (4.61)$$

The proof of this corollary is obtained following the same procedure shown in Corollary 1. Reordering and rewriting Eq. (4.57) in vector form, Eq. (4.60) is straightforwardly derived.

Corollary 3: Consider the q th surface S_q composed on r th boundary points (defined each point as P_r) and the measurement datum S_m . Given the deviation of the local CS from surface S_q w.r.t. S_m after inspection, defined by the vector $\mathbf{y}_{S_q}^{S_m}$, and assuming that CSs of boundary points are oriented similar to the local CS, the deviation of the r th boundary point of the inspected surface w.r.t. the measurement datum can be expressed as:

$$\mathbf{y}_{P_r}^{S_m} = \begin{pmatrix} \mathbf{I}_{3 \times 3} & -(\hat{\mathbf{t}}_{P_r}^{S_q}) \\ \mathbf{0}_{3 \times 3} & \mathbf{I}_{3 \times 3} \end{pmatrix} \cdot \mathbf{y}_{S_q}^{S_m}, \quad (4.62)$$

where $\hat{\mathbf{t}}_{P_r}^{S_q}$ is the skew matrix of the position vector $\mathbf{t}_{P_r}^{S_q}$ which describes the position of the point P_r w.r.t. CS S_q .

Proof of Corollary 3: From Corollary 1, given the deviation of CS S_q w.r.t. CS S_m , denoted as $\mathbf{x}_{S_q}^{S_m}$, and the deviation of the CS of the r th boundary point in surface S_q w.r.t. CS S_q , denoted as $\mathbf{x}_{P_r}^{S_q}$, the deviation of the CS of the r th boundary point in surface S_q w.r.t. S_m can be defined as:

$$\mathbf{x}_{P_r}^{S_m} = \begin{pmatrix} \left(\mathbf{R}_{P_r}^{S_q}\right)^T & -\left(\mathbf{R}_{P_r}^{S_q}\right)^T \cdot \left(\hat{\mathbf{t}}_{P_r}^{S_q}\right) & \mathbf{I}_{3 \times 3} & \mathbf{0}_{3 \times 3} \\ \mathbf{0}_{3 \times 3} & \left(\mathbf{R}_{P_r}^{S_q}\right)^T & \mathbf{0}_{3 \times 3} & \mathbf{I}_{3 \times 3} \end{pmatrix} \cdot \begin{pmatrix} \mathbf{x}_{S_q}^{S_m} \\ \mathbf{x}_{P_r}^{S_q} \end{pmatrix}. \quad (4.63)$$

As the r th boundary point is not deviated from the S_q surface since it is assumed that the part behaves as a solid rigid, $\mathbf{x}_{P_r}^{S_q}$ is equal to zero. As it is assumed that CS of boundary points and the surface CS are oriented similarly, matrix $\mathbf{R}_{P_r}^{S_q}$ is equal to the 3×3 identity matrix. Therefore, Eq. (4.63) is straight forward rewritten as Eq. (4.62), substituting the deviation vector \mathbf{x} by \mathbf{y} since we are referring to deviations from the inspection process.

Corollary 4: Consider a surface defined by its substitute surface S_i and the nominal surface N_i . Consider the SDT of this surface as $\{\mathbf{T}_{S_i, N_i}\}_D$:

$$\{\mathbf{T}_{S_i, N_i}\}_D = \left\{ \begin{array}{c} \boldsymbol{\Omega}_{S_i} \\ \mathbf{D}_{S_i} \end{array} \right\}, \quad (4.64)$$

which means the small translational and orientational deviation of S_i expressed in the D frame. This SDT at point P_r on the surface S_i , expressed in the frame F (see Figure 4.12), is defined as:

$$\{\mathbf{T}_{P_r, S_i}\}_F = \left\{ \begin{array}{c} \mathbf{R}_D^F \cdot \boldsymbol{\Omega}_{S_i} \\ \mathbf{R}_D^F \cdot (\mathbf{D}_{S_i} + ((\mathbf{R}_D^F)^T \cdot \mathbf{t}_{S_i}^{P_r}) \times \boldsymbol{\Omega}_{S_i}) \end{array} \right\}, \quad (4.65)$$

where \mathbf{R}_D^F is the rotation matrix from the F CS to the D CS; $\mathbf{t}_{S_i}^{P_r}$ is the translation vector from P_r to S_i expressed in the D CS; and \times is the cross product operator.

Proof of Corollary 4: The SDT $\{\mathbf{T}_{S_i, N_i}\}_D$ can be evaluated at the point P_r of the surface S_i defining the following SDT:

$$\{\mathbf{T}_{P_r, S_i}\}_D = \left\{ \begin{array}{c} \boldsymbol{\Omega}_{S_i} \\ \mathbf{D}_{S_i} + \boldsymbol{\Omega}_{S_i} \times \mathbf{t}_{P_r}^{S_i} \end{array} \right\}, \quad (4.66)$$

where $\mathbf{t}_{P_r}^{S_i}$ is the translation vector from S_i to P_r expressed in the D CS. This SDT can be expressed in the frame F as:

$$\{\mathbf{T}_{P_r, S_i}\}_F = \left\{ \begin{array}{c} \mathbf{R}_D^F \cdot \boldsymbol{\Omega}_{S_i} \\ \mathbf{R}_D^F \cdot (\mathbf{D}_{S_i} + \boldsymbol{\Omega}_{S_i} \times \mathbf{t}_{P_r}^{S_i}) \end{array} \right\}. \quad (4.67)$$

The translational deviation of Eq. (4.67) is the same as that in Eq. (4.65) by the following derivation:

$$\begin{aligned} \mathbf{R}_D^F \cdot (\mathbf{D}_{S_i} + \boldsymbol{\Omega}_{S_i} \times \mathbf{t}_{P_r}^{S_i}) &= \mathbf{R}_D^F \cdot (\mathbf{D}_{S_i} - \mathbf{t}_{P_r}^{S_i} \times \boldsymbol{\Omega}_{S_i}) \\ &= \mathbf{R}_D^F \cdot (\mathbf{D}_{S_i} + ((\mathbf{R}_D^F)^T \cdot \mathbf{t}_{S_i}^{P_r}) \times \boldsymbol{\Omega}_{S_i}). \end{aligned} \quad (4.68)$$

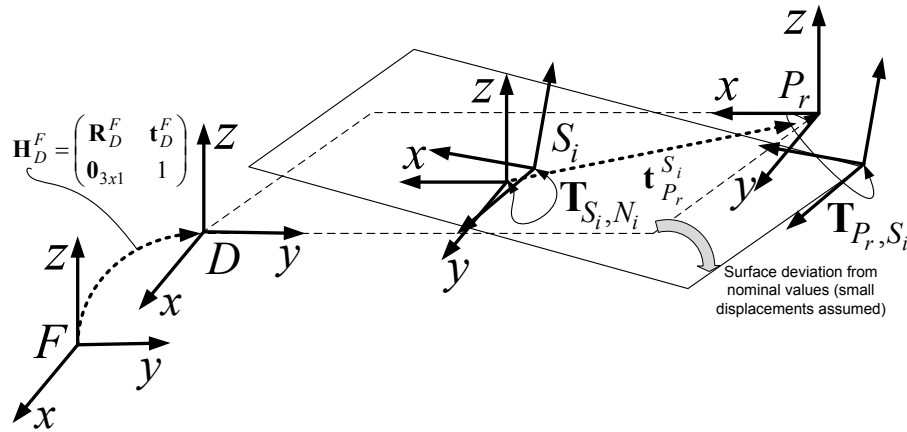


Figure 4.12: Surface S_i with a torsor deviation and frames D and F .

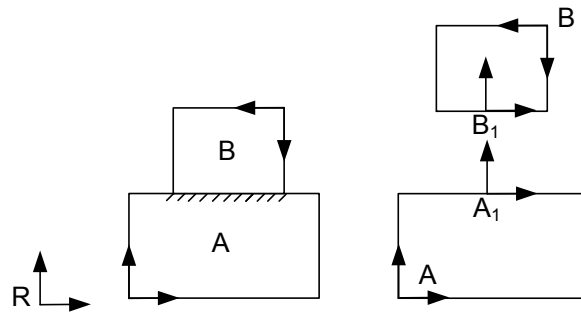


Figure 4.13: Example for analyzing small displacements using SDTs and DMVs.

4.8 Appendix 4.2: Comparison of SDTs with DMVs

To illustrate the different use of SDTs and DMVs, we present a simple example of an assembly composed of two parts, A and B , linked through a joint that it is considered without any degree of freedom (a solid rigid joint), as shown in Fig. 4.13. In order to evaluate the deviation of part B w.r.t. R , expressed in the frame R , let us apply both approaches.

- SDTs: Denoting the part torsor of part A w.r.t. R as $\mathbf{T}_{R,A}$, the surface torsors of surface A_1 and B_1 as \mathbf{T}_{A,A_1} and \mathbf{T}_{B,B_1} , respectively, and the joint of parts as a perfect rigid pair so \mathbf{T}_{A_1,B_1} is $\{\mathbf{0}_{3 \times 1} \quad \mathbf{0}_{3 \times 1}\}$, then, the part torsor of B is evaluated as

$$\begin{aligned} \mathbf{T}_{R,B} &= \mathbf{T}_{R,A} + \mathbf{T}_{A,A_1} + \mathbf{T}_{A_1,B_1} + \mathbf{T}_{B_1,B} \\ &= \mathbf{T}_{R,A} + \mathbf{T}_{A,A_1} - \mathbf{T}_{B,B_1}. \end{aligned} \quad (4.69)$$

Note that all torsors are expressed in the global frame R . Graphically, the fact of computing the torsors is shown in Fig. 4.14. The resulting torsor is obtained considering the following properties of SDTs.

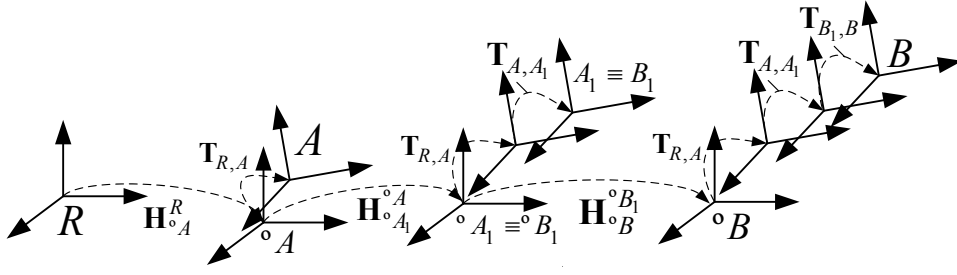


Figure 4.14: Torsors involved in the example for deriving $\mathbf{T}_{R,B}$.

◦ Property 1:

$$\forall a \in \mathfrak{R}; a + U = U, \quad (4.70)$$

◦ Property 2:

$$\forall a, b \in \mathfrak{R}; a \cdot U + b \cdot U = U. \quad (4.71)$$

- DMVs: The deviation of part B w.r.t. R can be expressed by a DMV as \mathbf{x}_B^R . Note that a generic DMV \mathbf{x}_2^1 denotes the deviation of 2 w.r.t. 1 expressed in the local frame 2. For this example, the chain of CSs is shown in Fig. 4.15. Denoting the DMVs \mathbf{x}_A^R , $\mathbf{x}_{A_1}^A$, $\mathbf{x}_{B_1}^{B_1}$ and \mathbf{x}_B^R , the DMV $\mathbf{x}_{A_1}^R$ can be evaluated applying Corollary 1 as

$$\mathbf{x}_{A_1}^R = \begin{pmatrix} (\mathbf{R}_{\circ A_1}^A)^T & -(\mathbf{R}_{\circ A_1}^A)^T \cdot (\hat{\mathbf{t}}_{\circ A_1}^A) & \mathbf{I}_{3 \times 3} & \mathbf{0}_{3 \times 3} \\ \mathbf{0}_{3 \times 3} & (\mathbf{R}_{\circ A_1}^A)^T & \mathbf{0}_{3 \times 3} & \mathbf{I}_{3 \times 3} \end{pmatrix} \cdot \begin{pmatrix} \mathbf{x}_A^R \\ \mathbf{x}_{A_1}^A \end{pmatrix}. \quad (4.72)$$

Then, \mathbf{x}_B^R can be evaluated applying again Corollary 1 as

$$\mathbf{x}_B^R = \begin{pmatrix} (\mathbf{R}_{\circ B}^{B_1})^T & -(\mathbf{R}_{\circ B}^{B_1})^T \cdot (\hat{\mathbf{t}}_{\circ B}^{B_1}) & \mathbf{I}_{3 \times 3} & \mathbf{0}_{3 \times 3} \\ \mathbf{0}_{3 \times 3} & (\mathbf{R}_{\circ B}^{B_1})^T & \mathbf{0}_{3 \times 3} & \mathbf{I}_{3 \times 3} \end{pmatrix} \cdot \begin{pmatrix} \mathbf{x}_{A_1}^R \\ \mathbf{x}_{B_1}^{B_1} \end{pmatrix}. \quad (4.73)$$

Note that, for this example, it is assumed that A_1 and B_1 are coincident (rigid pair). Substituting Eq. (4.72) in Eq. (4.73), the DMV \mathbf{x}_B^R is obtained as a function of \mathbf{x}_A^R , $\mathbf{x}_{A_1}^A$ and $\mathbf{x}_{B_1}^{B_1}$.

In general, SDTs are more recommended when analyzing the propagation of small displacements in assemblies using a global frame. This approach allows for modelling different types of joints between parts. Unlike SDTs, DMVs are more recommended when analyzing the propagation of small displacement between different surfaces of the same part, using local frames for the propagation.

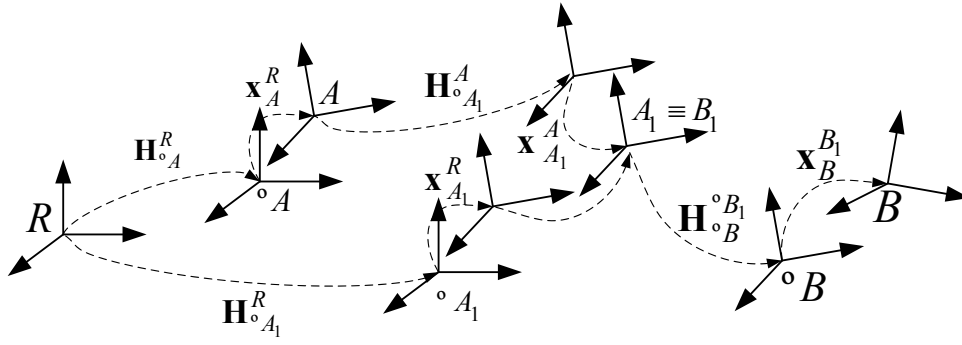


Figure 4.15: DMVs involved in the example for deriving \mathbf{x}_B^R .

4.9 Appendix 4.3: Derivation of SoV matrices

As it is presented in [3], the SoV matrices \mathbf{A}_k and \mathbf{B}_k can be derived following the methodology shown in Figure 4.16. The methodology is composed of six steps. The first step evaluates the relocation of the workpiece from station $k - 1$ to station k . The second step calculates the datum-induced error, which is caused by dimensional errors generated in previous stations. The third and the fourth steps calculate the contribution of fixture-induced errors and machining-induced errors on the features machined at station k . The fifth step combines all errors together (datum-, fixture- and machining-induced errors) to obtain the deviation of the newly generated features. Finally, at the sixth step, the newly generated features are combined with the feature deviations from previous stations. The detailed derivations are as follows.

- Step 1. The workpiece comes from station $k - 1$, and the vector with the feature deviations is \mathbf{x}_{k-1} . This DMV is defined w.r.t. the part reference CS at station $k - 1$, denoted as R_{k-1} , and thus, \mathbf{x}_{k-1} is also expressed as $\mathbf{x}_{k-1}^{R_{k-1}}$. CS R_{k-1} is equal to the CS of the primary datum at station $k - 1$. Due to the relocation, the feature deviations will be expressed w.r.t. the primary locating datum surface at station k , denoted as CS R_k . These feature deviations can be evaluated applying Corollary 2 from Appendix 4.1. Thus, feature deviations from station $k - 1$ expressed at station k will be defined as:

$$\mathbf{x}_{k-1}^{R_k} = \mathbf{A}_k^1 \cdot \mathbf{x}_{k-1}^{R_{k-1}}, \quad (4.74)$$

where \mathbf{A}_k^1 is defined as

$$\mathbf{A}_k^1 = \begin{pmatrix} \mathbf{I}_{6 \times 6} & \cdots & \mathbf{0}_{6 \times 6} & \cdots & \mathbf{D}_{S_1}^{R_k} & \cdots & \mathbf{0}_{6 \times 6} \\ \cdots & \cdots & \cdots & \cdots & \cdots & \cdots & \cdots \\ \mathbf{0}_{6 \times 6} & \cdots & \mathbf{I}_{6 \times 6} & \cdots & \mathbf{D}_{S_j}^{R_k} & \cdots & \mathbf{0}_{6 \times 6} \\ \cdots & \cdots & \cdots & \cdots & \cdots & \cdots & \cdots \\ \mathbf{0}_{6 \times 6} & \cdots & \mathbf{0}_{6 \times 6} & \cdots & \mathbf{D}_{S_M}^{R_k} & \cdots & \mathbf{I}_{6 \times 6} \end{pmatrix}_{6M \times 6M}, \quad (4.75)$$

and $\mathbf{D}_{S_i}^{R_k}$ is defined as

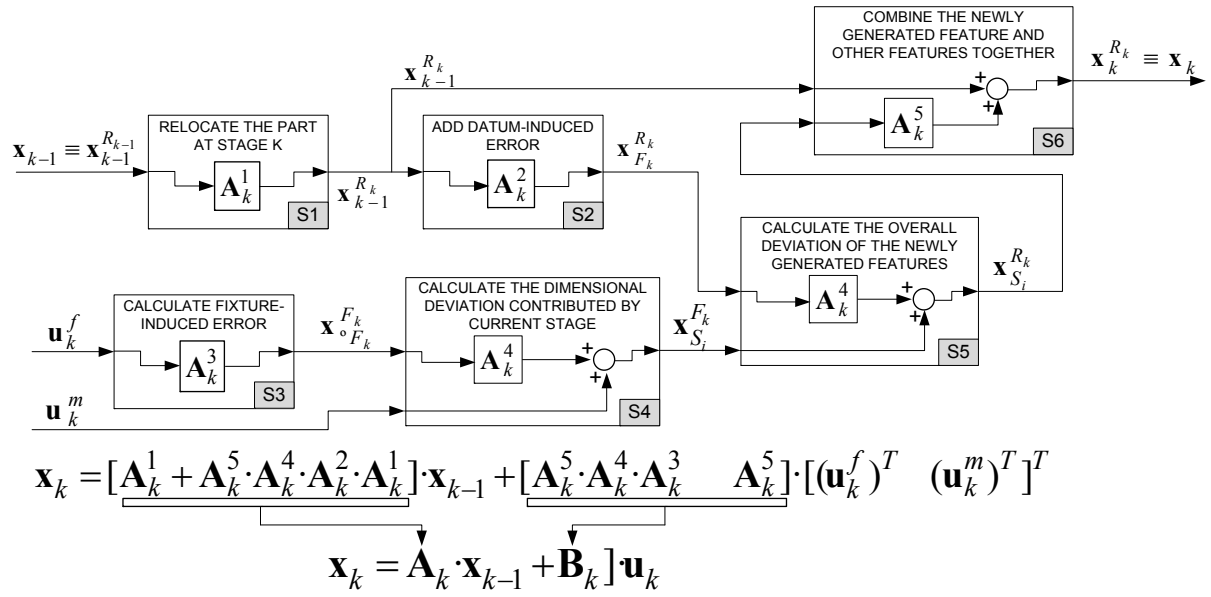


Figure 4.16: Steps for deriving the SoV matrices \mathbf{A}_k and \mathbf{B}_k .

$$\mathbf{D}_{S_j}^{R_k} = \begin{cases} \begin{pmatrix} -(\mathbf{R}_{\circ S_j}^{\circ R_k})^T & (\mathbf{R}_{\circ S_j}^{\circ R_k})^T \cdot (\hat{\mathbf{t}}_{\circ S_j}^{\circ R_k}) \\ \mathbf{0}_{3 \times 3} & -(\mathbf{R}_{\circ S_j}^{\circ R_k})^T \end{pmatrix}, & \text{If } S_j \text{ previous to stat. } k \\ \mathbf{0}_{6 \times 6}, & \text{Otherwise} \end{cases} \quad (4.76)$$

- Step 2. At station k , the fixture CS will be deviated w.r.t. the primary datum due to secondary and tertiary datum errors, as it was shown in Chapter 3. Thus, the deviation of F_k w.r.t. R_k is defined as

$$\mathbf{x}_{F_k}^{R_k} = \mathbf{A}_k^2 \cdot \mathbf{x}_{k-1}^{R_k}. \quad (4.77)$$

Matrix \mathbf{A}_k^2 is defined as

$$\mathbf{A}_k^2 = [\mathbf{0}_{6 \times 6} \quad \dots \quad \mathbf{\Phi}_k^1 \quad \dots \quad \mathbf{0}_{6 \times 6} \quad \dots \quad \mathbf{\Phi}_k^2 \quad \dots]_{6 \times 6M}, \quad (4.78)$$

where $\mathbf{\Phi}_k^1$ and $\mathbf{\Phi}_k^2$ are related to datum-induced errors at secondary and tertiary datums, respectively. These matrices can be derived according to the fixture layout, as shown in Chapter 3, Sub-section 3.2.2.

- Step 3. Due to locator errors, the fixture CS will be deviated from nominal values. As it was shown in Chapter 3, the deviation of fixture CS due to locator errors is expressed as

$$\mathbf{x}_{\circ F_k}^{F_k} = \mathbf{A}_k^3 \cdot \mathbf{u}_k^f, \quad (4.79)$$

where \mathbf{A}_k^3 can be derived according to the fixture layout, as shown in Chapter 3, Sub-section 3.2.1, and \mathbf{u}_k^f is the vector of locator deviations.

- Step 4. Since the cutting-tool path in machining is calibrated w.r.t. the nominal fixture CS, the generic cutting-tool path deviation is expressed w.r.t. the nominal fixture CS. Due to fixture-induced errors, the fixture CS is deviated. Thus, in order to expressed the machining errors at station k , the cutting-tool path deviations w.r.t. to current fixture CS needs to be evaluated. Applying Corollary 1 from Appendix 4.1, this deviation is defined as

$$\mathbf{x}_{S_i}^{F_k} = \mathbf{A}_k^4 \cdot \mathbf{x}_{F_k}^{F_k} + \mathbf{u}_k^m, \quad (4.80)$$

Matrix \mathbf{A}_k^4 is defined as

$$\mathbf{A}_k^4 = [\dots \ (\mathbf{G}_k^{S_i})^T \ \dots]_{6P \times 6}^T, \quad (4.81)$$

where $\mathbf{G}_k^{S_i}$ is defined as

$$\mathbf{G}_k^{S_i} = \begin{pmatrix} \left(\left(\mathbf{R}_{\circ S_i}^{F_k} \right)^T - \left(\mathbf{R}_{\circ S_i}^{F_k} \right)^T \cdot \left(\hat{\mathbf{t}}_{\circ S_i}^{F_k} \right) \right) \\ \mathbf{0}_{3 \times 3} \quad \left(\mathbf{R}_{\circ S_i}^{F_k} \right)^T \end{pmatrix}, \quad (4.82)$$

and S_i is a machined surface at station k , and P is the number of features machined at station k .

- Step 5. Considering the deviation of the fixture CS due to datum errors, and the deviation of the cutting-tool path due to fixture errors and machining errors w.r.t. the fixture CS, the final deviation of the feature machined w.r.t. the primary datum at station k can be evaluated applying Corollary 2 from Appendix 4.1. This deviation is defined as

$$\mathbf{x}_{S_i}^{R_k} = \mathbf{A}_k^4 \cdot \mathbf{x}_{F_k}^{R_k} + \mathbf{x}_{S_i}^{F_k}, \quad (4.83)$$

- Step 6. Finally, after station k the feature deviations is obtained combining the feature deviations from previous stations and the deviations of the machined features at station k . Thus, the final feature deviation after station k is defined as

$$\mathbf{x}_k^{R_k} = \mathbf{x}_{k-1}^{R_k} + \mathbf{A}_k^5 \cdot \mathbf{x}_{S_i}^{R_k}. \quad (4.84)$$

Matrix \mathbf{A}_k^5 is the selector matrix defined as

$$\mathbf{A}_k^5 = \begin{pmatrix} \mathbf{0}_{6 \times 6} & \dots & \mathbf{0}_{6 \times 6} \\ \dots & \dots & \dots \\ \mathbf{I}_{6 \times 6} & \dots & \mathbf{0}_{6 \times 6} \\ \dots & \dots & \dots \\ \mathbf{0}_{6 \times 6} & \dots & \mathbf{I}_{6 \times 6} \\ \dots & \dots & \dots \\ \mathbf{0}_{6 \times 6} & \dots & \mathbf{0}_{6 \times 6} \end{pmatrix}_{6M \times 6P}. \quad (4.85)$$

Note that \mathbf{A}_k^5 is a $6M \times 6P$ matrix. The block matrix $\mathbf{I}_{6 \times 6}$ are placed on the corresponding machined feature location.

As a conclusion, and expressing the propagation variation model in the state space form

$$\mathbf{x}_k = \mathbf{A}_k \cdot \mathbf{x}_{k-1} + \mathbf{B}_k \cdot \mathbf{u}_k + \mathbf{w}_k, \quad k = 1, \dots, N, \quad (4.86)$$

matrices \mathbf{A}_k and \mathbf{B}_k are evaluated, respectively, as follows

$$\mathbf{A}_k = [\mathbf{A}_k^1 + \mathbf{A}_k^5 \cdot \mathbf{A}_k^4 \cdot \mathbf{A}_k^2 \cdot \mathbf{A}_k^1]_{6M \times 6M}, \quad (4.87)$$

$$\begin{aligned} \mathbf{B}_k &= \begin{bmatrix} \mathbf{B}_k^f & \mathbf{B}_k^m \end{bmatrix} \\ &= [\mathbf{A}_k^5 \cdot \mathbf{A}_k^4 \cdot \mathbf{A}_k^3 \quad \mathbf{A}_k^5]_{6M \times (\lambda + 6P)}. \end{aligned} \quad (4.88)$$

Note that the dimension $\lambda + 6P$ refers to λ sources of errors due to fixture-induced deviations and $6P$ sources of errors due to machining-induced deviations during machining the P features.

Similarly, matrix \mathbf{C}_k can be also derived following a similar reasoning. The inspection station can be viewed as a special machining station where only a relocation is conducted since there is no machining operation. Thus, \mathbf{C}_k is defined as

$$\mathbf{C}_k = [\mathbf{C}_k^1 \cdot \mathbf{A}_k^1]_{6\mu \times 6M}, \quad (4.89)$$

where \mathbf{C}_k^1 is the selector matrix similar to \mathbf{A}_k^5 to indicate the features inspected (μ is the number of features inspected), and \mathbf{A}_k^1 is the relocating matrix that relates the primary datum surface at station k with the primary datum surface at the inspection station, placed after station k .

4.10 Appendix 4.4: SoV matrices for the case study

Applying the methodology shown in Section 4.4.1 to derive the SoV model for the 2D case study, the following matrices \mathbf{A}_k , \mathbf{B}_k and \mathbf{C}_k and the vector \mathbf{u}_k for each station were obtained:

- Station 1:

$$\mathbf{A}_1 = \begin{pmatrix} \begin{array}{cccc|cccc} \mathbf{I}_{24 \times 24} & & & & & & & \mathbf{0}_{24 \times 18} \\ \mathbf{0}_{1 \times 18} & 0 & 0 & 0 & 0 & 1 & 0 & \mathbf{0}_{1 \times 18} \\ \mathbf{0}_{1 \times 18} & -1 & 0 & 0 & 0 & 2.5 & 1 & \mathbf{0}_{1 \times 18} \\ \hline & & \mathbf{0}_{16 \times 24} & & & & & \mathbf{I}_{16 \times 18} \end{array} \end{pmatrix}_{42 \times 42} \quad (4.90)$$

- Station 3 (inspection station for KPC_1 and KPC_3 measurement):

$$\mathbf{C}_3 = \left(\begin{array}{c|cccccc|c|c|c} & -1 & 0 & 0 & 0 & 0 & -5 & & & \\ & 0 & -1 & 0 & 0 & 0 & 32.5 & & & \\ \mathbf{0}_{6 \times 12} & 0 & 0 & -1 & 5 & -32.5 & 0 & \mathbf{0}_{6 \times 12} & \mathbf{I}_{6 \times 6} & \mathbf{0}_{6 \times 6} \\ & 0 & 0 & 0 & -1 & 0 & 0 & & & \\ & 0 & 0 & 0 & 0 & -1 & 0 & & & \\ & 0 & 0 & 0 & 0 & 0 & -1 & & & \end{array} \right)_{6 \times 42} \quad (4.96)$$

- Station 4 (inspection station for KPC_2 measurement):

$$\mathbf{C}_4 = \left(\begin{array}{c|cccccc|c|c} & -1 & 0 & 0 & 0 & 0 & -10 & & & \\ & 0 & -1 & 0 & 0 & 0 & -22.5 & & & \\ \mathbf{0}_{6 \times 6} & 0 & 0 & -1 & 10 & 22.5 & 0 & \mathbf{0}_{6 \times 24} & \mathbf{I}_{6 \times 6} & \\ & 0 & 0 & 0 & -1 & 0 & 0 & & & \\ & 0 & 0 & 0 & 0 & -1 & 0 & & & \\ & 0 & 0 & 0 & 0 & 0 & -1 & & & \end{array} \right)_{6 \times 42} \quad (4.97)$$

4.11 Appendix 4.5: SDTs for the case study

The resulting torsors that define the MoMP for the 2D case study presented in Section 4.4.2 are shown in Tables 4.12, 4.13 and 4.14.

Table 4.12: SDTs for station 1.

| | |
|---|---|
| SDT of raw part surfaces | |
| $\{\mathbf{T}_{D,S_1}\}_D = \{\mathbf{0}_{3 \times 1} \quad \mathbf{0}_{3 \times 1}\}$ | $\{\mathbf{T}_{D,S_3}\}_D = \{\mathbf{0}_{3 \times 1} \quad \mathbf{0}_{3 \times 1}\}$ |
| $\{\mathbf{T}_{D,S_2}\}_D = \{\mathbf{0}_{3 \times 1} \quad \mathbf{0}_{3 \times 1}\}$ | $\{\mathbf{T}_{D,S_4}\}_D = \{\mathbf{0}_{3 \times 1} \quad \mathbf{0}_{3 \times 1}\}$ |
| SDT of part-holder surfaces | |
| $\{\mathbf{T}_{F_1,H_1}\}_{F_1} = \begin{Bmatrix} 0 & U \\ 0 & v_{H_1}^1 \\ \gamma_{H_1}^1 & 0 \end{Bmatrix}$ | $\{\mathbf{T}_{F_1,H_2}\}_{F_1} = \begin{Bmatrix} 0 & v_{H_2}^1 \\ 0 & U \\ \gamma_{H_2}^1 & 0 \end{Bmatrix}$ |
| SDT of joint workpiece/part-holder | |
| $\{\mathbf{T}_{H_1,S_3}\}_{F_1} = \begin{Bmatrix} 0 & U \\ 0 & 0 \\ 0 & 0 \end{Bmatrix}$ | $\{\mathbf{T}_{H_2,S_4}\}_{F_1} = \begin{Bmatrix} 0 & v_{H_2,S_4}^1 \\ 0 & U \\ \gamma_{H_2,S_4}^1 & 0 \end{Bmatrix}$ |
| Positioning deviation torsor | |
| $\{\mathbf{T}_{F_1,D}\}_{F_1} = \begin{Bmatrix} 0 & v_{H_2}^1 - 10\gamma_{H_2}^1 + 20\gamma_{H_1}^1 \\ 0 & v_{H_1}^1 - 37.5\gamma_{H_1}^1 \\ \gamma_{H_1}^1 & 0 \end{Bmatrix}$ | |
| Machining deviation torsor | |
| $\{\mathbf{T}_{F_1,S_5}\}_{F_1} = \begin{Bmatrix} 0 & U \\ 0 & v_{M_5}^1 \\ \gamma_{M_5}^1 & 0 \end{Bmatrix}$ | |
| Part surface deviation torsor | |
| $\{\mathbf{T}_{D,S_5}\}_D = \begin{Bmatrix} 0 & U \\ 0 & v_{M_5}^1 - v_{H_1}^1 + 37.5 \cdot (\gamma_{H_1}^1 - \gamma_{M_5}^1) \\ \gamma_{M_5}^1 - \gamma_{H_1}^1 & 0 \end{Bmatrix}$ | |

Table 4.14: SDTs for inspection station.

| | |
|--|--|
| Gauge positioning deviation torsor for inspecting KPC_1 and KPC_3 | |
| $\{\mathbf{T}_{D,G}\}_D = \begin{Bmatrix} 0 & U \\ 0 & 0 \\ 0 & 0 \end{Bmatrix}$ | |
| SDT between tolerance zone and real toleranced surface S_6 | |
| $\{\mathbf{T}_{TZ,S_6}\}_D = \begin{Bmatrix} 0 & & & U \\ 0 & & v_{M_5}^1 + v_{H_3}^2 - v_{H_1}^1 - v_{M_6}^2 & -32.5 \cdot (\gamma_{H_3}^2 + \gamma_{H_1}^1 - \gamma_{M_5}^1) \\ \gamma_{M_6}^2 - \gamma_{H_3}^2 + \gamma_{M_5}^1 - \gamma_{H_1}^1 & & & 0 \end{Bmatrix}$ | |
| Gauge positioning deviation torsor for inspecting KPC_2 | |
| $\{\mathbf{T}_{D,G}\}_D = \begin{Bmatrix} 0 & U \\ 0 & 0 \\ 0 & 0 \end{Bmatrix}$ | |
| SDT between tolerance zone and real toleranced surface S_7 | |
| $\{\mathbf{T}_{TZ,S_7}\}_D = \begin{Bmatrix} 0 & & & U \\ 0 & & +u_{M_7}^2 + v_{H_4}^2 - 10\gamma_{H_4}^2 & -22.5 \cdot (\gamma_{H_3}^2 - \gamma_{M_5}^1 + \gamma_{H_1}^1) \\ \gamma_{M_7}^2 - \gamma_{H_3}^2 + \gamma_{M_5}^1 - \gamma_{H_1}^1 & & & 0 \end{Bmatrix}$ | |

Table 4.13: SDTs for station 2.

| | |
|--|---|
| SDT of part-holder surfaces | |
| $\{\mathbf{T}_{F_2,H_3}\}_{F_2} = \begin{Bmatrix} 0 & U \\ 0 & v_{H_3}^2 \\ \gamma_{H_3}^2 & 0 \end{Bmatrix}$ | $\{\mathbf{T}_{F_2,H_4}\}_{F_2} = \begin{Bmatrix} 0 & v_{H_4}^2 \\ 0 & U \\ \gamma_{H_4}^2 & 0 \end{Bmatrix}$ |
| SDT of joint workpiece/part-holder | |
| $\{\mathbf{T}_{H_3,S_5}\}_{F_2} = \begin{Bmatrix} 0 & U \\ 0 & 0 \\ 0 & 0 \end{Bmatrix}$ | $\{\mathbf{T}_{H_4,S_2}\}_{F_2} = \begin{Bmatrix} 0 & v_{H_4,S_2}^2 \\ 0 & U \\ \gamma_{H_4,S_2}^2 & 0 \end{Bmatrix}$ |
| Positioning deviation torsor | |
| $\{\mathbf{T}_{F_2,D}\}_{F_2} = \begin{Bmatrix} 0 & & v_{H_4}^2 - 10\gamma_{H_4}^2 + 20 \cdot (\gamma_{H_3}^2 - \gamma_{M_5}^1 + \gamma_{H_1}^1) \\ 0 & & v_{H_3}^2 + v_{M_5}^1 - v_{H_1}^1 + 37.5 \cdot (\gamma_{H_1}^1 - \gamma_{M_5}^1 + \gamma_{H_3}^2) \\ \gamma_{H_3}^2 - \gamma_{M_5}^1 + \gamma_{H_1}^1 & & 0 \end{Bmatrix}$ | |
| Machining deviation torsor | |
| $\{\mathbf{T}_{F_2,S_6}\}_{F_2} = \begin{Bmatrix} 0 & U \\ 0 & v_{M_6}^2 \\ \gamma_{M_6}^2 & 0 \end{Bmatrix}$ | $\{\mathbf{T}_{F_2,S_7}\}_{F_2} = \begin{Bmatrix} 0 & u_{M_7}^2 \\ 0 & U \\ \gamma_{M_7}^2 & 0 \end{Bmatrix}$ |
| Part surface deviation torsor | |
| $\{\mathbf{T}_{D,S_6}\}_D = \begin{Bmatrix} 0 & & & U \\ 0 & & -70\gamma_{M_6}^2 - v_{M_6}^2 + v_{H_3}^2 + v_{M_5}^1 - v_{H_1}^1 + 37.5 \cdot (\gamma_{H_3}^2 - \gamma_{M_5}^1 + \gamma_{H_1}^1) & \\ \gamma_{M_6}^2 - \gamma_{H_3}^2 + \gamma_{M_5}^1 - \gamma_{H_1}^1 & & & 0 \end{Bmatrix}$ | |
| $\{\mathbf{T}_{D,S_7}\}_D = \begin{Bmatrix} 0 & & & U \\ 0 & & 20 \cdot (\gamma_{H_1}^1 - \gamma_{M_5}^1 + \gamma_{H_3}^2) - 10\gamma_{H_4}^2 + 2.5\gamma_{M_7}^2 + v_{H_4}^2 + u_{M_7}^2 & \\ \gamma_{M_7}^2 - \gamma_{H_3}^2 + \gamma_{M_5}^1 - \gamma_{H_1}^1 & & & 0 \end{Bmatrix}$ | |

References

- [1] J. S. Agapiou, E. A. Steinhilper, J. M. Alden, A. Anagonye, P. Bandyopadhyay, F. Gu, P. Hilbert, Predictive modeling of machining line variation, U.S. Patent Number 7, 209, 799 (B2).

-
- [2] K. Ogata, *Modern Control Engineering*, 4th Edition, Prentice Hall, 2001.
- [3] S. Zhou, Q. Huang, J. Shi, State space modeling of dimensional variation propagation in multistage machining process using differential motion vectors, *IEEE Transactions on Robotics and Automation* 19 (2) (2003) 296–309.
- [4] Q. Huang, J. Shi, J. Yuan, Part dimensional error and its propagation modeling in multi-operational machining processes, *Journal of Manufacturing Science and Engineering* 125 (2) (2003) 255–262.
- [5] D. Djurdjanovic, J. Ni, Dimensional errors of fixtures, locating and measurement datum features in the stream of variation modeling in machining, *Journal of Manufacturing Science and Engineering* 125 (4) (2003) 716–730.
- [6] J. P. Loose, S. Zhou, D. Ceglarek, Kinematic analysis of dimensional variation propagation for multistage machining processes with general fixture layouts, *IEEE Transactions on Automation Science and Engineering* 4 (2) (2007) 141–152.
- [7] J. P. Loose, Q. Zhou, S. Zhou, D. Ceglarek, Integrating GD&T into dimensional variation models for multistage machining processes, *International Journal of Production Research* 48 (10-12) (2010) 3129–3149.
- [8] M. Zhang, D. Djurdjanovic, J. Ni, Diagnosability and sensitivity analysis for multi-station machining processes, *International Journal of Machine Tools and Manufacture* 47 (3-4) (2007) 646–657.
- [9] J. Liu, J. Shi, S. J. Hu, Quality-assured setup planning based on the stream-of-variation model for multi-stage machining processes, *IIE Transactions* 41 (2009) 323–334(12).
- [10] H. Wang, Q. Huang, R. Katz, Multi-operational machining processes modeling for sequential root cause identification and measurement reduction, *Journal of Manufacturing Science and Engineering* 127 (3) (2005) 512–521.
- [11] Y. Ding, J. Shi, D. Ceglarek, Diagnosability analysis of multi-station manufacturing processes, *Journal of Dynamic Systems, Measurement, and Control* 124 (1) (2002) 1–13.
- [12] S. Zhou, Y. Chen, Y. Ding, J. Shi, Diagnosability study of multistage manufacturing processes based on linear mixed-effects models, *Technometrics* 45 (4) (2003) 312–325.
- [13] S. Y. Zhou, Y. Chen, J. Shi, Statistical estimation and testing for variation root-cause identification of multistage manufacturing processes, *IEEE Transactions on Automation Science and Engineering* 1 (1) (2004) 73–83.
- [14] Z. G. Li, S. Y. Zhou, Y. Ding, Pattern matching for variation-source identification in manufacturing processes in the presence of unstructured noise, *IIE Transactions* 39 (3) (2007) 251–263.

-
- [15] Y. Ding, P. Kim, D. Ceglarek, J. Jin, Optimal sensor distribution for variation diagnosis in multistation assembly processes, *IEEE Transactions on Robotics and Automation* 19 (4) (2003) 543–556.
- [16] D. Djurdjanovic, J. Ni, Measurement scheme synthesis in multi-station machining systems, *Journal of Manufacturing Science and Engineering* 126 (1) (2004) 178–188.
- [17] D. Djurdjanovic, J. Ni, Bayesian approach to measurement scheme analysis in multistation machining systems, *Proceedings of the Institution of Mechanical Engineers Part B-Journal of Engineering Manufacture* 217 (8) (2003) 1117–1130.
- [18] D. Djurdjanovic, J. Ni, Stream-of-variation (SoV)-based measurement scheme analysis in multistation machining systems, *IEEE Transactions on Automation Science and Engineering* 3 (4) (2006) 407–422.
- [19] L. Izquierdo, J. Shi, S. Hu, C. Wampler, Feedforward control of multistage assembly processes using programmable tooling, *NAMRI/SME Transactions* 35 (2007) 295–302.
- [20] D. Djurdjanovic, J. Zhu, Stream of variation based error compensation strategy in multi-stage manufacturing processes, *ASME Conference Proceedings*.
- [21] D. Djurdjanovic, J. Ni, Online stochastic control of dimensional quality in multistation manufacturing systems, *Proceedings of the Institution of Mechanical Engineers, Part B: Journal of Engineering Manufacture* 221 (5) (2007) 865–880.
- [22] Y. Chen, Y. Ding, J. Jin, D. Ceglarek, Integration of process-oriented tolerancing and maintenance planning in design of multistation manufacturing processes, *IEEE Transactions on Automation Science and Engineering* 3 (4) (2006) 440–453.
- [23] Y. Ding, J. H. Jin, D. Ceglarek, J. Shi, Process-oriented tolerancing for multi-station assembly systems, *IIE Transactions* 37 (6) (2005) 493–508.
- [24] B. Shirinzadeh, Flexible fixturing for workpiece positioning and constraining, *Assembly Automation* 22 (2) (2002) 112–120.
- [25] Y. Ding, D. Ceglarek, J. H. Jin, J. J. Shi, Process-oriented tolerance synthesis for multistage manufacturing systems, *Journal of Manufacturing Science and Engineering* 11 (2000) 15–22.
- [26] E. Ballot, P. Bourdet, A computational method for the consequences of geometric errors in mechanisms, in: *Proceedings of the 4th CIRP Seminar on Computer Aided Tolerancing*, Tokyo, Japan, 1997, pp. 137–148.
- [27] K. W. Chase, J. Gao, S. P. Magleby, General 2-D tolerance analysis of mechanical assemblies with small kinematic adjustments, *Journal of Design and Manufacturing* 5 (1995) 263–274.
- [28] K. W. Chase, J. Gao, S. P. Magleby, C. D. Sorensen, Including geometric feature variations in tolerance analysis of mechanical assemblies, *IIE Transactions* 28 (1996) 795–807.

- [29] J. K. Davidson, A. Mujezinovic, J. J. Shah, A new mathematical model for geometric tolerances as applied to round faces, *Journal of Mechanical Design* 124 (4) (2002) 609–622.
- [30] F. Villeneuve, O. Legoff, Y. Landon, Tolerancing for manufacturing: a three-dimensional model, *International Journal of Production Research* 39 (8) (2001) 1625–1648.
- [31] A. Desrochers, Modeling three-dimensional tolerance zones using screw parameters, in: *Proceedings of ASME 25th Design Automation Conference, DAC-8587, Las-Vegas, 1999*.
- [32] A. Desrochers, W. Ghie, L. Laperriere, Application of a unified jacobian–torsor model for tolerance analysis, *Journal of Computing and Information Science in Engineering* 3 (1) (2003) 2–14.
- [33] F. Villeneuve, F. Vignat, Simulation of the manufacturing process in a tolerancing point of view: Generic resolution of the positioning problem, in: *Models for Computer Aided Tolerancing in Design and Manufacturing, 2007*, pp. 179–189.
- [34] M. K. Nejad, F. Vignat, F. Villeneuve, Simulation of the geometrical defects of manufacturing, *The International Journal of Advanced Manufacturing Technology* 45 (2009) 631–648.
- [35] F. Villeneuve, F. Vignat, Manufacturing process simulation for tolerance analysis and synthesis, in: *Advances in Integrated Design and Manufacturing in Mechanical Engineering, 2005*, pp. 189–200.
- [36] M. K. Nejad, Propositions de résolution numérique des problèmes d’analyse de tolérance en fabrication: approche 3D. PhD Thesis (2010).
- [37] F. Vignat, F. Villeneuve, 3D transfer of tolerances using a SDT approach: Application to turning process, *Journal of Computing and Information Science in Engineering* 3 (1) (2003) 45–53.
- [38] M. K. Nejad, F. Vignat, A. Desrochers, F. Villeneuve, 3D simulation of manufacturing defects for tolerance analysis, *Journal of Computing and Information Science in Engineering* 10 (2) (2010) 021001.
- [39] J. Louati, B. Ayadi, Z. Bouaziz, M. Haddar, Three-dimensional modelling of geometric defaults to optimize a manufactured part setting, *The International Journal of Advanced Manufacturing Technology* 29 (2006) 342–348.
- [40] B. Ayadi, B. Anselmetti, Z. Bouaziz, A. Zghal, Three-dimensional modelling of manufacturing tolerancing using the ascendant approach, *The International Journal of Advanced Manufacturing Technology* 39 (2008) 279–290.
- [41] F. Vignat, F. Villeneuve, A numerical approach for 3D manufacturing tolerances synthesis, in: *10th CIRP Conference on Computer Aided Tolerancing Specification and Verification for Assemblies, Erlangen (Germany), 2007*.

-
- [42] J. Liu, J. Shi, S. J. Hu, Engineering-driven factor analysis for variation source identification in multistage manufacturing processes, *Journal of Manufacturing Science and Engineering* 130 (4) (2008) 041009.

Part II

**Extension of the Stream of Variation
model in multi-station machining
processes**

Limitations of the current SoV model due to machining-induced variations

The Stream of Variation (SoV) model has been recently proposed as an engineering-driven technique for part quality prediction in multi-station machining processes (MMPs). The current SoV model incorporates fixture and datum variations in the multi-station variation propagation, without explicitly considering common machining-induced variations such as machine-tool thermal distortions, cutting-tool wear, cutting-tool deflections, etc. This chapter shows the limitations of the current SoV model through an experimental case study where the effect of the spindle thermal expansion, cutting-tool flank wear and locator errors are introduced.

5.1 Introduction

As it was exposed in Chapter 4, the Stream of Variation (SoV) model as well as the Model of Manufactured Part (MoMP) have been successfully applied for part quality prediction and improvement in MMPs. Although both 3D manufacturing variation propagation models present their own advantages and drawbacks, both models incorporate the machining variation into the model as a theoretical variability of the cutting-tool tip during machining. In other words, the machining variation is modeled as a generic cutting-tool path deviation from nominal values due to the effect of all potential sources of variation during the machining operation. In some research works presented in the literature, the machining variation is assumed to be very small in comparison with datum or fixture errors and thus, negligible [1]. In many others, the machining variation is assumed to be known according to machine-tool precision specifications without specifying at which operation conditions that precision holds [2–5]. However, as it was exposed in Chapter 2 and 3, there is a clear analytical relationship between the cutting-tool path deviation during machining and specific sources of machining errors such as geometric-kinematic errors, thermal errors, force-induced errors, tooling wear errors, etc. Therefore, the integration of these analytical relationships into manufacturing variation models could notably improve the accuracy of part quality prediction in MMPs since the specific conditions of each machining operation at each machining station would be considered.

In this chapter, an experimental study is presented to show how important is the impact of machining-induced variations on the final part quality. The effect of specific machining-induced deviations such as the spindle thermal expansion and the cutting-tool flank wear is analyzed showing the importance of each machining-induced deviation and their relationship. The study compares the expected part quality using the SoV model assuming negligible the machining-induced errors, and the actual part quality. By this experimentation it seems clear that the application of current 3D manufacturing variation models is limited in those applications where important machining-induced errors are present. For these cases, the 3D manufacturing variation models should be expanded to deal with specific machining sources of variation. In Chapter 6 it is proposed the extension of the SoV model to include these machining sources of variation.

5.2 Theoretical limitations of current SoV model

As it was shown in Chapter 4, the SoV model for a N -station machining process is formulated as

$$\mathbf{x}_k = \mathbf{A}_k \cdot \mathbf{x}_{k-1} + \mathbf{B}_k \cdot \mathbf{u}_k + \mathbf{w}_k, \quad (5.1)$$

$$\mathbf{y}_k = \mathbf{C}_k \cdot \mathbf{x}_k + \mathbf{v}_k, \quad (5.2)$$

where $\mathbf{A}_k \cdot \mathbf{x}_{k-1}$, $k = 1, 2, \dots, N$, represents the deviations transmitted by datum features generated at upstream stations; $\mathbf{B}_k \cdot \mathbf{u}_k$ represents the deviations introduced within station k due to fixture errors which are expressed as Key Control Characteristics (KCCs) defined by the vector \mathbf{u}_k ; the deviations of KPCs are the linear combination of the deviations of features on workpieces, as represented by $\mathbf{C}_k \cdot \mathbf{x}_k$; \mathbf{w}_k and \mathbf{v}_k are the un-modeled system noise and measurement noise, respectively. These equations describe the relationship between the measured dimensional quality of a machined workpiece with the process level variation sources defined as KCCs and its propagation. In current model formulation, only the fixture variations and a generic cutting-tool path deviation are considered as KCCs.

The variation sources vector \mathbf{u}_k is defined as $\left[(\mathbf{u}_k^f)^T, (\mathbf{u}_k^m)^T \right]^T$. The term \mathbf{u}_k^f refers to fixture sources of error, and it is defined as $[\Delta l_1^k \ \Delta l_2^k \ \Delta l_3^k \ \Delta l_4^k \ \Delta l_5^k \ \Delta l_6^k \ \mathbf{u}_m^k]^T$, where Δl_i^k , $i = 1, 2, \dots, 6$, are the random deviations of fixture locators from their nominal position considering a 3-2-1 fixture scheme at station k . The term \mathbf{u}_k^m refers to a generic cutting-tool path deviation, defined as three translational and three orientation deviations. As it can be noted, this formulation does not include explicitly any machining source of error, such as geometric/kinematic errors, cutting-tool wear-induced errors or spindle thermal errors. The omission of modeling any machining error into the SoV model may limit the capability of the SoV model for accurate predictions when machining-induced errors are not negligible. For instance, consider a two-station machining process shown in Figure 5.1, where a face milling operation is conducted at the first station and the surface generated is used later as a datum feature at the second station for an end milling operation. Considering the dimensions d and e as two KPCs, it can be observed that besides the variations of fixture locators, $i)$ and $iv)$, the machining-induced variation sources that also affect KPC dimensional quality include: cutting-tool wear-induced variations, $ii)$ and $v)$, and spindle thermal-induced variations, $iii)$ and $vi)$. Note that only the variations of datum features are considered as the datum-induced variations (Figure 5.1). For this example, it

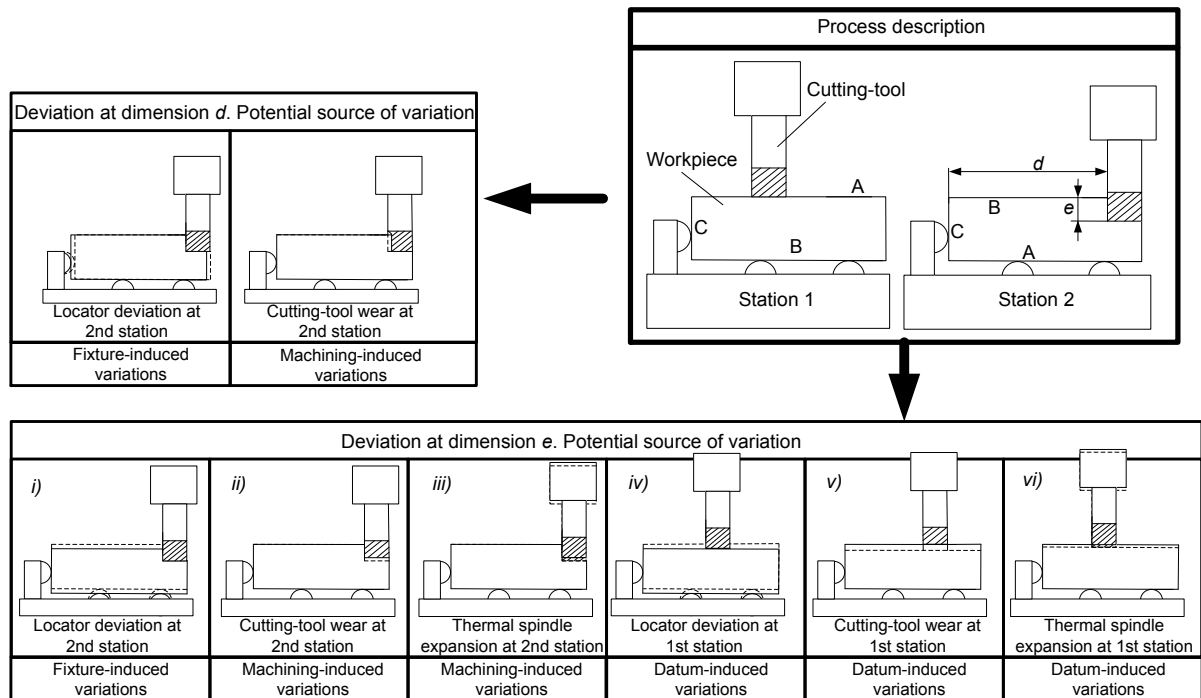


Figure 5.1: Example of sources of variation in a MMP.

is worthy noted that overlooking the explicit derivation of machining-induced variations will prevent to accurately predict the final part quality and ensure parts within specifications.

In the next section, a case study is conducted to analyze the accuracy of the current SoV model when machining-induced variations are present. The Matlab code that evaluates the SoV model is shown in Chapter 11.

5.3 Experimental study

A case study composed of the Aluminium 6061 reference part is conducted, as shown in Figure 5.2. The 3-station machining process is illustrated in Figure 5.3, with the datum features and the surfaces to be machined summarized in Table 5.1. The locations of locators that compose the fixture at each machining station is defined in Table 5.2. The nominal location and orientation of each surface is presented in Table 5.3. After station 3, the machined part is moved to the fourth station, where the CMM is used to measure the KPCs defined by the dimensional location of features S_2 , S_3 and S_8 .

With the defined MMP, three experiments were conducted in order to evaluate the prediction accuracy of the SoV model due to machining-induced variations. First, a workpiece with dimensions $95 \times 95 \times 47 \text{ mm}$ was machined according to the proposed MMP with minimum fixture and machining-induced variations. For this purpose, the fixture locators were calibrated in the machine-tool table with a touch probe ensuring fixture assembly

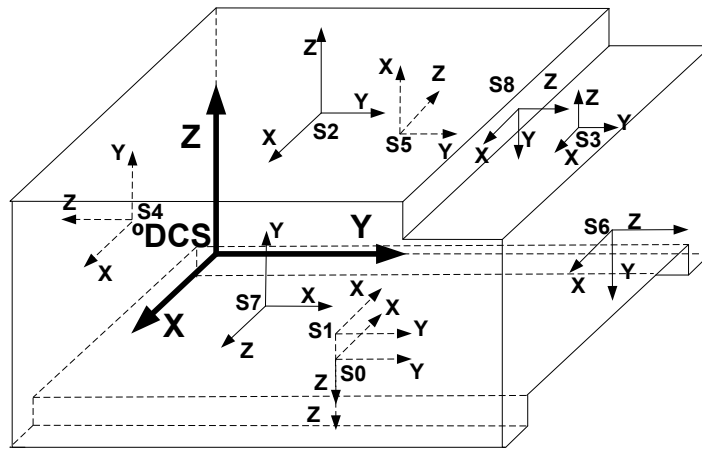


Figure 5.2: Case study. Coordinate systems of surfaces S_0 - S_8 .

errors less than $\pm 0.015 \text{ mm}$. The machining operation was conducted with a spindle temperature close to 25°C . The possible spindle temperature variations were compensated by a linear compensation algorithm provided by the machine-tool manufacturer. To control cutting-tool wear-induced errors, a new cutting-tool was used in the experimentation with dimensions of length and diameter of 111.322 mm and 24.856 mm , respectively. Both cutting length and diameter were measured by a mechanical touch probe, and a slot operation was conducted in aluminium blocks to measure the length and diameter deviations from the mechanical calibration procedure by CMM measurements. These deviations were added into the nominal cutting-tool length and diameter. In addition, the workpiece clamping procedure at each station was conducted by a torque wrench to apply a constant clamping torque of $10 \text{ N} \cdot \text{m}$, which was enough to ensure workpiece stability and minimize locator marks in the workpiece. Due to clamping forces, locators p_1 and p_2 are slightly bent, so locators positions are deviated from the nominal ones. An inductive sensor with precision $\pm 0.010 \text{ mm}$ was used to measure locator deviations in order to compensate the actual locators position before machining. The deviations measured were 18 and 30 microns at locator p_1 and p_2 respectively, whereas locator p_3 was not considered since for the case study, there is no KPC where a p_3 deviation influences. By these conditions, the MMP should generate high quality parts, where only geometrical errors, off-sets from calibration procedures and cutting-tool deflections could prevent the generation of “perfect” machined parts.

The second experimentation only dealt with fixture errors, keeping under control the machining-induced variations. The experimentation procedure was conducted similar to experimentation 1, except that deviations were intentionally introduced to several locators, as shown in Table 5.4. These locators errors were measured in the machine-tool table by the touch probe. Note that the forced errors were small (41 and 96 microns in locators L_1 and L_2 respectively) in order to simulate common fixture errors due to wear or slight assembly variations. For this experimentation, the KPC deviations are mostly generated by the fixture errors, and it should be predicted by the SoV model whose matrices \mathbf{A}_k , \mathbf{B}_k , and \mathbf{C}_k are calculated according to Chapter 4.

Table 5.1: Machined features and datum features according to the 3-2-1 locating scheme at each station.

| Station | Datum features | Machined features | Cutting-tool |
|---------|-------------------|-------------------|---|
| 1 | $S_0 - S_4 - S_5$ | S_2 | ADHX 110305, PVD TiAlN $\varnothing = 24.856$, $L = 111.322$ |
| 2 | $S_2 - S_6 - S_5$ | S_1 | ADHX 110305, PVD TiAlN $\varnothing = 24.856$, $L = 111.322$ |
| 3 | $S_1 - S_4 - S_5$ | S_3, S_8 | ADHX 110305, PVD TiAlN $\varnothing = 24.856$, $L = 111.322$ |
| 4 | $S_0 - S_4 - S_5$ | – | Inspection station |

\varnothing : Tool diameter (mm); L : Tool length (mm).

Table 5.2: Nominal location ($\mathbf{t}_{F_k}^{\circ D}$) and orientation ($\varphi_{F_k}^{\circ D}$) of fixture CS at each station and fixture layout.

| Station | $\varphi_{F_k}^{\circ D}$ (rad) | $\mathbf{t}_{F_k}^{\circ D}$ (mm) | Locators w.r.t. F_k (mm) |
|---------|---------------------------------|-----------------------------------|--|
| 1 | $[-\pi/2, \pi, 0]$ | $[0, 0, 0]$ | $L_{1x} = 10, L_{1y} = 30, L_{2x} = 50, L_{2y} = 70, L_{3x} = 90, L_{3y} = 30,$ $p_{1y} = 30, p_{1z} = -35, p_{2y} = 70, p_{2z} = -35, p_{3x} = 50, p_{3z} = -20$ |
| 2 | $[-\pi/2, 0, 0]$ | $[0, 95, 45]$ | $L_{1x} = 10, L_{1y} = 30, L_{2x} = 50, L_{2y} = 70, L_{3x} = 90, L_{3y} = 30,$ $p_{1y} = 30, p_{1z} = -35, p_{2y} = 70, p_{2z} = -35, p_{3x} = 50, p_{3z} = -20$ |
| 3 | $[-\pi/2, \pi, 0]$ | $[0, 0, 2.5]$ | $L_{1x} = 10, L_{1y} = 30, L_{2x} = 50, L_{2y} = 70, L_{3x} = 90, L_{3y} = 30,$ $p_{1y} = 30, p_{1z} = -35, p_{2y} = 70, p_{2z} = -35, p_{3x} = 50, p_{3z} = -20$ |

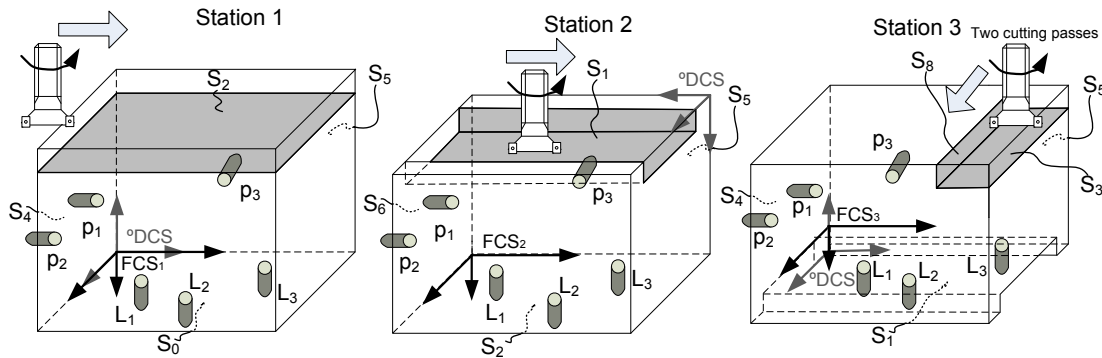


Figure 5.3: Case study. MMP adopted to manufacture the part.

Finally, a third experimentation was conducted to evaluate the effect of machining-induced variations. For this purpose, the locators errors and clamping procedure were kept identically as the experimentation 2, but a cutting-tool worn and a significant change of machine-tool thermal conditions (spindle temperature 29°C) without machine-tool thermal compensation were included in the experimental setup. By these new conditions, the deviation prediction of the SoV model should be higher than the experimentation 2 due to the influence of machining-induced variations on the KPCs. CMM measurements after experimentation 1, 2 and 3 and model predictions are shown in Table 5.5 and 5.6 respectively.

Table 5.3: Nominal location ($\mathbf{t}_{S_i}^{\circ D}$) and orientation ($\varphi_{S_i}^{\circ D}$) of each feature.

| Feature | $\varphi_{S_i}^{\circ D}$ (rad) | $\mathbf{t}_{S_i}^{\circ D}$ (mm) |
|---------|---------------------------------|-----------------------------------|
| S_0 | $[0, \pi, 0]$ | $[47.5, 47.5, 0]$ |
| S_1 | $[0, \pi, 0]$ | $[47.5, 47.5, 2.5]$ |
| S_2 | $[0, 0, 0]$ | $[47.5, 42.5, 45]$ |
| S_3 | $[0, 0, 0]$ | $[47.5, 90, 40]$ |
| S_4 | $[\pi/2, -\pi/2, -\pi/2]$ | $[47.5, 0, 22.5]$ |
| S_5 | $[0, -\pi/2, 0]$ | $[0, 47.5, 22.5]$ |
| S_6 | $[\pi/2, \pi/2, -\pi/2]$ | $[47.5, 95, 20]$ |
| S_7 | $[0, \pi/2, \pi/2]$ | $[95, 47.5, 22.5]$ |
| S_8 | $[\pi/2, \pi/2, -\pi/2]$ | $[47.5, 85, 42.5]$ |

Table 5.4: Locators errors measured in machine-tool table before conducting experiment 1, 2 and 3. Note that locators errors apply to station 1, 2 and 3.

| | Δl_1 (mm) | Δl_2 (mm) | Δl_3 (mm) | Δp_1 (mm) | Δp_2 (mm) | Δp_3 (mm) |
|------------|-------------------|-------------------|-------------------|-------------------|-------------------|-------------------|
| Exp. 1 | -0.008 | 0.000 | 0.012 | -0.018 | -0.004 | 0.000 |
| Exp. 2 – 3 | -0.041 | 0.000 | 0.096 | -0.018 | -0.004 | 0.000 |

Table 5.5: CMM results after experimentation 1, 2 and 3.

| | Experimentation 1 | | | Experimentation 2 | | | Experimentation 3 | | |
|----------|-------------------|--------|--------|-------------------|--------|--------|-------------------|--------|--------|
| | S_2 | S_3 | S_8 | S_2 | S_3 | S_8 | S_2 | S_3 | S_8 |
| x (mm) | – | – | – | – | – | – | – | – | – |
| y (mm) | – | – | 85.014 | – | – | 84.972 | – | – | 85.015 |
| z (mm) | 44.991 | 40.048 | – | 44.984 | 40.253 | – | 44.975 | 40.196 | – |

Table 5.6: SoV model prediction according to locator errors.

| | Experimentation 1 | | | Experimentation 2 – 3 | | |
|----------|-------------------|--------|--------|-----------------------|--------|--------|
| | S_2 | S_3 | S_8 | S_2 | S_3 | S_8 |
| x (mm) | – | – | – | – | – | – |
| y (mm) | – | – | 85.008 | – | – | 84.986 |
| z (mm) | 44.999 | 40.032 | – | 45.003 | 40.229 | – |

Table 5.7: Model prediction error after experimentation 1, 2 and 3.

| | Experimentation 1 | | | Experimentation 2 | | | Experimentation 3 | | |
|----------|-------------------|-------------|-------------|-------------------|-------------|-------------|-------------------|-------------|-------------|
| | Error S_2 | Error S_3 | Error S_8 | Error S_2 | Error S_3 | Error S_8 | Error S_2 | Error S_3 | Error S_8 |
| x (mm) | – | – | – | – | – | – | – | – | – |
| y (mm) | – | – | 0.006 | – | – | -0.014 | – | – | 0.029 |
| z (mm) | -0.008 | 0.016 | – | -0.019 | 0.024 | – | -0.028 | -0.033 | – |

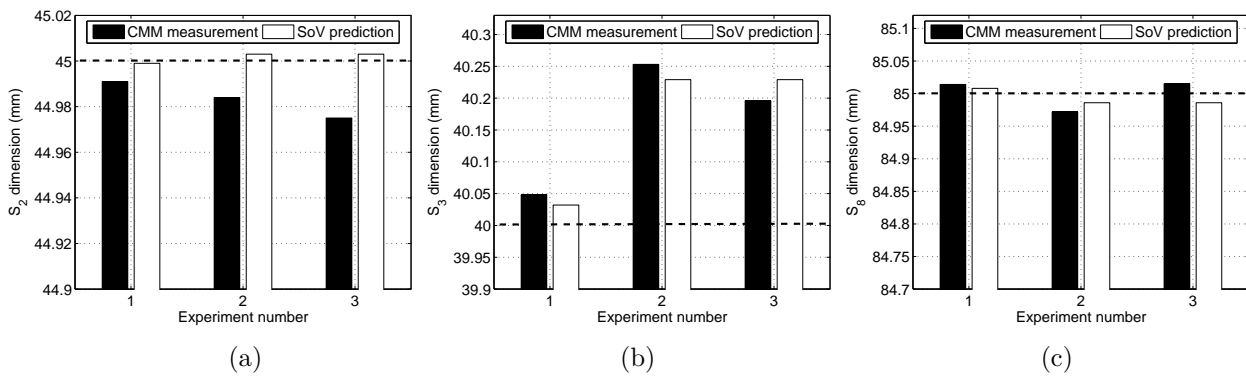


Figure 5.4: CMM measurements and SoV model predictions after experimentation 1, 2 and 3 for each KPC.

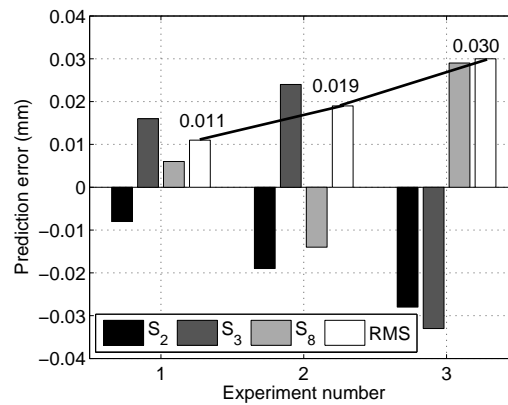


Figure 5.5: Prediction errors of the SoV model after experimentation 1, 2 and 3 for each KPC.

5.4 Discussion

After conducting experimentation 1, one can observe the difficulties to control all factors to ensure high quality machined parts. In spite of the control of locator errors, spindle expansion errors, cutting-tool wear-induced errors, cutting-tool length and diameter calibration and clamping errors, the machined parts have still uncontrol sources of error which prevent the manufacture of “perfect” parts. Besides the remaining locator errors, these factors could be geometrical-thermal axis errors, cutting-tool deflections, workpiece deformations due to cutting forces, etc. The maximum error is shown in feature S_3 where the KPC is deviated from 40.000 to 40.048 mm. Considering the remaining locator errors, the SoV model predicted fairly well the features S_2 , S_3 and S_8 , with prediction errors of -0.008 , 0.016 and 0.006 mm, respectively (Table 5.7).

For experimentation 2, the machined part presents an important deviation from the nominal dimensions as it is shown in Table 5.5 and Figure 5.4, where features S_2 , S_3 and

S_8 are deviated to 44.984, 40.253 and 84.972 *mm* respectively. These deviations are the results of the previous errors listed in the experimentation 1 and the effect of the locator errors introduced at locators L_1 and L_3 . The SoV model approximates the expected part quality reasonably, validating the model for propagating errors in MMPs due to locator errors. The predictions of features S_2 , S_3 and S_8 were 45.003, 40.229 and 84.986 as it is shown in Table 5.6. The prediction error for each KPC is shown in Table 5.7, and it is similar in magnitude to prediction errors in experimentation 1.

The addition of machining-induced variations such as spindle thermal expansion and cutting-tool wear-induced errors in experimentation 3 reveals the limitation of the SoV model predictions under these conditions. The spindle thermal expansion and cutting-tool wear seems to be important sources of error for the manufacture of features S_2 and S_3 since the actual values of both features are lower than those measured after experimentation 2. On the other hand, the machining-induced variations added produce an increase of S_8 in Z direction which is probably due to the cutting-tool wear of the cutting-tool edge during the end-milling operation. The deviations of these results with respect to those from experimentation 2 show the impact of machining-induced variations and suggest that, when machining-induced variations are present, the prediction error of SoV model will tend to be higher.

For comparison purposes, Figure 5.5 shows the prediction error at experimentation 1, 2 and 3 for each KPC, and the root-mean-squared (RMS) error. The first and second experimentation have a reduced RMS error since only locator errors are present. The RMS error at the second experimentation increases from 0.011 to 0.019 with respect to experimentation 1 due to higher locator errors. The RMS error at third experimentation error increases from 0.019 to 0.030 with respect to the second experimentation due to the machining-induced variations added. Therefore, the operation variations added in this case study involves the 57.9% of the RMS error in the SoV model predictions. The results from experimentation 1 – 3 confirm that the State Space model should be extended to include specific machining-induced variations, where additional KCCs should be added. For instance, the experimentation 3 reveals the great impact on part quality due to spindle thermal errors and cutting-tool wear errors.

5.5 Conclusions

In spite of the success of the SoV model for variation propagation modeling in MMPs, the absence of machining-induced variations into the model could be an important factor to limit the use of this model for accurate variation prediction. This chapter has experimentally shown the limitations of the SoV model when machining-induced variations are present. The case study analyzed at first and second experimentation has shown a reasonable accuracy of part quality prediction when locator errors are present and at the same time the machining-induced variations are controlled. The third experimentation conducted showed the limitation of the SoV model when machining-induced variations are present together with locator errors during normal fixture operation. The effect of the spindle thermal expansion and the cutting-tool errors increased the root-mean-squared prediction model error to 57.9%.

References

- [1] D. Djurdjanovic, J. Ni, Dimensional errors of fixtures, locating and measurement datum features in the stream of variation modeling in machining, *Journal of Manufacturing Science and Engineering* 125 (4) (2003) 716–730.
- [2] S. Zhou, Q. Huang, J. Shi, State space modeling of dimensional variation propagation in multistage machining process using differential motion vectors, *IEEE Transactions on Robotics and Automation* 19 (2) (2003) 296–309.
- [3] Q. Huang, J. Shi, Simultaneous tolerance synthesis through variation propagation modeling of multistage manufacturing processes, *NAMRI/SME Transactions*, 31 (2003) 515–522.
- [4] S. F. Zhang, Z. H. Sha, R. K. Kang, A physical machining accuracy predicting model in turning, *Key Engineering Materials* 329 (2007) 675–680.
- [5] J. Liu, J. Shi, S. J. Hu, Quality-assured setup planning based on the stream-of-variation model for multi-stage machining processes, *IIE Transactions* 41 (2009) 323–334(12).

Extension of the SoV model considering machining-induced variations

In spite of the success of the stream of variation (SoV) approach to modeling variation propagation in multi-station machining processes (MMPs), the absence of machining-induced variations could be an important factor that limits its application in accurate variation prediction, as shown in Chapter 5. Such machining-induced variations are caused by geometric-thermal effects, cutting-tool wear, etc. In this chapter, a generic framework for machining-induced variation representation based on differential motion vectors is presented. Based on this representation framework, machining-induced variations can be explicitly incorporated into the SoV model. An experimentation is designed and implemented to estimate the model coefficients related to spindle thermal-induced variations and cutting-tool wear-induced variations. The proposed model is compared with the conventional SoV model resulting in an average improvement on quality prediction of 67%. This result verifies the advantage of the proposed extended SoV model. The application of the extended model can lead to the investigation of new problems of quality improvement in MMPs such as machining error diagnosis, comprehensive manufacturing tolerance allocation (studied in Chapter 9), or new maintenance strategies.

6.1 Introduction

As it was exposed in Chapter 5, it is desirable to develop a process-level methodology to include machining-induced variations from different sources in the state space model. According to the literature, four main sources of machining-induced variations can be distinguished [1, 2]: geometric-kinematic variations, thermal-induced variations, cutting force-induced variations, and cutting-tool wear-induced variations. In single station, many research works have been conducted to model these machining sources of variation [3–10], and most of them were reported in Chapter 3. In general, these models require experimental procedures since the model derivation depends on the specific machining operation condition (cutting parameters, coolant types, machine-tool conditions, etc.). For instance, the evaluation of geometric-kinematic variations requires positioning errors, straightness errors and angular errors of machine-tool axes and squareness errors between axes, which

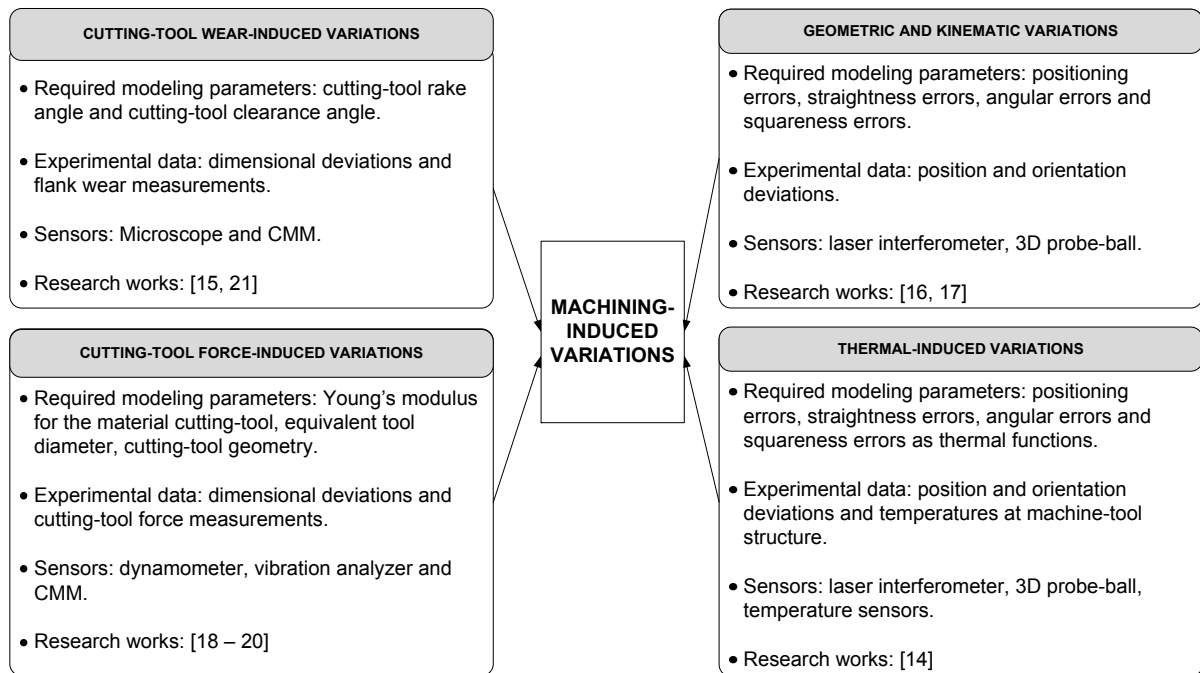


Figure 6.1: Required modeling parameters for estimating machining-induced variations.

can be measured with laser interferometers [5] or 3D probe-balls [6]. The evaluation of thermal-induced variations also requires an experimental procedure with the use of several temperature sensors throughout the machine-tool structure [3]. Other machining-induced variations, such as those related to cutting forces and tooling wear require parameters of cutting-tool geometry and frequency response properties, which can be estimated from experimental data [4, 7–10], and a coordinate measuring machine (CMM) for accurate part inspection. Figure 6.1 summarizes some of the required parameters to model machining-induced variations and some research works conducted for single station modeling.

In this chapter, a generic framework following the state space formulation based on differential motion vectors (DMVs) is proposed to explicitly model the induction and propagation of machining-induced variations. In addition, an experimentation is designed and implemented to estimate the model coefficients corresponding to cutting-tool wear-induced and spindle thermal-induced variations. The proposed model will provide quality improvement practitioners with a more comprehensive tool for more accurate and precise evaluation, monitoring and diagnosis of MMPs. This chapter is organized as follows. Section 6.2 summarizes the formulation of the state space model and the deviation representation mechanism adopted in this chapter. Section 6.3 presents the proposed generic framework for machining variation modeling, together with the detailed experimental procedure to model spindle thermal-induced variations and cutting-tool wear-induced variations through flank wear and spindle temperature measurements. A case study is conducted and summarized in Section 6.4 for model validation. Concluding remarks and potential model applications are discussed in Section 6.5.

6.2 Random Deviation Representation

In the conventional SoV model, datum-, machining- and fixture-induced variations are considered. These types of variations are induced by and transmitted among seven key elements of machining stations, named: i) machine-tool structure, ii) axes of the machine-tool, iii) machine-tool spindle, iv) cutting-tool, v) fixture locators, vi) workpiece datum features, and vii) manufacturing features. Describing the SoV is equivalent to represent the transmission and transformation of those types of variations among these elements.

6.2.1 Coordinate System Definition

In order to represent the dimensional variations of the seven elements involved in the SoV model, different CSs are defined.

Design Coordinate System (DCS). The nominal DCS, denoted as ${}^{\circ}D$, define the reference for the workpiece features during design. The definition of ${}^{\circ}D$ usually depends on the nominal geometry of the part and it is usually defined at an accessible corner. As this CS is only used in design, this CS cannot be deviated.

Reference Coordinate System (RCS). The nominal and true RCS, denoted as ${}^{\circ}R_k$ and R_k , respectively, define the reference for the workpiece features (Figure 6.2 (d)) at the station k . To facilitate the model derivation, the R_k is defined as the local CS of the primary datum feature at station k . In a 3-2-1 fixture layout, the primary datum is the main workpiece surface used to locate the part at the machine-tool table [11]. The R_k is defined similarly according to the actual part geometry.

Fixture Coordinate System (FCS). The nominal and true FCS at station k , denoted as ${}^{\circ}F_k$ and F_k , respectively, define the physical position and orientation of the fixture device according to the fixture layout. Figure 6.2 (d) shows the FCS for a fixture layout based on the 3-2-1 locating scheme.

Local Coordinate System (LCS^j). The nominal and true LCS^j at station k , denoted as ${}^{\circ}L_k^j$ and L_k^j , define the physical position and orientation of the j th nominal and actual surface of the part respectively (Figure 6.2 (c)). For planar surfaces the Z -axis of ${}^{\circ}L_k^j$ is commonly defined normal to the surface.

Machine-Tool Coordinate System (MCS). The MCS at station k , denoted as ${}^{\circ}M_k$, define the physical position and orientation of the reference CS for machine-tool movements. The origin of the ${}^{\circ}M_k$ is located at the locating origin of the nominal machine-tool table, with its Z -axis normal to the table and pointing upward, its X -axis parallel to the long axis of the table and pointing to its positive direction, and its Y -axis defined according to the right hand rule (RHR), as shown in Figure 6.2 (a). In this chapter, it is assumed that ${}^{\circ}M_k$ serves as the reference at station k and thus will not deviate.

Axis Coordinate System (ACSⁱ). The nominal and true ACS of the i th axis used at station k , denoted as ${}^{\circ}A_k^i$ and A_k^i , respectively, define the physical position and orien-

tation of the i th machine-tool axis. The origin of the ${}^{\circ}A_k^i$ is located at the geometrical center of the joint of the i th axis. For prismatic joints, the axes of the ${}^{\circ}A_k^i$ have the same orientation as that of the ${}^{\circ}M_k$. For revolute joints, the Z -axis of the ${}^{\circ}A_k^i$ coincides with the rotation axis with the same positive direction. Its X - and Y -axis are parallel to the axes of ${}^{\circ}M_k$ and their orientations are defined according to the RHR. For a 5-axis machine-tool, the CSs of machine-tool axes are shown in Figure 6.2 (a). The A_k^i is similarly defined for an actual axis.

Spindle Coordinate System (SCS). The nominal and true SCS at station k , denoted as ${}^{\circ}S_k$ and S_k , respectively, define the physical position and orientation of the spindle during machining. The origin of the ${}^{\circ}S_k$ is located at the geometrical center of the spindle and the orientations of axes are identical to that of the Z -axis of the machine-tool, as shown in Figure 6.2 (b). The S_k is defined similarly for the actual spindle.

Cutting-Tool Coordinate System (CCS). The nominal and true CCS at station k , denoted as ${}^{\circ}C_k$ and C_k , respectively, define the physical position and orientation of the cutter tip center during machining. The origin of the ${}^{\circ}C_k$ is located at the cutter tip center and the orientations of its axes are identical to that of the S_k , as shown in Figure 6.2 (c). The C_k is defined similarly for the actual cutting-tool.

Cutting-Tool Tip Coordinate System (TPCS). The nominal and true TPCS at station k , denoted as ${}^{\circ}P_k$ and P_k , respectively, defines the physical position and orientation of the cutting-tool tip. The origin of the ${}^{\circ}P_k$ is located at the center of the cutting edge that is used to generate a feature j , and the orientations of its axes are identical to that of ${}^{\circ}L_k^j$. Please note that, when machining a feature j at station k , the cutting-tool tip removes material generating the machined feature which is defined by the L_k^j . Thus, the position and orientation of the P_k define the position and orientation of L_k^j , as shown in Figure 6.2 (c).

The CSs defined above establish a generic framework for representing the variation induction and transmission from the cutting-tool tip to the j th manufacturing feature, i.e., from P_k to ${}^{\circ}D$. The whole framework is composed of two sub-chains. The first chain, defined from ${}^{\circ}M_k$ to P_k , represents how machining-induced variations deviate the cutting-tool tip w.r.t. the machine-tool CS. The most common machining-induced variations are due to geometric and kinematic errors of machine-tool axes, thermal distortions, cutting-tool deflections and cutting-tool wear, which induce deviations of CSs A_k^i , S_k , C_k and P_k , respectively. The second chain, defined from ${}^{\circ}M_k$ to ${}^{\circ}D$, represents how fixture- and datum-induced variations deviate the workpiece location w.r.t. the machine-tool CS.

6.2.2 Variation Representation

The position and the orientation of a CS can be defined by a vector consisting of a positioning vector and an orientation vector w.r.t. a certain CS. For instance, CS_1 can be defined, w.r.t. CS_2 , as $\mathbf{r}_1^2 = [(\mathbf{t}_1^2)^T \ (\mathbf{q}_1^2)^T]^T$, where $\mathbf{t}_1^2 = [x_1^2 \ y_1^2 \ z_1^2]^T$ and $\mathbf{q}_1^2 = [\alpha_1^2 \ \beta_1^2 \ \gamma_1^2]^T$. This indicates that the projections of CS_1 on the three coordinates of CS_2 , X_2 , Y_2 and Z_2 , are x_1^2 , y_1^2 and z_1^2 , respectively. The orientation of the axes X_1 , Y_1 and Z_1 can be obtained

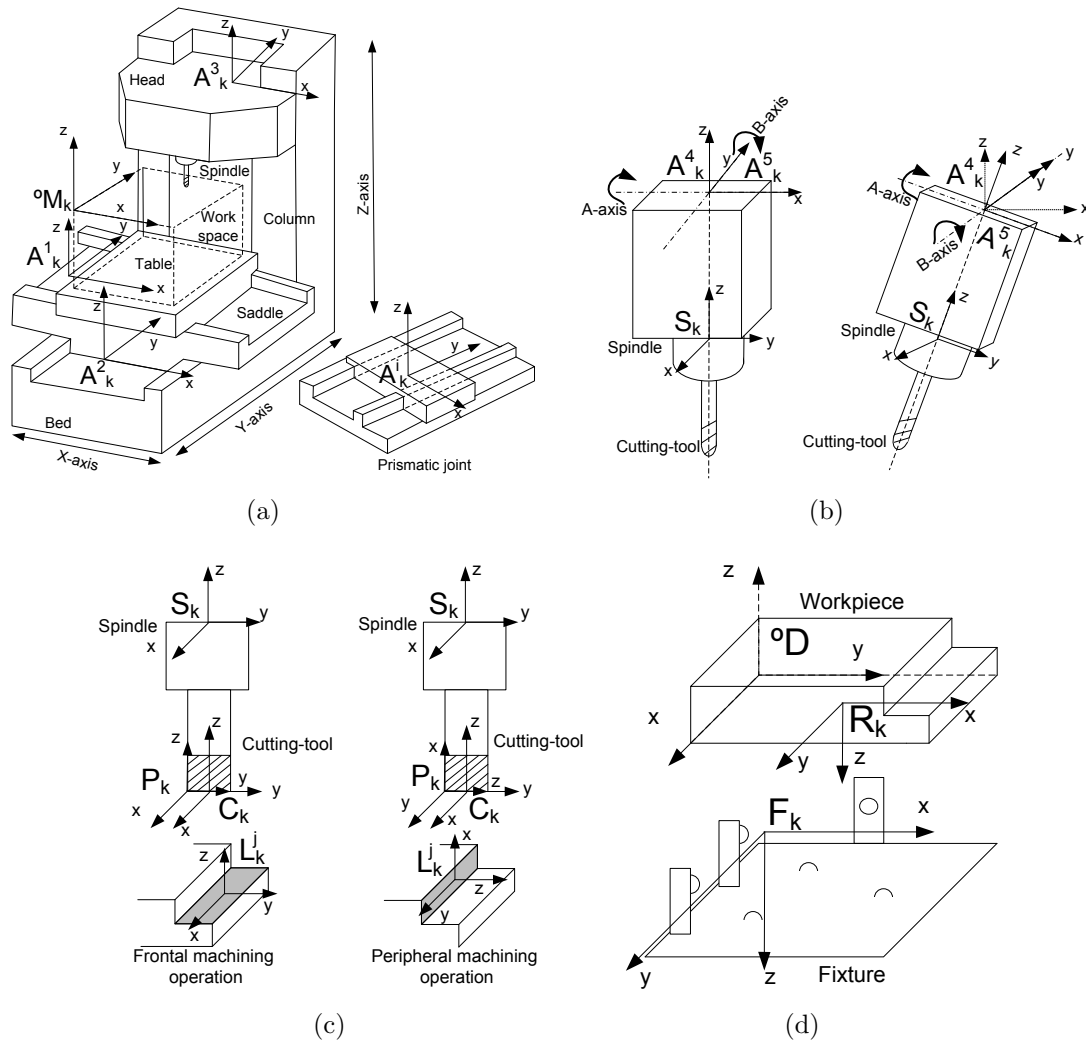


Figure 6.2: Example of the CSs involved in a 5-axis CNC machine-tool (type X-Y-Z-A-B).

by sequentially rotating CS_2 around Z_2 , Y_2' (after the first rotation) and Z_2'' (after the second rotation) with Euler angles of α_1^2 , β_1^2 and γ_1^2 , respectively.

Based on the CS definitions and the vectorial CS representations, the random deviation of an element involved in the machining process, e.g., a machine-tool spindle, can be represented by a DMV [12] of its own CS w.r.t. another CS. For instance, CS_1 is the SCS of a spindle and CS_2 is the MCS of a machine-tool. The nominal position and orientation of the spindle of a machine-tool is defined by \mathbf{r}_1^2 . The random deviation of the spindle w.r.t. the machine-tool can be defined by the DMV \mathbf{x}_1^2 , where $\mathbf{x}_1^2 = [(\mathbf{d}_1^2)^T \ (\mathbf{s}_1^2)^T]^T$, \mathbf{d}_1^2 contains three small position deviations, i.e., $\mathbf{d}_1^2 = [\Delta x_1^2 \ \Delta y_1^2 \ \Delta z_1^2]^T$, and \mathbf{s}_1^2 contains three small orientation deviations, i.e., $\mathbf{s}_1^2 = [\Delta \alpha_1^2 \ \Delta \beta_1^2 \ \Delta \gamma_1^2]^T$.

The DMV representation of random deviations among CSs creates the basis of the

variation propagation model. The induction, transmission and accumulation of deviations are modeled along the chain of CSs as a series of transformations of DMVs among different CSs. These transformations are linearized by assuming that the magnitudes of DMV elements are small, and are mathematically represented by the following lemma [13]:

Lemma 1. *Consider the CSs R , 1 and 2, with CSs 1 and 2 deviating from their nominal positions and orientations. Noting the deviation of CS 1 from nominal values as \mathbf{x}_1^R and the deviation of CS 2 w.r.t. CS 1 as \mathbf{x}_2^1 , then, the deviation of CS 2 from nominal values can be formulated as*

$$\begin{aligned}\mathbf{x}_2^R &= \begin{pmatrix} (\mathbf{R}_{\circ 2}^{\circ 1})^T & -(\mathbf{R}_{\circ 2}^{\circ 1})^T \cdot (\hat{\mathbf{t}}_{\circ 2}^{\circ 1}) & \mathbf{I}_{3 \times 3} & \mathbf{0}_{3 \times 3} \\ \mathbf{0}_{3 \times 3} & (\mathbf{R}_{\circ 2}^{\circ 1})^T & \mathbf{0}_{3 \times 3} & \mathbf{I}_{3 \times 3} \end{pmatrix} \cdot \begin{pmatrix} \mathbf{x}_1^R \\ \mathbf{x}_2^1 \end{pmatrix}, \\ &= \mathbf{T}_2^1 \cdot \mathbf{x}_1^R + \mathbf{x}_2^1.\end{aligned}\quad (6.1)$$

where $\mathbf{R}_{\circ 2}^{\circ 1}$ is the rotation matrix of $\circ 2$ w.r.t. $\circ 1$, $\mathbf{I}_{3 \times 3}$ is a 3×3 identity matrix and $\hat{\mathbf{t}}_{\circ 2}^{\circ 1}$ is the skew matrix of vector $\mathbf{t}_{\circ 2}^{\circ 1}$.

The proof of this lemma can be found in [13], and it is shown in the Appendix 6.1. This lemma is intensively used in this chapter to derive the deviation transmission among different CSs.

6.3 Extension of the State Space Model

Based on the vectorial deviation representation with DMVs, variation propagation in an N -station MMP can be described with the variation propagation model [13]

$$\mathbf{x}_k = \mathbf{A}_k \cdot \mathbf{x}_{k-1} + \mathbf{B}_k \cdot \mathbf{u}_k + \mathbf{w}_k, \quad (6.2)$$

$$\mathbf{y}_k = \mathbf{C}_k \cdot \mathbf{x}_k + \mathbf{v}_k, \quad (6.3)$$

where $k = 1, 2, \dots, N$. In the station transition equation (6.2), $\mathbf{A}_k \cdot \mathbf{x}_{k-1}$ represents the deviations transmitted by datum features generated at upstream stations; $\mathbf{B}_k \cdot \mathbf{u}_k$ represents the deviations introduced within station k , including those from fixture locators and by machining operations. In the observation equation (6.3), $\mathbf{C}_k \cdot \mathbf{x}_k$ represents the deviations of KPCs. The terms \mathbf{w}_k and \mathbf{v}_k define the un-modeled system errors (e.g., linearization errors) and the measurement noise, respectively.

In the conventional SoV model formulation [13], only the fixture-induced variations and an overall cutting-tool path variations are considered in \mathbf{u}_k . In that model, \mathbf{u}_k is defined as $\mathbf{u}_k = \left[(\mathbf{u}_k^f)^T, (\mathbf{u}_k^m)^T \right]^T = [\Delta l_1^k, \Delta l_2^k, \Delta l_3^k, \Delta l_4^k, \Delta l_5^k, \Delta l_6^k, (\mathbf{u}_k^m)^T]^T$, where \mathbf{u}_k^f is the deviation of the fixture components (Δl_i^k is the deviation of the i th fixture locator from their nominal position at station k), and \mathbf{u}_k^m is the overall cutting-tool path deviation that models the overall deviation of the j th machined feature CS, L_k^j , from the nominal fixture CS, $\circ F_k$, i.e., $\mathbf{x}_{L_k^j}^{\circ F_k}$. However, this formulation does not explicitly model any specific

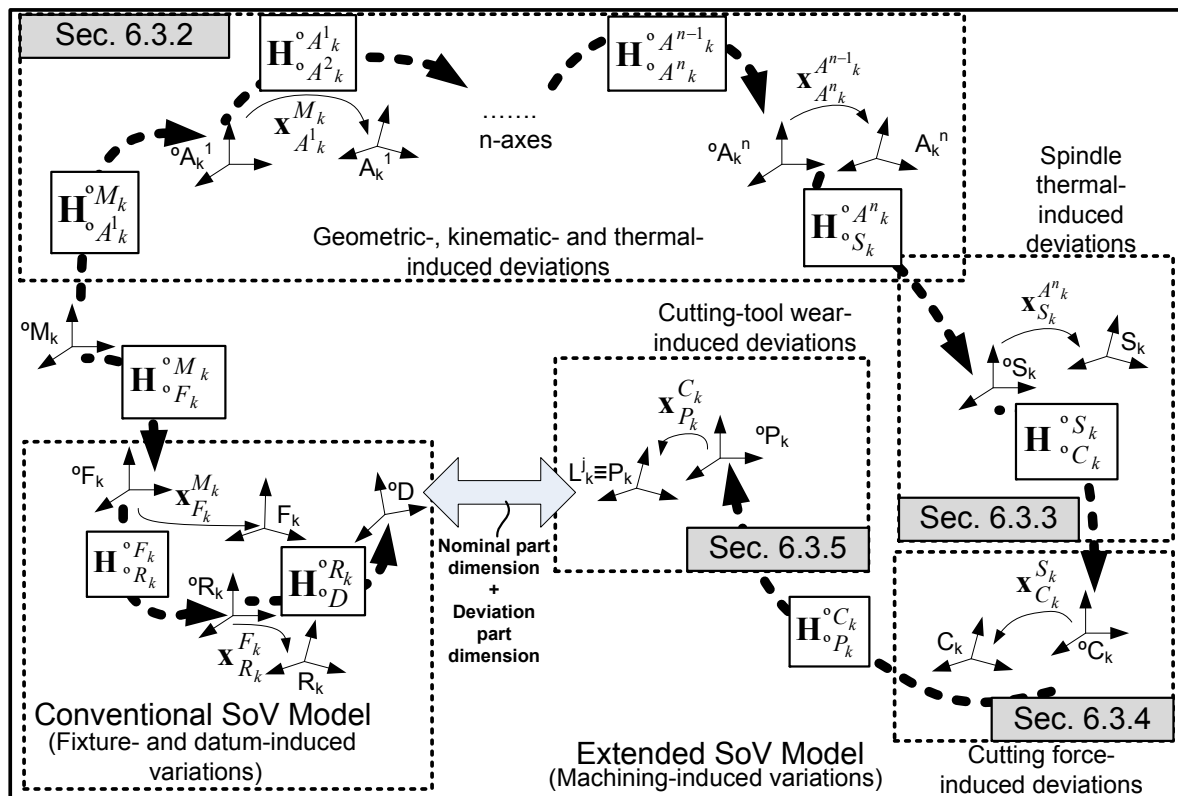


Figure 6.3: Relationships between the different CSs in a n -axis machine-tool.

machining-induced variation, such as those due to geometric-thermal effects, cutting-tool wear or cutting-tool deflections. In the next section, an extension of the conventional state space model to incorporate machining-induced variations will be proposed.

6.3.1 Framework for Incorporating Machining-Induced Variations

In this chapter, the manufacturing features are obtained from material removal by the cutting-tool edge. Thus, the overall cutting-tool path deviation of a manufacturing feature, $x_{L_k^j}^{F_k}$, is equivalent to the deviation of the cutting-tool edge, represented by the TPCS P_k , from the nominal fixture CS, $x_{P_k}^{F_k}$, i.e., $x_{L_k^j}^{F_k} \equiv x_{P_k}^{F_k}$. In this context, the incorporation of machining-induced variations can be built upon investigating the variations along the chain of CSs from the TPCS, P_k , to the nominal FCS, oF_k , at station k .

Figure 6.3 shows the relationship between the different CSs at station k where a generic n -axis machine-tool is used. All the elements involved in that station are defined by their corresponding CSs, composing a chain of CSs. Every nominal CS is defined w.r.t. its previous nominal CS in the chain, through an homogeneous transformation matrix (HTM). Due to fixture- and machining-induced variations, the CSs are deviated from their nominals by a DMV. Thus, at station k , the final cutting-tool path deviation defined by the

DMV $\mathbf{x}_{P_k}^{\circ F_k}$ will be affected by the DMVs of all CSs in the chain. Applying Lemma 1 repeatedly, one can express the total cutting-tool path deviation $\mathbf{x}_{P_k}^{\circ F_k}$ as a function of all CSs' deviations according to the following expression:

$$\mathbf{x}_{P_k}^{\circ F_k} = \mathbf{x}_{P_k}^{\circ M_k} = \mathbf{T}_{P_k}^{C_k} \cdot (\mathbf{T}_{C_k}^{S_k} \cdot (\mathbf{T}_{S_k}^{A_k^n} \cdot \mathbf{x}_{A_k^n}^{\circ M_k} + \mathbf{x}_{S_k}^{A_k^n}) + \mathbf{x}_{C_k}^{S_k}) + \mathbf{x}_{P_k}^{C_k}, \quad (6.4)$$

where the DMV terms refer to the following machining-induced variations:

(i) The geometric, kinematic and thermal variations of machine-tool axes, represented as a DMV, $\mathbf{x}_{A_k^n}^{\circ M_k}$, of the true ACS, A_k^n , w.r.t. the nominal MCS, ${}^{\circ}M_k$. It is modeled as

$$\mathbf{x}_{A_k^n}^{\circ M_k} = \mathbf{B}_k^{m_1} \cdot [\Delta T_1^k \quad \dots \quad \Delta T_m^k \quad \Delta \mathbf{r}^k]^T. \quad (6.5)$$

The deviation at the n th axis of a machine-tool is calculated from the temperature deviations at m different locations on the machine-tool structure, i.e., $\Delta T_1^k, \dots, \Delta T_m^k$. It is also determined by the deviations of the placement of the workpiece on the machine-tool table from nominal values along the n th machine-tool axis ($\Delta \mathbf{r}^k$). Please note that the nominal values of temperatures and placement of the workpiece are defined for the linearization of the geometric-thermal variations. As this chapter is focused on modeling and analyzing random deviations in MMPs, we discard the systematic deviations due to linearization since they can be compensated by calibration. The derivation of $\mathbf{B}_k^{m_1}$ is introduced in Section 6.3.2.

(ii) The spindle-thermal variation, represented as a DMV, $\mathbf{x}_{S_k}^{A_k^n}$, of the true SCS, S_k , w.r.t. the true ACS, A_k^n . It is modeled as

$$\mathbf{x}_{S_k}^{A_k^n} = \mathbf{B}_k^{m_2} \cdot [\Delta T_s^k]. \quad (6.6)$$

The deviation of the spindle due to its thermal expansion is a function of the spindle temperature variation ΔT_s^k . The derivation of $\mathbf{B}_k^{m_2}$ is introduced in Section 6.3.3.

(iii) The cutting force-induced variation, represented as a DMV, $\mathbf{x}_{C_k}^{S_k}$, of the true CCS, C_k , w.r.t. the true SCS, S_k . It is modeled as

$$\mathbf{x}_{C_k}^{S_k} = \mathbf{B}_k^{m_3} \cdot [\Delta F_x^k \quad \Delta F_y^k]^T. \quad (6.7)$$

The deviation of the cutting-tool due to deflections is a function of the variations of the cutting forces ΔF_x^k and ΔF_y^k . The derivation of $\mathbf{B}_k^{m_3}$ is introduced in Section 6.3.4.

(iv) The cutting-tool wear-induced variations, represented as a DMV, $\mathbf{x}_{P_k}^{C_k}$, of the true TPCS, P_k , w.r.t. the true CCS, C_k .

$$\mathbf{x}_{P_k}^{C_k} = \mathbf{B}_k^{m_4} \cdot [V_{B_{ij}}^k]. \quad (6.8)$$

The deviation of the cutting-tool tip is a function of the cutting-tool wear at the cutting edge $V_{B_{ij}}^k$ where i and j refers to the i th cutting edge of the j th cutting-tool. The derivation of $\mathbf{B}_k^{m_4}$ is introduced in Section 6.3.5.

Based on the elaboration of the four DMV terms, Eq. (6.4) can be re-written as:

$$\begin{aligned} \mathbf{x}_{P_k}^{\circ F_k} = & \left[\mathbf{T}_{P_k}^{C_k} \cdot \mathbf{T}_{C_k}^{S_k} \cdot \mathbf{T}_{S_k}^{A_k^n} \cdot \mathbf{B}_k^{m_1} \quad \vdots \quad \mathbf{T}_{P_k}^{C_k} \cdot \mathbf{T}_{C_k}^{S_k} \cdot \mathbf{B}_k^{m_2} \quad \vdots \quad \mathbf{T}_{P_k}^{C_k} \cdot \mathbf{B}_k^{m_3} \quad \vdots \quad \mathbf{B}_k^{m_4} \right] \cdot \\ & \cdot \left[\Delta T_1^k \quad \dots \quad \Delta T_m^k \quad \Delta x^k \quad \Delta y^k \quad \Delta z^k \quad \Delta \alpha^k \right. \\ & \left. \Delta \beta^k \quad \vdots \quad \Delta T_s^k \quad \vdots \quad \Delta F_x^k \quad \Delta F_y^k \quad \vdots \quad V_{B_{ij}}^k \right]^T. \end{aligned} \quad (6.9)$$

This formulation can be incorporated into the model (6.2), where $\mathbf{B}_k \cdot \mathbf{u}_k$ is defined as

$$\mathbf{B}_k \cdot \mathbf{u}_k = [\mathbf{B}_f^k \quad \vdots \quad \mathbf{B}_m^k] \cdot [\mathbf{u}_k^f \quad \vdots \quad \mathbf{u}_k^m]^T, \quad (6.10)$$

and \mathbf{B}_f^k models the impacts of the deviations of fixture locators, \mathbf{u}_k^f ; \mathbf{B}_m^k is a selector matrix (see Appendix 4.3), to specify the feature machined at station k ; and \mathbf{u}_k^m is the DMV $\mathbf{x}_{L_k^j}^{\circ F_k}$, which is equivalent to the DMV $\mathbf{x}_{P_k}^{\circ F_k}$ in this chapter. Therefore, the conventional SoV model can be extended by plugging Eq. (6.9) into Eq. (6.10). The term $\mathbf{B}_k \cdot \mathbf{u}_k$ in the extended SoV model is

$$\begin{aligned} \mathbf{B}_k \cdot \mathbf{u}_k = & \left[\mathbf{B}_f^k \quad \vdots \quad \mathbb{A}_5^k \cdot \mathbf{T}_{P_k}^{C_k} \cdot \mathbf{T}_{C_k}^{S_k} \cdot \mathbf{T}_{S_k}^{A_k^n} \cdot \mathbf{B}_k^{m_1} \quad \vdots \quad \mathbb{A}_5^k \cdot \mathbf{T}_{P_k}^{C_k} \cdot \mathbf{T}_{C_k}^{S_k} \cdot \mathbf{B}_k^{m_2} \quad \vdots \right. \\ & \left. \mathbb{A}_5^k \cdot \mathbf{T}_{P_k}^{C_k} \cdot \mathbf{B}_k^{m_3} \quad \vdots \quad \mathbb{A}_5^k \cdot \mathbf{B}_k^{m_4} \right] \cdot \left[\left(\mathbf{u}_k^f \right)^T \quad \vdots \quad \Delta T_1^k \quad \dots \quad \Delta T_m^k \quad \Delta x^k \quad \Delta y^k \right. \\ & \left. \Delta z^k \quad \Delta \alpha^k \quad \Delta \beta^k \quad \vdots \quad \Delta T_s^k \quad \vdots \quad \Delta F_x^k \quad \Delta F_y^k \quad \vdots \quad V_{B_{ij}}^k \right]^T. \end{aligned} \quad (6.11)$$

A summary of the procedure to obtain the state space model incorporating machining-induced variations is shown in Figure 6.4. As it can be noted, part of the procedure is based on the conventional procedure to derive the state space model, described in Chapter 4 and presented in [13]. The rest of the procedure, is the proposed extension model where each machining-induced variation is modeled and added into the state space model.

The following subsections elaborate the derivation of the DMVs and the corresponding coefficient matrices defined from Eq. (6.5) to Eq. (6.8) by modeling each type of machining-induced variations.

6.3.2 Geometric, kinematic and thermal variations of machine-tool axes

As it was explained in Chapter 3, for an n -axis machine-tool, the final position of the A_k^n w.r.t. the ${}^\circ M_k$ can be defined as

$$\mathbf{H}_{A_k^n}^{\circ M_k} = \mathbf{H}_{A_k^n}^{\circ M_k} \cdot \delta \mathbf{H}_{A_k^n}^{\circ M_k} = \mathbf{H}_{A_k^1}^{\circ M_k} \cdot \delta \mathbf{H}_{A_k^1}^{\circ M_k} \cdot \prod_{i=2}^n \mathbf{H}_{A_k^i}^{\circ A_k^{i-1}} \cdot \delta \mathbf{H}_{A_k^i}^{\circ A_k^{i-1}}, \quad (6.12)$$

where \mathbf{H}_b^a is the HTM of CS b w.r.t. CS a , and $\delta \mathbf{H}_b^a$ is the HTM that defines the small position and orientation deviations of CS b w.r.t. a due to the deviation from nominal values of b and a . With the assumption of rigid-body kinematics and small-angle approximation,

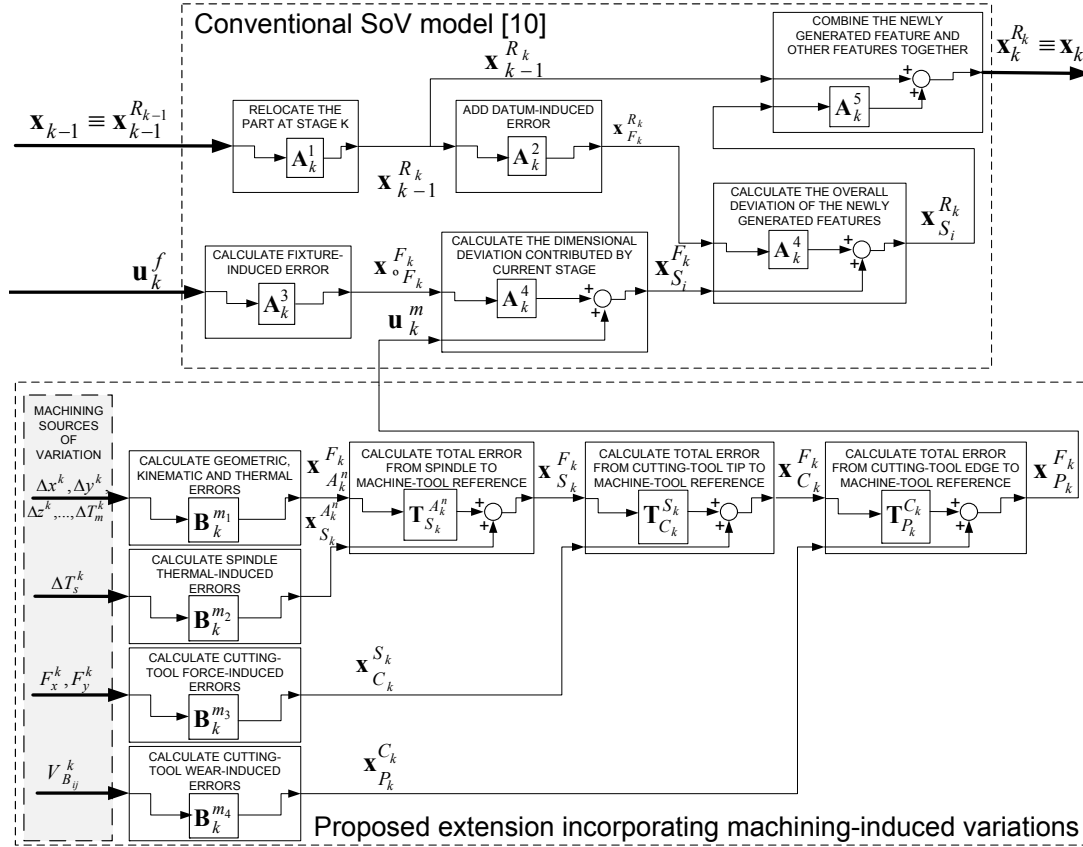


Figure 6.4: Summary of the procedure to derive the extended state space model.

any differential transformation matrix $\delta \mathbf{H}_{A_k}^{A_k^{i-1}}$ can be generally defined as a product of three HTMs [3, 6, 14], i.e.,

$$\delta \mathbf{H}_{A^i}^{A^{i-1}} = \begin{pmatrix} 1 & -\varepsilon_{zi} & \varepsilon_{yi} & \delta_{xi} \\ \varepsilon_{zi} & 1 & -\varepsilon_{xi} & \delta_{yi} \\ -\varepsilon_{yi} & \varepsilon_{xi} & 1 & \delta_{zi} \\ 0 & 0 & 0 & 1 \end{pmatrix} \cdot \begin{pmatrix} 1 & -\varepsilon_z(i) & \varepsilon_y(i) & \delta_x(i) \\ \varepsilon_z(i) & 1 & -\varepsilon_x(i) & \delta_y(i) \\ -\varepsilon_y(i) & \varepsilon_x(i) & 1 & \delta_z(i) \\ 0 & 0 & 0 & 1 \end{pmatrix} \cdot \begin{pmatrix} 1 & -\varepsilon_z^t(t, T_1, \dots, T_m, q) & \varepsilon_y^t(t, T_1, \dots, T_m, q) & \delta_x^t(t, T_1, \dots, T_m, q) \\ \varepsilon_z^t(t, T_1, \dots, T_m, q) & 1 & -\varepsilon_x^t(t, T_1, \dots, T_m, q) & \delta_y^t(t, T_1, \dots, T_m, q) \\ -\varepsilon_y^t(t, T_1, \dots, T_m, q) & \varepsilon_x^t(t, T_1, \dots, T_m, q) & 1 & \delta_z^t(t, T_1, \dots, T_m, q) \\ 0 & 0 & 0 & 1 \end{pmatrix}. \quad (6.13)$$

The first HTM describes the mounting errors of the i th axis w.r.t. the previous $(i-1)$ th axis. The mounting errors are position and orientation errors due to assembly errors and they are not dependent on the carriage position. Mounting errors can be represented by two of three possible angular deviations ε_{xi} (rotation around the X -axis), ε_{yi} (rotation around the Y -axis) and ε_{zi} (rotation around the Z -axis), and three offsets (δ_{xi} , δ_{yi} , δ_{zi}). The second HTM represents the motional deviations, which include the terms $\delta_p(q)$ and the terms $\varepsilon_p(q)$. $\delta_p(q)$ refers to the positional deviation in the P -axis direction when the prismatic joint moves along the Q -axis and is a function of the position of the Q -axis. $\varepsilon_p(q)$ refers to the angular deviation around the P -axis when the Q -axis moves and it is also a function of the position of the Q -axis. The third HTM describes the geometrical deviations due to thermal effects, whose components are defined as $\delta_p^t(t, T_1, \dots, T_m, q)$ and

$\varepsilon_p^t(t, T_1, \dots, T_m, q)$ for position and angular deviations, respectively. Mathematically, these terms are defined by the expressions [3]

$$\delta_p^t(t, T_1, \dots, T_m, q) = f_0^{pq}(T_1, \dots, T_m, t) + f_1^{pq}(T_1, \dots, T_m, t) \cdot q + f_2^{pq}(T_1, \dots, T_m, t) \cdot q^2 + \dots (6.14)$$

$$\varepsilon_p^t(t, T_1, \dots, T_m, q) = g_0^{pq}(T_1, \dots, T_m, t) + g_1^{pq}(T_1, \dots, T_m, t) \cdot q + g_2^{pq}(T_1, \dots, T_m, t) \cdot q^2 + \dots (6.15)$$

The terms $f_0^{pq}(T_1, \dots, T_m, t)$ and $g_0^{pq}(T_1, \dots, T_m, t)$ are the PITE components that model the position deviation on the P -axis when the Q -axis moves and it is a function of the operation time from the startup, t , and the temperatures T_1, \dots, T_m at different locations on the machine-tool structure. The terms $f_1^{pq}(T_1, \dots, T_m, t) \cdot q + f_2^{pq}(T_1, \dots, T_m, t) \cdot q^2 + \dots$ and $g_1^{pq}(T_1, \dots, T_m, t) \cdot q + g_2^{pq}(T_1, \dots, T_m, t) \cdot q^2 + \dots$ are the PDTE components that model the position and angular deviation on the P -axis when the Q -axis moves and it is a function of time, machine-tool temperatures and position at the Q -axis, denoted as q .

Eq. (6.13) shows that geometrical deviations due to kinematic and thermal effects may present non-linear relationships. In order to include these sources of variation into the SoV model, a linearization should be conducted based on three important assumptions. Firstly, it is assumed that the geometric-thermal deviations are modeled when the machine-tool is warmed-up adequately and thus, the effect of time on the thermal deviations can be neglected. Secondly, it is assumed that the workpiece is repeatedly placed in the same region inside the allowable work space of the machine-tool table and thus, only small deviations at the placement of the workpiece are expected. Thirdly, it is assumed that geometric, kinematic and thermal deviations do not change drastically along the travels at any axis (the experimentation in [3] supports this assumption). As a result, the geometric-thermal deviations in the machine-tool axis can be linearized without significant loss of precision. Under these assumptions, the motional deviations $\delta_p(q)$ and $\varepsilon_p(q)$ are linearized as $\delta_p(q_0) + \frac{\delta(\delta_p(q))}{\delta q} \Big|_{q=q_0} \cdot \Delta q$ and $\varepsilon_p(q_0) + \frac{\delta(\varepsilon_p(q))}{\delta q} \Big|_{q=q_0} \cdot \Delta q$, respectively, where q_0 is the nominal placement of the workpiece on the Q -axis, and Δq is the deviation of the workpiece placement on the machine-tool table along the Q -axis. On the other hand, the thermal-induced deviations $\delta_p^t(t, T_1, \dots, T_m, q)$ and $\varepsilon_p^t(t, T_1, \dots, T_m, q)$ from Eqs.(6.14) and (6.15) can be linearized as

$$\delta_p^t(t, T_1, \dots, T_m, q) = C_0^{pq} + C_1^{pq} \cdot \Delta T_1 + \dots + C_m^{pq} \cdot \Delta T_m + C_{m+1}^{pq} \cdot \Delta q, \quad (6.16)$$

$$\varepsilon_p^t(t, T_1, \dots, T_m, q) = D_0^{pq} + D_1^{pq} \cdot \Delta T_1 + \dots + D_m^{pq} \cdot \Delta T_m + D_{m+1}^{pq} \cdot \Delta q, \quad (6.17)$$

where $C_{(\cdot)}^{pq}$ and $D_{(\cdot)}^{pq}$ are constants, ΔT_c is the deviation of the c th temperature point at the machine-tool structure from its nominal values T_{c_0} where $c = 1, \dots, m$.

As a conclusion, the resulting position and orientation deviations defined by the matrix $\delta \mathbf{H}_{A_k^n}^{\circ M_k}$, considering the linearization, can be obtained from Eq. (6.12). This matrix will be defined in the form of

$$\delta \mathbf{H}_{A_k^n}^{\circ M_k} = \begin{pmatrix} 1 & -\theta_{A_k^n z}^{\circ M_k} & \theta_{A_k^n y}^{\circ M_k} & d_{A_k^n z}^{\circ M_k} \\ \theta_{A_k^n z}^{\circ M_k} & 1 & -\theta_{A_k^n x}^{\circ M_k} & d_{A_k^n y}^{\circ M_k} \\ -\theta_{A_k^n y}^{\circ M_k} & \theta_{A_k^n x}^{\circ M_k} & 1 & d_{A_k^n z}^{\circ M_k} \\ 0 & 0 & 0 & 1 \end{pmatrix}, \quad (6.18)$$

Eq. (6.18) can be rewritten in a DMV as

$$\mathbf{x}_{A_k^n}^{\circ M_k} = \mathbf{B}_k^{m_1} \cdot [\Delta T_1^k, \dots, \Delta T_m^k, \Delta \mathbf{r}^k]^T. \quad (6.19)$$

In Eq. (6.19), $\Delta \mathbf{r}^k$ denotes the deviation of the workpiece placement on the machine-tool table along the n th axes. In case a 5-axis machine-tool with A -axis and B -axis is modeled, $\Delta \mathbf{r}^k = [\Delta x^k, \Delta y^k, \Delta z^k, \Delta \alpha^k, \Delta \beta^k]$, where $\Delta \alpha$ and $\Delta \beta$ denote the deviation of the workpiece placement on A -axis and B -axis from linearized values, respectively. Please note that we discard the systematic deviations due to linearization such as the terms C_0^{pq} , D_0^{pq} , $\delta_p(q_0)$, $\varepsilon_p(q_0)$, since they can be eliminated by an initial calibration.

For practical purposes, geometric and thermal parameters related to geometric-thermal induced variations can be estimated from experimental data. Research works [3, 15–17] show in detail the derivation of these parameters.

6.3.3 Spindle thermal-induced variations

The spindle thermal variations are an important contributor to the total thermal variations during machining due to the large amounts of heat generated at high-speed revolutions [18]. Spindle thermal errors produce three positioning and two rotational drifts to the spindle CS [3]. This deviation is represented as the deviation of the $^{\circ}SCS$ w.r.t. ACS^n and is proportional to the increase of the spindle temperature, ΔT_s , from nominal conditions. At station k , this deviation is defined by the DMV

$$\begin{aligned} \mathbf{x}_{S_k}^{A_k^n} &= [f_1^k(\Delta T_s^k) \quad f_2^k(\Delta T_s^k) \quad f_3^k(\Delta T_s^k) \quad f_4^k(\Delta T_s^k) \quad f_5^k(\Delta T_s^k) \quad f_6^k(\Delta T_s^k)]^T \\ &\approx [C f_x^k \quad C f_y^k \quad C f_z^k \quad C f_\alpha^k \quad C f_\beta^k \quad 0]^T \cdot \Delta T_s^k = \mathbf{B}_k^{m_2} \cdot \Delta T_s^k, \end{aligned} \quad (6.20)$$

where $f_i^k(\cdot)$ is a function that relates position and orientation errors of S_k with the deviation of the spindle temperature from nominal conditions. $C f_i^k$ are proportional coefficients linearizing the $f_i^k(\cdot)$ functions and the $f_6^k(\Delta T_s^k)$ is considered 0 since it is assumed that the cutting-tool rotations axis is Z . These coefficients can be obtained through experimentation.

The experimentation to be conducted for modeling the spindle dimensional variations due to thermal effects consists of milling different workpiece surfaces at different spindle thermal states as it is shown in Figure 6.5 (a). To avoid fixture-induced variations, a workpiece with accurate datum surfaces should be mounted on a 3-2-1 fixture scheme during all the experiment. Several end milling operations are conducted with new cutting inserts at different spindle temperatures. The end milling operations are defined to manufacture the workpiece in the form of a “ladder” to make later possible the measurement of the surfaces generated at each operation. The spindle temperature is measured by a temperature sensor and for each end milling operation the temperature of the spindle is increased by rotating the spindle at high-speed revolutions. After milling at different temperatures, the workpiece is measured in a CMM and the dimensional deviations of manufacturing features can be linearly fitted to the spindle temperature.

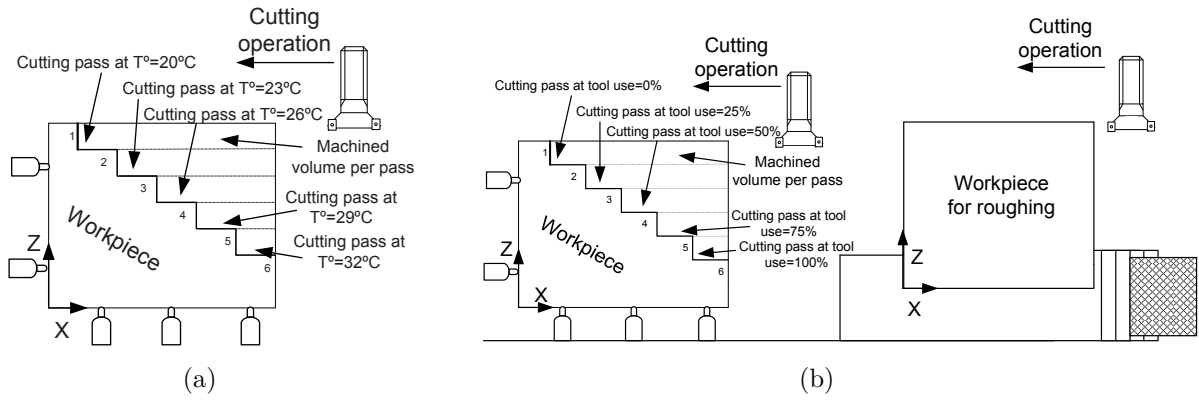


Figure 6.5: Experimentation to model machining-induced variations due to a) spindle thermal effects, and b) cutting-tool wear.

6.3.4 Cutting force-induced variations

The geometric variations of the machined workpieces due to cutting force-induced variations can be modeled by the cutting-tool deflection during the machining process. Various methods for cutting-tools with different complexity have been applied to model the deflection deviation as shown in Chapter 3. To represent these variations in the SoV model, it is necessary to describe the position and orientation deviations of the cutting-tool due to the deflection. Assuming finishing operations where the depth of cut is considered insignificant in comparison to the length of the cutting-tool overhang, and simplifying that the cutting force acts at the tool tip, the cutting-tool can be modeled as a unique cantilever beam defined by the equivalent tool diameter [9]. Then, the displacement of the cutting-tool perpendicular to the cutting-tool axis is proportional to the cutting force according to the equation [19, Chapter 7]:

$$\delta_r = \frac{F \cdot L^3}{3 \cdot E \cdot I} = \frac{64 \cdot F \cdot L^3}{3 \cdot \pi \cdot E \cdot D^4}, \quad (6.21)$$

where E is the Young's Modulus for the material tool; L^3/D^4 is the tool slenderness parameter, where D is the equivalent tool diameter and L is the overhang length; and F is the cutting force perpendicular to the tool axis. Furthermore, the rotation of the tool tip along the axis θ perpendicular to the cutting-tool axis is defined as [19, Chapter 7]:

$$\delta_\theta = \frac{F \cdot L^2}{2 \cdot E \cdot I} = \frac{64 \cdot F \cdot L^2}{2 \cdot \pi \cdot E \cdot D^4}, \quad (6.22)$$

where F is the force applied at the tool tip perpendicular to the plane defined by the axis θ and the cutting-tool axis. Thus, the true cutting-tool CS CCS is deviated from the nominal °CCS due to the cutting force-induced deflection. The deviation of CCS w.r.t. SCS at station k can be expressed by the DMV

$$\mathbf{x}_{C_k}^{S_k} = \mathbf{B}_k^{m_3} \cdot [\Delta F_x^k \quad \Delta F_y^k]^T, \quad (6.23)$$

where $\mathbf{B}_k^{m_3} = [C_1, 0; 0, C_1; 0, 0; 0, C_2; C_2, 0; 0, 0]$, and C_1 and C_2 are defined by the cutting-tool characteristics at station k by the expression $C_1 = \frac{64L^3}{3\pi ED^4}$ and $C_2 = \frac{3C_1}{2L}$. ΔF_x^k and

ΔF_y^k are the variation of the cutting force in X and Y direction from nominal conditions, respectively.

The parameters required to model the force-induced variations can be obtained directly by the geometry of the cutting-tool. For example, the equivalent tool diameter for end mills is considered 0.8 times the nominal cutting-tool diameter since the cutting flutes reduce the resistant section [9]. In order to obtain the Young's modulus, an experimentation is required since the manufacturers of cutting-tools do not usually provide this value. In [9], two experimental methods are proposed to obtain the value of Young's modulus for cutting-tools.

6.3.5 Cutting-tool wear-induced variations

According to the CSs defined previously, the V_B modifies the geometry of the tool tip and causes the deviation of TPCS from $^\circ$ TPCS. The wear of the cutting-tool tip will result in a loss of effective radial and axial depth of cut that generates dimensional deviations. In order to model the effect of V_B on part quality, the following assumptions are considered: i) flank wear is homogeneous; ii) there is no other factors on the cutting-tool edge such as the generation of a built-up edge or similar; and iii) the cutting-tool edge is a sharp edge. Under these assumptions, the deviation of the machined surface in its normal direction (and thus, in Z direction of CS L_k^j) from its nominal values is formulated as follows

$$\delta_z = \frac{\tan(\alpha)}{(1 - \tan(\gamma) \cdot \tan(\alpha))} \cdot V_B, \quad (6.24)$$

where α and γ are the clearance angle and the rake angle of the cutting inserts. According to Eq. (6.24), dimensional deviations are proportional to the flank wear magnitude and thus, the dimensional quality deviation can be described by a proportional coefficient that relates the influence of tool wear flank with the dimensional deviation of a manufacturing feature for a specific cutting operation and cutting-tool geometry [20].

Assuming that cutting-tool flank wear remains constant during the same cutting operation of one workpiece (this assumption holds in case that the workpiece to be machined is small-medium size), the cutting-tool wear-induced deviation is modeled as the DMV of P_k w.r.t. C_k as follows

$$\begin{aligned} \mathbf{x}_{P_k}^{C_k} &= [g_1^k(V_{B_{ij}}^k) \quad g_2^k(V_{B_{ij}}^k) \quad g_3^k(V_{B_{ij}}^k) \quad g_4^k(V_{B_{ij}}^k) \quad g_5^k(V_{B_{ij}}^k) \quad g_6^k(V_{B_{ij}}^k)]^T \\ &\approx \begin{bmatrix} 0 & 0 & C f_{V_{B_{ij}}^k}^k & 0 & 0 & 0 \end{bmatrix}^T \cdot V_{B_{ij}}^k = \mathbf{B}_k^{m_4} \cdot V_{B_{ij}}^k, \end{aligned} \quad (6.25)$$

where $g_i^k(\cdot)$ is a function that relates position and orientation errors of P_k with the flank wear of the cutting-tool. In Eq. (6.25), $V_{B_{ij}}^k$ refers to the flank wear of the i th cutting edge of the j th cutting-tool at the k th machining station and $C f_{V_{B_{ij}}^k}^k$ is a proportional coefficient that linearizes the $g_i^k(\cdot)$ function. The $C f_{V_{B_{ij}}^k}^k$ coefficients can be obtained from experimentation. Note that cutting-tool wear can also generate tool deflections due to the increase of cutting forces. These force-induced effects are modeled following Section 6.3.4.

The experimentation to be conducted for modeling the variations induced by the cutting-tool wear consists in milling different workpiece surfaces at different cutting-tool wear rates as it is shown in Figure 6.5 (b). To avoid fixture-induced variations, a workpiece with accurate datum surfaces should be mounted on a 3-2-1 fixture scheme during all the experiment. Similarly, to avoid thermal-induced variations the spindle temperature should be kept constant during the machining operations, cooling or heating if the temperature varies from the nominal. In addition to this workpiece, a second workpiece is placed at the machine-tool table in order to conduct continuous machining operations to wear the cutting-tool. The experimental procedure consists on conducting a cutting pass on the first workpiece with new cutting-tool inserts keeping the spindle temperature constant. Then, several cutting passes are performed on the second workpiece to wear the cutting-tool. After that, V_B is measured without removing the cutting insert from the cutting-tool and the procedure is then repeated until the cutting-tool is totally worn. Each cutting-pass at the first workpiece is conducted to manufacture the workpiece in a “ladder” form in order to measure later the surfaces generated at each cutting pass. When the tool is totally worn, the workpiece is removed and placed in a CMM using the same workpiece setup, and a linear regression between the cutting-tool wear and the dimensional deviations measured can be fitted. From this regression, the proportional coefficient $Cf_{V_{B..}}$ can be obtained.

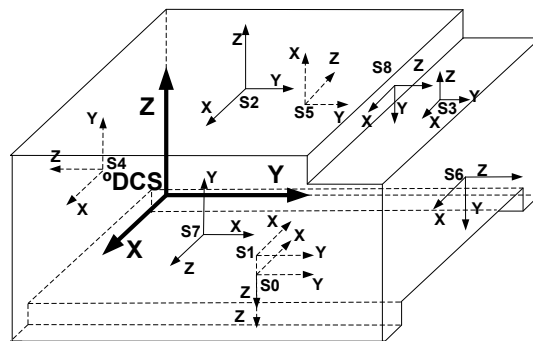


Figure 6.6: Aluminum 6061 part investigated by the case study. Surface CSs from S_0 to S_8 .

6.4 Case Study

To validate the extended SoV model, consider the case study composed of the Aluminum 6061 part shown in Figure 6.6 and the three-station machining process illustrated in Figure 6.7, with the datum features and the surfaces to be machined summarized in Table 6.1. The location of each fixture locator is defined in Table 6.2. The nominal position and orientation of each workpiece surface is presented in Table 6.3. After station 3, the machined part is moved to the inspection station to measure the three KPCs defined by the manufacturing features S_2 , S_3 and S_8 . To simplify the machining experimentation, the three machining stations presented in the case study are defined by the same machine-tool, cutting-tool and fixture layout but with different datum features, as illustrates the

process plan shown in Figure 6.7. In order to compare both conventional and extended SoV models, five machining conditions were tested considering both fixture-induced and machining-induced variations. The Matlab code for deriving the extended SoV model applied to the case study is shown in Chapter 11.

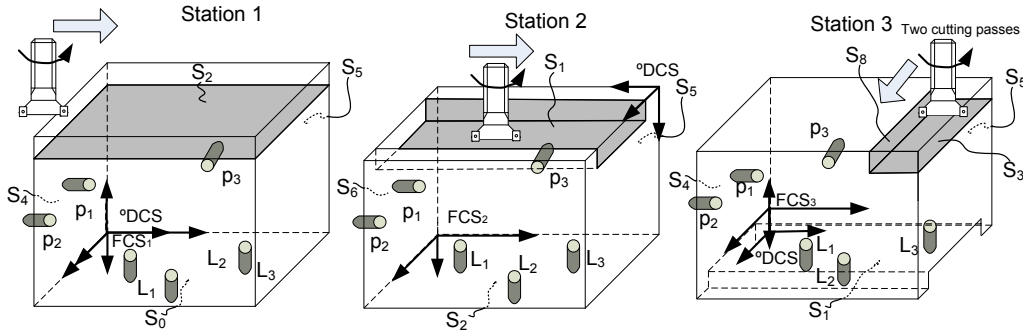


Figure 6.7: Case study. Part to be machined in a 3-station machining process.

Table 6.1: Machined features and datum features according to the 3-2-1 locating scheme at each station.

| Station | Datum features | Machined features | Cutting-tool |
|---------|-------------------|-------------------|---|
| 1 | $S_0 - S_4 - S_5$ | S_2 | ADHX 110305, PVD TiAlN $\varnothing = 24.856$, $L = 111.322$ |
| 2 | $S_2 - S_6 - S_5$ | S_1 | ADHX 110305, PVD TiAlN $\varnothing = 24.856$, $L = 111.322$ |
| 3 | $S_1 - S_4 - S_5$ | S_3, S_8 | ADHX 110305, PVD TiAlN $\varnothing = 24.856$, $L = 111.322$ |
| 4 | $S_0 - S_4 - S_5$ | – | Inspection station |

\varnothing : Tool diameter (mm); L : Tool length (mm).

Table 6.2: Nominal location ($\mathbf{t}_{F_k}^{\circ D}$) and orientation ($\varphi_{F_k}^{\circ D}$) of fixture CS at each station and fixture layout.

| Station | $\varphi_{F_k}^{\circ D}$ (rad) | $\mathbf{t}_{F_k}^{\circ D}$ (mm) | Locators w.r.t. F_k (mm) |
|---------|---------------------------------|-----------------------------------|---|
| 1 | $[-\pi/2, \pi, 0]$ | $[0, 0, 0]$ | $L_{1x} = 10, L_{1y} = 30, L_{2x} = 50, L_{2y} = 70, L_{3x} = 90, L_{3y} = 30$ $p_{1y} = 30, p_{1z} = -35, p_{2y} = 70, p_{2z} = -35, p_{3x} = 50, p_{3z} = -20$ |
| 2 | $[-\pi/2, 0, 0]$ | $[0, 95, 45]$ | $L_{1x} = 10, L_{1y} = 30, L_{2x} = 50, L_{2y} = 70, L_{3x} = 90, L_{3y} = 30$ $p_{1y} = 30, p_{1z} = -35, p_{2y} = 70, p_{2z} = -35, p_{3x} = 50, p_{3z} = -20$ |
| 3 | $[-\pi/2, \pi, 0]$ | $[0, 0, 2.5]$ | $L_{1x} = 10, L_{1y} = 30, L_{2x} = 50, L_{2y} = 70, L_{3x} = 90, L_{3y} = 30$ $p_{1y} = 30, p_{1z} = -35, p_{2y} = 70, p_{2z} = -35, p_{3x} = 50, p_{3z} = -20$ |

In the first experiment, a workpiece was machined according to the process plan with minimum fixture and machining variations. For this purpose, the fixture locators were calibrated on the machine-tool table with a touch probe to ensure fixture assembly deviations less than ± 0.015 mm. The machining operation was conducted with a spindle temperature close to 21°C . The possible spindle temperature variations were compensated

Table 6.3: Nominal location ($\mathbf{t}_{S_i}^{\circ D}$) and orientation ($\varphi_{S_i}^{\circ D}$) of each feature.

| Feature | $\varphi_{S_i}^{\circ D}$ (rad) | $\mathbf{t}_{S_i}^{\circ D}$ (mm) |
|---------|---------------------------------|-----------------------------------|
| S_0 | $[0, \pi, 0]$ | $[47.5, 47.5, 0]$ |
| S_1 | $[0, \pi, 0]$ | $[47.5, 47.5, 2.5]$ |
| S_2 | $[0, 0, 0]$ | $[47.5, 42.5, 45]$ |
| S_3 | $[0, 0, 0]$ | $[47.5, 90, 40]$ |
| S_4 | $[\pi/2, -\pi/2, -\pi/2]$ | $[47.5, 0, 22.5]$ |
| S_5 | $[0, -\pi/2, 0]$ | $[0, 47.5, 22.5]$ |
| S_6 | $[\pi/2, \pi/2, -\pi/2]$ | $[47.5, 95, 20]$ |
| S_7 | $[0, \pi/2, \pi/2]$ | $[95, 47.5, 22.5]$ |
| S_8 | $[\pi/2, \pi/2, -\pi/2]$ | $[47.5, 85, 42.5]$ |

by a linear compensation algorithm provided by the machine-tool manufacturer. To control the impact of cutting-tool wear effects, a new cutting-tool was used in the experiment whose dimensions were also calibrated with a mechanical touch probe on the machine-tool table. In addition, the workpiece clamping procedure at each station was conducted by a torque wrench to ensure a constant clamping force. With these settings, the MMP should generate high quality parts.

The second experiment only dealt with fixture-induced variations, keeping under control the machining-induced variations. The experiment was conducted in a similar way to the first experiment, except that some locator deviations were intentionally introduced, as shown in Table 6.4. These locator deviations were measured on the machine-tool table by a touch probe. For this experiment, the KPC deviations are mostly generated by the fixture-induced variations, and it should be predicted by the conventional SoV model.

The third, the fourth and the fifth experiments were conducted to evaluate the effect of machining-induced variations. In these experiments, the clamping procedure was kept identically as the second experiment but other locator deviations were introduced. In the third experiment, the temperature at the machine-tool spindle was increased up to $25^{\circ}C$ without using any thermal compensation algorithm so a thermal deviation was present at all stations. The cutting-tool used was a new one in order to avoid cutting-tool wear effects. In the fourth experiment, the cutting operation at all stations was conducted with a worn cutting-tool and without thermal variations. The cutting-tool flank wear was measured at both cutting-tool edges, with the resulting values of 0.9 mm and 0.5 mm for the primary and secondary cutting edges respectively. Finally, in the fifth experiment the spindle temperature was increased up to $30^{\circ}C$ and a worn cutting-tool was used with a flank wear of 0.3 mm at both primary and secondary edges, keeping the same locator deviations as in the second experiment. In the third, the fourth and the fifth experiments, the prediction errors of the conventional SoV model is expected to be higher than those in the second experiment due to the influence of the machining-induced variations. Furthermore, in these experiments the extended SoV model is expected to be more accurate than the conventional one due to its ability to deal with the machining-induced variations.

Table 6.4: Experimental conditions. Note that all deviations apply to stations 1, 2 and 3.

| Exp ID | Error Type | Δl_1 <i>mm</i> | Δl_2 <i>mm</i> | Δl_3 <i>mm</i> | Δp_1 <i>mm</i> | Δp_2 <i>mm</i> | Δp_3 <i>mm</i> | ΔT_s $^{\circ}C$ | $V_{B_{11}}$ <i>mm</i> | $V_{B_{21}}$ <i>mm</i> |
|--------|---------------|---------------------------|---------------------------|---------------------------|---------------------------|---------------------------|---------------------------|-----------------------------|---------------------------|---------------------------|
| 1 | None | -0.008 | 0.000 | 0.012 | -0.018 | -0.004 | 0.000 | 0 | 0 | 0 |
| 2 | LC | -0.041 | 0.000 | 0.096 | -0.018 | -0.004 | 0.000 | 0 | 0 | 0 |
| 3 | LC and TH | -0.024 | 0.000 | -0.037 | -0.018 | -0.004 | 0.000 | 10 | 0 | 0 |
| 4 | LC and TW | -0.024 | 0.000 | -0.037 | -0.018 | -0.004 | 0.000 | 0 | 0.9 | 0.5 |
| 5 | LC, TH and TW | -0.041 | 0.000 | 0.096 | -0.018 | -0.004 | 0.000 | 15 | 0.3 | 0.3 |

LC: Locator deviation; TW: Cutting-tool wear; TH: Spindle thermal expansion

6.4.1 Results and Discussion

In order to integrate the machining-induced variations due to the spindle thermal expansion and the cutting-tool wear effects into the SoV model, an experimentation for modeling purposes was conducted according to the steps mentioned in Section 6.3. For spindle thermal variations, only the spindle thermal expansion in Z direction was studied discarding other positional and angular errors during the spindle warm-up. The spindle temperature was measured by a PT-100 sensor and the machine-tool was warmed up by keeping the spindle rotating at 10,000 r.p.m. After milling at different temperatures, the workpiece was measured in a CMM and the deviation between the machined features were linearly adjusted with the spindle temperature (Figure 6.8). From the experimental results, the thermal coefficients were adjusted as: $Cf_x^k = Cf_y^k = Cf_z^k = Cf_{\alpha}^k = Cf_{\beta}^k = Cf_{\gamma}^k \approx 0$ and $Cf_z^k = -0.0052 \text{ mm}/^{\circ}C$ for $k = 1, 2, 3$. Note that the negative sign indicates that a thermal increase impacts on the deviation of the SCS along $-Z$ direction of the SCS and therefore, along the $-Z$ direction of the LCS^{*j*}.

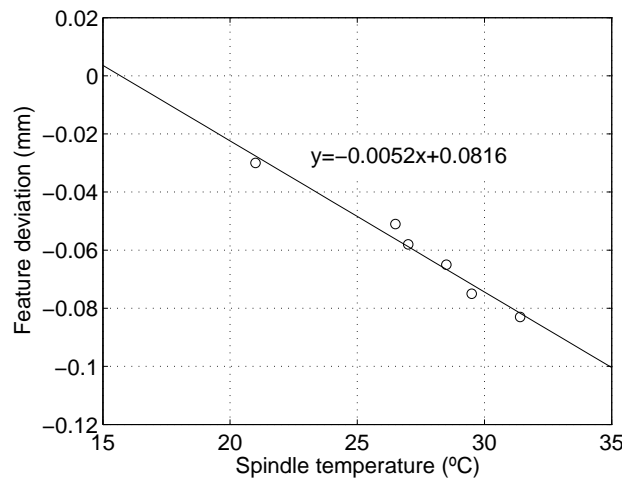


Figure 6.8: Machined feature deviations measured experimentally along spindle thermal expansion.

On the other hand, in order to model the cutting-tool wear effects, several end milling

operations were conducted with different cutting-tool flank wear values. The experimentation was conducted on a calibrated fixture device and keeping the spindle temperature at 25°C . The end mill modeled was a cutter plate composed of inserts ADHX 110305, PVD TiAlN. The resulting linear relationships between flank wear values at primary and secondary cutting edges and the dimensional deviation of the machined features are shown in Figure 6.9. From the experimental results, the cutting-tool wear coefficients were adjusted as: $Cf_{VB_{11}}^1 = Cf_{VB_{11}}^2 = Cf_{VB_{11}}^3 = 0.125$ and $Cf_{VB_{21}}^3 = 0.135$.

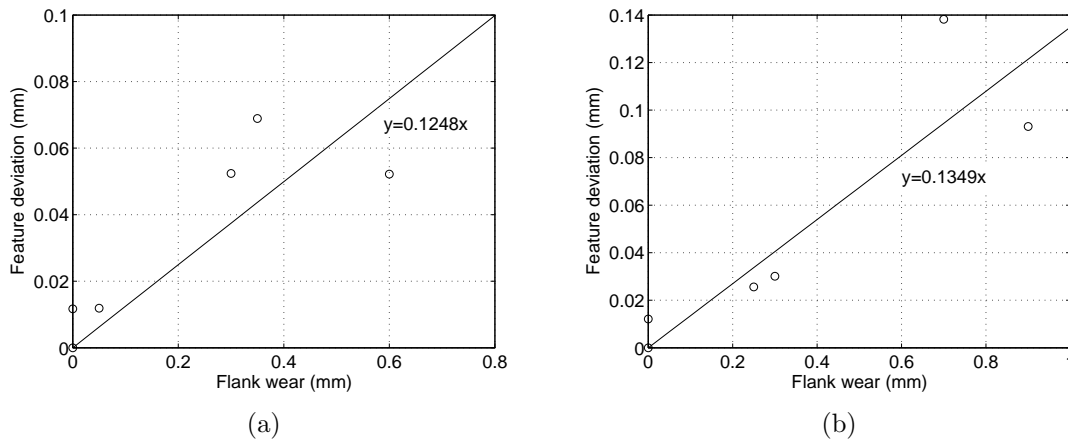


Figure 6.9: Machined feature deviations measured when machining with: a) flank wear at the primary cutting-tool edge and b) flank wear at the secondary cutting-tool edge.

According to the experimental results, the quality of the machining operation is closely related to the cutting-tool wear, especially for features generated by the secondary cutting-tool edge (e.g., the machined feature S_8). The influence of the spindle thermal expansion is also important since, with a reasonable thermal spindle expansion of $\pm 5^{\circ}\text{C}$, a feature deviation around $\pm 0.026\text{ mm}$ is expected. Other machining-induced variations, such as the geometric, kinematic and thermal variations of machine-tool axes or cutting-tool deflections during machining, could also be considered. However, for this case study one can expect that some of these sources of variation will be less important. For instance, if the workpieces are placed always in the same region of the machine-tool table, and the workpieces are small, one can expect that the geometric-kinematic variations during machining will be low. On the other hand, if the cutting-tools used are cutter plate tools, which are more robust than slender solid end mills, one can expect that cutting force-induced variations will be lower than those from slender solid end mills. In other words, the specific characteristics of the machining operation have to be considered in order to ensure if some of these machining-induced variations may be assumed negligible in comparison with others.

After modeling the relationships between machining-induced variations and part quality, the five experiments were conducted. After each cutting experiment, the average prediction error of the three KPCs was computed according to the estimations from both

conventional and extended SoV models. The average prediction error for each cutting condition is shown in Figure 6.10. Analyzing the results from the experiment 1, one can observe the difficulties to control all factors to ensure high quality machined parts. In spite of the control of locator deviations, spindle thermal expansion, cutting-tool wear, cutting-tool length and diameter calibration and clamping deviations, the machined parts have still uncontrolled sources of variation which produce an average prediction error of 0.010 mm . Mainly, these factors could be dimensional deviations due to geometric-thermal effects on machine-tool axis, cutting-tool deflections or workpiece deformations due to cutting forces. For the second experiment, the machined part is deviated from its nominal values due to the locator deviations introduced at locators L_1 and L_3 . The SoV model approximates the expected part quality fairly well with an average prediction error of 0.019 mm , validating the model for propagating errors in MMPs due to fixture-induced variations. The addition of machining-induced variations such as those due to spindle thermal expansion and cutting-tool wear in the third, the fourth and the fifth experiments reveal the limitation of the conventional SoV model predictions under these conditions. The extended SoV model is able to partially deal with these deviations and reduces the prediction error considerably. As shown in Figure 6.10, the prediction improvement in the third, the fourth and the fifth experimental conditions was 62.5%, 74.7% and 64.4% respectively, which means an average prediction improvement of 67% with respect to the conventional SoV when machining-induced variations are applied.

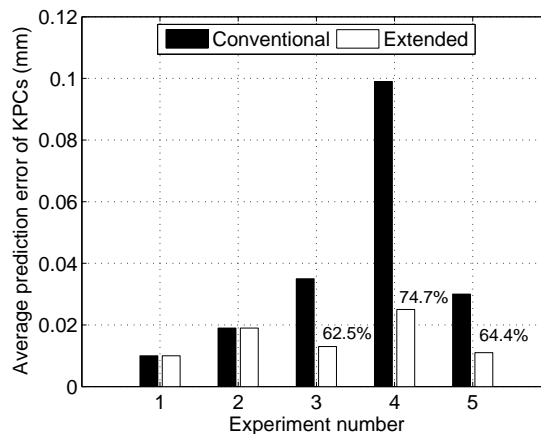


Figure 6.10: Average prediction error of the three KPCs for both conventional and extended SoV models in the five tested experimental conditions.

6.5 Conclusions

In spite of the success of the SoV approach for variation propagation modeling in MMPs, the fact of not including machining-induced variations into the model could be an important factor to limit the use of this methodology for accurate variation prediction. In order to improve the conventional SoV methodology, it is desirable to additionally represent the machining-induced variations such as those due to geometric-thermal deviations

of machine-tool axes, cutting force-induced deviations, cutting-tool wear, etc., in a comprehensive model. In this chapter, a generic framework for machining-induced variation representation based on DMVs is presented, based on which, machining-induced variations can be explicitly incorporated into the conventional SoV model. This generic framework requires experiments for the estimation of empirical models of machining-induced variations which are based on measurements of temperature sensors, interferometers, probe-balls, etc., and predict the corresponding variation. Consequently, the approach is in particular interesting for applications in mass production where the costs for the initial calculation of the models can be compensated by the reduction of measurements of the variations during and after the multi-station machining process.

The proposed model is compared with the conventional SoV model when different machining-induced variations are added in a MMP case of study. The machining-induced variations modeled and added into the experimentation were related to spindle thermal expansion and cutting-tool wear. Different machining-induced variations were combined in the experimentation and the resulting prediction errors from the extended SoV model were notably lower (a 67% on average less) than those from the conventional SoV model, verifying the potential use of the proposed extended SoV model.

A fundamental assumption underlying the proposed methodology is the small magnitude of the variations. The extended model will keep under reasonable accuracy when the main sources of variation present small deviations from their nominal values. Following the proposed framework, additional types of machining-induced variations can be included into the extended model considering how they affect to any of the CSs defined in this chapter and propagating their effects, by a previous linearization, through the chain of CSs that composes the machine-tool. Furthermore, the applicability of the proposed comprehensive state space model can be considered under two approaches: i) to improve the accurateness of the conventional SoV model by considering new sources of variations, and ii) to deal with some problems in MMPs that have not been investigated yet. In the first approach, conventional SoV applications, such as design evaluation of MMPs, tolerance analysis and sensor placement, can be significantly improved by adding new variation sources into the model. In the second approach, the inclusion of these new variation sources can aid the investigation of new problems, such as machining fault diagnosis, a complete manufacturing tolerance allocation (studied in Chapter 9), and new maintenance strategies integrating both fixture maintenance and cutting-tool replacement policies.

6.6 Appendix 6.1: Proof of Lemma 1

Noting $\mathbf{H}_1^R = \mathbf{H}_{o_1}^R \cdot \delta\mathbf{H}_1^R$, we have $\mathbf{H}_R^1 = (\mathbf{H}_1^R)^{-1} = (\delta\mathbf{H}_1^R)^{-1} \cdot \mathbf{H}_R^{o_1}$. Then, considering $\mathbf{H}_2^1 = \mathbf{H}_R^1 \cdot \mathbf{H}_2^R$ we have:

$$\mathbf{H}_2^1 = (\mathbf{H}_1^R)^{-1} \cdot \mathbf{H}_2^R = (\delta\mathbf{H}_1^R)^{-1} \cdot \mathbf{H}_R^{o_1} \cdot \mathbf{H}_2^R. \quad (6.26)$$

As $\mathbf{H}_2^R = \mathbf{H}_{\circ 2}^R \cdot \delta \mathbf{H}_2^R$, Eq. (6.26) is rewritten as:

$$\mathbf{H}_2^1 = (\delta \mathbf{H}_1^R)^{-1} \cdot \mathbf{H}_R^{\circ 1} \cdot \mathbf{H}_{\circ 2}^R \cdot \delta \mathbf{H}_2^R. \quad (6.27)$$

Noting $\delta \mathbf{H}_2^R$ as

$$\delta \mathbf{H}_2^R = \mathbf{I}_{4 \times 4} + \Delta_2^R, \quad (6.28)$$

where Δ_2^R is the differential transformation matrix defined as

$$\Delta_2^R = \begin{pmatrix} \hat{\boldsymbol{\theta}}_2^R & \mathbf{d}_2^R \\ \mathbf{0}_{1 \times 3} & 0 \end{pmatrix}, \quad (6.29)$$

where $\hat{\boldsymbol{\theta}}_2^R$ is the skew matrix of $\boldsymbol{\theta}_2^R$ and it is defined as

$$\hat{\boldsymbol{\theta}}_2^R = \begin{pmatrix} 0 & -\theta_{2z}^R & \theta_{2y}^R \\ \theta_{2z}^R & 0 & -\theta_{2x}^R \\ -\theta_{2y}^R & \theta_{2x}^R & 0 \end{pmatrix}, \quad (6.30)$$

and considering the small motion assumption (then, $\Delta_1^1 = -\Delta_1^R$, as shown in [13]), Eq. (6.27) can be rewritten as:

$$\mathbf{H}_2^1 = (\mathbf{I}_{4 \times 4} - \Delta_1^R) \cdot \mathbf{H}_{\circ 2}^{\circ 1} \cdot (\mathbf{I}_{4 \times 4} + \Delta_2^R). \quad (6.31)$$

As $\mathbf{H}_2^1 = \mathbf{H}_{\circ 2}^{\circ 1} \cdot \delta \mathbf{H}_2^1$, from Eq. (6.31) we can derive $\delta \mathbf{H}_2^1$ as:

$$\delta \mathbf{H}_2^1 = (\mathbf{H}_{\circ 2}^{\circ 1})^{-1} \cdot (\mathbf{H}_{\circ 2}^{\circ 1} - \Delta_1^R \cdot \mathbf{H}_{\circ 2}^{\circ 1} + \mathbf{H}_{\circ 2}^{\circ 1} \cdot \Delta_2^R - \Delta_1^R \cdot \mathbf{H}_{\circ 2}^{\circ 1} \cdot \Delta_2^R). \quad (6.32)$$

Neglecting the second-order small values and re-ordering

$$\Delta_2^R = (\mathbf{H}_{\circ 2}^{\circ 1})^{-1} \cdot \Delta_1^R \cdot \mathbf{H}_{\circ 2}^{\circ 1} + \delta \mathbf{H}_2^1 - \mathbf{I}_{4 \times 4}. \quad (6.33)$$

As $\Delta_2^1 = \delta \mathbf{H}_2^1 - \mathbf{I}_{4 \times 4} =$ Eq. (6.33) is rewritten as

$$\Delta_2^R = (\mathbf{H}_{\circ 2}^{\circ 1})^{-1} \cdot \Delta_1^R \cdot \mathbf{H}_{\circ 2}^{\circ 1} + \Delta_2^1. \quad (6.34)$$

Considering the components of the matrices, Eq. (6.34) becomes

$$\begin{aligned} \begin{pmatrix} \hat{\boldsymbol{\theta}}_2^R & \mathbf{d}_2^R \\ \mathbf{0}_{1 \times 3} & 0 \end{pmatrix} &= \begin{pmatrix} (\mathbf{R}_{\circ 2}^{\circ 1})^T & -(\mathbf{R}_{\circ 2}^{\circ 1})^T \cdot \mathbf{t}_{\circ 2}^{\circ 1} \\ \mathbf{0}_{1 \times 3} & 1 \end{pmatrix} \cdot \begin{pmatrix} \hat{\boldsymbol{\theta}}_1^R & \mathbf{d}_1^R \\ \mathbf{0}_{1 \times 3} & 0 \end{pmatrix} \cdot \begin{pmatrix} \mathbf{R}_{\circ 2}^{\circ 1} & \mathbf{t}_{\circ 2}^{\circ 1} \\ \mathbf{0}_{1 \times 3} & 1 \end{pmatrix} + \begin{pmatrix} \hat{\boldsymbol{\theta}}_2^1 & \mathbf{d}_2^1 \\ \mathbf{0}_{1 \times 3} & 0 \end{pmatrix}, \\ &= \begin{pmatrix} (\mathbf{R}_{\circ 2}^{\circ 1})^T \cdot \hat{\boldsymbol{\theta}}_1^R \cdot \mathbf{R}_{\circ 2}^{\circ 1} + \hat{\boldsymbol{\theta}}_2^1 & (\mathbf{R}_{\circ 2}^{\circ 1})^T \cdot \hat{\boldsymbol{\theta}}_1^R \cdot \mathbf{t}_{\circ 2}^{\circ 1} + (\mathbf{R}_{\circ 2}^{\circ 1})^T \cdot \mathbf{d}_1^R + \mathbf{d}_2^1 \\ \mathbf{0}_{1 \times 3} & 0 \end{pmatrix}. \end{aligned} \quad (6.35)$$

Therefore,

$$\hat{\boldsymbol{\theta}}_2^R = (\mathbf{R}_{\circ 2}^{\circ 1})^T \cdot \hat{\boldsymbol{\theta}}_1^R \cdot \mathbf{R}_{\circ 2}^{\circ 1} + \hat{\boldsymbol{\theta}}_2^1 \quad (6.36)$$

$$\mathbf{d}_2^R = (\mathbf{R}_{\circ 2}^{\circ 1})^T \cdot \hat{\boldsymbol{\theta}}_1^R \cdot \mathbf{t}_{\circ 2}^{\circ 1} + (\mathbf{R}_{\circ 2}^{\circ 1})^T \cdot \mathbf{d}_1^R + \mathbf{d}_2^1. \quad (6.37)$$

Considering that $\hat{\mathbf{a}} \cdot \mathbf{b} = -\hat{\mathbf{b}} \cdot \mathbf{a}$, and that if $\mathbf{c} = \mathbf{B} \cdot \mathbf{a}$, the skew matrix of \mathbf{c} is $\hat{\mathbf{c}} = |\mathbf{B}| \cdot (\mathbf{B}^T)^{-1} \cdot \hat{\mathbf{a}} \cdot (\mathbf{B})^{-1}$, then Eq. (6.33) can be rewritten in a vector form resulting in Eq. (6.1).

References

- [1] R. Ramesh, M. A. Mannan, A. N. Poo, Error compensation in machine tools - a review part I: geometric, cutting-force induced and fixture-dependent errors, *International Journal of Machine Tools and Manufacture* 40 (9) (2000) 1235–1256.
- [2] R. Ramesh, M. A. Mannan, A. N. Poo, Error compensation in machine tools - a review part II: thermal errors, *International Journal of Machine Tools and Manufacture* 40 (9) (2000) 1257–1284.
- [3] J. S. Chen, J. Yuan, J. Ni, Thermal error modelling for real-time error compensation, *International Journal of Advanced Manufacturing Technology* 12 (1996) 266–275.
- [4] M. A. E. Baradie, The effect of varying the workpiece diameter on the cutting tool clearance angle in tool-life testing, *Wear* 195 (1-2) (1996) 201 – 205.
- [5] S.-H. Suh, E.-S. Lee, S.-Y. Jung, Error modelling and measurement for the rotary table of five-axis machine tools, *The International Journal of Advanced Manufacturing Technology* 14 656–663.
- [6] W. T. Lei, Y. Y. Hsu, Accuracy test of five-axis CNC machine tool with 3D probe-ball. part I: design and modeling, *International Journal of Machine Tools and Manufacture* 42 (10) (2002) 1153 – 1162.
- [7] G. M. Kim, B. H. Kim, C. N. Chu, Estimation of cutter deflection and form error in ball-end milling processes, *International Journal of Machine Tools and Manufacture* 43 (2003) 917–924.
- [8] T. A. Dow, E. L. Miller, K. Garrard, Tool force and deflection compensation for small milling tools, *Precision Engineering* 28 (2004) 31–45.
- [9] L. N. López de Lacalle, A. Lamikiz, J. A. Sanchez, M. A. Salgado, Effects of tool deflection in the high-speed milling of inclined surfaces, *International Journal of Advanced Manufacturing Technology* 24 (2004) 621–631.
- [10] X. Bi, Y. Liu, Y. Liu, Analysis and control of dimensional precision in turning process, in: *Control and Decision Conference*, 2009, pp. 3456 –3459.
- [11] P. Joshi, *Jigs and Fixtures Design Manual*, McGraw-Hill, 2003.
- [12] R. Paul, *Robot Manipulator: Mathematics, Programming, and Control*, Cambridge, MA, MIT Press, 1981.
- [13] S. Zhou, Q. Huang, J. Shi, State space modeling of dimensional variation propagation in multistage machining process using differential motion vectors, *IEEE Transactions on Robotics and Automation* 19 (2) (2003) 296–309.
- [14] J. P. Choi, S. J. Lee, H. D. Kwon, Roundness error prediction with a volumetric error model including spindle error motions of a machine tool, *International Journal of Advanced Manufacturing Technology* 21 (2003) 923–928.

- [15] G. Chen, J. Yuan, J. Ni, A displacement measurement approach for machine geometric error assessment, *International Journal of Machine Tools and Manufacture* 41 (1) (2001) 149 – 161.
- [16] S. H. Yang, K. H. Kim, Y. K. Park, S. G. Lee, Error analysis and compensation for the volumetric errors of a vertical machining centre using a hemispherical helix ball bar test, *International Journal of Advanced Manufacturing Technology* 23 (2004) 495–500.
- [17] P. C. Tseng, A real-time thermal inaccuracy compensation method on a machining centre, *International Journal of Advanced Manufacturing Technology* 13 (3) (1997) 182–190.
- [18] Z. Haitao, Y. Jianguo, S. Jinhua, Simulation of thermal behavior of a CNC machine tool spindle, *International Journal of Machine Tools and Manufacture* 47 (6) (2007) 1003–1010.
- [19] J. M. Gere, S. P. Timoshenko, *Mecanics of Materials*, PWS Publishers; Second Edition, 1984.
- [20] A. K. Sheikh, A. Raouf, U. A. Sekerdey, M. Younas, Optimal tool replacement and resetting strategies in automated manufacturing systems, *International Journal of Production Research* 37 (4) (1999) 917–937.

Part III

Novel applications of the SoV model

Quality prediction and compensation in multi-station machining processes using sensor-based fixtures

New fixture technologies, such as sensor-based fixtures, will significantly improve part quality through cutting-tool path compensations in multi-station machining processes (MMPs). Successful application of sensor-based fixtures depends on the development of new variation reduction methodologies to predict part quality in MMPs and detect the critical machining stations whose critical manufacturing variations can be estimated by installing a suitable sensor-based fixture. In this chapter, a methodology is proposed to facilitate the implementation of sensor-based fixtures in MMPs. This methodology involves three key steps: (1) an identification of station-induced variations; (2) a sensor placement optimization method for designing sensor-based fixtures; and (3) a compensability analysis. A case study is conducted to demonstrate the effectiveness of the methodology.

7.1 Introduction

Manufacturers in the 21st century will increasingly face frequent and unpredictable market changes. These changes include the frequent introduction of new products, increased demand for new products, and above all, new process technologies. In multi-station machining processes (MMPs), reconfigurable manufacturing systems (RMSs) and flexible manufacturing systems (FMSs) with flexible fixturing methodologies will be critical to adapt manufacturing processes to the changes necessary for continuous new product development [1]. In FMSs, fixturing flexibility becomes an important issue and several flexible fixturing methodologies have been studied in past years [2–4]. Among these methodologies, modular fixtures are probably the most widely used in industry [2]. The use of modular fixtures decreases the tooling cost and storage space and shortens lead time. However, many factors, such as lack of stiffness, clearances between modular assemblies, tolerances of modular components, and variations in fastening forces and clamping forces, increase the location variations of modular fixtures and impair the final product quality [3]. To overcome these limitations and improve part quality, new fixture technologies, such as sensor-based fixtures, have been developed and deployed in computer numerical

controlled (CNC) machining centers to actively compensate fixturing variations through cutting-tool path modifications [5]. Despite the success of sensor-based fixtures in single-station machining processes, their applications in MMPs has not been investigated. Part of the reason is that the quality-process relationship, especially the variation propagation in MMPs is extremely complex and traditional modeling techniques are not effective [6]. The recent developed SoV model presented in Chapter 4 let engineers estimate part quality in MMPs and it could be applied together with sensor-based fixtures to improve part quality through cutting-tool path compensations.

In the literature, the SoV model has been already applied for active control for variation reduction, where expected dimensional variations generated at upstream stations are compensated at downstream stations [7–12]. Specifically, active control for variation reduction is referred to the automatic adjustments of the tooling (locators, cutting tool paths, etc.) settings to minimize the process variability, based on in-line measurements [13, Chapter 18]. Two basic approaches have been investigated in controlling variation magnitude in MMPs: feed-back and feed-forward control. Feed-back control makes use of information from downstream measurements to determine control actions at upstream stations. For instance, after inspecting the quality of a sample of parts at the last station, a mean shift of a key product characteristic (KPC) may be detected. The corresponding control action for the parts to be manufactured is determined and performed at an intermediate station. Alternatively, feed-forward control requires in-process measurements prior to the stations where adjustments will be made. Unlike the feed-back control strategy, this strategy allows the dimensional adjustments for either a batch of parts or an individual part. Therefore, feed-forward control is more preferable in variation reduction for the MMPs and most of the research works in this field are focused on this control strategy. Both feed-back and feed-forward control strategies are shown in Figure 7.1.

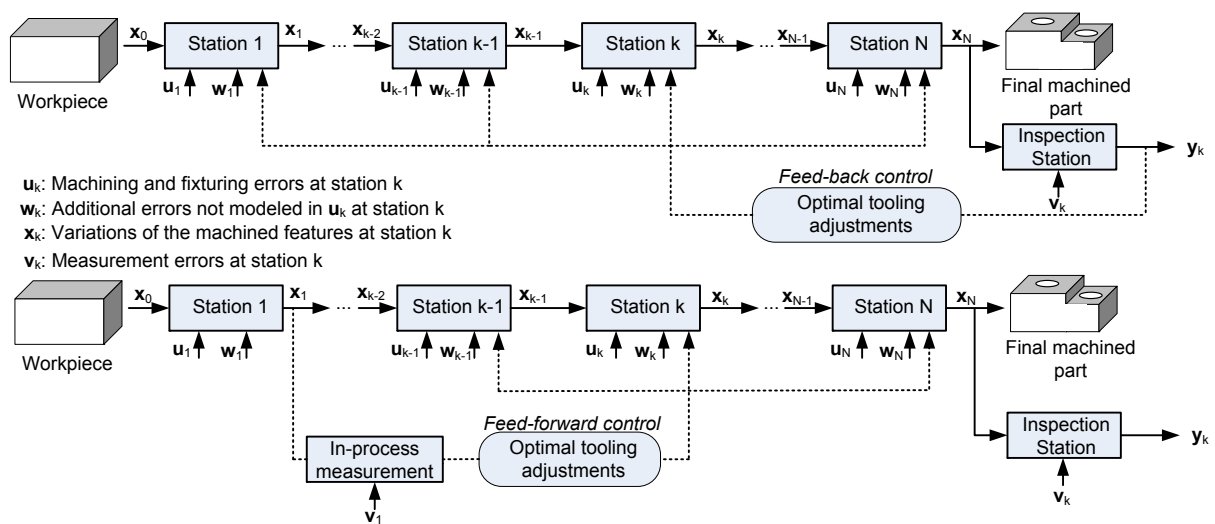


Figure 7.1: Active control for variation reduction: feed-back and feed-forward control strategies.

The first work in the field of active control for variation reduction was conducted

by Djurdjanovic and Zhu [7]. The feed-back and feed-forward control strategies for the placement of stations with dimensional adjustment capability was proposed. Innovatively addressing the dimension compensation problem, this work considers only the deterministic effects, neglecting the noise due to the linearization, unmodeled effects, process noise, and sensor imperfection. Furthermore, the concept of *compensability* was introduced to quantitatively evaluate the capability of variation compensation in a specific system. This concept is equivalent to the concept of *controllability* from control theory [14] and enables the identification of the compensable variation sources. Izquierdo *et al.* [8] extended the feed-forward control strategy to include parts/process requirements and specific engineering constraints on the magnitudes of control actions, such as physical limits and inaccuracy of tooling adjustments.

Previous works were focused on the study of feed-forward control with a full control of all tooling elements. This assumption may not be realistic, since tooling adjustments through flexible fixtures or CNC machine-tools may only be assigned to selected stations in the system due to their high costs. Thus, Djurdjanovic and Ni [9] proposed a feed-forward control strategy with distributed actuation capabilities, taking into consideration the actuation accuracy and noise. However, they only select the best placement from the potential and distributed tooling adjustments, without considering the interaction of multiple tooling adjustments. Metaheuristic optimization approaches were used in [10, 11], where the research work in [9] was extended to deal with variation reduction considering multiple tooling adjustments. The placement of flexible fixtures at multiple stations was analyzed for adjusting tooling elements after multiple in-process measurements. The optimization of the flexible fixtures allocation in the MMP was conducted using a genetic algorithm.

The aforementioned model-based feed-forward control strategies assume that the underlying variation propagation models used for deriving the control action are precise and accurate. However, the models used in designing the control actions are typically obtained from the nominal product and process design information. In practice, unavoidable random errors may lead to random deviations of the actual model from the nominal model. Zhong *et al.* [12] investigated the impact of model uncertainty on the control performance in MMPs and proposed a feed-forward predictive control methodology, with model uncertainty explicitly considered.

From the previous literature review, it is shown that the feed-forward control has been investigated for flexible tooling in order to compensate the expected variations that are estimated from in-process measurements. This chapter presents the application of sensor-based fixtures (modular fixtures with precision sensors [5]) in FMSs for dimensional variation reduction with a feed-forward control strategy. The use of these advanced fixtures devices requires the integration of the sensor-based fixture design into the control law derivation in order to maximize the compensability of part quality variations. Basically, this chapter addresses the following research problems that have not been studied previously: (i) the optimal allocation of sensor-based fixtures to machining stations; (ii) the optimal selection of the number of sensors; and (iii) the optimal distribution of sensors within fixtures. Different from previous research, the in-process measurements considered

in this chapter are from sensor-based fixtures, which provide information from fixture locator variations and datum variations. Furthermore, the collection of in-process measurements is not time consuming since they are obtained after clamping the workpiece in the fixture device.

The chapter is organized as follows. Section 7.2 proposes a SoV-based methodology to study the potential use of sensor-based fixtures for improving part quality through cutting-tool path compensations. The methodology involves three key steps: (1) an identification of station-induced variations; (2) a sensor-based fixture design algorithm for optimal sensor placement; and (3) a compensability analysis. A case study is presented in Section 7.3 to demonstrate the effectiveness of the proposed methodology and conclusions are given in Section 7.4.

7.2 Active control for variation reduction

In this section, the proposed methodology for quality prediction and compensation in MMPs with sensor-based fixtures and CNC machine-tools is introduced in detail. The methodology, outlined in Figure 7.2, is based on three key steps: (1) identification of station-induced variations; (2) sensor-based fixture design algorithm for optimal sensor placement; and (3) compensability analysis.

7.2.1 Step 1: identification of station-induced variations

The first step of the proposed methodology deals with the identification of critical machining stations that contribute significantly to the final part quality variation, i.e., the random variations embedded in \mathbf{y}_N . This identification gives the engineer a general idea of which stations would be more suitable to install a sensor-based fixture. However, the decision of where to place the sensor-based fixture also depends on the sensor-based fixture layout and the capability of subsequent CNC machine-tools to compensate the variations identified.

As it was presented in Chapter 4, the SoV model is defined in its input–output form as:

$$\mathbf{Y} = \mathbf{\Gamma}^f \cdot \mathbf{U}^f + \mathbf{\Gamma}^m \cdot \mathbf{U}^m + \boldsymbol{\varepsilon}, \quad (7.1)$$

where vectors \mathbf{Y} , \mathbf{U}^f and \mathbf{U}^m are the stacking quality vectors and input vectors of fixture and machining variations, respectively, from stations $k = 1, 2, \dots, N$, defined as $\mathbf{Y} = [\mathbf{y}_1^T, \mathbf{y}_2^T, \dots, \mathbf{y}_N^T]^T$, $\mathbf{U}^f = [(\mathbf{u}_1^f)^T, (\mathbf{u}_2^f)^T, \dots, (\mathbf{u}_N^f)^T]^T$ and $\mathbf{U}^m = [(\mathbf{u}_1^m)^T, (\mathbf{u}_2^m)^T, \dots, (\mathbf{u}_N^m)^T]^T$. The matrices $\mathbf{\Gamma}^f$, $\mathbf{\Gamma}^m$ and $\boldsymbol{\varepsilon}$ are defined as

$$\mathbf{\Gamma}^f = \begin{pmatrix} \mathbf{M}_{1,1} & 0 & \dots & 0 \\ \mathbf{M}_{2,1} & \mathbf{M}_{2,2} & \dots & 0 \\ & & \vdots & \\ \mathbf{M}_{N,1} & \mathbf{M}_{N,2} & \dots & \mathbf{M}_{N,N} \end{pmatrix}, \quad \mathbf{\Gamma}^m = \begin{pmatrix} \widetilde{\mathbf{M}}_{1,1} & 0 & \dots & 0 \\ \widetilde{\mathbf{M}}_{2,1} & \widetilde{\mathbf{M}}_{2,2} & \dots & 0 \\ & & \vdots & \\ \widetilde{\mathbf{M}}_{N,1} & \widetilde{\mathbf{M}}_{N,2} & \dots & \widetilde{\mathbf{M}}_{N,N} \end{pmatrix}, \quad (7.2)$$

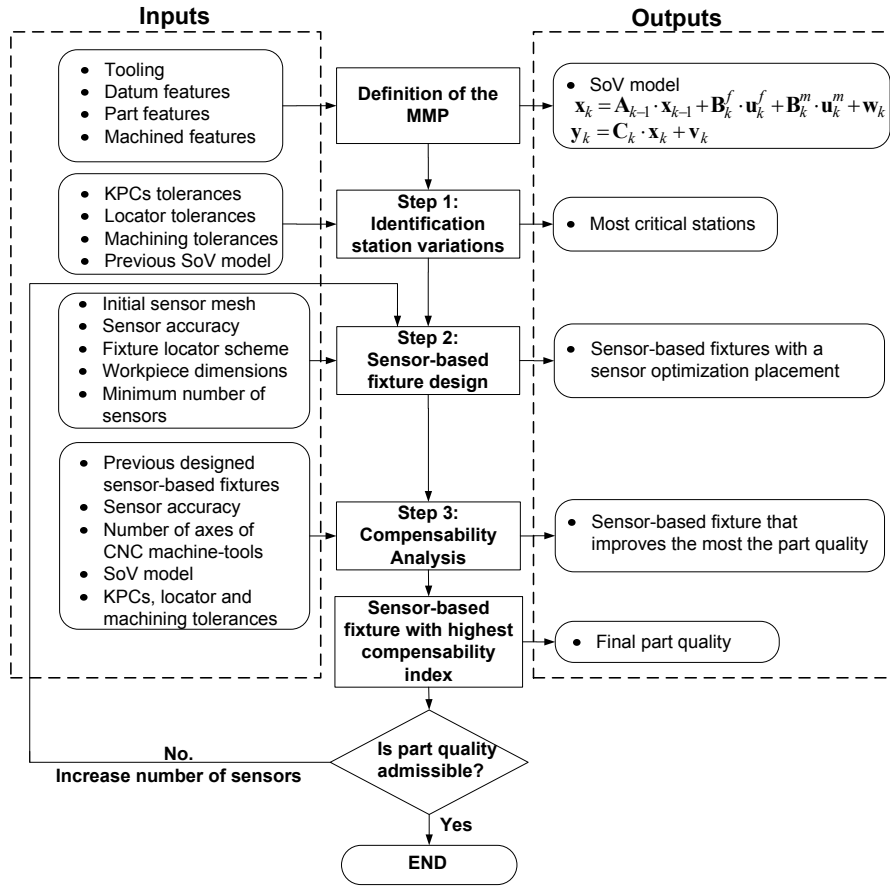


Figure 7.2: Diagram of the methodology conducted for quality prediction and compensation with sensor-based fixtures

$$\boldsymbol{\varepsilon} = \begin{pmatrix} \bar{\mathbf{M}}_{1,1} & 0 & \dots & 0 \\ \bar{\mathbf{M}}_{2,1} & \bar{\mathbf{M}}_{2,2} & \dots & 0 \\ & & \vdots & \\ \bar{\mathbf{M}}_{N,1} & \bar{\mathbf{M}}_{N,2} & \dots & \bar{\mathbf{M}}_{N,N} \end{pmatrix} \cdot \begin{pmatrix} \mathbf{w}_1 \\ \mathbf{w}_2 \\ \vdots \\ \mathbf{w}_N \end{pmatrix} + \begin{pmatrix} \mathbf{v}_1 \\ \mathbf{v}_2 \\ \vdots \\ \mathbf{v}_N \end{pmatrix}, \quad (7.3)$$

where

$$\mathbf{M}_{i,j} = \mathbf{C}_i \cdot \boldsymbol{\Phi}_{i,j} \cdot \mathbf{B}_j^f, \quad i \geq j, \quad (7.4)$$

$$\widetilde{\mathbf{M}}_{i,j} = \mathbf{C}_i \cdot \boldsymbol{\Phi}_{i,j} \cdot \mathbf{B}_j^m, \quad i \geq j, \quad (7.5)$$

$$\bar{\mathbf{M}}_{i,j} = \mathbf{C}_i \cdot \boldsymbol{\Phi}_{i,j}, \quad i \geq j, \quad (7.6)$$

$$\boldsymbol{\Phi}_{i,j} = \begin{cases} \mathbf{A}_{i-1} \cdot \mathbf{A}_{i-2} \cdots \mathbf{A}_j, & i > j \\ \mathbf{I}, & i = j \end{cases} \quad (7.7)$$

Therefore, Eq. (7.1) defines the relationship between the measured variations of the KPCs and the root causes of those variations. Analyzing Eq. (7.1) in terms of covariances and assuming machining variations are independent of fixture variations, one can estimate

the final part quality variation according to the expected locator fixture and cutting-tool path variations by the following equation:

$$\Sigma_{\mathbf{Y}} = \Gamma^f \cdot \Sigma_{\mathbf{U}^f} \cdot (\Gamma^f)^T + \Gamma^m \cdot \Sigma_{\mathbf{U}^m} \cdot (\Gamma^m)^T + \Sigma_{\boldsymbol{\varepsilon}}, \quad (7.8)$$

where $\Sigma_{\mathbf{Y}}$, $\Sigma_{\mathbf{U}^f}$, $\Sigma_{\mathbf{U}^m}$ and $\Sigma_{\boldsymbol{\varepsilon}}$ are the covariance matrices of the KPC measurements, the fixture variations, the machining variations, and the unmodeled system and measurement noise, respectively.

In order to evaluate the impact of fixture and machining variations on KPCs, the following indices can be derived according to Eq. (7.8):

$$\eta_f = \frac{\|\Sigma_{\mathbf{Y}}^f\|}{\|\Sigma_{\mathbf{Y}}\|}, \quad (7.9)$$

$$\eta_m = \frac{\|\Sigma_{\mathbf{Y}}^m\|}{\|\Sigma_{\mathbf{Y}}\|}, \quad (7.10)$$

where $\|\cdot\|$ denotes the Euclidean norm. In Eqs. (7.9) and (7.10), the terms $\Sigma_{\mathbf{Y}}^f$ and $\Sigma_{\mathbf{Y}}^m$ are defined respectively as:

$$\Sigma_{\mathbf{Y}}^f = \Gamma^f \cdot \Sigma_{\mathbf{U}^f} \cdot (\Gamma^f)^T + \Sigma_{\boldsymbol{\varepsilon}}, \quad (7.11)$$

$$\Sigma_{\mathbf{Y}}^m = \Gamma^m \cdot \Sigma_{\mathbf{U}^m} \cdot (\Gamma^m)^T + \Sigma_{\boldsymbol{\varepsilon}}. \quad (7.12)$$

By evaluating Eq. (7.9) and Eq. (7.10), one can differentiate the criticalities of fixture-induced variations and machining-induced variations. In order to identify critical stations, additional indices should be evaluated. In this chapter, as we are focused on FMSs, the use of modular fixtures tends to produce higher fixture-induced variations than in massive manufacturing systems where dedicated fixtures are used [3]. In FMSs, the main sources of variations are related more to fixtures than to machining operations, due to the use of accurate CNC machine-tools. Therefore, assuming that fixture-induced variations are expected to be more critical than machining variations, the following indices are defined:

$$\eta_{f,k} = \frac{\|\Sigma_{\mathbf{Y}}^{f,k}\|}{\|\Sigma_{\mathbf{Y}}\|} \quad k = 1, \dots, N, \quad (7.13)$$

where

$$\Sigma_{\mathbf{Y}}^{f,k} = \Gamma^f \cdot \Sigma_{\mathbf{U}^{f,k}} \cdot (\Gamma^f)^T + \Sigma_{\boldsymbol{\varepsilon}}, \quad (7.14)$$

and $\Sigma_{\mathbf{U}^{f,k}}$ is the covariance matrix of $\mathbf{U}^{f,k}$ which defines only the fixture-induced variations at the k th station. Assuming fixtures based on locators distributed according to the 3-2-1 locating scheme [15], $\mathbf{U}^{f,k}$ is defined as $[(\mathbf{0}_{6 \times 1})^T, \dots, (\mathbf{u}_k^f)^T, \dots, (\mathbf{0}_{6 \times 1})^T]^T$. By evaluating the index $\eta_{f,k}$ for $k = 1, \dots, N$, engineers can identify the station that contributes the most to the final part variations. Therefore, those stations with high $\eta_{f,k}$ indices will be candidates for the installation of sensors in order to compensate fixture-induced variations at that station or at its downstream stations through cutting-tool path adjustments. Note that the optimal sensor-fixture placement requires the compensability analysis discussed in Section 7.2.3, since the sensor-based fixture design is integrated with the control law derivation and thus, with the compensability of the sources of variation in the MMP. The index $\eta_{f,k}$ is used as a first step to identify critical and thus, potential stations where sensor-based fixtures can be applied.

7.2.2 Step 2: Sensor-based fixture design

Sensor measurements according to fixture and datum variations

A sensor-based fixture is a modular fixture composed of S sensors that can detect the variations of the workpiece from its nominal location. Figure 7.3 shows an example of a sensor-based fixture composed of a set of inductive precision sensors. The sensors will measure the variations of the workpiece when: i) fixture locators deviate from their nominal positions; or ii) the datum surfaces (primary, secondary and tertiary datums are defined in 3-2-1 locating schemes) on a workpiece deviate from their nominal positions due to the dimensional variations induced at upstream machining stations. According to these two possible situations, the sensor measurements will indicate random deviations from nominal values. Please note that in this chapter, it is assumed that workpiece surfaces are perfect planar and thus, the form errors are assumed negligible.

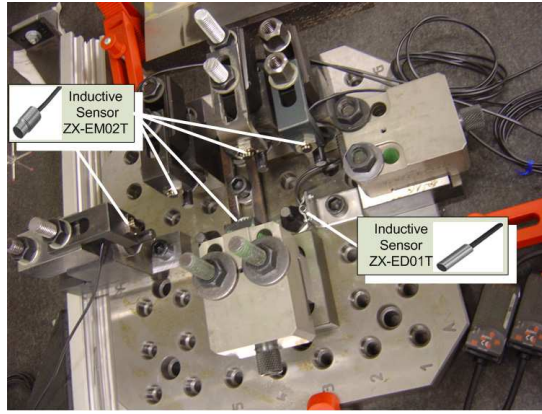


Figure 7.3: Example of a sensor-based fixture with inductive precision sensors mounted on a 3-2-1 locating scheme.

First, consider the situation where only fixture locator variations are present without any datum variations. As the fixture locators are distributed according to the 3-2-1 locating scheme, the workpiece is located deterministically according to the fixture locator layout plus the fixture locator variations. For a fixture composed of six locators, the locator j 's position can be defined with a position vector, \mathbf{r}_j , and a normal vector, \mathbf{n}_j . Both of these two vectors are defined at the contact point between locator and workpiece surface, w.r.t. the nominal fixture coordinate system (FCS), as shown in Figure 7.4. As it was shown in Chapter 3 (Sub-section 3.2.1), a small variation of a fixture locator in the direction of movement constraint, i.e., \mathbf{n}_j , denoted as Δl_j , will cause a small perturbation in the FCS, denoted as $\mathbf{x}_F^{\circ F}$. This small perturbation can be mathematically expressed as:

$$\Delta l_j = \mathbf{t}_j^T \cdot \mathbf{x}_F^{\circ F}, \quad (7.15)$$

where

$$\mathbf{t}_j^T = [\mathbf{n}_j^T, (\mathbf{r}_j \times \mathbf{n}_j)^T], \quad (7.16)$$

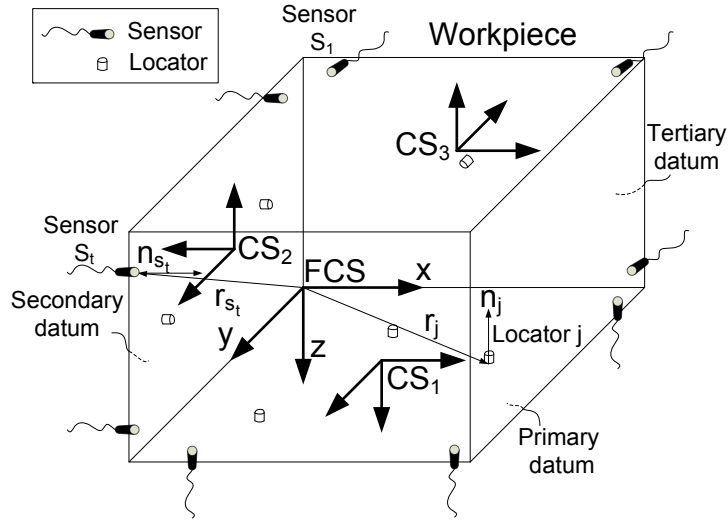


Figure 7.4: Sensor-based fixture scheme. Position and normal vectors of locators and sensors.

and \times is the cross product operator. Δl_j is defined by the equation:

$$\Delta l_j = \mathbf{n}_j^T \cdot \Delta \mathbf{r}_j, \quad (7.17)$$

where $\Delta \mathbf{r}_j$ is the position variation of locator j . The deterministic localization condition (a unique solution of $\mathbf{x}_F^{\circ F}$) requires that Eq. (7.15) is satisfied for all locators. Thus, considering all locator variations, Eq. (7.15) becomes:

$$\Delta \mathbf{l} = \mathbf{G}_l^T \cdot \mathbf{x}_F^{\circ F}, \quad (7.18)$$

where $\Delta \mathbf{l} = [\Delta l_1, \Delta l_2, \dots, \Delta l_6]^T$ and $\mathbf{G}_l = [\mathbf{t}_1, \mathbf{t}_2, \dots, \mathbf{t}_6]$, which is called *locator matrix* in [16]. In order to ensure a deterministic localization, the locator matrix \mathbf{G}_l must be non-singular, i.e., $\mathbf{t}_1, \mathbf{t}_2, \dots, \mathbf{t}_6$ are linearly independent [16], and thus, matrix \mathbf{G}_l is invertible. The variation of FCS is then related to the variations of fixture locators by

$$\mathbf{x}_F^{\circ F} = (\mathbf{G}_l^T)^{-1} \cdot \Delta \mathbf{l}. \quad (7.19)$$

Following a similar procedure, the variations of the workpiece location can be related to the sensor measurements distributed along the datum surfaces. Assuming that S sensors are mounted in the sensor-based fixture, the vector containing the sensor measurements is defined as $\Delta \mathbf{s} = [\Delta s_1 \dots \Delta s_S]^T$. $\Delta \mathbf{s}$ is related to the variations of workpiece location by

$$\Delta \mathbf{s} = \mathbf{G}_s^T \cdot \mathbf{x}_F^{\circ F}, \quad (7.20)$$

where

$$\mathbf{G}_s = [\mathbf{t}_{s_1}, \mathbf{t}_{s_2}, \dots, \mathbf{t}_{s_S}], \quad (7.21)$$

and

$$\mathbf{t}_{s_\tau} = [\mathbf{n}_{s_\tau}^T, (\mathbf{r}_{s_\tau} \times \mathbf{n}_{s_\tau})^T]^T. \quad (7.22)$$

In Eq. (7.22), \mathbf{n}_{s_τ} defines the normal vector of the workpiece surface at the τ th sensor point w.r.t. the nominal FCS, and \mathbf{r}_{s_τ} is the position vector of the workpiece point that is measured by the τ th sensor w.r.t. the nominal FCS. Therefore, the relationship between sensor measurements and fixture locator variations is expressed by combining Eqs. (7.19) and (7.20), i.e.,

$$\Delta \mathbf{s} = \mathbf{G}_s^T \cdot (\mathbf{G}_l^T)^{-1} \cdot \Delta \mathbf{l}. \quad (7.23)$$

Note that the matrix $\mathbf{G}_s^T \cdot (\mathbf{G}_l^T)^{-1}$ is full column-rank if, according to the 3-2-1 locating scheme, the sensor distribution has at least 3 sensors at the primary datum, 2 sensors at the secondary datum and one sensor at the tertiary datum.

Second, consider the situation where only datum variations are present at the machining station. Given a workpiece located with a 3-2-1 locating scheme, the primary datum is placed over the three locators that constrain the translation along Z -axis and the rotation around X - and Y -axis of the FCS, as shown in Figure 7.4. At the primary datum surface, none of the sensors placed on this datum can measure any workpiece datum variation. Then, the workpiece is moved over the primary datum keeping the contact between the primary datum and the locators until the workpiece surface is blocked due to the contact between the other two locators. At the secondary datum surface, the sensors can measure the secondary datum variations w.r.t. the primary datum. Specifically, the sensors can detect the rotation variation of the secondary datum w.r.t. the primary datum around the Y axis of the FCS. Finally, the workpiece is moved over the five locators until the tertiary datum is blocked by the sixth fixture locator. At the tertiary datum surface, the sensors can measure the rotation variation of the tertiary datum w.r.t. the primary datum around the X - and Z - axis of the FCS. With these considerations, the orientation variation of the secondary datum surface w.r.t. the primary datum surface can be detected. The coordinate systems that define the secondary and tertiary datums are CS_2 and CS_3 , respectively, as shown in Figure 7.4. Following the reasoning shown above, the sensor measurements will be related to the datum variations of the CS_2 by

$$\Delta \mathbf{s}_2 = \mathbf{G}_{D_2}^T \cdot \mathbf{x}_2^1. \quad (7.24)$$

where $\Delta \mathbf{s}_2$ denotes sensor measurements on the secondary datum; \mathbf{x}_2^1 is the variation of the secondary datum surface w.r.t. the primary datum surface; and \mathbf{G}_{D_2} is the matrix:

$$\mathbf{G}_{D_2} = [\mathbf{t}_{s_1}^2, \mathbf{t}_{s_2}^2, \dots, \mathbf{t}_{s_{d_2}}^2], \quad (7.25)$$

where

$$\mathbf{t}_{s_\tau}^2 = [(\mathbf{n}_{s_\tau}^2)^T, (\mathbf{r}_{s_\tau}^2 \times \mathbf{n}_{s_\tau}^2)^T]^T. \quad (7.26)$$

Note that the superscript 2 indicates that the vectors are defined w.r.t. CS_2 , and s_{d_2} denotes the last sensor installed on the secondary datum surface. Similarly, the sensor measurements corresponding to the datum variations on the tertiary datum are defined as:

$$\Delta \mathbf{s}_3 = \mathbf{G}_{D_3}^T \cdot \mathbf{x}_3^1. \quad (7.27)$$

Therefore, the influence of datum variations on sensor measurements is described as:

$$\begin{aligned} [(\Delta \mathbf{s}_2)^T, (\Delta \mathbf{s}_3)^T]^T &= \begin{pmatrix} \mathbf{G}_{D_2}^T & \mathbf{0}_{s_{d_2} \times 6} \\ \mathbf{0}_{s_{d_3} \times 6} & \mathbf{G}_{D_3}^T \end{pmatrix} \cdot [(\mathbf{x}_2^1)^T, (\mathbf{x}_3^1)^T]^T \\ &= \mathbf{G}_{D_2 D_3}^T \cdot [(\mathbf{x}_2^1)^T, (\mathbf{x}_3^1)^T]^T \end{aligned} \quad (7.28)$$

Note that matrix $\mathbf{G}_{D_2 D_3}^T$ is full column-rank if there are at least 3 sensors installed on both the secondary and the tertiary datum surfaces. Assuming that a sensor-based fixture is placed at station P , Eq. (7.28) can be generalized by including the sensors at all datum surfaces and the variations of all the workpiece features generated at station $P - 1$. The vectors defined w.r.t. station P are expressed as:

$$\begin{aligned} [(\Delta \mathbf{s}_1)^T, (\Delta \mathbf{s}_2)^T, (\Delta \mathbf{s}_3)^T]^T &= \begin{pmatrix} \dots & \mathbf{0}_{6 \times 1} & \mathbf{0}_{6 \times 1} & \dots \\ \dots & \dots & \dots & \dots \\ \vdots & \mathbf{G}_{D_2}^T & \mathbf{0}_{s_{d_2} \times 6} & \vdots \\ \vdots & \mathbf{0}_{s_{d_3} \times 6} & \mathbf{G}_{D_3}^T & \vdots \\ \dots & \dots & \dots & \dots \\ \dots & \mathbf{0}_{6 \times 1} & \mathbf{0}_{6 \times 1} & \dots \end{pmatrix} \cdot \mathbf{x}_{P-1}^P, \quad (7.29) \\ \Delta \mathbf{s} &= \mathbf{G}_D^T \cdot \mathbf{x}_{P-1}^P. \end{aligned} \quad (7.30)$$

Due to manufacturing variation propagation, datum variations will be related to manufacturing variations (fixture and machining variations) from upstream stations. According to the SoV model described by Eq. (7.1), datum variations after station $P - 1$ are defined as:

$$\mathbf{x}_{P-1}^{P-1} = \mathbf{\Gamma}_{1 \dots P-1}^f \cdot \mathbf{U}_{1 \dots P-1}^f + \mathbf{\Gamma}_{1 \dots P-1}^m \cdot \mathbf{U}_{1 \dots P-1}^m + \boldsymbol{\omega}_{1 \dots P-1}, \quad (7.31)$$

where $\mathbf{\Gamma}_{1 \dots P-1}^f$, $\mathbf{\Gamma}_{1 \dots P-1}^m$, $\mathbf{U}_{1 \dots P-1}^f$ and $\mathbf{U}_{1 \dots P-1}^m$ are, respectively, the part of the matrices $\mathbf{\Gamma}^f$, $\mathbf{\Gamma}^m$, \mathbf{U}^f and \mathbf{U}^m that correspond to the stations from 1 to $P - 1$, and $\boldsymbol{\omega}_{1 \dots P-1}$ is:

$$\boldsymbol{\omega}_{1 \dots P-1} = [\bar{\mathbf{M}}_{P-1,1} \quad \bar{\mathbf{M}}_{P-1,2} \quad \dots \quad \bar{\mathbf{M}}_{P-1,P-1}] \cdot [\mathbf{w}_1^T \quad \mathbf{w}_2^T \quad \dots \quad \mathbf{w}_{P-1}^T]^T. \quad (7.32)$$

Eq. (7.31) is rewritten as:

$$\mathbf{x}_{P-1}^{P-1} = \mathbf{\Gamma}_{1 \dots P-1} \cdot \mathbf{U}_{1 \dots P-1} + \boldsymbol{\omega}_{1 \dots P-1}, \quad (7.33)$$

where $\mathbf{U}_{1 \dots P-1}$ denotes the fixture and machining variations from station 1 to station $P - 1$. At station P , the workpiece will be relocated, so the datum variations w.r.t. the primary datum surface at station P will be defined as:

$$\mathbf{x}_{P-1}^P = \mathbf{A}_{P-1} \cdot \mathbf{x}_{P-1}^{P-1}, \quad (7.34)$$

and substituting Eq. (7.33) in Eq. (7.34):

$$\mathbf{x}_{P-1}^P = \mathbf{A}_{P-1} \cdot \mathbf{\Gamma}_{1 \dots P-1} \cdot \mathbf{U}_{1 \dots P-1} + \mathbf{A}_{P-1} \cdot \boldsymbol{\omega}_{1 \dots P-1}. \quad (7.35)$$

Finally, $\Delta \mathbf{s}$ can be achieved by substituting Eq. (7.35) in Eq. (7.30), i.e.,

$$\Delta \mathbf{s} = \mathbf{G}_D^T \cdot \mathbf{A}_{P-1} \cdot \mathbf{\Gamma}_{1\dots P-1} \cdot \mathbf{U}_{1\dots P-1} + \mathbf{G}_D^T \cdot \mathbf{A}_{P-1} \cdot \boldsymbol{\omega}_{1\dots P-1}. \quad (7.36)$$

As shown in Eq. (7.36), sensor measurements in the sensor-based fixture at station P will indicate manufacturing variations induced at upstream stations.

Considering that the second term on the right hand side of Eq. (7.36) can be neglected, by superposition $\Delta \mathbf{s}$ can be expressed considering Eq. (7.23) and Eq. (7.36) as

$$\begin{aligned} \Delta \mathbf{s} &= [\mathbf{G}_D^T \cdot \mathbf{A}_{P-1} \cdot \mathbf{\Gamma}_{1\dots P-1}, \mathbf{G}_s^T \cdot (\mathbf{G}_l^T)^{-1}] \cdot [(\mathbf{U}_{1\dots P-1})^T, (\Delta \mathbf{l})^T]^T + \mathbf{e}_s, \\ &= \mathbf{D} \cdot \mathbf{E}_{1\dots P} + \mathbf{e}_s, \end{aligned} \quad (7.37)$$

where $\mathbf{E}_{1\dots P}$ represents the variations of both fixture and machining operations at stations 1 to $P - 1$, and the fixture variations induced at station P ; \mathbf{e}_s is the measurement errors of the fixture sensors with a covariance matrix $\boldsymbol{\Sigma}_{\mathbf{e}_s}$.

Identification of the most significant sensors

Ideally, the number of sensors required to estimate the fixture locator variations if datum variations are not present is six, assuming that these sensors are distributed in a 3-2-1 locating scheme. However, when datum variations are present, the minimum number of sensors is increased to nine, with three sensors at each datum surface. In addition to fixture variations and datum variations, sensor accuracy is another factor that increases the number of sensors. In order to define the minimum number of sensors that maximize the measurement-noise ratio and minimize the error in estimating fixture variations, the sensor placement optimization method proposed by Kammer [17, 18] is applied. This method, named the effective independence (Efi) sensor placement method, was successfully applied by Wang and Nagarkar [19] in placing sensors in a coordinate checking fixture for extrusion processes and by Camelio *et al.* [20] in placing probes of a coordinate machine measurement for diagnosing multiple faults in fixturing compliant parts. The Efi method is essentially an iterative numerical method that finds the most effective sensor locations by (i) starting with a large number of candidate locations, and (ii) eliminating the least effective sensor at each step of the iteration until a minimum number of sensors is reached. In the Efi method, the least effective sensors eliminated from the initial candidates are not reconsidered in the process afterwards so the resulting most effective sensors cannot guarantee a global optimum sensor location. In order to increase the efficiency of the Efi method, the use of genetic algorithms has been presented by other researchers [21].

As shown in the previous subsection, the relationship between the sources of variations and the sensor measurements is defined by Eq. (7.37). In order to analyze the most significant sensors in the sensor-based fixture, Eq. (7.37) should consider the range of the expected sources of variations in the MMP. Thus, Eq. (7.37) can be modified as:

$$\begin{aligned} \Delta \mathbf{s} &= (\mathbf{D} \cdot \mathbf{T}) \cdot (\mathbf{T}^{-1} \cdot \mathbf{E}_{1\dots P}) + \mathbf{e}_s, \\ &= \tilde{\mathbf{D}} \cdot \tilde{\mathbf{E}}_{1\dots P} + \mathbf{e}_s, \end{aligned} \quad (7.38)$$

where \mathbf{T} is the diagonal matrix, $diag\{\mathbf{u}_1^{tol_f}, \mathbf{u}_1^{tol_m}, \dots, \mathbf{u}_{P-1}^{tol_f}, \mathbf{u}_{P-1}^{tol_m}, \mathbf{u}_P^{tol_f}\}$, and $\mathbf{u}_k^{tol_f}$ and $\mathbf{u}_k^{tol_m}$ are the fixture locator tolerances and machining tolerances at station k , respectively.

From Eq. (7.38), the Fisher information matrix is defined as [17]:

$$\mathbf{Q} = \tilde{\mathbf{D}}^T \cdot \Sigma_{\mathbf{e}_s}^{-1/2} \cdot \Sigma_{\mathbf{e}_s}^{-1/2} \cdot \tilde{\mathbf{D}} = \bar{\mathbf{D}}^T \cdot \bar{\mathbf{D}}. \quad (7.39)$$

The Fisher information matrix should be maximized to provide the sensor placement that best estimate the normalized manufacturing variations $\tilde{\mathbf{E}}_{1\dots P}$. For this purpose, Kammer [17] proposed the evaluation of the information provided from a sensor distribution by analyzing the matrix:

$$\mathbf{\Omega} = \bar{\mathbf{D}} \cdot [\bar{\mathbf{D}}^T \cdot \bar{\mathbf{D}}]^{-1} \cdot \bar{\mathbf{D}}^T. \quad (7.40)$$

Kammer showed that the ρ th diagonal term of $\mathbf{\Omega}$ represents the fractional contribution of the ρ th sensor location to the linear independence of the columns of $\bar{\mathbf{D}}$. Furthermore, the ρ th diagonal term of $\mathbf{\Omega}$, named the Efl of the ρ th sensor location, is related to the determinant of the Fisher information matrix as [22]:

$$\Omega_{\rho,\rho} = \frac{|\mathbf{Q}| - |\mathbf{Q}_\rho|}{|\mathbf{Q}|}, \quad (7.41)$$

where \mathbf{Q}_ρ represents the Fisher information matrix with the ρ th candidate sensor location removed.

Therefore, the Efl sensor placement method from an initial mesh of sensors evaluates the diagonal terms of $\mathbf{\Omega}$ and removes the ρ th sensor that presents the lowest value of $\Omega_{\rho,\rho}$. For the remaining mesh of sensors, the Fisher information matrix is updated and the evaluation of the Efl's sensors is repeated until a reasonable minimum number of sensors is reached. This minimum number of sensors will compose the sensor-based fixture system. Two criteria can be applied for choosing the appropriate number of sensors: i) a predefined number of sensors from the designer; and ii) the minimum number of sensors that, in case that any of them is removed, the uncertainty of the estimation of manufacturing variations highly increases. Unlike the first criterion which is straight forward, the second criterion requires to formulate the covariance matrix of $(\mathbf{E}_{1\dots P} - \hat{\mathbf{E}}_{1\dots P})$. According to [9], this covariance matrix is defined as:

$$\Sigma_{\mathbf{E}_{1\dots P} - \hat{\mathbf{E}}_{1\dots P}} = \Sigma_{\mathbf{E}_{1\dots P}} - \Sigma_{\mathbf{E}_{1\dots P}} \cdot \mathbf{D}^T \cdot [\mathbf{D} \cdot \Sigma_{\mathbf{E}_{1\dots P}} \cdot \mathbf{D}^T + \Sigma_{\mathbf{e}_s}]^+ \cdot \mathbf{D} \cdot \Sigma_{\mathbf{E}_{1\dots P}}, \quad (7.42)$$

where \mathbf{H}^+ denotes the Moore-Penrose inverse of a matrix \mathbf{H} . In order to evaluate the increase of the uncertainty in the manufacturing variation estimation after a sensor is deleted from the fixture, the following ratio is defined:

$$I_u = \frac{\|\Sigma_{\mathbf{E}_{1\dots P} - \hat{\mathbf{E}}_{1\dots P}}^{S-1}\|}{\|\Sigma_{\mathbf{E}_{1\dots P} - \hat{\mathbf{E}}_{1\dots P}}^S\|}, \quad (7.43)$$

where the superscript S refers to the number of the sensors remaining in the fixture. By limiting this ratio during the optimization procedure, the most significant sensors can be kept in the fixture. Figure 7.5 summarizes the methodology proposed to design a sensor-based fixture with optimal sensor distribution.

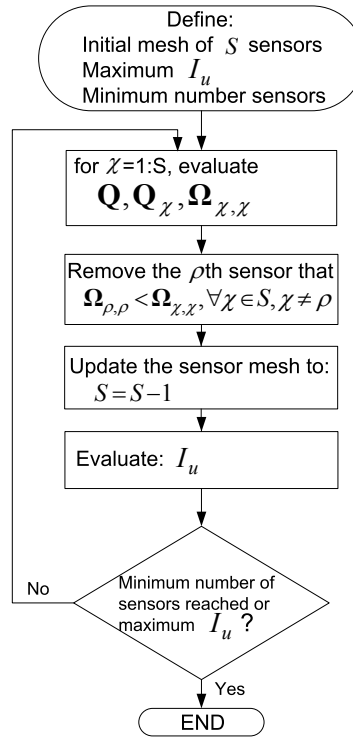


Figure 7.5: Algorithm to place the optimal number of sensors in the sensor-based fixture.

7.2.3 Step 3: Compensability Analysis

In order to study the compensability analysis of an N -station machining process, we consider station P as the station where the sensor-based fixture is placed and stations P to N as the stations where CNC machine-tools are placed capable to conduct cutting-tool path compensations. According to Eq. (7.1), for this N -station machining process the variations of the KPCs at the end of the MMP is defined as:

$$\mathbf{Y}_N = \mathbf{\Gamma}_{N,1\dots P} \cdot \mathbf{E}_{1\dots P} + \mathbf{\Gamma}_{N,P\dots N} \cdot \mathbf{U}_{P\dots N} + \mathbf{\Gamma}_{N,P\dots N} \cdot \mathbf{U}_{P\dots N}^C + \boldsymbol{\varepsilon}_N, \quad (7.44)$$

where $\mathbf{E}_{1\dots P}$ represents the sources of variations from station 1 to station $P - 1$ and the fixture variations from station P ; $\mathbf{U}_{P\dots N}$ represents the machining variations from station P and the sources of variations from stations $P + 1$ to N ; $\mathbf{U}_{P\dots N}^C$ is the cutting-tool path compensation conducted at station P through station N where CNC machine-tool are placed; and the matrices $\mathbf{\Gamma}_{N,1\dots P}$, $\mathbf{\Gamma}_{N,P\dots N}$ are the corresponding block matrices from matrix $\mathbf{\Gamma}$ in Eq. (7.1). Since only the estimated variations from the sensor-based fixture measurements can be propagated at downstream stations in order to be compensated by CNC machine-tools, the rest of sources of variations can be considered as un-compensable. For this reason, Eq. (7.44) can be re-written as:

$$\mathbf{Y}_N = \mathbf{\Gamma}_{N,1\dots P} \cdot \mathbf{E}_{1\dots P} + \mathbf{\Gamma}_{N,P\dots N} \cdot \mathbf{U}_{P\dots N}^C + \boldsymbol{\nu}_N, \quad (7.45)$$

where

$$\boldsymbol{\nu}_N = \boldsymbol{\Gamma}_{N,P\dots N} \cdot \mathbf{U}_{P\dots N} + \boldsymbol{\varepsilon}_N. \quad (7.46)$$

With the information collected from the sensor-based fixture, $\mathbf{E}_{1\dots P}$ can be estimated by Eq. (7.37) according to the sensor measurements. Assuming that machining and fixture variations follow normal distributions, the linear least squares estimator of $\mathbf{E}_{1\dots P}$ is defined as [9]:

$$\hat{\mathbf{E}}_{1\dots P} = \boldsymbol{\Sigma}_{\mathbf{E}_{1\dots P}} \cdot \mathbf{D}^T \cdot [\mathbf{D} \cdot \boldsymbol{\Sigma}_{\mathbf{E}_{1\dots P}} \cdot \mathbf{D}^T + \boldsymbol{\Sigma}_{\mathbf{e}_s}]^+ \cdot \Delta \mathbf{s}. \quad (7.47)$$

From Eq. (7.45), the term $\mathbf{U}_{P\dots N}^C$ will be defined to eliminate part quality variations at the end of the MMP. In order to make \mathbf{Y}_N equal to zero in Eq. (7.45), $\mathbf{U}_{P\dots N}^C$ is defined as:

$$\mathbf{U}_{P\dots N}^C = -\boldsymbol{\Gamma}_{N,P\dots N}^+ \cdot \boldsymbol{\Gamma}_{N,1\dots P} \cdot \hat{\mathbf{E}}_{1\dots P}. \quad (7.48)$$

Substituting Eq. (7.37) and (7.47) in Eq. (7.48):

$$\mathbf{U}_{P\dots N}^C = -\boldsymbol{\Gamma}_{N,P\dots N}^+ \cdot \boldsymbol{\Gamma}_{N,1\dots P} \cdot [\boldsymbol{\Sigma}_{\mathbf{E}_{1\dots P}} \cdot \mathbf{D}^T \cdot [\mathbf{D} \cdot \boldsymbol{\Sigma}_{\mathbf{E}_{1\dots P}} \cdot \mathbf{D}^T + \boldsymbol{\Sigma}_{\mathbf{e}_s}]^+ \cdot (\mathbf{D} \cdot \mathbf{E}_{1\dots P} + \mathbf{e}_s)]. \quad (7.49)$$

Finally, substituting Eq. (7.49) in Eq. (7.45):

$$\begin{aligned} \mathbf{Y}_N &= [\boldsymbol{\Gamma}_{N,1\dots P} - \boldsymbol{\Gamma}_{N,P\dots N} \cdot \boldsymbol{\Gamma}_{N,P\dots N}^+ \cdot \boldsymbol{\Gamma}_{N,1\dots P} \cdot [\boldsymbol{\Sigma}_{\mathbf{E}_{1\dots P}} \cdot \mathbf{D}^T \cdot [\mathbf{D} \cdot \boldsymbol{\Sigma}_{\mathbf{E}_{1\dots P}} \cdot \mathbf{D}^T + \boldsymbol{\Sigma}_{\mathbf{e}_s}]^+ \cdot \\ &\quad \mathbf{D}]] \cdot \mathbf{E}_{1\dots P} + \tilde{\boldsymbol{\nu}}_N, \\ &= \mathbf{C} \cdot \mathbf{E}_{1\dots P} + \tilde{\boldsymbol{\nu}}_N. \end{aligned} \quad (7.50)$$

where

$$\tilde{\boldsymbol{\nu}}_N = \boldsymbol{\nu}_N - \boldsymbol{\Gamma}_{N,P\dots N} \cdot \boldsymbol{\Gamma}_{N,P\dots N}^+ \cdot \boldsymbol{\Gamma}_{N,1\dots P} \cdot [\boldsymbol{\Sigma}_{\mathbf{E}_{1\dots P}} \cdot \mathbf{D}^T \cdot [\mathbf{D} \cdot \boldsymbol{\Sigma}_{\mathbf{E}_{1\dots P}} \cdot \mathbf{D}^T + \boldsymbol{\Sigma}_{\mathbf{e}_s}]^+ \cdot \mathbf{e}_s. \quad (7.51)$$

In [7], matrix \mathbf{C} is named the uncompensable space matrix. In order to make the term $\mathbf{C} \cdot \mathbf{E}_{1\dots P}$ equal to zero for any value of $\mathbf{E}_{1\dots P}$, the following two conditions need to be satisfied:

$$\boldsymbol{\Gamma}_{N,P\dots N} \cdot \boldsymbol{\Gamma}_{N,P\dots N}^+ = \mathbf{I}, \quad (7.52)$$

$$\boldsymbol{\Sigma}_{\mathbf{E}_{1\dots P}} \cdot \mathbf{D}^T \cdot [\mathbf{D} \cdot \boldsymbol{\Sigma}_{\mathbf{E}_{1\dots P}} \cdot \mathbf{D}^T + \boldsymbol{\Sigma}_{\mathbf{e}_s}]^+ \cdot \mathbf{D} = \mathbf{I}, \quad (7.53)$$

where \mathbf{I} is an identity matrix. Considering that the Moore-Penrose inverse satisfies the following properties [23]

$$\mathbf{H}^+ = \mathbf{H}^T \cdot (\mathbf{H} \cdot \mathbf{H}^T)^{-1}, \quad (7.54)$$

$$\mathbf{H}^+ = (\mathbf{H}^T \cdot \mathbf{H})^{-1} \cdot \mathbf{H}^T, \quad (7.55)$$

when \mathbf{H} is a full row-rank matrix and full column-rank matrix, respectively, the two conditions shown in Eqs. (7.52) and (7.53) are defined as follows [7]. The first condition

holds when $\Gamma_{N,P\dots N}$ is a full row-rank matrix. This indicates the capability of the system to compensate the estimated variations according to sensor-based fixture measurements at downstream stations (stations from P to N). This condition is analogous to the well-known controllability concept in control theory [14]. The second condition holds when (i) sensor measurements errors \mathbf{e}_s are negligible in comparison with workpiece surface variations and (ii) when $(\mathbf{D} \cdot (\boldsymbol{\Sigma}_{\mathbf{E}_{1\dots P}})^{1/2})^+ \cdot (\mathbf{D} \cdot (\boldsymbol{\Sigma}_{\mathbf{E}_{1\dots P}})^{1/2})$ and $(\mathbf{D} \cdot (\boldsymbol{\Sigma}_{\mathbf{E}_{1\dots P}})^{1/2})^T \cdot ((\mathbf{D} \cdot (\boldsymbol{\Sigma}_{\mathbf{E}_{1\dots P}})^{1/2})^T)^+$ are identity matrices, which means that $\mathbf{D} \cdot (\boldsymbol{\Sigma}_{\mathbf{E}_{1\dots P}})^{1/2}$ is a full column-rank matrix. This fact is proved by neglecting $\boldsymbol{\Sigma}_{\mathbf{e}_s}$ and thus Eq. (7.53) is rewritten as

$$\boldsymbol{\Sigma}_{\mathbf{E}_{1\dots P}} \cdot \mathbf{D}^T \cdot [\mathbf{D} \cdot (\boldsymbol{\Sigma}_{\mathbf{E}_{1\dots P}})^{1/2} \cdot (\mathbf{D} \cdot ((\boldsymbol{\Sigma}_{\mathbf{E}_{1\dots P}})^{1/2})^T)^T]^+ \cdot \mathbf{D} = \mathbf{I}. \quad (7.56)$$

Considering that the Moore-Penrose inverse satisfies the property $(\mathbf{H} \cdot \mathbf{H}^T)^+ = (\mathbf{H}^T)^+ \cdot \mathbf{H}^+$, Eq. (7.56) becomes

$$\begin{aligned} & (\boldsymbol{\Sigma}_{\mathbf{E}_{1\dots P}})^{1/2} \cdot (\boldsymbol{\Sigma}_{\mathbf{E}_{1\dots P}})^{1/2} \cdot \mathbf{D}^T \cdot ((\mathbf{D} \cdot (\boldsymbol{\Sigma}_{\mathbf{E}_{1\dots P}})^{1/2})^T)^+ \cdot (\mathbf{D} \cdot (\boldsymbol{\Sigma}_{\mathbf{E}_{1\dots P}})^{1/2})^+ \cdot \\ & (\mathbf{D} \cdot (\boldsymbol{\Sigma}_{\mathbf{E}_{1\dots P}})^{1/2}) \cdot (\boldsymbol{\Sigma}_{\mathbf{E}_{1\dots P}})^{-1/2} = \mathbf{I}, \end{aligned} \quad (7.57)$$

Since $\boldsymbol{\Sigma}_{\mathbf{E}_{1\dots P}}$ is a symmetric and positive-definite matrix, Eq. (7.57) is finally rewritten as

$$\begin{aligned} & (\boldsymbol{\Sigma}_{\mathbf{E}_{1\dots P}})^{1/2} \cdot (\mathbf{D} \cdot (\boldsymbol{\Sigma}_{\mathbf{E}_{1\dots P}})^{1/2})^T \cdot ((\mathbf{D} \cdot (\boldsymbol{\Sigma}_{\mathbf{E}_{1\dots P}})^{1/2})^T)^+ \cdot (\mathbf{D} \cdot (\boldsymbol{\Sigma}_{\mathbf{E}_{1\dots P}})^{1/2})^+ \cdot \\ & (\mathbf{D} \cdot (\boldsymbol{\Sigma}_{\mathbf{E}_{1\dots P}})^{1/2}) \cdot (\boldsymbol{\Sigma}_{\mathbf{E}_{1\dots P}})^{-1/2} = \mathbf{I}, \end{aligned} \quad (7.58)$$

As it can be observed in Eq. (7.58), this condition holds if $\mathbf{D} \cdot (\boldsymbol{\Sigma}_{\mathbf{E}_{1\dots P}})^{1/2}$ is a full column-rank matrix. This second condition corresponds to the diagnosability of the system from station 1 to P . This condition is analogous to the well-known observability condition in control theory [14].

Therefore, in order to compensate manufacturing variations at downstream stations, it is required to be able to diagnose these variations and also be able to compensate the effect of these variations at downstream stations through cutting-tool path modifications. In [7], the evaluation of the rank of the uncompensable space matrix is used to indicate the presence of uncompensable sources of manufacturing variations in MMPs.

Besides the uncompensable space matrix, a compensability index can be defined to quantitatively describe the part variation that can be compensated by applying a sensor-based fixture at a specific machining station. The compensability index at station k can be formulated as [10, 11]

$$\Upsilon_k = \frac{\|\boldsymbol{\Sigma}_{\mathbf{Y}}^{NC}\| - \|\boldsymbol{\Sigma}_{\mathbf{Y}}^C\|}{\|\boldsymbol{\Sigma}_{\mathbf{Y}}^{NC}\|}, \quad (7.59)$$

where $\boldsymbol{\Sigma}_{\mathbf{Y}}^C$ and $\boldsymbol{\Sigma}_{\mathbf{Y}}^{NC}$ are the resulting $\boldsymbol{\Sigma}_{\mathbf{Y}}$ matrix in case that a sensor-based fixture is placed or not in the MMP, respectively. Note that when $\Upsilon_k \rightarrow 0$, there is no quality improvement and the variation of the KPCs cannot be reduced through compensation. Otherwise, when $\Upsilon_k \rightarrow 1$, there is a significant quality improvement and the variation of the KPCs tends to be 0. The evaluation of this ratio for different placements of sensor-based fixtures and different number of sensors and layouts is conducted to detect the best

compensation scheme that minimizes the variation of the KPCs.

Rewriting Eq. (7.50), \mathbf{Y}_N can be expressed in the following useful form:

$$\mathbf{Y}_N = (\mathbf{\Gamma}_{N,1\dots P} - \mathbf{\Gamma}_{N,1\dots P}^+ \cdot \mathbf{\Gamma}_{N,1\dots P}) \cdot \mathbf{E}_{1\dots P} + \mathbf{\Gamma}_{N,1\dots P}^+ \cdot \mathbf{\Gamma}_{N,1\dots P} \cdot (\mathbf{E}_{1\dots P} - \hat{\mathbf{E}}_{1\dots P}) + \boldsymbol{\nu}_N \quad (7.60)$$

where it can be noted that the final part quality variation depends on three terms. The first term on the right hand side defines the part quality variation due to uncompensable variations generated at stations $1, \dots, P$, since sensor-based fixtures provide a limited information from previous manufacturing stations. The second term defines the part quality variation due to those previous manufacturing variations that, although they are compensable, the total variation is not compensated due to their estimation errors. The third term defines the inherent part quality variation due to machining variations at station P , manufacturing variations at stations $P+1, \dots, N$, and unmodeled and linearization errors.

7.3 Case Study

In order to demonstrate the effectiveness of the proposed methodology and the potential benefits of the sensor-based fixtures, a case study is conducted. The MMP analyzed is shown in Figure 7.6 and the resulting machined part is shown in Figure 7.7. The datum features and the surfaces machined at each station are presented in Table 7.1. The location of each fixture locator at each machining station is defined in Table 7.2 and the nominal position and orientation of each surface is presented in Table 7.3. The KPCs to be measured are the distance between the features S_3 and S_0 and the distance between S_8 and S_6 . For this MMP, it is assumed that all machining stations are CNC machine-tools where cutting-tool path adjustments can be conducted, since we are analyzing a MMP in the context of FMSs. Furthermore, it is assumed that fixture locator variations are independent of each other with a locator tolerance of 0.1 mm . Machining variations are also assumed to be independent of each other and independent of fixture locator variations. At all stations, the position and orientation tolerances of cutting-tool paths are assumed to be 0.02 mm and 0.001 rad , respectively.

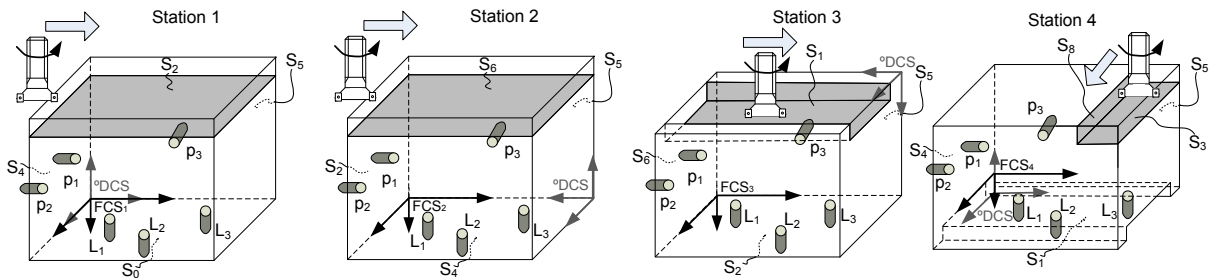


Figure 7.6: Case study. Part to be machined in a 4-station machining process.

The SoV methodology is employed to predict the final part quality. Applying Eq. (7.8), the predicted variations of S_3 w.r.t. S_0 and S_8 w.r.t. S_6 were $\pm 0.64 \text{ mm}$ and $\pm 0.55 \text{ mm}$,

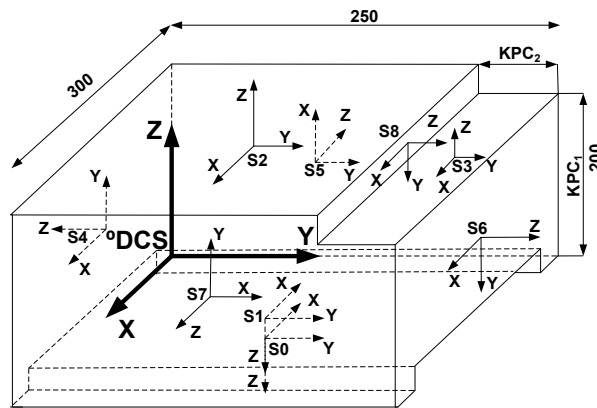


Figure 7.7: Case study. Surfaces S_0 to S_8 . Dimensions in mm .

respectively, considering a six sigma coverage. In order to reduce the variance, the proposed methodology is applied. Firstly, the stations with a higher contribution to the final part quality variations are identified. Secondly, the optimal sensor placement algorithm is applied to design a sensor-based fixture with optimal sensor placement. Please note that for illustrative purposes, at this case study the placement of a sensor-based fixture is analyzed at every station even if its variation contribution is low. With each sensor-based fixture design, a compensability analysis is conducted, evaluating the tooling adjustment capability to reduce part quality variation. After evaluating the different compensability indices for each potential sensor-based fixture design, the one with the highest index is selected. Finally, for that fixture configuration the expected part quality at the end of the MMP is evaluated.

Furthermore, for comparison purposes, the final part variation is analyzed considering four situations: (1) without compensation; (2) with compensation and a sensor-based fixture composed of minimum number of sensors with non-optimal sensor placement; (3) with compensation and a sensor-based fixture composed of minimum number of sensors with optimal sensor placement; and (4) with compensation and a sensor-based fixture composed of a higher number of sensors with optimal sensor placement.

Table 7.1: Machined features and datum features according to the 3-2-1 locating scheme at each station.

| Station | Datum features | Machined features |
|---------|-------------------|--------------------|
| 1 | $S_0 - S_4 - S_5$ | S_2 |
| 2 | $S_4 - S_2 - S_5$ | S_6 |
| 3 | $S_2 - S_6 - S_5$ | S_1 |
| 4 | $S_1 - S_4 - S_5$ | S_3, S_8 |
| 5 | $S_0 - S_4 - S_5$ | Inspection station |

Table 7.2: Nominal location ($\mathbf{t}_{F_k}^{\circ D}$) and orientation ($\varphi_{F_k}^{\circ D}$) of fixture CS at each station and fixture layout.

| Station | $\varphi_{F_k}^{\circ D}$ (rad) | $\mathbf{t}_{F_k}^{\circ D}$ (mm) | Locators w.r.t. F_k (mm) |
|---------|---------------------------------|-----------------------------------|---|
| 1 | $[-\pi/2, \pi, 0]$ | $[0, 0, 0]$ | $L_{1x} = 125, L_{1y} = 50, L_{2x} = 50, L_{2y} = 250, L_{3x} = 200, L_{3y} = 250,$ $p_{1y} = 50, p_{1z} = -100, p_{2y} = 250, p_{2z} = -100, p_{3x} = 125, p_{3z} = -100$ |
| 2 | $[\pi/2, -\pi/2, \pi]$ | $[0, 0, 200]$ | $L_{1x} = 100, L_{1y} = 50, L_{2x} = 50, L_{2y} = 150, L_{3x} = 150, L_{3y} = 150,$ $p_{1y} = 50, p_{1z} = -125, p_{2y} = 250, p_{2z} = -125, p_{3x} = 100, p_{3z} = -125$ |
| 3 | $[-\pi/2, 0, 0]$ | $[0, 250, 200]$ | $L_{1x} = 125, L_{1y} = 50, L_{2x} = 50, L_{2y} = 250, L_{3x} = 200, L_{3y} = 250,$ $p_{1y} = 50, p_{1z} = -100, p_{2y} = 250, p_{2z} = -100, p_{3x} = 125, p_{3z} = -100$ |
| 4 | $[-\pi/2, \pi, 0]$ | $[0, 0, 20]$ | $L_{1x} = 125, L_{1y} = 50, L_{2x} = 50, L_{2y} = 250, L_{3x} = 200, L_{3y} = 250,$ $p_{1y} = 50, p_{1z} = -100, p_{2y} = 250, p_{2z} = -100, p_{3x} = 125, p_{3z} = -100$ |
| 5 | $[-\pi/2, \pi, 0]$ | $[0, 0, 0]$ | - |

Table 7.3: Nominal location ($\mathbf{t}_{S_i}^{\circ D}$) and orientation ($\varphi_{S_i}^{\circ D}$) of each feature.

| Feature | $\varphi_{S_i}^{\circ D}$ (rad) | $\mathbf{t}_{S_i}^{\circ D}$ (mm) |
|---------|---------------------------------|-----------------------------------|
| S_0 | $[0, \pi, 0]$ | $[150, 125, 0]$ |
| S_1 | $[0, \pi, 0]$ | $[150, 125, 20]$ |
| S_2 | $[0, 0, 0]$ | $[150, 75, 200]$ |
| S_3 | $[0, 0, 0]$ | $[150, 225, 180]$ |
| S_4 | $[\pi/2, -\pi/2, -\pi/2]$ | $[150, 0, 100]$ |
| S_5 | $[0, -\pi/2, 0]$ | $[0, 75, 100]$ |
| S_6 | $[\pi/2, \pi/2, -\pi/2]$ | $[150, 250, 75]$ |
| S_7 | $[0, \pi/2, \pi/2]$ | $[300, 125, 100]$ |
| S_8 | $[\pi/2, \pi/2, -\pi/2]$ | $[150, 200, 190]$ |

7.3.1 Identification of station-induced variations

Applying the first step of the proposed methodology, the impact of fixture and machining variations on KPCs can be analyzed. The results of the indices presented in Section 7.2.1 are shown in Figure 7.8. According to the results, the fixture-induced variations are more critical than machining variations ($\eta_f = 0.93$ and $\eta_m = 0.07$). Analyzing the influence of fixture-induced variations on part quality at each station, it is noted that fixture-induced variations at station 2 produces higher variations on the KPCs since the resulting indices were $\eta_{f,1} = 0.30$, $\eta_{f,2} = 0.42$, $\eta_{f,3} = 0.13$ and $\eta_{f,4} = 0.33$. As a conclusion, it can be expected that an improvement of the fixture system at station 2 by installing a sensor-based fixture can lead to a greater improvement in product quality than in any other station. However, this expectation may be incorrect since we need to conduct a compensability analysis for a specific sensor-based fixture in order to analyze which part of the potential variation detected by the sensors can be compensated downstream stations by tooling adjustments in the CNC machine-tools. This analysis will be conducted in next subsections.

7.3.2 Sensor-based fixture design and compensability analysis

In this case study, a sensor-based fixture is designed and deployed at each machining station to evaluate all possible compensability indices. The algorithm for optimal sensor placement was run for each machining station until a sensor-based fixture with a minimum

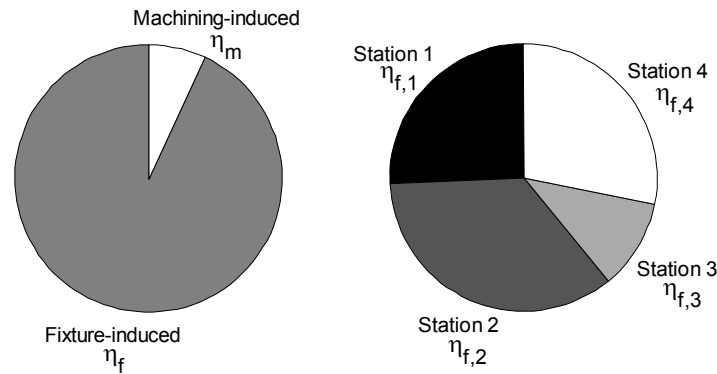


Figure 7.8: Identification of the impact of station-induced variations on the final part quality.

number of sensors was reached. In the algorithm, the sensor mesh was initialized with a 20 mm between-sensor distance at each datum surface. In addition, the errors of each sensor measurement were assumed to be identical and independent of each other, so the covariance matrix of the sensor measurement errors was defined as $\Sigma_{e_s} = \text{diag}\{\sigma_s^2, \sigma_s^2, \dots, \sigma_s^2\}$, with $\sigma_s = 0.03$ mm. Table 7.4 shows an example of sensor distribution for a sensor-based fixture placed at station 4.

A compensability analysis is conducted for each sensor based fixture. The results of this analysis can be found in Table 7.5. According to these results, the placement of a sensor-based fixture with minimum number of sensors and optimal distribution at station 4 provides the best compensability index and thus, the highest part quality variation reduction. Interestingly, it can be noticed from the table that the rank of the uncompensable space matrix increases as the placement of the sensor-based fixture is done closer to the end of the manufacturing line. This is because the manufacturing is propagated along the MMP and thus, workpiece variations at those stations are generated by a larger number of sources of variation. The higher the number of sources of variation that cannot be compensated, the higher the rank of the uncompensable space matrix.

7.3.3 Comparison of part quality variation according to sensor accuracy and sensor distribution

The compensability analysis shows that the highest part quality improvement could be attained with the sensor-based fixture located at station 4. As the sensors have limited precision, the compensation capability is greatly related to sensor placement, number of

Table 7.4: Sensor distribution for the sensor-based fixture at station 4.

| St. | Coordinates of the sensors w.r.t. the FCS (in mm) |
|-----|--|
| 4 | $s_1 = [10, 10, 0]$; $s_2 = [240, 290, 0]$; $s_3 = [10, 290, 0]$; $s_4 = [0, 10, -10]$; $s_5 = [0, 290, -190]$; $s_6 = [0, 290, -10]$; $s_7 = [240, 0, -190]$; $s_8 = [240, 0, -10]$; $s_9 = [10, 0, -190]$ |

Table 7.5: Results of the compensability analysis for the case study.

| Sensor-based fixture station | Rank of \mathbb{C} | Υ_k | KPC_1 variation | KPC_2 variation | $\ \Sigma_{\mathbf{E}_{1..P}-\hat{\mathbf{E}}_{1..P}}\ $ |
|------------------------------|----------------------|--------------|-------------------|-------------------|--|
| 1 | 4 | 0.12 | 0.50 mm | 0.54 mm | $9.42 \cdot 10^{-6} \text{ mm}^2$ |
| 2 | 6 | 0.20 | 0.60 mm | 0.29 mm | $2.78 \cdot 10^{-4} \text{ mm}^2$ |
| 3 | 7 | 0.11 | 0.54 mm | 0.52 mm | $2.78 \cdot 10^{-4} \text{ mm}^2$ |
| 4 | 8 | 0.21 | 0.47 mm | 0.47 mm | $2.78 \cdot 10^{-4} \text{ mm}^2$ |

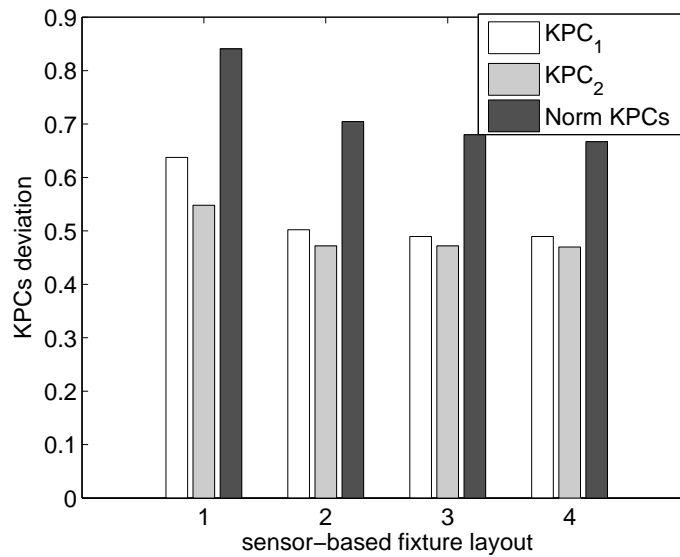


Figure 7.9: Variation of KPCs according to sensor-based fixture designs: (1) Non-sensor-based fixture; (2) sensor-based fixture with nine non-optimal sensors; (3) sensor-based fixture with nine optimal sensors; (4) sensor-based fixture with 14 optimal sensors.

sensors and sensor precision itself. For comparison purposes, the part quality variation at the end of the MMP is analyzed considering four situations: (1) without compensation; (2) with compensation and a sensor-based fixture at station 4 composed of minimum number of sensors with non-optimal sensor placement; (3) with compensation and a sensor-based fixture at station 4 composed of minimum number of sensors with optimal sensor placement; and (4) with compensation and a sensor-based fixture at station 4 composed of a higher number of sensors with optimal sensor placement. The resulting part quality variation for each case is shown in Figure 7.9. The figure presents interesting results. First, the important reduction of part quality variation with a sensor-based fixture is shown. The Euclidean norm of the vector of KPCs when the MMP manufactures parts without a sensor-based fixture is 0.84 mm whereas using an optimal sensor-based fixture at the 4 station with minimum number of sensors this value is reduced to 0.68 mm. The results from other sensor-based fixture configurations also reveal that, although the sensor distribution is important, it is not really important when the sensor measurement error is not

high. In fact, the sensor-based fixture with minimum number of sensors with non-optimal distribution presents a value of 0.70 mm whereas the sensor-based fixture with 14 optimal distributed sensors presents a value of 0.66 mm .

In order to show the influence of sensor precision on the final KPC variation and on the resulting compensability index, the same sensor-based fixture layouts were analyzed for different sensor precisions. The results shown in Figure 7.10 and Figure 7.11 reveal that there are no relevant differences between both sensor-based fixtures when sensors are accurate enough, specially when they are optimally placed. However, as sensor inaccuracy increases, the performance of the fixture with minimum number of sensors which are not optimally placed decreases rapidly. For those optimally placed, their performance is more robust, specially the one with a higher number of sensors.

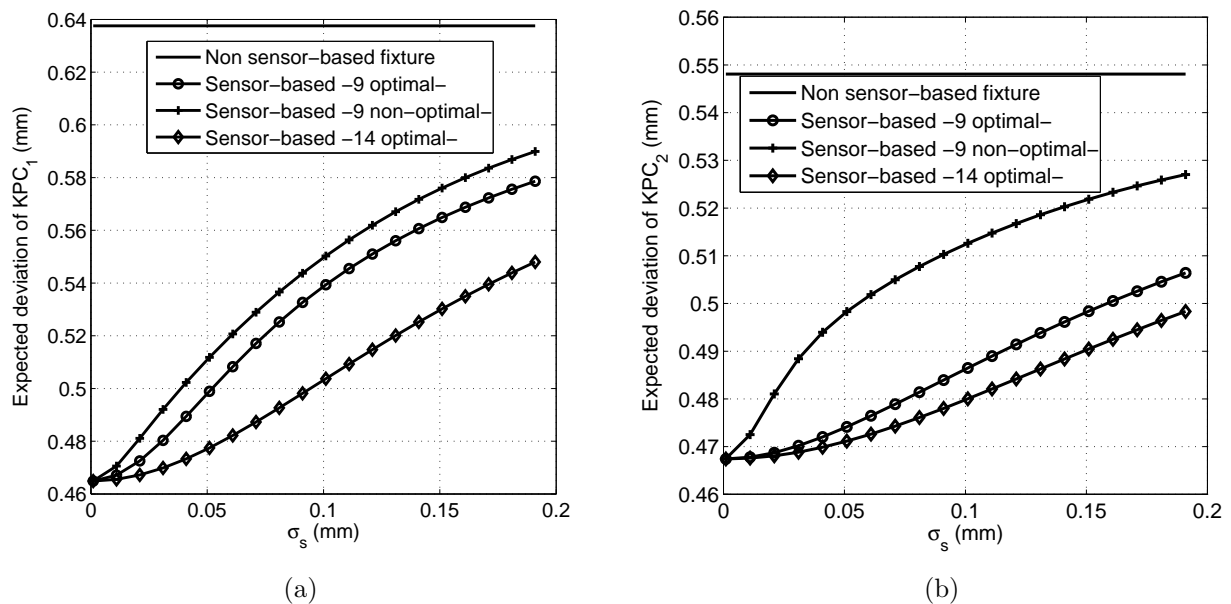


Figure 7.10: Variation of a) KPC_1 and b) KPC_2 according to different sensor-based fixtures.

7.4 Conclusions

Sensor-based fixtures can notably improve machined part quality through cutting-tool path compensations in FMSs. In order to facilitate the application of sensor-based fixtures and evaluate their potential benefits, a 3 step methodology has been proposed. The methodology deals with (1) the identification of station-induced variations, (2) the sensor placement optimization method for designing sensor-based fixtures, and (3) the compensability analysis. A case study with four machining stations was used to illustrate the effectiveness of the methodology. The results of the case study validate the potential use of sensor-based fixtures and highlight the importance of sensor placement and sensor precision in improving the final part quality in FMSs.

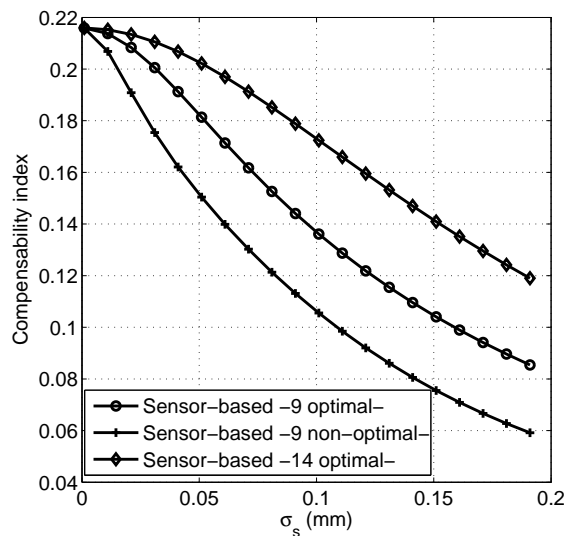


Figure 7.11: Compensability index according to sensor precision and the sensor-based fixture design.

References

- [1] D. Ceglarek, W. Huang, S. Zhou, Y. Ding, R. Kumar, Y. Zhou, Time-based competition in multistage manufacturing: Stream-of-variation analysis (SOVA) methodology - review, *International Journal of Flexible Manufacturing Systems* 16 (1) (2004) 11–44.
- [2] Y. Rong, *Computer-aided fixture design*, Marcel Dekker, New York, 1999.
- [3] Z. M. Bi, W. J. Zhang, Flexible fixture design and automation: Review, issues and future directions, *International Journal of Production Research* 39 (13) (2001) 2867–2894.
- [4] B. Shirinzadeh, Flexible fixturing for workpiece positioning and constraining, *Assembly Automation* 22 (2) (2002) 112–120.
- [5] E. C. DeMeter, M. J. Hockenberger, The application of tool path compensation for the reduction of clamping-induced geometric errors, *International Journal of Production Research* 35 (12) (1997) 3415–3432.
- [6] J. Liu, Variation reduction for multistage manufacturing processes: a comparison survey of statistical-process-control vs stream-of-variation methodologies, *Quality and Reliability Engineering International* 26 (7).
- [7] D. Djurdjanovic, J. Zhu, Stream of variation based error compensation strategy in multi-stage manufacturing processes, *ASME Conference Proceedings* 2005 (42231) (2005) 1223–1230.

-
- [8] L. Izquierdo, J. Shi, S. Hu, C. Wampler, Feedforward control of multistage assembly processes using programmable tooling, *NAMRI/SME Transactions* 35 (2007) 295–302.
- [9] D. Djurdjanovic, J. Ni, Online stochastic control of dimensional quality in multistation manufacturing systems, *Proceedings of the Institution of Mechanical Engineers Part B-Journal of Engineering Manufacture* 221 (5) (2007) 865–880.
- [10] Y. Jiao, D. Djurdjanovic, Allocation of flexible tooling for optimal stochastic multistation manufacturing process quality control, *ASME Conference Proceedings* 2008 (48524) (2008) 161–169.
- [11] Y. Jiao, D. Djurdjanovic, Joint allocation of measurement points and controllable tooling machines in multistage manufacturing processes, *IIE Transactions* 42 (10) (2010) 703–720.
- [12] J. Zhong, J. Liu, J. Shi, Predictive control considering model uncertainty for variation reduction in multistage assembly processes, *IEEE Transactions on Automation Science and Engineering* 7 (4) (2010) 724–735.
- [13] J. Shi, *Stream of Variation Modeling and Analysis for Multistage*, CRC Press Taylor and Francis Group, 2007.
- [14] K. Ogata, *Modern Control Engineering*, 4th Edition, Prentice Hall, 2001.
- [15] P. Joshi, *Jigs and Fixtures Design Manual*, McGraw-Hill, 2003.
- [16] M. Y. Wang, Characterizations of positioning accuracy of deterministic localization of fixtures, in: *IEEE International Conference on Robotics and Automation*, Vol. 3, 2002, pp. 2894–2899.
- [17] D. Kammer, Sensor placement for on-orbit modal identification and correlation of large space structures, *Journal of Guidance, Control, and Dynamics* 14 (2) (1991) 251–259.
- [18] D. C. Kammer, Optimal sensor placement for modal identification using system-realization methods, *Journal of Guidance, Control, and Dynamics* 19 (3) (1996) 729–731.
- [19] M. Y. Wang, S. Nagarkar, Locators and sensors for automated coordinate checking fixtures, Report. Available via <http://hdl.handle.net/1903/5885>. Accessed 28 Nov 2009 (1997).
- [20] J. A. Camelio, S. J. Hu, H. Yim, Sensor placement for effective diagnosis of multiple faults in fixturing of compliant parts, *Journal of Manufacturing Science and Engineering* 127 (1) (2005) 68–74.
- [21] L. Yao, W. A. Sethares, D. C. Kammer, Sensor placement for on-orbit modal identification via a genetic algorithm, *AIAA Journal* 31 (1993) 1922–1928.

- [22] W. L. Poston, R. H. Tolson, Maximizing the determinant of the information matrix with the effective independence method, *Journal of Guidance, Control, and Dynamics* 15 (1992) 1513–1514.
- [23] K. B. Petersen, M. S. Pedersen, *The matrix cookbook*, Available via <http://matrixcookbook.com>. Accessed 30 May 2011 (2007).

Design of multi-station machining processes by integrating the SoV model and shop-floor data

Process design has been intensively studied to reduce dimensional variability of products produced in multi-station machining processes (MMPs). Most of the existing studies focus on predicting variation propagation and evaluating process robustness. However, these studies overlook the potential use of historical shop-floor quality data of existing MMPs in order to extract the actual manufacturing operation capabilities from each station, and then, to evaluate more accurately the expected dimensional variability of new candidate process plans. In this chapter a methodology to improve process plan selection is proposed based on three steps: i) based on historical shop-floor data from the stations of an existing MMP, the process capabilities of the stations to be used for the new product are inferred; ii) a sensitivity analysis of candidate process plans is carried out to identify critical fixtures and manufacturing stations/operations; and iii) an optimal selection of candidate process plans. A case study is presented to demonstrate the effectiveness of the methodology.

8.1 Introduction

Process planning is the systematic determination of the detailed methods by which parts can be manufactured from raw material to finished products [1]. Due to the possibility of multiple candidate machines, setups and processes for manufacturing the same product, it is critical to optimally select the process plan to multiple objectives, such as minimizing the number of setups, the number of processing operations, the number of cutting-tools, the machining time, the manufacturing cost, and the variability of product quality characteristics. Kusiak and Finke [2] studied the selection of process plans by minimizing the manufacturing cost and the number of tools and auxiliary devices. Noto La Diega *et al.* [3] presented a multi-objective approach which takes into account four group of requirements: competitive targets (manufacturing cost); technology requirements (equipment capabilities); production requirements (utilization of manufacturing resources); and market requirements (product quality). The decision to select the most appropriate process plan is conducted by maximizing a suitability function, which is based on the use

of fuzzy set theory to deal with the high level of vagueness and uncertainty in defining the requirements. Wei *et al.* [4] proposed the use of a throughput profit function for the selection of manufacturing process plans. This function integrates the measurements of production efficiency and manufacturing cost, and is defined as the total revenue from the parts that are produced during a production planning period minus the total associated manufacturing cost.

The satisfactory delivering of designated product quality is one of the most significant criteria in comparison of candidate process plans. Product quality is evaluated by dimensional and geometrical variations of a group of key product characteristics (KPCs). The acceptable level of KPC variations is specified by the GD&T specifications in the design drawing and should be controlled in multi-station machining processes (MMPs) with a variety of variation sources.

Research on process plan evaluation and selection for minimal product variability has been mainly conducted through engineering-driven methods, which are based on the Stream of Variation (SoV) models. Based on the SoV model, a variety of methodologies have been proposed for process plan evaluation in MMPs. Ding *et al.* [5] developed a group of hierarchical process-oriented sensitivity indices to evaluate the robustness of process plan candidates at three different levels: process level, station level and fixture level. Using and comparing this group of indices, the most robust process plan candidate to fixture-induced variations can be selected. Zhang *et al.* [6] presented similar sensitivity analyses based on the SoV model to assess how sensitive are the KPCs to certain fixture-induced variations in the manufacturing of an automotive cylinder head. However, these previous works were limited by the modeling capability, where only datum- and fixture-induced variations were included, assuming that machining-induced variations at machining stations were negligible. Furthermore, the sensitivity indices were applied to detect critical fixture components in a process plan candidate, but there is no systematic methodology to guide the process planner in redefining the process plan candidates. Liu *et al.* [7] developed a methodology to select the process plan that minimizes the cost related to process precision and satisfies the quality specifications. Their methodology was based on the SoV considering all potential setup sequences and datum schemes although the potential use of different machine-tools with different process capabilities at each station was omitted.

Process planning evaluation has also been conducted by process capability analysis. Since products possess multiple, rather than a single, quality characteristics, process capability analysis is based on a multivariate capability index. A variety of multivariate capability indices, such as those presented in [8–11], among others, have been proposed for assessing capability. The introduction of these indices can be found in [12, Chapter 16]. These indices were also implemented for MMP analysis using the SoV model. For instance, Wang and Ceglarek [13] presented a methodology to select the process plan that is less sensitive to part and tool variations in a multi-station assembly line using the multivariate process capability index defined in [8]. Ding *et al.* [14] evaluated the process capability of a multi-station assembly line by adopting the multivariate process capability ratio proposed in [9]. Frey *et al.* [15] proposed the estimation of the process capability

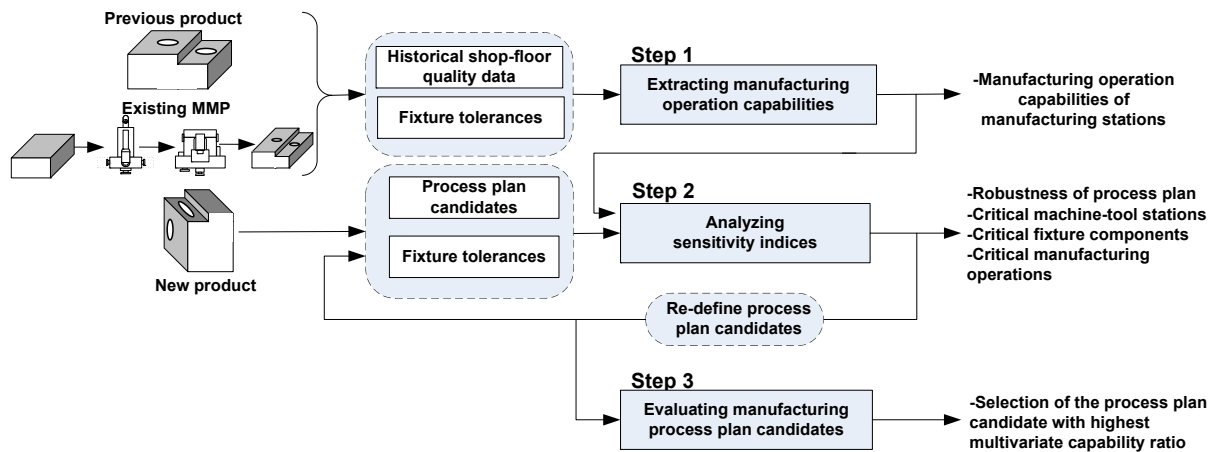


Figure 8.1: Three-step methodology proposed for process plan evaluation, adjustment and selection.

of manufacturing systems through a process capability matrix which is constructed by estimating the sensitivity of each quality characteristic to small changes in each variable related to manufacturing variation. However, despite of many proposed works including different multivariate process capability indices, industrial applications are limited [16]. This is because those process capability indices are obtained by considering only fixture-induced variations.

In practice, the process capability depends on all the manufacturing station capabilities which are the combination of the fixture capability, and the manufacturing operation capability, which depends on the machine-tool's capability to perform a specific manufacturing operation at specific manufacturing conditions (e.g., high cutting speeds, use of coolants, etc.). Overlooking the manufacturing operation capability, which is inversely related to the operation-induced variations, will make the estimation of the manufacturing station capability over-optimistic, and the process plan evaluation will be not realistic. Furthermore, manufacturing operation capability cannot be estimated through general specifications from machine-tool vendors, since it also depends on many other factors such as the type of manufacturing operation, components wear, thermal effects, deflections and cutting conditions. For instance, in Chapter 5 the machining-induced deviations were investigated on a vertical machining center with a position accuracy of $\pm 5 \mu m$. A $10^\circ C$ temperature increase caused the thermal expansion of the spindle and produced a $50 \mu m$ deviation on the machined surface, whereas in other experiments a $0.3 mm$ tool flank wear generated a $37 \mu m$ machined surface deviation. The impacts of these factors on process capability can often be estimated from historical shop-floor quality data. Thus, the combination of proper shop-floor quality data and the SoV model will provide a more reliable estimate of process capabilities.

In this chapter, we propose a systematic methodology, as shown in Figure 8.1, that integrates process plan evaluation, adjustment and selection through three steps. The first step deals with the extraction of the manufacturing capabilities from available shop-floor quality data from an existing MMP whose manufacturing stations are expected to be

used for manufacturing the new product. With the estimation of manufacturing capabilities and fixture-induced variations, candidate process plans of a new MMP can be analyzed through a sensitivity analysis at the second step. At this step, a flowchart is defined to guide the process planner in detecting critical components in each process plan candidate and to propose process plan modifications. The third step evaluates each process plan candidate through a process capability analysis according to part specifications. At this step, the process plan candidate with the largest capability ratio is selected as the optimal process plan candidate.

The rest of this chapter is organized as follows. In Section 8.2, the SoV model for process plan evaluation is briefly described. In Section 8.3, the methodology proposed for process plan evaluation, adjustment and selection is presented in detail. Finally, Section 8.4 presents a case study to demonstrate the applicability of the proposed methodology and Section 8.5 concludes the chapter.

8.2 SoV model for process planning evaluation

For the purpose of process plan evaluation, the following nomenclature is adopted in this chapter. Without loss of generality, consider a generic MMP related to a machining production line, with all the potential process plan candidates to manufacture a specific part as it is shown in Figure 8.2. For this generic case, the following variables are defined:

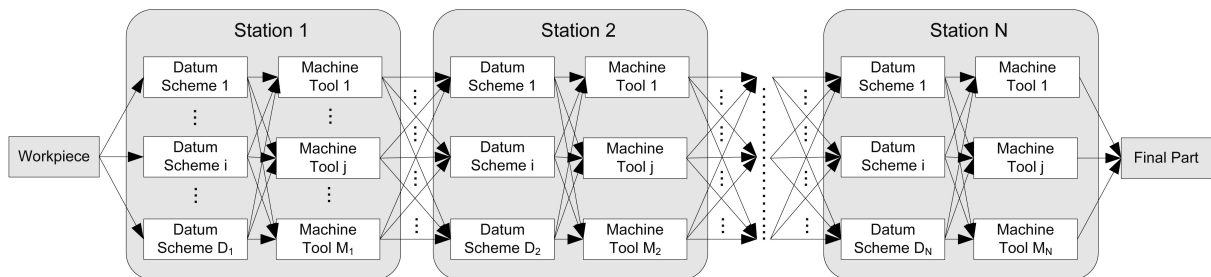


Figure 8.2: Generic MMP with all potential datum schemes and machine-tools to be applied at each station.

1. The datum scheme (DS) at station k ($k = 1, 2, \dots, N$) is denoted as DS d_k ($d_k = 1, 2, \dots, D_k$, where D_k is the total number of feasible datum scheme options for station k). A datum scheme refers to a specific fixture layout and group of datum surfaces, within which the machining process can be performed.
2. The machine-tool (MT) at station k ($k = 1, 2, \dots, N$) is denoted as MT m_k ($m_k = 1, 2, \dots, M_k$, where M_k is the total number of feasible machine-tools for station k). Note that for a specific manufacturing operation, different machine-tools can be applied, and their selection defines a specific manufacturing variability due to machining-induced variations. Furthermore, a specific machine-tool selection determines the use of other machine-tools in the subsequent manufacturing operations.

3. Corresponding to a selected DS, d_k , and a MT, m_k , at station k , the quality of all features are denoted by a state vector $\mathbf{x}_k^{d_k, m_k}$, with each element representing the dimensional deviation from its nominal value.
4. The random deviation of process variables at station k are denoted by $\mathbf{u}_k^{d_k}$ and $\mathbf{u}_k^{m_k}$. The term $\mathbf{u}_k^{d_k}$ refers to random deviations of fixture components associated with a selected datum scheme d_k , whereas the term $\mathbf{u}_k^{m_k}$ refers to random deviations of the cutting-tool path due to machining-induced variations associated with a selected machine-tool m_k and its cutting parameters. The elements in $\mathbf{u}_k^{d_k}$ and $\mathbf{u}_k^{m_k}$ are called process variables or KCCs and are treated as independent system input data that follow a multivariate normal distribution.
5. The un-modeled system noises at station k are represented by \mathbf{w}_k , and are assumed to be independent of any component of $\mathbf{u}_k^{d_k}$ and $\mathbf{u}_k^{m_k}$. Also, the elements of \mathbf{w}_k are assumed to be zero mean and independent of each other.
6. Since the features are measured in the coordinate system defined by the selected datum scheme d_k , the measurements of quality are denoted as $\mathbf{y}_k^{d_k}$. In this chapter, it is assumed that the measurements of product quality are conducted on-machine using the same datum scheme as the one used in the last machining operation. In case that another datum scheme was used, an additional station $k + 1$ would be defined and the measurements would be defined as $\mathbf{y}_{k+1}^{d_{k+1}}$. It is assumed that M features are inspected. Furthermore, the measurements are assumed to be multivariate normal.
7. The measurement noise is denoted by a random vector \mathbf{v}_k , which is independent of $\mathbf{x}_k^{d_k, m_k}$, $\mathbf{u}_k^{d_k}$, $\mathbf{u}_k^{m_k}$ and \mathbf{w}_k . The components of \mathbf{v}_k are assumed to be zero mean and independent of each other.

By adopting the assumptions of rigid parts and small errors, a linear state space model can be constructed to associate the part quality with a sequence of setups according to the process plan as follows:

$$\mathbf{x}_k^{d_k, m_k} = \mathbf{A}_k^{d_k} \cdot \mathbf{x}_{k-1}^{d_{k-1}, m_{k-1}} + \mathbf{B}_k^{d_k} \cdot \mathbf{u}_k^{d_k} + \mathbf{B}_k^{m_k} \cdot \mathbf{u}_k^{m_k} + \mathbf{w}_k, \quad (8.1)$$

$$\mathbf{y}_k^{d_k} = \mathbf{C}_k^{d_k} \cdot \mathbf{x}_k^{d_k, m_k} + \mathbf{v}_k, \quad k = 1, 2, \dots, N, \quad (8.2)$$

where $\mathbf{A}_k^{d_k} \cdot \mathbf{x}_{k-1}^{d_{k-1}, m_{k-1}}$, represents the deviations transmitted from upstream stations through the datum scheme d_k selected at station k ; $\mathbf{B}_k^{d_k} \cdot \mathbf{u}_k^{d_k}$ represents the deviations introduced within station k due to fixture-induced variations which are defined by the vector $\mathbf{u}_k^{d_k}$; $\mathbf{B}_k^{m_k} \cdot \mathbf{u}_k^{m_k}$ represents the deviations introduced within station k due to the machining-induced variations defined by the vector $\mathbf{u}_k^{m_k}$ such as geometric-thermal deviations, cutting force-induced deviations, etc.; $\mathbf{C}_k^{d_k} \cdot \mathbf{x}_k^{d_k, m_k}$ is the deviations of the KPCs measured at station k on the selected datum scheme; \mathbf{w}_k and \mathbf{v}_k are the system noise and measurement noise, respectively. These equations can be re-written in the input-output form in order to describe the relationship between the KPCs and the KCCs. The input-output equation is defined as:

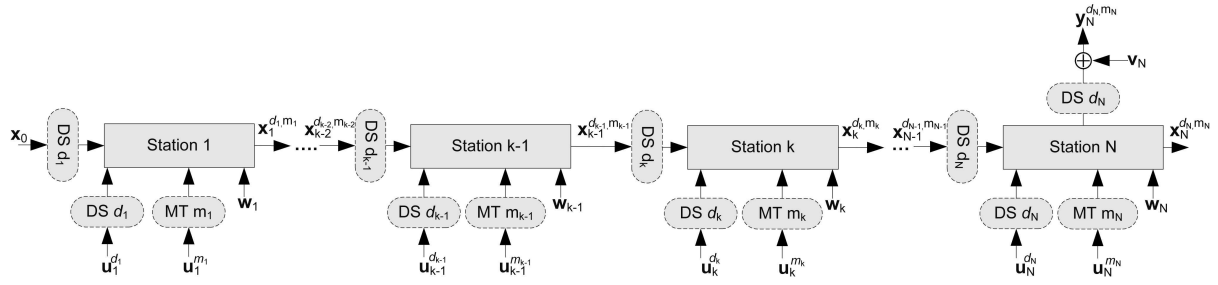


Figure 8.3: Representation of the MMP according to the SoV nomenclature.

$$\begin{aligned}
 \mathbf{y}_k^{d_k} &= \sum_{i=1}^k \mathbf{C}_k^{d_k} \cdot \Phi_{k,i}^{(\bullet)} \cdot \mathbf{B}_i^{d_i} \cdot \mathbf{u}_i^{d_i} + \sum_{i=1}^k \mathbf{C}_k^{d_k} \cdot \Phi_{k,i}^{(\bullet)} \cdot \mathbf{B}_i^{m_i} \mathbf{u}_i^{m_i} + \mathbf{C}_k^{d_k} \cdot \Phi_{k,0}^{(\bullet)} \cdot \mathbf{x}_0 \\
 &+ \sum_{i=1}^k \mathbf{C}_k^{d_k} \cdot \Phi_{k,i}^{(\bullet)} \cdot \mathbf{w}_i + \mathbf{v}_k,
 \end{aligned} \tag{8.3}$$

where $\Phi_{k,i}^{(\bullet)}$ is the state transition matrix tracing the datum schemes transformation from station i to k ; $\Phi_{k,i}^{(\bullet)} = \mathbf{A}_k^{d_k} \cdot \mathbf{A}_{k-1}^{d_{k-1}} \dots \mathbf{A}_i^{d_i}$ for $i < k$, and $\Phi_{k,k}^{(\bullet)} = \mathbf{I}$. The initial state vector \mathbf{x}_0 represents the original deviations of the features on a part that enters the first station of the process. These original deviations are generated by previous manufacturing processes (i.e. bulk forming processes). For a selected datum scheme, d_k , and the decisions on datum schemes for upstream stations $\{d_1, d_2, \dots, d_{k-1}\}$, the coefficient matrices, $\mathbf{A}_k^{d_k}$, $\mathbf{B}_k^{d_k}$, $\mathbf{C}_k^{d_k}$, and $\Phi_{k,i}^{(\bullet)}$ ($i = 1, 2, \dots, k$), can be derived following the procedure presented in Chapter 4, Appendix 4.3. In this chapter, the vector $\mathbf{u}_k^{m_k}$ will only be referred as a generic cutting-tool path deviation in the machine-tool m_k selected at station k , and it will be defined as $\mathbf{u}_k^{m_k} = [\delta_x^{m_k}, \delta_y^{m_k}, \delta_z^{m_k}, \delta_\alpha^{m_k}, \delta_\beta^{m_k}, \delta_\gamma^{m_k}]^T$, denoting the deviations of the cutting-tool at the three translational degrees of freedom (d.o.f) (x, y, z) and three rotational d.o.f (α, β, γ). On the other hand, matrix $\mathbf{B}_k^{m_k}$ will be defined as the machined feature selector matrix described in Chapter 4, Appendix 4.3.

Without loss of generality, let us consider that the KPCs are measured at the end of the production line, in the station N , as shown in Figure 8.3. Thus, Eq. (8.3) can be re-written in a vector form as:

$$\mathbf{Y}_N = \Gamma_N^f \cdot \mathbf{U}_N^f + \Gamma_N^m \cdot \mathbf{U}_N^m + \Gamma_N^w \cdot \mathbf{W}_N + \mathbf{v}_N, \tag{8.4}$$

where

$$\Gamma_N^f = [[\mathbf{C}_N^{d_N} \cdot \Phi_{N,1}^{(\bullet)} \cdot \mathbf{B}_1^{d_1}] \quad [\mathbf{C}_N^{d_N} \cdot \Phi_{N,2}^{(\bullet)} \cdot \mathbf{B}_2^{d_2}] \quad \dots \quad [\mathbf{C}_N^{d_N} \cdot \Phi_{N,N}^{(\bullet)} \cdot \mathbf{B}_N^{d_N}]], \tag{8.5}$$

$$\Gamma_N^m = [[\mathbf{C}_N^{d_N} \cdot \Phi_{N,1}^{(\bullet)} \cdot \mathbf{B}_1^{m_1}] \quad [\mathbf{C}_N^{d_N} \cdot \Phi_{N,2}^{(\bullet)} \cdot \mathbf{B}_2^{m_2}] \quad \dots \quad [\mathbf{C}_N^{d_N} \cdot \Phi_{N,N}^{(\bullet)} \cdot \mathbf{B}_N^{m_N}]], \tag{8.6}$$

$$\Gamma_N^w = [[\mathbf{C}_N^{d_N} \cdot \Phi_{N,1}^{(\bullet)}] \quad [\mathbf{C}_N^{d_N} \cdot \Phi_{N,2}^{(\bullet)}] \quad \dots \quad [\mathbf{C}_N^{d_N} \cdot \Phi_{N,N}^{(\bullet)}]], \tag{8.7}$$

and $\mathbf{U}_N^f = [(\mathbf{u}_1^{d_1})^T, \dots, (\mathbf{u}_N^{d_N})^T]^T$, $\mathbf{U}_N^m = [(\mathbf{u}_1^{m_1})^T, \dots, (\mathbf{u}_N^{m_N})^T]^T$, $\mathbf{Y}_N = \mathbf{y}_N^{d_N}$, $\mathbf{W}_N = [(\mathbf{w}_1)^T, \dots, (\mathbf{w}_N)^T]^T$.

Eq. (8.4) can be used by the process planner to predict the part quality variability of a process plan candidate according to the specific datum schemes and machine-tools applied and their respective fixture and machining-induced variations. Assuming that \mathbf{U}_N^f , \mathbf{U}_N^m , \mathbf{W}_N and \mathbf{v}_N are independent of each other, Eq. (8.4) can be analyzed in terms of covariances as

$$\Sigma_{\mathbf{Y}_N} = \Gamma_N^f \cdot \Sigma_{\mathbf{U}_N^f} \cdot (\Gamma_N^f)^T + \Gamma_N^m \cdot \Sigma_{\mathbf{U}_N^m} \cdot (\Gamma_N^m)^T + \Gamma_N^w \cdot \Sigma_{\mathbf{W}_N} \cdot (\Gamma_N^w)^T + \Sigma_{\mathbf{v}_N}, \quad (8.8)$$

where $\Sigma_{\mathbf{Y}_k}$ is the covariance matrix of the KPCs, $\Sigma_{\mathbf{U}_k^f}$ is the covariance matrix of the fixture-induced variations; $\Sigma_{\mathbf{U}_k^m}$ is the covariance matrix of machining-induced variations; $\Sigma_{\mathbf{W}_k}$ is the covariance matrix of un-modeled source of variations; and $\Sigma_{\mathbf{v}_k}$ is the covariance matrix of measurement noise. Note that it is assumed that there is no mean-shift in any source of variation, since at process planning stage, process planners are more focused on the variation propagation.

8.3 Methodology

The methodology proposed in this chapter combines a SoV model for modeling both fixture- and machining-induced variations with historical shop-floor quality data from existing MMPs in order to evaluate, adjust and select the best process plan from a group of process plan candidates. The methodology, summarized in Figure 8.1, is composed of the following steps:

- *Step 1: extracting manufacturing operation capabilities from historical shop-floor quality data:* manufacturing operation capability can be derived from machine-tool specifications, such as precision, or position repeatability at each axis. However, these specifications provided by vendors do not consider the real manufacturing operation in which thermal effects, components' wear or deflections may deteriorate manufacturing operation capability. The use of historical data can lead to a more accurate estimation of the manufacturing operation capability.
- *Step 2: sensitivity analysis for adjusting process plan candidates:* the different process plan candidates are analyzed through a sensitivity analysis considering the expected fixture-induced variations from maintenance data (note that a calibration action is required when the fixture presents an excessive deviation from its nominal due to wear, deformations, etc.) and the expected machining-induced variations extracted in step 1. The information obtained from the sensitivity analysis can help the process planner to introduce changes to each process plan candidate in order to minimize its sensitivity indices and increase its robustness to fixture- or machining-induced variations.
- *Step 3: process plan evaluation and selection:* each process plan candidate will be evaluated with a multivariate capability ratio MC_p^χ , which represents the capability of the manufacturing process plan candidate χ to manufacture the part within specifications.

8.3.1 Extracting manufacturing capabilities from historical shop-floor quality data

Let us consider a new MMP using existing machining stations. Consider a part with M KPCs manufactured in that MMP with N stations and a fixture layout at each station based on the common 3-2-1 locating principle applied in machining processes [17]. The term $\Sigma_{\mathbf{U}_N^m}$ in Eq. (8.8) defines the machining-induced variations of the manufacturing stations and indirectly, their manufacturing operation capabilities. In order to extract their capabilities, Eq. (8.8) can be simplified by removing the term $\Gamma_N^w \cdot \Sigma_{\mathbf{W}_N^f} \cdot (\Gamma_N^w)^T$, since it contains second or higher order terms whose contribution to product variability is much smaller than that of fixture-induced and machining-induced variations. Thus, manufacturing operation capabilities can be extracted from Eq. (8.8) defining the matrices Γ_N^f , Γ_N^m , $\Sigma_{\mathbf{U}_N^f}$, $\Sigma_{\mathbf{Y}_N}$, and $\Sigma_{\mathbf{v}_N}$. Matrices Γ_N^f and Γ_N^m are defined through process plan and product knowledge from the MMP, as it is shown in Chapter 4. Matrix $\Sigma_{\mathbf{v}_N}$ can be assumed negligible compared to product variability. Otherwise, process planner can define this covariance matrix by estimating the measuring errors according to the calibration of the measuring instruments. The matrix $\Sigma_{\mathbf{U}_N^f}$, which refers to the variance of the fixture locators, can be obtained from previous production and maintenance data. In this chapter, it is assumed that the variances of fixture locators are known from historical fixture maintenance data. Specifically, it is assumed that the deviations of fixture locators are randomly distributed and independent of each other, and the fixtures placed in different stations are also assumed to be independent of each other. Under these assumptions, $\Sigma_{\mathbf{U}_N^f} = \text{diag}\{\Sigma_{\mathbf{u}_{f1}}, \Sigma_{\mathbf{u}_{f2}}, \dots, \Sigma_{\mathbf{u}_{fN}}\}_{6N \times 6N}$, where $\Sigma_{\mathbf{u}_{fk}} = \text{diag}\{\sigma_{l_1}^2, \sigma_{l_2}^2, \dots, \sigma_{l_6}^2\}$ for $k = 1, \dots, N$. The terms $\sigma_{l_j}^2$, $j = 1, \dots, 6$, are the variance of each fixture locator at a specific machining station and they can be determined as $\sigma_{l_j} = T_j/6$. T_j is the tolerance assigned to the j th fixture locator and it is assumed to be known. The covariance matrix of the KPCs, $\Sigma_{\mathbf{Y}_N}$, can be estimated from the historical shop-floor product quality data.

After defining the matrices, the manufacturing operation capability matrix $\Sigma_{\mathbf{U}_N^m}$ of each machining station can be estimated vectorizing the matrices from Eq. (8.8). Thus, the manufacturing operation capability can be obtained by solving the equation:

$$\text{vec}(\Sigma_{\mathbf{U}_N^m}) = (\Gamma_N^m \otimes \Gamma_N^m)^{-1} \cdot \text{vec}(\Sigma_{\mathbf{Y}_N} - \Gamma_N^f \cdot \Sigma_{\mathbf{U}_N^f} \cdot (\Gamma_N^f)^T - \Sigma_{\mathbf{v}_N}), \quad (8.9)$$

where $\text{vec}(\bullet)$ denotes the vectorisation of the matrix \bullet formed by stacking the columns of \bullet into a single vector, and \otimes is the Kronecker product operator. Note that the dimensions of matrices $\text{vec}(\Sigma_{\mathbf{U}_N^m})$, Γ_N^m , $\Sigma_{\mathbf{Y}_N}$, Γ_N^f , $\Sigma_{\mathbf{U}_N^f}$ and $\Sigma_{\mathbf{v}_N}$ are $36N^2 \times 1$, $6M \times 6N$, $6M \times 6M$, $6M \times 6N$, $6N \times 6N$ and $6N \times 6N$, respectively. It is important to remark that Eq. (8.9) estimates the covariance matrix $\Sigma_{\mathbf{U}_N^m}$ with the covariance matrices $\Sigma_{\mathbf{Y}_N}$ and $\Sigma_{\mathbf{U}_N^f}$, which are estimated from historical shop-floor data and maintenance data, respectively. In order to ensure that the resulting $\Sigma_{\mathbf{U}_N^m}$ is a positive definite matrix, the following assumptions should be verified in practice: i) the sample size of the historical shop-floor quality data set is larger than the number of quality variables and process variables; ii) the shop-floor quality data set is collected from a statistically in-control process and thus is well-conditioned and contains no outliers or missing data; iii) the magnitude of measurement error is significantly smaller than the magnitudes of the potential variations of

the KPCs induced by the fixtures and/or machining operations; and iv) in estimating the fixture locator tolerance, the magnitude of estimation error is significantly smaller than that of fixture locator variability. As a result, the variances of KPCs contributed by such estimation errors are significantly smaller than that induced by the machining operations. In practice of new design of an existing MMP, these assumptions can be reasonably made. If these assumptions do not hold for some special cases, the positive definitiveness of $\Sigma_{\mathbf{U}_N^m}$ can still be ensured by applying smoothing techniques [18].

According to Eq. (8.9), the problem of extracting the manufacturing operation capability can be classified into three cases:

- Case 1: when the number of KPCs and that of the stations are the same ($6N = 6M$), Γ_N^m is a square matrix. If it is full-rank, Eq. (8.9) has a unique solution. This is common when one feature is machined at each station without removing any of the previous machined features, and at the end of the process, all the machined features are inspected. Otherwise, if Γ_N^m is not column wise full rank, it is necessary to investigate the interrelationships among elements in \mathbf{U}_N^m , remove the dependent machining-induced deviations, and solve the problem applying the method for Case 2. If Γ_N^m is not row wise full rank, the measurement plan should be re-examined by introducing more independent KPC measurements, as introduced in Case 3.
- Case 2: when there are more KPCs than potential machining-induced deviations ($6N < 6M$), Γ_N^m is not square and its rank is lower than $6M$. Thus, there are more equations than unknown variables. For this case, if the column wise rank of Γ_N^m is $6N$, Eq. (8.9) is modified to extract manufacturing capabilities by the minimum least squares algorithm. This solution would be obtained by solving the following equation:

$$vec(\Sigma_{\mathbf{U}_N^m}) = (\mathbb{B}^T \cdot \mathbb{B})^{-1} \cdot \mathbb{B}^T \cdot vec(\Sigma_{\mathbf{Y}_N} - \Gamma_N^f \cdot \Sigma_{\mathbf{U}_N^f} \cdot (\Gamma_N^f)^T - \Sigma_{\mathbf{v}_N}), \quad (8.10)$$

where $\mathbb{B} = \Gamma_N^m \otimes \Gamma_N^m$. In case that the column wise rank of Γ_N^m is $6S$, where $S < N$, then the same equation applies but not all the manufacturing operation capabilities can be extracted since there are $N - S$ stations that do not influence on the KPC variability.

- Case 3: when there are less KPCs than potential machining-induced deviations ($6N > 6M$), Γ_N^m is not square. It means that there is not enough information from the KPCs variability to extract all manufacturing operation capabilities. Thus, it is necessary to introduce more product quality data to infer the manufacturing operation capability of all machining stations.

8.3.2 Sensitivity analysis for adjusting process plan candidates

The sensitivity analysis is employed to assess the impact of each source of variation on part quality during the design phase. It is used as a decision making support tool for re-defining datum schemes and improving the proposed process plan candidates. This analysis depends on both fixture and manufacturing operation capabilities that are estimated in step 1.

The analysis follows the flowchart shown in Figure 8.4 to detect the critical sources of variations that impact the KPCs. This three-phase process is based on the analysis of different sensitivity indices at different levels which are defined in the following subsections. At phase I, fixture sensitivity indices, $S_{f,process}^Y$, and operation sensitivity indices, $S_{m,process}^Y$, are evaluated to determine the main source of variation (fixture- or machining-induced) in the candidate process plan.

At phase II, additional sensitivity indices of individual KPCs will be compared with the average sensitivity index scaled by a factor C_b to identify the critical KPCs. Finally, at phase III, the identified critical KPC will be further analyzed to identify the critical station and the critical KCCs to obtain that KPC. This information can lead the process planner to re-define the process plan candidate and increase its robustness.

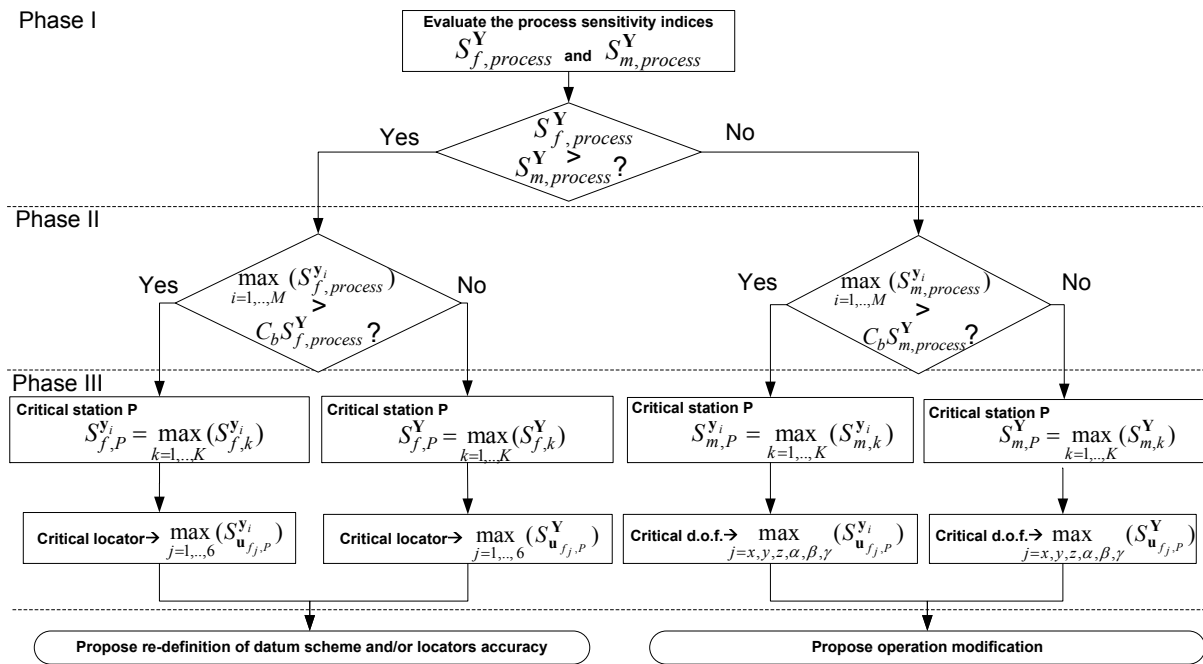


Figure 8.4: Flowchart for process plan adjustment through sensitivity analysis.

The different sensitivity indices applied in the proposed flowchart are extensions of widely accepted indices. Basically, a sensitivity index of a generic variable H with respect to a generic parameter ϱ can be described by the differential equation

$$S_{\varrho}^H = \frac{\delta H}{\delta \varrho} \frac{\Delta \varrho}{\Delta H}, \quad (8.11)$$

where ΔH and $\Delta \varrho$ denote the admissible deviation of variable H and the nominal deviation of parameter ϱ , respectively. For a MMP process design problem, the admissible deviation of a variable H is related to a KPC and it can be defined by its tolerance from the design drawing, denoted by H^{tol} . The nominal deviation of a generic parameter ϱ is related to fixture- or machining-induced variations, and it can be defined by its expected range of variation denoted by ϱ^{tol} and defined as $6\sigma_{\varrho}$ (99.73% of confidence level), where

σ_ρ is the standard deviation of this source of variation. Thus, the sensitivity analysis is re-written as

$$S_\rho^H = \frac{\delta H}{\delta \rho} \frac{\rho^{tol}}{H^{tol}}. \quad (8.12)$$

Let us consider the design of a new MMP composed of N stations, each of which is equipped with a 3-2-1 fixture device. Each locator of a fixture is denoted by the index j ($j = 1, \dots, 6$). Consider that this MMP will be used to manufacture a product composed of M KPCs, and each KPC is denoted by the index i ($i = 1, \dots, M$). According to Eq. (8.12), a series of sensitivity indices can be defined as shown in the following subsections. Additionally, a summary of these indices and their respective meaning is shown in Table 8.1.

Fixture sensitivity index

Locator sensitivity index: this type of index evaluates the impact of the variability of each fixture locator in the station k . Two indices can be distinguished: that with respect to (w.r.t.) an individual KPC, as defined in Eq. (8.13), and that w.r.t. a product, as defined in Eq. (8.14).

$$S_{\mathbf{u}_{f_j,k}}^{\mathbf{y}_i} = \text{abs} \left(\frac{\delta \mathbf{y}_i}{\delta \mathbf{u}_{f_j,k}} \frac{\mathbf{u}_{f_j,k}^{tol}}{\mathbf{y}_i^{tol}} \right) = \text{abs} \left(\Gamma_{i,j}^f \frac{\mathbf{u}_{f_j,k}^{tol}}{\mathbf{y}_i^{tol}} \right), \quad (8.13)$$

$$S_{\mathbf{u}_{f_j,k}}^{\mathbf{Y}} = \frac{1}{M} \sum_{i=1}^M S_{\mathbf{u}_{f_j,k}}^{\mathbf{y}_i}, \quad (8.14)$$

where $\text{abs}(A)$ denotes the absolute value of A ; $\Gamma_{i,j}^f$ denotes the element at the i th row and the j th column of the matrix Γ_N^f ; \mathbf{y}_i^{tol} is the product dimensional tolerance of the KPC \mathbf{y}_i ; $\mathbf{u}_{f_j,k}^{tol}$ is the tolerance of the j th fixture locator component in the station k . This sensitivity index is defined according to Eq. 8.12 by substituting H , ρ , H^{tol} and ρ^{tol} with \mathbf{y}_i , $\mathbf{u}_{f_j,k}$, \mathbf{y}_i^{tol} , and $\mathbf{u}_{f_j,k}^{tol}$, respectively. $S_{\mathbf{u}_{f_j,k}}^{\mathbf{y}_i}$ refers to the impact of the variability of the j th locator in the station k on the i th KPC, whereas $S_{\mathbf{u}_{f_j,k}}^{\mathbf{Y}}$ refers to the impact on the average of all KPCs.

Fixture sensitivity index: this type of indices evaluates the impact of the fixture-induced variations in a specific datum scheme at station k . Fixture sensitivity index w.r.t. a KPC ($S_{f,k}^{\mathbf{y}_i}$) and w.r.t. the product ($S_{f,k}^{\mathbf{Y}}$) are defined, respectively, as:

$$S_{f,k}^{\mathbf{y}_i} = \frac{1}{6} \sum_{j=1}^6 S_{\mathbf{u}_{f_j,k}}^{\mathbf{y}_i}, \quad (8.15)$$

$$S_{f,k}^{\mathbf{Y}} = \frac{1}{M} \sum_{i=1}^M S_{f,k}^{\mathbf{y}_i}. \quad (8.16)$$

Sensitivity index of manufacturing operation

Dof Sensitivity index: this type of index evaluates the impact of the variability of a specific d.o.f when conducting a specific machining operation at station k due to machining-induced variations. Two indices are defined w.r.t. a KPC ($S_{\mathbf{u}_{m_j,k}}^{\mathbf{y}_i}$) and w.r.t. the product ($S_{\mathbf{u}_{m_j,k}}^{\mathbf{Y}}$), respectively, as:

$$S_{\mathbf{u}_{m_j,k}}^{\mathbf{y}_i} = \text{abs} \left(\frac{\delta \mathbf{y}_i}{\delta \mathbf{u}_{m_j,k}} \frac{\mathbf{u}_{m_j,k}^{\text{tol}}}{\mathbf{y}_i^{\text{tol}}} \right) = \text{abs} \left(\Gamma_{i,j}^m \frac{\mathbf{u}_{m_j,k}^{\text{tol}}}{\mathbf{y}_i^{\text{tol}}} \right), \quad (8.17)$$

$$S_{\mathbf{u}_{m_j,k}}^{\mathbf{Y}} = \frac{1}{M} \sum_{i=1}^M S_{\mathbf{u}_{m_j,k}}^{\mathbf{y}_i}, \quad (8.18)$$

where $\Gamma_{i,j}^m$ denotes the element in the i th row and j th column of the matrix Γ_N^m ; $\mathbf{u}_{m_j,k}^{\text{tol}}$ defines the machining-induced variations of the j th d.o.f at the k th station and the index $j = 1, \dots, 6$, is referred to the six d.o.f of the machine-tool related to the translations X , Y , Z and rotations α , β , γ , respectively. Note that these machining-induced variations are subjected to a specific machining operation at specific cutting conditions and it is related to the manufacturing operation capability $\Sigma_{\mathbf{U}_{N'}^m}$ extracted from step 1, where N' is the number of stations in the existing MMP. Assuming that the q th machining station in an existing MMP is being used in the new process planning for the new MMP as the k th manufacturing station, the expected machining-induced variations of the j th d.o.f at the k th station is defined by the expression

$$\mathbf{u}_{m_j,k}^{\text{tol}} = 6 \cdot \sqrt{\Sigma_{\mathbf{u}_{q'}^{m_{q'}}}(j, j)}, \quad (8.19)$$

where

$$\Sigma_{\mathbf{U}_{N'}^m} = \text{diag}\{\Sigma_{\mathbf{u}_{1'}^{m_{1'}}}, \dots, \Sigma_{\mathbf{u}_{q'}^{m_{q'}}}, \dots, \Sigma_{\mathbf{u}_{N'}^{m_{N'}}}\}, \quad (8.20)$$

and the term $\Sigma_{\mathbf{u}_{q'}^{m_{q'}}}(j, j)$ refers to the (j, j) element of the covariance matrix. Note that the type of operation and cutting conditions from the existing MMP should be similar to those to be conducted in the new MMP. For example, similar cutting speeds, cutting-tools and coolants.

Manufacturing operation sensitivity index: this type of index evaluates the impact of the variability of a specific manufacturing operation with specific conditions at station k . Two indices are defined w.r.t. a KPC ($S_{m,k}^{\mathbf{y}_i}$) and w.r.t. the product ($S_{m,k}^{\mathbf{Y}}$), respectively, as:

$$S_{m,k}^{\mathbf{y}_i} = \frac{1}{6} \sum_{j=1}^6 S_{\mathbf{u}_{m_j,k}}^{\mathbf{y}_i}, \quad (8.21)$$

$$S_{m,k}^{\mathbf{Y}} = \frac{1}{M} \sum_{i=1}^M S_{m,k}^{\mathbf{y}_i}. \quad (8.22)$$

Station sensitivity index

Station sensitivity index: this type of index evaluates the impact of the variability of the datum scheme and the manufacturing operation at station k . Two indices are defined w.r.t. a KPC ($S_{\mathbf{u}_k}^{\mathbf{y}_i}$) and w.r.t. the product ($S_{\mathbf{u}_k}^{\mathbf{Y}}$), respectively, as:

$$S_{\mathbf{u}_k}^{\mathbf{y}_i} = \frac{S_{f,k}^{\mathbf{y}_i} + S_{m,k}^{\mathbf{y}_i}}{2}, \quad (8.23)$$

$$S_{\mathbf{u}_k}^{\mathbf{Y}} = \frac{S_{f,k}^{\mathbf{Y}} + S_{m,k}^{\mathbf{Y}}}{2}. \quad (8.24)$$

Process sensitivity indices

Process sensitivity index considering fixture-induced variations: this type of index evaluates the impact of fixture-induced variations along a MMP. Two indices are defined w.r.t. a KPC ($S_{f,process}^{\mathbf{y}_i}$) and w.r.t. the product ($S_{f,process}^{\mathbf{Y}}$), respectively, as

$$S_{f,process}^{\mathbf{y}_i} = \frac{1}{K} \sum_{k=1}^K S_{f,k}^{\mathbf{y}_i}, \quad (8.25)$$

$$S_{f,process}^{\mathbf{Y}} = \frac{1}{M} \sum_{i=1}^M S_{f,process}^{\mathbf{y}_i}. \quad (8.26)$$

Process sensitivity index considering machining-induced variations: this type of index evaluates the impact of machining-induced variations along a MMP. Two indices are defined w.r.t. a KPC ($S_{m,process}^{\mathbf{y}_i}$) and w.r.t. the product ($S_{m,process}^{\mathbf{Y}}$), respectively, as:

$$S_{m,process}^{\mathbf{y}_i} = \frac{1}{K} \sum_{k=1}^K S_{m,k}^{\mathbf{y}_i}, \quad (8.27)$$

$$S_{m,process}^{\mathbf{Y}} = \frac{1}{M} \sum_{i=1}^M S_{m,process}^{\mathbf{y}_i}. \quad (8.28)$$

Global process sensitivity index: this type of index evaluates the impact of both fixture- and machining-induced variations along a MMP. Two indices are defined w.r.t. a KPC ($S_{process}^{\mathbf{y}_i}$) and w.r.t. the product ($S_{process}^{\mathbf{Y}}$), respectively, as:

$$S_{process}^{\mathbf{y}_i} = \frac{S_{f,process}^{\mathbf{y}_i} + S_{m,process}^{\mathbf{y}_i}}{2}, \quad (8.29)$$

$$S_{process}^{\mathbf{Y}} = \frac{S_{f,process}^{\mathbf{Y}} + S_{m,process}^{\mathbf{Y}}}{2}. \quad (8.30)$$

Note that in the flowchart shown in Figure 8.4, the indices $S_{\mathbf{u}_k}^{\mathbf{y}_i}$, $S_{process}^{\mathbf{y}_i}$ and their corresponding indices w.r.t. product are not evaluated since the purpose of the sensitivity analysis is to analyze separately the variability of each process plan due to fixture- and machining-induced variations in order to propose process plan adjustments.

Table 8.1: Summary of the sensitivity indices and physical meaning.

| Sensitivity index | KPC | Product | Rationale for definition |
|---|---|---------------------------------------|---|
| Locator index | $S_{\mathbf{u}_{f_j,k}}^{\mathbf{Y}_i}$ | $S_{\mathbf{u}_{f_j,k}}^{\mathbf{Y}}$ | Identifies the most important locator on KPC/product variability |
| Fixture index | $S_{\mathbf{u}_f,k}^{\mathbf{Y}_i}$ | $S_{\mathbf{u}_f,k}^{\mathbf{Y}}$ | Identifies the most important fixture on KPC/product variability |
| Dof index | $S_{\mathbf{u}_{m_j,k}}^{\mathbf{Y}_i}$ | $S_{\mathbf{u}_{m_j,k}}^{\mathbf{Y}}$ | Identifies the most important d.o.f on KPC/product variability |
| Manufact. index | $S_{\mathbf{m},k}^{\mathbf{Y}_i}$ | $S_{\mathbf{m},k}^{\mathbf{Y}}$ | Identifies the most important operation on KPC/product variability |
| Station index | $S_{\mathbf{u}_k}^{\mathbf{Y}_i}$ | $S_{\mathbf{u}_k}^{\mathbf{Y}}$ | Identifies the most important station on KPC/product variability |
| Process index due to fixture deviations | $S_{f,process}^{\mathbf{Y}_i}$ | $S_{f,process}^{\mathbf{Y}}$ | Evaluates the influence of the whole manufact. process on KPC/product variability considering only fixture-induced variations |
| Process index due to operation deviations | $S_{m,process}^{\mathbf{Y}_i}$ | $S_{m,process}^{\mathbf{Y}}$ | Evaluates the influence of the whole manufact. process on KPC/product variability considering only machining-induced variations |
| Global process index | $S_{process}^{\mathbf{Y}_i}$ | $S_{process}^{\mathbf{Y}}$ | Evaluates the influence of the whole process on KPC/product variability |

8.3.3 Process plan evaluation and selection

A widely used process capability index for a single KPC in industry is defined as $C_p = (USL - LSL)/6\sigma$, where USL and LSL are the upper and lower specification limits of a quality characteristic, respectively; and σ is its standard deviation. However, in MMPs, there are always multiple KPCs, and the use of advanced capability indices is a challenging issue to estimate the process capability [16].

In this chapter, the multivariate process capability ratio proposed by Chen [9] is adopted for evaluating the manufacturing capability of each process plan candidate. The use of this ratio is justified by its successful implementation by previous authors [19, Chapter 13] in similar multi-station processes with the use of the SoV methodology. Focusing only on the variations in the KPC measurements, \mathbf{Y}_N , the multivariate process capability index for a process plan candidate χ can be expressed as

$$MC_p^{\chi}(N) = \frac{1}{r_0}, \quad (8.31)$$

where r_0 is a value that has the probability, $Pr(\max(|\mathbf{Y}_{i,N}^c|/r_{i,N}, i = 1, \dots, M) \leq r_0)$, equal to $1 - \alpha$, and α is the allowable expected proportion of non-conforming products from the process. $\mathbf{Y}_{i,N}^c$ is the c th component of the i th KPC measured at station N , and $r_{i,N}$ is the tolerance value for this component. The r_0 value can be obtained by Monte Carlo simulations of Eq. (8.4), where the fixture-induced variations (\mathbf{U}_N^f) are assumed normally distributed with the standard deviations defined from the fixture tolerances and the machining-induced variations (\mathbf{U}_N^m) are assumed normally distributed with the standard deviations estimated from step 1. The un-modeled errors (\mathbf{W}_N) and the measurement errors (\mathbf{v}_N) are set according to process planner's knowledge about the process and measurement devices.

Through this formulation, an index value of $MC_p^{\chi}(N) = 1.0$ corresponds to an expected proportion of conforming product of exactly $1 - \alpha$. A larger $MC_p^{\chi}(N)$ indicates a lower expected proportion of non-conforming products or a more capable process plan. Therefore, these interpretations enable the MC_p^{χ} ratio to have a similar meaning to the univariate ratio C_p [19].

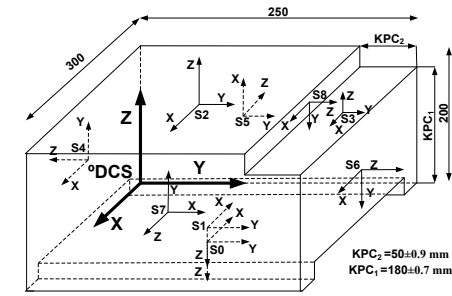
8.4 Case study

8.4.1 Problem description

To demonstrate the effectiveness of the proposed methodology, a case study is conducted for planning a MMP that manufactures the part shown in Table 8.2. The engineer proposes three candidate process plans, each of which consists of four machining stations, as illustrated in Figure 8.5. The third candidate plan has the same datum scheme as that of the second candidate plan, but the machine-tool used at station 3 is $M4$ whereas that at station 4 is $M3$. For the sake of simplicity, the 3-2-1 fixture layout at each station are kept the same for all candidate process plans. Only the datum features and the features to be machined at the last two machining stations vary among different candidate plans. The location of locators that compose the fixtures at machining stations are defined in Table 8.3 and their admissible deviations are assumed to be normally distributed with variance $\sigma_{l_j}^2 = (0.017)^2 \text{ mm}^2$, where $j = 1, \dots, 6$. The KPCs to be measured are the distance between the features S_3 and S_0 , denoted as KPC_1 , and the normal distance between S_8 and S_6 , denoted as KPC_2 . The dimensional tolerance requirement for KPC_1 and KPC_2 are $\pm 0.7 \text{ mm}$ and $\pm 0.9 \text{ mm}$, respectively.

Table 8.2: Nominal location ($\mathbf{t}_{S_i}^{\circ D}$) and orientation ($\varphi_{S_i}^{\circ D}$) of each feature.

| Feature | $\varphi_{S_i}^{\circ D}$ (rad) | $\mathbf{t}_{S_i}^{\circ D}$ (mm) |
|---------|---------------------------------|-----------------------------------|
| S_0 | $[0, \pi, 0]$ | $[150, 125, 0]$ |
| S_1 | $[0, \pi, 0]$ | $[150, 125, 20]$ |
| S_2 | $[0, 0, 0]$ | $[150, 75, 200]$ |
| S_3 | $[0, 0, 0]$ | $[150, 225, 180]$ |
| S_4 | $[\pi/2, -\pi/2, -\pi/2]$ | $[150, 0, 100]$ |
| S_5 | $[0, -\pi/2, 0]$ | $[0, 75, 100]$ |
| S_6 | $[\pi/2, \pi/2, -\pi/2]$ | $[150, 250, 75]$ |
| S_7 | $[0, \pi/2, \pi/2]$ | $[300, 125, 100]$ |
| S_8 | $[\pi/2, \pi/2, -\pi/2]$ | $[150, 200, 190]$ |



It is assumed that an existing MMP with four machine-tools M_1, \dots, M_4 are used to carry out machining operations as described in Figure 8.6 and the information about the machined part and the fixture layout applied at each station are shown in Tables 8.4 and 8.5, respectively. The next subsections will present the methodology proposed in this chapter step by step.

8.4.2 Step 1: Estimation of manufacturing operation capabilities

In order to extract manufacturing operation capabilities from the existing MMP, a set of product-quality data needs to be sampled from the shop-floor. For illustrative purposes, the data-set was generated from the SoV model that is defined according to the process and product data in Tables 8.4 and Table 8.5. In practice, such data will be provided by

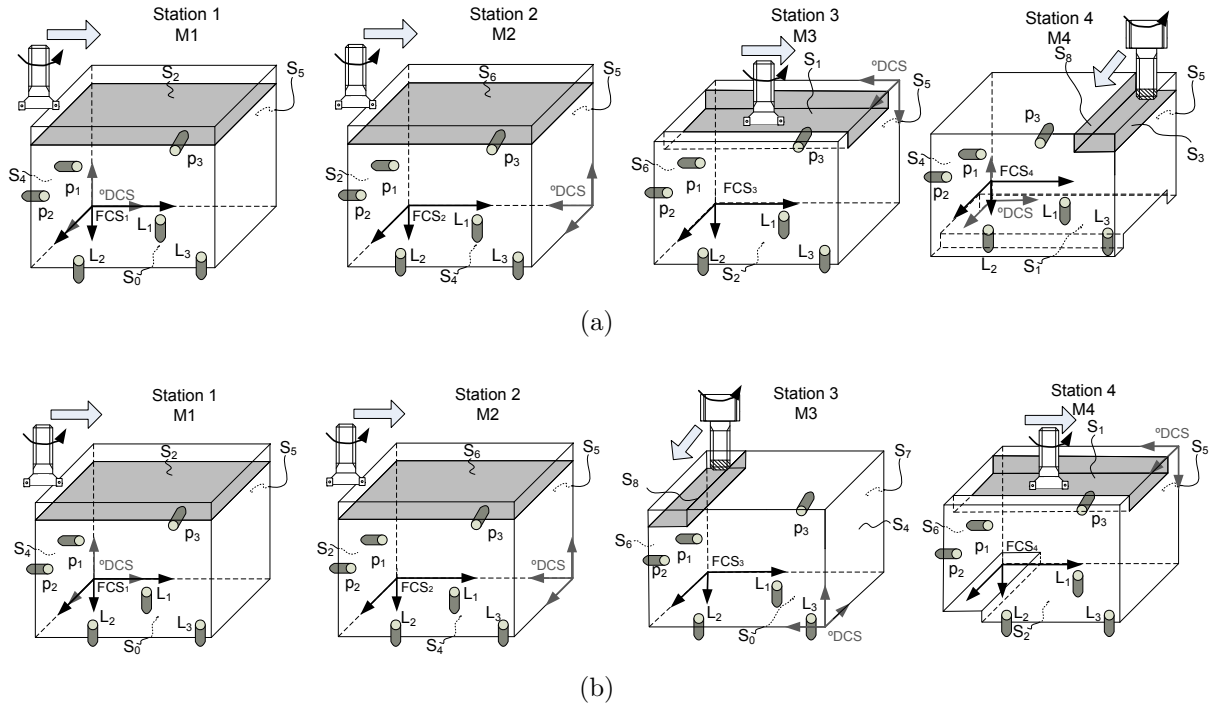


Figure 8.5: Case study. a) Proposed process plan number 1. b) Proposed process plan number 2. Process plan number 3 is the same than number 2 but machine-tool $M4$ is placed at the third station and machine-tool $M3$ at the fourth station.

Table 8.3: Nominal location ($\mathbf{t}_{F_k}^{\circ D}$) and orientation ($\varphi_{F_k}^{\circ D}$) of fixture CS at each station and fixture layout. PP1: process plan 1; PP2,3: process plan 2 and 3.

| Station | $\varphi_{F_k}^{\circ D}$ (rad) | $\mathbf{t}_{F_k}^{\circ D}$ (mm) | Locators w.r.t. F_k (mm) |
|-----------|---------------------------------|-----------------------------------|---|
| 1 | $[-\pi/2, \pi, 0]$ | $[0, 0, 0]$ | $L_{1x} = 125, L_{1y} = 50, L_{2x} = 50, L_{2y} = 250, L_{3x} = 200, L_{3y} = 250,$ $p_{1y} = 50, p_{1z} = -100, p_{2y} = 250, p_{2z} = -100, p_{3x} = 125, p_{3z} = -100$ |
| 2 | $[\pi/2, -\pi/2, \pi]$ | $[0, 0, 200]$ | $L_{1x} = 100, L_{1y} = 50, L_{2x} = 50, L_{2y} = 150, L_{3x} = 150, L_{3y} = 150,$ $p_{1y} = 50, p_{1z} = -125, p_{2y} = 250, p_{2z} = -125, p_{3x} = 100, p_{3z} = -125$ |
| 3 (PP1) | $[-\pi/2, 0, 0]$ | $[0, 250, 200]$ | $L_{1x} = 125, L_{1y} = 50, L_{2x} = 50, L_{2y} = 250, L_{3x} = 200, L_{3y} = 250,$ $p_{1y} = 50, p_{1z} = -100, p_{2y} = 250, p_{2z} = -100, p_{3x} = 125, p_{3z} = -100$ |
| 3 (PP2,3) | $[\pi/2, \pi, 0]$ | $[300, 250, 0]$ | $L_{1x} = 125, L_{1y} = 50, L_{2x} = 50, L_{2y} = 250, L_{3x} = 200, L_{3y} = 250,$ $p_{1y} = 50, p_{1z} = -100, p_{2y} = 250, p_{2z} = -100, p_{3x} = 125, p_{3z} = -100$ |
| 4 (PP1) | $[-\pi/2, \pi, 0]$ | $[0, 0, 20]$ | $L_{1x} = 125, L_{1y} = 50, L_{2x} = 50, L_{2y} = 250, L_{3x} = 200, L_{3y} = 250,$ $p_{1y} = 50, p_{1z} = -100, p_{2y} = 250, p_{2z} = -100, p_{3x} = 125, p_{3z} = -100$ |
| 4 (PP2,3) | $[-\pi/2, 0, 0]$ | $[0, 250, 200]$ | $L_{1x} = 125, L_{1y} = 50, L_{2x} = 50, L_{2y} = 250, L_{3x} = 200, L_{3y} = 250,$ $p_{1y} = 50, p_{1z} = -100, p_{2y} = 250, p_{2z} = -100, p_{3x} = 125, p_{3z} = -100$ |
| 5 | $[-\pi/2, \pi, 0]$ | $[0, 0, 0]$ | - |

Table 8.4: Nominal location ($\mathbf{t}_{S_i}^{\circ D}$) and orientation ($\varphi_{S_i}^{\circ D}$) of each feature for the previous part produced.

| Feature | $\varphi_{S_i}^{\circ D}$ (rad) | $\mathbf{t}_{S_i}^{\circ D}$ (mm) |
|---------|---------------------------------|-----------------------------------|
| S_A | $[0, \pi, 0]$ | $[150, 125, 0]$ |
| S_B | $[0, 0, 0]$ | $[150, 125, 200]$ |
| S_C | $[\pi/2, -\pi/2, -\pi/2]$ | $[150, 0, 100]$ |
| S_D | $[0, -\pi/2, 0]$ | $[0, 75, 100]$ |
| S_E | $[\pi/2, \pi/2, -\pi/2]$ | $[150, 250, 100]$ |
| S_F | $[0, \pi/2, \pi/2]$ | $[300, 125, 100]$ |
| S_G | $[0, \pi/2, \pi/2]$ | $[280, 125, 25]$ |
| S_H | $[0, \pi, 0]$ | $[290, 125, 50]$ |

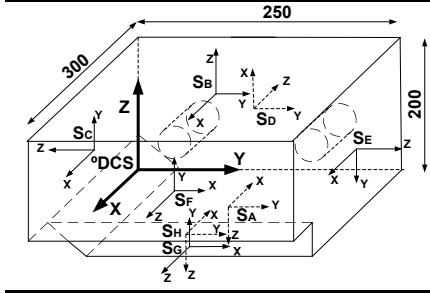


Table 8.5: Nominal location ($\mathbf{t}_{F_k}^{\circ D}$) and orientation ($\varphi_{F_k}^{\circ D}$) of fixture CS at each station and fixture layout for the previous production line.

| Station | $\varphi_{F_k}^{\circ D}$ (rad) | $\mathbf{t}_{F_k}^{\circ D}$ (mm) | Locators w.r.t. F_k (mm) |
|-------------------|---------------------------------|-----------------------------------|---|
| 1 | $[-\pi/2, \pi, 0]$ | $[0, 0, 0]$ | $L_{1x} = 125, L_{1y} = 50, L_{2x} = 50, L_{2y} = 250, L_{3x} = 200, L_{3y} = 250,$ $p_{1y} = 50, p_{1z} = -100, p_{2y} = 250, p_{2z} = -100, p_{3x} = 125, p_{3z} = -100$ |
| 2 | $[\pi/2, -\pi/2, \pi]$ | $[0, 0, 250]$ | $L_{1x} = 100, L_{1y} = 50, L_{2x} = 50, L_{2y} = 150, L_{3x} = 150, L_{3y} = 150,$ $p_{1y} = 50, p_{1z} = -125, p_{2y} = 250, p_{2z} = -125, p_{3x} = 100, p_{3z} = -125$ |
| 3A, 3B, 4A, 4B | $[\pi, \pi/2, 0]$ | $[0, 250, 200]$ | $L_{1x} = 125, L_{1y} = 50, L_{2x} = 50, L_{2y} = 250, L_{3x} = 200, L_{3y} = 250,$ $p_{1y} = 50, p_{1z} = -100, p_{2y} = 250, p_{2z} = -100, p_{3x} = 125, p_{3z} = -100$ |
| 5 | $[-\pi/2, \pi, 0]$ | $[0, 0, 0]$ | - |

the manufacturers based on their previous production and maintenance records. The data was generated through Monte Carlo simulations, with the following assumptions:

- The random variations of fixture locators follow a normal distribution with zero-mean and variance of $\sigma_{l_j^p}^2 = (0.075)^2 \text{ mm}^2$.
- The displacement variations and angular variations induced by face milling operations performed at machine-tools $M1, M2$ and $M4$ follow normal distributions with zero-means and variance of $(0.06)^2 \text{ mm}^2$ and $(0.003)^2 \text{ rad}^2$, respectively.
- The displacement variations and angular variations induced by end milling operations performed at machine-tool $M4$ follow normal distributions with zero-mean and variance of $(0.09)^2 \text{ mm}^2$ and $(0.009)^2 \text{ rad}^2$, respectively, for peripheral surface, and $(0.075)^2 \text{ mm}^2$ and $(0.0075)^2 \text{ rad}^2$ for frontal surfaces.
- The displacement and angular variations induced by face milling operations performed at machine-tool $M3$ follow normal distributions with zeros-means and variance of $(0.03)^2 \text{ mm}^2$ and $(0.001)^2 \text{ rad}^2$, respectively.
- The displacement and angular variations induced by end milling operations performed at machine-tool $M3$ follow normal distributions with zeros-means and variance of $(0.05)^2 \text{ mm}^2$ and $(0.005)^2 \text{ rad}^2$, respectively, for peripheral surfaces, and $(0.035)^2 \text{ mm}^2$ and $(0.0035)^2 \text{ rad}^2$, respectively, for frontal surfaces.

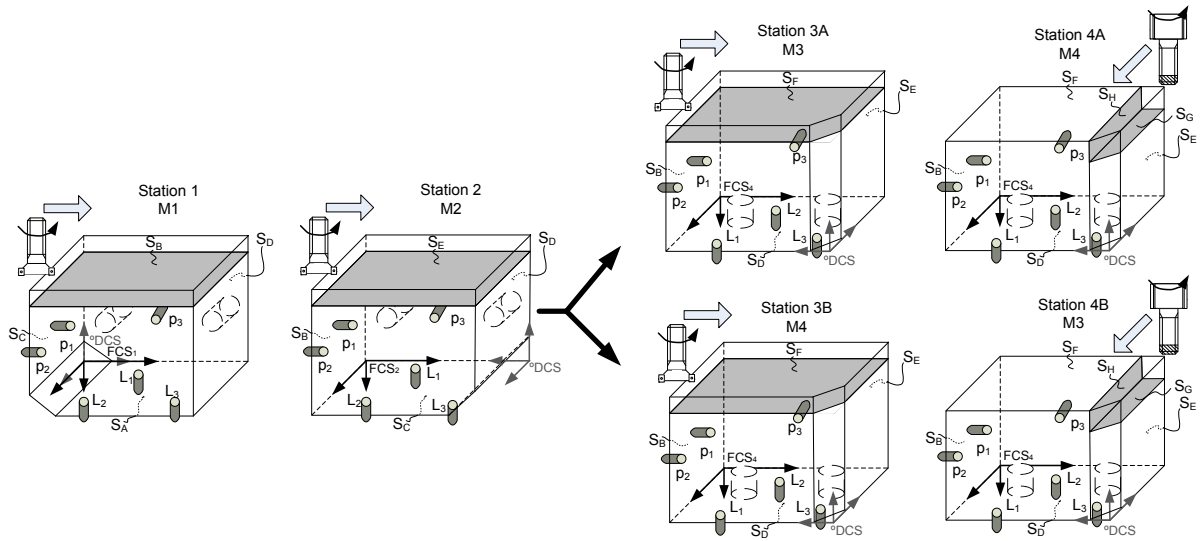


Figure 8.6: Case study. Previous production line.

- The noises are normally distributed with zero-mean and variance $(0.003)^2 \text{ mm}^2$ for translational measurements and $(5 \cdot 10^{-5})^2 \text{ rad}^2$ for angular measurements.
- Furthermore, all source of variations were assumed to be independent.

After generating 1,000 product-quality data using Eq. (8.4), the manufacturing operation capabilities were estimated by solving Eq. (8.9). The estimation results are shown in Figure 8.7 and their deviations from actual values can be explained by the measurement errors added in the simulations and the limited number of product quality data generated (1,000 simulations, which is a reasonable quantity for historical data). Note that the values extracted are the variance of the machining-induced deviations which indicate the manufacturing operation capability of each machine-tool for a specific operation and cutting conditions. The variance of the machining-induced deviations for linear and angular displacement at the manufacturing station k define the diagonal values of the covariance matrix $\Sigma_{\mathbf{u}_k}^{m_k}$.

For this configuration, a high accuracy is achieved in the estimation of the variance of the machining-induced deviations as it is shown in Figure 8.7. However, if the measurement noise increases notably, the estimation error of these variances can prevent the extraction of the manufacturing operation capabilities with enough accuracy to analyze and adjust the process plan candidates in the next steps.

8.4.3 Step 2: Sensitivity analysis

The sensitivity analysis for adjusting process plan candidates was conducted with the results shown in Figure 8.8. For process plan candidate 1, the manufacturing operation capability is more critical than the inaccuracy of the applied datum schemes ($S_{m,process}^{\mathbf{Y}} > S_{f,process}^{\mathbf{Y}}$). The sensitivity indices report higher dimensional variation on the KPC_1 than

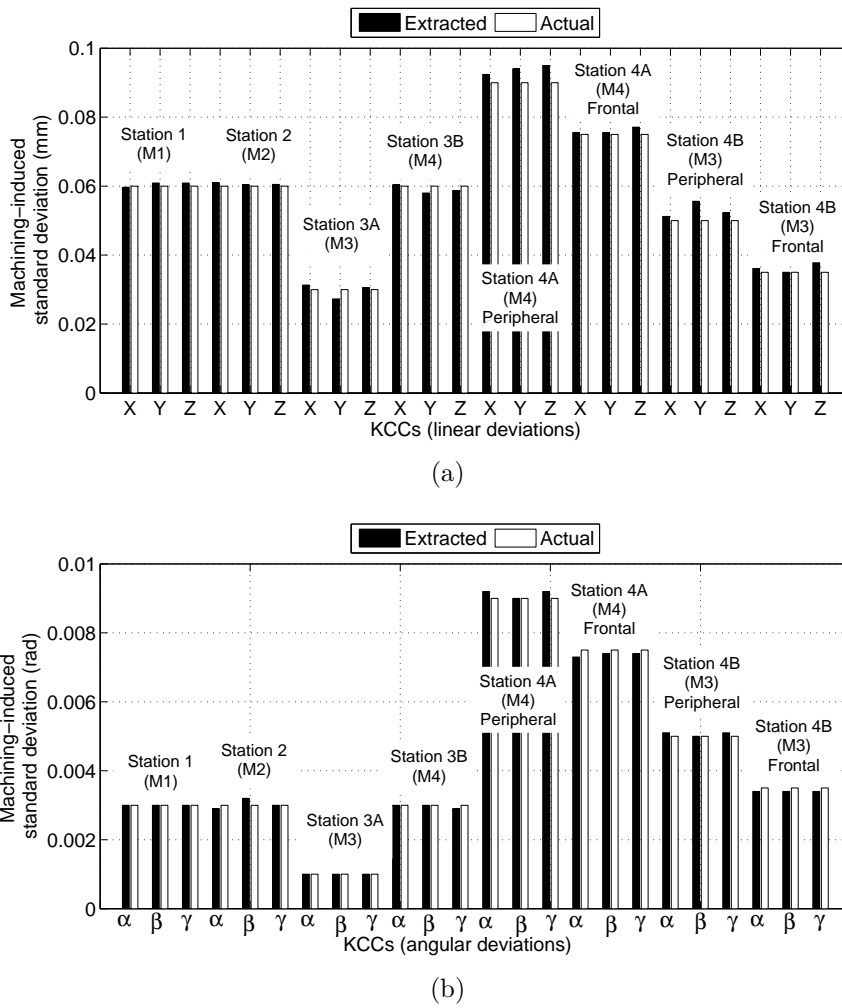


Figure 8.7: Comparison of actual and extracted values of the machining-induced variations at each manufacturing station. Figures a) and b) refer to linear and angular deviations respectively.

the average of all KPCs ($S_{m,process}^{KPC_1} > C_b S_{m,process}^Y$, with $C_b=1.3$), and the 76% of the variability at this KPC due to machining-induced variations is generated at station 1. In this station, the random deviations of the cutting-tool path along Z -axis and β orientation are the main factors that produce the variability at the KPC_1 . Especially, the angular deviations on β reports the main source of variation to the final dimensional quality of KPC_1 . The sensitivity analysis of the process plan candidate 2 reported that the fixture-induced variations are more critical to the final product quality ($S_{f,process}^Y > S_{m,process}^Y$). At this process plan, there is no special KPC with an important variability w.r.t. other KPCs, and the sensitivity indices w.r.t. product were analyzed. Similar to the process plan 1, the station 3 is the most critical station since it generates almost the 95% of the fixture-induced variations. The analysis of this station revealed that the locator 3 is the most important source of variation and it accounts around the 38% of the fixture-induced variations at the station 3. For the process plan candidate 3, the sensitivity analysis was

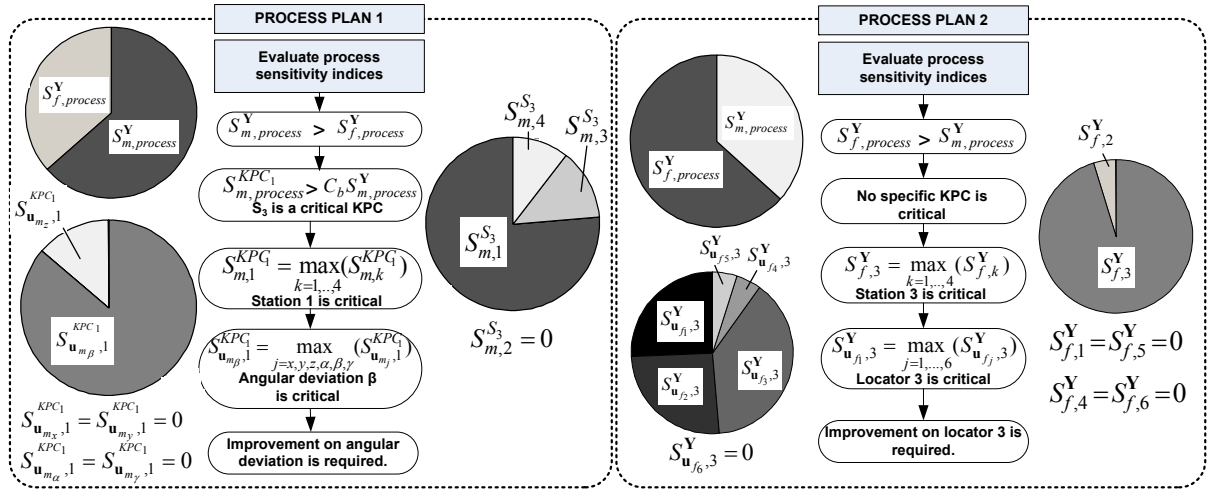


Figure 8.8: Sensitivity analysis results for process plans 1 and 2.

very similar to process plan candidate 2, and the required adjustment of the fixture layout at station 3 was also reported.

Through these analyses, the process planner can propose adjustments at each process plan to decrease the impact of the source of variations related to the fixture or the machining operation.

8.4.4 Step 3: Process plan evaluation and selection

A capability analysis of each process plan was conducted to evaluate the process plan candidates according to its capability to keep parts within specifications. The multivariate process capability ratio defined in Eq. (8.31) was evaluated for each process plan candidate by running the Eq. (8.4) for 1,000 Monte Carlo simulations. At these simulations, each component of the fixture-induced deviations \mathbf{U}_k^f was normally distributed with a standard deviation of 0.017 mm ; each component of the machining-induced deviations \mathbf{U}_k^m was normally distributed according to the variance of these deviations extracted from the step 1 of the proposed methodology; the measurement error was assumed normally distributed with mean 0 and variance $(0.003)^2 \text{ mm}^2$ for positional location and with mean 0 and variance of $(5 \cdot 10^{-5})^2 \text{ rad}^2$ for angular location; and the term related to non-linear errors was assumed negligible.

Considering the expected proportion of conforming products as $1 - \alpha = 0.95$, the capability indices obtained were $MC_p^1 = 0.27$, $MC_p^2 = 1.96$ and $MC_p^3 = 0.84$ for process plan candidates 1, 2 and 3 respectively. The results show that the first and third process plans are not capable to keep the 95% within specifications whereas the second process plan is capable. As it can be seen, although the second and third process plans share the same datum schemes, the selection of a proper machine-tool with high manufacturing operation capability at the third station is a key issue to keep parts within specifications. Figure 8.9 shows graphically these process capability indices.

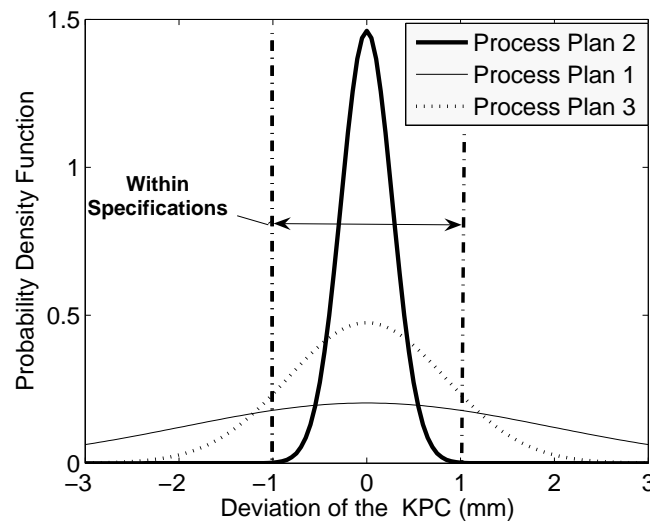


Figure 8.9: Graphical representation of the multivariate process capability indices of process plans 1, 2 and 3.

8.5 Conclusions

A new methodology has been proposed for process plan evaluation, adjustment and selection in a MMP in order to minimize product variability. Unlike existing works, the proposed methodology considers the potential impact of the machining-induced variations of each machining station on part quality and guides the process planner to adjust process plan candidates according to a sensitivity analysis. The methodology consisted of three steps. The first step consists of analyzing an existing MMP whose manufacturing stations are expected to be used for manufacturing the new product in a new MMP. Analyzing historical shop-floor quality data, the manufacturing operation capabilities of each station can be extracted. In the second step, the extracted manufacturing operation capabilities are used together with the fixture tolerances to analyze the robustness of each process plan candidate. This step is conducted through a sensitivity analysis by a flowchart that guides the process planner to redefine and adjust each process plan candidate to increase their robustness to manufacturing variations. Finally, the third step consists of evaluating the process plan candidates through a multivariate capability ratio. At this step, the best process plan candidate is the one with the largest ratio, which is the most robust process plan candidate to manufacturing variations. To illustrate the validation of the methodology, a case study was presented.

References

- [1] H. C. Zhang, S. H. Huang, A fuzzy approach to process plan selection, *International Journal of Production Research* 32 (6) (1994) 1265–1279.
- [2] A. Kusiak, G. Finke, Selection of process plans in automated manufacturing systems, *IEEE Journal of Robotics and Automation* 4 (4) (1988) 397–402.

-
- [3] S. Noto La Diega, G. Perrone, M. Piacentini, Multiobjectives approach for process plan selection in IMS environment, *CIRP Annals - Manufacturing Technology* 45 (1) (1996) 471–474.
 - [4] S. Y. Wei, C. C. Lo, C. A. Chang, Using throughput profit for selecting manufacturing process plan, *Computers and Industrial Engineering* 32 (4) (1997) 939–948.
 - [5] Y. Ding, J. J. Shi, D. Ceglarek, Diagnosability analysis of multi-station manufacturing processes, *Journal of Dynamic Systems Measurement and Control* 124 (1) (2002) 1–13.
 - [6] M. Zhang, D. Djurdjanovic, J. Ni, Diagnosibility and sensitivity analysis for multi-station machining processes, *International Journal of Machine Tools and Manufacture* 47 (2007) 646–657.
 - [7] J. Liu, J. Shi, S. J. Hu, Quality-assured setup planning based on the stream-of-variation model for multi-stage machining processes, *IIE Transactions* 41 (12) (2009) 323–334.
 - [8] W. Taam, P. Subbaiah, J. W. Liddy, A note on multivariate capability indices, *Journal of Applied Statistics* 20 (3) (1993) 339–351.
 - [9] H. F. Chen, A multivariate process capability index over a rectangular solid tolerance zone, *Statistica Sinica* 4 (2) (1994) 749–758.
 - [10] F. K. Wang, J. C. Chen, Capability indices using principle components analysis, *Quality Engineering* 11 (1) (1998) 21–27.
 - [11] F. K. Wang, T. C. T. Du, Using principle component analysis in process performance for multivariate data, *Omega* 28 (2) (2000) 185–194.
 - [12] W. L. Pearn, S. Kotz, *Encyclopedia And Handbook of Process Capability Indices: A Comprehensive Exposition of Quality Control Measures*, World Scientific Publishing Company, 2006.
 - [13] H. Wang, D. Ceglarek, Quality-driven sequence planning and line configuration selection for compliant structure assemblies, *CIRP Annals-Manufacturing Technology* 54 (1) (2005) 31–35.
 - [14] Y. Ding, D. Ceglarek, J. Shi, Design evaluation of multi-station assembly processes by using state space approach, *Journal of Mechanical Design* 124 (3) (2002) 408–418.
 - [15] D. D. Frey, K. N. Otto, J. A. Wysocki, Evaluating process capability during the design of manufacturing systems, *Journal of Manufacturing Science and Engineering* 122 (3) (2000) 513–519.
 - [16] S. Kotz, N. L. Johnson, Process capability indices - a review, 1992-2000, *Journal of Quality Technology* 34 (1) (2002) 2–19.
 - [17] P. Joshi, *Jigs and Fixtures Design Manual*, McGraw-Hill, 2003.

-
- [18] K. A. Bollen, J. S. Long, *Testing Structural Equation Models*, Sage Publications, Inc, 1993.
- [19] J. Shi, *Stream of Variation Modeling and Analysis for Multistage*, CRC Press Taylor and Francis Group, 2007.

Process-oriented tolerancing using the extended Stream of Variation model

Current research works on process-oriented tolerancing in multi-station machining processes (MMPs) have been mainly focused on fixture tolerances and the integration of fixture maintenance policies. In this chapter, the process-oriented tolerancing is expanded based on the extended Stream of Variation (SoV) model presented in Chapter 6, which explicitly represents the machining-induced variations in the variation propagation along MMPs. With this modeling capability extension, a complete process-oriented tolerancing can be conducted where important process variables such as the admissible cutting-tool wear, accuracy of fixture components, spindle thermal expansion and so on, can be taken into account. This approach also leads to the incorporation of a variety of manufacturing costs, such as those related to cutting-tool replacement policies, in order to reach a real minimum manufacturing cost. A case study presents the potential application of the proposed methodology and demonstrates its advantages over conventional methods.

9.1 Introduction

Machining operations are inherently imperfect in fabricating parts. This is due to the numerous process variables that affect the final quality of products, such as machine-tool thermal expansion, cutting-tool wear, fixture error, etc. The inherent variability of machining processes requires to specify dimensional and geometrical tolerances on raw and machined surfaces to ensure final product functionality. Product tolerancing defines the variability allowed for each key variable that characterizes the functional requirements of the product, named the key product characteristics (KPCs). There are two basic directions in tolerancing research: (a) tolerance analysis and (b) tolerance synthesis. Tolerance analysis predicts the variation of the final product given the tolerance of each part using a mathematical model of tolerance accumulation such as the worst-case or the statistical model [1, Chapter 9]. Tolerance synthesis, or tolerancing, focuses on assigning tolerance specifications to individual manufacturing features on a part to ensure product functionality and minimize manufacturing cost. In the literature, the traditional tolerancing approach is product-oriented. This approach is mainly focused on assigning tolerances

to product variables, such as dimensions of final product and parts. However, this approach only considers limited a priori knowledge about manufacturing capabilities and manufacturing costs of specific operations, and does not explicitly specify the allowable variability of the process variables, such as those related to tooling variations due to wear, thermal distortions or manufacturing accuracy. Recently, the process-oriented tolerancing approach was proposed by [2]. This approach is essentially a tolerance transfer method where the quality specification of the final product is ensured by optimally assigning tolerances of process variables throughout the manufacturing process.

In a MMP, the process variables, also referred as key control characteristics (KCCs), are the main root fault causes of the process that negatively impact on the KPCs. These KCCs define the working condition of the tools (machine-tools, fixtures and cutting-tools) that are used to fabricate a part. In the process-oriented tolerancing approach, the incorporation of KCCs into tolerance models leads to the integration of tolerancing with process maintenance and operation strategies. As a result, a more comprehensive function cost can be considered to find out the optimal tolerance allocation that minimizes the total manufacturing cost.

In the literature, only few works have been focused on process-oriented tolerancing using the SoV model [2–5]. Ding *et al.* [2] applied the process-oriented tolerancing approach to allocate product and process tolerances in a multi-station assembly process (MAP). The KCCs modeled were the variability of fixture locators caused by their degradation. Considering reciprocal functions as cost-tolerance functions, the optimal tolerance of KCCs with the minimum manufacturing cost was allocated by solving a constrained optimization problem. Similar problem was described by Chen *et al.* [3], who expanded Ding *et al.*'s work to integrate the process-oriented tolerancing with fixture maintenance planning. Tool fabrication cost, fixture maintenance cost and quality loss functions were considered together to optimize the process tolerance allocation and the frequency of fixture maintenance operations in MAPs. In machining systems, Huang and Shi [4] developed a similar tolerance allocation methodology considering as KCCs the locators' variability at each station. Recently, Liu *et al.* [5] studied the use of the SoV model to evaluate the robustness of different candidate setup plans for a MMP. By analyzing different process plan candidates and allocating the locators' tolerance optimally, the best process plan candidate can be defined.

However, in the formulations of these recent efforts, only the fixture-induced variations were explicitly considered, leaving the incorporation of other significant machining-induced variations unaddressed. As shown in Chapter 2, such machining-induced variations can be introduced by machine-tool geometric deviations, thermal variations, force-induced deviations, tooling wear and dynamic deviations. These variations, together with those induced by fixture deviations, will deteriorate the dimensional integrity of the features generated within a station affecting the final product quality. For process-oriented tolerancing purposes, the omission of these machining-induced variations may potentially lead to wider tolerances on fixture components which will not be able to keep parts within specifications.

To illustrate this potential problem, one may consider an example of the two-station machining process shown in Figure 9.1. At the first station, the dimension of the machined feature D_2 is deviated from its nominal value due to the locator tolerance, denoted by $\pm T_2$, and the machining-induced variations due to the cutting-tool wear, denoted by $\pm T_3$, and those induced by the spindle thermal expansion, denoted by $\pm T_4$. Thus, considering the worst-case deviation, the tolerance of D_2 is defined by $T_1 = T_2 + T_3 + T_4$. The workpiece is then setup at station 2, where the dimension of the feature to be machined, D_3 , will be deviated from nominal values in a similar way and thus, its final tolerance will be defined by $T_5 = T_6 + T_7 + T_8$. As a result, the KPC of this part defined by the dimension of the feature D_4 will depend on all previous fixture and machining-induced variations. Its tolerance will be defined as $T_{10} = T_1 + T_5 + T_9 = T_2 + T_3 + T_4 + T_6 + T_7 + T_8 + T_9$, which means that if machining-induced variations are not negligible with respect to fixture-induced variations, the achievable tolerance of this KPC depends on the variability of six different KCCs defined by the tolerances $\{T_2, T_3, T_4, T_6, T_7, T_8\}$. Note that the tolerance T_9 refers to the tolerance of the dimension D_1 (raw material) so it is not related to a fixture or machining-induced variation. Neglecting the machining-induced variations will result in allocating a higher tolerance value for fixture locators. However, if in reality machining-induced variations are not negligible, the locator tolerances allocated will generate parts outside specifications since additional sources of variation are present. As a conclusion, a reliable process-oriented tolerancing requires the incorporation of all those KCCs related to machining-induced variations that directly influence on part quality.

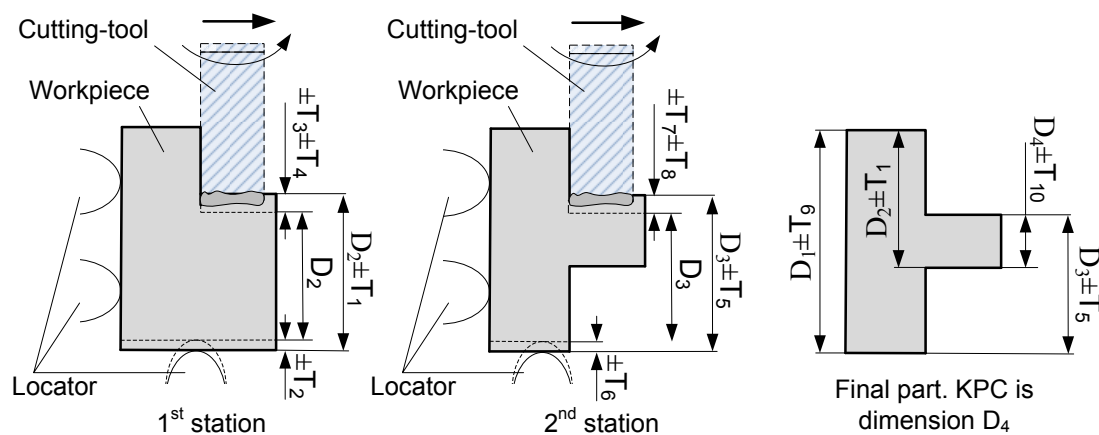


Figure 9.1: Example of the influence of machining-induced variations on the tolerance allocation problem.

In this chapter, we propose a process-oriented tolerancing methodology, considering the fixture-induced variations and two of the most critical machining-induced variations, named the spindle thermal-induced variations and the cutting-tool wear-induced variations. For this purpose, the extended SoV model presented in Chapter 6 is applied, distinguishing two different kind of process variables: i) maintainable KCCs, which are those variables whose maximum variations can be limited or controlled through corrective actions (hard-time maintenance actions), and ii) non-maintainable KCCs, which are those variables whose variations cannot be limited or controlled although their variability can

be known from shop-floor knowledge or can be estimated according to historical shop-floor data. Unlike previous process-oriented tolerancing methodologies, the proposed methodology ensures product quality with a minimum manufacturing cost by considering the cost related to both fixture maintenance strategies and cutting-tool replacement policies.

This chapter is organized as follows. Section 9.2 formulates the assumptions considered in the process-oriented tolerance allocation problem. Section 9.3 describes the tolerance allocation problem, and Sections 9.4 and 9.5 expose the manufacturing cost functions and the constraints of the problem. In Section 9.6, a summary of the optimization problem for process-oriented tolerance allocation is presented. A case study is shown in Section 9.7 to demonstrate the effectiveness of the proposed process-oriented tolerancing approach. Finally, Section 9.8 presents the conclusions of the chapter.

9.2 Assumptions

In this chapter, the following assumptions are made to facilitate the model formulation and derivation:

- Machined workpiece behaves as a rigid body and the magnitudes of all random deviations are small.
- The sources of process variations are assumed to be independent of each other.
- Variability of process variables may be not normally distributed due to their nature.
- There are no dominant process variables that impact on the KPC deviations and thus, the variance of KPCs due to the variance of any process variable is very small in comparison to the total variance of the KPCs due to the rest of process variables.
- According to the above assumptions and the Lindeberg's central limit theorem [6, 7], the resultant random deviations of the KPCs can be approximated by a normal distribution if a large number of process variables is considered.
- The manufacturing process is assumed to be centered and thus, it is assumed that there is no mean-shift of KPCs.
- In a fixture device, when the maximum admissible wear of a locator is reached, a fixture maintenance action is carried out to replace and calibrate all fixture locators.

9.3 Problem formulation

Without loss of generality, two machining-induced variations are considered in the variation propagation model in this chapter: i) machining-induced variations due to cutting-tool wear and ii) machining-induced variations due to spindle thermal expansion. Focusing the research work on small-medium workpiece size with the use of cutter insert plates, these two machining-induced variations can be considered as the most critical KCCs for tolerancing rather than other variation sources, such as cutting-tool deflections or geometric

deviations of machine-tool axes, as it was shown in Chapter 5. According to the extended SoV model shown in Chapter 6, the terms \mathbf{B}_k and \mathbf{u}_k from the conventional SoV model can be expanded in the form of $\mathbf{B}_k = [\mathbf{B}_k^f \ \mathbf{B}_k^s \ \mathbf{B}_k^w]$ and $\mathbf{u}_k = [\mathbf{u}_k^f \ \Delta T_k^s \ V_k]^T$. Through this model extension, the KPC variations can be related to that of the KCCs, including the fixture locator variations (\mathbf{u}_k^f), the spindle thermal expansion (ΔT_k^s) and the cutting-tool wear state (V_k).

For tolerance allocation purposes, we reformulate the matrix \mathbf{B}_k as $[\mathbf{B}_k^f \ \mathbf{B}_k^f \ \mathbf{B}_k^s \ \mathbf{B}_k^w]$ and the vector \mathbf{u}_k as $\left[(\mathbf{u}_k^{fi})^T, (\mathbf{u}_k^{fw})^T, \Delta T_k^s, V_k \right]^T$ in order to separate the fixture deviation in two independent components: the component due to the accuracy of each locator after mounting and calibrating the fixture device (defined by the term \mathbf{u}_k^{fi}) and the component due to the degradation of each fixture locator during normal operation (defined by the term \mathbf{u}_k^{fw}). If the machined part is inspected at the end of the machining process, the SoV model in an input–output form is defined as:

$$\mathbf{Y} = \mathbf{\Gamma} \cdot \mathbf{U} + \boldsymbol{\varepsilon}, \quad (9.1)$$

where $\mathbf{U} = [(\mathbf{u}_1)^T, \dots, (\mathbf{u}_N)^T]^T$ is the vector of the KCCs of all stations, and $\mathbf{Y} = [y_1, \dots, y_M]^T$ is the vector of the M KPC measurements collected at the end of a MMP. $\mathbf{\Gamma}$ and $\boldsymbol{\varepsilon}$ can be obtained as shown in Chapter 4.

The process-oriented tolerancing consists of defining the tolerances for all KCCs that minimize the total manufacturing cost and ensure part quality specifications. Thus, the optimal process-oriented tolerance allocation can be formulated as the following optimization problem:

$$\min_{\mathbf{T}_U} \{C_T(\mathbf{T}_U)\}, \quad \text{subjected to } \boldsymbol{\Psi}, \quad (9.2)$$

where C_T is the total manufacturing cost which is a function of \mathbf{T}_U ; $\mathbf{T}_U = [T_1, T_2, \dots, T_\eta]^T$ is a vector where the element T_χ represents the tolerance of the χ th KCC defined in \mathbf{U} ; and $\boldsymbol{\Psi}$ is a set of constraints.

Considering two types of machining-induced variations (due to tool wear and spindle thermal expansion) and the fixture-induced variations, the objective is to minimize the total manufacturing cost for allocating: i) the initial precision of fixture locators, ii) the admissible maximum wear of fixture locators before a maintenance operation is carried out, and iii) the admissible maximum wear of cutting-tools before a cutting-tool replacement is conducted. The tolerance allocation problem is thus composed of the following cost functions: i) fixture precision cost, ii) fixture maintenance cost, iii) cutting-tool replacement cost, and iv) quality loss cost. Furthermore, the vector of constraints is composed of: i) constraints of the non-maintainable KCCs, ii) constraints of the maintainable KCCs, and iii) constraints related to part quality specifications. The following subsections will describe the manufacturing cost functions and the constraints in detail.

9.4 Definition of manufacturing cost functions

9.4.1 Fixture precision cost

The first group of manufacturing costs is related to the precision of the fixtures to be used. Tighter tolerances of fixturing elements result in higher tooling fabrication and assembly costs. Several algebraic functions have been proposed to calculate fixture precision costs, such as reciprocal, reciprocal power, negative exponential and reciprocal squared functions [1]. For tolerance allocation, the reciprocal function and negative exponential function are widely accepted [3]. In this chapter, we assume a fixture layout at each station based on the common 3-2-1 locating principle applied in machining processes [8]. For this fixture layout, the cost function for the j th fixture component (locator) installed at station k is chosen to be a reciprocal function as

$$C_{j,k}^L = \frac{w_{j,k}^D}{\Delta l_{j,k}^D}, \quad k = 1, \dots, N, \quad j = 1, \dots, 6, \quad (9.3)$$

where $\Delta l_{j,k}^D$ is the tolerance assigned to the j th locator at station k , and $w_{j,k}^D$ is a weighting coefficient related to its fabrication and assembly cost.

9.4.2 Fixture maintenance cost

The second group of manufacturing costs defines the cost due to the fixture maintenance. For a new fixture, the allowable varying ranges of locators position are determined by their design tolerances. Thus, the j th locator of a manufactured fixture should match an initial precision defined by the design tolerance $\Delta l_{j,k}^D$. However, due to the gradual degradation, the dimension of a locator at station k will decrease until it reaches a limit specified by the admissible maximum wear Δl_k^w . Then, a maintenance operation should be carried out. Such operations are commonly referred to as hard-time maintenance actions in industry. The time between fixture maintenance actions is defined by t_k^a , which can be estimated from maintenance data or fixture specifications.

Intuitively, a low frequency of maintenance actions imposes a higher precision of the initial locator dimensions (design tolerances) to keep parts within specifications for a longer period of time and thus, higher precision costs and lower fixture maintenance costs.

According to [3], the long-run average maintenance cost of a fixture at station k can be expressed as:

$$C_k^M = \frac{\left(\sum_{j=1}^6 C_{j,k}^L \right) + C_k^f}{t_k^a}, \quad (9.4)$$

where

$$t_k^a = \min_{j=1, \dots, 6} (t_k^{a_j}), \quad (9.5)$$

$$t_k^{a_j} = f_k^j(\Delta l_k^w), \quad k = 1, \dots, N, \quad j = 1, \dots, 6; \quad (9.6)$$

C_k^f is the fixed cost related to the maintenance operation at station k ; and t_k^{aj} is the time required to wear the j th locator at station k up to a wear value of Δl_k^w , and it is modeled by the function $f_k^j(\cdot)$

9.4.3 Cutting-tool replacement cost

A cutting-tool replacement is conducted when the admissible maximum wear value of the cutting-tool is reached. The time to replace the τ th cutting-tool at station k , called $t_{\tau,k}^b$, basically depends on two factors: i) the deviation generated on the machined feature due to the cutting-tool wear, and ii) the maximum flank wear recommended by the tool manufacturing vendor to avoid breakage or unsafe operations. In general, two terms define the cutting-tool replacement cost. The first term refers to the residual cost of the cutting-tool which is the cost of under-using the cutting-tool due to an early replacement before the maximum cutting-tool wear is reached. The second term refers to the cost of the cutting-tool replacement itself that involves the replacement of cutting-inserts or cutting-tools by operators.

Intuitively, a high replacement frequency decreases the dimensional variability of the machined features but increases the replacement cost. Therefore, cutting-tool replacement policies seek a trade-off between the dimensional variability of the feature machined due to tool-wear and the replacement cost of the cutting-tool. In this chapter, the cost of cutting-tool replacement is defined as follows:

$$C_{\tau,k}^w = (w_k^{res\tau} \cdot R_{\tau,k} + w_k^{rep\tau}) / t_{\tau,k}^b, \quad (9.7)$$

where

$$R_{\tau,k} = \min_{\varrho=1,\dots,\mu_{\tau,k}} \left(\frac{(V_{\tau,k}^{max\varrho} - V_{\tau,k}^{\varrho})}{V_{\tau,k}^{max\varrho}} \right) \quad (9.8)$$

$$t_{\tau,k}^b = \min_{\varrho=1,\dots,\mu_{\tau,k}} \left(t_{\tau,k}^{b\varrho} \right), \quad (9.9)$$

$$t_{\tau,k}^{b\varrho} = g_k(V_{\tau,k}^{\varrho}), \quad k = 1, \dots, N \quad (9.10)$$

where $w_k^{res\tau}$ is the residual cost of under-using a cutting-tool edge in the τ th cutting-tool at station k ; $w_k^{rep\tau}$ is the cost related to replace or turn the τ th cutting-tool in order to use a new cutting-tool edge at station k ; $R_{\tau,k}$ is the residual life of the cutting-tool in terms of percentage; $t_{\tau,k}^{b\varrho}$ is the time required to wear the ϱ th edge of the τ th cutting-tool at station k up to a flank wear value of $V_{\tau,k}^{\varrho}$, and it is modeled by the function $g_k(\cdot)$; and $V_{\tau,k}^{max\varrho}$ is the admissible maximum tool wear in the ϱ th edge of the τ th cutting-tool to avoid a breakage or an unsafely machining operation at station k . It is noted that τ , $\tau = 1, \dots, \kappa_k$, is the index of cutting-tools used at station k , and ϱ , $\varrho = 1, \dots, \mu_{\tau,k}$, is the index of cutting edges which remove material simultaneously (e.g. end mills use two cutting edges simultaneously).

9.4.4 Quality loss cost

According to [9], even if a product is well within specifications, the product has a quality loss if its quality characteristic value is not at the ideal performance target. In manu-

facturing, the quality loss associated may include the cost of scrap or rework. As this chapter deals with variation propagation and the SoV model predicts the variability of the KPCs, the ideal target value of the KPC variations is zero, which means that no variation occurs. The Taguchi quality loss function for this case is the “smaller-the-better” function [9]. The equation used to describe this quality loss function of one part is:

$$L = \frac{I_0 \cdot y_i^2}{(T_{y_i}/2)^2}, \quad (9.11)$$

where I_0 is the loss in monetary units per unit of time when the 0.27% of parts manufactured are out of specifications; y_i is the deviation of the i th KPC from its target; and T_{y_i} is the dimensional tolerance of the i th KPC.

9.5 Definition of constraints

9.5.1 Constraints of non-maintainable KCCs

Many KCCs that contribute to final KPC variations can not be cost-effectively maintained or controlled since their variation ranges cannot be reduced through correction actions in an feasible way. However, although the variation range of these KCCs, named non-maintainable KCCs, cannot be reduced, they can be estimated when shop-floor data is available. In the process-oriented tolerancing problem, the variability of each non-maintainable KCC is restricted to a constant range. For instance, one common non-maintainable KCC is generally related to the temperature variations of the machine-tool spindle. In practice, it is infeasible to maintain or control the temperature of the machine-tool spindle during machining. However one can estimate, using historical data, the temperature variation range of the machine-tool in normal conditions. Thus, the deviation of the spindle temperature with respect to the nominal temperature can be restricted by the six-sigma range as:

$$-3 \cdot \sigma_{T_k^s} \leq \Delta T_k^s \leq +3 \cdot \sigma_{T_k^s}, \quad k = 1, \dots, N, \quad (9.12)$$

where $\sigma_{T_k^s}$ is the standard deviation of the spindle temperature at station k under normal manufacturing conditions, which is estimated from empirical shop-floor data or a priori knowledge. Other non-maintainable KCCs such as cutting-tool deflections due to cutting force variations or geometrical axis deviations due to straightness errors or misalignments can be defined by similar constraints.

9.5.2 Constraints of maintainable KCCs

Unlike non-maintainable KCCs, the maintainable KCCs can be kept within a range of variation by adequate corrective actions. Two common types of maintainable KCCs are related to the initial precision of fixture locators and the wear of cutting-tools. Constraints of these maintainable KCCs are: i) the initial precision of locators cannot be lower than a minimum tolerance, denoted by Δl_{min}^D , which is defined by manufacturing and assembly limitations of fixture components; ii) the initial precision of locators, in case that a non-accurate locator were needed, cannot be higher than a maximum tolerance range, denoted

by Δl_{max}^D ; and iii) the maximum cutting-tool wear cannot exceed its maximum allowable value, denoted by $V_{\tau,k}^{max\varrho}$, which is set to avoid cutting-tool breakage or unsafely operations. These constraints can be written as:

$$0 \leq V_{\tau,k}^{\varrho} \leq V_{\tau,k}^{max\varrho}, \quad (9.13)$$

$$\Delta l_{min}^D \leq \Delta l_{j,k}^D \leq \Delta l_{max}^D, \quad (9.14)$$

for $k = 1, \dots, N$, $j = 1, \dots, 6$, $\tau = 1, \dots, \kappa_k$ and $\varrho = 1, \dots, \mu_{\tau,k}$.

9.5.3 Part quality constraints

Process tolerances will be set in order to ensure part design specifications. For this purpose, any part design specification should be mathematically expressed by constraint equations. A widely accepted approach is transforming the GD&T specifications shown in part design drawings into VD&T specifications [10–12], defining the maximum values of the DMVs for the toleranced feature. For dimensional tolerances, the following methodology to translate a GD&T specification into constraints of DMVs can be applied:

- Step 1: Identify the controlled feature (S_q), the measurement datum feature (S_D) and the GD&T reference datum feature (S_m). A controlled feature is defined as the toleranced feature whose dimensional tolerance needs to be translated into constraints. A measurement datum feature refers to the feature used as a datum in the inspection station where the inspection of part quality is conducted. A GD&T reference datum feature is the datum feature applied in the toleranced feature definition.
- Step 2: Identify the boundary points $\{P_1^{S_q}, \dots, P_P^{S_q}\}$ that define the controlled feature. For a plane, its P extreme points are considered as the boundary points since they are most likely to be out of specifications due to orientation deviations.
- Step 3: Determine the quality constraints according to the type of measurement conducted to verify the specifications. These measurements can be direct, when the GD&T reference datum feature and the measurement datum feature are the same, or indirect, when they are different. For each type of measurements, the constraints are defined as follows:
 - (a) Specification verified by direct measurements. According to the SoV model in Eq. (9.1), if we assume that measurement and linearization errors in comparison with part dimension deviations are negligible, the variability of the controlled feature S_q is defined by the covariance matrix:

$$\Sigma_{\mathbf{Y}_{S_q}} = \mathbf{\Gamma}_{S_q} \cdot \Sigma_{\mathbf{U}} \cdot \mathbf{\Gamma}_{S_q}^T, \quad (9.15)$$

where $\Sigma_{\mathbf{U}}$ is the covariance matrix of the s independent process variables defined by the vector \mathbf{U} (e.g. the locator deviation due to its initial precision and its degradation, cutting-tool wear, etc.), and it has the form $diag\{Var(u_1),$

$\dots, Var(u_s)\}$ where $Var(\bullet)$ is the variance of \bullet ; and $\mathbf{\Gamma}_{S_q}$ is a block matrix of $\mathbf{\Gamma}$ that corresponds to the deviation of feature S_q , obtained from Eq. (9.1). From Eq. (9.15), the variability of the boundary point P_p in the controlled feature S_q can be defined as:

$$\Sigma_{\mathbf{Y}_{P_p}^{S_q}} = (\mathbf{C}_{P_p} \cdot \mathbf{\Gamma}_{S_q}) \cdot \Sigma_{\mathbf{U}} \cdot (\mathbf{C}_{P_p} \cdot \mathbf{\Gamma}_{S_q})^T \quad (9.16)$$

where matrix \mathbf{C}_{P_p} is defined in Appendix 9.1. By the Lindeberg's central limit theorem, it is assumed that the variability of the KPCs can be approximated to a normal distribution, so the variability constraints of each boundary point at the direction where the tolerance applies can be defined as follows:

$$\Sigma_{\mathbf{Y}_{P_p}^{S_q}}(\rho, \rho) = (\mathbf{C}_{P_p} \cdot \mathbf{\Gamma}_{S_q}) \cdot \Sigma_{\mathbf{U}} \cdot (\mathbf{C}_{P_p} \cdot \mathbf{\Gamma}_{S_q})^T(\rho, \rho) \leq \left(\frac{T}{6}\right)^2, \quad \forall P_p \in S_q, \quad (9.17)$$

where $\Sigma_{(\cdot)}(\rho, \rho)$ refers to the (ρ, ρ) element of the covariance matrix $\Sigma_{(\cdot)}$; $\rho = 1, 2, 3$ according to the direction where the dimensional tolerance applies (e.g. $\rho = 1$ for x direction, etc.); and T is the tolerance for this dimensional tolerance specification.

- (b) Specification verified by indirect measurements. For this case, the variability of the boundary point P_p in the controlled feature S_q is defined by the covariance matrix:

$$\Sigma_{\mathbf{Y}_{P_p}^{S_q}} = (\mathbf{C}_{P_p} \cdot \mathbf{K} \cdot [\mathbf{\Gamma}_{S_q} \quad \mathbf{\Gamma}_{S_m}]^T) \cdot \Sigma_{\mathbf{U}} \cdot (\mathbf{C}_{P_p} \cdot \mathbf{K} \cdot [\mathbf{\Gamma}_{S_q} \quad \mathbf{\Gamma}_{S_m}]^T)^T, \quad (9.18)$$

where matrix \mathbf{K} is defined in Appendix 9.2. Thus, the variability constraints of each boundary point at the direction where the tolerance applies can be defined as follows:

$$\Sigma_{\mathbf{Y}_{P_p}^{S_q}}(\rho, \rho) = (\mathbf{C}_{P_p} \cdot \mathbf{K} \cdot [\mathbf{\Gamma}_{S_q} \quad \mathbf{\Gamma}_{S_m}]^T) \cdot \Sigma_{\mathbf{U}} \cdot (\mathbf{C}_{P_p} \cdot \mathbf{K} \cdot [\mathbf{\Gamma}_{S_q} \quad \mathbf{\Gamma}_{S_m}]^T)^T(\rho, \rho) \leq \left(\frac{T}{6}\right)^2, \quad \forall P_p \in S_q \quad (9.19)$$

Eq. (9.17) and Eq. (9.19) are quality constraints for a boundary point P_p in the controlled feature S_q in case that the inspection is conducted by a direct or indirect measurement respectively. If the controlled feature is defined with $p = 1, \dots, P$ boundary points, then P quality constraints will be defined. As a general form, the quality constraints are defined by the inequality:

$$\mathbf{D}_p^q \leq \left(\frac{T_q}{6}\right)^2, \quad \forall P_p \in S_q, \quad (9.20)$$

where T_q is the tolerance specification of the controlled feature S_q , and the term \mathbf{D}_p^q is defined as shown above according to the type of measurement conducted to verify the part specification.

9.6 Summary of the optimization problem

As presented above, the process-oriented tolerancing becomes the generic optimization problem defined in Eq. (9.2). Its resolution assigns the tolerances of the maintainable KCCs in order to make the manufacturing cost minimum and keep the parts within specifications. Based on the set of various costs defined in previous subsections, this optimization problem can be re-formulated as:

$$\min_{\Delta l_{j,k}^D, \Delta l_k^w, V_{\tau,k}^\varrho} \left[\sum_{k=1}^N w_k^M \cdot \frac{(\sum_{j=1}^6 \frac{w_{j,k}^D}{\Delta l_{j,k}^D}) + C_k^f}{t_k^a} + \sum_{k=1}^N \sum_{\tau=1}^{\kappa_k} w_k^\tau \cdot \left(w_k^{res_\tau} \cdot \min_{\varrho=1, \dots, \mu_{\tau,k}} \left(\frac{(V_{\tau,k}^{max_\varrho} - V_{\tau,k}^\varrho)}{V_{\tau,k}^{max_\varrho}} \right) / t_{\tau,k}^b + \frac{w_k^{rep_\tau}}{t_{\tau,k}^b} \right) + \sum_{i=1}^M \frac{I_0 \cdot y_i^2}{(T_{yi}/2)^2} \right], \quad (9.21)$$

subjected to:

$$\begin{aligned} -3 \cdot \sigma_{T_k^s} &\leq \Delta T_k^s \leq +3 \cdot \sigma_{T_k^s}, \\ 0 &\leq V_{\tau,k}^\varrho \leq V_{\tau,k}^{max_\varrho}, \\ \Delta l_{min}^D &\leq \Delta l_{j,k}^D \leq \Delta l_{max}^D, \\ \mathbf{D}_{p,r}^q &\leq \left(\frac{T_r}{6} \right)^2, \end{aligned} \quad (9.22)$$

where $j = 1, \dots, 6$; $k = 1, \dots, N$; $i = 1, \dots, M$; $q = 1, \dots, Q$; $p = 1, \dots, P$; ϱ refers to the cutting edge of the τ th cutting-tool at the k th station with $\varrho = 1, \dots, \mu_{\tau,k}$ and $\tau = 1, \dots, \kappa_k$; \mathbf{D}_p^q refers to the constraints due to dimensional tolerance specifications; T_q the tolerance value applied to the controlled feature; and w_k^M and w_k^τ are weighting coefficients for the costs related to fixture maintenance actions and cutting-tool replacements respectively. The optimization problem is summarized in Figure 9.2.

9.7 Case study

9.7.1 Problem description

To demonstrate the proposed process-oriented tolerancing methodology, a case study that manufactures parts was conducted as shown in Figure 9.3, with a 3-station machining process, as illustrated in Figure 9.4. The datum features and the surfaces to be machined are summarized in Table 9.1. The position of fixture locators at each machining station is defined in Table 9.2. The KPCs of the part are the normal distance between S_3 and S_0 , denoted as KPC_1 , and the normal distance between S_8 and S_6 , denoted as KPC_2 . The dimensional tolerance requirements for both KPCs are $\pm 0.05 \text{ mm}$. The extended SoV model presented in Chapter 6 is applied to model the variation propagation along this MMP. In this extended model, the KCCs modeled are the deviation of the fixture locators, the wear of the cutting-tools and the spindle thermal expansion of the machine-tools. For

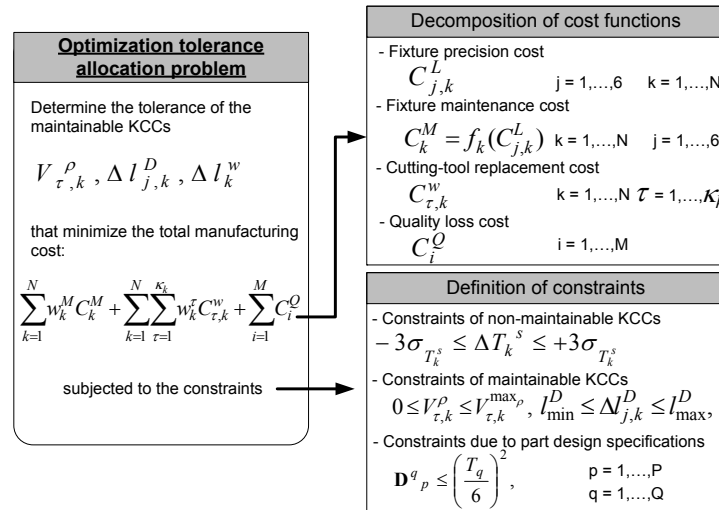


Figure 9.2: Process-oriented tolerancing problem.

this case study, the process-oriented tolerancing is formulated as:

$$\min_{\Delta l_{j,k}^D, \Delta l_k^w, V_{1,k}^{\rho}} \left[\sum_{k=1}^3 w_k^M \cdot \frac{(\sum_{j=1}^6 \frac{w_{j,k}^D}{\Delta l_{j,k}^D}) + C_k^f}{t_k^a} + \sum_{k=1}^3 w_k^1 \cdot \left(w_k^{res1} \cdot \min_{\varrho=1,2} \left(\frac{(V_{1,k}^{\max \varrho} - V_{1,k}^{\varrho})}{V_{1,k}^{\max \varrho}} \right) / t_{1,k}^b + \frac{w_k^{rep1}}{t_{1,k}^b} \right) + \sum_{i=1}^2 \frac{I_0 \cdot y_i^2}{(T_{y_i}/2)^2} \right], \quad (9.23)$$

for $j = 1, \dots, 6$; $k = 1, 2, 3$; $i = 1, 2$ and $\varrho = 1, 2$. One cutting-tool is used at each station, and each cutting-tool has two cutting edges ($\varrho = 1, 2$). Furthermore, the two edges of the cutting-tool are only used at station 3 (end milling operation), while in the first two stations, only one cutting edge is used (face milling operations). This cost function should be minimized subjected to the following 15 constraints:

- 3 constraints on the admissible thermal variation of the machine-tool spindle at each station. As these process variables are non-maintainable KCCs, it is assumed that the specific thermal variation range at each station in normal conditions is known from the shop-floor knowledge.
- 4 constraints on the maximum cutting-tool wear, one for each cutting-tool edge used. Note that in the third station, primary and secondary cutting-tool edges are used to machine the features S_8 and S_3 . Thus, two constraints should be defined at that station.
- 4 constraints on the dimensional tolerance of the KPC_1 , one constraint for each point that defines the boundaries of the S_3 plane (points P_1, P_2, P_3, P_4).
- 4 constraints on the dimensional tolerance of the KPC_2 , one constraint for each point that defines the boundaries of the S_8 plane (points P_1, P_4, P_5, P_6).

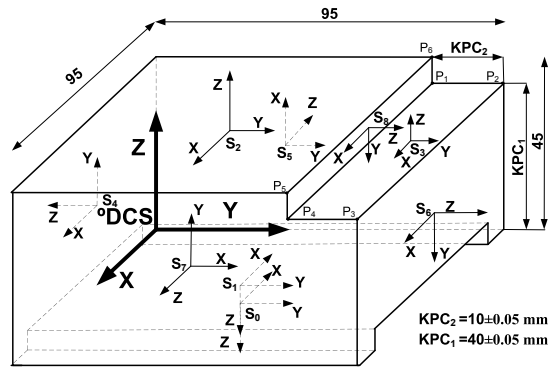


Figure 9.3: Final machined part for the case study (unit: mm).

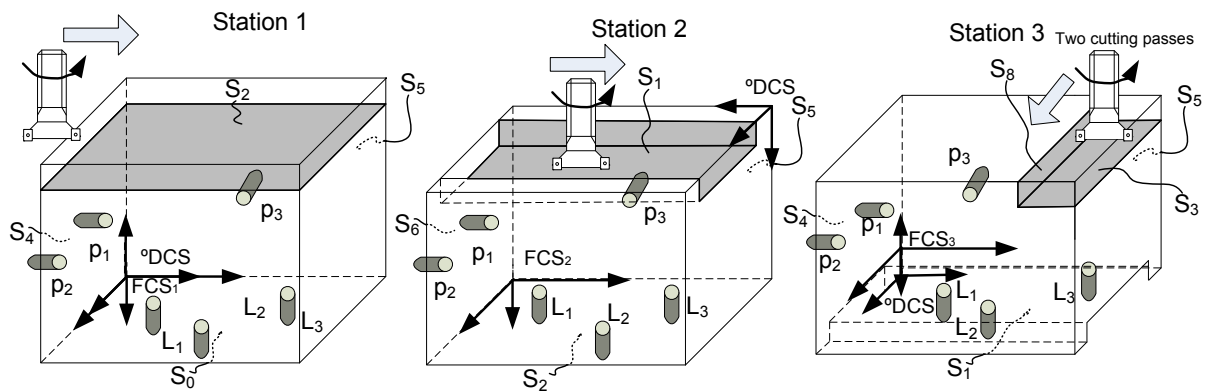


Figure 9.4: Case study. Part to be machined in a 3-station machining process.

Table 9.1: Machined features and datum features according to the 3-2-1 locating scheme at each station.

| Station | Datum features | Machined features | Cutting-tool |
|---------|----------------|-------------------|---|
| 1 | $S_0-S_4-S_5$ | S_2 | ADHX 110305, PVD TiAlN $\varnothing = 24.856$, $L = 111.322$ |
| 2 | $S_2-S_6-S_5$ | S_1 | ADHX 110305, PVD TiAlN $\varnothing = 24.856$, $L = 111.322$ |
| 3 | $S_1-S_4-S_5$ | S_3, S_8 | ADHX 110305, PVD TiAlN $\varnothing = 24.856$, $L = 111.322$ |
| 4 | $S_0-S_4-S_5$ | | Inspection station |

\varnothing : Tool diameter (mm); L : Tool length (mm)

Table 9.2: Nominal location ($\mathbf{t}_{F_k}^{\circ D}$) and orientation ($\varphi_{F_k}^{\circ D}$) of fixture CS at each station and fixture layout.

| Station | $\varphi_{F_k}^{\circ D}$ (rad) | $\mathbf{t}_{F_k}^{\circ D}$ (mm) | Locators w.r.t. F_k (mm) |
|---------|---------------------------------|-----------------------------------|--|
| 1 | $[-\pi/2, \pi, 0]$ | $[0, 0, 0]$ | $L_{1x} = 10, L_{1y} = 30, L_{2x} = 50, L_{2y} = 70, L_{3x} = 90, L_{3y} = 30,$ $p_{1y} = 30, p_{1z} = -35, p_{2y} = 70, p_{2z} = -35, p_{3x} = 50, p_{3z} = -20$ |
| 2 | $[-\pi/2, 0, 0]$ | $[0, 95, 45]$ | $L_{1x} = 10, L_{1y} = 30, L_{2x} = 50, L_{2y} = 70, L_{3x} = 90, L_{3y} = 30,$ $p_{1y} = 30, p_{1z} = -35, p_{2y} = 70, p_{2z} = -35, p_{3x} = 50, p_{3z} = -20$ |
| 3 | $[-\pi/2, \pi, 0]$ | $[0, 0, 2.5]$ | $L_{1x} = 10, L_{1y} = 30, L_{2x} = 50, L_{2y} = 70, L_{3x} = 90, L_{3y} = 30,$ $p_{1y} = 30, p_{1z} = -35, p_{2y} = 70, p_{2z} = -35, p_{3x} = 50, p_{3z} = -20$ |

Table 9.3: Nominal location ($\mathbf{t}_{S_i}^{\circ D}$) and orientation ($\varphi_{S_i}^{\circ D}$) of each feature.

| Feature | $\varphi_{S_i}^{\circ D}$ (rad) | $\mathbf{t}_{S_i}^{\circ D}$ (mm) |
|---------|---------------------------------|-----------------------------------|
| S_0 | $[0, \pi, 0]$ | $[47.5, 47.5, 0]$ |
| S_1 | $[0, \pi, 0]$ | $[47.5, 47.5, 2.5]$ |
| S_2 | $[0, 0, 0]$ | $[47.5, 42.5, 45]$ |
| S_3 | $[0, 0, 0]$ | $[47.5, 90, 40]$ |
| S_4 | $[\pi/2, -\pi/2, -\pi/2]$ | $[47.5, 0, 22.5]$ |
| S_5 | $[0, -\pi/2, 0]$ | $[0, 47.5, 22.5]$ |
| S_6 | $[\pi/2, \pi/2, -\pi/2]$ | $[47.5, 95, 20]$ |
| S_7 | $[0, \pi/2, \pi/2]$ | $[95, 47.5, 22.5]$ |
| S_8 | $[\pi/2, \pi/2, -\pi/2]$ | $[47.5, 85, 42.5]$ |

For this case study, the following assumptions are considered in relation with the progressive degradation in fixture devices and cutting-tools. In fixture devices, material wear rates are constant along the time as it can be observed in any maintenance handbook (e.g. [13]). However, fixture components are usually coated with special materials to minimize the wear rate. Thus, fixture devices usually tend to present a very low wear rate at the beginning of the production but increases when the coating is removed or deteriorated. In this case study and for the sake of simplicity, it is assumed that the fixture degradation at all stations can be modeled as a quadratic curve with the production time. Furthermore, it is assumed that all locators are degraded identically along the manufacturing process. Thus, the admissible maximum wear of fixture locators at station k can be modeled as $\Delta l_k^w = G_k \cdot (t_k^a)^2$, where G_k is a constant that indicates the wear rate of locators at station k and t_k^a is the operation time when a fixture maintenance action is conducted. In cutting-tools, tool wear is commonly modeled as a third-order polynomial function of machining time [14], although for high cutting speeds the wear rate increases and the flank wear tends to follow a second-order function [15]. In this case study, and without loss of generality, it is assumed that the cutting-tool flank wear curve follows a second-order polynomial function with machining time. Thus, the admissible maximum wear of the τ th cutting-tool at the station k can be modeled as $V_{\tau,k}^e = E_{\tau,k}^e \cdot t_k^b + F_{\tau,k}^e \cdot (t_k^b)^2$, where t_k^b is the machining time when a cutting-tool replacement is conducted. For this equation, $E_{\tau,k}^e$ and $F_{\tau,k}^e$ are coefficients that model the wearing rate of the ρ th cutting-tool edge of the τ th cutting-tool at station k .

Table 9.4: Numerical values for manufacturing tolerance allocation in the case study.

| STATION 1 & 2 ($k = 1, 2$) | | | | STATION 3 ($k = 3$) | | | |
|------------------------------|------------------------|--------------------|-------------------------------------|------------------------|-------------------------------------|------------------------|------------------------|
| Par. | Value | Par. | Value | Par. | Value | Par. | Value |
| $w_{j,k}^D$ | 3 u | C_k^f | 500 u | $w_{j,k}^D$ | 3 u | C_k^f | 500 u |
| w_k^{res1} | 20 u | w_k^{rep1} | 10 u | w_k^{res1} | 20 u | w_k^{rep1} | 10 u |
| w_k^M | 1 | w_k^1 | 1 | w_k^M | 1 | w_k^1 | 1 |
| $V_{1,k}^{max1}$ | 0.4 mm | G_k | $1.9 \cdot 10^{-7} \frac{mm}{hr^2}$ | $V_{1,k}^{max1}$ | 0.4 mm | $V_{1,k}^{max2}$ | 0.4 mm |
| $E_{1,k}^1$ | $0.0113 \frac{mm}{hr}$ | $F_{1,k}^1$ | $0.0019 \frac{mm}{hr^2}$ | G_k | $1.9 \cdot 10^{-7} \frac{mm}{hr^2}$ | $E_{1,k}^1, E_{1,k}^2$ | $0.0113 \frac{mm}{hr}$ |
| Δl_{min}^D | 0.010 mm | Δl_{max}^D | 0.4 mm | $F_{1,k}^1, F_{1,k}^2$ | $0.0019 \frac{mm}{hr^2}$ | $\pm 3\sigma_{T_k^s}$ | $\pm 5^\circ C$ |
| $\pm 3\sigma_{T_k^s}$ | $\pm 5^\circ C$ | | | Δl_{min}^D | 0.010 mm | Δl_{max}^D | 0.4 mm |

Par: Parameter. Additionally, $I_0 = 9.45 \text{ u/hr}$

9.7.2 Numerical analysis

A numerical analysis was conducted with the values presented in Table 9.4. The optimization problem with 24 variables (6 variables for each locator design tolerance at each station -18 variables in total-, one variable for the admissible maximum wear of fixture locators at each station -3 variables in total- and one variable for the admissible maximum wear of each cutting-tool edge -3 variables in total-) and 15 constraints was solved using two algorithms sequentially. Firstly, a genetic algorithm (GA) was run in Matlab from an initial population of 60 individuals for 15 generations in order to find a region close to the optimal solution. The initial population was created randomly by uniform distributions. Secondly, the solution provided by the GA algorithm was used as the initial point in a mesh adaptive direct search (MADS) algorithm for tuning the optimal result. The MADS algorithm was run until the tolerance mesh reached a value of $8 \cdot 10^{-3}$. The optimization procedure was repeated five times to ensure the convergence of the solution. Table 9.5 shows the parameters applied for both optimization algorithms according to the recommendations of the optimization toolbox user's guide from Matlab [16].

9.7.3 Comparison with a traditional process - oriented tolerancing methodology

The case study was analyzed by applying the proposed methodology and a process-oriented tolerancing methodology without the extended SoV model. The latter will be named traditional methodology hereafter. In the traditional methodology, the effects of other KCCs such as the cutting-tool wear and the thermal spindle expansion on part quality are not considered. The results of both methodologies are shown in Figure 9.5. Note that tolerances of locators p_1 , p_2 and p_3 at stations 2 and 3 and locator p_3 at station 3 are not shown since they do not affect any of the KPCs analyzed in this study and thus, they are set to the maximum tolerance range (Δl_{max}^D). In terms of costs, the proposed methodology estimates a manufacturing cost of 52.3 u/hr , where the fixture maintenance cost, the cutting-tool replacement cost and the expected part quality cost are 24.4 u/hr , 17.3 u/hr and 10.6 u/hr , respectively. On the other hand, the traditional methodology

Table 9.5: Parameters applied in the GA and the MADS algorithm.

| Genetic Algorithm (GA) | | | |
|--|--------------------|----------------------|------------------------------|
| Parameter | Value | Parameter | Value |
| Variables to optimize | 24 | Initial population | 60 |
| Initial population distributions | | Reproduction options | |
| $\Delta l_k^w, (\forall k)$ | Unif(0.002, 0.040) | Elite count | 10 |
| $\Delta l_{j,k}^D, (\forall j, \forall k)$ | Unif(0.010, 0.040) | Crossover fraction | 0.8 |
| $V_{1,k}^e, (\forall \varrho, \forall k)$ | Unif(0, 0.4) | Crossover function | Heuristic (ratio= 1.2) |
| Scaling function | Rank | Mutation function | Uniform ($P = 0.05$) |
| Selection options | Roulette | Stop criterium | Generations: 15 |
| Mesh Adaptive Direct Search Algorithm (MADS) | | | |
| Parameter | Value | Parameter | Value |
| Variables to optimize | 24 | Contraction | 0.5 |
| Initial mesh size | 1 | Poll method | Positive basis 2N |
| Maximum mesh size | Inf | Polling order | Consecutive |
| Maximum function evaluations | Inf | Stop criterium | Tol. mesh: $8 \cdot 10^{-3}$ |
| Expansion | 2 | | |

estimates a manufacturing cost of 21.0 u/hr , where the fixture maintenance cost, cutting-tool replacement cost and the expected part quality cost are 11.2 u/hr , 2.7 u/hr and 7.1 u/hr , respectively.

The results from both methodologies show some interesting conclusions. As it was expected, the traditional methodology underestimates the variability of the manufacturing process, so it tends to loose the tolerances allocated in the optimization problem resulting in a lower manufacturing cost. It expects a quality loss cost of 10.6 u/hr , however this result will be misleading since it overlooks other sources of variation, such as the thermal spindle expansion or the cutting-tool wear effect on part dimensions. Thus, the traditional methodology presents a locators design with lower precision (higher initial tolerances -see Figure 9.5 (a)-) with a lower frequency of maintenance actions (higher times between fixture maintenance actions -see Figure 9.5 (b)-) than the proposed methodology. Another important difference of both methodologies is presented in the cutting-tool replacement cost and thus, in the admissible cutting-tool wear values. The results show that the traditional methodology replaces the cutting-tools when the maximum tool wear is reached (0.4 mm of tool-wear according to vendor's recommendations) since this methodology only takes into account the admissible tool wear in the cost term of the optimization function (under-use cutting-tool cost and replacement cost) and overlooks its effect on dimensional part quality. Instead, the proposed methodology restricts the admissible tool wear (0.060, 0.057 and 0.057 mm in the first, second and third station respectively, see Figure 9.5 (c)) to ensure part quality but the cutting-tool replacement cost is increased.

In order to demonstrate the improvements of the proposed methodology over its traditional counterpart, 10,000 Monte Carlo simulations of two MMPs designed by the two

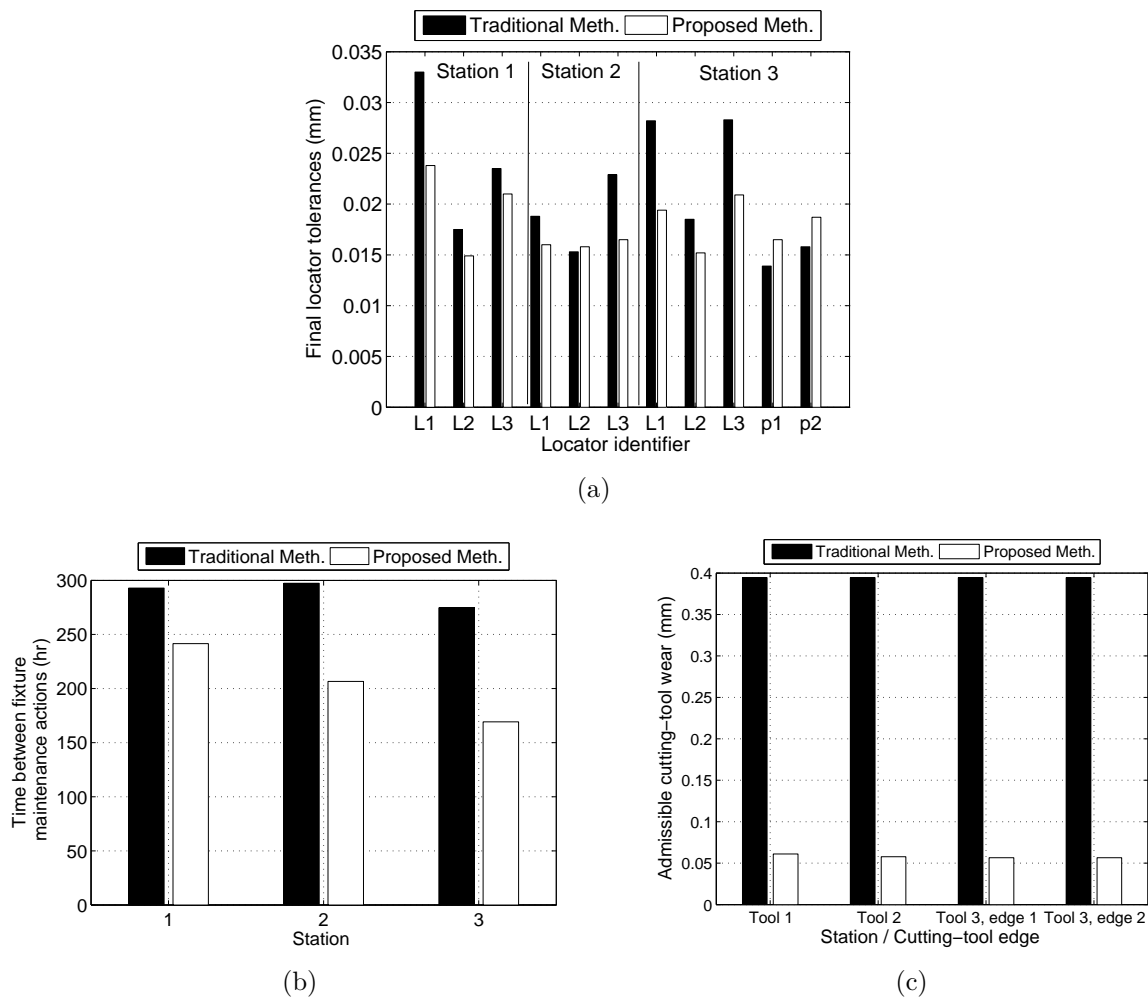


Figure 9.5: a) Design tolerances for fixture locators; b) Time between two consecutive fixture maintenance actions (in hours) at each machining station; c) Admissible cutting-tool wear at each cutting-tool edge before a cutting-tool replacement is conducted.

different tolerancing methodologies were conducted. For each simulation, a random value for each KCC is calculated according to its probability distribution function (p.d.f). For this case study, the initial locator precision is assumed normally distributed with mean 0 and standard deviation $\Delta l_{j,k}^D/6$; the fixture wear and cutting-tool wear are random variables with the p.d.f derived in Appendix 9.3; the measurement noise and un-modeled noise are also assumed normally distributed with mean 0's and standard deviation $0.005/6$ mm and $1.05 \cdot 10^{-3}/6$ rad for dimensional and orientational noise, respectively. The simulation results concluded that the number of conforming parts was notably different for the two methodologies, indicating the importance of the incorporation of process variations, such as thermal and cutting-tool wear variations, in the process-oriented tolerancing. The proposed methodology kept the 99.21% of the parts conforming to the dimensional specifications of KPC_1 and KPC_2 . However, the traditional methodology can only ensure a conforming rate of 82.45%. Therefore, by including the cutting-tool wear and spindle ther-

mal expansion effects on part quality, the process-oriented tolerance allocation improve the conforming rate by 16.76%. This result is also shown in the actual cost related to part quality loss. Although the expected quality loss is 10.6 u/hr and 7.1 u/hr for the proposed and traditional methodology respectively, both methodologies will present a higher quality loss cost due to the components added in the Monte Carlo simulation to simulate the effect of measurement noise and un-modeled components of the variation propagation itself. Besides these factors, the traditional methodology will present an additional component that will increase the actual quality loss cost since its variation propagation model does not consider the effect of cutting-tool wear or thermal variations, so one can expect a higher number of non-conforming parts. After Monte Carlo simulations, the actual quality loss for the proposed and the traditional methodology was 17.63 u/hr and 52.23 u/hr , respectively. This means that the final manufacturing cost by allocating the tolerances of the KCCs with the proposed methodology is increased to 59.41 u/hr , and with the traditional methodology, the manufacturing cost is increased to 66.16 u/hr , a 11.36% higher than the proposed one.

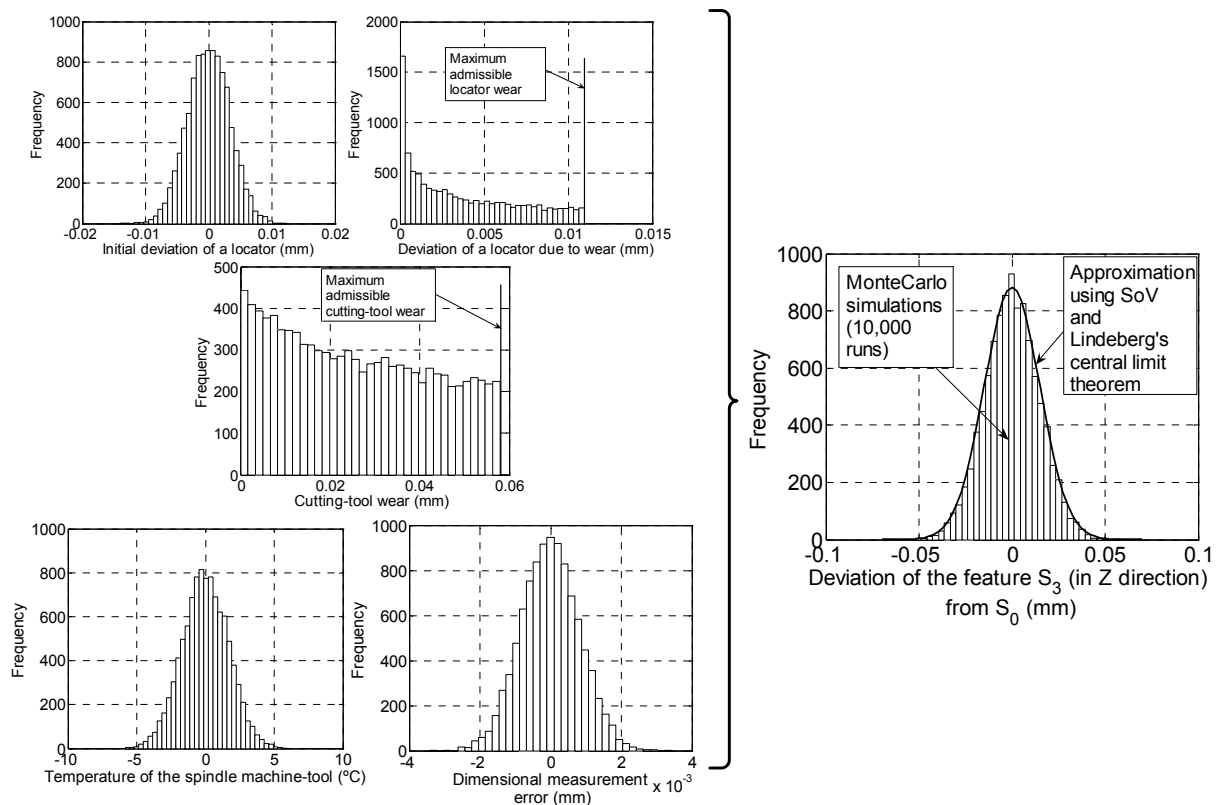


Figure 9.6: P.d.f of some of the KCCs for the case study and p.d.f of the resulting deviation of feature S_3 .

The Monte Carlo simulations also confirm that, for the case study, the Lindeberg's central limit theorem holds and the variability of the KPCs can be approximated to a normal distribution despite some KCCs are not normally distributed. Figure 9.6 shows the p.d.f of the deviation of feature S_3 in Z direction according to Monte Carlo simulations

and according to the approximation used in the chapter assuming that Lindeberg's central limit theorem holds.

9.8 Conclusions

In this chapter, a process-oriented tolerancing methodology has been developed to incorporate additional KCCs and cost elements that had not been included in previous works. In order to add these additional elements, the extended SoV model was applied. Through this model, the process-oriented tolerancing can deal with maintainable KCCs, such as the allowable cutting-tool wear or the tolerances of the fixture locators, and non-maintainable KCCs, such as the thermal state of the machine-tool spindle. For tolerance allocation purposes, only the maintainable KCCs are considered whereas the variability range of non-maintainable KCCs are estimated through shop-floor knowledge. Furthermore, the integration of the fixture maintenance policies and the cutting-tool replacement policies into the process-oriented tolerance allocation problem is also conducted in order to reach a real minimum manufacturing cost. A case study was conducted to demonstrate the potential of the proposed process-oriented tolerancing methodology. The results revealed that, without including KCCs related to thermal state of the spindles and cutting-tool wear, the tolerance allocation decisions may be misleading, increasing both the number of non-conforming parts and the final manufacturing cost.

9.9 Appendix 9.1: Part quality constraints in direct measurements

The dimensional deviation of features inspected by a direct measurement can be estimated by Eq. (9.1) (and their variance with Eq. (9.15)) if one can estimate the deviations of process variables. However, these equations express the deviation of the local coordinate system (LCS) of the feature inspected w.r.t. the GD&T reference datum, but the deviation of all boundary points of the feature inspected is needed in order to analyze if the feature is within the tolerance specification. Thus, the boundary point deviations w.r.t. the GD&T reference datum must be evaluated knowing the LCS deviation of the inspected feature. This relationship can be known applying the Corollary 1 presented in Appendix 4.1. According to this corollary, given two features 1 and 2 and a global coordinate system R , and given the deviation of the feature 1 w.r.t. R , \mathbf{x}_1^R , and the deviation of feature 2 w.r.t. feature 1, \mathbf{x}_2^1 , then:

$$\mathbf{x}_2^R = \begin{pmatrix} (\mathbf{R}_{o_2}^{\circ 1})^T & -(\mathbf{R}_{o_2}^{\circ 1})^T \cdot (\hat{\mathbf{t}}_{o_2}^{\circ 1}) & \mathbf{I}_{3 \times 3} & \mathbf{0}_{3 \times 3} \\ \mathbf{0}_{3 \times 3} & (\mathbf{R}_{o_2}^{\circ 1})^T & \mathbf{0}_{3 \times 3} & \mathbf{I}_{3 \times 3} \end{pmatrix} \begin{pmatrix} \mathbf{x}_1^R \\ \mathbf{x}_2^1 \end{pmatrix}, \quad (9.24)$$

where $\mathbf{R}_{o_2}^{\circ 1}$ is the nominal rotational matrix between feature 1 and 2; $\hat{\mathbf{t}}_{o_2}^{\circ 1}$ is the skew symmetric matrix obtained from the nominal location vector $\mathbf{t}_{o_2}^{\circ 1} = [t_{o_2x}^{\circ 1}, t_{o_2y}^{\circ 1}, t_{o_2z}^{\circ 1}]$ and it is defined as $\hat{\mathbf{t}}_{o_2}^{\circ 1} = [[0, -t_{o_2z}^{\circ 1}, t_{o_2y}^{\circ 1}]; [t_{o_2z}^{\circ 1}, 0, -t_{o_2x}^{\circ 1}]; [-t_{o_2y}^{\circ 1}, t_{o_2x}^{\circ 1}, 0]]$; and $\mathbf{I}_{3 \times 3}$ is a 3×3 identity matrix.

Applying this corollary and assuming rigid parts, the deviation of the boundary points defined in step 2 w.r.t. the GD&T reference datum ($\mathbf{x}_{P_p^{S_q}}^{S_m}$) is related to the deviation of the LCS attached to the controlled feature w.r.t. the GD&T reference datum ($\mathbf{x}_{S_q}^{S_m}$) by the matrix \mathbf{C}_{P_p} according to the following equation:

$$\mathbf{x}_{P_p^{S_q}}^{S_m} = \mathbf{C}_{P_p} \cdot \mathbf{x}_{S_q}^{S_m}, \quad \forall P_p \in S_q, \quad (9.25)$$

where

$$\mathbf{C}_{P_p} = \begin{pmatrix} \mathbf{I}_{3 \times 3} & -\left(\hat{\mathbf{t}}_{P_p^{S_q}}^{\circ S_q} \right) \\ \mathbf{0}_{3 \times 3} & \mathbf{I}_{3 \times 3} \end{pmatrix}. \quad (9.26)$$

This result is obtained straightforwardly from Corollary 1 in Appendix 4.1 since by assuming rigid parts, the DMV $\mathbf{x}_{P_p^{S_q}}^{S_q}$ is always zero.

9.10 Appendix 9.2: Part quality constraints in indirect measurements

For indirect measurements, a controlled feature and a GD&T reference datum feature are measured in the inspection station w.r.t. the measurement datum. Thus, Eq. (9.1) gives us the deviation of the LCS of both features w.r.t. the measurement datum. However, the deviation of the boundary points of the controlled feature w.r.t. the GD&T reference datum feature is needed. Thus, the deviation of the LCS of the controlled feature must be expressed w.r.t. the LCS of the GD&T reference datum feature. For this purpose, the Corollary 2 presented in Appendix 4.1 can be applied. According to this corollary, given two features 1 and 2 and a global coordinate system R , and given the deviation of feature 1 w.r.t. R , \mathbf{x}_1^R , and the deviation of feature 2 w.r.t. R , \mathbf{x}_2^R , then:

$$\mathbf{x}_2^1 = \begin{pmatrix} -(\mathbf{R}_{\circ 2}^{\circ 1})^T & (\mathbf{R}_{\circ 2}^{\circ 1})^T \cdot \left(\hat{\mathbf{t}}_{\circ 2}^{\circ 1} \right) & \mathbf{I}_{3 \times 3} & \mathbf{0}_{3 \times 3} \\ \mathbf{0}_{3 \times 3} & -(\mathbf{R}_{\circ 2}^{\circ 1})^T & \mathbf{0}_{3 \times 3} & \mathbf{I}_{3 \times 3} \end{pmatrix} \begin{pmatrix} \mathbf{x}_1^R \\ \mathbf{x}_2^R \end{pmatrix}. \quad (9.27)$$

Applying this corollary, the DMV of the controlled feature w.r.t. the GD&T reference datum ($\mathbf{x}_{S_q}^{S_m}$) is related to the DMVs of the GD&T reference datum and the controlled feature w.r.t. the measurement datum feature ($\mathbf{x}_{S_m}^{S_D}$ and $\mathbf{x}_{S_q}^{S_D}$ respectively) by the matrix \mathbf{K} as follows:

$$\mathbf{x}_{S_q}^{S_m} = \mathbf{K} \cdot [\mathbf{x}_{S_m}^{S_D} \quad \mathbf{x}_{S_q}^{S_D}]^T, \quad (9.28)$$

where

$$\mathbf{K} = \begin{pmatrix} -\left(\mathbf{R}_{\circ S_q}^{\circ S_m} \right)^T & \left(\mathbf{R}_{\circ S_q}^{\circ S_m} \right)^T \cdot \left(\hat{\mathbf{t}}_{\circ S_q}^{\circ S_m} \right) & \mathbf{I}_{3 \times 3} & \mathbf{0}_{3 \times 3} \\ \mathbf{0}_{3 \times 3} & -\left(\mathbf{R}_{\circ S_q}^{\circ S_m} \right)^T & \mathbf{0}_{3 \times 3} & \mathbf{I}_{3 \times 3} \end{pmatrix}. \quad (9.29)$$

9.11 Appendix 9.3: P.d.f. of tooling wear variables

Fixture wear.

Fixture wear is assumed to follow a quadratic curve with operation time expressed by the equation

$$w_k^l = G_k \cdot (t_k^{op})^2, \quad (9.30)$$

where w_k^l is the locator wear at the operation time t_k^{op} (note that if $t_k^{op} = t_k^a$, then the locator wear is the admissible maximum wear and thus, $w_k^l = \Delta l_k^w$), and $t_k^{op} \in [0, t_k^a]$. Assuming a production of a large number of parts and a random inspection process during production, the variable t_k^{op} related to the inspected parts can be considered as a uniform random variable in the range of $[0, t_k^a]$. Thus, the p.d.f of fixture wear in the k th station can be obtained by the change of variable formula [6]. By this formula, if $y = r(x)$ where r is differentiable and $f_X(x)$ is the p.d.f of x , then the p.d.f of y is calculated as:

$$g(y) = f_X(r^{-1}(y)) \cdot \left| \frac{dr^{-1}(y)}{dy} \right|. \quad (9.31)$$

Applying this formula, the p.d.f of fixture wear is

$$g(w_k^l) = \frac{1}{t_k^a} \cdot \left| \frac{1}{\sqrt{4G_k \cdot w_k^l}} \right|, \quad (9.32)$$

where $w_k^l \in [0, \Delta l_k^w]$ and $\Delta l_k^w = G_k \cdot (t_k^a)^2$. For the numerical values applied in the case study (Table 9.4), the mean and variance value of this process variable can be obtained as:

$$E(w_k^l) = 0.169 \cdot 10^{-9} \cdot (t_k^a)^3, \quad (9.33)$$

$$Var(w_k^l) = 0.175 \cdot 10^{-24} \cdot (t_k^a)^5 (429 \cdot (t_k^a)^2 - 326000 \cdot t_k^a + 0.112 \cdot 10^9). \quad (9.34)$$

Cutting-tool wear.

The cutting-tool wear variable is assumed to follow a quadratic curve with the machining time in the form:

$$w_{\tau,k}^e = E_{\tau,k}^e \cdot t_{\tau,k}^m + F_{\tau,k}^e \cdot (t_{\tau,k}^m)^2, \quad (9.35)$$

where $w_{\tau,k}^e$ is the cutting-tool wear at the machining time $t_{\tau,k}^m$, and $t_{\tau,k}^m \in [0, t_{\tau,k}^{b_e}]$. Following the same procedure as shown above, the p.d.f of the cutting-tool wear variable is defined as:

$$h(w_{\tau,k}^e) = \frac{1}{t_{\tau,k}^{b_e}} \cdot \left| \frac{1}{\sqrt{(E_{\tau,k}^e)^2 + 4 \cdot F_{\tau,k}^e \cdot w_{\tau,k}^e}} \right|, \quad (9.36)$$

where $w_{\tau,k}^e \in [0, V_{\tau,k}^e]$ and $V_{\tau,k}^e = E_{\tau,k}^e \cdot t_{\tau,k}^{b_e} + F_{\tau,k}^e \cdot (t_{\tau,k}^{b_e})^2$. For the numerical case study, the

mean and variance value of this process variable are defined as follows:

$$\begin{aligned}
 E(w_{\tau,k}^e) &= 0.00322 + \left(\sqrt{12800 + 8590t_{\tau,k}^{b_e} + 1440(t_{\tau,k}^{b_e})^2} \right) \cdot \left(2.85 \cdot 10^{-5} + 0.959 \cdot 10^{-5}t_{\tau,k}^{b_e} + 0.161 \cdot 10^{-5} \left(t_{\tau,k}^{b_e} \right)^2 \right), \quad (9.37) \\
 Var(w_{\tau,k}^e) &= \left(\sqrt{12800 + 8590t_{\tau,k}^{b_e} + 1440 \left(t_{\tau,k}^{b_e} \right)^2} \right) \cdot \left(0.857 \cdot 10^{-6} - 0.271 \cdot 10^{-6}t_{\tau,k}^{b_e} + 0.105 \cdot 10^{-7} \left(t_{\tau,k}^{b_e} \right)^2 + 0.209 \cdot 10^{-7} \left(t_{\tau,k}^{b_e} \right)^3 \right. \\
 &\quad + 0.260 \cdot 10^{-8} \left(t_{\tau,k}^{b_e} \right)^4 + 0.171 \cdot 10^{-9} \left(t_{\tau,k}^{b_e} \right)^5 + 0.955 \cdot 10^{-11} \left(t_{\tau,k}^{b_e} \right)^6 + 0.857 \cdot 10^{-6} \left. \right) - 9.69 \cdot 10^{-5} - 0.196 \cdot 10^{-5}t_{\tau,k}^{b_e} \\
 &\quad + 0.910 \cdot 10^{-5} \left(t_{\tau,k}^{b_e} \right)^2 + 0.135 \cdot 10^{-5} \left(t_{\tau,k}^{b_e} \right)^3 - 0.647 \cdot 10^{-6} \left(t_{\tau,k}^{b_e} \right)^4 - 0.153 \cdot 10^{-6} \left(t_{\tau,k}^{b_e} \right)^5 - 0.858 \cdot 10^{-8} \left(t_{\tau,k}^{b_e} \right)^6 \quad (9.38)
 \end{aligned}$$

References

- [1] P. Drake, Dimensioning and tolerancing handbook, McGraw-Hill, 1999.
- [2] Y. Ding, J. Jin, D. Ceglarek, J. Shi, Process-oriented tolerancing for multi-station assembly systems, IIE Transactions 37 (2005) 493–508.
- [3] Y. Chen, Y. Ding, J. Jin, D. Ceglarek, Integration of process-oriented tolerancing and maintenance planning in design of multistation manufacturing processes, IEEE Transactions on Automation Science and Engineering 3 (4) (2006) 440–453.
- [4] Q. Huang, J. Shi, Simultaneous tolerance synthesis through variation propagation modeling of multistage manufacturing processes, NAMRI/SME Transactions 31 (2003) 515–522.
- [5] J. Liu, J. Shi, S. J. Hu, Quality-assured setup planning based on the stream-of-variation model for multi-stage machining processes, IIE Transactions 41 (12) (2009) 323–334.
- [6] F. M. Dekking, C. Kraaikamp, H. P. Lopuhaä, L. E. Meester, A Modern Introduction to Probability and Statistics: Understanding Why and How, Springer, 2005.
- [7] P. Billingsley, Probability and measure, 3rd Edition, John Wiley & Sons Inc., New York, 1995.
- [8] P. Joshi, Jigs and Fixtures Design Manual, McGraw-Hill, 2003.
- [9] G. Taguchi, S. Chowdhury, Y. Wu, Taguchi's Quality Engineering Handbook, John Wiley and Sons Ltd, 2004.
- [10] J. Shi, Stream of Variation Modeling and Analysis for Multistage, CRC Press Taylor and Francis Group, 2007.
- [11] S. Zhang, Z. Sha, R. Kang, A physical machining accuracy predicting model in turning, Key Engineering Materials 329 (2007) 675–680.
- [12] J. P. Loose, Q. Zhou, S. Y. Zhou, D. Ceglarek, Integrating GD&T into dimensional variation models for multistage machining processes, International Journal of Production Research 48 (11) (2010) 3129–3149.

-
- [13] H. P. Bloch, F. K. Geitner, Machinery Component Maintenance and Repair, Gulf Professional Publishing, 2003.
 - [14] D. Wang, M. Zuo, K. Qi, M. Liang, On-line tool adjustment with adaptive tool wear function identification, International Journal of Production Research 34:9 (1996) 2499–2515.
 - [15] ASM-Handbook, ASM Metals Handbook, 9th Edition, Vol. 16 Machining, 2003.
 - [16] The Mathworks, Matlab Optimization Toolbox User's Guide, Available via <http://www.mathworks.com/help/toolbox/gads/>. Accessed 15 March 2011 (2011).

Conclusions and future work

The research presented in this dissertation is concluded by summarizing the main achievements and original contributions. Potential future studies are also discussed in this section.

10.1 Conclusions

Present and future markets demand significantly shorter new product realization cycles and higher performance in manufacturing systems. A key issue to reduce total production time (product development time, manufacturing lead time and ramp-up time) and improve part quality is the integration of product and process knowledge. This product-process integration enables engineers to: i) shrink both product and process development time and launch time significantly; ii) eliminate or reduce changes in product design after the design phase; and iii) rapidly identify and isolate root causes of all faults during ramp-up time. Nowadays, the lack of comprehensive knowledge-based methods for predicting and improving product quality and process performance is one of the major barriers to achieving further progress in manufacturing variation reduction, and the main cause preventing manufacturers from achieving high rates of correct products the first time they are produced. Future manufacturing practices are expected to become more of a science, where the fundamental understanding of manufacturing will enable many future improvements in product and process design, modeling and simulation. The advances in the understanding and modeling of complex manufacturing processes such as multi-station machining processes will be able to make the first and every product correct avoiding expensive and time-consuming practices of trial and error in product and process design.

Recent research efforts have been aimed toward deriving mathematical models to relate manufacturing sources of variation with part quality errors in multi-station machining systems in order to integrate design and manufacturing knowledge. Such integration would make it possible to create a large number of applications to improve product and process design and manufacturing in areas such as fault diagnosis, best placement of inspection stations, process planning, dimensional control and process-oriented tolerancing. However, nowadays there are still important limitations on the development of these models and even some of their potential applications have still not been studied in detail. The comprehensive research work described in this dissertation contributes to overcome some of the current limitations by extending the manufacturing variation models to include specific

sources of errors related to machine-tools and machining operations. Furthermore, novel applications for process and product design improvement that have not yet been studied in the literature have also been proposed, studied and validated. The major contributions of this dissertation can be summarized as follows.

The first part of the dissertation presented a comprehensive literature review in order to conduct a detailed analysis of the sources of machining errors that produce macro- and/or micro-geometric errors on machined surfaces. The literature review reported not only the main sources of errors in machining processes but also the main analytical/physical models applied to estimate the resulting part quality. The formulation of the models analyzed was adapted in order to be consistent and the relationships between the models were described to facilitate the prediction of final part quality. In addition to the main physical models applied in the literature, more complex models based on regressions and artificial intelligence were also briefly described in order to provide a general picture of part quality prediction in uni-station machining systems. In this part of the dissertation, besides the study of sources of errors and models in uni-station systems, a review of part quality prediction in multi-station machining systems was also conducted. At this point, two 3D manufacturing variation models applied in the literature (the Stream of Variation model – SoV – and the Model of Manufactured Part – MoMP) were presented and analyzed in detail. The derivation of both models for practical purposes was described using two examples and the main advantages, drawbacks and potential applications of each model were studied. Therefore, the first part of the dissertation offered a comprehensive literature review for the prediction of geometric part quality in uni- and multi-station machining processes.

The second and third parts of the dissertation deal with the extension and application of the SoV model for part quality prediction and improvement in multi-station machining processes. In the second part, an experimental study showed how important part quality errors due to machining-induced errors, such as thermal errors or cutting-tool wear-induced errors, can be. This experimental work confirmed the necessary inclusion of physical models of machining-induced errors into the SoV model. This inclusion means the extension of the current SoV model, including new key control characteristics in the model derivation, such as the thermal variation of the machine-tool structure, the admissible cutting-tool wear during the process, etc. The extension of the SoV model is formulated in detail at the end of the second part of the thesis, and opens up an important field of application for part quality prediction and improvement in multi-station machining processes.

Finally, the third part of the dissertation presents some potential applications of the current SoV model and its extended version for part quality improvement. The first application showed how to apply the SoV model together with sensor-based fixtures when there are CNC machine-tools in the multi-station machining system in order to modify the cutting-tool path and partially compensate the expected part quality error. In this research work the design of sensor-based fixtures was also studied in order to maximize the information obtained from sensors about fixture-induced errors. The second application dealt with the evaluation and improvement of manufacturing process plans by

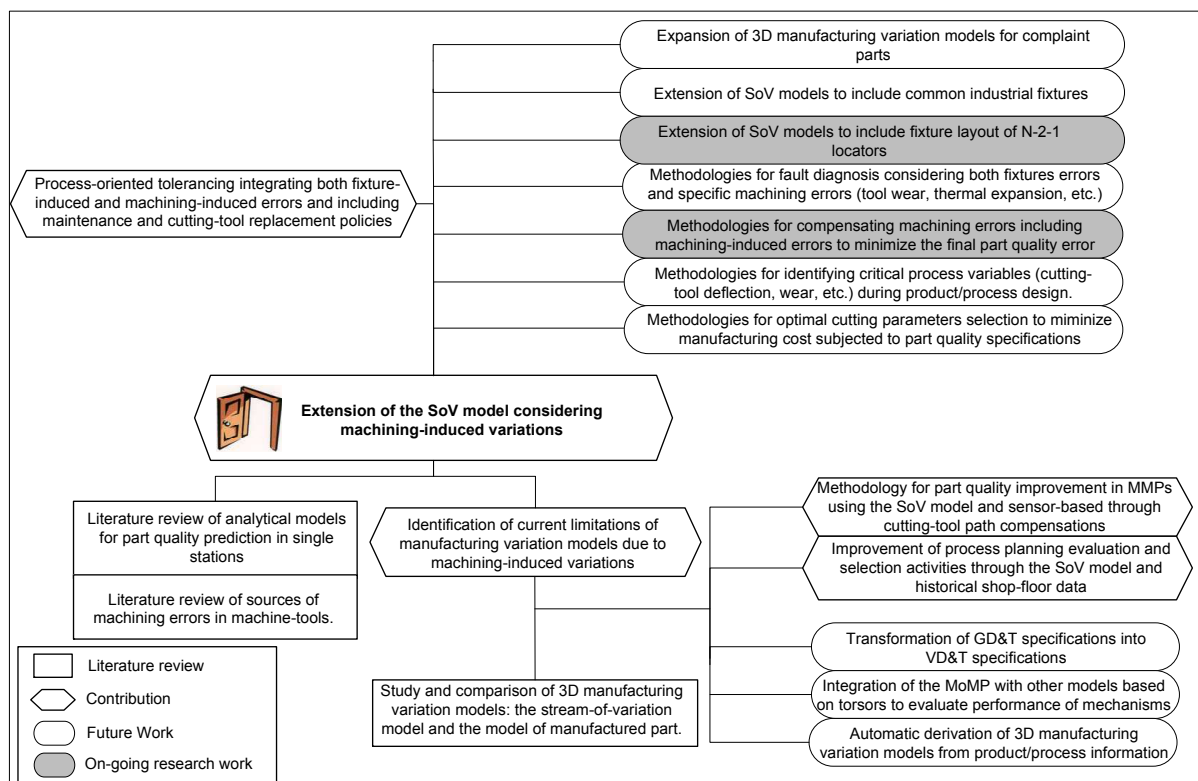


Figure 10.1: Summary of thesis contributions, suggested future work and on-going research work.

integrating the SoV model and historical shop-floor quality data. The main contribution of this work was the use of shop-floor quality data to extract machine-tool capabilities and the development of a systematic methodology based on sensitivity indices to detect critical components (critical locators and critical machine-tool capabilities) for each process plan. Finally, the third application showed the use of the extension of the SoV model to improve process-oriented tolerancing in multi-station machining processes. It was remarked that current practices in process-oriented tolerancing only allocated the admissible variability of fixture locators to ensure a specific geometric part quality minimizing the manufacturing cost. Thus, other important sources of variability such as those related to machining-induced variations were not taken into account and so part quality could not be ensured and the total manufacturing cost is not a real minimum. The application of the extended SoV model, which includes the machining-induced errors in the 3D manufacturing variation model, contributes to the development of a more general process-oriented tolerance allocation problem. This is accomplished by the fact that, in the allocation problem, it considers new variables such as the admissible cutting-tool wear or spindle thermal expansion in the machining stations to ensure geometric part quality with a minimum manufacturing cost.

Figure 10.1 summarizes the contributions of the dissertation and outlines the potential future works as well as the on-going research being carried out at Universitat Jaume I.

10.2 Suggestions for future work

This dissertation has presented the topic of part quality prediction and improvement in multi-station machining processes. Besides the study of different 3D manufacturing variation models and the extension of one of them, three important applications have been presented in detail for the improvement of multi-station machining processes. These three applications are only a sample of the potential improvement of multi-station processes that could be achieved with the application of the current SoV model and its extended version. In the author's opinion, novel applications with the SoV extended model can be numerous, since it is an emerging field of research. For instance, some issues worth investigating are:

- Fault diagnosis in MMPs when faults due to machining-induced errors occur. Currently, fault diagnosis has been mainly focused only on fixture faults. An example of this fault diagnosis would be the identification of an excessive cutting-tool wear in one station that produces a part quality error at the end of the process.
- Identification during the manufacturing design process of critical process variables that can prevent the desired part quality from being reached. This information can help the designer to evaluate alternatives such as the use of robust cutting-tools (e.g., milling cutters instead of end mills to avoid cutting-deflections), the use of machine-tools with thermal compensations, and the definition of admissible cutting-tool wear values in specific machining operations.
- Compensations of machining errors (others than fixture errors) to minimize the final part quality error at the end of the MMP. For instance, the estimation of how a specific level of cutting-tool wear or cutting-force values may deviate the final functional feature of a part at the end of the MMP can lead to the modification of cutting-tool trajectories in order to compensate for their impact. This topic is an on-going research work currently being carried out at Universitat Jaume I.
- Global optimization of cutting parameters, such as depth of cut, cutting speed, feed rates, etc., in order to minimize the manufacturing cost subjected to part quality specifications. For instance, the selection of a specific feed rate and depth of cut may produce an increase in cutting-tool deflection and thus an important part quality error can be produced. The consideration of how cutting parameters influence on the process variables in the MMP, such as spindle thermal expansion, cutting-tool wear or cutting-tool deflections, can be included in the manufacturing variation model to analyze the global optimum of the manufacturing process.

Besides the investigation of the potential applications of the extended SoV model listed above, this doctoral research also encourages investigation in other fields that are promising due to the lack of research work presented in the literature. Among them, the following research topics are remarked:

- Current 3D manufacturing variation models (SoV and MoMP) should be expanded to analyze manufacturing variation when complaint parts are machined. Currently, these models are restricted to solid rigid parts.

- Current 3D manufacturing variation models (SoV and MoMP) should be expanded to incorporate form errors. Currently, these models assumed that datum surfaces and locating surfaces are perfect in form (only dimensional and orientation errors are present) and the error at the machined surface does not include form errors.
- SoV models only deal with fixtures composed of locators, but their extension to cover common industrial fixtures such as vises or chucks should also be addressed. This extension is partly conducted in Chapter 3, where fixture and datum feature errors using fixtures based on locating surfaces are modeled. However, this modelization should be included into the derivation of the SoV model.
- SoV models can deal with non-orthogonal 3-2-1 fixture layouts but common over-constrained fixture schemes in industry, such as N-2-1 layouts, remain unaddressed. This topic is an on-going research work currently being conducted at Universitat Jaume I.
- Despite the recent efforts in transforming GD&T specifications related to positional, orientation and form tolerances into VD&T, SoV models require the transformation of other GD&T specifications, such as the profile of a surface or the inclusion of material condition modifiers.
- The MoMP model should be integrated with models for variation analysis in mechanisms based on the SDT approach. This integration can lead to the evaluation of the performance of a mechanism by considering the manufacturing variability in each part of the mechanism, and analyzing the impact of fixture or machine-tool capabilities on the mechanism performance.
- The complex derivation of 3D manufacturing variation models should be overcome by developing algorithms for their automatic derivation given data from product design and manufacturing processes.

These future research topics will help reduce total production time and improve part quality in multi-station machining systems leading the manufacturers to be able to transit from design concept to a finished product with absolute certainty of a correct result from the first unit onward.

Appendix: Matlab code

11.1 SoV model and case study of Chapter 5

```
%%%%%%%%%%%%%%%%%%%%%%%%%%%%%%%%%%%%%%%%%%%%%%%%%%%%%%%%%%%%%%%%%%%%%%%%
% CHAPTER 5: LIMITATIONS OF THE CURRENT SOV. CASE STUDY
%%%%%%%%%%%%%%%%%%%%%%%%%%%%%%%%%%%%%%%%%%%%%%%%%%%%%%%%%%%%%%%%%%%%%%%%
% MAIN PROGRAM %%%%%%%%%%%%%%%%%%%%%%%%%%%%%%%%%%%%%%%%%%%%%%%%%%%%%%%%%%%%%%%%%%%%%%%%%
%%%%%%%%%%%%%%%%%%%%%%%%%%%%%%%%%%%%%%%%%%%%%%%%%%%%%%%%%%%%%%%%%%%%%%%%

clear all;

%%%%%%%%%%%%%%%%%%%%%%%%%%%%%%%%%%%%%%%%%%%%%%%%%%%%%%%%%%%%%%%%%%%%%%%%
% General parameters %%%%%%%%%%%%%%%%%%%%%%%%%%%%%%%%%%%%%%%%%%%%%%%%%%%%%%%%%%%%%%%%%%%%%%%%%

parameters;

%%%%%%%%%%%%%%%%%%%%%%%%%%%%%%%%%%%%%%%%%%%%%%%%%%%%%%%%%%%%%%%%%%%%%%%%
% Homogeneous transformations %%%%%%%%%%%%%%%%%%%%%%%%%%%%%%%%%%%%%%%%%%%%%%%%%%%%%%%%%%%%%%%%%%%%%%%%%

H_transforms;

%%%%%%%%%%%%%%%%%%%%%%%%%%%%%%%%%%%%%%%%%%%%%%%%%%%%%%%%%%%%%%%%%%%%%%%%
% Derivation of the SoV model for the case study %%%%%%%%%%%%%%%%%%%%%%%%%%%%%%%%%%%%%%%%%%%%%%%%%%%%%%%%%%%%%%%%%%%%%%%%%

%%%%%%%%%%%%%%%%%%%%%%%%%%%%%%%%%%%%%%%%%%%%%%%%%%%%%%%%%%%%%%%%%%%%%%%%
% STATION 1 %%%%%%%%%%%%%%%%%%%%%%%%%%%%%%%%%%%%%%%%%%%%%%%%%%%%%%%%%%%%%%%%%%%%%%%%%

% Sources of variation at station 1. Locator errors.
%Station{1}.uf=[-0.041 0 0.096 -0.018 -0.0042 0];
%Station{1}.uf=[-0.008 0 0.012 -0.018 -0.0042 0];
%Station{1}.uf=[-0.024 0 -0.037 -0.018 -0.0042 0];
Station{1}.uf=[0 0 0 0 0 0];

% Matrix A(1) and B(1)
matrix_station_1;

%%%%%%%%%%%%%%%%%%%%%%%%%%%%%%%%%%%%%%%%%%%%%%%%%%%%%%%%%%%%%%%%%%%%%%%%
% STATION 2 %%%%%%%%%%%%%%%%%%%%%%%%%%%%%%%%%%%%%%%%%%%%%%%%%%%%%%%%%%%%%%%%%%%%%%%%%

% Sources of variation at station 2. Locator errors.
```



```

% CHAPTER 5: LIMITATIONS OF THE CURRENT SOV. CASE STUDY
%%%%%%%%%%%%%%%%%%%%%%%%%%%%%%%%%%%%%%%%%%%%%%%%%%%%%%%%%%%%%%%%%%%%%%%%
% SUBPROGRAM: PARAMETERS.M %%%%%%%%%
%%%%%%%%%%%%%%%%%%%%%%%%%%%%%%%%%%%%%%%%%%%%%%%%%%%%%%%%%%%%%%%%%%%%%%%%

% Number of features
M=9;

%%%%%%%%%%%%%%%%%%%%%%%%%%%%%%%%%%%%%%%%%%%%%%%%%%%%%%%%%%%%%%%%%%%%%%%%
% Position and orientation of each feature w.r.t. R. Euler rotation ZYZ order
%%%%%%%%%%%%%%%%%%%%%%%%%%%%%%%%%%%%%%%%%%%%%%%%%%%%%%%%%%%%%%%%%%%%%%%%

% Feature S0
alfa_R_S0=0;
beta_R_S0=pi;
gamma_R_S0=0;
t1x_R_S0=47.5;
t1y_R_S0=47.5;
t1z_R_S0=0;

% Feature S1
alfa_R_S1=0;
beta_R_S1=pi;
gamma_R_S1=0;
t1x_R_S1=47.5;
t1y_R_S1=47.5;
t1z_R_S1=2.5;

% Feature S2
alfa_R_S2=0;
beta_R_S2=0;
gamma_R_S2=0;
t1x_R_S2=47.5;
t1y_R_S2=42.5;
t1z_R_S2=45;

% Feature S3
alfa_R_S3=0;
beta_R_S3=0;
gamma_R_S3=0;
t1x_R_S3=47.5;
t1y_R_S3=90;
t1z_R_S3=40;

% Feature S4
alfa_R_S4=pi/2;
beta_R_S4=-pi/2;
gamma_R_S4=-pi/2;
t1x_R_S4=47.5;
t1y_R_S4=0;

```

```

t1z_R_S4=22.5;

% Feature S5
alfa_R_S5=0;
beta_R_S5=-pi/2;
gamma_R_S5=0;
t1x_R_S5=0;
t1y_R_S5=47.5;
t1z_R_S5=22.5;

% Feature S6
alfa_R_S6=pi/2;
beta_R_S6=pi/2;
gamma_R_S6=-pi/2;
t1x_R_S6=47.5;
t1y_R_S6=95;
t1z_R_S6=20;

% Feature S7
alfa_R_S7=0;
beta_R_S7=pi/2;
gamma_R_S7=pi/2;
t1x_R_S7=95;
t1y_R_S7=47.5;
t1z_R_S7=22.5;

% Feature S8
alfa_R_S8=pi/2;
beta_R_S8=pi/2;
gamma_R_S8=-pi/2;
t1x_R_S8=47.5;
t1y_R_S8=85;
t1z_R_S8=42.5;

%%%%%%%%%%%%%%%%%%%%%%%%%%%%%%%%%%%%%%%%%%%%%%%%%%%%%%%%%%%%%%%%%%%%%%%%
% Position and orientation of FCS at each station w.r.t. R. Euler rotation ZYZ order
%%%%%%%%%%%%%%%%%%%%%%%%%%%%%%%%%%%%%%%%%%%%%%%%%%%%%%%%%%%%%%%%%%%%%%%%

% Station 1
Station1_alfa_R_FCS=-pi/2;
Station1_beta_R_FCS=pi;
Station1_gamma_R_FCS=0;
Station1_t1x_R_FCS=0;
Station1_t1y_R_FCS=0;
Station1_t1z_R_FCS=0;

% Station 2
Station2_alfa_R_FCS=-pi/2;
Station2_beta_R_FCS=0;

```

```

Station2_gamma_R_FCS=0;
Station2_t1x_R_FCS=0;
Station2_t1y_R_FCS=95;
Station2_t1z_R_FCS=45;

% Station 3
Station3_alfa_R_FCS=-pi/2;
Station3_beta_R_FCS=pi;
Station3_gamma_R_FCS=0;
Station3_t1x_R_FCS=0;
Station3_t1y_R_FCS=0;
Station3_t1z_R_FCS=2.5;

%%%%%%%%%%%%%%%%%%%%%%%%%%%%%%%%%%%%%%%%%%%%%%%%%%%%%%%%%%%%%%%%%%%%%%%%
% CHAPTER 5: LIMITATIONS OF THE CURRENT SOV. CASE STUDY
%%%%%%%%%%%%%%%%%%%%%%%%%%%%%%%%%%%%%%%%%%%%%%%%%%%%%%%%%%%%%%%%%%%%%%%%
% SUBPROGRAM: H_TRANSFORMS.M
%%%%%%%%%%%%%%%%%%%%%%%%%%%%%%%%%%%%%%%%%%%%%%%%%%%%%%%%%%%%%%%%%%%%%%%%

%%%%%%%%%%%%%%%%%%%%%%%%%%%%%%%%%%%%%%%%%%%%%%%%%%%%%%%%%%%%%%%%%%%%%%%%
% Homogeneous Transformations Matrices
%%%%%%%%%%%%%%%%%%%%%%%%%%%%%%%%%%%%%%%%%%%%%%%%%%%%%%%%%%%%%%%%%%%%%%%%

% HTM H^R_S0
alfa=alfa_R_S0;
beta= beta_R_S0;
gamma=gamma_R_S0;
param=[alfa,beta,gamma];
oRotate_R_S0=Euler_rotation(param);
oTraslate_R_S0=[ t1x_R_S0; t1y_R_S0; t1z_R_S0]';
H_R_S0=[ oRotate_R_S0 oTraslate_R_S0'; 0 0 0 1];

% HTM H^R_S1
alfa=alfa_R_S1;
beta= beta_R_S1;
gamma=gamma_R_S1;
param=[alfa,beta,gamma];
oRotate_R_S1=Euler_rotation(param);
oTraslate_R_S1=[ t1x_R_S1; t1y_R_S1; t1z_R_S1]';
H_R_S1=[ oRotate_R_S1 oTraslate_R_S1'; 0 0 0 1];

% HTM H^R_S2
alfa=alfa_R_S2;
beta= beta_R_S2;
gamma=gamma_R_S2;
param=[alfa,beta,gamma];
oRotate_R_S2=Euler_rotation(param);
oTraslate_R_S2=[ t1x_R_S2; t1y_R_S2; t1z_R_S2]';
H_R_S2=[ oRotate_R_S2 oTraslate_R_S2'; 0 0 0 1];

% HTM H^R_S3

```

```
alfa=alfa_R_S3;
beta= beta_R_S3;
gamma=gamma_R_S3;
param=[alfa,beta,gamma];
oRotate_R_S3=Euler_rotation(param);
oTraslate_R_S3=[ t1x_R_S3; t1y_R_S3; t1z_R_S3]';
H_R_S3=[ oRotate_R_S3 oTraslate_R_S3'; 0 0 0 1];

% HTM H^R_S4
alfa=alfa_R_S4;
beta= beta_R_S4;
gamma=gamma_R_S4;
param=[alfa,beta,gamma];
oRotate_R_S4=Euler_rotation(param);
oTraslate_R_S4=[ t1x_R_S4; t1y_R_S4; t1z_R_S4]';
H_R_S4=[ oRotate_R_S4 oTraslate_R_S4'; 0 0 0 1];

% HTM H^R_S5
alfa=alfa_R_S5;
beta= beta_R_S5;
gamma=gamma_R_S5;
param=[alfa,beta,gamma];
oRotate_R_S5=Euler_rotation(param);
oTraslate_R_S5=[ t1x_R_S5; t1y_R_S5; t1z_R_S5]';
H_R_S5=[ oRotate_R_S5 oTraslate_R_S5'; 0 0 0 1];

% HTM H^R_S6
alfa=alfa_R_S6;
beta= beta_R_S6;
gamma=gamma_R_S6;
param=[alfa,beta,gamma];
oRotate_R_S6=Euler_rotation(param);
oTraslate_R_S6=[ t1x_R_S6; t1y_R_S6; t1z_R_S6]';
H_R_S6=[ oRotate_R_S6 oTraslate_R_S6'; 0 0 0 1];

% HTM H^R_S7
alfa=alfa_R_S7;
beta= beta_R_S7;
gamma=gamma_R_S7;
param=[alfa,beta,gamma];
oRotate_R_S7=Euler_rotation(param);
oTraslate_R_S7=[ t1x_R_S7; t1y_R_S7; t1z_R_S7]';
H_R_S7=[ oRotate_R_S7 oTraslate_R_S7'; 0 0 0 1];

% HTM H^R_S8
alfa=alfa_R_S8;
beta= beta_R_S8;
gamma=gamma_R_S8;
param=[alfa,beta,gamma];
```

```

oRotate_R_S8=Euler_rotation(param);
oTraslate_R_S8=[ t1x_R_S8; t1y_R_S8; t1z_R_S8]';
H_R_S8=[ oRotate_R_S8 oTraslate_R_S8'; 0 0 0 1];

%%%%%%%%%%%%%%%%%%%%%%%%%%%%%%%%%%%%%%%%%%%%%%%%%%%%%%%%%%%%%%%%%%%%%%%%
% CHAPTER 5: LIMITATIONS OF THE CURRENT SOV. CASE STUDY
%%%%%%%%%%%%%%%%%%%%%%%%%%%%%%%%%%%%%%%%%%%%%%%%%%%%%%%%%%%%%%%%%%%%%%%%
% SUBPROGRAM: MATRIX_STATION_1.M %%%%%%%%%
%%%%%%%%%%%%%%%%%%%%%%%%%%%%%%%%%%%%%%%%%%%%%%%%%%%%%%%%%%%%%%%%%%%%%%%%

% Locator coordenates w.r.t. FCS at station 1
L1x=10;
L1y=30;
L2x=50;
L2y=70;
L3x=90;
L3y=30;
p1y=30;
p1z=-35;
p2y=70;
p2z=-35;
p3x=50;
p3z=-20;

%%%%%%%%%%%%%%%%%%%%%%%%%%%%%%%%%%%%%%%%%%%%%%%%%%%%%%%%%%%%%%%%%%%%%%%%
% Calculus of matrices T1, T2, T3 according to Zhou's methodology %%%%%%%%%
%%%%%%%%%%%%%%%%%%%%%%%%%%%%%%%%%%%%%%%%%%%%%%%%%%%%%%%%%%%%%%%%%%%%%%%%

% FIXTURE ERROR %%%%%%%%%
% Calculus of matrix T3
C=L3x*L1y-L1y*L2x+L3y*L2x+L2y*L1x-L2y*L3x-L3y*L1x;

T3=[[ (L2y-L3y)*p2z/C (L3y-L1y)*p2z/C (L1y-L2y)*p2z/C -p2y/(p1y-p2y) p1y/(p1y-p2y) 0];
    [(L3x-L2x)*p3z/C (L1x-L3x)*p3z/C (L2x-L1x)*p3z/C p3x/(p1y-p2y) -p3x/(p1y-p2y) 1];
    [(L3y*L2x-L2y*L3x)/C (L3x*L1y-L3y*L1x)/C (L2y*L1x-L1y*L2x)/C 0 0 0 ];
    [-(L2x-L3x)/C -(L3x-L1x)/C -(L1x-L2x)/C 0 0 0];
    [-(L2y-L3y)/C (-L3y+L1y)/C (-L1y+L2y)/C 0 0 0];
    [0 0 0 -1/(p1y-p2y) +1/(p1y-p2y) 0]];

% Calculus of matrix Gqi necessary for evaluating A4

gamma_R_FCS=Station1_gamma_R_FCS;
beta_R_FCS=Station1_beta_R_FCS;
alfa_R_FCS=Station1_alfa_R_FCS;
t1x_R_FCS=Station1_t1x_R_FCS;
t1y_R_FCS=Station1_t1y_R_FCS;
t1z_R_FCS=Station1_t1z_R_FCS;

% Position and orientation of the newly feature machined. The feature
%machined is S2, so q1=S2
gamma_R_q1=gamma_R_S2;

```

```

beta_R_q1=beta_R_S2;
alfa_R_q1=alfa_R_S2;
t1x_R_q1=t1x_R_S2;
t1y_R_q1=t1y_R_S2;
t1z_R_q1=t1z_R_S2;

alfa=alfa_R_FCS;
beta= beta_R_FCS;
gamma=gamma_R_FCS;

param=[alfa,beta,gamma];
oRotate_R_FCS=Euler_rotation(param);

oTraslate_R_FCS=[ t1x_R_FCS; t1y_R_FCS; t1z_R_FCS]';
H_R_FCS=[ oRotate_R_FCS oTraslate_R_FCS'; 0 0 0 1];

alfa=alfa_R_q1;
beta= beta_R_q1;
gamma=gamma_R_q1;
param=[alfa,beta,gamma];
oRotate_R_q1=Euler_rotation(param);

oTraslate_R_q1=[ t1x_R_q1; t1y_R_q1; t1z_R_q1]';
H_R_q1=[ oRotate_R_q1 oTraslate_R_q1'; 0 0 0 1];

H_FCS_q1=pinv(H_R_FCS)*H_R_q1;

oRotate_FCS_q1=H_FCS_q1(1:3,1:3);
oTraslate_FCS_q1=H_FCS_q1(1:3,4);
oTraslate_FCS_q1_circun=[0 -oTraslate_FCS_q1(3) oTraslate_FCS_q1(2);
oTraslate_FCS_q1(3) 0 -oTraslate_FCS_q1(1);
-oTraslate_FCS_q1(2) oTraslate_FCS_q1(1) 0];

Gq1=[[oRotate_FCS_q1'] [-oRotate_FCS_q1'*oTraslate_FCS_q1_circun];
      [zeros(3,3)] [oRotate_FCS_q1']];

%%%%%%%%% DATUM FEATURE ERROR %%%%%%%%%%
% Calculus T1 and T2

%Position and orientation of secondary datum. Secondary datum = S4
gamma_R_2=gamma_R_S4;
beta_R_2=beta_R_S4;
alfa_R_2=alfa_R_S4;
t1x_R_2=t1x_R_S4;
t1y_R_2=t1y_R_S4;
t1z_R_2=t1z_R_S4;

%Position and orientation of tertiary datum. Tertiary datum = S5
gamma_R_3=gamma_R_S5;

```



```

beta_R_3=beta_R_S5;
alfa_R_3=alfa_R_S5;
t1x_R_3=t1x_R_S5;
t1y_R_3=t1y_R_S5;
t1z_R_3=t1z_R_S5;

%Calculus of Homogeneous transformations matrices

alfa=alfa_R_2;
beta= beta_R_2;
gamma=gamma_R_2;

param=[alfa,beta,gamma];
oRotate_R_2=Euler_rotation(param);

oTraslate_R_2=[ t1x_R_2; t1y_R_2; t1z_R_2]';
H_R_2=[ oRotate_R_2 oTraslate_R_2'; 0 0 0 1];

alfa=alfa_R_3;
beta= beta_R_3;
gamma=gamma_R_3;

param=[alfa,beta,gamma];
oRotate_R_3=Euler_rotation(param);

oTraslate_R_3=[ t1x_R_3; t1y_R_3; t1z_R_3]';
H_R_3=[ oRotate_R_3 oTraslate_R_3'; 0 0 0 1];

H_2_F=pinv(H_R_2)*H_R_FCS;
H_3_F=pinv(H_R_3)*H_R_FCS;

% Rotation of LCS of secondary and tertiary datums to express LCS according
% to T1 and T2

alfa=Station1_alfa_Ref_2;
beta=Station1_beta_Ref_2;
gamma=Station1_gamma_Ref_2;

param=[alfa,beta,gamma];
oRotate_Ref_2=Euler_rotation(param);

K_Ref_2=[eye(3) zeros(3);
         zeros(3) oRotate_Ref_2];

alfa=Station1_alfa_Ref_3;
beta=Station1_beta_Ref_3;
gamma=Station1_gamma_Ref_3;

param=[alfa,beta,gamma];

```

```

oRotate_Ref_3=Euler_rotation(param);

K_Ref_3=[eye(3) zeros(3);
        zeros(3) oRotate_Ref_3];

oTraslate_2_F=H_2_F(1:3,4);
oTraslate_2_F_mod=oRotate_Ref_2*oTraslate_2_F;
ot2_Fx_mod=oTraslate_2_F_mod(1);
ot2_Fy_mod=oTraslate_2_F_mod(2);

oTraslate_3_F=H_3_F(1:3,4);
oTraslate_3_F_mod=oRotate_Ref_3*oTraslate_3_F;
ot3_Fx_mod=oTraslate_3_F_mod(1);
ot3_Fy_mod=oTraslate_3_F_mod(2);

% Matrix T1
T1=[[0 0 -1 -ot2_Fy_mod (p2z+ot2_Fx_mod+(p2y*(p2z-p1z)/(p1y-p2y))) 0];
     [0 0 0 -p3x (p3x*(p1z-p2z)/(p1y-p2y)) 0];
     [0 0 0 0 0 0 ];
     [0 0 0 0 0 0 ];
     [0 0 0 0 0 0 ];
     [0 0 0 1 -(p1z-p2z)/(p1y-p2y) 0]];

% Matrix T2
T2=[[0 0 0 0 0 0];
     [0 0 -1 (-p3z-ot3_Fy_mod) (p3x+ot3_Fx_mod) 0];
     [0 0 0 0 0 0];
     [0 0 0 0 0 0];
     [0 0 0 0 0 0];
     [0 0 0 0 0 0]];

%%% Derivation of matrices A1, A2, A3, A4, A5 %%%%%%%%%%%%%%%

% MATRIX A1. RELOCATION MATRIX
% Relocate the part. As it is the first station, A1 is the identity matrix
Station{1}.A1=eye(6*M);

% MATRIX A2. DATUM-INDUCED ERROR
%T1 and T2 multiply the features which are the second and tertiary datum
%plane.
Station{1}.A2=[zeros(6,6*4) T1 T2 zeros(6,6*3)];

% MATRIX A3. FIXTURE-INDUCED ERROR
Station{1}.A3=-T3;

% MATRIX A4. OVERALL DEVIATION OF NEWLY GENERATED FEATURES
Station{1}.A4=[Gq1];

```



```

gamma_R_FCS=Station2_gamma_R_FCS;
beta_R_FCS=Station2_beta_R_FCS;
alfa_R_FCS=Station2_alfa_R_FCS;
t1x_R_FCS=Station2_t1x_R_FCS;
t1y_R_FCS=Station2_t1y_R_FCS;
t1z_R_FCS=Station2_t1z_R_FCS;

% Position and orientation of the newly feature machined. The feature
%machined is S2, so q1=S1
gamma_R_q1=gamma_R_S1;
beta_R_q1=beta_R_S1;
alfa_R_q1=alfa_R_S1;
t1x_R_q1=t1x_R_S1;
t1y_R_q1=t1y_R_S1;
t1z_R_q1=t1z_R_S1;

alfa=alfa_R_FCS;
beta= beta_R_FCS;
gamma=gamma_R_FCS;

param=[alfa,beta,gamma];
oRotate_R_FCS=Euler_rotation(param);

oTraslate_R_FCS=[ t1x_R_FCS; t1y_R_FCS; t1z_R_FCS]';
H_R_FCS=[ oRotate_R_FCS oTraslate_R_FCS'; 0 0 0 1];

alfa=alfa_R_q1;
beta= beta_R_q1;
gamma=gamma_R_q1;

param=[alfa,beta,gamma];
oRotate_R_q1=Euler_rotation(param);

oTraslate_R_q1=[ t1x_R_q1; t1y_R_q1; t1z_R_q1]';
H_R_q1=[ oRotate_R_q1 oTraslate_R_q1'; 0 0 0 1];

H_FCS_q1=pinv(H_R_FCS)*H_R_q1;

oRotate_FCS_q1=H_FCS_q1(1:3,1:3);
oTraslate_FCS_q1=H_FCS_q1(1:3,4);
oTraslate_FCS_q1_circun=[0 -oTraslate_FCS_q1(3) oTraslate_FCS_q1(2);
oTraslate_FCS_q1(3) 0 -oTraslate_FCS_q1(1);
-oTraslate_FCS_q1(2) oTraslate_FCS_q1(1) 0];

Gq1=[[oRotate_FCS_q1'] [-oRotate_FCS_q1'*oTraslate_FCS_q1_circun];
[zeros(3,3) [oRotate_FCS_q1']]];

%%%%%%%%% DATUM FEATURE ERROR %%%%%%%%%%
% Calculus T1 and T2

```

```

%Position and orientation of secondary datum. Secondary datum = S6
gamma_R_2=gamma_R_S6;
beta_R_2=beta_R_S6;
alfa_R_2=alfa_R_S6;
t1x_R_2=t1x_R_S6;
t1y_R_2=t1y_R_S6;
t1z_R_2=t1z_R_S6;

%Position and orientation of tertiary datum. Tertiary datum = S5
gamma_R_3=gamma_R_S5;
beta_R_3=beta_R_S5;
alfa_R_3=alfa_R_S5;
t1x_R_3=t1x_R_S5;
t1y_R_3=t1y_R_S5;
t1z_R_3=t1z_R_S5;

%Calculus of Homogeneous transformations matrices

alfa=alfa_R_2;
beta= beta_R_2;
gamma=gamma_R_2;

param=[alfa,beta,gamma];
oRotate_R_2=Euler_rotation(param);

oTraslate_R_2=[ t1x_R_2; t1y_R_2; t1z_R_2]';
H_R_2=[ oRotate_R_2 oTraslate_R_2'; 0 0 0 1];

alfa=alfa_R_3;
beta= beta_R_3;
gamma=gamma_R_3;

param=[alfa,beta,gamma];
oRotate_R_3=Euler_rotation(param);

oTraslate_R_3=[ t1x_R_3; t1y_R_3; t1z_R_3]';
H_R_3=[ oRotate_R_3 oTraslate_R_3'; 0 0 0 1];

H_2_F=pinv(H_R_2)*H_R_FCS;
H_3_F=pinv(H_R_3)*H_R_FCS;

% Rotation of LCS of secondary and tertiary datums to express LCS according
% to T1 and T2

alfa=Station2_alfa_Ref_2;
beta=Station2_beta_Ref_2;
gamma=Station2_gamma_Ref_2;

```

```

param=[alfa,beta,gamma];
oRotate_Ref_2=Euler_rotation(param);

K_Ref_2=[eye(3) zeros(3);
         zeros(3) oRotate_Ref_2];

alfa=Station2_alfa_Ref_3;
beta=Station2_beta_Ref_3;
gamma=Station2_gamma_Ref_3;

param=[alfa,beta,gamma];
oRotate_Ref_3=Euler_rotation(param);

K_Ref_3=[eye(3) zeros(3);
         zeros(3) oRotate_Ref_3];

oTraslate_2_F=H_2_F(1:3,4);
oTraslate_2_F_mod=oRotate_Ref_2*oTraslate_2_F;
ot2_Fx_mod=oTraslate_2_F_mod(1);
ot2_Fy_mod=oTraslate_2_F_mod(2);

oTraslate_3_F=H_3_F(1:3,4);
oTraslate_3_F_mod=oRotate_Ref_3*oTraslate_3_F;
ot3_Fx_mod=oTraslate_3_F_mod(1);
ot3_Fy_mod=oTraslate_3_F_mod(2);

% Matrix T1
T1=[[0 0 -1 -ot2_Fy_mod (p2z+ot2_Fx_mod+(p2y*(p2z-p1z)/(p1y-p2y))) 0];
     [0 0 0 -p3x (p3x*(p1z-p2z)/(p1y-p2y)) 0];
     [0 0 0 0 0 0];
     [0 0 0 0 0 0];
     [0 0 0 0 0 0];
     [0 0 0 1 -(p1z-p2z)/(p1y-p2y) 0]];

% Matrix T2
T2=[[0 0 0 0 0 0];
     [0 0 -1 (-p3z-ot3_Fy_mod) (p3x+ot3_Fx_mod) 0];
     [0 0 0 0 0 0];
     [0 0 0 0 0 0];
     [0 0 0 0 0 0];
     [0 0 0 0 0 0]];

%%% Derivation of matrices A1, A2, A3, A4, A5 %%%%%%%%%%%%%%%

% MATRIX A1. RELOCATION MATRIX
% Relocate the part. Previous station-->Feature S4. Current station--> Feature
% S2

```

```

H_S2_S0=pinv(H_R_S2)*H_R_S0;
oRotate_S2_S0=H_S2_S0(1:3,1:3);
oTraslate_S2_S0=H_S2_S0(1:3,4);
oTraslate_S2_S0_circun=[0 -oTraslate_S2_S0(3) oTraslate_S2_S0(2);
oTraslate_S2_S0(3) 0 -oTraslate_S2_S0(1);
-oTraslate_S2_S0(2) oTraslate_S2_S0(1) 0];
Q_S2_S0=[-[oRotate_S2_S0'] [oRotate_S2_S0'*oTraslate_S2_S0_circun];
[zeros(3,3) -[oRotate_S2_S0']];

```

```

H_S2_S1=pinv(H_R_S2)*H_R_S1;
oRotate_S2_S1=H_S2_S1(1:3,1:3);
oTraslate_S2_S1=H_S2_S1(1:3,4);
oTraslate_S2_S1_circun=[0 -oTraslate_S2_S1(3) oTraslate_S2_S1(2);
oTraslate_S2_S1(3) 0 -oTraslate_S2_S1(1);
-oTraslate_S2_S1(2) oTraslate_S2_S1(1) 0];
Q_S2_S1=[-[oRotate_S2_S1'] [oRotate_S2_S1'*oTraslate_S2_S1_circun];
[zeros(3,3) -[oRotate_S2_S1']];

```

```

H_S2_S3=pinv(H_R_S2)*H_R_S3;
oRotate_S2_S3=H_S2_S3(1:3,1:3);
oTraslate_S2_S3=H_S2_S3(1:3,4);
oTraslate_S2_S3_circun=[0 -oTraslate_S2_S3(3) oTraslate_S2_S3(2);
oTraslate_S2_S3(3) 0 -oTraslate_S2_S3(1);
-oTraslate_S2_S3(2) oTraslate_S2_S3(1) 0];
Q_S2_S3=[-[oRotate_S2_S3'] [oRotate_S2_S3'*oTraslate_S2_S3_circun];
[zeros(3,3) -[oRotate_S2_S3']];

```

```

H_S2_S4=pinv(H_R_S2)*H_R_S4;
oRotate_S2_S4=H_S2_S4(1:3,1:3);
oTraslate_S2_S4=H_S2_S4(1:3,4);
oTraslate_S2_S4_circun=[0 -oTraslate_S2_S4(3) oTraslate_S2_S4(2);
oTraslate_S2_S4(3) 0 -oTraslate_S2_S4(1);
-oTraslate_S2_S4(2) oTraslate_S2_S4(1) 0];
Q_S2_S4=[-[oRotate_S2_S4'] [oRotate_S2_S4'*oTraslate_S2_S4_circun];
[zeros(3,3) -[oRotate_S2_S4']];

```

```

H_S2_S5=pinv(H_R_S2)*H_R_S5;
oRotate_S2_S5=H_S2_S5(1:3,1:3);
oTraslate_S2_S5=H_S2_S5(1:3,4);
oTraslate_S2_S5_circun=[0 -oTraslate_S2_S5(3) oTraslate_S2_S5(2);
oTraslate_S2_S5(3) 0 -oTraslate_S2_S5(1);
-oTraslate_S2_S5(2) oTraslate_S2_S5(1) 0];
Q_S2_S5=[-[oRotate_S2_S5'] [oRotate_S2_S5'*oTraslate_S2_S5_circun];
[zeros(3,3) -[oRotate_S2_S5']];

```

```

H_S2_S6=pinv(H_R_S2)*H_R_S6;
oRotate_S2_S6=H_S2_S6(1:3,1:3);
oTraslate_S2_S6=H_S2_S6(1:3,4);
oTraslate_S2_S6_circun=[0 -oTraslate_S2_S6(3) oTraslate_S2_S6(2);

```



```
%%%%%%%%%%%%%%%%%%%%%%%%%%%%%%%%%%%%%%%%%%%%%%%%%%%%%%%%%%%%%%%%%%%%%%%%% DERIVATION OF A(2), B(2), U(2) %%%%%%%%%%%%%%%%%%%%%%%%%%%%%%%%%%%%%%%%%%%%%%%%%%%%%%%%%%%%%%%%%%%%%%%%%%
```

```
Station{2}.A=[Station{2}.A1+Station{2}.A5*Station{2}.A4*(Station{2}.A2*Station{2}.A1)];
Station{2}.B=[Station{2}.A5*Station{2}.A4*Station{2}.A3 ];
Station{2}.U=[Station{2}.uf'];
```

```
%%%%%%%%%%%%%%%%%%%%%%%%%%%%%%%%%%%%%%%%%%%%%%%%%%%%%%%%%%%%%%%%%%%%%%%%%
% CHAPTER 5: LIMITATIONS OF THE CURRENT SOV. CASE STUDY
%%%%%%%%%%%%%%%%%%%%%%%%%%%%%%%%%%%%%%%%%%%%%%%%%%%%%%%%%%%%%%%%%%%%%%%%%
SUBPROGRAM: MATRIX_STATION_3.M %%%%%%%%%%%%%%%%%%%%%%%%%%%%%%%%%%%%%%%%%%%%%%%%%%%%%%%%%%%%%%%%%%%%%%%%%%
%%%%%%%%%%%%%%%%%%%%%%%%%%%%%%%%%%%%%%%%%%%%%%%%%%%%%%%%%%%%%%%%%%%%%%%%%
```

```
% Locator coordenates w.r.t. FCS at station 3
```

```
L1x=10;
L1y=30;
L2x=50;
L2y=70;
L3x=90;
L3y=30;
p1y=30;
p1z=-35;
p2y=70;
p2z=-35;
p3x=50;
p3z=-20;
```

```
%%%%%%%%%%%%%%%%%%%%%%%%%%%%%%%%%%%%%%%%%%%%%%%%%%%%%%%%%%%%%%%%%%%%%%%%%
%%%%%%%%%%%%%%%%%%%%%%%%%%%%%%%%%%%%%%%%%%%%%%%%%%%%%%%%%%%%%%%%%%%%%%%%% Calculus of matrices T1, T2, T3 according to Zhou's methodology %%%%%%%%%%%%%%%%%%%%%%%%%%%%%%%%%%%%%%%%%%%%%%%%%%%%%%%%%%%%%%%%%%%%%%%%%%
```

```
%%%%%%%%%%%%%%%%%%%%%%%%%%%%%%%%%%%%%%%%%%%%%%%%%%%%%%%%%%%%%%%%%%%%%%%%% FIXTURE ERROR %%%%%%%%%%%%%%%%%%%%%%%%%%%%%%%%%%%%%%%%%%%%%%%%%%%%%%%%%%%%%%%%%%%%%%%%%%
```

```
% Calculus of matrix T3
```

```
C=L3x*L1y-L1y*L2x+L3y*L2x+L2y*L1x-L2y*L3x-L3y*L1x;
```

```
T3=[[ (L2y-L3y)*p2z/C (L3y-L1y)*p2z/C (L1y-L2y)*p2z/C -p2y/(p1y-p2y) p1y/(p1y-p2y) 0];
     [(L3x-L2x)*p3z/C (L1x-L3x)*p3z/C (L2x-L1x)*p3z/C p3x/(p1y-p2y) -p3x/(p1y-p2y) 1];
     [(L3y*L2x-L2y*L3x)/C (L3x*L1y-L3y*L1x)/C (L2y*L1x-L1y*L2x)/C 0 0 0 ];
     [-(L2x-L3x)/C -(L3x-L1x)/C -(L1x-L2x)/C 0 0 0];
     [-(L2y-L3y)/C (-L3y+L1y)/C (-L1y+L2y)/C 0 0 0];
     [0 0 0 -1/(p1y-p2y) +1/(p1y-p2y) 0]];
```

```
% Calculus of matrix Gqi necessary for evaluating A4.
```

```
gamma_R_FCS=Station3_gamma_R_FCS;
beta_R_FCS=Station3_beta_R_FCS;
alfa_R_FCS=Station3_alfa_R_FCS;
t1x_R_FCS=Station3_t1x_R_FCS;
t1y_R_FCS=Station3_t1y_R_FCS;
t1z_R_FCS=Station3_t1z_R_FCS;
```

```
% Position and orientation of the newly feature machined. The feature
```

```

%machined is S8, so q1=S8
gamma_R_q1=gamma_R_S8;
beta_R_q1=beta_R_S8;
alfa_R_q1=alfa_R_S8;
t1x_R_q1=t1x_R_S8;
t1y_R_q1=t1y_R_S8;
t1z_R_q1=t1z_R_S8;

alfa=alfa_R_FCS;
beta= beta_R_FCS;
gamma=gamma_R_FCS;

param=[alfa,beta,gamma];
oRotate_R_FCS=Euler_rotation(param);

oTraslate_R_FCS=[ t1x_R_FCS; t1y_R_FCS; t1z_R_FCS]';
H_R_FCS=[ oRotate_R_FCS oTraslate_R_FCS'; 0 0 0 1];

alfa=alfa_R_q1;
beta= beta_R_q1;
gamma=gamma_R_q1;

param=[alfa,beta,gamma];
oRotate_R_q1=Euler_rotation(param);

oTraslate_R_q1=[ t1x_R_q1; t1y_R_q1; t1z_R_q1]';
H_R_q1=[ oRotate_R_q1 oTraslate_R_q1'; 0 0 0 1];

H_FCS_q1=pinv(H_R_FCS)*H_R_q1;

oRotate_FCS_q1=H_FCS_q1(1:3,1:3);
oTraslate_FCS_q1=H_FCS_q1(1:3,4);
oTraslate_FCS_q1_circun=[0 -oTraslate_FCS_q1(3) oTraslate_FCS_q1(2);
oTraslate_FCS_q1(3) 0 -oTraslate_FCS_q1(1);
-oTraslate_FCS_q1(2) oTraslate_FCS_q1(1) 0];

Gq1_A=[[oRotate_FCS_q1'] [-oRotate_FCS_q1'*oTraslate_FCS_q1_circun];
[zeros(3,3)] [oRotate_FCS_q1']];

% Position and orientation of the newly feature machined. The feature
%machined is S3, so q1=S3

gamma_R_q1=gamma_R_S3;
beta_R_q1=beta_R_S3;
alfa_R_q1=alfa_R_S3;
t1x_R_q1=t1x_R_S3;
t1y_R_q1=t1y_R_S3;
t1z_R_q1=t1z_R_S3;

```

```

alfa=alfa_R_FCS;
beta= beta_R_FCS;
gamma=gamma_R_FCS;

param=[alfa,beta,gamma];
oRotate_R_FCS=Euler_rotation(param);

oTraslate_R_FCS=[ t1x_R_FCS; t1y_R_FCS; t1z_R_FCS]';
H_R_FCS=[ oRotate_R_FCS oTraslate_R_FCS'; 0 0 0 1];

alfa=alfa_R_q1;
beta= beta_R_q1;
gamma=gamma_R_q1;

param=[alfa,beta,gamma];
oRotate_R_q1=Euler_rotation(param);

oTraslate_R_q1=[ t1x_R_q1; t1y_R_q1; t1z_R_q1]';
H_R_q1=[ oRotate_R_q1 oTraslate_R_q1'; 0 0 0 1];

H_FCS_q1=pinv(H_R_FCS)*H_R_q1;

oRotate_FCS_q1=H_FCS_q1(1:3,1:3);
oTraslate_FCS_q1=H_FCS_q1(1:3,4);
oTraslate_FCS_q1_circun=[0 -oTraslate_FCS_q1(3) oTraslate_FCS_q1(2);
oTraslate_FCS_q1(3) 0 -oTraslate_FCS_q1(1);
-oTraslate_FCS_q1(2) oTraslate_FCS_q1(1) 0];

Gq1_B=[[oRotate_FCS_q1' [-oRotate_FCS_q1'*oTraslate_FCS_q1_circun];
[zeros(3,3) [oRotate_FCS_q1']]];

%%%%%%%%% DATUM FEATURE ERROR %%%%%%%%%%
% Calculus T1 and T2

%Position and orientation of secondary datum. Secondary datum = S4
gamma_R_2=gamma_R_S4;
beta_R_2=beta_R_S4;
alfa_R_2=alfa_R_S4;
t1x_R_2=t1x_R_S4;
t1y_R_2=t1y_R_S4;
t1z_R_2=t1z_R_S4;

%Position and orientation of tertiary datum. [gamma,beta,alfa]. S5
gamma_R_3=gamma_R_S5;
beta_R_3=beta_R_S5;
alfa_R_3=alfa_R_S5;
t1x_R_3=t1x_R_S5;
t1y_R_3=t1y_R_S5;
t1z_R_3=t1z_R_S5;

```

```

%Calculus of Homogeneous transformations

alfa=alfa_R_2;
beta= beta_R_2;
gamma=gamma_R_2;

param=[alfa,beta,gamma];
oRotate_R_2=Euler_rotation(param);

oTraslate_R_2=[ t1x_R_2; t1y_R_2; t1z_R_2]';
H_R_2=[ oRotate_R_2 oTraslate_R_2'; 0 0 0 1];

alfa=alfa_R_3;
beta= beta_R_3;
gamma=gamma_R_3;

param=[alfa,beta,gamma];
oRotate_R_3=Euler_rotation(param);

oTraslate_R_3=[ t1x_R_3; t1y_R_3; t1z_R_3]';
H_R_3=[ oRotate_R_3 oTraslate_R_3'; 0 0 0 1];

H_2_F=pinv(H_R_2)*H_R_FCS;
H_3_F=pinv(H_R_3)*H_R_FCS;

ot2_Fx_mod=-H_2_F(2,4);
ot2_Fy_mod=H_2_F(1,4);
ot3_Fx_mod=H_3_F(2,4);
ot3_Fy_mod=-H_3_F(1,4);

% Matrix T1
T1=[[0 0 -1 -ot2_Fy_mod (p2z+ot2_Fx_mod+(p2y*(p2z-p1z)/(p1y-p2y))) 0];
     [0 0 0 -p3x (p3x*(p1z-p2z)/(p1y-p2y)) 0];
     [0 0 0 0 0 0];
     [0 0 0 0 0 0];
     [0 0 0 0 0 0];
     [0 0 0 1 -(p1z-p2z)/(p1y-p2y) 0]];

% Matrix T2
T2=[[0 0 0 0 0 0];
     [0 0 -1 (-p3z-ot3_Fy_mod) (p3x+ot3_Fx_mod) 0];
     [0 0 0 0 0 0];
     [0 0 0 0 0 0];
     [0 0 0 0 0 0];
     [0 0 0 0 0 0]];

```

```

%% Derivation of matrices A1, A2, A3, A4, A5 %%%%%%%%%%%

% MATRIX A1. RELOCATION MATRIX
% Relocate part. Previous station-->Feature S2. Current station--> Feature
% S1

H_S1_S0=pinv(H_R_S1)*H_R_S0;
oRotate_S1_S0=H_S1_S0(1:3,1:3);
oTraslate_S1_S0=H_S1_S0(1:3,4);
oTraslate_S1_S0_circun=[0 -oTraslate_S1_S0(3) oTraslate_S1_S0(2);
oTraslate_S1_S0(3) 0 -oTraslate_S1_S0(1);
-oTraslate_S1_S0(2) oTraslate_S1_S0(1) 0];
Q_S1_S0=[- [oRotate_S1_S0'] [oRotate_S1_S0'*oTraslate_S1_S0_circun];
[zeros(3,3)] -[oRotate_S1_S0']];

H_S1_S2=pinv(H_R_S1)*H_R_S2;
oRotate_S1_S2=H_S1_S2(1:3,1:3);
oTraslate_S1_S2=H_S1_S2(1:3,4);
oTraslate_S1_S2_circun=[0 -oTraslate_S1_S2(3) oTraslate_S1_S2(2);
oTraslate_S1_S2(3) 0 -oTraslate_S1_S2(1);
-oTraslate_S1_S2(2) oTraslate_S1_S2(1) 0];
Q_S1_S2=[- [oRotate_S1_S2'] [oRotate_S1_S2'*oTraslate_S1_S2_circun];
[zeros(3,3)] -[oRotate_S1_S2']];

H_S1_S3=pinv(H_R_S1)*H_R_S3;
oRotate_S1_S3=H_S1_S3(1:3,1:3);
oTraslate_S1_S3=H_S1_S3(1:3,4);
oTraslate_S1_S3_circun=[0 -oTraslate_S1_S3(3) oTraslate_S1_S3(2);
oTraslate_S1_S3(3) 0 -oTraslate_S1_S3(1);
-oTraslate_S1_S3(2) oTraslate_S1_S3(1) 0];
Q_S1_S3=[- [oRotate_S1_S3'] [oRotate_S1_S3'*oTraslate_S1_S3_circun];
[zeros(3,3)] -[oRotate_S1_S3']];

H_S1_S4=pinv(H_R_S1)*H_R_S4;
oRotate_S1_S4=H_S1_S4(1:3,1:3);
oTraslate_S1_S4=H_S1_S4(1:3,4);
oTraslate_S1_S4_circun=[0 -oTraslate_S1_S4(3) oTraslate_S1_S4(2);
oTraslate_S1_S4(3) 0 -oTraslate_S1_S4(1);
-oTraslate_S1_S4(2) oTraslate_S1_S4(1) 0];
Q_S1_S4=[- [oRotate_S1_S4'] [oRotate_S1_S4'*oTraslate_S1_S4_circun];
[zeros(3,3)] -[oRotate_S1_S4']];

H_S1_S5=pinv(H_R_S1)*H_R_S5;
oRotate_S1_S5=H_S1_S5(1:3,1:3);
oTraslate_S1_S5=H_S1_S5(1:3,4);
oTraslate_S1_S5_circun=[0 -oTraslate_S1_S5(3) oTraslate_S1_S5(2);
oTraslate_S1_S5(3) 0 -oTraslate_S1_S5(1);
-oTraslate_S1_S5(2) oTraslate_S1_S5(1) 0];
Q_S1_S5=[- [oRotate_S1_S5'] [oRotate_S1_S5'*oTraslate_S1_S5_circun];

```

```

[zeros(3,3)] -[oRotate_S1_S5'];

H_S1_S6=pinv(H_R_S1)*H_R_S6;
oRotate_S1_S6=H_S1_S6(1:3,1:3);
oTraslate_S1_S6=H_S1_S6(1:3,4);
oTraslate_S1_S6_circun=[0 -oTraslate_S1_S6(3) oTraslate_S1_S6(2);
oTraslate_S1_S6(3) 0 -oTraslate_S1_S6(1);
-oTraslate_S1_S6(2) oTraslate_S1_S6(1) 0];
Q_S1_S6=-[oRotate_S1_S6'] [oRotate_S1_S6'*oTraslate_S1_S6_circun];
[zeros(3,3)] -[oRotate_S1_S6'];

H_S1_S7=pinv(H_R_S1)*H_R_S7;
oRotate_S1_S7=H_S1_S7(1:3,1:3);
oTraslate_S1_S7=H_S1_S7(1:3,4);
oTraslate_S1_S7_circun=[0 -oTraslate_S1_S7(3) oTraslate_S1_S7(2);
oTraslate_S1_S7(3) 0 -oTraslate_S1_S7(1);
-oTraslate_S1_S7(2) oTraslate_S1_S7(1) 0];
Q_S1_S7=-[oRotate_S1_S7'] [oRotate_S1_S7'*oTraslate_S1_S7_circun];
[zeros(3,3)] -[oRotate_S1_S7'];

H_S1_S8=pinv(H_R_S1)*H_R_S8;
oRotate_S1_S8=H_S1_S8(1:3,1:3);
oTraslate_S1_S8=H_S1_S8(1:3,4);
oTraslate_S1_S8_circun=[0 -oTraslate_S1_S8(3) oTraslate_S1_S8(2);
oTraslate_S1_S8(3) 0 -oTraslate_S1_S8(1);
-oTraslate_S1_S8(2) oTraslate_S1_S8(1) 0];
Q_S1_S8=-[oRotate_S1_S8'] [oRotate_S1_S8'*oTraslate_S1_S8_circun];
[zeros(3,3)] -[oRotate_S1_S8'];

Q=eye(6*M);
Q(6+1:6*2,6+1:6*2)=zeros(6);
Q(6*6+1:6*7,6+1:6*2)=Q_S1_S6;
Q(6*2+1:6*3,6+1:6*2)=Q_S1_S2;
Q(1:6,6+1:6*2)=Q_S1_S0;
Q(6*4+1:6*5,6+1:6*2)=Q_S1_S4;
Q(6*5+1:6*6,6+1:6*2)=Q_S1_S5;

Station{3}.A1=Q;

% MATRIX A2. DATUM-INDUCED ERROR
%T1 and T2 multiply the features which are the second and tertiary datum
%plane.

Station{3}.A2=[zeros(6,6*4) T1 T2 zeros(6,6*3)];

% MATRIX A3. FIXTURE-INDUCED ERROR
Station{3}.A3=-T3;

% MATRIX A4. OVERALL DEVIATION OF NEWLY GENERATED FEATURES

```



```

Q_S0_S3=[-[oRotate_S0_S3'] [oRotate_S0_S3'*oTraslate_S0_S3_circun];
         [zeros(3,3)] -[oRotate_S0_S3']];

H_S0_S4=pinv(H_R_S0)*H_R_S4;
oRotate_S0_S4=H_S0_S4(1:3,1:3);
oTraslate_S0_S4=H_S0_S4(1:3,4);
oTraslate_S0_S4_circun=[0 -oTraslate_S0_S4(3) oTraslate_S0_S4(2);
oTraslate_S0_S4(3) 0 -oTraslate_S0_S4(1);
-oTraslate_S0_S4(2) oTraslate_S0_S4(1) 0];
Q_S0_S4=[-[oRotate_S0_S4'] [oRotate_S0_S4'*oTraslate_S0_S4_circun];
         [zeros(3,3)] -[oRotate_S0_S4']];

H_S0_S5=pinv(H_R_S0)*H_R_S5;
oRotate_S0_S5=H_S0_S5(1:3,1:3);
oTraslate_S0_S5=H_S0_S5(1:3,4);
oTraslate_S0_S5_circun=[0 -oTraslate_S0_S5(3) oTraslate_S0_S5(2);
oTraslate_S0_S5(3) 0 -oTraslate_S0_S5(1);
-oTraslate_S0_S5(2) oTraslate_S0_S5(1) 0];
Q_S0_S5=[-[oRotate_S0_S5'] [oRotate_S0_S5'*oTraslate_S0_S5_circun];
         [zeros(3,3)] -[oRotate_S0_S5']];

H_S0_S6=pinv(H_R_S0)*H_R_S6;
oRotate_S0_S6=H_S0_S6(1:3,1:3);
oTraslate_S0_S6=H_S0_S6(1:3,4);
oTraslate_S0_S6_circun=[0 -oTraslate_S0_S6(3) oTraslate_S0_S6(2);
oTraslate_S0_S6(3) 0 -oTraslate_S0_S6(1);
-oTraslate_S0_S6(2) oTraslate_S0_S6(1) 0];
Q_S0_S6=[-[oRotate_S0_S6'] [oRotate_S0_S6'*oTraslate_S0_S6_circun];
         [zeros(3,3)] -[oRotate_S0_S6']];

H_S0_S7=pinv(H_R_S0)*H_R_S7;
oRotate_S0_S7=H_S0_S7(1:3,1:3);
oTraslate_S0_S7=H_S0_S7(1:3,4);
oTraslate_S0_S7_circun=[0 -oTraslate_S0_S7(3) oTraslate_S0_S7(2);
oTraslate_S0_S7(3) 0 -oTraslate_S0_S7(1);
-oTraslate_S0_S7(2) oTraslate_S0_S7(1) 0];
Q_S0_S7=[-[oRotate_S0_S7'] [oRotate_S0_S7'*oTraslate_S0_S7_circun];
         [zeros(3,3)] -[oRotate_S0_S7']];

H_S0_S8=pinv(H_R_S0)*H_R_S8;
oRotate_S0_S8=H_S0_S8(1:3,1:3);
oTraslate_S0_S8=H_S0_S8(1:3,4);
oTraslate_S0_S8_circun=[0 -oTraslate_S0_S8(3) oTraslate_S0_S8(2);
oTraslate_S0_S8(3) 0 -oTraslate_S0_S8(1);
-oTraslate_S0_S8(2) oTraslate_S0_S8(1) 0];
Q_S0_S8=[-[oRotate_S0_S8'] [oRotate_S0_S8'*oTraslate_S0_S8_circun];
         [zeros(3,3)] -[oRotate_S0_S8']];

Q=eye(6*M);

```



```

%%%%%%%%%% STATION 1 %%%%%%%%%%%

% Sources of variation at station 1. Locator errors.
Station{1}.uf=[-0.041 0 0.096 -0.018 -0.0042 0]; % Locator errors
Station1_Delta_T=15; %Thermal deviation from nominal in spindle
Station1_Delta_Vb=0.3; %Tool flank wear in this operation (units, mm)

% Matrix A(1) and B(1)
matrix_station_1;
matrix_station_1_ext;

%%%%%%%%%% STATION 2 %%%%%%%%%%%

% Sources of variation at station 2. Locator errors.
Station{2}.uf=[-0.041 0 0.096 -0.018 -0.0042 0];% Locator errors
Station2_Delta_T=15; %Thermal deviation from nominal in spindle
Station2_Delta_Vb=0.3; %Tool flank wear in this operation (units, mm)

% Matrix A(2) and B(2)
matrix_station_2;
matrix_station_2_ext;

%%%%%%%%%% STATION 3 %%%%%%%%%%%

% Sources of variation at station 3. Locator errors.
Station{3}.uf=[-0.041 0 0.096 -0.018 -0.0042 0];% Locator errors
Station3_Delta_T=15; %Thermal deviation from nominal in spindle
Station3_Delta_Vb_f1=0.3; %Tool flank wear in this operation (units, mm)
Station3_Delta_Vb_f2=0.3; %Tool flank wear in this operation (units, mm)

% Matrix A(3) and B(3)
matrix_station_3;
matrix_station_3_ext;

%%%%%%%%%% INSPECTION STATION %%%%%%%%%%%
% Matrix C4
matrix_inspection;

%%%%%%%%%%%%%%%%%%%%%%%%%%%%%%%%%%%%%%%%%%%%%%%%%%%%%%%%%%%%%%%%%%%%%%%%%%
%%%%%%%%%% QUALITY PREDICTION USING SOV
%%%%%%%%%%%%%%%%%%%%%%%%%%%%%%%%%%%%%%%%%%%%%%%%%%%%%%%%%%%%%%%%%%%%%%%%%%

% Raw part errors.
Station{1}.X=[zeros(6*M,1)];

% Error propagation

for (i=1:3)

```



```

%%%%%%%%%%%%%%%%%%%%%%%%%%%%%%%%%%%%%%%%%%%%%%%%%%%%%%%%%%%%%%%%%%%%%%%%%%%%%%
%%%%%%%%%%%%%% CHAPTER 6:  EXTENSION SOV MODEL %%%%%%%%%%%%%%%
%%%%%%%%%%%%%% SUBPROGRAM: MATRIX_STATION_1_EXT.M %%%%%%%%%%%%%%%
%%%%%%%%%%%%%%%%%%%%%%%%%%%%%%%%%%%%%%%%%%%%%%%%%%%%%%%%%%%%%%%%%%%%%%%%%%%%%%

%%%%%%%%%%%%%%%%%%%%%%%%%%%%%%%%%%%%%%%%%%%%%%%%%%%%%%%%%%%%%%%%%%%%%%%%%%%%%%
%%%%%%%% MACHINING ERRORS: HOMOGENEOUS TRANSFORMATION MATRICES %%%%
%%%%%%%%%%%%%%%%%%%%%%%%%%%%%%%%%%%%%%%%%%%%%%%%%%%%%%%%%%%%%%%%%%%%%%%%%%%%%%

Tool_diameter=Tool_diameter_station_1;
Tool_length=Tool_length_station_1;

% HTM: The tool tip CS is equal to the qi CS
Station1_alfa_R_TTCS=alfa_R_S2;
Station1_beta_R_TTCS=beta_R_S2;
Station1_gamma_R_TTCS=gamma_R_S2;
Station1_t1x_R_TTCS=t1x_R_S2;
Station1_t1y_R_TTCS=t1y_R_S2;
Station1_t1z_R_TTCS=t1z_R_S2;

% The tool CS is equal to the tool tip CS if the operation is a face
% milling. If the operation is a end milling, the CS is deviated the tool
% diameter in Z direction
Station1_alfa_R_TCS=Station1_alfa_R_FCS;
Station1_beta_R_TCS=Station1_beta_R_FCS;
Station1_gamma_R_TCS=Station1_gamma_R_FCS;
Station1_t1x_R_TCS=Station1_t1x_R_TTCS;
Station1_t1y_R_TCS=Station1_t1y_R_TTCS;
Station1_t1z_R_TCS=Station1_t1z_R_TTCS;

% The Spindle CS is equal to the tool CS but it is deviated in Z direction
% by the cutting-tool length
Station1_alfa_R_SCS=Station1_alfa_R_TCS;
Station1_beta_R_SCS=Station1_beta_R_TCS;
Station1_gamma_R_SCS=Station1_gamma_R_TCS;
Station1_t1x_R_SCS=Station1_t1x_R_TCS;
Station1_t1y_R_SCS=Station1_t1y_R_TCS;
Station1_t1z_R_SCS=Station1_t1z_R_TCS-Tool_length;

gamma_R_TTCS=Station1_gamma_R_TTCS;
beta_R_TTCS=Station1_beta_R_TTCS;
alfa_R_TTCS=Station1_alfa_R_TTCS;
t1x_R_TTCS=Station1_t1x_R_TTCS;
t1y_R_TTCS=Station1_t1y_R_TTCS;
t1z_R_TTCS=Station1_t1z_R_TTCS;

alfa=alfa_R_TTCS;
beta= beta_R_TTCS;
gamma=gamma_R_TTCS;

```

```

param=[alfa,beta,gamma];
oRotate_R_TTCS=Euler_rotation(param);

oTraslate_R_TTCS=[ t1x_R_TTCS; t1y_R_TTCS; t1z_R_TTCS]';
H_R_TTCS=[ oRotate_R_TTCS oTraslate_R_TTCS'; 0 0 0 1];

gamma_R_TCS=Station1_gamma_R_TCS;
beta_R_TCS=Station1_beta_R_TCS;
alfa_R_TCS=Station1_alfa_R_TCS;
t1x_R_TCS=Station1_t1x_R_TCS;
t1y_R_TCS=Station1_t1y_R_TCS;
t1z_R_TCS=Station1_t1z_R_TCS;

alfa=alfa_R_TCS;
beta= beta_R_TCS;
gamma=gamma_R_TCS;

param=[alfa,beta,gamma];
oRotate_R_TCS=Euler_rotation(param);

oTraslate_R_TCS=[ t1x_R_TCS; t1y_R_TCS; t1z_R_TCS]';
H_R_TCS=[ oRotate_R_TCS oTraslate_R_TCS'; 0 0 0 1];

H_TCS_TTCS=pinv(H_R_TCS)*H_R_TTCS;

oRotate_TCS_TTCS=H_TCS_TTCS(1:3,1:3);
oTraslate_TCS_TTCS=H_TCS_TTCS(1:3,4);
oTraslate_TCS_TTCS_circun=[0 -oTraslate_TCS_TTCS(3) oTraslate_TCS_TTCS(2);
oTraslate_TCS_TTCS(3) 0 -oTraslate_TCS_TTCS(1);
-oTraslate_TCS_TTCS(2) oTraslate_TCS_TTCS(1) 0];

gamma_R_SCS=Station1_gamma_R_SCS;
beta_R_SCS=Station1_beta_R_SCS;
alfa_R_SCS=Station1_alfa_R_SCS;
t1x_R_SCS=Station1_t1x_R_SCS;
t1y_R_SCS=Station1_t1y_R_SCS;
t1z_R_SCS=Station1_t1z_R_SCS;

alfa=alfa_R_SCS;
beta= beta_R_SCS;
gamma=gamma_R_SCS;

param=[alfa,beta,gamma];
oRotate_R_SCS=Euler_rotation(param);

oTraslate_R_SCS=[ t1x_R_SCS; t1y_R_SCS; t1z_R_SCS]';
H_R_SCS=[ oRotate_R_SCS oTraslate_R_SCS'; 0 0 0 1];

H_SCS_TCS=pinv(H_R_SCS)*H_R_TCS;

```



```

%%%%%%%%%%%%%%%%%%%%%%%%%%%%%%%%%%%%%%%%%%%%%%%%%%%%%%%%%%%%%%%%%%%%%%%%
%%% MACHINING ERRORS: HOMOGENEOUS TRANSFORMATION MATRICES %%%
%%%%%%%%%%%%%%%%%%%%%%%%%%%%%%%%%%%%%%%%%%%%%%%%%%%%%%%%%%%%%%%%%%%%%%%%

```

```

Tool_diameter=Tool_diameter_station_2;
Tool_length=Tool_length_station_2;

```

```

% HTM: The tool tip CS is equal to the qi CS
Station2_alfa_R_TTCS=alfa_R_S1;
Station2_beta_R_TTCS=beta_R_S1;
Station2_gamma_R_TTCS=gamma_R_S1;
Station2_t1x_R_TTCS=t1x_R_S1;
Station2_t1y_R_TTCS=t1y_R_S1;
Station2_t1z_R_TTCS=t1z_R_S1;

```

```

% The tool CS is equal to the tool tip CS if the operation is a face
% milling. If the operation is a end milling, the CS is deviated the tool
% diameter in Z direction
Station2_alfa_R_TCS=Station2_alfa_R_FCS;
Station2_beta_R_TCS=Station2_beta_R_FCS;
Station2_gamma_R_TCS=Station2_gamma_R_FCS;
Station2_t1x_R_TCS=Station2_t1x_R_TTCS;
Station2_t1y_R_TCS=Station2_t1y_R_TTCS;
Station2_t1z_R_TCS=Station2_t1z_R_TTCS;

```

```

% The Spindle CS is equal to the tool CS but it is deviated in Z direction
% by the cutting-tool length
Station2_alfa_R_SCS=Station2_alfa_R_TCS;
Station2_beta_R_SCS=Station2_beta_R_TCS;
Station2_gamma_R_SCS=Station2_gamma_R_TCS;
Station2_t1x_R_SCS=Station2_t1x_R_TCS;
Station2_t1y_R_SCS=Station2_t1y_R_TCS;
Station2_t1z_R_SCS=Station2_t1z_R_TCS-Tool_length;

```

```

gamma_R_TTCS=Station2_gamma_R_TTCS;
beta_R_TTCS=Station2_beta_R_TTCS;
alfa_R_TTCS=Station2_alfa_R_TTCS;
t1x_R_TTCS=Station2_t1x_R_TTCS;
t1y_R_TTCS=Station2_t1y_R_TTCS;
t1z_R_TTCS=Station2_t1z_R_TTCS;

```

```

alfa=alfa_R_TTCS;
beta= beta_R_TTCS;
gamma=gamma_R_TTCS;

```

```

param=[alfa,beta,gamma];
oRotate_R_TTCS=Euler_rotation(param);

```

```

oTraslate_R_TTCS=[ t1x_R_TTCS; t1y_R_TTCS; t1z_R_TTCS]';
H_R_TTCS=[ oRotate_R_TTCS oTraslate_R_TTCS'; 0 0 0 1];

gamma_R_TCS=Station2_gamma_R_TCS;
beta_R_TCS=Station2_beta_R_TCS;
alfa_R_TCS=Station2_alfa_R_TCS;
t1x_R_TCS=Station2_t1x_R_TCS;
t1y_R_TCS=Station2_t1y_R_TCS;
t1z_R_TCS=Station2_t1z_R_TCS;

alfa=alfa_R_TCS;
beta= beta_R_TCS;
gamma=gamma_R_TCS;

param=[alfa,beta,gamma];
oRotate_R_TCS=Euler_rotation(param);

oTraslate_R_TCS=[ t1x_R_TCS; t1y_R_TCS; t1z_R_TCS]';
H_R_TCS=[ oRotate_R_TCS oTraslate_R_TCS'; 0 0 0 1];

H_TCS_TTCS=pinv(H_R_TCS)*H_R_TTCS;

oRotate_TCS_TTCS=H_TCS_TTCS(1:3,1:3);
oTraslate_TCS_TTCS=H_TCS_TTCS(1:3,4);
oTraslate_TCS_TTCS_circun=[0 -oTraslate_TCS_TTCS(3) oTraslate_TCS_TTCS(2);
oTraslate_TCS_TTCS(3) 0 -oTraslate_TCS_TTCS(1);
-oTraslate_TCS_TTCS(2) oTraslate_TCS_TTCS(1) 0];

gamma_R_SCS=Station2_gamma_R_SCS;
beta_R_SCS=Station2_beta_R_SCS;
alfa_R_SCS=Station2_alfa_R_SCS;
t1x_R_SCS=Station2_t1x_R_SCS;
t1y_R_SCS=Station2_t1y_R_SCS;
t1z_R_SCS=Station2_t1z_R_SCS;

alfa=alfa_R_SCS;
beta= beta_R_SCS;
gamma=gamma_R_SCS;

param=[alfa,beta,gamma];
oRotate_R_SCS=Euler_rotation(param);

oTraslate_R_SCS=[ t1x_R_SCS; t1y_R_SCS; t1z_R_SCS]';
H_R_SCS=[ oRotate_R_SCS oTraslate_R_SCS'; 0 0 0 1];

H_SCS_TCS=pinv(H_R_SCS)*H_R_TCS;

oRotate_SCS_TCS=H_SCS_TCS(1:3,1:3);
oTraslate_SCS_TCS=H_SCS_TCS(1:3,4);

```



```

Tool_diameter=Tool_diameter_station_3;
Tool_length=Tool_length_station_3;

% HTM: The tool tip CS is equal to the qi CS. qi=S3
Station3_alfa_R_TTCS=alfa_R_S3;
Station3_beta_R_TTCS=beta_R_S3;
Station3_gamma_R_TTCS=gamma_R_S3;
Station3_t1x_R_TTCS=t1x_R_S3;
Station3_t1y_R_TTCS=t1y_R_S3;
Station3_t1z_R_TTCS=t1z_R_S3;

% The tool CS is equal to the tool tip CS if the operation is a face
% milling. For S3, is a face milling (frontal) operation
Station3_alfa_R_TCS=Station3_alfa_R_FCS;
Station3_beta_R_TCS=Station3_beta_R_FCS;
Station3_gamma_R_TCS=Station3_gamma_R_FCS;
Station3_t1x_R_TCS=Station3_t1x_R_TTCS;
Station3_t1y_R_TCS=Station3_t1y_R_TTCS;
Station3_t1z_R_TCS=Station3_t1z_R_TTCS;

% The Spindle CS is equal to the tool CS but it is deviated in Z direction
% by the cutting-tool length
Station3_alfa_R_SCS=Station3_alfa_R_TCS;
Station3_beta_R_SCS=Station3_beta_R_TCS;
Station3_gamma_R_SCS=Station3_gamma_R_TCS;
Station3_t1x_R_SCS=Station3_t1x_R_TCS;
Station3_t1y_R_SCS=Station3_t1y_R_TCS;
Station3_t1z_R_SCS=Station3_t1z_R_TCS-Tool_length;

gamma_R_TTCS=Station3_gamma_R_TTCS;
beta_R_TTCS=Station3_beta_R_TTCS;
alfa_R_TTCS=Station3_alfa_R_TTCS;
t1x_R_TTCS=Station3_t1x_R_TTCS;
t1y_R_TTCS=Station3_t1y_R_TTCS;
t1z_R_TTCS=Station3_t1z_R_TTCS;

alfa=alfa_R_TTCS;
beta= beta_R_TTCS;
gamma=gamma_R_TTCS;

param=[alfa,beta,gamma];
oRotate_R_TTCS=Euler_rotation(param);

oTraslate_R_TTCS=[ t1x_R_TTCS; t1y_R_TTCS; t1z_R_TTCS]';
H_R_TTCS=[ oRotate_R_TTCS oTraslate_R_TTCS'; 0 0 0 1];

gamma_R_TCS=Station3_gamma_R_TCS;
beta_R_TCS=Station3_beta_R_TCS;

```

```

alfa_R_TCS=Station3_alfa_R_TCS;
t1x_R_TCS=Station3_t1x_R_TCS;
t1y_R_TCS=Station3_t1y_R_TCS;
t1z_R_TCS=Station3_t1z_R_TCS;

alfa=alfa_R_TCS;
beta= beta_R_TCS;
gamma=gamma_R_TCS;

param=[alfa,beta,gamma];
oRotate_R_TCS=Euler_rotation(param);

oTraslate_R_TCS=[ t1x_R_TCS; t1y_R_TCS; t1z_R_TCS]';
H_R_TCS=[ oRotate_R_TCS oTraslate_R_TCS'; 0 0 0 1];

H_TCS_TTCS=pinv(H_R_TCS)*H_R_TTCS;

oRotate_TCS_TTCS=H_TCS_TTCS(1:3,1:3);
oTraslate_TCS_TTCS=H_TCS_TTCS(1:3,4);
oTraslate_TCS_TTCS_circun=[0 -oTraslate_TCS_TTCS(3) oTraslate_TCS_TTCS(2);
oTraslate_TCS_TTCS(3) 0 -oTraslate_TCS_TTCS(1);
-oTraslate_TCS_TTCS(2) oTraslate_TCS_TTCS(1) 0];

gamma_R_SCS=Station3_gamma_R_SCS;
beta_R_SCS=Station3_beta_R_SCS;
alfa_R_SCS=Station3_alfa_R_SCS;
t1x_R_SCS=Station3_t1x_R_SCS;
t1y_R_SCS=Station3_t1y_R_SCS;
t1z_R_SCS=Station3_t1z_R_SCS;

alfa=alfa_R_SCS;
beta= beta_R_SCS;
gamma=gamma_R_SCS;

param=[alfa,beta,gamma];
oRotate_R_SCS=Euler_rotation(param);

oTraslate_R_SCS=[ t1x_R_SCS; t1y_R_SCS; t1z_R_SCS]';
H_R_SCS=[ oRotate_R_SCS oTraslate_R_SCS'; 0 0 0 1];

H_SCS_TCS=pinv(H_R_SCS)*H_R_TCS;

oRotate_SCS_TCS=H_SCS_TCS(1:3,1:3);
oTraslate_SCS_TCS=H_SCS_TCS(1:3,4);
oTraslate_SCS_TCS_circun=[0 -oTraslate_SCS_TCS(3) oTraslate_SCS_TCS(2);
oTraslate_SCS_TCS(3) 0 -oTraslate_SCS_TCS(1);
-oTraslate_SCS_TCS(2) oTraslate_SCS_TCS(1) 0];

% Matrices to be added into the current SoV model. SoV extension

```

```

Extended_SoV_A=[[oRotate_TCS_TTCS'] [-oRotate_TCS_TTCS'*oTraslate_TCS_TTCS_circun];
               [zeros(3,3) [oRotate_TCS_TTCS']]];

Extended_SoV_B=eye(6);

Extended_SoV_C=[[oRotate_SCS_TCS'] [-oRotate_SCS_TCS'*oTraslate_SCS_TCS_circun];
               [zeros(3,3) [oRotate_SCS_TCS']]];

Extended_SoV_M=[[Extended_SoV_A*Extended_SoV_C] [Extended_SoV_B]];

Extended_SoV_Phi=[Station_alfa_x 0;
                  Station_alfa_y 0;
                  Station_alfa_z 0;
                  Station_beta_x 0;
                  Station_beta_y 0;
                  Station_beta_z 0;
                  0 0;
                  0 0;
                  0 Station3_gamma_z_3f1;
                  0 0;
                  0 0;
                  0 0;];

% Derivation of the machining-induced error related to feature S3
Station3_um_S3=[Extended_SoV_M]*[Extended_SoV_Phi]*[Station3_Delta_T
            Station3_Delta_Vb_f1]';

% Machining-induced errors for qi=S8. Previous calculus is repeated for the Feature S8.
Station3_alfa_R_TTCS=alfa_R_S8;
Station3_beta_R_TTCS=beta_R_S8;
Station3_gamma_R_TTCS=gamma_R_S8;
Station3_t1x_R_TTCS=t1x_R_S8;
Station3_t1y_R_TTCS=t1y_R_S8;
Station3_t1z_R_TTCS=t1z_R_S8;

% If the operation is a end milling, the CS is deviated the tool
% diameter in Z direction. For S8, is a end-milling (pheriferical) operation
Station3_alfa_R_TCS=Station3_alfa_R_FCS;
Station3_beta_R_TCS=Station3_beta_R_FCS;
Station3_gamma_R_TCS=Station3_gamma_R_FCS;

Station3_t1x_R_TCS=Station3_t1x_R_TTCS;
Station3_t1y_R_TCS=Station3_t1y_R_TTCS+Tool_diameter/2;
Station3_t1z_R_TCS=Station3_t1z_R_TTCS;

% The Spindle CS is equal to the tool CS but it is deviated in Z direction
% by the cutting-tool length
Station3_alfa_R_SCS=Station3_alfa_R_TCS;

```

```

Station3_beta_R_SCS=Station3_beta_R_TCS;
Station3_gamma_R_SCS=Station3_gamma_R_TCS;
Station3_t1x_R_SCS=Station3_t1x_R_TCS;
Station3_t1y_R_SCS=Station3_t1y_R_TCS;
Station3_t1z_R_SCS=Station3_t1z_R_TCS-Tool_length;

gamma_R_TTCS=Station3_gamma_R_TTCS;
beta_R_TTCS=Station3_beta_R_TTCS;
alfa_R_TTCS=Station3_alfa_R_TTCS;
t1x_R_TTCS=Station3_t1x_R_TTCS;
t1y_R_TTCS=Station3_t1y_R_TTCS;
t1z_R_TTCS=Station3_t1z_R_TTCS;

alfa=alfa_R_TTCS;
beta= beta_R_TTCS;
gamma=gamma_R_TTCS;

param=[alfa,beta,gamma];
oRotate_R_TTCS=Euler_rotation(param);

oTraslate_R_TTCS=[ t1x_R_TTCS; t1y_R_TTCS; t1z_R_TTCS]';
H_R_TTCS=[ oRotate_R_TTCS oTraslate_R_TTCS'; 0 0 0 1];

gamma_R_TCS=Station3_gamma_R_TCS;
beta_R_TCS=Station3_beta_R_TCS;
alfa_R_TCS=Station3_alfa_R_TCS;
t1x_R_TCS=Station3_t1x_R_TCS;
t1y_R_TCS=Station3_t1y_R_TCS;
t1z_R_TCS=Station3_t1z_R_TCS;

alfa=alfa_R_TCS;
beta= beta_R_TCS;
gamma=gamma_R_TCS;

param=[alfa,beta,gamma];
oRotate_R_TCS=Euler_rotation(param);

oTraslate_R_TCS=[ t1x_R_TCS; t1y_R_TCS; t1z_R_TCS]';
H_R_TCS=[ oRotate_R_TCS oTraslate_R_TCS'; 0 0 0 1];

H_TCS_TTCS=pinv(H_R_TCS)*H_R_TTCS;

oRotate_TCS_TTCS=H_TCS_TTCS(1:3,1:3);
oTraslate_TCS_TTCS=H_TCS_TTCS(1:3,4);
oTraslate_TCS_TTCS_circun=[0 -oTraslate_TCS_TTCS(3) oTraslate_TCS_TTCS(2);
oTraslate_TCS_TTCS(3) 0 -oTraslate_TCS_TTCS(1);
-oTraslate_TCS_TTCS(2) oTraslate_TCS_TTCS(1) 0];

```

```

gamma_R_SCS=Station3_gamma_R_SCS;
beta_R_SCS=Station3_beta_R_SCS;
alfa_R_SCS=Station3_alfa_R_SCS;
t1x_R_SCS=Station3_t1x_R_SCS;
t1y_R_SCS=Station3_t1y_R_SCS;
t1z_R_SCS=Station3_t1z_R_SCS;

alfa=alfa_R_SCS;
beta= beta_R_SCS;
gamma=gamma_R_SCS;

param=[alfa,beta,gamma];
oRotate_R_SCS=Euler_rotation(param);

oTraslate_R_SCS=[ t1x_R_SCS; t1y_R_SCS; t1z_R_SCS]';
H_R_SCS=[ oRotate_R_SCS oTraslate_R_SCS'; 0 0 0 1];

H_SCS_TCS=pinv(H_R_SCS)*H_R_TCS;

oRotate_SCS_TCS=H_SCS_TCS(1:3,1:3);
oTraslate_SCS_TCS=H_SCS_TCS(1:3,4);
oTraslate_SCS_TCS_circun=[0 -oTraslate_SCS_TCS(3) oTraslate_SCS_TCS(2);
oTraslate_SCS_TCS(3) 0 -oTraslate_SCS_TCS(1);
-oTraslate_SCS_TCS(2) oTraslate_SCS_TCS(1) 0];

% Matrices to be added into the current SoV model. SoV extension

Extended_SoV_A=[[oRotate_TCS_TTCS'] [-oRotate_TCS_TTCS'*oTraslate_TCS_TTCS_circun];
[zeros(3,3)] [oRotate_TCS_TTCS']];

Extended_SoV_B=eye(6);

Extended_SoV_C=[[oRotate_SCS_TCS'] [-oRotate_SCS_TCS'*oTraslate_SCS_TCS_circun];
[zeros(3,3)] [oRotate_SCS_TCS']];

Extended_SoV_M=[[Extended_SoV_A*Extended_SoV_C] [Extended_SoV_B]];

Extended_SoV_Phi=[Station_alfa_x 0;
Station_alfa_y 0;
Station_alfa_z 0;
Station_beta_x 0;
Station_beta_y 0;
Station_beta_z 0;
0 0;
0 0;
0 Station3_gamma_z_3f2;
0 0;
0 0;
0 0;];

```

```

% Derivation of the machining-induced error related to S8
Station3_um_S8=[Extended_SoV_M]*[Extended_SoV_Phi]*[Station3_Delta_T
  Station3_Delta_Vb_f2]';

Station{3}.um=[Station3_um_S3;
  Station3_um_S8];

%%%%%%%%%%%%%%%%%%%%%%%%%%%%%%%%%%%%%%%%%%%%%%%%%%%%%%%%%%%%%%%%%%%%%%%%
%%%%%%%%%%%%%%%%%%%%%%%%%%%%%%%%%%%%%%%%%%%%%%%%%%%%%%%%%%%%%%%%%%%%%%%%
%%%%%%%%%%%%%%%%%%%%%%%%%%%%%%%%%%%%%%%%%%%%%%%%%%%%%%%%%%%%%%%%%%%%%%%% DERIVATION OF A(3), B(3), U(3) %%%%%%%%%
%%%%%%%%%%%%%%%%%%%%%%%%%%%%%%%%%%%%%%%%%%%%%%%%%%%%%%%%%%%%%%%%%%%%%%%%

Station{3}.A=[Station{3}.A1+Station{3}.A5*Station{3}.A4*(Station{3}.A2*Station{3}.A1)];
Station{3}.B=[Station{3}.A5*Station{3}.A4*Station{3}.A3 Station{3}.A5];
Station{3}.U=[Station{3}.uf';
  Station{3}.um];

```

